'86 MASSIVE NEUTRINOS

in Astrophysics and in Particle Physics

International Advisory Committee :

K. Bergkvist (Stockholm)
J. D. Bjorken (FNAL)
F. Boehm (CALTEC)
A. Dar (Haifa)
E. Fiorini (Milano)
T. Kotani (Osaka)
D. Schramm (FNAL)
F. Sciully (CALTEC)
J. Steinberger (CERN)
R. Turlay (Saclay)
F. Wilczek (Santa Barbara)

Organizing Committee :

O. Fackler (Rockefeller)
M. Mugge (FNAL)
J. Trân Thanh Vân (Orsay)
F. Vannucci (Paris)

Sponsored by :

Institute for Geophysical
and Planetary Science
Lawrence Livermore
National Laboratory
Centre National de la Recherche Scientifique
Commissariat à l'Energie Atomique

Associated Editor : O. Lebey

Proceedings of the
SIXTH MORIOND WORKSHOP
Tignes - Savoie - France January 25 - February 1st, 1986

SPS
CERN
BIBLIOTHEQUE
NW
41
48
1986

'86 MASSIVE NEUTRINOS in Astrophysics and in Particle Physics

edited by
O. Fackler
J. Trân Thanh Vân

Editions Frontières

- 12332

'86 MASSIVE NEUTRINOS
IN ASTROPHYSICS AND IN PARTICLE PHYSICS

VIth Moriond Workshop

Tignes, Savoie, France - January 25 - February 1st, 1986

ISBN - 2 - 86332 - 040 - 8

Copyright 1986 by Editions Frontières

All rights reserved. This book, or parts thereof, may not be produced in any form or by any means, electronic or mechanical, including photocopying, recording or any information storage and retrieval system now known or to be invented, without written permission from the Publisher.

EDITIONS FRONTIERES
B. P. 44
91190 GIF sur YVETTE - France

Printed in Singapore by Kim Hup Lee Printing Co. Pte. Ltd.

FOREWORD

The Sixth Moriond Workshop of the XXIst Rencontres de Moriond was held at Tignes, Savoie (France) from January 25 to February 1st, 1986. It was attended by 110 participants from 17 countries.

The main purpose of the Rencontres de Moriond is to discuss recent developments in contemporary physics and also to promote effective collaboration between experimentalists and theorists in similar fields By bringing together a relatively small number of participants, we hope to develop better human relations as well as a more thorough and detailed discussion of the contributions in an informal and friendly atmosphere.

Two years ago, a Moriond Workshop was devoted to the study of the theoretical and experimental consequences of Massive Neutrinos in Astrophysics and in Particle Physics. The success of the meeting and the unanimous wish of the participants to discuss this subject again within two years encouraged us to organize this year Workshop on the subject of Massive Neutrinos. Since the last meeting, many new experiments have been started and new results become available and are presented - some of them for the first time - at the meeting.

The success of this workshop is due to the presence of almost all active physicists working in this field, to the efforts of the speakers to give pedagogical and enlighting lectures as well as to the lively discussions which followed the presentations. I would like to thank all the participants, the advisory committee members : K. Bergkvist, J. D. Bjorken, F. Boehm, A. Dar, E. Fiorini, T. Kotani, D. Schramm, F. Sciully, J. Steinberger, R. Turlay and F. Wilczek, and the organizing committee members : M. Mugge and F. Vannucci and particularly O. Fackler for their hard work in preparing the scientific as well as the material organization of this Workshop.

I am also grateful to Mr Baudin, Mayor of Tignes, Mr Debart and Mr Dorval for their help at Tignes, to the hotel owners : Mrs Baudin, Mrs Devilaine, Mr Mazzega and Mr Reymond for their hospitality at Tignes and to the Conference secretaries : S. Bouhet, K. Douplitzki, O. Lebey, N. Lesbre, Lê van Suu, L. Norry, A. Ramos and E. Trân Thanh Tâm who have devoted much of their time and energy to the success of this meeting.

The '86 Moriond Workshop is sponsored for the first time by both french and american institutions : Institute for Geophysical and Planetary Science, Lawrence Livermore National Laboratory, Centre National de la Recherche Scientifique and Commissariat à l'Energie Atomique. I sincerely hope that this cooperation between the two countries (and also with others countries) can continue and develop in the future.

J. Trân Thanh Vân

CONTENTS

S. P. ROSEN	"Introductory talk"	1

I. COSMOLOGICAL AND ASTROPHYSICAL CONSTRAINTS ON NEUTRINO MASS

F. R. KLINKHAMER	"Structure in the universe from massive neutrinos"	33
G. STEIGMAN	"Closing the door on dark matter candidates"	51
K. KANG	"Cosmology and heavy unstable particles"	63
D. N. SCHRAMM	"The resurrection of neutrinos as dark matter"	75
S. CAHEN	"Standard solar models : a search for consistency"	83
L. J. HALL	"Millicharged matter in the galactic halo"	93
P. LANGACKER	"The electron neutrino mass and neutrinoless double beta decay"	101
D. N. SPERGEL	"Experimental limits on cold dark matter"	113

II. SOLAR AND COSMIC NEUTRINOS

T. KIRSTEN	"Status report on the GALLEX solar neutrino project"	119
M. SPIRO	"Neutrino oscillations in matter and solar neutrino experiments"	129
W. C. HAXTON	"The molybdenum solar neutrino experiment"	143
J. J. SIMPSON	"SNO : The Sudbury neutrino observatory"	**151**
M. BALDO-CEOLIN	"Solar neutrino detection in ICARUS"	**159**
E. BELLOTTI	"The NUSEX experiment at Mont Blanc"	**165**
G. CHARDIN	"Search for high energy muons from Cygnus X3 in the Frejus detector"	**173**
A. Y. SMIRNOV	"Baksan underground data on Cygnus X-3 at $E_\mu > 200$ GeV and $E_\mu > 500$ GeV"	**181**

III. THEORETICAL ASPECTS OF MASSIVE NEUTRINOS

S. T. PETCOV	"Massive neutrinos and neutrino mixing"	**187**
A. HALPRIN	"Sneutrinos in rare kaon decay"	**207**
M. ROOS	"On the possible astrophysical evidence for a radiatively decaying neutrino"	**213**

IV. SEARCHES FOR HEAVY NEUTRAL LEPTONS

D. S. KOLTICK	"Limits on the tau neutrino mass"	219
G. SANTONI	"Searches for decays of heavy neutrinos in the charm experiment"	229
J. M. LEVY	"Limits on neutrinos mixing parameters from a heavy neutrino decay search"	235
R. ALEKSAN	"Search for heavy neutral leptons at Cello"	241
M. SHAEVITZ	"A search for heavy neutral leptons in υ_μ-N interactions"	253

V. NEUTRINO OSCILLATIONS

M. SHAEVITZ	"Neutrino oscillation experiments at accelerators"	259
K. KLEINKNECHT	"Experimental constraints on lepton mixing angles and neutrino mass differences for three simultaneously oscillating neutrino flavours"	271
S. KATSANEVAS	"Results on neutrino oscillations from an appearance experiment in BEBC"	279
E. S. SMITH	"Search for neutrino oscillations at LAMPF"	287
R. MASCHUW	"Search for neutrino oscillations with KARMEN"	293
J. M. LOSECCO	"Neutrino physics with a massive underground detector"	301
K. SCHRECKENBACH	"Experimental methods for the determination of the neutron lifetime"	313
J. L. VUILLEUMIER	"The oscillation experiment at the GOESGEN reactor"	321
J. BOUCHEZ	"Bugey Collaboration"	331
H. W. SOBEL	"Two position results from the Irvine mobile neutrino oscillation detector"	339
P. O. LAGAGE	"Studying reactor antineutrino oscillations with large underground dectectors ?"	349
A. Y. SMIRNOV	"Neutrino oscillations in matter with varying density"	355
A. MESSIAH	"Treatment of υ_e-oscillations in solar matter: The MSW effect."	373

VI. NEW NEUTRINOS DETECTORS

K. RIISAGER	"Thermal pulse detection of photons and charged particles"	391
V. ZACEK	"The superconducting tunnel junction - A new high resolution dectector in the Kev range"	397
D. TWERENBOLD	"Superconducting tunnelling junctions as high-resolution X-ray detectors"	407
D. N. SPERGEL	"Detecting dark matter with superconducting grains"	415
B. CABRERA	"Cryogenic particle detectors for magnetic monopoles and neutrinos"	423

VII. DIRECT MASS MEASUREMENTS

V. LUBIMOV	"The neutrino mass from beta spectrum (ITEP-85)"	441
K. E. BERGKVIST	"Some notes on a matter of controversy regarding the ITEP claims of evidence of finite neutrino mass"	465
J. W. PETERSEN	"An upper limit for the electron antineutrino mass from the Zurich experiment on tritium β-decay"	469
J. F. WILKERSON	"The Los Alamos free molecular and atomic tritium beta decay experiment"	483
H. KAWAKAMI	"Neutrino mass measurement at INS"	503
W. KOLOS	"Molecular effects in the neutrino mass determination from beta-decay of the tritium molecule"	517
M. MUGGE	"A status report on the Livermore-Rockefeller-Fermilab neutrino mass experiment"	529
M. DAUM	"New upper limit for the muon neutrino mass"	535
B. TASIAUX	"Nuclear-muon capture in ^{3}He and massive neutrino search in the 10-100 MEV range"	541
D. S. KOLTICK	"Search for neutral heavy leptons"	547
K. RIISAGER	"Limits for the electron neutrino mass from internal bremsstrahlung"	557

J. J. SIMPSON "Evidence for a 17-kev neutrino in ^{3}H and ^{35}S b spectra" 565

S. YASUMI "Measurement of the mass of the electron neutrino using electron capture in ^{163}Ho" 579

VIII. DOUBLE BETA DECAY

T. H. HO "2β-Decay and the pion induced double charge exchange nuclear reaction" 585

E. TAKASUGI "New theoretical developments on the double beta decay and the pattern of neutrino mixings" 589

H. V. KLAPDOR "Double beta decay rates and the neutrino mass" 597

P. VOGEL "Double beta decay and nuclear structure" 607

P. FISCHER "A low background study of Ge^{76} neutrinoless double beta decay in the St. Gothard tunnel" 615

E. FIORINI "Present and future experiments on double beta decay" 623

Y. NAGAI "Neutrinoless double beta decays of ^{76}Ge and the present status of ^{100}Mo double beta decays" 631

A. A. POMANSKI "Comment on the importance of the two neutrino double beta decay study for understanding of the internal structure nuclei" 639

IX. NEW INTERACTIONS

S. L. GLASHOW "The fifth force" 643

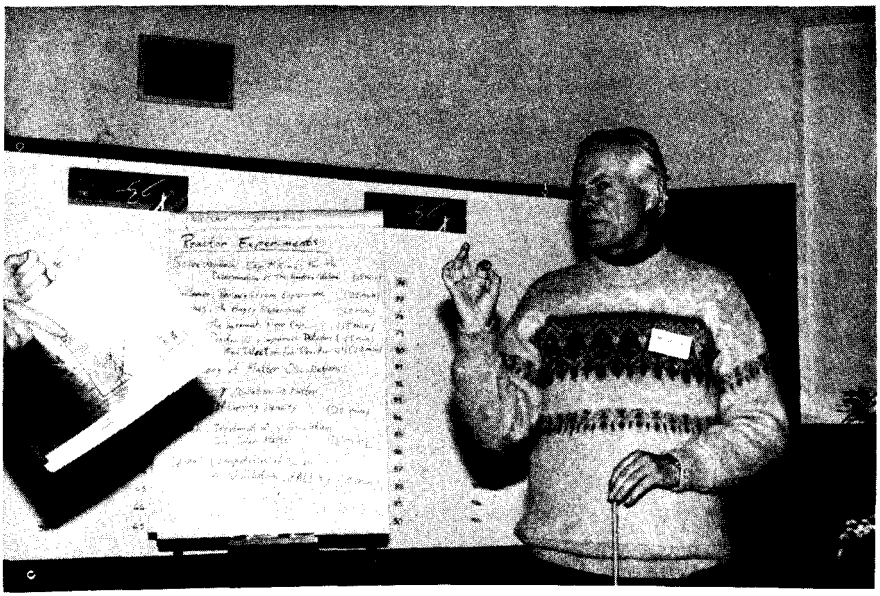
X. SUMMARY AND CONCLUSIONS

E. FIORINI "Summary talk" 653

G. STEIGMAN "Theoretical summary talk" 681

List of participants 695



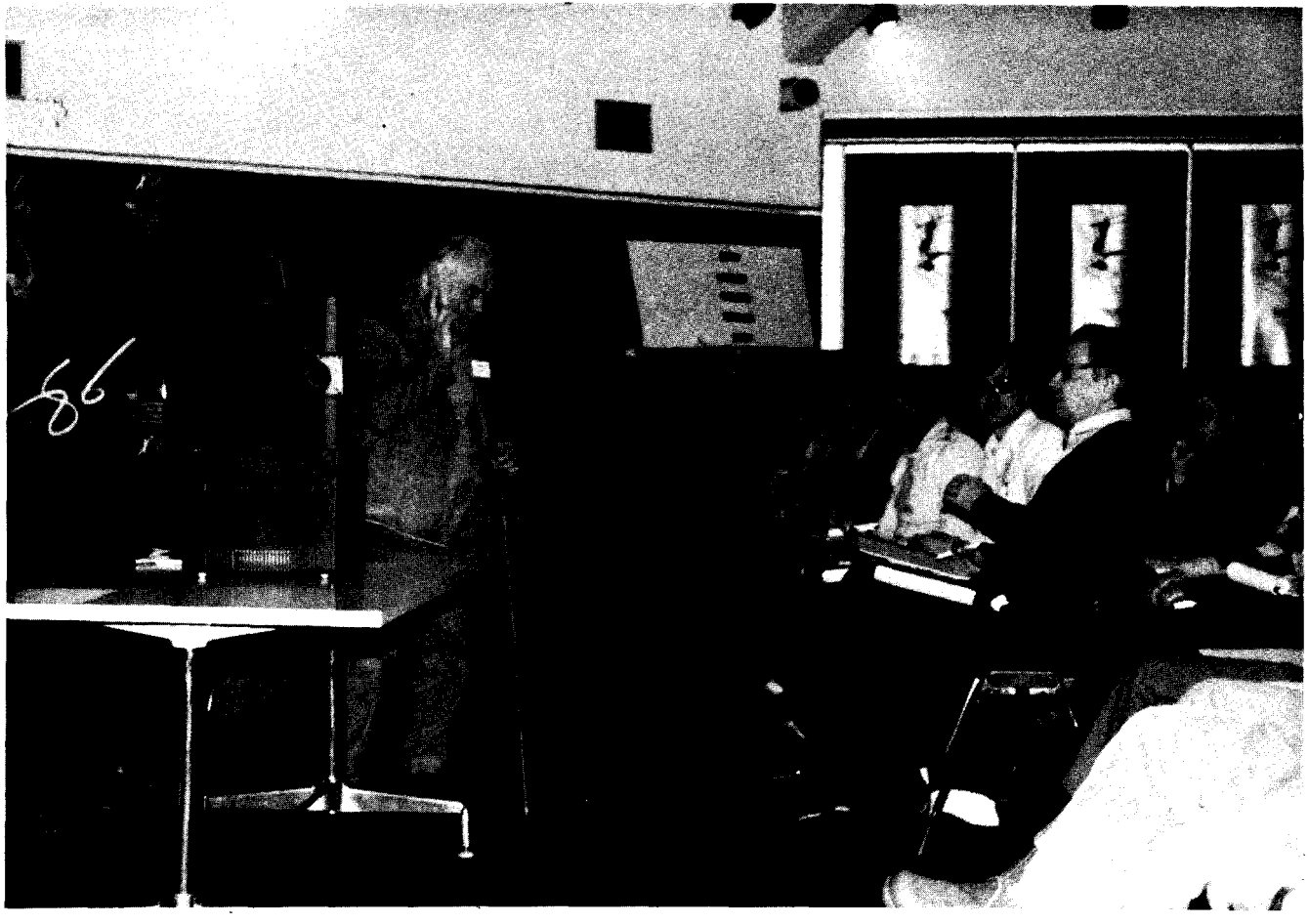

Positive Experiences















INTRODUCTORY TALK
VI. MORIOND WORKSHOP
MASSIVE NEUTRINOS IN PARTICLE PHYSICS AND ASTROPHYSICS

S. P. Rosen
Los Alamos National Laboratory
Los Alamos, NM 87545, U.S.A.

Abstract

We review the concepts of Majorana and Dirac neutrinos from an operational point of view and survey the experimental search for neutrino mass. We also review the work of Mikheyev and Smirnov on the enhancement of neutrino oscillations via the mechanism of Wolfenstein matter oscillations. Results of an extensive computation of MSW effects in the sun are described.

Introduction

The "desperate remedy" put forward by Pauli to save the principle of energy conservation in the 1930's has blossomed into an exceedingly rich phenomenon with important consequences for physics and astrophysics. But we are still asking some of the same questions posed by the founding fathers:

What is the mass of the neutrino? What is the relationship between the neutrino and its anti-particle?

Fortunately we have many more tools with which to answer them today than were available fifty years ago.

In the heavens, we have cosmology and astrophysics to provide us with arguments concerning the structure and evolution of the Universe, and the role played therein by massive neutrinos. Here on earth we have laboratories, reactors and accelerators at which to measure the spectra of β-decay and electron capture, π- and τ-decay; and at which to search for neutrino oscillations. Down below, we have deep underground experiments studying solar and atmospheric neutrinos and searching for no-neutrino double beta decay.

When might we know the answers? Well, I would hope that we might learn something about them at this workshop, and have the final, definitive words before I retire, a decade hence.

Pauli[1] expected the mass of neutrino to be small, but not necessarily zero. Fermi[2], in 1934, used his theory of beta decay to show that the mass of the neutrino had to be less than that of the electron. In the era of parity nonconservation (1957-60), we thought we had found a principle leading to:

$$m_\nu \simeq 0 \qquad (1.1)$$

namely the invariance of the charged-current (V-A) interaction under the replacement of any single field by γ_5 times itself (γ_5-invariance[3]). But this principle was soon lost: first to the discovery[4] of CP nonconservation in 1964, and then to discovery of neutral currents (1973).

Today, the mass of ν_e is known to be at least four orders of magnitude smaller than Fermi's original bound, while the bounds on

m_{ν_μ} and m_{ν_τ} are looser. The questions remains, however: how different are they from zero?

In 1937, Majorana[6] invented a "symmetrical" theory for electrons and positrons. He noted that, were his theory applied to neutrinos, it would imply that the same neutral particle would be emitted in β^+- and β^-- decay, instead of the ν_e with β^+- and ν_e^c ($\equiv\bar{\nu}_e$) with β^--decay. Racah[7], in the same year, invented the basic test for Majorana neutrinos, which consists of making the neutrino emitted by one nuetron stimulate the decay of a second neutron:

$$n_1 \rightarrow p_1 + e_1^- + "\nu" \quad , "\nu" + n_2 \rightarrow p_2 + e_2^- \tag{1.2}$$

and Furry[8] (1939) realized that the intermediate neutrino exchanged between n_1 and n_2 could be a virtual, instead of a real particle, thereby inventing the process of no-neutrino double beta decay:

$$(A,Z) \rightarrow (A,Z+2) + 2e^- \tag{1.3}$$

Fifty years later we are still looking for evidence that the sequence in eq. (1.2) acutally occurs. Its modern significance is that it is yet another signal for neutrino mass.

What I would like to do in this introduction is to review, briefly and from an operational point of view, the concepts mentioned above and the experimental status of neutrino mass as we begin this meeting. I would then like to discuss the beautiful, new work by Mikheyev and Smirnov[9] regarding resonance amplification of neutrino oscillations in the sun; it is based upon the extremely clever notion of matter oscillations introduced by Lincoln Wolfenstein[10] and it opens up the possiblility of a new interpretation of the solar neutrino problem.

2. Dirac and Majorana Neutrinos

In keeping with an operational point of view, we distinguish between Dirac and Majorana neutrinos on the basis of the relationship between the neutrinos emitted with negatively charged leptons and those emitted with positively charged leptons. Let us denote these neutrinos as "ν_ℓ^-" and "ν_ℓ^+" respectively:

$$
\begin{array}{l|\,|l}
n \to p e^- \text{ ``}\nu_e^-\text{''} & p \to n e^+ \text{ ``}\nu_e^+\text{''} \\
\pi^- \to \mu^- \text{ ``}\nu_\mu^-\text{''} & \pi^+ \to \mu^+ \text{ ``}\nu_\mu^+\text{''} \\
F^- \to \tau^- \text{``}\nu_\tau^-\text{''} & F^+ \to \tau^+ \text{ ``}\nu_\tau^+\text{''}
\end{array} \qquad (2.1)
$$

In the Dirac case "ν_ℓ^-" and ν_ℓ^+" are distinct particles:

$$\text{``}\nu_\ell^-\text{''} \neq \text{``}\nu_\ell^+\text{''} \quad \text{(Dirac)} \qquad (2.2a)$$

The Racah sequence of eq. (1.2) cannot occur, and we have a conservation law for total lepton number. Consequently no-neutrino double beta decay is forbidden and only the two-neutrino mode can take place.

In the Majorana case, "ν_ℓ^-" and "ν_ℓ^+" are identical particles:

$$\text{``}\nu_\ell^-\text{''} \equiv \text{``}\nu_\ell^+\text{''} \quad \text{(Majorana)} \qquad (2.2b)$$

The Racah sequence now becomes a possibility and there is no conservation law for lepton number. However, we must impose a serious caveat regarding massless neutrinos because, in the limit of exact (V-A) for charged currents and zero mass for neutrinos, the "ν_ℓ^-" has perfect positive helicity and the "ν_ℓ^+" has perfect negative helicity. The Racah sequence is forbidden no matter whether the neutrino is a Majorana particle or not, and the distinction between Majorana and Dirac neutrinos has no operational meaning.

For the distinction to be meaningful either: (i) charged currents must have an admixture of (V+A) when $m_\nu = 0$; or (ii) charged currents are pure (V-A), but $m_\nu \neq 0$. In a general sense these two possibilities go hand-in-hand because an admixture of (V+A) charged currents in lowest order can give rise to a non-zero neutrino mass in higher orders and vice versa. The practical question, however, is which of these two possibilities is likely to be the dominant effect. Gauge theories tend not to favor the first alternative because the neutrino flavor eignestates coupling to (V-A) and (V+A) charged currents are, in most

cases, orthogonal to one another. This orthogonality can only be broken if the neutrino mass matrix has one, or more non-zero and nondegenerate eigenvalues, and so the distinction between Majorana and Dirac neutrinos is only meaningful when the neutrino mass is not zero. Conversely, positive evidence that the neutrino is a Majorana particle would imply that, in the framework of gauge theories, the neutrino has a non-zero mass.

3. Dirac and Majorana Mass Terms

The typical mass term in a Lagrangian always couples a left-handed field ν_L to a right-handed one N_R:

$$-\mathcal{L} = \frac{1}{2} m \, \bar{\nu}_L \, N_R + \text{Hermitian Conj.} \tag{3.1}$$

Let us suppose ν_L is always the neutrino that couples to e^-_L in the charged weak current: then, if N_R couples to e^-_R in another charged weak current, the Lagrangian will be invariant under a global phase transformation:

$$\begin{pmatrix} e^-_{L,R} \\ \nu_L \\ N_R \end{pmatrix} \rightarrow e^{i\phi} \begin{pmatrix} e^-_{L,R} \\ \nu_L \\ N_R \end{pmatrix} \tag{3.2}$$

We therefore have a lepton conservation law and Dirac neutrinos. Exactly the same holds true if N_R and e^-_R are singlets with respect to the gauge group. The mass term for this case is known as a Dirac mass term.

Now suppose that N_R couples to e^+_R in a charged current, as does $(\nu_{eL})^c \equiv (\nu_e{}^c)_R$. We can no longer make the Lagrangian invariant under a global phase transformation, and so we no longer have a lepton conservation law. Such a mass term has Majorana neutrinos as its eigenstates, and hence it is known as a Majorana mass term. This is a "Unique, for neutrinos only" possibility which is not available for electrically charged fermions.

In general, both Dirac and Majorana terms are present in the Lagrangian:

$$-\mathcal{L} = \frac{1}{2} \; (\bar{\nu}_L, \; \bar{N}^C_L) \begin{bmatrix} m_L & m_D \\ m_D & m_R \end{bmatrix} \begin{pmatrix} \nu^C_R \\ N_R \end{pmatrix} + \text{H.C.} \tag{3.3}$$

The eigenstates of this Lagrangian are Majorana neutrinos as long as $m_L + m_R \neq 0$. When

$$m_L + m_R = 0 \tag{3.4}$$

the Majorana terms m_L and m_R can be "rotated" into the Dirac terms m_D, and hence the mass eigenstates are Dirac neutrinos.

One way of understanding eq. (3.4) is as a "pseudo-condition" for cancellation between the contributions of ν_L and N_R to the amplitude for no-neutrino double beta decay. We say "pseudo-condition" because the electron helicities change from the ν_L to the N_R contributions, and there is little interference between them. Another way of understanding eq. (3.4) is as a condition for a global phase invarance: the mass matrix is a vector in an SU(2) space and is invariant under all rotations having this vector as axis.

4. The Problem of Neutrino Mass

The essential problem of neutrino mass is that while there is no known theoretical principle which implies that the neutrino must have zero mass, its mass is certainly much smaller than that of any other fermion and may even be zero. Why is this so?

It is true that in the standard Glashow-Weinberg-Salam (G-W-S) theory with minimal Higgs-boson and fermion content, the Dirac mass of the neutrino vanishes because there is no ν_R field in the theory. There is, however, a right-handed change conjugate field, $(\nu_L)^C \equiv \nu^C_R$ in the theory, and so by adding weak isovector Higgs boson to the G-W-S model, one can generate a Majorana mass term.

In a more general context, theories which embed the G-W-S model into a larger gauge group tend either to add an extra right-handed neutrino to the fermion spectrum, or to provide a mechanism for

generating a Majorana mass, or to contain both of these features. Thus we expect theories beyond the standard model to generate mass for the neutrinos.

Unfortunately these theories give us very little guidance as to the magnitudes of neutrino masses, and in particular they do not explain why neutrino masses are much smaller than those of their charged lepton counterparts. One simple mechanism which might explain this fact is the see-saw of Gell-Mann, Ramond, and Slansky[11] and of Yanagida[12]. It is based upon the unique property of neutrinos, namely the Majorana mass term, and it makes use of this property to split the neutrino mass spectrum into two parts: very light fields coupling to e^-_L and very heavy ones coupling to e^-_R.

Let us suppose that, in addition to the ν_L which couples to e^-_L in the charged weak current, there does indeed exist an N_R which couples to e^-_R. The mass of N_R must be greater than, say, 10 GeV, or else we would have seen it by now. We can then construct a mass matrix exactly as in eq. (3.3) which the following choice of entries:

$$m_L \sim 0 \quad , m_R \sim M_{gut} \quad , m_D \sim m_f \tag{4.1}$$

where M_{gut} is the mass of the grand unification scale and m_f is the mass of an appropriate fermion. It could be the mass of the corresponding charged lepton, or it could be the mass of the appropriate up-quark, which has the same quantum numbers under the weak gauge group as the neutrino. Since M_{gut} is of order 10^{14} geV, the eigenvalues of the mass matrix separate into one very light one,

$$m_L \sim \frac{m_f^2}{M_{gut}} \tag{4.2}$$

and one very heavy one

$$m_R \sim M_{gut} \tag{4.3}$$

As m_f varies between the masses of the corresponding charged lepton and up-quark, so the ranges of values for m_L are:

$$m_{Le} \sim 10^{-11} - 10^{-9} \text{ ev}$$

$$m_{L\mu} \sim 10^{-7} - 10^{-5} \text{ eV} \qquad (4.4)$$

$$m_{L\tau} \sim 10^{-4} - 10^{-2} \text{ eV}$$

Both the L and the R mass eigenstates are Majorana neutrinos, and hence they can give rise to no-neutrino double beta. However one mass is much too small, and the other much too big to give rise to observable effects[13].

5. Double Beta Decay

We turn now to the only practical method of establishing the existence of Majorana neutrinos, namely the search for no-neutrino double beta decay.[14] It is customary to discuss two modes of nuclear double beta decay, the two-neutrino mode,

$$(A,Z) \rightarrow (A,Z+2) + 2e^- + 2\bar{\nu}_e \qquad (5.1)$$

which is expected to occur as a second order effect of the single beta-decay interaction Hamiltonian, and no-neutrino double beta decay,

$$(A,Z) \rightarrow (A,Z+2) + 2e^- \qquad (5.2)$$

which does not conserve lepton number ($\Delta L=2$). In principle, the no-neutrino mode could be engendered by some new, hitherto unknown, interaction, but this possibility is theoretically unattractive unless one has an independent argument establishing the strength of the new interaction. We therefore take the point of view that the no-neutrino mode, should it occur, must be due to the exchange of a virtual neutrino between two neutrons inside the nucleus. Clearly such a neutrino must be Majorana particle.

In recent years, a third possible mode of double beta decay has been discussed. It also violates the conservation of lepton number, but involves three particles in the final state, two electrons and a scalar

boson called the Majoron[15]. This hypothetical particle is the Goldstone boson which would be engendered by the spontaneous breakdown of lepton number conservation as a global rather than a local, symmetry.

From a purely phenomenological point of view, the amplitude for the no-neutrino decay mode arising from virtual neutrino exchange will not vanish provided that: either (i) the neutrino has a non-vanishing rest mass; or (ii) there exist right-handed currents; or (iii) both of these conditions are satisfied. From the gauge theoretic point of view, the neutrino must have a non-vanishing mass for any one of these conditions to be realized. Because the average separation between nucleons provides a cut-off on the momentum of the virtual neutrino, we must consider separately the cases in which the neutrino mass m_ν is much less than, or greater than its average momentum $\langle p_\nu \rangle$.

In the light neutrino case ($m_\nu \ll \langle p_\nu \rangle \tilde{\sim} 50$ MeV), the nuclear matrix elements are independent of m_ν and we should extract the same value of m_ν from the measured lifetimes of all double beta decay parent nuclei. In the heavy neutrino case ($m_\nu \gtrsim \langle p_\nu \rangle \tilde{\sim} 50$ MeV), the nuclear matrix elements vary with A because they involve a Yukawa-like "potential":

$$\text{Nuclear Matrix element} \sim \langle f | \text{Spin-Isospin Operator} \cdot \frac{e^{-mr}}{r} | i \rangle \qquad (5.3)$$

knowing the dependence upon A, we should again be able to extract the same mass from the lifetimes of all nuclei.

This will not be true if the process of no-neutrino double beta decay involves the exchange of two neutrinos, one light and one heavy. Under such conditions we find that the "effective mass" extracted from measured lifetimes does depend upon A[16], the general trend being the heavier A, the lighter "m_ν". Thus it could happen that the effective mass for ^{130}Te could be close to zero while that for ^{48}Ca is of order 30 eV.

With these ideas in mind, we now examine the current experimental situation. Several experimental groups[17] are searching for the no-neutrino mode of $^{76}\text{Ge} \rightarrow {}^{76}\text{Se}$, and one of them[17] has recently set a lower limit on the half-life of

$$T_{\frac{1}{2}}(0\nu) > 2.5 \times 10^{23} \text{ years} \qquad (5.4)$$

This is the most sensitive limit obtained so far, and from the theoretically calculated nuclear matrix elements, it follows that the effective mass is bounded by

$$\langle m_\nu \rangle_{\beta\beta} \lesssim 1\text{-}2.5 \text{ eV} \tag{5.5}$$

However, these same theoretical calculations underestimate the half-lives for the two-neutrino double beta decay mode by an order of magnitude; thus it might be safer to multiply the above bound by a factor 3 and set

$$\langle m_\nu \rangle_{\beta\beta} \lesssim 3\text{-}7.5 \text{ eV} \tag{5.6}$$

from ^{76}Ge decay.

Another method of setting limits on the effective mass consists of comparing the total half-lives of ^{128}Te → ^{128}Xe and ^{130}Te → ^{130}Xe.[19] The energy released in the first decay is roughly one third of that released in the second, 0.87 MeV as compared with 2.53 MeV. Consequently the ratio of the phases spaces for the no-neutrino mode of each decay is roughly proportional to $(3)^5$, while the phase space ratio for the two-neutrino mode is roughly $(3)^{10}$. If we now assume that the nuclear matrix elements for the two isotopes are equal to one another, we find that the ratio of half-lives is a very sensitive function of the effective neutrino mass varying from about 6×10^4 when $\langle m_\nu \rangle_{\beta\beta}$ is zero to 3×10^2 when $\langle m_\nu \rangle_{\beta\beta} \sim m_e$. From the latest limit on the half-life ratio, we learn that[20]

$$\langle m_\nu \rangle_{\beta\beta} \lesssim 5.7 \text{ eV} \tag{5.7}$$

Both of the limits in eqs. (5.6 and 7) are consistent with one another, but they are in conflict with the best value obtained by ITEP[21]:

$$m_\nu \sim 30 \text{ eV} \tag{5.8}$$

Before discussing the implications of this conflict, we should say a word about another conflict, namely that between the theoretical calculations of lifetimes and the geochemically measured ones.

The lifetime for the two-neutrino decay mode of eq. (5.1) is usually calculated by summing over intermediate nuclear states by means of closure and then using the shell model, or some variant thereof, to evaluate the resulting nuclear matrix element. Almost invariably the calculated lifetimes are an order of magnitude shorter than the lifetimes measured by geochemical means; in the case of ^{130}Te they have been as much as two orders of magnitude shorter[22], but Grotz and Klapdor[23] have recently reduced this discrepancy to one order with the aid of various correlations in the nucleus. Obviously, if we cannot compute the nuclear matrix elements for two-neutrino decay correctly, we cannot have much confidence in the matrix elements for no-neutrino decay, and hence we cannot deduce reliable limits on neutrino masses from experimental limits on the no-neutrino lifetime. A rough measure of our uncertainty is the factor 3 between eqs. 5.5 and 5.6.

A critical experiment in this regard is being carried out by Elliott, Hahn, and Moe[33] at the University of California, Irvine. They use a TPC to observe the two-neutrino mode of $^{82}\text{Se} \rightarrow {}^{82}\text{Kr}$, and even though they are in the midst of a valiant battle against the minutest of backgrounds, they are able to set a lower limit which compares quite well with the geochemical value, namely:

$$T_{\frac{1}{2}}(2\nu, {}^{82}\text{Se}) > 1.1 \times 10^{20} \text{ yr (69\% C.L.)} \tag{5.8a}$$

as compared with

$$T_{\frac{1}{2}}({}^{82}\text{Se})_{\text{geo}} = (1.7 \pm 0.3) \times 10^{20} \text{ yr.} \tag{5.8b}$$

This suggests that, insofar as ^{82}Se is concerned, the geochemical measurements are correct and that the theoretical estimates are overly optimistic. While it may not necessarily be the case, one is inclined to presume that the same holds true for ^{128},^{130}Te and for several other isotopes that have been investigated. The only isotope for which the theoretical calculations are in general agreement with experiment appears to be ^{48}Ca, and here one has a well-understood selection rule to

keep the matrix element down at a reasonable value[14]. Why the other theoretical nuclear matrix elements are much larger than they should be becomes a serious question for nuclear structure physics.

Setting these reservations aside for the moment, let us compare double beta decay with the present situation in tritium beta decay.

6. Tritium Beta Decay and Some Possible Implications

The present hunt for neutrino mass at the end of the Kurie plot, began with the report of a positive sighting by the ITEP group in 1980[25]. Up to, and including the time of this talk, it is still the only group reporting numbers; however, we hope that this will change as the meeting progresses.

A major problem in the interpretation of the ITEP experiment arises from the matrix in which the tritium is embedded. It is a complicated molecule known as valine and it can have the effect of changing the spectrum of final states of the ^{3}He daughters of tritium decay. Such changes could simulate a neutrino mass, at least in first approximation. For this reason, ITEP quote: (i) a "model independent" limit on the mass, which is the most conservative statement to be made; (ii) a "realistic" range for m_ν which makes use of the best available knowledge of the final state spectrum; and (iii) a "best" value, which has the best X^2 value. These results are:

$$\begin{array}{lll} m\nu > 9 \text{ eV} & \text{"model independent"} & \\ 40 > m_\nu > 20 \text{ eV} & \text{"realistic"} & (6.1) \\ m_\nu \sim 30 \text{ eV} & \text{best value} & \end{array}$$

Many other experiments have been undertaken since the original ITEP announcement, and they have taken different approaches to the matrix plus final state problem. The Los Alamos experimental group[26] has begun to use a molecular beam, very accurate computations of the molecular final states having been made, and eventually it will switch to an atomic beam. The Livermore group[27] plans to use frozen molecular tritium, while the Zurich-SIN group[28] uses a carbon matrix and the INS Tokyo[29] group another organic compound. We hope to hear new results from some these groups at this meeting.

If we assume that the ITEP best value of 30 eV is indeed the mass of the electron-type neutrino, then there is a conflict between it and the most conservative bound extracted from double beta decay, which is about 8 eV. The simplest conclusion to be drawn is that the neutrino is a Dirac particle, but this is not an attractive notion in the context of gauge theories. It has therefore been suggested that the electron neutrino might be an admixture of at least two mass eigenstates m_1 and m_2, which have opposite CP eigenvalues to ensure that they interfere destructively in the amplitude for no-neutrino double beta decay.

In tritium β-decay, one measures the average of the masses weighted by the mixing angle θ:

$$m_\nu \equiv m_1 \cos^2\theta + m_2 \sin^2\theta \tag{6.2}$$

and in no-neutrino decay one measures the weighted difference

$$m_{\beta\beta} \equiv m_1 \cos^2\theta - m_2 \sin^2\theta \tag{6.3a}$$

so long as m_1 and m_2 are light compared with the mean momentum of the exchanged neutrino. Should one mass, say m_1, be light and the other m_2, heavy, then one must take into account the difference between the propagation of light and heavy neutrinos through the nuclear medium. The effective mass for double beta decay now becomes[16)]

$$\langle m_{\beta\beta} \rangle = m_1 \cos^2\theta - F\, m_2 \sin^2\theta \tag{6.3b}$$

where the propagation factor F has the effect of making $\langle m_{\beta\beta} \rangle$ dependent on the nuclear species in which it is measured. Langacker, Sathiapalan, and Steigman[30)] have recently used a series of laboratory and cosmological constraints to show that if $m_1 \sim 27$ eV, then there are two small windows open for a stable heavy neutrino

$$m_2 \sim 40 \text{ MeV} \quad \text{or} \quad 1.7\text{-}2.1 \text{ geV} \tag{6.4}$$

What will the heavy lepton searches have to tell us for such neutrinos?

7. Neutrino Oscillations

Neutrino oscillations provide us with another imortant arena in the search for neutrino mass. Detection of the phenomenon itself would immediately establish that at least one neutrino has a non-zero mass, and the present limits on its existence allow us to explore much smaller mass differences than can be detected with present techniques in tritium beta decay or double beta decay.

Experiments searching for oscillations have been, and continue to be carried out at reactors, accelerators and underground detectors. At reactors the neutrinos, $\bar{\nu}_e$, have at most a few MeV of energy, and so one can only look for the disappearance $\bar{\nu}_e \to \nu_x$. While hints of oscillations have appeared from time to time, no definitive observations have been made and one can only set limits on the squared mass difference Δm^2 and the mixing angle $\sin^2 2\theta$. These limits extend down to 0.02 $(eV)^2$ for Δm^2 and somewhere between 0.1 and 0.2 for $\sin^2 2\theta$.[31]

Accelerators extend to much higher energies than reactors and they allow us to look for appearance modes $\nu_\mu \to \nu_\tau$ and $\nu_\mu \to \nu_e$ as well as for the disappearance $\nu_\mu \to \nu_x$. For large Δm^2, the appearance experiments can set much tighter limits on the mixing angles than can the disappearance ones; for example, present limits on $\nu_\mu \to \nu_e$ imply that $\sin^2 2\theta \lesssim 5\times 10^{-3}$ for large Δm^2[32]. The corresponding bounds on Δm^2 for $\sin^2 2\theta \sim 1$ are about an order of magnitude larger ($\Delta m^2 \lesssim 0.3$ ev^2) than those obtained at reactors.

By far the most sensitive experiments for extremely small Δm^2 is the disappearance of solar neutrinos $\nu_e \to \nu_x$. The long baseline ($\tilde{\sim} 1.5 \times 10^{11}$m) coupled with the low energy of solar neutrinos ($E \lesssim 14$ MeV) allows one to probe values of Δm^2 as low as $10^{-10} - 10^{-12}$ eV^2. Indeed the conventional approach to the solar neutrino problem is that, given the apparently large suppression observed by Davis and his colleagues in the $^{37}Cl \to {}^{37}Ar$ experiment, it is either caused by nonstandard solar dynamics, or by neutrino oscillations with large mixing angles and terrestrially inaccessible mass differences, possibly as small as $\Delta m^2 \sim (10^{-10} - 10^{-12})eV^2$.

In a beautiful paper, Mikheyev and Smirnov[9] have recently shown that a new interpretation of the solar neutrino problem might be possible. They point out that, given the high densities of matter

encountered in the sun, oscillations with small mixing angles ($\sin^2 2\theta \sim 10^{-3} - 10^{-1}$) can greatly be enhanced through the mechanism of Wolfenstein matter oscillations[10] and the effective mixing angle can become maximal or close to it. Thus a neutrino born as a ν_e in the core of the sun can emerge as almost a pure ν_μ even though the in vacuo mixing angle is small. This Mikheyev-Smirnov-Wolfenstein (MSW) effect comes into play for a range of mass differences which is larger than the large angle case, namely $\Delta m^2 \sim 10^{-4} - 10^{-8}$ eV^2, but still not accessible to reactor or accelerator experiments. In the following section I shall discuss an extensive series of computations of the MSW effect which has just been performed at Los Alamos by J. Gelb and myself.[33]

In concluding this section I want to remark that, once we obtain definitive evidence for the existence of oscillations, we will have to adapt a 3-state analysis rather than the 2-state analysis customarily used. The 2-state analysis is excellent for the purpose of demonstrating the essential physics of oscillations, but if and when oscillations are found, we will no longer be able to evade the full complexity and parametrization of a three (and possibly more) neutrino system.[34]

8. The MSW Enhancement Effect and Solar Neutrinos

In essence, the solar neutrino problem is simply that the standard solar model predicts a capture rate for ^{8}B neutrinos (plus a small component of ^{7}Be neutrinos) in the reaction

$$\nu + {}^{37}\mathrm{Cl} \rightarrow e^- + {}^{37}\mathrm{Ar} \qquad (8.1)$$

of[35]

$$(C.R)_{Th} = 5.9 \pm 2.2 \quad \text{SNU}$$

while the experiment by Ray Davis and his colleagues has detected, over a period of 10-15 years, an average capture rate of[36]

$$(C.R)_{expt} = 2.1 \pm 0.3 \quad \text{SNU} \qquad (8.2)$$

Is this discrepancy of a factor 2-4 between theory and experiment due to some dynamical feature of the sun not taken into account in the standard model, or is it due to neutrino oscillations? Here I am going to take the point of view that oscillations are responsible and describe the implications of the MSW effect.

Let me remind you that matter oscillations arise because electron-type neutrinos can scatter coherently from matter through one particular diagram that is not open to muon- and tau-type neutrinos. In so far as neutral current reactions are concerned, there is thought to be no difference between the three types of neutrino when they exchange a neutral Z-boson with quarks and leptons; but an electron-type neutrino can also scatter from electrons through the exchange of a charged W-boson. This additional diagram gives rise to a difference in the refractive index of the electron-neutrino as compared with muon- and tau-neutrinos; alternatively one can think of a difference in the effective masses of the neutrinos as they propagate through a material medium.

If we denote by $\nu_e(t)$ and $\nu_\mu(t)$ the probability amplitudes for a given neutrino to be an electron-type or a muon-type neutrino respectively at time t, then the differential equation governing their time development is[10]

$$i\frac{d}{dt}\begin{pmatrix}\nu_e\\ \nu_\mu\end{pmatrix}=\begin{bmatrix}A' + \sqrt{2}GN_e & B\\ B & D\end{bmatrix}\begin{pmatrix}\nu_e\\ \nu_\mu\end{pmatrix}$$

where A′, B, D are the usual in vacuo parameters

$$A' = \frac{m_1^2c^2 + m_2^2s^2}{2E} \quad ; \quad D = \frac{m_1^2 s^2 + m_2^2c^2}{2E}$$

$$B = \frac{\left(m_2^2 - m_1^2\right) cs}{2E} \equiv \frac{\Delta m^2}{2E} cs \qquad (8.4)$$

$$\nu_e = c\nu_1 + s\nu_2 \quad ; \quad \nu_\mu = -s\nu_1 + c\nu_2$$

$$c \equiv \cos\theta \quad , \quad s \equiv \sin\theta$$

and $\sqrt{2}\ GN_e$ is the contribution of the charged W-boson diagram to the coherent forward scattering of electron-type neutrinos by electrons. Here G is the Fermi constant for weak interactions and N_e is the electron density. The sign of the matter oscillation term in eq. (8.3) is different from that originally given by Wolfenstein, but a consensus of three independent arguments now agrees with the change.

One such argument is a direct calculation by Langacker[37]; another, given by Wolfenstein[38] himself is based on the observation that the forward amplitude for $\bar{\nu}_e$-e scattering below the W-pole in the Δ-channel must have a definite sign; and the third is based upon the properties that, in the Glashow-Weinberg-Salam model, the W-exchange and Z-exchange diagrams have opposite signs[39], and Z exchange gives rise to an attractive force between ν_e and e.

The condition for maximal mixing between ν_e, ν_μ and the eigenmodes of eq. (8.3) is that the diagonal elements in the "Hamiltonian" matrix be equal to one another:

$$\sqrt{2}\ GN_e = D-A' = \frac{\Delta m^2}{2E}\cos 2\theta \tag{8.5}$$

Since G and N_e are both positive, the signs of Δm^2 and $\cos 2\theta$ must be the same for maximal mixing to occur; in turn this requires $\nu_e \equiv c\nu_1 + s\nu_2$ to be composed principally of the lighter of the two mass eigenstates.

In general, the effective mixing angle in matter, $\sin^2 2\theta_m$, is related to the in vacuo mixing angle $\sin^2 2\theta$ by[10]:

$$\sin^2 2\theta_m = \frac{\sin^2 2\theta}{\left[\sin^2 2\theta + (L/L_0 - \cos 2\theta\right]^2} \tag{8.6}$$

where

$$L = \frac{4\pi E}{\Delta m^2} \equiv \frac{2.5\ (E(\text{MeV}))}{\Delta m^2(\text{eV})^2}\ \text{meters}$$

$$L_0 = \frac{2\pi}{\sqrt{2}GN_e} = \frac{2.5}{\sqrt{2}} \cdot \frac{10^7}{\rho_e}\ \text{meters} \quad ; \quad N = 6 \times 10^{23}\rho_e \tag{8.7}$$

Equation (8.6) shows that $\sin^2 2\theta_m$ has its maximum value at $L/L_0 = \cos 2\theta$, which is the same condition as in eq. (8.5), and that it drops to 1/2 at a distance

$$\Delta\left(L/L_0\right) \equiv L/L_0 - \cos 2\theta = \pm \sin 2\theta \tag{8.8}$$

Thus the peak in the curve for $\sin^2 2\theta_m$ as a function of (L/L_0) gets narrower and narrower as $\sin^2 2\theta$ gets smaller and smaller. We shall make use of this property below to develop a simple model for the MSW effect, but for the moment let us turn to the results of the computations.

At Los Alamos, Jim Gelb and I have carried out a program in which we assume that the reduction by a factor ~ 3 in the ^{37}Cl experiment is due to the MSW effect. We determine those values of $\sin^2 2\theta$ and Δm^2 which yield this reduction, especially in the small mixing angle regime, and then for each set of parameters we predict:

(a) the capture rate for pp + ^{7}Be neutrinos in ^{71}Ga; and

(b) the spectrum at the earth of electron-type neutrinos coming from ^{8}B decay in the sun. Our results are shown in Figs. (1)-(3).

We find that there are two classes of solution for the ^{37}Cl problem (see Fig. 1):

1) one with $\Delta m^2 \tilde{\sim} 10^{-4}$ for all small θ;

and

2) $(\sin^2 2\theta) \times \Delta m^2 \tilde{\sim} 10^{-7.5}$.

Solutions belonging to the first class predict that the ^{71}Ga capture rate will be the same as in the standard solar model. Solutions belonging to the second class show a steady decrease in the ^{71}Ga capture as $\sin^2 2\theta$ increases from 10^{-3} up to 10^{-1}; this decrease becomes as large as a factor of 10 at the upper end of the $\sin^2 2\theta$ range (see Table I).

Table I. Predicted (pp + ^{7}Be)ν Capture Rates (SNU) in ^{71}Ga. Standard Model Predicts 110.

Δm^2 \ $\sin^2 2\theta$	10^{-3}	$10^{-2.5}$	10^{-2}	$10^{-1.5}$	10^{-1}	$10^{-0.5}$
7.8×10^{-5}	(110)	(110)	(110)	(110)	(110)	(110)
4×10^{-5}	(110)	110	110	110	110	110
1.1×10^{-5}	100	(100)	105	100	95	95
4×10^{-6}	90	85	(85)	80	75	65
1.1×10^{-6}	60	40	30	(30)	30	35
4×10^{-7}	80	45	10	5	(10)	25
1.3×10^{-7}	95	95	30	10	10	(25)

We also find that the spectra of ^{8}B electron-type neutrinos arriving at earth are different for the two classes of solutions. In the first class, the low energy neutrinos are virtually unchanged by the MSW effect, while the high energy ones are almost completely turned into muon type neutrinos; the separation between "high" and"low" occurs in the neighborhood of 5-7 MeV depending on the value of $\sin^2 2\theta$ (see Fig. 2). In the second class of solutions, neutrinos of all energies are partially converted into muon neutrinos, but the conversion is especially marked for the low and intermediate energies. Since the pp and ^{7}Be neutrinos have low energies, we see that the difference in their spectra accounts for the difference in the predictions of the two classes for the ^{71}Ga capture rate.

Under certain circumstances, the spectrum of electron-type neutrinos arriving at earth may play a critical role in the choice between different explanations for the solar neutrino problem. Suppose for example that the outcome of the ^{71}Ga experiment slows a definite reduction in capture rate as compared with the standard solar model, but that the reduction factor is either much less than that in the ^{37}Cl experiment (e.g. 3/2 instead of 3), or much greater than ^{37}Cl (e.g. 5 instead of 3.) In such a case there could be little doubt that the neutrino is oscillating and that the MSW effect is coming into play through the second class of solutions; a measurement of the spectrum would serve to confirm this.

But now suppose instead, that the reduction factor for the ^{71}Ga capture rate is about the same as in $^{37}C\ell$: in this case we would have to choose between solutions with large mixing angles and those with small angles enhanced by MSW. Since the spectrum changes markedly from one case to another, it becomes the only tool available for picking the appropriate solution.

Another situation in which the spectrum of electron neutrinos reaching the earth becomes important will occur if the ^{71}Ga experiment should yield a capture rate consistent with the predictions of the standard model. We would then have to choose between the MSW effect and solar dynamics as the cause of the $^{37}C\ell$ anomaly. A change in solar dynamics vis-a-vis the standard model would change the normalization of $^{8}8$ neutrinos, but not their spectral shape, while the MSW changes the shape. Thus again the spectrum becomes the tool with which one can choose between the two possible explanations. From this argument, it becomes clear that after the ^{71}Ga experiment, the most important measurement of solar neutrinos will be the spectrum of the electron-type neutrino component reaching the earth.

9. Theoretical Comments on the MSW Effect.

Having discussed the implications of the MSW effect for solar neutrino physics, let us turn to the theory of the effect. Since the density of the sun falls (approximately exponentially) as one moves out from the core of the sun to the edge, an electron neutrino born in the core will pass through three distinct regions on its journey out of the sun. In the first region, the in vacuo oscillation length L is much larger than L_0, the density induced "scattering length" (see eq. (8.7)), and so the effective mixing angle (eq. (8.6)), is close to zero. In the second region L is roughly equal to L_0 and so the maximal mixing condition of eq. (8.5) is close to being fulfilled. Finally the neutrino moves into a region in which L is much smaller than L_0, and the effective mixing angle is approximately the same as the in vacuo mixing angle. Thus one expects no oscillations to occur in the first region, large oscillations in the second region, and in vacuo type oscillations in the third region and then all the way to earth. As can be seen from Figs. (4), the computations confirm this picture very well, especially in the small angle case.

Now the solution of the "equations of motion" for $\nu_e(t)$ and $\nu_\mu(t)$ (eq. 8.3) depends upon a comparison between the size, $2\Delta R_0$, of the second region as compared with the effective oscillation length L_m of the neutrino in matter:

$$L_m = L/\{\sin^2 2\theta + (L/L_0 - \cos 2\theta)^2\}^{\frac{1}{2}} \tag{9.1}$$

If $2\Delta R_0$ is much larger the L_m, the eigenvectors of the Hamiltonian in eq. (8.3) will rotate relatively slowly as the neutrino moves through the second region, and we can use the adiabatic approximation to solve for $\nu_e(t)$ (see talk by Messiah[40] below); if, on the other hand, $2\Delta R_0$ is much smaller than L_m, then the sudden approximation must be used. We will argue below that of the two solutions found for the solar neutrino problem, the first one, with $\Delta m^2 \sim 10^{-4}$ eV^2, corresponds to the adiabatic solution, and the second to the sudden approximation.

To make this analysis more precise, let us consider the second region to be one in which $\sin^2 2\theta_m$ is greater than, or equal to one-half. In terms of L/L_0 it is centered at $(L/L_0) = \cos 2\theta$ and extends a distance $\Delta(L/L_0) = \pm \sin 2\theta$ on either side of it. For a fixed $E/\Delta m^2$ for the neutrino, the density at the central position is

$$\rho_0(R_0) = \frac{10^7}{\sqrt{2}} \frac{\Delta m^2}{E} \cos 2\theta \tag{9.2}$$

and the change at the end-points is

$$\pm\Delta\rho_0 = \pm\rho_0 \tan 2\theta \tag{9.3}$$

Thus the spatial extent of this region is

$$2\Delta R_0 = 2\Delta\rho_0 / \frac{d\rho}{dR_0} = \frac{2\tan 2\theta}{h_0} \quad ; \quad h_0 = \left| \frac{1}{\rho} \frac{d\rho}{dR_0} \right| \tag{9.4}$$

At the central point of the second region, the effective oscillation length is

$$L_m = L/\sin 2\theta = (4\pi E/\Delta m^2 \sin 2\theta) \tag{9.5}$$

Therefore the criterion for the sudden approximation ($2\Delta R_0 \ll L_m$) can be written as

$$\frac{\Delta m^2}{2E} \sin 2\theta \tan 2\theta \quad \ll \quad \pi\, h \tag{9.6}$$

The criterion for the adiabatic approximation is obtained by reversing the inequality in eq. (9.6).

A good approximation to the density profile of the sun, except possibly for the first 10% which corresponds to the core, is the exponential distribution

$$\rho(R) = \rho_c\, e^{-R/R_c} \; ; \quad R_c = (R_{sun}/10) \sim 7\times 10^7 m \tag{9.7}$$

Thus the scale height h_0 of eq. (9.4) is given by

$$h_0 = (1/7\times 10^7 m)$$

and the criterion for the sudden approximation becomes (in the small angle limit)

$$\sin^2 2\theta \left(\frac{\Delta m^2(eV)}{E(MeV)}\right)^2 \lesssim 10^{-7.7} \tag{9.8}$$

For the adiabatic approximation we reverse the inequality of eq. (9.8).

We have already made the point that the enhancement region, the second region encountered by the neutrino, is relatively narrow for small mixing angles. We can now use this property to construct a simple model for the sudden approxmation in the small angle limit in which the neutrino undergoes no oscillations in either the first or the third regions of its journey, but oscillates maximally in the narrow central region, the frequency being

$$w = \frac{\Delta m^2}{4E} \sin 2\theta \tag{9.9}$$

From arguments of continuity across the boundaries of the regions, the probability amplitude p_e is given in this model by[33)]

$$p_e(R) = \begin{cases} e^{i\alpha} & \text{Region I} \\ e^{i\alpha}\cos\, w(R-R_0+\Delta R_0) & \text{Region II} \\ e^{i\alpha}\cos\, w(2\Delta R_0) & \text{Region III} \end{cases} \qquad (9.10)$$

Hence the probability that a neutrino arrives at earth as an electron-type neutrino is given by

$$P_{earth}(\nu_e \to \nu_e) = \cos^2 (2w\Delta R_0) \sim \cos^2\left(\frac{\Delta m^2}{2E}\,\frac{(2\theta)^2}{h_0}\right) \qquad (9.11)$$

From the criterion for validity of our sudden approximation (eq. 9.6), we see that the argument of the cosine function in eq. (9.11) never exceeds π. Thus as a function of $E/\Delta m^2$, P_{earth} $(\nu_e \to \nu_e)$ begins at a value close to one, then declines to zero as the argument decreases from π to $\pi/2$, and then climbs steadily back to one as $E/\Delta m^2$ increases and the argument approaches zero. The scale for this behavior is determined by the factor $(2\theta)^2$, or more properly $(\sin^2(2\theta)/\cos 2\theta)$: The smaller $(2\theta)^2$, the more rapidly the probability passes from one to zero and back to one again. This behavior is nicely illustrated in Figure (5) below.

Another application of this result concerns not a monoenergetic neutrino, but the integral over a spectrum of energies. This is of course the situation one encounters in the case of ^8B neutrinos incident upon $^{37}C\ell$. The total capture rate is given by

$$R = \int_0^{Emax} F(E)\, \sigma(E)\, P_{earth}(\nu_e \to \nu_e) dE \qquad (9.12)$$

where $F(E)$ and $\sigma(E)$ are the flux and capture cross-sections respectively for neutrinos of energy E, and P_{earth} is the probability that such neutrinos are of the correct type to be captured via the charged current reaction $\nu + n \to p + e^-$. We evaluate R and obtain

$$R = \frac{1}{2} R_s + \frac{1}{2} \int_0^{E_{max}} \cos\left(\frac{\Delta m^2 (2\theta)^2}{E h_0}\right) F(E)\sigma(E)dE$$

$$= \frac{1}{2}R_s + \frac{1}{2} \int_{\infty}^{Q} \cos\chi \; F(\chi)\sigma(\chi) \; \frac{dE}{d\chi} \; d\chi \qquad (9.13)$$

where

$$\chi = \frac{\Delta m^2}{E} \cdot \frac{(2\theta)^2}{h_0} \quad , \quad Q = \frac{\Delta m^2}{E max} \cdot \frac{(2\theta)^2}{h_0} \qquad (9.14)$$

and R_s in the capture rate in the standard model.

If we now assert that R is some fraction, say 1/3, of the capture rate in the standard model, then we determine a specific value Q_0 for the upper limit of integration in eq. (9.13). This means that we obtain a relation between Δm^2 and $(2\theta)^2$:

$$\Delta m^2 \; (2\theta^2) \; \sim Q_0 \; h_0 \; E_{max} \sim Q_0 \times 10^{-7.4} \qquad (9.15)$$

Since Q_0 is a number of order unity, we find that this relation fits the second class of solutions for the ^{37}Cl experiment extremely well.

For most of the solutions satisfying eq. (9.15), the enhancement region (or slab) occurs in the main body of the sun rather than in the core. Obviously the other solution in which $\Delta m^2 \sim 10^{-4}$ eV^2 for all small $\sin^2 2\theta$ corresponds to a situation in which the enhancement occurs in the core (see the density profile, Fig. 6 and eq. (9.2)). To account for this solution as another manifestation of the sudden approximation we would have to assume that the density in the core falls off much more slowly than the exponential decline we have used for the body of the sun. A more likely explanation is that this solution arises from the adiabatic approximation, a point which will be discussed in detail by Messiah[40] at this meeting, and which has recently been emphasized by Bethe[41].

The principal feature of the adiabatic solution is that the probability p_{earth} $(\nu_e \to \nu_e)$ remains close to unity for $E/\Delta m^2$ in the

neighborhood of 10^2 - 10^4, then falls rapidly to an asymptotic value of $\sin^2\theta$ in the neighborhood of $E/\Delta m^2 \sim 10^5$ and then remains small as $E/\Delta m^2$ increases beyond this range of values. Thus for a fixed suppression in the Davis experiment, the adiabatic solution will always yield a value of Δm^2 which will not be very sensitive to the mixing angle and will lie in the vicinity of 10^{-4}. In addition, the impact of this solution upon the spectrum of ^8B neutrinos will be to leave unchanged electron neutrinos in the lower half of the energy range and to convert almost all the neutrinos in the upper half into muon-type neutrinos.

In conclusion let me express my own view that MSW is such a beautiful phenomenon that Nature would be well advised to use it. After all, it may eventually give us the unambiguous, incontrovertible, uncontestable, clear and definitive evidence we so eagerly seek that the neutrino has mass.

References

1) L. M. Brown, Physics Today, September 1978, p. 23.

2) E. Fermi, reprinted in P. K. Kabir, Development of Weak Interaction Theory, P. 1-21 (Gordon & Breach, 1963).

3) R. Feynman and M. Gell-Mann, Phys. Rev. 109, 1983 (1958); R. Marshak and E. Sudarshan ibid 109 1860 (1958); and J. J. Sakurai N. Cimento 7, 649 (1958).

4) J. Christenson, J. Cronin, V. Fitch and R. Turlay, Phys. Rev. Lett. 13, 138 (1964).

5) F. Hasert et al, Phys. Lett. 46B, 138 (1973).

6) E. Majorana, Nuovo Cimento 14, 171 (1937).

7) G. Racah, Nuovo Cimento 14, 322 (1937).

8) W. H. Furry, Phys. Rev. 56, 1184 (1939).

9) S. P. Mikheyev and A. Smirnov; see A. Smirnov in this volume.

10) L. Wolfenstein, Phys. Rev. D17, (1978).

11) M. Gell-Mann, P. Ramond, and R. Slansky, in Supergravity (North-Holland, 1979).

12) T. Yanagida, Workshop on Unified Theory and Baryon Number of Universe, (Japan, 1979).

13) A. Halprin, P. Minkowski, H. Primakoff and S. P. Rosen, Phys. Rev. D13, 2567 (1976).

14) Recent reviews of double beta decay have been given by: W. C. Haxton and G. J. Stephenson, Jr., Prog. Part. and Nuclear Phys. 12, 409 (1984); M. Doi, T. Kotani, and E. Takasugi, Osaka University Preprint OS-GE 85-03 (1985); and D. Caldwell UCSB preprint. See also J. Vergados, Physics Reports.

15) Y. Chikashige, R. N. Mohapatra, and R. D. Peccei, Phys. Lett. 98B, 265 (1981).

16) A. Halprin, S. Petcov, and S. P. Rosen, Phys. Lett. 125B, 335 (1983); J. D. Vergados, Phys. Rev. D28, 2887 (1983).

17) Collaborations working on ^{76}Ge experiments include Milano, LBL-UC Santa Barbara Battelle N. W.-University of South Carolina, and CalTech-SIN.

18) D. Caldwell et al, UC Santa Barbara Preprint (1986).

19) B. Pontecorvo, Phys. Lett. 26B, 630 (1968); H. Primakoff and S. P. Rosen, Phys. Rev. 184, 1925 (1981).

20) T. Kirsten, Proc. of the XIth International Conference on Neutrino Physics and Astrophysics (World Scientific, Singapore, 1984).

21) V. A. Lubimnov, Proceedings of XXII International Conference on High Energy Physics, Leipzig 1984.

22) W. C. Haxton, G. J. Stephenson Jr., and D. Strottman Phys. Rev. D25, 2360 (1982).

23) H. V. Klapdor and H. V. Grotz, Phys. Lett. 142B 323 (1984); and H. Klapdor, these proceedings.

24) S. R. Elliott, A. A. Hahn, and M. K. Moe, UC Irvine preprint (1986); and A. Hahn these proceedings.

25) V. A. Lubimov et al, Phys. Lett. 94B, 266 (1980).

26) T. Bowles, D. Knapp, R. H. Robertson and J. Wilkerson; see J. Wilkerson, these proceedings.

27) O. Fackler and H. Mugge, these proceedings.

28) See talk by Dr. Petersen, these proceedings.

29) See talk by Dr. Ejiri, these proceedings.

30) P. Langacker, A. Sathiapalan and G. Steigman, University of Pennsylvania Preprint (1985).

31) V. Zacek et al, Phys. Lett. 164B, 1983 (1985).

32) H. White, private communication.

33) S. P. Rosen, and J. Gelb, Los Alamos preprint LA-UR-86-804.

34) C. Kim and H. Nishiura, Johns Hopkins Preprint (1985).

35) Report of NSAC Subpanel, R. Vandenbosch, Chairman; J. Bahcall et al, Rev. Mod. Phys. 54, (1982).

36) R. Davis, Proceedings of Miniworkshop on Low-Energy Neutrino-Nucleus Interactions, Madison, Wisconsin, December 1984.

37) P. Langacker, private communication.

38) L. Wolfenstein, private communication.

39) See for example, B. Kayser et al, Phys. Rev. D20, 87 (1979).

40) A. Messiah, these proceedings.

41) H. A. Bethe, Phys. Rev. Lett. 56, 1305 (1986).

Figure Captions

Fig. 1: Values of Δm^2 and $\sin^2 2\theta$ that reduce the capture rate in the ^{37}Cl experiment by factors of 2,3,4 respectively. The two classes of solution for small mixing angles are clearly displayed.

Fig. 2: Values of Δm^2 and $\sin^2 2\theta$ that reduce the capture rate in the ^{71}Ga experiment by factors of 2,3,4 respectively.

Fig. 3: Probability for arrival of electron type neutrinos from ^8B decay at earth as a function of energy for the cases of: (i) the first class of solutions with $\Delta m^2 \sim 10^{-4}$ eV^2 (denoted by stars); and (ii) the second class of solutions with $\Delta m^2 2\theta \sim 10^{-7.5}$ (denoted by circles).

Fig. 4: Probability for $\nu_e \to \nu_e$ as the neutrino travels through the sun. The three regions in which oscillations are suppressed, amplified, and then behave as in vacuo are readily seen. In this example, $\sin^2 2\theta = 10^{-3}$.

Fig. 5: Probability at earth for $\nu_e \to \nu_e$ as a function of $E/\Delta m^2$. The range of large suppression grows with $\sin^2 2\theta$ and shrinks slightly at the lower $E/\delta m^2$ values when the spatial distribution of neutrino production is taken into account. Here $\sin^2 2\theta = 10^{-2}$.

Fig. 6: Density profile of the sun (courtesy of Dr. A. Cox).

Fig. 1

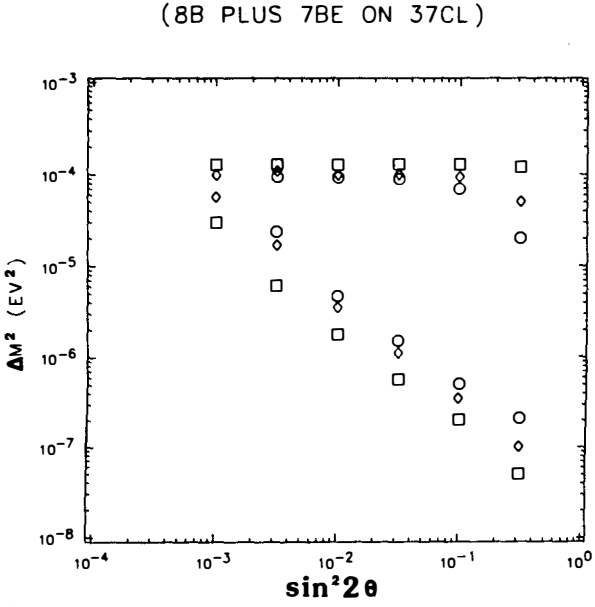

(8B PLUS 7BE ON 37CL)
10^{-3}
10^{-4}
10^{-5}
10^{-6}
10^{-7}
10^{-8}
ΔM^2 (EV^2)
10^{-4}
10^{-3}
10^{-2}
10^{-1}
10^{0}
$\sin^2 2\theta$

Fig. 2

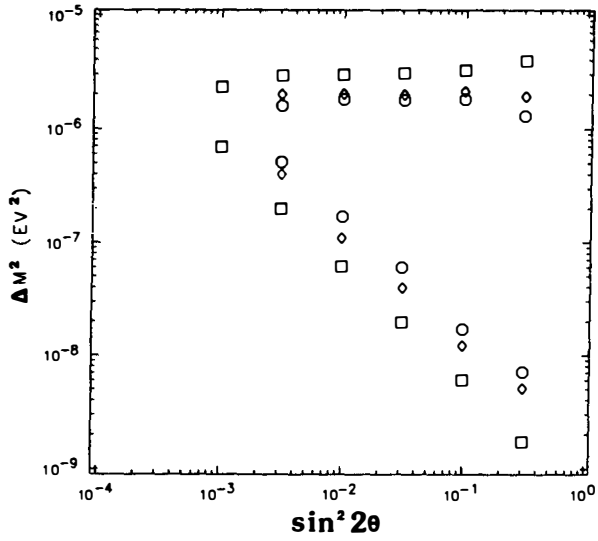

(PP PLUS 7BE ON 71GA)
10^{-5}
10^{-6}
10^{-7}
10^{-8}
10^{-9}
ΔM^2 (EV^2)
10^{-4}
10^{-3}
10^{-2}
10^{-1}
10^{0}
$\sin^2 2\theta$

Fig. 3

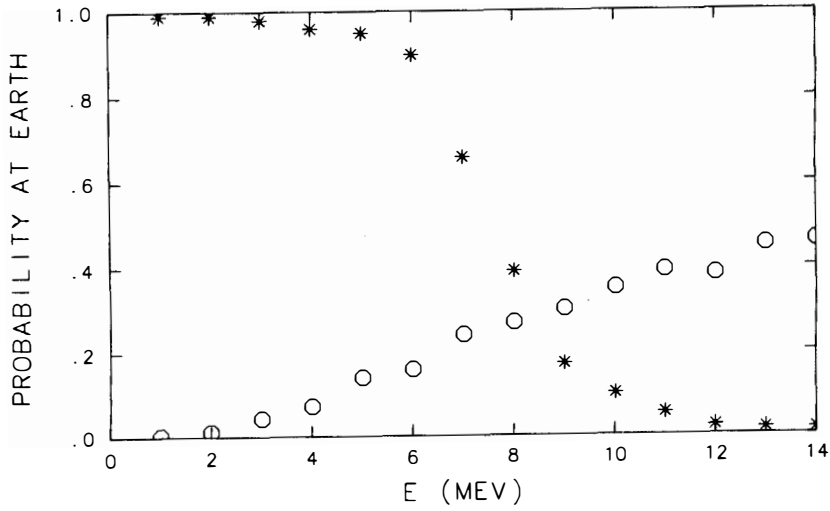

PROBABILITY AT EARTH
1.0
.8
.6
.4
.2
.0
0
2
4
6
8
10
12
14
E (MEV)

Fig. 4

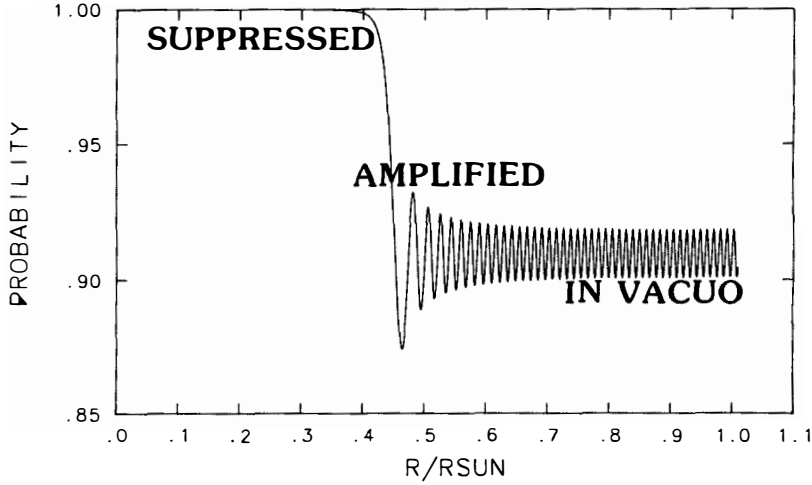

SUPPRESSED
AMPLIFIED
IN VACUO
PROBABILITY
1.00
.95
.90
.85
.0
.1
.2
.3
.4
.5
.6
.7
.8
.9
1.0
1.1
R/RSUN

Fig. 5

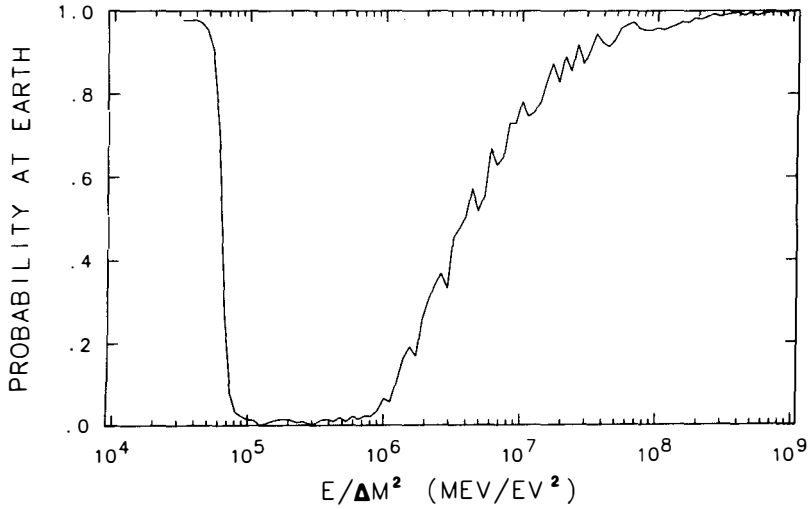
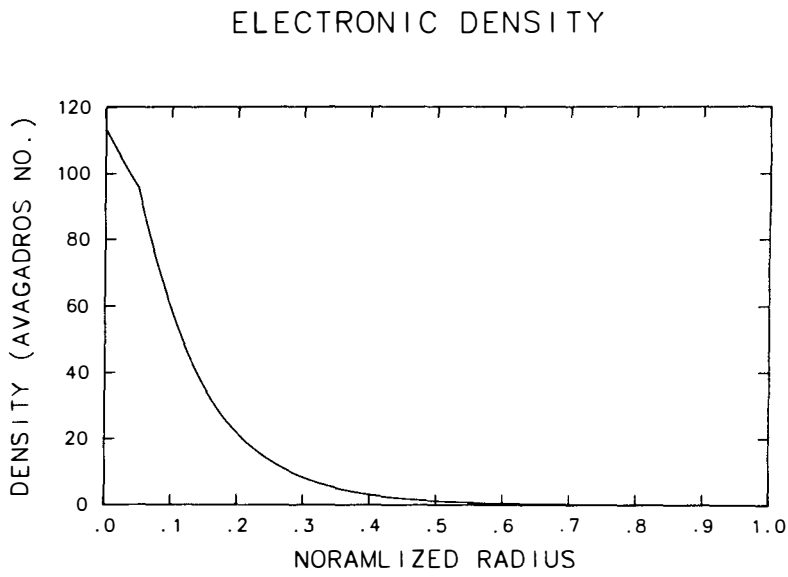

PROBABILITY AT EARTH
1.0
.8
.6
.4
.2
.0
10^4
10^5
10^6
10^7
10^8
10^9
E/ΔM² (MEV/EV²)

Fig. 6


ELECTRONIC DENSITY
DENSITY (AVAGADROS NO.)
120
100
80
60
40
20
0
.0
.1
.2
.3
.4
.5
.6
.7
.8
.9
1.0
NORAMLIZED RADIUS

STRUCTURE IN THE UNIVERSE FROM MASSIVE NEUTRINOS

Frans R. Klinkhamer*
Nuclear Science Division
Lawrence Berkeley Laboratory
Berkeley, CA 94720



ABSTRACT

A neutrino with hypothetical mass of order 10 eV may have an important role in the formation of large-scale structure in the Universe.

*This work was supported by the U.S. Department of Energy under Contract No. DE-AC03-76SF00098.

Introduction

Physical sciences have often progressed by making a judicial simplification of the problem at hand. A prime example is modern cosmology, where we disregard all fine structure and treat the Universe as perfectly homogeneous. According to our present knowledge the history of the Universe has two crucial ingredients:

(i) expansion, which idea goes back to Friedmann,[1] who first (1922) considered non-static solutions of the cosmological equations;

(ii) radiation epoch, which was discussed originally (1927) by Lemaitre[1] and later explored by Gamov,[1] who in particular studied the synthesis of heavier nuclei from protons and neutrons in the hot soup of the early Universe.

These two ingredients of our standard cosmology are reflected in its popular name: the Hot Big Bang. For a better understanding of what follows let me recall the basic assumptions and arguments leading to the standard model. The first two steps involve the relevant physics:

(i) General Relativity is the theory appropriate to describe the selfgravitation of the Universe. The Einstein field equations are in standard notation[2]

$$R_{\mu\nu} - \frac{1}{2} g_{\mu\nu} R = -8\pi G T_{\mu\nu} \qquad (1)$$

and relate the curvature of the space-time metric ($g_{\mu\nu}$) on the left-hand side to the energy-momentum tensor ($T_{\mu\nu}$) on the right-hand side via the Newton gravitational coupling constant (G);

(ii) Particle and nuclear physics to provide the correct expression for the energy-momentum tensor in (1).

The following two steps in the argument introduce the crucial simplifications, which make the problem tractable:

(iii) Homogeneity and isotropy, which reduce the metric to the Robertson-Walker form, greatly simplifying the set of 10 equations in (1);

(iv) Thermal equilibrium and entropy conservation of the matter content of the Universe, which leads to dependence on the overall thermodynamic quantities only, e.g., the temperature T.

These steps combined lead to simple differential equations, which describe the evolution of the Universe, see for example Chapter 15 of Weinberg's book.[2] Radio source counts and especially observations of the cosmic background radiation (CBR) support the assumptions (iii) and (iv). This

part of cosmology, which I would like to call "smooth cosmology," is in great shape. In fact, we dare to use the success of the model to constrain possible modifications of the particle physics. Specifically, the more or less correctly predicted abundances of ^2D, ^4He, ^7Li from cosmic nucleosynthesis would restrict the number (N_ν) of neutrino types (and hence the number of families) to 4 or 5 at most.[3] The reason for this is as follows: a larger number N_ν would lead to faster expansion, which leaves less time for the neutrons to decay and thus results in a higher abundance of ^4He. [It may be that for specific values of neutrino mass differences and mixing angles this upper bound on N_ν is raised[4].] Hopefully, measurement of the Z° width at SLC and LEP will confirm that N_ν is close to the presently known value of 3 and not very much larger.

Up till now I have briefly reviewed the stretching and evolution of the canvas of the Universe without any attention to the fine print on it. Nevertheless we do observe "ripples" to be present, i.e. galaxies, groups, clusters and superclusters ranging in mass from some $10^{11}M_\odot$ to $10^{16}M_\odot$. Many questions arise in what I would like to call "ripple cosmology":

(i) What determined the amplitude and shape of the primordial spectrum of the density perturbations, which grew into the presently observed structure?

(ii) Are there interrelations between the different entities, for example do galaxies arise as fragments in a larger system or do the galaxies form first and then agregate into clusters?

(iii) What sets the mass scale? Recall that the mass scale of stars arises from balancing the inward pull of gravitation with the thermal and radiation pressure of the interior of the star (Eddington in Ref. 1). We would like to have the same understanding for the typical mass of the ripples.

Furthermore, all we see is not all there is: dark matter seems to be 10 times more abundant than the visible matter.[5] In fact, our present estimates for the density ratio are

$$\Omega_{\text{luminous}} \sim 0.01 \tag{2a}$$

$$\Omega_{\text{dynamical}} \sim 0.1 - 1 \ . \tag{2b}$$

I take the opportunity to introduce some notation; the present density ratio, critical density and the Hubble expansion parameter are[2]

$$\Omega \equiv \rho/\rho_{crit}$$

$$\rho_{crit} \equiv \frac{3H_o^2}{8\pi G} = 2.\ 10^{-29}\ h^2\ g\ cm^{-3}$$

$$H_o \equiv 100\ h\ km\ s^{-1}\ Mpc^{-1} = (10^{10}\ h^{-1}\ yr)^{-1}$$

and for Ω <1 or >1 the Universe is open or closed and will expand for ever or contract again, respectively. Observations show h to lie between approximately 1/2 and 3/4. Let us return to the density ratios in (2), which have been deduced from the study of many different systems. As an example, I take the first such study, namely Zwicky's[1] analysis (1937) of the Coma cluster. Its mass can be determined in two ways:

(a) counting the galaxies or measuring their luminosity and then multiplying by a typical galaxy mass or mass to light ratio gives the cluster mass $M_{Coma}^{(a)}$;

(b) using the virial theorem with the observed velocities and orbits of the cluster galaxies gives the mass $M_{Coma}^{(b)}$.

Surprisingly $M_{Coma}^{(b)}$ turned out to be more than 100 times larger than $M_{Coma}^{(a)}$, or in other words, most of the matter in the Coma cluster is invisible! Adding up similar mass estimates of other systems leads to the overall mass densities reported in (2a,b). For dynamics dark matter is the most important and at best the visible galaxies may serve as tracers of the overall gravitational potential. But what is this dark matter made of? We do not know yet. Probably it is not baryonic, since the cosmic nucleosynthesis results[3] do not allow for such a large baryon density $\Omega_b \sim 0.1 - 1$. An ideal candidate, truly dark and collisionless, would be a massive neutrino. Only the heaviest neutrino would matter cosmologically, which in the absence of mixing may be the τ-type neutrino. [Let me indulge in some numerology: if the neutrinos follow the charged lepton (e^-, μ^-, τ^-) mass ratios their masses could be in the ballpark 0.01:3:50 eV.]

Alas, there is no definitive experimental result on neutrino mass. Of course, this should not, and did not, deter astrophysicists from speculating "what if..." and in the following I will summarize the results of their wishful thinking. Henceforth, I will assume $N_\nu = 3$ neutrino types and one dominant neutrino mass m_{ν_1}.

Massive Neutrinos in Cosmology

The implications of possible massive neutrinos for "smooth cosmology" were first discussed by Gershtein and Zeldovich,[6] who derived an important bound on the sum of the masses

$$\Sigma \equiv \sum_{i=1}^{N_\nu} m_{\nu i} \lesssim 100 \text{ eV} \quad . \tag{3}$$

The argument is very simple: since the neutrinos participated in the thermal equilibrium before they decoupled at $T \sim 1$ MeV, we know their present number density ($n_{\nu i} \sim \frac{1}{3} n_{\gamma CBR}$); multiplying with the mass $m_{\nu i}$ gives the present energy density ratio $\Omega_{\nu i} = 1.36\ (m_{\nu i}/100 \text{ eV})$ and in order to avoid a prohibitively large total density of the Universe or, equivalently, a too short age of the Universe the bound (3) must hold. The same argument gives mass limits of other weakly interacting particles (gravitinos...), provided their lifetime is large enough. Later it was noted[7] that massive neutrinos could provide Zwicky's "missing mass" in the Coma cluster and others. But the real breakthrough in understanding the role of massive neutrinos for "ripple cosmology" occurred in 1980, just after the first ITEP result on non-zero neutrino mass was announced. It was realized more or less simultaneously by different collaborations, located in the three superpowers the Netherlands,[8] the US,[9] and the USSR,[10,11] that massive neutrinos have two nice properties:

(i) a <u>damping scale</u> of order

$$1.8\ M_p^3/m_{\nu 1}^2 \sim 3\ 10^{14} \left(\frac{100 \text{ eV}}{m_{\nu 1}}\right)^2 M_\odot \quad , \tag{4}$$

where the Planck mass is $M_p \equiv (\hbar c/G)^{1/2} = 1.22\ 10^{28}$ eV = $2.17\ 10^{-5}$ g, this would give the desired mass scale of the ripples of our Universe;

(ii) only a <u>small initial amplitude</u> of the primordial (adiabatic) density perturbations is needed

$$\delta_{\nu 1}^{in} \equiv \left(\frac{\rho_{\nu 1} - \bar{\rho}_{\nu 1}}{\bar{\rho}_{\nu 1}}\right)^{in} \sim \frac{1 + z_{GF}}{1 + z_{\gamma\nu}} \sim 2\ 10^{-4}\ \frac{100 \text{ eV}}{m_{\nu 1}}\ \frac{1 + z_{GF}}{6} \tag{5}$$

and hence only small residual fluctuations in the CBR at the arcminute scale are to be expected.

In (5) $z_{\gamma\nu}$ and z_{GF} are the respective redshifts of the epoch when the neutrino mass becomes dominant and when the galaxies form ($\delta_{\nu 1} = 1$).

Recall that the redshift is given by $z \equiv (\lambda_{obs} - \lambda_{em})/\lambda_{em}$ and that $1 + z = a_{obs}/a_{em}$, where a is the scale factor of the Universe and "obs" and "em" refer to the present observer and the emission epoch.

For a neutrino mass of several tens of eV the scenario would be as follows: neutrinos ν_1 collapse into large systems and shortly afterwards the baryonic gas, which was dragged along, dissipates its energy and fragments into galaxies. I will now discuss in somewhat more detail how structure could have arisen in this way. In addition to Ref. 8-11 I will only give the reference of the best calculation to date of a particular problem.

Linear Growth Period

We have no definitive idea on the origin of the primordial density fluctuations, which grow into the observed structures of the Universe, and for simplicity we will use a scale-free initial spectrum

$$|\delta_k|^2 \propto k^n \quad , \tag{6}$$

where δ_k is the Fourier transform of $\delta \equiv (\rho - \bar{\rho})/\bar{\rho}$ with $\bar{\rho}$ the average density. The Harrison-Zeldovich spectrum with n = 1 is a special case, in that all different wavelength perturbations have the same rms gravitational potential depth. Spectra with n>1 or <1 would lead to strong inhomogeneities on small scales (black holes) or ultimately on large scales, unless there is a cut-off in (6). For this reason most astrophysicists prefer to use n = 1, but the reader should keep in mind our total lack of understanding of the initial perturbations. [An inflation scenario may lead to a n = 1 spectrum, but its amplitude appears too large;[12] nevertheless this is an interesting hint.] In this section we consider the period when $\delta_{\nu_1} << 1$, which allows us to linearize the perturbation equations. Before we look at the neutrino perturbations, we must consider in more detail the global evolution of the Universe. A neutrino mass m_{ν_1} is irrelevant for the very early epoch ($T >> m_{\nu_1}$). It may be that the light (lefthanded) neutrino ν_L has a super heavy (right-handed) partner ν_R, but it can be shown[13] that this partner does not upset standard nucleosynthesis or baryogenesis (creation of net baryon number at temperatures of the Grand Unification scale). For the later evolution Fig. 1 gives the energy densities of the relevant particles vs. the photon temperature (now 2.7 K): first the photons (and relativistic neutrinos) dominate, but for $T < m_{\nu_1}$ the massive non-relativistic

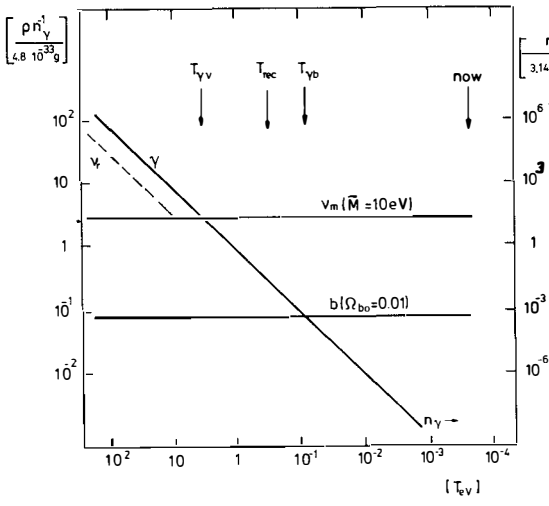


Fig.1 Thermal history of energy densities of photons, relativistic neutrinos and rest masses of neutrinos and baryons (see Klinkhamer and Norman 1981). Procedure to calculate the energy density of one component at a certain temperature: multiply $n_\gamma(T)$ from the ordinate at the right by the $\rho/n_\gamma(T)$ ratio of the component of the ordinate at the left. Note that the ρ/n_γ ratio of rest masses of neutrinos and baryons depends linearly on $\tilde{M} = \sum/3$ and Ω_{bo} respectively. We thus see that the cooling Universe first was dominated by radiation and relativistic particles and then by rest mass either from neutrinos ($T_{\gamma\nu}$) or baryons ($T_{\gamma b}$). In the latter epoch density fluctuations probably grew into the presently observed structure, leaving a trace in the cosmic background radiation which decoupled from the baryons at $T_{rec} \sim 4500$, when recombination of the ionized gas occurred. Note that for $T \lesssim 1$ MeV the neutrinos were a collisionless gas

neutrinos take over and now ($z < z_{\gamma\nu}$) the neutrino density perturbations can grow. This growth occurs earlier than would be the case for simple baryonic perturbations (in Fig. 1 $z_{\gamma b}$ is 100 times less than $z_{\gamma\nu}$). Since δ grows now as the scale factor a (if $\Omega_o < 1$ then the growth stops for $1 + z < \Omega_o^{-1}$, so that we must have $z_{GF} > \Omega_o^{-1} - 1$) the required initial amplitude to have condensation at z_{GF} is given by (5). After recombination the baryonic gas catches up rapidly with the neutrino perturbation. The small neutrino fluctuations are accompanied by fluctuations in the photons, which are free streaming after recombination of the nuclei (p^+, He^{++}) and the electrons (e^-) at $T \sim 4500$ K. Hence there will be small fluctuations in the CBR. Observational limits[14] are $\Delta T/T_{CBR} < 2\ 10^{-5}$ and calculations[15] show that small enough initial neutrino fluctuations are possible, provided

$$z_{GF} < 8.7 \quad \text{for } \Omega_o = 1,\ h = 0.75 \qquad (7)$$

$$z_{GF} < 3.5 \quad \text{for } \Omega_o = 1,\ h = 0.50$$

and Fig. 2 shows the expected $\Delta T/T$ for $\Omega_o = 1$, $h = 0.75$, $z_{GF} = 3$ (these calculations were for a $n = 1$ spectrum). Standard adiabatic perturbations without massive neutrinos require an initial amplitude larger than (5) and the resulting CBR fluctuations would violate the observational limits.

Now we turn to the emergence of a mass scale (4). In a normal collisional gas we know that for perturbations with wavelength λ larger

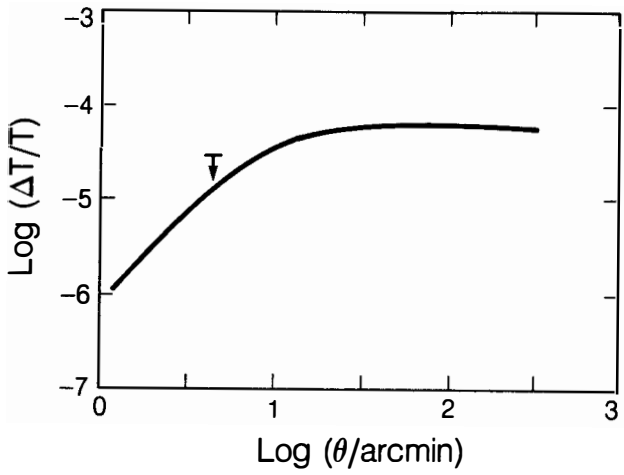


Fig. 2. Temperature fluctuations[15] of the cosmic background radiation vs. angular scale for a massive neutrino with $\Omega = 1$, $\Omega_b = 0.03$, $h = 0.75$ and $z_{GF} = 3$ and for the same experimental setup as in Ref. 14, which gave the upper limit (95% c.l.) shown by the arrow.

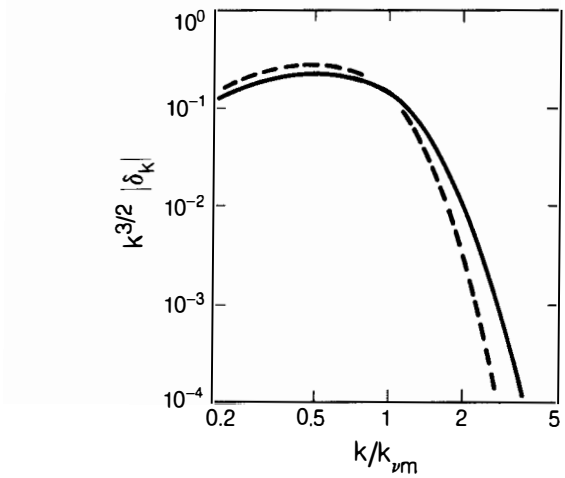


Fig. 3. Collisionless damping[16] of neutrino perturbations (full curve: a single massive neutrino, dashed: three equally massive neutrinos). The final result (at $z \tilde{\sim} 75$) for an initial spectrum (6) follows by multiplication of $(k/k_{\nu m})^{n/2}$.

than the Jeans length λ_J the amplitude grows by gravitational instability, whereas smaller wavelengths oscillate as an acoustic wave with constant amplitude, the profile being maintained by the collisions. Things are different in a collisionless gas, such as the one of our massive neutrinos. Again for large wavelengths there is growth, but now for $\lambda <$ "λ_J" there is <u>damping</u> arising from the freestreaming of the particles and also from directional dispersion, which occurs in $d > 1$ dimensions. The critical wavelength turns out to be (its value at the present is given)

$$\lambda_{\nu m} = 41 \ \frac{30 \text{ eV}}{m_{\nu 1}} \ \text{Mpc} \tag{8a}$$

and the masscale is

$$M_{\nu m} \equiv \frac{\pi}{3} \rho_{\nu 1} \lambda_{\nu m}^3 = 3.2 \ 10^{15} \left(\frac{30 \text{ eV}}{m_{\nu 1}} \right)^2 M_\odot \ . \tag{8b}$$

The transfer function which describes the small scale damping has been calculated in detail[16] and is shown in Fig. 3.

To summarize, during the relativistic epoch perturbations with small wavelengths are damped, so that the final spectrum has a cut-off (8a) determined from the moment when the neutrinos become non-relativistic. Since the growth period is long the initial amplitude δ^{in} can be rather small and is consistent with present limits on the C8R fluctuations. We now turn to the precise structure that this spectrum gives rise to later.

Nonlinear Growth Period

We can follow analytically the growth of the neutrino perturbations as long as $\delta << 1$. When stronger contrasts occur the linear approximation breaks down. Presently the only way to follow the further evolution is through numerical simulations (N-body methods). There are severe restrictions by computer limitations, but nevertheless a number of interesting results have been obtained.

It is clear that the cutoff (8a) in the spectrum will have significant effects.[17] To illustrate this we present in Figs. 4a,b and 4c,d the result of a calculation[18] with a $n = 0$ spectrum without and with the sharp cut off. The resulting structure is very different in the two cases. When there is a cutoff a structure of filaments and cells appears, which is rather similar to that observed on the supercluster scale.[19] In

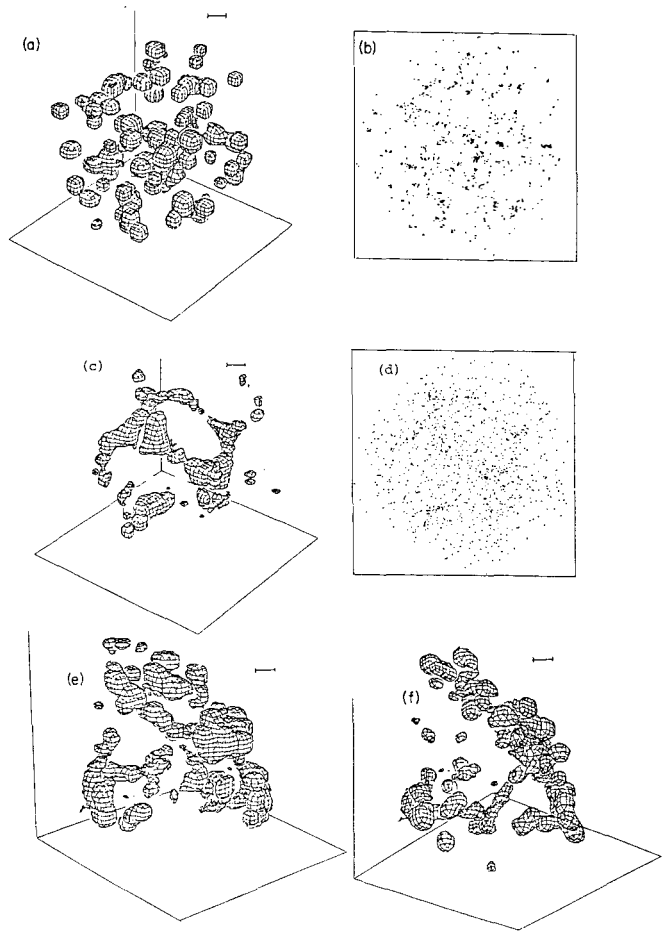


Fig. 4: Isodensity surfaces (at 4 times the mean density) and projected point distributions from massive neutrino models (h = 0.78, Ω = 1) from Ref. 18. The bar on the right-hand upper corner represents 10 Mpc.
a,b: n = 0 spectrum without small scale cut-off
c,d: n = 0 spectrum with the cut-off (8a)
e,f: real galaxy distributions from the CfA survey (Ref. 20).

Fig. 4e,f the Center for Astrophysics redshift survey[20] of galaxies in our Northern neighborhood is plotted in the same way as the model results.

I will now discuss the interesting numerical results of White, Frenk and Davis[21] (WFD). These authors start (a = 1) from the n = 1 spectrum calculated in Ref. 16 with an amplitude of 22%. Figure 5 shows in the left frames the neutrino density pattern after expansion by a factor 4, 6 and 10. Since the neutrinos are invisible, one should try to identify the regions where the galaxies would form, but this is precisely the subject we understand least about. The (reasonable) procedure adopted by WFD is to look for volume cells of the initial grid that have gone through collapse and to tag the corresponding particles as "galaxies." The underlying idea is that the baryon gas dragged along would have shocked there, possibly triggering galaxy formation.[17] At a = 2.9 already 1% of the particles have had a collapsed volume element and this moment is defined to be the onset of galaxy formation (GF; note this is a different convention than $\delta = 1$ used in the previous section). Later frames can be interpreted as the present day situation if galaxy formation occurred at a redshift $z_{GF} = a/2.9 - 1$. The frames on the right of Fig. 5 show that the epoch with filamentary structure is rather ephemeral ($z_{GF} = 1.1$) and that at later epochs only strong clusters remain. In Fig. 6 the resulting correlation functions $\xi(r)$ are given. Recall that $\xi(r)$ is the excess probability over random to find at a distance r of a given galaxy another one. Observations of the sky learn that for real galaxies this function is given by

$$\xi(r) \sim (r/R_o)^{-1.8} \tag{9a}$$

$$R_o \sim 5\ h^{-1}\ \text{Mpc} \tag{9b}$$

Figure 6b shows that the lengthscale (R_o) of the candidate "galaxies" is much too large, which was to be expected from a comparison of (9b) with the neutrino scale (8a). In Fig. 7 we give on the right the final distribution of the "galaxies," which should be compared with the real galaxy distribution on the left. Qualitatively two problems of the neutrino scenario are clear:

(i) too large voids;

(ii) too large clusters.

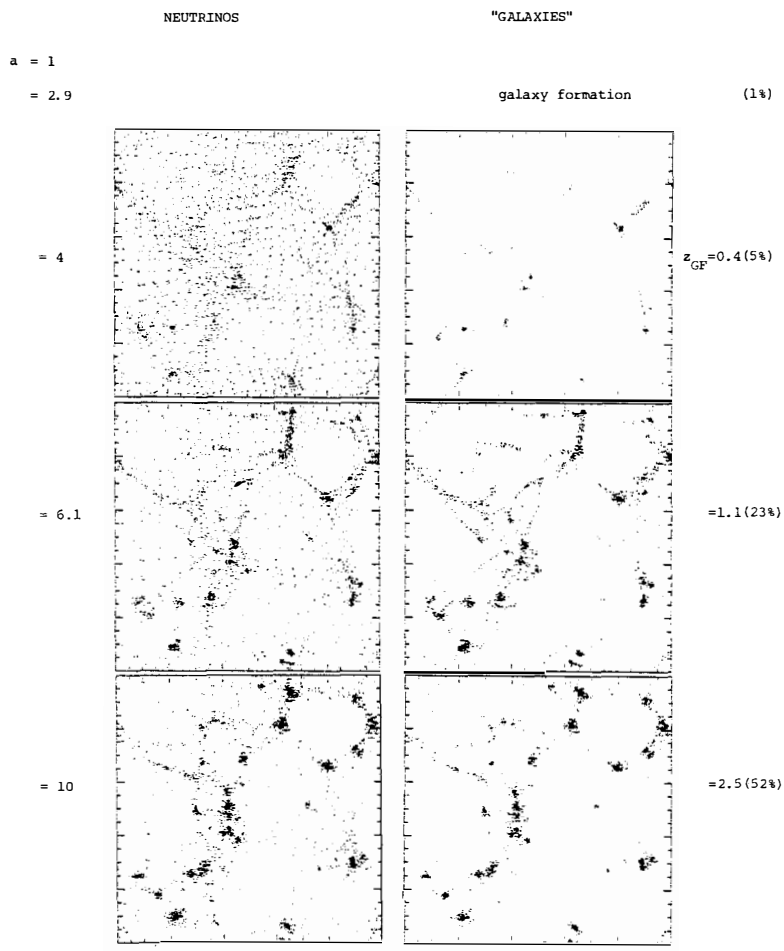


Fig. 5: Projected particle distributions in a massive neutrino model (Ω = 1) from Ref. 21. The left-hand panels show all particles, the right-hand panels those tagged as "galaxies," see text. The expansion factor a is shown on the left while for the "galaxy" picture the redshifts of galaxy formation z_{GF} and the fraction of tagged particles are shown on the right.

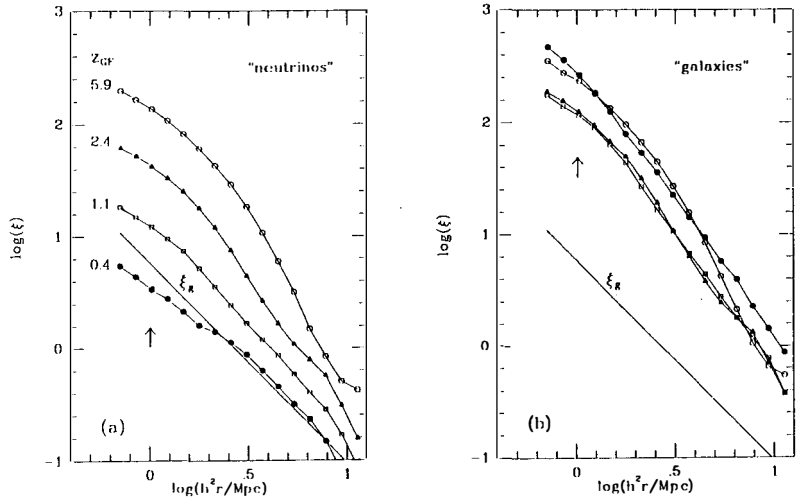


Fig. 6: Correlation functions for the models of Fig. 5. The straight line is the observed function (9).

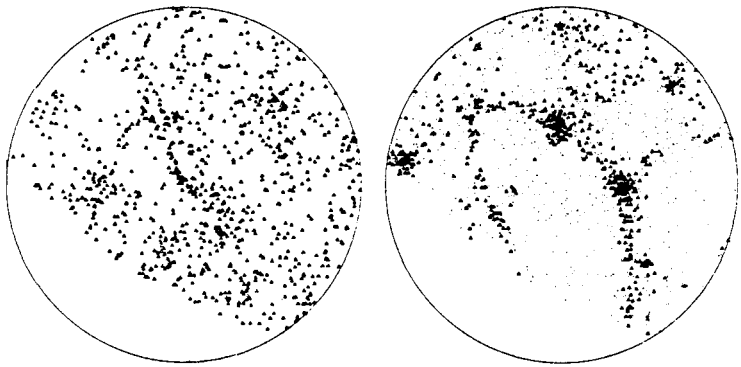


Fig. 7: On the right distribution of "galaxies" in a massive neutrino model (z_{GF} = 2.5, h = 0.54, Ω = 1), on the left the real galaxies of the CfA survey (Ref. 20).

In order to proceed more quantitatively WFD consider the clustering scale R_c, which turns out to be close to R_o, defined by

$$R_c^{-3} \int_0^{R_c} \xi(r) r^2 dr = 1 \qquad (10)$$

For real galaxies $R_c \sim 5\ h^{-1}$ Mpc and with the equation (8a) for $\lambda_{\nu m}$ one then gets the relation

$$[R_c/\lambda_{\nu m}]_{model} = 0.4\ \Omega h\ \theta^{-2} \quad , \qquad (11)$$

where $\theta \equiv T_{CBR}/2.7$ K. The numerical calculations give the number on the left-hand side of (11), which implies a value for $\Omega h \theta^{-2}$, depending on z_{GF}, of course. Figure 8 shows the required value of $h\theta^{-2}$ for given Ω. Other observations[2] lead us to expect $h\theta^{-2} \sim 0.5 - 0.75$, since θ is close to 1. Also many quasars are observed at $z = 3$, so that we must have galaxy formation at z_{GF} of at least 3. Taking Fig. 8 at face value would rule out models with $n = 1$, $\Omega \leq 1$, possibly allowing those with $n = 4$. WFD conclude that "the conventional neutrino-dominated picture appears to be ruled out." I would agree that things do not look great, but I find their

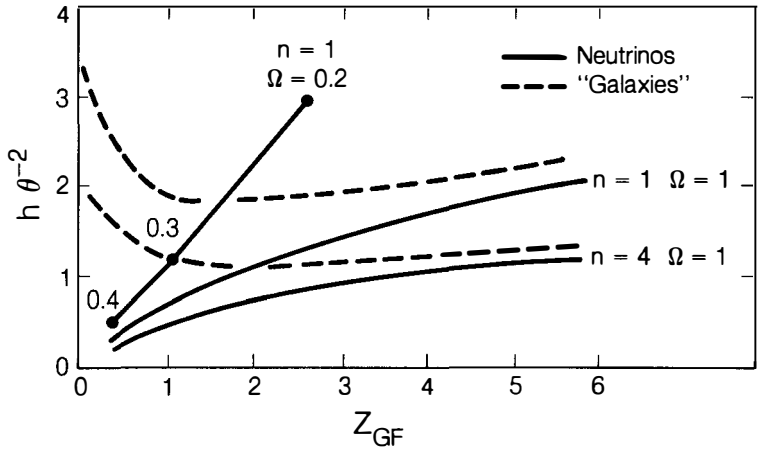


Fig. 8: Values of $h\theta^{-2}$ implied by equation (11) for massive neutrino models (Ref.21).

conclusion too severe. Since we do not know how real galaxies form let us just look at the "neutrino" curves in Fig. 8 to get a rough idea. Then the n = 1 - 4, Ω = 1 curves are in the ballpark ($h\theta^{-2} \sim 1$, $z_{GF} \sim 3$). This may be all the accuracy we could hope for since we do not know the correct primordial perturbation spectrum, nor, as said above, where and when the galaxies visible to us form. In fact, it might be that galaxy formation is not an entirely fair tracer of the neutrino density. Still, for $\Omega_o = 1$ the age of the Universe

$$t_o = \frac{2}{3} H_o^{-1} = 6.7\ h^{-1}\ 10^9\ \text{yr} \qquad (12)$$

may be uncomfortably short for h ~ 1, considering the ages quoted for globular clusters of at least 12 10^9 yr. [t_o could be larger than (12) if there were a nonzero cosmological constant, see Ref. 2].

Independent of the uncertainties of galaxy formation there is another problem for the massive neutrino scenario, namely the large neutrino clusters mentioned above and in Fig. 7. The following numbers[22] (for the case n = 1, but n = 4 gives similar results) speak for themselves:

	Neutrino Clusters		Abell Clusters
	$z_{GF} = 2.5$	$z_{GF} = 6$	
mean spacing (Mpc)	65	70	50
mass fraction of Universe	0.39	0.61	<0.01
mass (10^{15} $M_\odot$)	26	54	1
X-luminosity (10^{45} erg/s)[a]	8	30	0.5
number expected in HEAO-1	500	2000	≤ 7[b]

[a] Using $\Omega_b = 0.1$

[b] Unidentified sources in the X-ray survey of the HEAO satellite.

Further details can be found in Ref. 22, but it is clear from this table that these objects are not likely to constitute such an important part of our present Universe and escape detection. On the other hand, unless the neutrino structures condense very recently (z ~ 1 in Fig. 5), it seems hard to avoid having such neutrino clusters.

Conclusions

The reason for the two severe problems of the massive neutrino scenario encountered in the previous section can be phrased as follows: the non-linear collapse of the neutrinos is too fast if we also want them to trigger galaxy formation at a redshift z_{GF} of at least 3. Still, galaxy formation may have some surprises in store for us theorists, so I would not dismiss massive neutrinos entirely.* There is the possibility, albeit a rather unattractive one, that galaxies originate from a different kind of seeds than the large-scale structure.

Cosmology provides an upper limit of ~100 eV for the neutrino mass and for neutrinos to be important dynamically requires a lower "limit" of several eV. It is intriguing that a neutrino mass in this narrow range could generate a mass scale (4,8) and structure (Figs. 4 c,d, and 5) corresponding to precisely the largest structures observed in the Universe. Although "ripple cosmology" would not dare to predict a neutrino mass of tens of eV, astrophysicists could probably live (and be happy) with it, were such a mass to be found in laboratory experiments.

Acknowledgments

I would like to thank Marc Davis for informative discussions over the years and to congratulate the organizers of this workshop, especially J. Tran Thanh Van and Orrin Fackler, for bringing about such a lively and interesting meeting.

References

1. K.R. Lang and O. Gingerich (eds.), A Source Book in Astronomy and Astrophysics 1900-1975 (Harvard UP, 1979).

2. S. Weinberg, Gravitation and Cosmology (Wiley, 1972).

3. A.M. Boesgaart and G. Steigman, Ann. Rev. Astron. Astrophys., 23, 319 (1985).

4. Smirnov in these Proceedings.

5. S.M. Faber and J.S. Gallagher, Ann. Rev. Astron. Astrophys., 17, 135 (1979).

6. S.S. Gershtein and Ya. B. Zeldovich, JETP Lett. 4, 120 (1966).

---

* Note that other dark matter candidates (gravitinos, axions...) also have their share of problems.[23]

7. A.S. Szalay and G. Marx, Astron. Astrophys. 49, 437 (1976).

8. F.R. Klinkhamer and C.A. Norman, Astrophys. J. 243, L1, E245, L97 (1981); F.R. Klinkhamer, Astron. Astrophys. 107, 235 (1982).

9. J.R. Bond, G. Efstathiou and J. Silk, Phys. Rev. Lett. 45, 1980 (1980).

10. G.S. Bisnovaty-Kogan and I.D. Novikov, Astron. Zh. 57, 899 (1986).

11. A.G. Doroshkevich, M. Yu. Khlopov, R.A. Sunyaev, A.S. Szalay, and Ya. B. Zeldovich, 10th Texas Symposium, Ann. New York Academy of Sciences 375, 32 (1981) and ref. herein.

12. W. Fischler, B. Ratra and L. Susskind, Nucl. Phys. B259, 730 (1985) and ref. herein.

13. F.R. Klinkhamer, G. Branco, J.P. Derendinger, P. Hut, and A. Masiero, Astron. Astrophys. 94, L19 (1981); J.A. Harvey, E.W. Kolb, D.B. Reiss and S. Wolfram, Nucl. Phys. B177, 456 (1981).

14. J.M. Uson and D. Wilkinson, Astrophys. J. 277, L1 (1984).

15. J.R. Bond and G. Efstathiou, Astrophys. J. 285, L45 (1984).

16. J.R. Bond and A.S. Szalay, Astrophys. J. 274, 443 (1983).

17. Ya. B. Zeldovich, Astron. Astrophys. 5, 84 (1970); in M.S. Longair and J. Einasto (eds.), The Large Scale Structure of the Universe (Reidel, 1978).

18. C.S. Frenk, S.M. White and M. Davis, Astrophys. J. 271, 417 (1983).

19. J.H. Oort, Ann. Rev. Astron. Astrophys. 21, 373 (1983).

20. M. Davis, J. Huchra, D. Latham, and J. Tonry, Astrophys. J. 253, 423 (1982); M. Davis and P.J.E. Peebles, Astrophys. J. 267, 465 (1983).

21. S.D.M. White, C.S. Frenk and M. Davis, Astrophys. J. 274, L1 (1983); S.D.M. White, in M. Turner and R. Kolb (eds.), Proceedings of the Inner Space-Outer Space Workshop, Fermilab 1984 (Chicago UP).

22. S.D.M. White, M. Davis and C.S. Frenk, M.N.R.A.S. 209, 15P (1984).

23. M. Davis, G. Efstathiou, C.S. Frenk and S.D.M. White, Astrophys. J. 292, 371 (1985); Steigman in these Proceedings.

CLOSING THE DOOR ON DARK MATTER CANDIDATES

Gary Steigman
Bartol Research Foundation
University of Delaware
Newark, DE 19716, USA



ABSTRACT

Cold dark matter candidates - if they exist - will be present in, and perhaps dominate the mass density of, the halo of our Galaxy. As they pass the vicinity of the Sun, such halo particles will be focussed gravitationally, pass through the Sun and - occassionally - be captured and accumulate in the solar core. When the density in the core of the Sun of dark matter candidates has increased sufficiently, they will annihilate and among the annihilation products will be energetic ($\geq$GeV) "ordinary" neutrinos (ν_e, ν_μ, ν_τ) which are detectable in deep underground experiments. The event rates in such detectors from the capture and annihilation of various dark matter candidates (Dirac and Majorana neutrinos, Sneutrinos and Photinos) are presented and it is shown how comparison with data may lead to constraints on (or, the exclusion of) the masses of these particles.

INTRODUCTION

The problem is that most of the Universe is dark [1]. For example, in the vicinity of the Sun in the disk of our Galaxy, the "seen" or "luminous" mass is only ~ 1/2 the total mass inferred from the motions of stars. On larger scales, the problem is worse. Within the "shining" parts of galaxies ($\lesssim$ Holmberg radius) the luminous mass only accounts for ~ 20% of the total mass (inferred from the dynamics of stars or gas). On the scales of rich clusters, only ~ 10% of the mass shines. Although ordinary nucleons may, indeed, account for all of the mass inferred on scales up to that of clusters and superclusters (including the dark mass), primordial nucleosynthesis[2] constrains the nucleon density to be less than ~ 10% of the critical density.

Various exotica from the particle physics zoo have been proposed as candidates for the dark matter which dominates the density of the Universe. It is convenient to group the particles according to their clustering properties. "Hot" particles such as ~ 30eV neutrinos cannot cluster on small scales and are not expected to dominate the mass on the scale of galactic halos. In contrast, "cold" particles such as very massive ($\gtrsim$ GeV) photinos, sneutrinos, Dirac or Majorana neutrinos will cluster on all scales from much smaller than a galaxy on up. In this context, it is worth noting that axions[3] are "cold" despite being very light (~ 10^{-5}eV); axions are <u>not</u> relevant to our subsequent discussion and are excluded from the constraints to be presented below. "Warm" dark matter candidates, such as axinos of mass 0.1 - 1 keV, have clustering properties intermediate to those of hot and cold particles; warm particles too are excluded from further discussion here.

Although <u>dark</u>, massive cold dark matter candidates such as neutrinos, sneutrinos and photinos are not <u>invisible</u>. If such a

particle, denoted by X in the following, exists, it may provide the mass density which dominates the halo of the Galaxy: $\rho_X \sim \rho_H \sim 0.3$ GeV/cm^3. Such particles would have collapsed along with the ordinary nucleonic matter in the formation of the Galaxy and, through collective gravitational interactions ("violent relaxation"), relaxed to fill the halo with Xs whose velocity distribution is typical of that of the halo: $v_X = v_H \simeq 300 \text{kms}^{-1}$. In their lonely passage through the Galaxy, Xs will occassionally pass in the vicinity of the Sun. Those which come sufficiently close will by focussed by the solar gravitational field to pass through the Sun. Those which pass through the Sun may scatter off a nucleus in the Sun and lose an amount of kinetic energy large enough so that they remain gravitationally bound - they are captured by the Sun. Over the age of the Sun (~ 4.5 Gyr) such captured Xs accumulate in the solar core (although the lighter Xs may evaporate from the Sun) and, when their density is high enough, they will begin annihilating in collisions with each other (photinos with photinos, sneutrinos with sneutrinos, Majorana neutrinos with Majorana neutrinos, but, Dirac neutrinos with Dirac antineutrinos). Among the debris of X annihilation will be some ordinary neutrinos (ν_e, ν_μ, ν_τ) of sufficiently high energy ($\gtrsim$ GeV) to be detectable in deep underground experiments. In death, the dark matter candidates may become visible.

Below, the survival from the early Universe of Weekly Interacting Massive Particles (WIMPs) is reviewed and their expected density at present is calculated. Next, we turn to the capture rate by the Sun of Xs and estimate the flux of energetic ordinary neutrinos from annihilations in the solar core. The expected flux is folded with the cross section for neutrino-nucleon scattering to obtain the predicted event rate (per kiloton-year) in a deep underground detector.

Comparison with atmospheric background neutrinos leads to the conclusion that such experiments may detect the presence of these cold dark matter candidates; failure to do so will close the door on such dark matter candidates.

The results outlined below are from a collaborative effort with my Bartol colleague, T.K. Gaisser, and my student at the University of Delaware, S. Tilav. Since the details of our work will appear elsewhere[4], here I only summarize our results; for details and the appropriate references, see ref. 4.

Survival of WIMPs

The evolution of the abundance of WIMPs in the early Universe was first described by Zeldovich[5] and Chiu[5] and has been reviewed by Steigman[5]. At high temperatures, reactions occur sufficiently rapidly (compared to the universal expansion rate, the Hubble parameter H) to establish and maintain equilibrium. During this epoch the WIMP number density n_X is equal to its equilibrium value; for $x = M_X/T > 1$, $n_{eq} \propto T^3 x^{3/2} e^{-x}$ (T is the temperature). As the Universe expands and cools, n_X decreases exponentially (annihilation is dominating over pair production) until a stage is reached ($T = T_*$) when equilibrium can no longer be maintained. Deviations from equilibrium ($n_X > n_{eq}$) become significant for $T \lesssim T_*$ (it is often assumed - erroneously - that "freeze-out" occurs when $\Gamma = H$; since, for WIMPs, $x_* \simeq 20$, this is a poor approximation). The critical temperature, T_*, is found by solving [5]

$$x_*^{1/2} e^{x_*} \simeq 5 \times 10^{34}\, g_X M_X \langle \sigma v \rangle_* g_*^{-1/2}, \qquad (1)$$

where g_X is the number of X spin states, M_X is in GeV, $< \sigma v >_*$ is the thermally averaged annihilation rate coefficient (in units of $cm^3 s^{-1}$) and, g_* is the effective number of relativistic degrees of freedom at T_*. Below T_*, annihilations continue to reduce the X abundance. The final - frozen-out - abundance of Xs, compared to that at T_* is: $N_{X0}/N_{N*} \simeq x_*^{-1}$. The present ratio of Xs to photons is [5]

$$(N_X/N_\gamma)_0 \simeq (5\times10^{-35}/M_X<\sigma v>_*)\ (x_*/g_*^{\frac{1}{2}}). \qquad (2)$$

If Ω_X is the ratio of the X mass density to the critical density ($\rho_c \simeq 2\times10^{29}(H_0/100)^2 gcm^{-3}$; the Hubble parameter at present may be written as $H_0 = 50h_{1/2} kms^{-1}Mpc^{-1}$),

$$\Omega_X h_{\frac{1}{2}}^2 \simeq (1.9\times10^{-26}/<\sigma v>*)(x_*/20)\ (64/g_*)^{\frac{1}{2}}. \qquad (3)$$

For typical weak annihilation cross sections, $x_* \simeq 20$ and $\Omega_X h_{1/2}^2 \simeq O(1)$.

Capture of WIMPs

The capture of WIMPS has been studied in detail by Press and Spergel[6]; what follows is a qualitative description which elucidates the physics and displays the qualitative dependence of the capture rate on the various parameters. The detailed quantitative expressions are from Gaisser et al[4], following Press and Spergel[6]

After gravitational collapse and violent relaxation, the WIMPs fill the halo of the Galaxy with a velocity distribution,

$$n_X(v) \sim (v^2/v_H^3) \exp[-3/2\ (v/v_H)^2]. \tag{4}$$

The flux, at any point in the halo, of Xs is: $\phi_X(v) \sim v n_X(v) \sim v\rho(v)/M_X$. Since only relatively slow moving Xs will be captured, we may restrict attention to $v < v_* < v_H$. In this limit,

$$\phi_X(<v_*) \approx (\rho_X/M_X)\ (v_*^4/v_H^3) \tag{5}$$

If v_* is less than the escape velocity ($v_{esc} = 2GM/R$), Xs will be focussed; orbits with impact parameters $b \leq b_* = (v_{esc}/v_*)R$ will have a distance of closest approach less than R. The rate (per sec) at which WIMPs pass through, for example, the Sun is

$$\phi_X(<v_*)\pi b_*^2 \approx (\rho_X/M_X)\ R_\odot^2\ (v_{esc\odot}^2 v_*^2/v_H^3). \tag{6}$$

However, not all WIMPs passing through the Sun will be captured. To find the capture rate we must multiply (6) by f, the probability that a WIMP will - in passage through the Sun - suffer an elastic collision leading to capture. f is essentially (for $f \leq 1$) the "optical" depth to WIMP - nucleus scattering in the Sun.

$$f = \int n\sigma d\ell \approx (M_\odot/M_H)\ \sigma_{eff}/R_\odot^2, \tag{7}$$

where M_H is the hydrogen mass and the effective scattering cross section, σ_{eff}, is summed over all nuclei, weighted by their abundance,

$$\sigma_{eff} = X_{Hi} \Sigma\ (n_i/n_H)\ \sigma_{xi}. \tag{8}$$

In (8), X_H is the hydrogen mass fraction, n_i/n_H is the abundance - by number - of nucleus i and, σ_{xi} is the WIMP - nucleus cross section (in cm^2).

Collecting the above relations, we find that the capture rate $\dot{N}_X$ varies as,

$$\dot{N}_X \approx (\rho_X/M_X)\ (M_\odot/M_H)\ (v^2_{esc\odot}\ v_*{}^2/v^3{}_H)\ \sigma_{eff}. \qquad (9)$$

For the Sun, $v_{esc} \simeq 2v_H$ so that $v_* \simeq v_H$; a detailed calculation results in a capture rate,

$$\dot{N}_{X\odot} \simeq 9x10^{64}\ \sigma_{eff\odot}/M_X\ (s^{-1}). \qquad (10)$$

In (10) we have set $\rho_X = \rho_H$ and $v_X = v_H$.

Dirac neutrinos and Sneutrinos may scatter coherently from iron nuclei in the Earth and be captured. Since the Earth is always less important[4] - by a factor 20 or greater - than the Sun, we neglect such captures here.

Annihilation Of WIMPs

As the WIMPs accumulate in the solar core their density increases and they begin to annihilate. After a time $t_{eq} < t_\odot$, equilibrium between captures and annihilations is achieved and a steady-state is obtained in which the number of captures per second is balanced by (twice) the number of annihilations per second (two Xs disappear in each annihilation). If $N_\nu(E_\nu)$ is the number of ordinary neutrinos produced per annihilation with energy between E_ν and $E_\nu + dE_\nu$, then the differential flux at Earth due to annihilations in the Sun is

$$\phi_\nu(E_\nu) = \phi_{\bar{\nu}}(E_\nu) = N_\nu(E_\nu)/2\ (\dot{N}_X/4\pi d^2), \tag{11}$$

where d = 1AU is the Earth-Sun distance.

The annihilation produced neutrinos can be detected by scattering from the nucleons in a deep underground experiment. If N_N is the number of nucleons per kiloton times the number of seconds in a year ($N_N \simeq 1.9 \times 10^{40}$) then the differential event rate (per kiloton-year per GeV) in an underground detector is

$$R_\nu(E_\nu) = N_N \phi_\nu(E_\nu)[\sigma_{\nu N}(E_\nu) + \sigma_{\bar{\nu}N}(E_\nu)]. \tag{12}$$

For energies of interest ($\gtrsim$ GeV), $\sigma_{\nu N} \propto E_\nu$ and we find,

$$R_\nu(E_\nu) \simeq 10^4 (E_\nu/M_X)\ N_\nu(E_\nu)\ (\sigma_{eff}/\sigma_{crit})_\odot (\text{kt-yr-GeV})^{-1} \tag{13}$$

where $\sigma_{crit} = 4 \times 10^{-36} \text{cm}^2$. If we integrate over E_ν, the total event rate is

$$R_\nu \simeq 4 \times 10^3 N_\nu (\sigma_{eff}/\sigma_{crit})_\odot (\text{kt-yr})^{-1}. \tag{14}$$

In (14) we have used the result that $< E_\nu > \simeq M_X/3$. Actually, for "direct" neutrinos ($X\bar{X} \to \nu\bar{\nu}$), $< E_\nu > = M_X$, whereas for "prompt" neutrinos ($X\bar{X} \to f\bar{f} \to \nu\bar{\nu}$---), $< E_\nu >/M_X$ varies from ~ 0.30 to ~ 0.35.

Before presenting the results of the detailed calculations[4], some remarks are in order. Sufficiently light WIMPs will evaporate from the Sun before they annihilate. Thus, if M_X is decreased, at some point R_ν will decrease exponentially. We have found [4] that, typically,

$M_{xcrit} \simeq$ 3GeV so that our constraints will apply to WIMPs more massive than ~ 3 GeV. Finally, we have, up to now, assumed that the WIMPs provide the dark mass of the halo ($\rho_x = \rho_H$). However, even if they are dynamically unimportant, WIMPs - if present at all - will still be captured by the Sun. For $\rho_x < \rho_H$, the predicted event rate will be reduced by the ratio ρ_x/ρ_H. Constraints on the nucleon density from big bang nucleosynthesis[2] suggest that $\Omega_N h_{1/2}^2 > 0.04$ so that, for $\Omega_x < \Omega_N$, we will assume that $\rho_x/\rho_H = (\Omega_x h_{1/2}^2/0.04)$.

Dirac Neutrinos

We[4] have calculated the relic abundance of massive Dirac neutrinos and find that $\Omega_\nu h_{1/2}^2 = 1$ for $M_\nu = 3.6$ GeV. For smaller masses, $\Omega_\nu > 1$ so that $M_\nu < 3.6$ GeV is excluded (for stable, Dirac neutrinos). When M_ν increases to 17 GeV, $\Omega_\nu h_{1/2}^2 \simeq 0.04$ so that heavier neutrinos are dynamically negligible. For 3 GeV < M_ν < 40GeV, we find a total event rate ($\nu_e + \nu_\mu + \nu_\tau$) in excess of ~ 6 events per kiloton-year. Massive, stable Dirac neutrinos should have been detected.

Majorana Neutrinos

For Majorana neutrinos [4], $\Omega_\nu h_{1/2}^2 = 1$ for $M_\nu = 12.7$ GeV. Lighter Majorana neutrinos - if stable - lead to $\Omega_\nu > 1$ and, therefore, are excluded. For all masses in excess of ~13 GeV, the total event rate is between 5 and 6 events per kiloton-year. Majorana neutrinos - if massive and stable - should have been found.

It should, however, be noted that massive Dirac or Majorana neutrinos are <u>not</u> expected to be stable. Indeed, such massive neutrinos could decay via $\nu_x \to \mu^- \pi^+$ (or $e^- \pi^+$). The expected lifetime for this mode is,

$$\tau(\nu_X \to \ell^- \pi^+) \approx (2\times10^{-10}/M_X^3)|U_{X\ell}|^{-2}\text{sec.} \qquad (15)$$

Thus, unless the X-ℓ mixing is incredibly small, massive neutrinos (>GeV) should not be present today.

Sneutrinos

Sneutrinos may self annihilate ($\tilde{\nu}\tilde{\nu} \to \nu\nu$) via zino exchange. The cross section for this process depends on the majorana part of the zino mass. In general, sneutrinos are cosmologically uninteresting ($\Omega_\nu << \Omega_N$). If, however, it is arranged that $\Omega_\nu > \Omega_N$, so that $\rho_\nu = \rho_H$, the same rapid annihilation directly into ordinary neutrinos leads to an enormous predicted[4] event rate. If sneutrinos were the halo dark mass, the underground detectors would have been flooded with events.

Photinos

Photino annihilation proceeds via the exchange of scalar fermions. Thus, there are - at least - two parameters which determine $\Omega_{\tilde{\gamma}}$ and R_ν: the photino mass $M_{\tilde{\gamma}}$ and the scalar fermion mass M_S. Constraints on $\Omega_{\tilde{\gamma}}$ and R_ν permit us to exclude some - but not all - regions in the $M_{\tilde{\gamma}}$ - M_S plane. If we require that $\Omega_{\tilde{\gamma}} < 1$ and $R_\nu < 1(\text{kt-yr})^{-1}$, we exclude $M_{\tilde{\gamma}} < 30$ GeV and $M_S < 125$ GeV. For further details, see ref. 4.

Conclusions

Cold dark matter candidates (with the exception of axions) may be dark but not invisible. Such WIMPs will, through their weak

interactions with ordinary nuclei, be captured by the Sun. They will, if sufficiently massive (> 3GeV), languish in the core of the Sun until they encounter one of their own kind and annihilate. The energetic (>GeV) ordinary neutrinos (ν_e, ν_μ, ν_τ) from such annihilations are observable in the deep underground detectors. The absence of such events provides constraints on the possible presence of several candidate WIMPs. Massive, stable Dirac, or Majorana neutrinos as well as Sneutrinos can be ruled out. If photinos are to survive, they must be quite massive ($M_{\tilde{\gamma}} > 30$ GeV) and the mass of the lightest scalar fermion must be quite large ($M_S > 125$ GeV).

The door is closing on (most) cold dark matter candidates.

Acknowledgments

All the work described here has been done in collaboration with T.K. Gaisser and S. Tilav to whom I am indebted. I have benefitted greatly from discussions relating to this material with D. Seckel and D. Spergel. This research is supported at Bartol by DOE grant DE-AC02-78ER-05007.

References

1. S.M. Faber and J.S. Gallagher, Ann.Rev.Astron.Astrophys. 17, 135 (1979).

2. A.M. Boesgaard and G. Steigman, Ann.Rev.Astron.Astrophys. 23, 319 (1985).

3. S. Weinberg, Phys. Rev.Lett. 40, 223 (1978),
F. Wilczek, Phys. Rev.Lett. 40, 279, (1978),
M. Dine, W. Fischler and M. Srednicki, Phys.Lett. 104B, 199 (1981).

4. T.K. Gaisser, G. Steigman and S. Tilav, In Preparation (1986),
S. Tilav, University of Delaware M.Sc.Thesis (1986).

5. Ya.B. Zeldovich, Adv.Astron.Astrophys. 3, 241 (1965).
H.Y. Chiu, Phys. Rev. Lett. 17, 712 (1966),
G. Steigman, Ann. Rev. Nucl.Part. Sci. 29, 313 (1979).

6. W.H. Press and D.N. Spergel, Ap. J. 296, 679 (1985).

COSMOLOGY AND HEAVY UNSTABLE PARTICLES[†]

Kyungsik Kang
Department of Physics
Brown University
Providence, RI 02912 USA

ABSTRACT

After a brief review of the standard cosmology and cosmological implications of the grand unification in particle physics, I present the cosmological constraints for the heavy unstable particles based on the recent work in collaboration with K. Choi and Jihn Kim. The result is the restriction of the mass versus lifetime plot. Also discussed briefly is the grand unification effect on the stability of such heavy particle.

[†]Supported in part by the U. S. Department of Energy under Contract DE-AC02-76ER03130.A.020-Task A

1. Introduction

Advances in the unification of the forces acting on elementary particles have resulted in exciting interface between particle physics at superhigh energies and cosmology[1]. The developments in particle physics theoretical scheme allow us to actually calculate astrophysical and cosmological problems including the evolution of the universe, and cosmology provides probes of, and constraints on, the new ideas of the unification in particle theory. Indeed, the early universe has provided a valuable laboratory to test the grand unification idea of strong, electromagnetic and weak forces[2]. Refreshing answers[3] to the standard cosmological problems such as the matter-antimatter asymmetry, the large scale homogeneity and isotropy, and the flatness of the present universe have been provided by grand unification theory of strong-electroweak interactions. On the other hand, cosmology and astrophysics can render valuable constraints to grand unification model buildings. Invisible axions is a good example: the parameters of invisible axions are constrained by astrophysical data[4] while cosmological implication of unique automatic axion extends to constrain the number of the family generations of elementary particles, i.e., the quarks and leptons[5]. Another classic example is the mass of light or heavy neutrino. Cosmological reasonings set bounds for the massive neutrinos and provide constraints to limit the allowed interactions in the grand unified theories[6].

In this talk, I will briefly review the essential ingredients of cosmology and then discuss the cosmological constraints placed on the heavy unstable particles[7]. Stable heavy neutrinos[8] have been studied in connection with the energy density of the present universe. In composite models, another realm of the frontier particle physics, it is plausible to expect that a stable particle with a mass around the confining scale would appear. This is the case if the global vector symmetry $U(1)_v$ is unbroken[9] in composite models. The proton is such an example in quantum chromodynamics. For the cosmic temperature below the confinement scale, the relevant interaction is that of $SU(3)_c$ x SU(2) x U(1), which is so weak for the stable particles below the confinement scale as to be an effective annihilator in the expanding universe.

There is a well-known cosmological bound[6], $\sum_i m_{\nu i} \leq$ 50eV, from the restriction $\rho_c = 3H_0^2/8\pi G \cong 2 \times 10^{-29}$ g/cm^3. On the other hand, a stable heavy Dirac neutrino with $m_\nu \leq$ 2 GeV (about 10 GeV if the neutrino is a Mojorana type) has also been noted to be in conflict with the upper bound of the energy density of the universe[10]. Thus neutrinos in the mass range of 50 eV to about 10 GeV must be unstable. The lifetime of such neutrino will be constrained by the observed radiation backgrounds if the decay produces photons

and also by the entropy effect produced by decaying neutrinos on the primordial synthesis of deuterium[11].

Superheavy stable neutrinos show similar behavior as the light neutrinos and it has been shown that an absolutely stable superheavy neutrino with mass larger than 2.5×10^5GeV is again excluded by the upper bound of the critical energy density of the universe[8]. Basically heavy neutrinos in the mass range of 10 GeV to about 10 TeV can be stable, whereas those with mass larger than 10 TeV must be unstable.

Specifically I will present the recent results on the cosmological constraints for an unstable superheavy neutrino[7]. The instability of superheavy particles is generally expected in grand unified theories. Cosmological constraints will give mass-lifetime correlations and in general restrict the allowed region of mass-lifetime. Dilution of the cosmological baryon numbers and the effect of the unstable neutrino decay on nucleosynthesis are two cosmological constraints that restrict the lifetime of unstable neutrinos. In addition, the grand unification effect on the stability of such heavy particles is briefly discussed.

2. Cosmology

Homogeneous and issotropic universe (in large scale) is described by the Robertson-Walker metric involving the time-dependent scale factor $R(t)$, a constant κ related to the curvature sealar as $\kappa/R^2(t)$, and the comoving coordinates r, θ, and ϕ. By making use of this metric in the Ricci tensor, one obtains the field equation

$$\dot{R}^2 + \kappa = \frac{8\pi G}{3} \rho R^2 \tag{1}$$

In addition, the energy-momentum conservation constraint from the energy momentum tensor reduces to

$$\frac{d}{dR} (\rho R^3) = -3pR^2 \tag{2}$$

where ρ is the pressure density. Note that the energy density ρ decreases at least as fast as R^{-3} upon expansion as long as p stays positive. $\dot{R}^2 + \kappa$ from (1) then decreases at least as fast as R^{-1}. The third ingredient of the standard cosmological model is the equation of the state

$$p = = (\rho, V, T, \ldots) \tag{3}$$

If the universe is filled with non-relativistic matter with negligible pressure

$\rho \sim R^{-3}$, whereas with relativistic ideal gas, $p = \rho/3$, one gets $\rho \sim R^{-4}$.

Consider the early universe made of ideal gas consisting of different types of particles in thermal equilibrium. The total energy density and pressure density can be written as

$$\rho(T) = \sum_i \int E_i(q)\, n_i(q,T)\, dq \tag{4}$$

$$p(T) = \sum_i \int \left(\frac{q^2}{3E_i(q)}\right) n_i(q,T)\, dq \tag{5}$$

where $n_i(q,T)$ is the number density of particle type i in the mementum range $[q, q+dq]$ that gives the particle number density $n_i(T)$ by

$$n_i(T) = \int n_i(q,T)\, dq = \frac{4\pi}{h^3} g_i \int q^2 dq \, [e^{E_i(q)/kT} \pm 1]^{-1} \tag{6}$$

Here $\pm$ depend on the particle type i being fermion or boson and g_i is the number of spin states, i.e., $g=1$ for ν or $\bar{\nu}$ and $g = 2$ for photons, charged leptons and baryons. For nonrelativistic particles $E_i(q) = (m_i^2 + q^2)^{1/2}$ whereas for relativistic particles $E_i(q) = q$ so that $p(T) = \frac{1}{3}\rho(T)$ and $\rho \sim R^{-4}$ as expected. With $\rho \sim R^{-4}$, the field equation (1) reduces to

$$\dot{\rho}/\rho = -4\dot{R}/R = -4\left(\frac{8\pi G}{3}\rho\right)^{1/2} \tag{7}$$

so that

$$t = \left(\frac{32\pi G}{3}\rho\right)^{-1/2} + \text{const} = \frac{M_p}{T^2}\left(\frac{32\pi A}{3}\right)^{-1/2} + \text{const} \tag{8}$$

where M_p is the planck mass $M_p = G^{-1/2} = 1.2 \times 10^{19}$ GeV and A depends on the kind of particles in thermal equilibrium as $\rho = A T^4$. In addition from the second law of thermodynamics, the entropy of particles in thermal equilibrium at T in a volume V satisfies

$$dS(V,T) = \frac{1}{T}\{d(\rho V) + p dV\} \tag{9}$$

The integrability condition of the entropy reduces to

$$\frac{dp(T)}{dT} = \frac{1}{T}\,[\rho(T) + p(T)] \tag{10}$$

which may also be derived directly from (4) and (5). Combining with the energy conservation relation (2), (10) can be written as the entropy conservation law

$$\frac{d}{dt}\,[\frac{R^3}{T}\,\{\,\rho(T) + p(T)\,\}] = 0 \tag{11}$$

which reduces to

$$TR = \text{const} \tag{12}$$

for all highly relativistic particles in thermal equilibrium.

Since the scale factor is unobservable, it is preferable to describe the expanding universe by the age versus temperature. Once ρ (T) is known, t -T relation is possible from (8) in the radiation-dominated era. For a black body with temperature T, $\rho_\gamma(T) = \int \rho_\gamma\,(\nu,T)d\nu = aT^4$ with $a = (\frac{\pi^2}{15})\,\frac{kT^4}{\hbar c^3}$. Thus the total energy density of the universe containing different types of particles all in thermal equilibrium at temperature T is

$$\rho(T) = N_F\,\rho_i(T) = \frac{1}{2}\sum_i\,(g_i^B + \frac{7}{8}\,g_i^F)\,aT^4 \tag{13}$$

where g_i^B (g_i^F) is the total number of bosonic (fermionic) degrees of freedom. During the radiation dominated era then the age of the universe from (8) as function of the temperature is

$$t = \frac{M_p}{T^2}\left(\frac{32\pi a N_F}{3}\right)^{-1/2} \tag{14}$$

To develop some feelings for the age of the early universe, consider the new inflationary model[12] within the context of the minimal SU(5) grand unification at the unification energy scale $T \simeq 10^{14}$GeV = 1.16×10^{27} ^oK. There are three generations of quarks and leptons, an adjoint 24 gauge fields, an adjoint 24 Higgs scalar fields, two 5 Higgs scalars, and one radiatively induced Coleman-Weinberg type scalar. One may need another complex singlet Higgs scalar if the minimal model is to solve the strong CP problem by an invisible axion. This gives ρ (T) = $55T^4$ so that $t = M_p/(43T^2) = 0.24\ (10^{10}/T^oK)^2$ sec. At the unification energy the universe was 1.83×10^{-35} sec old and objects

which are apart from each other 10^{10} light-years today were seperated only about 6 cm at that time. Energy density would have been $\rho = 1.3 \times 10^{75}$ gr/cm^3 then. Consider the time when the universe got cooled down below the muon threshold. In the range of $m_\mu < T < m_e$, muons are rare enough to be neglected so that electrons, photons, three kinds of left-handed neutrinos, and their antiparticles are important constituents of the universe. Then $N_F = 43/8$, and $t \cong (10^{10}/T^\circ K)^2$ sec. The universe at $T = 1$ MeV $= 1.16 \times 10^{10}\ ^\circ K$ was about 1 sec old and $\rho = 10^2 gr/cm^3$. The universe would have had the horizon distance about 1 light-year.

We note that number density can change due to the expansion of the universe as well as due to physical reactions such as annihilations. Statistical equilibrium will involve certain conditions to be met by the expansion rate and annihilation rate. For a reaction with cross section $\sigma(E)$, the annihilation rate depends on the thermally averaged product of the cross section and the relative velocity $\langle \sigma v \rangle$. With a target number density $n \propto R^{-3} \propto T^3$, the annihilation rate is $\langle \sigma v \rangle\, n(T) \propto T^3 \langle \sigma v \rangle$. The statistical equilibrium is established and maintained when the reaction rate is much larger than the expansion rate $t^{-1}(t) \propto T^2$. For low energy annihilations, $\sigma \propto v^{-1}$ so that $\langle \sigma v \rangle$ is independent of T . At energies below the mass of the intermediate vector boson M_w, weak interaction cross sections behave like in the Fermi theory, $\sigma(E) \propto E^2$ whereas above M_w, $\sigma(E) \propto E^{-2}$ which is the case for the superheavy particles. It is then clear that in early universe, equilibrium was established because of high temperature and density. As the universe expanded and cooled, reaction rate became small whereby loosing the equilibrium gradually.

In discussing the unstable particle cosmology, there are three important temperatures that determine the evolution of the early universe. The first is the decoupling(or freezing out) temperature T_D which is defined by the condition that the expansion rate of the universe becomes the same as the annihilation rate of the particle and its antiparticle. The second is the temperature T_m below which the universe enters into the mass-dominated era and the nonrelativistic mass of the particle and its antiparticle starts to dominate the energy density of the universe. The third is the decay temperature T_d of the particle. If the particle is absolutely stable, then $T_d = 0$. If T_d is larger than T_D and T_m, the latter temperatures are meaningless in the thermal history of the universe. If T_d is between T_D and T_m , the universe does not enter the mass-dominated era. Thus the most interesting case is when $T_D > T_m > T_d$ as far as the cosmological constraints on the heavy particle is concerned. In general the type of particles whose

lifetime is much longer than the inverse mass can satisfy this inequality. The unstable particle that decays by the interactions around the grand unification scale belongs to this category.

3. Cosmological Constraints on Heavy Unstable Particles

The number density of any type of stable particles that are uniformly spread throughout a homogeneous universe must obey the rate equation [10,13]

$$\frac{dn}{dt} = -3\left(\frac{\dot{R}}{R}\right)n - \langle\sigma v\rangle\,(n^2 - n_0^2) \tag{15}$$

The first term accounts for the dilution in n due to the expansion of the universe, while the second term represents the annihilation and production of particles in reactions. n_0 in (15) is the number density of the particles in thermal equilibrium. Survival of particles in the cosmological context was discussed by Zel'dovich et al[13] and by Chiu[14] in mid 60's and studied numerically by Lee and Weinberg, by Wolfram and by others[10]. Let us redefine the total number of the heavy particles by $f = n/T^3$ as the total volume is behaving like T^{-3} with n(T) given from (6) in the unit $\hbar=c=k=1$,

$$f = \frac{n(T)}{T^3} = \frac{g}{2\pi^2}\int_0^\infty \frac{u^2\,du}{\exp\{[u^2+x^{-2}]^{1/2}\} \pm 1} \tag{16}$$

where $x = T/m$, m being the heavy particle mass. g accounts for the fermionic (bosonic) degrees of freedom with the upper (lower) sign in (16). Then Eq. (15) becomes

$$\frac{df}{dx} = Z[f^2(x) - f_0^2(x)] \tag{17}$$

where

$$Z = \left(\frac{45}{8\pi^3 G}\right)^{1/2}\frac{m\langle\sigma v\rangle}{N_F^{1/2}}$$

Here we have made use of Eqs (7) and (12) which hold for the radiation-dominated era. From (16), it is easy to see that the Boldzman factor is not important at high temperatures $T \gg M$ (or $x \gg 1$) so that $f(x) \sim$ const but at low temperatures $T \ll m$ (or $\ll 1$),

$$f(x) \simeq \frac{g}{(8\pi^3)^{1/2}}\, e^{-1/x}\, x^{-3/2} \tag{18}$$

Eq. (17) is to be solved subject to the initial condition $f(x=\infty) = f_0$.

It is expected that $f(x)$ remains approximately equal to $f_o(x)$ until the temperature drops to the decoupling temperature T_D or $df_o/dx = Zf_0^2$ at $x = x_D = T_D/m$ and that thereafter f follows approximately the equation

$$\frac{df}{dx} = Zf^2 \tag{19}$$

for $x < x_D$ with the initial condition $f(x_D) = f_o(x_D)$. Since $x_D < 1$, we can approximate f_o by the nonrelativistic formula (18) and insert it into (19) to obtain

$$x_D^{-1/2}\, e^{1/x_D} = \frac{8}{8\pi^3}\left[\frac{45}{N_F(x_D)}\right]^{1/2} mM_p\langle\sigma v\rangle\Big|_{x = xD} \tag{20}$$

so that T_D is determined approximately by

$$x_D^{-1} = \ell n\left[\frac{8}{8\pi^3}\left(\frac{45}{N_F}\right)^{1/2} mM_p\langle\sigma v\rangle\right]_{x = x_D} \tag{21}$$

If we assume that the massless degrees of freedom below the mass of the super heavy particle m are those of the standard model, then $N_F = 427/4$.

The mass dominated temperature T_m can be obtained from equating the energy density of the heavy particles to that of all other particles, Eq. (13), at $x_m = T_m/m$,

$$\frac{\pi^2 N_F}{15} T_m^4 = 2m\left(\frac{T_m}{T_D}\right)^3 n_0(T_D) = 2m\,\varepsilon\, T_m^3 f_0(x_D) \tag{22}$$

where $T_m < T_D$, $\varepsilon = 0.8$ to correct the analytic approximation compared to the numerical solution and 2 accounts for the Dirac type particle and its antiparticles. By making use of (18) and (20), we obtain T_m from (22),

$$T_m = \varepsilon\,\frac{N_F(T_D)}{N_F(T_m)}\left[\frac{160}{\pi N_F(T_D)}\right]^{1/2} \frac{m}{\alpha M_p}\,\frac{m}{x_D^2} \tag{23}$$

where we have parametrized $\langle\sigma v\rangle$ at x_D as α/m^2.

Finally the decay temperature T_d of the unstable heavy particle is related to the age of the universe t_m which is the lifetime of the particle. Since $T_d < T_m$, t_m can be obtained from Eqs (1) and (2) and (12) for $p << \rho$ and zero curvature

$$t_m = B/T_d^{3/2} \tag{24}$$

where B satifies

$$B/T_m^{3/2} = [45/32\pi^3 N_F(T_m)]^{1/2} M_p/T_m^2 \qquad (25)$$

as T_m is at the boundary between the radiation-dominated era and the matter dominated era. Then it follows from (23) - (25) that

$$t_m = (1.1 \times 10^{-4})\alpha^2 N_F(T_d)^{1.5} M_p^3 (x_D/m)^4 (\rho_m/\rho_R) T_d^{1.5} \qquad (26)$$

where we have expressed (T_m/T_d) by the ratio of the heavy particle energy density

$$\rho_m(T_d) = 2m\varepsilon n(T_D)(T_d/T_D)^3 = 2m\varepsilon n(T_D)(T_m/T_D)^3(T_d/T_m)^3$$

$$= \pi(\pi^2/15) N_F(T_m) T_m^4 \quad (T_d/T_m)^3$$

and the energy density of the other relativistic particles

$$\rho_R(T_d) = (\pi^2/15) N_F(T_d) T_d^4.$$

Eq. (26) gives a bound for the lifetime of the heavy particle t_m for a given m and a bound for the ratio of the energy densities ρ_m/ρ_R at T_d. Existing calculations[15] show that the grand unification models can explain the small baryon number density $n_N/n_\gamma \cong 10^{-9}$ and certainly no larger than 10^{-5}. Even if we tske this optomistic value, at T_d, the nucleon number n_N must not be diluted by a factor larger than 10^5 as all the energy of heavy particles will end up in the form of radiation. For $\rho_m/\rho_R \leq 10^5$ and a typical value $\alpha \simeq 1$, Eq. (26) gives an allowed region[16] of mass-lifetime plot whose boundary is approximately a straight line connecting the point ($m=10^8$GeV, $t_m \cong 1$ sec) and ($m = 10^{13}$GeV, $t_m = 10^{-16}$ sec).

Other constraints of heavy unstable particle decay is the effect on the nucleosynthesis[17] and photofission of light nuclei. The latter is satisfied once the first condition is met. If T_d <0.1 MeV, the heavy particle survives once the primordial nucleosynthesis is in progress and can increase expansion rate of the universe. This will eventually produce a large neutron to proton ratio leading to a larger He^4 abundance. In order to preserve the primordial He^4 production mechanism, it was suggested by Weinberg[17] that the reheating temperature after the heavy particle decay is to be greater than 0.4 MeV so

that any previously formed He^4 nuclei are broken up and the nucleosynthesis can start from scratch. In this case, the reheating temperature T_H is given by $\rho_m(T_d) = (\pi^2/15)N_F(T_H)T_H^4$. On the other hand

$$\rho_m(T_d) = 2\varepsilon m\, T_d^3 f_0(x_D) = 0.03\,\frac{M_P^2}{t_m^2} \tag{27}$$

by requiring $T_H > 0.4$ MeV for $T_d < 0.1$ MeV, we then obtain

$$t_m < 8.6 \times 10^{24}\ \text{GeV}^{-1} = 5.66\ \text{sec} \tag{28}$$

while from (24)

$$t_m > (1.4 \times 10^{33}) x_D^{\alpha 1/2}/m\ \text{sec}. \tag{29}$$

Eqs. (26), (28) and (29) are the constraints for the lifetime[18]. The latter two constraints modifies the mass-lifetime plot obtained from (26): below $m = 10^7$GeV, the boundary curve follows (29), for $M=10^7 \sim 10^8$GeV, it follows (28) and for $M > 10^8$ GeV it is given by (26).

Finally we can perform in analogy with the nucleon decay the operator analysis of heavy particle decay for a given unifying force for the unstable particle. Suppose that a d-dimensional operator for the decay is produced by the grand unification interaction. If the final states after the decay contain only the standard fermions of SU(3) x SU(2) x U(1), d will not be smaller than 6 and the corresponding lifetime due to grand unification interaction is parametrized by

$$t_G = \beta M_x^{2(d-4)}/m^{1+2(d-4)} \tag{30}$$

where M_x is the mass of the exchanged superheavy particle around 10^{15}GeV and β is a constant depending on the specific model. For $10^8 < M < 10^{12}$ GeV, $d \geq 9$ operators give t_G in the forbidden region, d=7 operators are barely allowed for $m > 10^{11}$ GeV and d = 6 operators allow heavy particles almost all values of $m > 10^{7.6}$ GeV. For $2.5 \times 10^5 < m < 10^{7.6}$ GeV, no grand unified models satisfy the cosmological constraints. The main constraints in this mass region come from the dilution of the already manufactured nucleon number density and nucleosynthesis.

Acknowledgments

I would like to thank Kiwoon Choi and Jinh E. Kims for their initiatives to numerically analyse the mass-lifetime relations for unstable particles in cosmology and to Gary Steigman for helpful criticism.

References and Footnotes

1. See, for example, Unity of Forces in the Universe. Vol II, Ed. A. Zee (World Scientific Pub. Co., 1982); G. Steigman, Ann. Rev. Nucl. Part Sci. 29, 313 (1979); Kyungsik Kang in the Proceedings of the Second Symposium on Theoretical Physics, Ed. H. S. Song (Min Eum Sa, Seoul, 1984).
2. Ya. B. Zel'dovich, Com. Astrophys. Space Phys. 2,12 (1970).
3. A. H. Guth, Phys. Rev. D23, 347(1981); M. Yoshimua, Phys Rev. Lett. 41, 281(1978).
4. M. Fukugita et al., Phys. Rev. D26, 1840(1982); K. Kang and A. Panziris, Phys. Rev. D (In press).
5. For example, S. Dimopoulos, et al., Phys. Lett. 117B, 185(1982); K. Kang and S. Ouvry, Phys.Rev. D28, 2662(1983).
6. R. Cowsik and J. McClelland, Phys. Rev. Lett. 29, 669(1972); J. E. Gunn et al., Astrophys. J. 223, 1015(1978).
7. K-Choi, K.Kang and J.E.Kim, Phys. Rev D32, 2822(1985).
8. I. Bars, M.J. Bowick, and K. Freese, Phys. Lett. 138B, 159(1984).
9. C. Vafa and E. Witten, Nucl Phys. B234,173(1984).
10. B. W. Lee and S. Weinberg, Phys. Rev. Lett.39,165(1977); D. A. Dicus, E. W. Kolb and V.L. Teplitz, ibid. 168(1977); S. Wolfram, Phys. Lett. 82B.65 (1979).
11. J. E. Gunn et al, (Ref 6).
12. A. Albricht and P. J. Steinhardt, Phys. Rev. Lett. 48, 1220(1982); A. D. Linde, Phys. Lett. 108B, 389(1982).
13. Ya, B. Zeldovich, L. B. Okun and S. B. Pikelner, Uspokhi 8, 702(1966).
14. H. Y. Chiu, Phys. Rev. Lett 17, 712(1966).
15. See, for example, M. Yoshimura in Grand Unified Theories and Related Topics, Ed. M. Konuma and T. Maskawa (World Scientific, 1981); A. Masiero et al., Z phys. C17. 33(1983).
16. If the dilution factor is reduced by a factor r so that $\rho_m/\rho_R = 10^5/r$, then the life-time will decrease by a factor $r^{1.5}$ and the allowed region will shrink accordingly.
17. S.Weinberg, Phys. Rev. Lett. 48, 1303(1983); E. W. Kolb and R. J. Scherra, Phys. Rev. D25, 1481(1982).
18. It was pointed out by M. Turner, Phys. Rev. D31, 681(1985) that the decaying particles may not heat up the universe so that Eq. (29) for $m < 10^7$GeV may not be necessary. I thank G. Steigman for bringing this to my attention.

THE RESURRECTION OF NEUTRINOS AS DARK MATTER

David N. Schramm
The University of Chicago and Fermilab



"Rumors of my death are greatly exaggerated" – Mark Twain

It is shown that new observations of large scale structure in the Universe (voids, foam, and large-scale velocity fields) are best understood if the dominant matter of the Universe is in the form of massive ($9eV \leq m_\nu \leq 35eV$) neutrinos. Cold dark matter, even with biasing, seems unable to duplicate the combination of these observations (although a fine-tuned loophole with cold matter and percolated explosions may also marginally work.) The previous fatal problems of galaxy formation with neutrinos can be remedied by combining them with either cosmic strings or explosive galaxy formation. The former naturally gives the scale-free correlation function for galaxies, clusters, and superclusters, and gives large, but not necessarily spherical voids. The latter naturally gives spherical voids, but requires fine tuning and percolation to get the large scales and the scale-free correlation function.

Massive neutrinos were once quite popular as candidates for solving the cosmological dark matter problem, since they were the least exotic of the non-baryonic options, and they naturally clustered only on large scales where the dark matter was needed, rather than on the small scales where the contribution of dark matter was known to be minimal (ref. 1 and references therein). They received a major boost with the preliminary reports of measured mass (ref. 2 and references therein) for ν_e (although probably only the most massive ν is cosmologically important, and that might well be ν_τ which could still have a $\sim 10eV$ mass, even if $m_{\nu_e} \ll 1eV$). Also, they gained strength when it was shown[3] that the neutrino Jean's mass was

$$M_J \sim \frac{3 \times 10^{18} M_\odot}{m_\nu^2(eV)} \text{ or } \lambda_J \sim \frac{1300 Mpc}{m_\nu(eV)}$$

which for $m_\nu \sim 10eV$ yielded $M \sim 10^{16} M_\odot$, and $\lambda \sim 30Mpc$, the mass and scale of superclusters.

Unfortunately, massive neutrinos fell into disrepute as dark matter when it was emphasized[4] that in the standard adiabatic model of galaxy formation with a random phase Zel'dovich fluctuation spectrum of the type expected by inflation, and with $\delta T/T$ constrained by microwave observations, galaxies did not form until redshift $z \lesssim 1$. This occurred because the initially formed pancakes with mass M_J took a while to fragment down to galaxy size. This contradicted the observations which showed that quasars existed back to $z \sim 3.5$. In addition, if baryons stay in gas form in the potential wells of the large ν pancakes, they light up in the x-rays beyond what is observed[5].

While some[6] have appealed to statistical tails, etc., to escape these conclusions, most cosmologists began abandoning neutrinos and adopting cold dark matter[7], which could enable rapid galaxy formation[8,9].

Cold matter also had its problems[10]. In the standard model, it would all cluster on small scales, and thus be measured by the dynamics of clusters, such as the Virgo infall. Since such measurements implied that $\Omega \sim 0.2 \pm 0.1$ on cluster scales, this meant that $\Omega_{cold} \lesssim 0.3$, and not unity. Remember that $\Omega_{baryon} \sim 0.1$, so observationally, non-baryonic dark matter is not required unless one wants an Ω of unity, so cold matter wasn't naturally solving one problem for which it was postulated. This constraint on cold matter could be escaped if it were *also* assumed that galaxy formation was biased[9,11] and did not occur everywhere.

Thus, there could be many clumps of cold matter and baryons that did not shine for some ad hoc reason. Biasing ran into problems when it could not explain the observation[12] of a very large cluster–cluster correlation function, ξ_{cc}, relative to the galaxy–galaxy correlation function[10,11], ξ_{gg}. With biasing $\xi_{cc} \propto \xi_{gg}$ but in all models $\xi_{gg} < 0$ for a few 10's of Mpc, whereas ξ_{cc} was observed to be positive out to scales $\gtrsim 50Mpc$.

Hardcore cold matter lovers had to argue that the ξ_{cc} data might be wrong, although no one has been able to disprove it. A way out of the ξ_{cc} problem was proposed in Reference 13. There we noted that the correlation functions appear to be scale free, thus implying that large-scale structure is dominated by something other than random noise and gravity, say either percolated explosions or strings. In fact, the scale-free structure is characterized by a fractal of dimension $D \sim 1.2$, not too different from the $D \sim 1$ that naive string theory might yield. String calculations[14] of galaxy formation indeed found support for such a fractal process with the appropriate dimension being valid from galaxy to supercluster scales.

Thus, there were already strong hints that something was wrong with the previous, in vogue, picture of biasing and cold matter with random noise initial fluctuations. To this we now add the new observations of many large voids[15,16] of diameter $50h_{1/2}Mpc$ ($h_{1/2} \equiv H_0/50km/sec/Mpc$), with most galaxies distributed on the walls of the voids, and the observation[17] that our local 40 Mpc region of space is moving with a coherent velocity field of $\sim 600km/sec$ toward Hydra-Centaurus. While at least one large void (in Böotes) had been observed before[18], using a pencil beam approach, until the Harvard redshift[15] survey work, it was not known how ubiquitous voids were. In fact, the Harvard data shows that almost all galaxies are distributed along the "walls" of voids; galaxies and clusters are not randomly distributed, but fit onto a well-ordered pattern.

While the Harvard work only goes out to $\sim 100Mpc$, there is substantial evidence that this sort of pattern persists to redshifts $z \sim 1$ from the Koo and Kron survey[16], as well as the earlier work of Tifft and others on distributions of quasar redshifts which showed "quantization". A simple explanation for the peaks and valleys in the distribution of galaxies and quasars with redshift is that one is looking through filaments or shells with voids in between, once again demonstrating that galaxies and clusters are not laid out randomly on the sky, but follow a pattern.

While statistical fluctuations with cold matter might yield a few large voids as well as many small voids[5,9], it is difficult to get all of space filled with large voids and have galaxies appear only at the boundaries unless some special form of "biasing" is used. However, the real killing blow for the cold matter plus biasing scheme comes from the velocity field work. Even if the biasing could be selected so as to give ubiquitous large voids, the velocities of a $40Mpc$ region of galaxies would be relatively small and random, rather than large and coherent[19]. Thus, it appears that the large-scale structure is telling us that we need something that gives us $\sim 40Mpc$ coherent patterns, and cold matter doesn't appear the way to go.

Since neutrinos naturally gave us patterns on this scale, maybe they should be reexamined. In addition, since the voids look rather spherical, and since explosions tend to produce

spherical holes after a few expansion times even if the initial explosion is asymmetric, perhaps an explosive mechanism should be considered also. Since the Ostriker–Cowie[20] explosion mechanism by itself cannot yield such large voids, the only way it could work is via a high density network of explosions which percolated[10,21]. However, to get $\Omega = 1$ with an exploding scenario would still require non-baryonic matter that did not cluster with the light emitting stuff. In principal, this could be either neutrinos or cold matter but at least with neutrinos an $\sim 40 Mpc$ scale might still be naturally imposed.

Of course, in order for neutrinos to work as the dominant matter, some mechanism to rapidly form galaxies must be imposed both to enable galaxies to exist at $z \sim 5$, and to condense out the gas before it falls into the forming deep potential wells, and emits x-rays. Two ways that might achieve this rapid formation are either via the aforementioned explosion scheme within the collapsing ν-pancakes, or via cosmic strings[22] which would act as nucleation sites for galaxy formation. Since strings are not free-streamed away by the relativistic neutrinos[23], the galaxy scale fluctuations remain within the ν-pancakes.

To summarize, the above possibilities leaves us with two viable options: 1. Neutrinos and strings; or 2. Neutrinos and percolated explosions. A third option of cold matter and percolated explosions cannot be completely dismissed, but does not naturally give us the $\sim 40 Mpc$ scale; however, the explosions could be a way of clearing the baryons out of the cold matter clumps in the voids and leave a critical density of matter not associated with the light emitting regions. In such a scenario, the voids would then be filled with clumps of cold matter.

It is interesting that the two most viable options involve the same two options that the scale-free cluster–cluster correlation function arguments point towards. Let us look at each of these scenarios in a little more detail and see if there might be ways of resolving whether either of them might actually be correct. Also, let us see what each requires for the physics of the early Universe.

Both of these scenarios have hot matter, presumably neutrinos as the dominant matter of the Universe. If $\Omega = 1$, as is necessary to avoid our living at a special epoch, and as agrees with the recent large-scale galaxy count arguments of Loh and Spillar (but disagrees with the direct dynamical arguments on scales of clusters and smaller, and with the baryonic measurements from nucleosynthesis), then $m_\nu \lesssim 35eV$. Since with $\Omega = 1$ the age of the Universe $t_0 = \frac{2}{3H_0}$, and since globular clusters and nucleochronology require $t_0 \gtrsim 11 \times 10^9 yr$ (with a best fit of $t_0 \sim 15 \times 10^9 yr$) we must say that $H_0^{-1} \gtrsim 17 \times 10^9 yr$. Thus, $H_0 \lesssim 60 km/sec/Mpc$, or $h_{1/2} \lesssim 1.2$. From the number of neutrinos and photons in the Universe, we know that the most massive neutrino is bounded by (see ref. 1 and references therein)

$$m_\nu \lesssim (25eV)\Omega h_{1/2}^2 \lesssim 35eV.$$

From the requirement that we want the neutrinos to give us the large-scale structure, $\lambda_J \sim 40 Mpc$, or $M_J \sim 10^{16} M_\odot$, we must have $m_\nu \gtrsim 10eV$. Also, we have a lower bound from the nucleosynthesis argument[26] that the number of neutrino species with $m_\nu \lesssim 10MeV$ is three

or at most four, since the sum of all neutrino masses cannot exceed the $35eV$ limit mentioned above. Since the lowest mass for the most massive one occurs when they are all equal, then if $N_\nu \leq 4$,

$$m_\nu \gtrsim 9eV.$$

The first scale to be able to condense and thus have their density grow will be the horizon scale when the neutrinos become non-relativistic, which is M_J. However, in the string option, loops of string will exist down to scales of galaxy size (scales smaller than galaxy size gravitationally radiate away[22]). So as the neutrinos slow down they can be trapped on smaller scales. The baryons will not be able to begin clustering until after recombination. However, the slow-moving baryons will rapidly fall on to the pre-existing loops of string plus neutrinos. Thus, galaxies will be able to form shortly after recombination, and well before $z \sim 1$.

The correlation functions of galaxies through superclusters will be characterized by the string picture[14] and will naturally yield a fractal near $D \sim 1$. The collapsing ν-pancakes on $\lambda_J \sim 40Mpc$ scales will create large voids on that scale, and leave galaxies in planes. Although actual detailed evolutionary calculations of ν-pancakes plus string-induced galaxy formation remain to be completed, probably this model would not naturally leave truly spherical voids.

Of course, in many models voids do tend towards a spherical shape after several expansion times. Thus, one might use the degree of sphericity versus z to say something about the nature of the origin of the voids.

While this string plus neutrino scenario naturally yields $D \sim 1$, it does not so naturally give $D = 1.2$. Fine tuning[28] of string parameters may enable such variation on the scale of the galaxy–galaxy correlation function, or some modification of the criteria for the formation of light-emitting regions around the strings may be necessary.

In this regard it should be remembered that because of possible systematic errors, not everyone agrees that 1.2 is significantly different from 1.0, even for the galaxy–galaxy correlation function, which is the best determined[30]. The uncertainties in the exponent of the cluster–cluster correlation functions are *far* larger, thus problems in trying to explain variations from $D = 1$ fractals are not serious at the present time. With strings there is the additional problem of tuning the primordial phase transition so as to inflate first, and then produce strings[38]. While not impossible, this is constraining.

The second way to get neutrinos to work involves explosive galaxy formation. Here we need initial seeds to lead to condensations which produce massive baryonic objects which explode. Under the third option, where the explosions are used with cold matter, the baryons might naturally collect around the growing small-scale (globular cluster mass) cold matter clumps. However, as mentioned before, such a model does not naturally give us $40Mpc$ structure. If we use neutrinos then the seeds must be in a form which does not get free-streamed away by the relativistic neutrinos. Strings don't work well here because the string scales that might lead to rapidly evolving baryonic objects are radiated away gravitationally. Thus, the seeds must come in some other isothermal-like form. Perhaps the best option

would be condensates from the quark–hadron transition, either planetary mass black holes[31] or Witten nuggets[32]. Both have formation problems[33] and the latter have survival problems[34] also. If such objects could form and survive, they do lead naturally[35] to very massive ($\sim 1000 M_\odot$) baryonic objects which would explode on rapid timescales.

The scale affected by explosions of single galaxy size[36] is at most a few Mpc; however, it has been shown[21] that at sufficiently high densities and high Trigger rates, the explosions can percolate at least out to scales of a few 10's of Mpc. The fractal dimension of such percolated ensembles is quite sensitive to parameter assumptions and usually varies with scale, thus showing that it is not a true scale-free fractal. If it is made to fit the small scale (few Mpc) with $D \sim 1$ it is usually larger $D \sim 2$ on scales of $\gtrsim 10 Mpc$. Since, as mentioned above, the exponent of the cluster–cluster correlation function is not, at present, well determined, such models cannot be ruled out. With such explosions percolating within ν-pancakes, we might naturally have their pattern superimposed on the $\sim 40 Mpc$ neutrino scale. In addition, although percolated explosions will initially be highly non-spherical, their shape will evolve towards sphericity with the smaller axes catching up in length to the largest one. In order for large-scale percolation to occur, several generations[21] of explosions must occur; however, cooling arguments and time to initial explosions, plus the need for condensed objects by $z \sim 4$ and the need to hide from present observers, the radiation produced by the explosions, severely restrict the possibility of such percolation and thus quite a bit of fine tuning is required to escape the constraints.

Thus, while we cannot explicitly rule out this latter case, unless some new physics can be developed to show how the fine-tuned parameters are natural for other reasons, we must lean towards the string option as the present frontrunner. Strings, of course, would have other observational consequences (see ref. 22 and references therein) like gravitational double lensing of distant objects and shifts in the 3° background across such a line of lenses, and a background of gravitational radiation from the evaporation of small-scale strings which might affect the millisecond pulsar. Thus, observations should eventually be able to confirm or deny this frontrunner.

In summary, we have come full circle and once again massive neutrinos are looking good. However, with them comes the need for galaxy and structure formation triggered by something other than random phase adiabatic fluctuations. The non-random phase fractal initial conditions such as produced by strings[37] or fractal generating explosions[20,21] seem to be the way to go. It is comforting that the exotica of cosmic strings do seem to be a natural consequence[39] of the current, in vogue, superstring Theories of Everything (T.O.E.).

Acknowledgements to co-workers J. Charlton, K. Olive, A. Melott, G. Steigman, A. Szalay, and M. Turner are gratefully given. This work was supported in part by NSF AST 85-15447, and by DOE DE-FG02-85ER40234 at the University of Chicago.

References

1. Schramm, D. and Steigman, G. 1981, *Ap.J.* **243**, 1.
2. Lubimov, A. 1986, in this volume.
3. .Bond, J., Efstathiou, G., and Silk, J. 1980, *Phys.Rev.Lett.* **45**, 1980.
4. Frenk, C., White, S., and Davis, M. 1983, *Ap.J.* **271**, 417.
5. Davis, M. 1986 *Proc. 1984 Inner Space/Outer Space*, University of Chicago Press.
6. Melott, A. 1986 *Proc. 1984 Inner Space/Outer Space*, University of Chicago Press.
7. Blumenthal, G., Faber, S., Primack, J., and Rees, M. 1984, *Nature* **311**, 517.
8. Melott, A., Einasto, J., Saar, E., Suisalu, I., Klypin, A., and Shandarin, S. 1983, *Phys.Rev.Lett* **51**, 935.
9. Efstathiou, G., Frenk, C., White, S., and Davis, M. 1985 *Ap.J.Suppl.* **57**, 241.
10. Schramm, D. 1985, *Proc. 1984 Rome Conf. on Microwave Background.*
11. Bardeen, J., Bond, J., Kaiser, N., and Szalay, A. 1985, submitted to *Ap.J.*.
12. Bahcall, N. and Soniero, R. 1983, *Ap.J.* **270**, 20; Klypin and Khlopov 1983, *Soviet Astron. Lett.* **9**, 41.
13. Szalay, A. and Schramm, D. 1985, *Nature* **314**, 718.
14. Turok, N. 1985, U.C. Santa Barbara preprint
15. Geller, M. and Huchra, J. 1986, Center for Astrophysics preprint
16. Koo, D. and Kron, R. 1986, in preparation.
17. Faber, S., Aaronson, M., Lynden-Bell, D. 1986, *Proc. of Hawaii Symposium on Large-Scale Structure.*
18. Kirschner, R., Oemler, G., Schecter, P., and Shectman, S. 1982, *Ap.J.* **248**, L57.
19. Melott, A. 1986, Univ. of Chicago preprint.
20. Ostriker, J. and Cowie, L. 1980, *Ap.J.* **243**, L127.
21. Charlton, J. and Schramm, D. 1986, submitted to *Ap.J.*.
22. Vilenkin, A. 1985, *Physics Reports* **121**, 1.
23. Vittorio, N. and Schramm, D. 1985, *Comments on Nuclear and Particle Physics* **15**, 1.
24. Loh, E. and Spillar, E. 1986, Princeton University preprint
25. Freese, K. and Schramm, D. 1984, *Nucl. Physics* **B233**, 167.
26. Yang, J., Turner, M., Steigman, G., Schramm, D., and Olive, K. 1984 *Ap.J.* **281**, 493.
27. Melott, A., Scherrer, R., and Schramm, D. 1986, in preparation.
28. Pagels, H. 1986, Rockefeller University preprint.
29. Geller, M. 1986, private communication.
30. Peebles, P.J.E. 1981, *The Large Scale Structure of the Universe*, Princeton University Press.
31. Crawford, M. and Schramm, D. 1982, *Nature* **298**, 538.
32. Witten, E. 1984, *Phys.Rev.* **D30**, 272.
33. Applegate, J. and Hogan, C. 1985, *Phys.Rev.* **D31**, 3037.
34. Alcock, C. and Fahri, J. 1985, MIT preprint.
35. Freese, K., Price, R., and Schramm, D. 1983, *Ap.J.* **275**, 405.
36. Vishniac, E., Ostriker, J., and Bertschinger, E. 1985, Princeton University preprint.
37. Turok, N. and Schramm, D. 1984, *Nature* **312**, 598.
38. Olive, K. and Seckel, D. 1986, FNAL preprint.
39. Witten, E. 1985, *Physics Letters* **B153**, 243.

STANDARD SOLAR MODELS: A SEARCH FOR CONSISTENCY

S. Cahen, C. Doom[1], and M. Cassé

Institut de Recherche Fondamentale, Service d'Astrophysique
Centre d'Etudes Nucléaires de Saclay
91191 Gif-sur-Yvette Cedex, France

[1]On leave from the Astrophysical Institute
Vrije Universiteit Brussels

presented by S. Cahen

ABSTRACT

A comparison of the standard solar models implemented by various authors with the recent Los Alamos radiative opacities is presented. These models differ in their input data- nuclear reaction rates and mass fraction Z of elements heavier than helium- and consequently in their results: neutrino fluxes and helium mass fraction Y. As a consistency check, it is shown that our numerical model reproduces with a satisfactory accuracy the published neutrino fluxes when the same key reaction rates and the same mass fraction of heavy elements, Z, are adopted. Good agreement is also obtained with all other teams but one on the value of Y required to fit the observed luminosity of the sun. On the basis of recent determinations of Z and of the reaction rates, we predict as a best estimate a flux of 5.3 10^{6} ^{8}B neutrinos.cm^{-2}.s^{-1} (about 25% higher than in Bahcall et al.[1], 1985) and a capture rate of 7.4 SNU on ^{37}Cl and 111 SNU on ^{71}Ga (using the ν capture cross section on ^{71}Ga from Ref.1)

1 - Introduction

A gallium solar neutrino detector will hopefully operate in the near future (Kirsten, this volume). An up-to-date determination of the expected capture rate on this detector becomes therefore a strong need. In the recent years, several conventional solar models have been published[1-7] based on recent Los Alamos opacities (Huebner et al.[8]). These models differ in their input data- nuclear reaction rates and heavy element mass fraction- and also in their results. We would like to trace back the origin of these variations. Are they entirely due to differences in the input physics or to deeper differences in computational strategies?

In section 2 we briefly present our model. The key nuclear reaction rates and the metallicity Z adopted by the various authors are presented in section 3 as well as the estimated sensitivity of the calculated neutrino fluxes to changes in these key input data. In section 4 we compare the previously published results with those provided by our model initiated with the same data input. Our best estimate model is shown in section 5 and conclusions are drawn in section 6.

2 - The solar model

The numerical model used in this study has already been described[9]. We recall that the solar structure is computed assuming spherical symmetry and the absence of rotation and magnetic field, starting from an initially homogeneous star with a given composition (mass fraction X of hydrogen, Y of helium and Z of heavier elements). Since Y is a poorly known value, we adopt, as usual, a value of Z consistent with photospheric estimates and adjust Y in order that the numerical sun reaches the solar luminosity ($3.86\ 10^{33}$ erg.s^{-1}) after an elapsed time of about $4.6\ 10^{9}$ yr. The solar radius is adjusted by varying the parameter α, which is the ratio of the mixing length ℓ[10] in the convective envelope of the sun to the pressure scale height H_p:

$$\alpha = \frac{\ell}{H_p} \quad , \quad \text{with } H_p^{-1} = \frac{1}{P}\left|\frac{dP}{dr}\right|$$

The nuclear energy production and the changes in the elemental abundances are computed in a fully consistent manner with the nuclear network presented in table I. Electron screening of the nuclear reactions is taken into account following the formalism of Graboske et al.[11]. The equation of state includes perfect gas, degenerate electron and radiation pressures, as well as partial ionization of hydrogen and helium in the convective envelope and Coulomb corrections according to the Debye-Hückel formalism.

TABLE I: THE NUCLEAR NETWORK

Reaction chain	Heat input (MeV)	Maximum neutrino energy (MeV)
$p(p,e^+\nu)D$	1.192	0.420
$p(pe^-,\nu)D$	0.001	1.440
$D(p,\gamma)^3He$	5.494	-
$^3He(^3He,2p)^4He$	12.860	-
$^3He(\alpha,\gamma)^7Be$	1.586	-
$^7Be(e^-,\nu)^7Li$	0.049	0.861
$^7Li(p,\alpha)^4He$	17.348	-
$^7Be(p,\gamma)^8B(e^+\nu)^8Be^*(\alpha)^4He$	11.017	14.06
$^{12}C(p,\gamma)^{13}N(e^+\nu)^{13}C$	3.455	1.20
$^{13}C(p,\gamma)^{14}N$	7.551	-
$^{14}N(p,\gamma)^{15}O(e^+\nu)^{15}N$	9.054	1.73
$^{15}N(p,\alpha)^{12}C$	4.966	-
$^{15}N(p,\gamma)^{16}O$	12.128	-
$^{16}O(p,\gamma)^{17}F(e^+\nu)^{17}O$	2.423	-
$^{17}O(p,\alpha)^{14}N$	1.193	-

3 - Nuclear reaction rates and metallicity

As already shown[2], the four reactions most influential for the production of the various neutrinos are $p(p,e^+\nu)^2H$, $^3He(^3He,2p)^4He$, $^3He(\alpha,\gamma)^7Be$, and $^7Be(p,\gamma)^8B$. The estimates of these key rates have significantly varied in the last years[12,13,14,15] except that of the $^3He(^3He,2p)^4He$ reaction. The values we adopt (Caughlan et al.[15] except for the p+p rate[14]) are close to that of Bahcall et al.[1] (1985). The reaction rates taken by the different authors (or equivalently the so-called S factors) are presented in table II.

Apart from the reaction rates, the authors differ in their choice of the initial solar metallicity Z. In this work we adopt the most recent value, given by Grevesse[17], $Z/X = 0.0284(1 \pm 0.05)$, based mainly on photospheric abundance determinations. As usual, it is assumed that the initial abundances in the entire sun are identical to the present photospheric ones.

Each of the key parameters presented above has it own impact on the neutrino flux arising from the different sources. A full discussion of this point requires to vary each one in order to estimate its influence on the neutrino flux. This is a systematic task that we have not yet accomplished. For the time being, we rely on the study of Bahcall et al.[2]. Table III, from these authors,

presents the relevant partial derivatives of the neutrino fluxes with respect to the key parameters discussed up to now. Note the high sensibility of the ^8B neutrino flux to changes in S_{11} and Z.

TABLE II: KEY INPUT DATA

Authors	p + p [a]	$^3He + ^4He$ [b]	$p + ^7Be$ [b]	Z
Bahcall et al.[2] 1982	3.88	0.52	0.029	0.0179
VandenBerg[4] 1983	FCZ 75	FCZ 75	FCZ 75	0.0169
Noels et al.[6] 1984	FCZ 75	FCZ 75	FCZ 75	{0.0180 0.0200
Bahcall et al.[1] 1985	4.03[c]	0.52	0.0238	0.0179
Lebreton and Maeder[7] 1986	HFCZ 83[d]	HFCZ 83[e]	HFCZ 83[d]	0.0200
This work: Reference model	4.07[f]	HFCZ 83[e]	0.024[g]	0.0200

FCZ 75 = Fowler et al.[16], HFCZ 83 = Harris et al.[13]. **a,b)** the numbers quoted in each column indicate the values of S(0) (see e.g. Parker[34]) for the reaction considered, in units of 10^{-25} MeV-barn for column a) and keV-barn for column b); **c)** this value is deduced from eq.(3) of Bahcall et al.[2] (1982) using the neutron half-life adopted by Bahcall et al.[1] (1985); **d)** Harris et al.[13] adopted the value of Bahcall et al.[2] (1982) (see first line) for this reaction; **e)** corresponds, according to Harris et al.[13] to S(0) = 0.56 keV-b and has not been revised by Caughlan et al.[15]; **f)** deduced from eq.(3) of Bahcall et al.[2] (1982) using the neutron half-life adopted by Filippone[14]; **g)** adopted by Filippone[14] and Caughlan et al.[15].

TABLE III
SENSIBILITY OF THE NEUTRINO FLUXES TO KEY PARAMETERS
(from Bahcall et al.[3] 1982)

ν source	$\frac{\partial \ln \varphi_i}{\partial \ln S_{11}}$	$\frac{\partial \ln \varphi_i}{\partial \ln S_{34}}$	$\frac{\partial \ln \varphi_i}{\partial \ln S_{17}}$	$\frac{\partial \ln \varphi_i}{\partial \ln Z}$
pp	0.1	-0.06	≃0.	-0.06
^7Be	-1.0	0.87	≃0.	0.68
^8B	-2.7	0.83	1.0	1.43

φ_i = neutrino flux arising from source i. S_{11}, S_{34} and S_{17} are the S factors (see e.g. Parker[34]) for the reactions p+p, $^3He+^4He$, and $p+^7Be$ respectively.

4 - Comparison with other models

We have tried to reproduce the results of VandenBerg[4], Bahcall et al.[2] (1982), Bahcall et al.[1] (1985), and Lebreton and Maeder[7], starting from their main input parameters (S_{11}, S_{34}, S_{17}, and Z, see table II). These authors, who have all used the Los Alamos opacities, give enough informations to allow a meaningful comparison with our results. The expected neutrino counting rates on chlorine and gallium are displayed in table IV, together with the metallicity, the inferred helium content and the central temperature and density of each model.

TABLE IV: COMPARISON OF THE MODELS

Authors	Z	Y	R_ν(Cl)	R_ν(Ga)	$\frac{T_c}{10^6 K}$	ρ_c g.cm^{-3}
VandenBerg[4] 1983	0.0169	0.27	8.3	a)	a)	a)
This work	0.0169	0.27	7.6	101 b)	15.38	143.6
Bahcall et al.[2] 1982	0.0179	0.25	7.6	106 b)	15.50	156.3
This work	0.0179	0.273	7.8	102 b)	15.60	147.5
Bahcall et al.[1] 1985	0.0179	0.25	5.8	107 c)	a)	a)
This work	0.0179	0.274	6.2	107 c)	15.52	145.5
Noels et al.[6] 1984	0.0180	0.274	a)	a)	15.63	150.2
Noels et al.[6] 1984	0.0200	0.282	a)	a)	15.75	151.5
Lebreton and Maeder[7] 1986	0.0200	0.282	13.3	a)	15.91	160.3
This work	0.0200	0.282	10.5	115 c)	15.77	150.7
This work: Reference model	0.0200	0.285	7.4	111 c)	15.64	145.8

a) Not specified ; b,c) Neutrino capture cross sections on ^{71}Ga from Bahcall[35] (b) and Bahcall et al.[1] (1985) (c). Z, Y, R_ν(Cl), R_ν(Ga), T_c and ρ_c denote the metallicity the helium mass fraction, the counting rate on chlorine and gallium and the central temperature and density. The neutrino counting rates are expressed in SNU (1 SNU = 10^{-36}capture/target atom/second)

It is gratifying to see in table IV that the expected neutrino counting rates on ^{37}Cl are reasonably reproducible despite their high sensitivity to central conditions, the maximum deviation being of the order of 30% (with respect to Lebreton and Maeder[7]), this being due in great part to their higher central temperature). Note that our central density is slightly lower than that of Bahcall et al.[2] (1982) and Lebreton and Maeder[7]. The agreement on the helium content Y (which is an adjusted parameter in all models) is impressive, with however the noticeable exception of Bahcall et al.[2,1], who require Y $\simeq$ 0.25 instead of Y $\simeq$ 0.274 for our work with the same Z. The cause of this discrepancy is not understood at the moment. Is it due to the simplified treatment of the solar atmosphere used by Bahcall et al.[2,1] compared to all other models? Indeed their solar structure is truncated at a point where the temperature is about 3

10^5K, and the outer zone ($\simeq 10^{-3}$ $M_\odot$) is described by a polytropic approximation. To get a clear-cut answer to this question we[18] will try to adapt the simplified atmospheric treatment of Bahcall et al.[2] to our solar model. If we except Bahcall et al.[2,1], all calculations show that Y and Z are positively correlated. Y is indeed sensitive to the opacity of the solar material and hence to Z (see e.g. Ref.19). We find $\partial \ln Y / \partial \ln(Z/X) \simeq 0.3$ in agreement with Noels et al.[6], but with a sign opposite to that printed in table X of Bahcall et al.[2]. Y is much less sensitive to the nuclear reaction rates: the most influential reaction is p + p for which the calculated partial derivative $\partial \ln Y / \partial \ln S_{11}$ is only 0.1 according to Bahcall et al.[2] (1982).

5 - Best estimates

The ability to reproduce the main results of most of the recent models (barring a disturbing exception, see above), can be considered as a calibration of our model or equivalently as a general coherence test of all the models considered. Having gained some confidence in our computational strategy we are now in position to produce a reference model based on updated data (see last row of table II).

The time evolution of various physical variables of our reference model, i.e. luminosity, photospheric radius and central values of temperature, density, hydrogen and ^{3}He mass fractions, and heat generation by nuclear reactions is shown in table V. Table VI shows the run of these physical quantities throughout the present sun. All these results are in reasonable agreement with those of Bahcall et al.[2] (1982) and Lebreton and Maeder[7], who published such detailed tables. We obtain a value $\alpha = 1.54$ for the mixing length parameter (see section 2) leading to a depth of the convective envelope of $1.86\ 10^5$ km at the base of which the temperature is $2.02\ 10^6$ km. Table VII presents the neutrino flux expected from each specific reaction and the total neutrino counting rate on chlorine, R_ν(Cl) and gallium, R_ν(Ga). We get R_ν(Cl) = 7.4 SNU and R_ν(Ga) = 111 SNU. Bahcall et al.[1] found $R_\nu(\mathrm{Cl}) = 5.8 \pm 2.2$ SNU and $R_\nu(\mathrm{Ga}) = 107^{+11}_{-7}$ SNU.

Work is in progress to evaluate the uncertainties on the capture rates following the general procedure presented in Bahcall et al.[1] (1982). As seen in table III, the 25% discrepancy in the ^{8}B neutrino flux between Bahcall et al.[1] and us could be almost entirely accounted for by the difference in Z, our value of Z (=0.20) being about 12% higher than the value adopted by these authors. Note that the neutrinos arising from ^{8}B have a non negligible contribution to the solar neutrino counting rate of a gallium detector when the revised cross section

TABLE V : TIME EVOLUTION OF THE REFERENCE MODEL

Age 10^9 yr	$\frac{L}{L_\odot}$	$\frac{R}{R_\odot}$	$\frac{T_c}{10^6 K}$	ρ_c g.cm^{-3}	$X_c(^1H)$	$X_c(^3He)$	ϵ_c erg.g^{-1}s^{-1}
0.144	0.726	0.886	13.58	81.66	0.6860	5.43E-05	16.6
0.249	0.733	0.889	13.60	82.60	0.6790	5.03E-05	15.7
0.397	0.741	0.893	13.65	83.95	0.6688	4.72E-05	15.4
0.596	0.751	0.897	13.72	85.72	0.6544	4.25E-05	14.6
0.855	0.763	0.903	13.81	88.13	0.6356	3.96E-05	14.7
1.180	0.780	0.909	13.93	91.26	0.6120	3.61E-05	14.8
1.575	0.800	0.918	14.07	95.39	0.5832	3.21E-05	14.9
1.662	0.807	0.920	14.13	96.87	0.5767	3.08E-05	15.0
1.808	0.814	0.923	14.18	98.54	0.5658	2.94E-05	15.1
2.110	0.831	0.930	14.32	102.3	0.5431	2.65E-05	15.3
2.470	0.853	0.939	14.48	107.1	0.5157	2.33E-05	15.5
2.832	0.875	0.948	14.65	112.3	0.4879	2.03E-05	15.7
3.256	0.903	0.959	14.86	119.0	0.4549	1.70E-05	16.0
3.661	0.930	0.971	15.08	126.2	0.4227	1.41E-05	16.3
3.888	0.947	0.978	15.21	130.6	0.4044	1.27E-05	16.5
4.134	0.965	0.985	15.36	135.6	0.3842	1.13E-05	16.9
4.355	0.982	0.993	15.50	140.6	0.3659	9.64E-06	16.9
4.574$\odot$	1.000	1.000	15.64	145.6	0.3474	8.52E-06	17.2
4.796	1.018	1.008	15.79	151.4	0.3283	7.30E-06	17.4
5.068	1.041	1.018	15.98	158.7	0.3046	5.98E-06	17.6
5.306	1.062	1.026	16.16	166.0	0.2836	5.05E-06	18.0

$\odot$: present sun. $L/L_\odot$, $R/R_\odot$ are respectively the luminosity and the radius in solar units. T_c, ρ_c, $X_c(^1H)$, $X_c(^3He)$ and ϵ_c denote the central values of temperature, density, hydrogen mass fraction, ^3He mass fraction and heat generation by nuclear reactions respectively. The first time steps from 0. to 0.144 10^9 yr are excluded due to small oscillations of L, ρ_c, T_c, and ϵ_c related to fast burning of D, ^3He, Li and Be before they reach their equilibrium abundance. At the beginning of hydrogen burning, the sun is about 30% less luminous than now, in agreement with Bahcall et al.[2] and Lebreton and Maeder[7].

TABLE VI : STRUCTURE OF THE REFERENCE MODEL AT $t = 4.57\ 10^9$yr

$\frac{M_r}{M_\odot}$	$\frac{r}{R_\odot}$	$\frac{T}{10^6 K}$	ρ g.cm^{-3}	$X(^1H)$	$X(^3He)$	ε erg.g^{-1}s^{-1}	$\frac{L_r}{L_\odot}$
0.0000	0.0000	15.64	145.8	0.3474	8.52E-06	1.72E+01	0.0000
0.0001	0.0099	15.61	145.2	0.3500	8.72E-06	1.71E+01	0.0009
0.0018	0.0262	15.42	139.1	0.3699	1.06E-06	1.64E+01	0.0156
0.0047	0.0363	15.22	133.2	0.3845	1.18E-05	1.55E+01	0.0392
0.0057	0.0388	15.16	131.6	0.3893	1.23E-05	1.52E+01	0.0469
0.0204	0.0611	14.53	115.1	0.4402	1.90E-05	1.29E+01	0.1531
0.0345	0.0742	14.09	104.8	0.4731	2.53E-05	1.13E+01	0.2409
0.0571	0.0902	13.50	92.67	0.5128	3.64E-05	9.41E+00	0.3618
0.0757	0.1010	13.10	84.94	0.5383	4.67E-05	8.17E+00	0.4463
0.1036	0.1151	12.56	75.61	0.5685	6.47E-05	6.65E+00	0.5527
0.1399	0.1310	11.95	65.95	0.5983	9.42E-05	5.11E+00	0.6626
0.1861	0.1492	11.26	56.23	0.6260	1.46E-04	3.66E+00	0.7664
0.2436	0.1699	10.50	46.67	0.6500	2.42E-04	2.39E+00	0.8552
0.3128	0.1935	9.676	37.45	0.6684	4.36E-04	1.38E+00	0.9214
0.3931	0.2204	8.825	28.77	0.6809	8.56E-04	7.14E-01	0.9638
0.4819	0.2510	7.976	20.98	0.6880	1.87E-03	3.35E-01	0.9870
0.5747	0.2859	7.146	14.38	0.6917	2.89E-03	9.44E-02	0.9970
0.6578	0.3218	6.402	9.643	0.6939	1.67E-03	2.46E-02	0.9993
0.7565	0.3752	5.483	5.292	0.6951	4.84E-04	5.52E-03	1.0000
0.8519	0.4502	4.478	2.313	0.6955	1.26E-04	7.19E-04	1.0000
0.9228	0.5455	3.520	0.8509	0.6955	7.99E-05	5.53E-05	1.0000
0.9633	0.6480	2.705	0.3130	0.6955	7.59E-05	3.13E-06	1.0000
0.9854	0.7565	1.790	0.1212	0.6955	7.56E-05	4.48E-08	1.0000
0.9949	0.8393	1.064	0.0542	0.6955	7.50E-05	4.22E-10	1.0000
0.9998	0.9522	0.2643	0.0063	0.6955	7.56E-05	0.00E+00	1.0000
1.0000	1.000	0.0058	0.0000	0.6955	7.56E-05	0.00E+00	1.0000

$M_r/M_\odot$ is the mass included in the sphere of radius $r/R_\odot$, and $L_r/L_\odot$ the energy leaving this sphere per second. T, ρ, $X(^1H)$, $X(^3He)$ and ε denote the values of temperature, density, hydrogen and ^{3}He mass fraction and heat generation by nuclear reactions respectively.

TABLE VII: NEUTRINOS FLUXES AND CAPTURE RATES

	Bahcall et al.[1] 1985			This work, reference model		
ν source	Flux[a]	^{37}Cl[b]	^{71}Ga[b]	Flux[a]	^{37}Cl[b]	^{71}Ga[b]
pp	6.10	0.	70.2	5.95	0.	68.4
pep	0.015	0.24	2.5	0.012	0.19	2.0
^{7}Be	0.40	0.95	27.0	0.46	1.1	31.4
^{8}B	0.00040	4.3	1.2	0.00053	5.7	1.6
^{13}N	0.05	0.08	2.6	0.06	0.09	3.2
^{15}O	0.04	0.24	3.5	0.05	0.32	4.7
Total	6.61	5.8	107.	6.53	7.4	111.

a) In units of $10^{10}\nu.cm^{-2}.s^{-1}$ at Earth. Neutrino capture cross sections are taken from Bahcall[35] for ^{37}Cl and Bahcall et al[1] (1985) for ^{71}Ga. b). Neutrino capture rates are expressed in SNU (see caption of table IV).

of the reaction $^{71}Ga(\nu,e^-)^{71}Ge$ at high energy is taken into account (see e.g. ref.20, 21, and Klapdor, this volume).

The value of Y = 0.285 derived in this work, which is supposed to reflect the helium mass fraction at the birth of the sun, $Y_{pre\odot}$, has interesting astrophysical consequences (see also Ref.9).

i) The revisited solar helium abundance is now closer to the value measured in the Orion nebula ($Y_{Orion} \simeq 0.28$ to 0.30, see e.g. ref. 22 and 23) the two values being expected to be similar [24,25]. Note that $Y = Y_{pre\odot} = 0.285$ is also consistent with the central value derived from the observations by Voyager 2 of Uranus[26] in which the helium abundance is supposed to be close to the presolar one: $Y_{Uranus} = 0.27 \pm 0.08$ (the quoted error, still preliminary, is probably overestimated[27]).

ii) This presolar helium abundance together with the primordial one, Y_p = 0.23 to 0.24, derived from the observation of extragalactic metal-poor HII regions[28,29,30], would imply that the increase of the helium mass fraction, ΔY, from the birth of the galaxy to the birth of the sun is $\simeq 0.05$, which is more than expected[31,32], but still explainable in the hypothesis of an active phase of star formation in the young galaxy[33].

6 - Conclusions

The various standard solar models implemented with recent Los Alamos opacities have been compared. The different neutrino fluxes calculated from these published models are reproduced with a reasonable accuracy if we adopt the same key input data (nuclear reaction rates and heavy element mass fraction Z). All models agree on an initial helium content $Y \simeq 0.28$ with $Z = 0.02$, with however a major exception: Bahcall et al.[2] (1982) infer $Y = 0.25 \pm 0.01$. This discrepancy is not understood at the moment. Using the best estimates of the nuclear reaction rates and of the solar metallicity we predict a neutrino counting rate of 7.4 SNU on chlorine and 111 SNU on gallium (using the neutrino capture cross sections of Bahcall et al.[1]), with a ^8B neutrino flux ($5.3\ 10^6$ $\nu.cm^{-2}.s^{-1}$ at Earth) about 25% higher than in Bahcall et al.[1] (1985). The revisited solar helium abundance (Y = 0.285) is consistent with the Orion value and sets interesting constraints on the chemical evolution of the Galaxy.

REFERENCES

1. Bahcall, J.N., Cleveland, B.T., Davis, R., Rowley, J.K.: 1985, *Astrophys. J.*, **292**, L79
2. Bahcall, J.N., Huebner, W.F., Lubow, S.H., Parker, P.D., Ulrich, R.K.: 1982, *Rev. Mod. Phys.*, **54**, 767

3. Filippone, B.W., Schramm, D.N.: 1982, *Astrophys. J.*, **253**, 393
4. VandenBergh, D.A., 1983: *Astrophys.J.Suppl.*, **51**, 29
5. Shibahashi, H., Noels, A., Gabriel, M.: 1984, *Astron. Astrophys.*, **123**, 283
6. Noels, A.,Scuflaire, R., Gabriel, M.: 1984, *Astron. Astrophys.*, **130**, 389
7. Lebreton, Y., Maeder, A.: 1985, *Astron. Astrophys.*, (in press)
8. Huebner, W.F., Merts, A.L., Magee, N.H., Jr, Argo, M.F.,:1977, *Astrophysical Opacity Library, UC-34b*
9. Cassé, M., Cahen, S., Doom, C.: 1986, in *Neutrinos and the Present Day Universe*, Congrès de la Société Francaise de Physique, eds. T. Montmerle, M. Spiro, CEA, C.E.N. Saclay
10. Böhm-Vitense, E.: 1958, *Zs. f. Ap.*, **46**, 108
11. Graboske, H.C., DeWitt, H.E., Grossman, A.S., Cooper, M.S.: 1973, *Astrophys. J.*, **181**, 457
12. Hampel, W.: 1983, Proceedings of the first Workshop on Nuclear Astrophysics, Ringberg Castle, Tegernsee, Germany, Max-Planck Institut ed.
13. Harris, M.J., Fowler, W.A., Caughlan, G.R, Zimmerman, B.A.: 1983, *Ann. Rev. Astron. Astrophys.*, **21**, 165
14. Filippone, B.W.: 1985, in *Solar Neutrinos and Neutrino Astronomy*, eds. M.L. Cherry, K. Lande, W.A. Fowler, American Institute of Physics, p.100
15. Caughlan, G. R., Fowler, W. A., Harris, M. J., Zimmerman, B. A.: 1985, *At. Data Nucl. Data Tables*, **32**, 197
16. Fowler, W.A., Caughlan, G.R., Zimmerman, B.A.: 1975, *Ann. Rev. Astron. Astrophys.*, **13**, 69
17. Grevesse, N.: 1984, in *Frontiers of Astronomy and Astrophysics* , Proceedings of the Seventh European Regional Astronomy Meeting, ed. R. Pallavicini, Florence, 1984, p.71
18. Cahen, S., Doom, C., Cassé, M.: 1986, in preparation
19. Iben, I., Jr.:1969, *Ann. of physics.*, **54**, 164
20. Mathews, G.J., Bloom, S.D., Fuller, G.M., Bahcall, J.N.: 1985, *Phys. Rev. C*, **32**, 796
21. Grotz, K., Klapdor, H.V., Metzinger, J.:1986, *Astron. Astrophys.*, **154**, L1
22. Yang, J., Turner, M.S., Steigman, G., Schramm, D.N., Olive, K.A., : 1984, *Astrophys. J.*, **281**, 493
23. Peimbert, M.: 1986, in *Star Forming Regions*, Symposium IAU No.115, M. Peimbert and J. Jugaku eds., Dordrecht, Reidel,
24. Steigman, G.: 1983, in *Primordial Helium*, ESO Workshop, eds. P. A. Shaver, D. Kunth, and K. Kjär, p.13
25. Olive, K.A., Schramm, D.N., Steigman, G., Turner, M.S., Yang, J.: 1981, *Astrophys. J.*, **246**, 557
26. Hanel, R., Conrath, B., Flasar, F.M., Kunde, V., Maguire, W., Pearl, J., Pirraglia, J., Samuelson, R., Cruikshank, D., Gautier, D., Gierasch, P., Horn, L., Schulte, P.: 1986, *Science*, in press
27. Gautier, D.: 1986, private communication
28. Kunth, D., Sargent, W.L.W.: 1983, *Astrophys. J.*, **273**, 81
29. Pagel, B.E.: 1985, paper given at the Royal Society Discussion Meeting on Material Content of the Universe
30. Peimbert, M., Pena, M., Torres-Peimbert, S.: 1985, *Astron.Astrophys.*, (submitted)
31. Maeder, A.: 1983, in *Primordial Helium*, ESO Workshop, eds. P.A. Shaver, D. Kunth, and K. Kjär, p.89
32. Delbourgo-Salvador, P., Gry, C., Malinie, G., Audouze, J.:1985, *Astron. Astrophys.*, **150**, 53
33. Vangioni-Flam, Audouze, J., Delbourgo-Salvador, P.: 1986, private communication
34. Parker, P.D.MacD.: 1986, in *Physics of the Sun*, ed. P.A. Sturrock, Vol.I, Reidel, Dordrecht, p.17
35. Bahcall, J.N.: 1978 , *Rev. Mod. Phys.*, Vol.50, No.4, p.881

MILLICHARGED MATTER IN THE GALACTIC HALO

Lawrence J. Hall
Lyman Laboratory of Physics
Harvard University
Cambridge, MA 02138
U.S.A.



Two models are proposed for strongly interacting particles which are the galactic halo dark matter. In one case these particles carry electric charge of order $10^{-3}e$, and in the other they are hydrogen-like bound states.

There is good evidence that many galaxies, including our own, possess halos which do not shine.[1] This galactic dark matter may have a mass which is a factor of ten larger than the luminous galactic mass.

In the standard particle physics model this matter would have to be baryonic; either in black holes or in various aggregations of atoms. It cannot be a cloud of free atoms since they interact strongly with each other, and the resulting dissipation allows the halo to collapse into a disk. There are arguments, although not iron-clad ones, against any baryonic interpretation.[2,3] The simple remedy of adding small (~10 eV) neutrino masses to the standard model does not work. While such neutrinos can contribute significantly to Ω, they do not clump on galactic scales[4] and hence cannot be the halos.

Of course much heavier ($\gtrsim$ GeV) neutrinos are a possible candidate. But these certainly are not much like the neutrinos we know, and hence are better classified with the list of exotic candidates: very heavy neutrinos, sneutrinos, axions...[4] These exotica do have a feature in common with ordinary neutrinos: their interaction cross-sections with each other and with matter are weak or smaller. In fact, to many physicists a dark matter candidate immediately means one that is weakly interacting. In this talk I will discuss shadow matter as a dark matter candidate. To many physicists, shadow matter is also synonymous for matter which interacts with us weakly. My model for the halo will depart from these conventional connotations; it will be a halo of strongly interacting shadow matter.

Halo dark matter particles could dissipate by scattering from ordinary matter, for example, from hydrogen with X-section σ_H. It is also possible that inelastic collisions between dark matter particles (σ_D) could dissipate their energy. Such dissipation will be small provided the mean free time for a dissipative collision is longer than the age of the galaxy. I find

$$\tau_{coll.} \simeq \frac{10^{10}\ \text{yrs.}}{\left(\frac{\sigma_D}{\frac{m}{3}\ 10^{-24}\ \text{cm}^2}\right) + \left(\frac{\sigma_H}{10^{-24}\ \text{cm}^2}\right)} \qquad (1)$$

where m is the mass of the dark matter particles in GeV. For m ~ 3 GeV, σ_D and $\sigma_H \lesssim 10^{-24}\ \text{cm}^2$ will lead to stable halo configurations. From this viewpoint the dark matter particles can be strongly interacting.

It has often been speculated that another world may occupy the space in which we live, and that this world may interact only weakly with us. Recent manifestations have these hidden[5] or shadow[6] worlds interact with us only via gravitational physics at the Planck scale. At energies accessible to us, the shadow world does not have any particles which have both ordinary and shadow gauge interactions (connector particles). In this case, any relic shadow particles which survive until today are expected to be extremely weakly interacting with us, and although they may lead to interesting cosmology and astrophysics[7,8], we will not be able to detect them directly.

In contrast to this, it has been shown recently that, even if there are no connector particles at low energies, shadow particles can interact

with us providing the shadow world has a massless photon which mixes with our photon[9,10]. This mixing arises whenever a connector particle exists, no matter how heavy it may be. Such a connector particle induces a one-loop photon wavefunction mixing term $\varepsilon F^{\mu\nu}F'_{\mu\nu}$. Redefining fields to get canonical kinetic energy terms then gives interactions $A(J+\varepsilon J') + A'(J'+\varepsilon J)$. Here A and A' are the photon and shadow photon fields, while J and J' are the ordinary and shadow electromagnetic currents. This is the symmetric basis: electrons emit $(A+\varepsilon A')$, shadow electrons emit $(A'+\varepsilon A)$. In situations where only ordinary matter is available it is convenient to go to an asymmetric basis with interactions: $AJ + (A'+2\varepsilon A)J'$. In this basis the shadow photon (A') does not interact with us. Thus, if shadow galaxies exist, they emit mainly shadow photons which pass straight through the earth undetected, however, they also emit our own photons with a strength $\propto \varepsilon^2$. We will always work in this asymmetric basis.

How large is ε? The one loop mixing diagram gives $\varepsilon \sim (ee'/16\pi^2)N$, where N is the degeneracy of the connector particle. Note that ε is independent of the connector mass M. If at scale M the U(1) and U(1)' are embedded in unbroken non-Abelian group factors, then this is no longer true: ε is suppressed by vv'/M^2 where v,v' are the symmetry breaking scales at which the U(1) factors appear. Thus ε can vary over a wide range. I will often consider the case of $\varepsilon \sim 10^{-3}$.

I consider two simple models for the low energy sector of the shadow world. One contains a single stable Dirac fermion of shadow charge e' (the shadow electron, e') while the other includes a second stable species of equal and opposite charge (the shadow proton, p'). These models turn out to have greatly differing properties: in the first, a cosmological asymmetry between e' and $\bar{e}'$ is impossible, so the halo contains equal numbers of e' and $\bar{e}'$. In the asymmetric basis the dark matter particles carry small ordinary electric charges. In the second model, a cosmological asymmetry between e' and $\bar{e}'$ is a necessity, the halo is composed of bound states e'p', shadow hydrogen. The rest of this talk is devoted to a brief sketch of the cosmology and astrophysics of these two models. For more details the reader should consult reference 11.

Consider the evolution of the shadow sector in the big bang in the case of just a single stable species: the shadow electron. At temperatures below the shadow electron mass, $m_{e'}$, the annihilation $e'\bar{e}' \to \gamma'\gamma'$ depletes the e' and $\bar{e}'$ densities until this process freezes out. As the temperature falls below $\alpha'^2 m_{e'}$ shadow positronium "recombination" takes

place. These will soon decay, leaving only the e' and $\bar{e}'$ which escaped recombination due to a relic ionization. For these e' and $\bar{e}'$ to be the dark matter in our halo, they must contribute about .1 to Ω. This fixes $m_{e'}$ to be about 1 TeV (for $\alpha' = 10^{-2}$, $\varepsilon = 10^{-3}$ which I shall use throughout).

As a digression it is interesting to consider the shadow background radiation. Compton scattering, $\gamma'e' \to \gamma'e'$, freezes out as soon as the e' have been depleted by annihilations. The γ' background radiation, in the asymmetric basis, actually contains a fraction $(1-\varepsilon^2)$ shadow photons which do not interact with ordinary matter and hence red-shift until today, and a fraction ε^2 ordinary photons. These are kept in thermal equilibrium by ordinary Compton scattering to a much lower temperature and hence become absorbed into our own 3°K background radiation. In a shadow world where $\gamma'e' \to \gamma'e'$ freezes out at such a low temperature that the ε^2 fraction of ordinary photons is also out of thermal contact with electrons and protons, there will be a second component to the ordinary photon background radiation. This component will have a spectrum which has a Planckian shape corresponding to some temperature T (not necessarily equal to 3°K) but an intensity which is ε^2 of the Planck intensity.

Is a halo made of equal numbers of e' and $\bar{e}'$ dissipationless and stable? At first sight, since the particles carry charges it seems unlikely. The annihilation cross section $\langle \sigma_A v \rangle$ for $e'\bar{e}' \to \gamma'\gamma'$ is $\pi\alpha'^2/m_{e'}^2$. This gives negligable depletion of the halo, and gives a flux of monochromatic TeV energy ordinary photons at the earth of $\sim 3.10^{-18}$ $cm^{-2}s^{-1}sr^{-1}$. This very high energy γ ray background is much too faint to have been observed. For example, Cygnus X-3 when viewed through a $1° \times 1°$ window has a corresponding flux of TeV photons of about 3.10^{-7} $cm^{-2}s^{-1}sr^{-1}$. The most dangerous dissipative process is radiative shadow Moller and Bhabha scattering: $e'e' \to e'e'\gamma'$ and $e'\bar{e}' \to e'\bar{e}'\gamma'$. The process $e'H \to e'H$ is down by $O(\varepsilon^2)$ compared with these and can be ignored. Even the non-radiative, elastic processes have energy transport cross-sections of about $10^{-25}cm^2$. Hence the radiative processes will certainly give $\sigma_D << 3.10^{-22}$ cm^2, so that from (1) we find that negligable dissipation occurs.

Finally, one might worry that, since all the e' and $\bar{e}'$ which are incident on the earth are captured by it, $e'\bar{e}' \to \gamma'\gamma'$ inside the earth would give a terrestrial intrinsic heat source greater than the observed value of 10^{-8} $erg\,gm^{-1}s^{-1}$. The energy at which energy is being produced in these annihilations is actually about 10^{-5} $erg\,gm^{-1}s^{-1}$. However, a fraction $(1-\varepsilon^2)$ of this does not interact with the material of the earth,

only $\varepsilon^2 \sim 10^{-6}$ of it produces actual heating and this is only 1/10% of the heating due to radioactive decay.

The case of two stable shadow species, e' and p', is considerably more complicated. I will define e' to be the lightest of the two species. I will later argue that $m_{e'}$ must be less than 5 GeV in this model. If there were no cosmic asymmetries, the process $e'\bar{e}' \to \gamma'\gamma'$ would occur to such a high degree in the Big Bang that the number of H' = e'p' bound states which could later form would be severely limited. For H' to contribute significantly to Ω, p' would have to be very heavy. In this case, $p'\bar{p}' \to \gamma'\gamma'$ occurs insufficiently and $\Omega(p') >> 1$. To avoid this we require a cosmic asymmetry of e' over $\bar{e}'$ and p' over $\bar{p}'$, and $m_{p'} \lesssim 1$ TeV. (This applies for $\alpha' = 10^{-2}$, larger $m_{p'}$ are possible for larger α').

Having ensured that the desired quantity of shadow matter survive until today we must next ask about the degree of shadow recombination: $e'p' \to H'$. Using the Saha equation, I find a degree of relic ionization of $10^{-2}(m_{e'}/\text{GeV})(m_{p'}/\text{TeV})$. Thus for parameters which we will find to be of interest, most of e' and p' end up as H'.

How small can $m_{e'}$ be? A lower limit of about an MeV comes from requiring that sufficient ^{4}He was made during Big Bang nucleosynthesis. Much more stringent lower limits result from considering H' scattering. Recall that the shadow Bohr radius $r' \sim 1/\alpha' m_{e'}$, and X-sections for H' scattering become very large when $m_{e'}$ is small.

The halo is not rotating. In order that HH' scattering does not produce a viscous drag on the baryonic disk $\sigma_{HH'}$ must be limited. Using a Born approximation calculation, this limit translates into $m_{e'} > 200$ MeV. The requirement that H'H' scattering give a σ_D suchthat $\tau_{\text{coll.}} > 10^{10}$ yrs (equation (1)) gives: $m_{e'} > \sqrt{250\ \text{GeV}/m_{p'}}$ GeV. For $m_{p'}$, taking its maximum value of 1 TeV, $m_{e'} > \frac{1}{2}$ GeV.

I have given two very different examples of halos composed of shadow matter. In each case the shadow matter interacts quite strongly with itself and with ordinary matter. Each model has a consistent cosmology and a stable halo configuration. An important question remains: would we have observed this dark matter directly on earth? This could be done in two ways: by searching for heavy non-relativistic particles incident on the earth yielding 1-100 keV recoil energies to nuclei which they strike. Alternatively one could search for an accummulation of e' or H' in the earth.

These questions are addressed elsewhere[11]. Here I mention briefly

the constraints on H' implied by recent experiments deep underground[13] and at the surface of the earth[14] using a germanium detector. At a depth of 4000 m.w.e. a background count rate of order 100 events $Kg^{-1}d^{-1}$ was obtained for Ge recoil energies of ~20-150 keV. This places stringent lower bounds on $m_{e'}$. As $m_{p'}$ is increased, so more collisions are required to bring H' to rest so that $m_{e'}$ must be made smaller. However, as $m_{e'}$ is made smaller the counting rate in the detector on the earth's surface increases. Combining the experiments, one finds that $m_{p'} \simeq 1$ TeV and $m_{e'} \simeq 5$ GeV are essentially determined! If $m_{p'} > 1$ TeV, $\Omega_{p'} > 1$; if $m_{p'} < 1$ TeV the H' flux increases and so does the surface counting rate. If $m_{e'} < 5$ GeV the H' scattering cross section goes up giving too large a surface counting rate. If $m_{e'} > 5$ GeV the H' scattering cross-section goes down so that H' penetrate deep underground more easily giving too high a counting rate at 4000 mwe. A similar discussion applies to other values of ε and α', although with differing resulting $m_{e'}$ and $m_{p'}$.

The dark matter in our galactic halo may be quite strongly interacting. A shadow sector of the universe may become visible to us if it has an unbroken U(1) gauge group. Combining these ideas, I have constructed models of strongly interacting shadow halos, for which direct searches can be made underneath, at and above the surface of the earth.

I thank my collaborator Haim Goldberg. I would also like to thank S. Glashow, D. Schramm, G. Steigman, and D. Spergel for useful conversations at this workshop. I have also benefitted from discussions with A. de Rújula, A. Drukier, G. Field, G. Gelmini, R. Jaffe, L. Krauss, K. Lane, and W. Press. This research was supported in part by the National Science Foundation under Grant No. PHY-82-15249 and by a Sloan Foundation Fellowship.

REFERENCES

1) V. C. Rubin, Science 220, 1339 (1983).

2) J. R. Primack, Lectures given at the International School of Physics "Enrico Fermi", Varenna, Italy, July 1984, SLAC-PUB-3387.

3) D. J. Hegyi and K. A. Olive, Phys. Lett. 126B, 28 (1983).

4) F. R. Klinkhamer and D. Schramm, Talks in these proceedings.

5) For a review, see L. J. Hall, Proceedings of Winter School at Mahabaleshwar, India, Lecture notes in Physics 208, Ed. P. Roy and V.

Singh, Springer Verlag (1984).

6) D. J. Gross, J. A. Harvey, E. Martinec, and R. Rohm, Phys. Rev. Lett. 54, 502 (1985).

7) E. W. Kolb, D. Seckel, and M. S. Turner, Nature 314, 415 (1985).

8) L. M. Krauss, A. H. Guth, D. N. Spergel, G. B. Field, and W. H. Press, Yale University preprint, YTP-85-16 (1985).

9) R. Holdom, Phys. Lett. 166B, 196 (1985).

10) S. Glashow, Phys. Lett. 167B, 35 (1986).

11) H. Goldberg and L. J. Hall, Harvard University preprint (1986).

12) A. M. Boesgaard and G. Steigman, Ann. Rev. Astron. Astrophys. 23, 319 (1985).

13) S. P. Ahlen, F. T. Avignone, R. L. Brodzinski, A. K. Drukier, G. Gelmini, and D. N. Spergel, preprint (1986).

14) F. T. Avignone, private communication.

THE ELECTRON NEUTRINO MASS AND NEUTRINOLESS DOUBLE BETA DECAY[1]

Paul Langacker
Department of Physics, University of Pennsylvania
Philadelphia, Pennsylvania 19104-6396



ABSTRACT

The ITEP tritium beta decay experiment[2] suggests a nonzero ν_e mass in the 17-40 eV range, while neutrinoless double beta decay ($\beta\beta_{0\nu}$) experiments set upper limits from 2-10 eV if the ν_e is an unmixed Majorana particle. It is argued that these constraints imply that either: (a) the ν_e is a Dirac or approximately Dirac neutrino. (b) The ν_e is a mixture of Majorana mass eigenstates (which cancel in the $\beta\beta_{0\nu}$) amplitude), with a heavy component either around 40 MeV or around 2 GeV. Or (c) the ν_e is a mixture of Majorana mass eigenstates and there is new physics to allow a fast invisible decay or annihilation for the heavy component. As a by-product, cosmological limits are obtained for heavy neutrinos that are mainly $SU_2 \times U_1$ singlets.

INTRODUCTION

Majorana and Dirac Masses

The known neutrinos of the first family are the left-handed electron neutrino ν_{eL} and the right-handed 'antineutrino' ν^c_{eR}, which are associated with the e^-_L and e^+_R, respectively, in ordinary charged-current weak interactions. These are not independent degrees of freedom, but are related by

$$\nu_L = C\overline{\nu^c_R}^T \tag{1}$$

where $C = i\gamma^2\gamma^0$, so that $\nu_{eL} \leftrightarrow \gamma^0 \nu^c_{eR}$ under CP.

Mass terms always take left- and right-handed fields into each other. If one introduces a new field N_R and its CP conjugate N^c_L to the theory, then one can write a Dirac (lepton number conserving) mass term

$$-L_{Dirac} = m_D \bar{\nu}_L N_R + \text{h.c.}, \tag{2}$$

which connects N_R and ν_L. In this case ν_L, N_R, N^c_L, and ν^c_R form a four component Dirac particle. Usually, the N_R is an $SU_2 \times U_1$ singlet, with m_D generated by an ordinary Higgs doublet, and $L = L_e + L_\mu + L_\tau$ is conserved in the three family generalization. This possibility is most similar to the way in which masses are generated for the other fermions (e^-, u, d, etc.) in the standard model, but it is difficult to understand why $m_{\nu e}$ is so small in this case. Another possibility[3] is that N_R is a known doublet neutrino, such as $\nu^c_{\tau R}$. This is a variation on the Konopinski-Mahmoud model.[4] Then ν_{eL}, $\nu^c_{\tau R}$, $\nu_{\tau L}$, and ν^c_{eR} can be combined to form a Dirac neutrino with $L_e - L_\tau$ conserved.

In a Majorana mass term one avoids the need for a new fermion field by coupling the ν_L to its CP conjugate ν^c_R

$$\begin{aligned} -L_M &= 1/2\ m\ \bar{\nu}_L\ \nu^c_R + \text{h.c.} \\ &= 1/2\ m\ \bar{\nu}_L C\ \bar{\nu}_L{}^T + \text{h.c.} \end{aligned} \tag{3}$$

ν_L and ν^c_R can be combined to form a two component Majorana neutrino. L_M can be thought of as creating or annihilating two neutrinos, and violates lepton number by $\Delta L = \pm 2$. m can be generated by the vacuum expectation value (VEV) of a new Higgs triplet[5] or as a higher order effective operator. Majorana masses are popular amongst theorists because they are so different from quark and lepton masses, and there is therefore the possibility of explaining why $m_{\nu e}$ is so small (if it is non-zero).

There are many models for neutrino mass[6], all of which have good and bad features. The major classes of models are listed in Table 1, along with the most natural scales for $m_{\nu e}$. None lead to $m_{\nu e} \sim 20$ eV naturally, but one can usually obtain $m_{\nu e}$ in this range by fine tuning.

Model	m_{ν_e}	$\langle m_{\nu_e} \rangle$
Dirac	1-10 MeV	0
Pure Majorana[5] (Higgs triplets)	arbitrary, but hierarchy problem if too large or small.	m_{ν_e}
Heavy seesaw[7,8] (1 light, 1 superheavy Majorana)	10^{-9} - 10^{-4} eV	m_{ν_e}
		(0 in Dirac variant[6])
Light Seesaw[1] (2 Light Majorana)	1-10 MeV	$\ll m_{\nu_e}$
Charged Higgs[9,6]	$\ll$ 1 eV	$\ll m_{\nu_e}$

Table 1. Major classes of neutrino mass models, along with their most natural scales for m_{ν_e} and $\langle m_{\nu_e} \rangle$.

In the seesaw model[7] one introduces an $SU_2 \times U_1$ singlet neutrino N_L^c with a (large) Majorana mass M (which can be bare or generated by a Higgs singlet) so that one has the mass term

$$-L = 1/2 \quad (\bar{\nu}_L \; \bar{N}_L^c) \begin{pmatrix} 0 & m_D \\ m_D & M \end{pmatrix} \begin{pmatrix} \nu_R^c \\ N_R \end{pmatrix} + \text{h.c.} \qquad (4)$$

where m_D is an ordinary Dirac mass. Diagonalizing (4) yields two Majorana mass eigenstates neutrinos ν_1 and ν_2 with

$$\nu_e = \nu_1 \cos\theta + \nu_2 \sin\theta$$
$$\nu_N = -\nu_1 \sin\theta + \nu_2 \cos\theta \qquad (5)$$

The physical masses are $m_1 \sim m_D^2/M \ll m_D$ and $m_2 \sim M$, and

$$\tan^2\theta = m_1/m_2 \simeq m_D^2/M \qquad (6)$$

In the ordinary seesaw model M is >> 1 GeV, so that a very tiny m_1 is obtained naturally. M is typically a GUT scale[7], but the seesaw can be implemented in non-GUT models as well.[8] In the light seesaw model[1] both m_D and M are $\ll$ 1 GeV (eg. M ~ 1 MeV). Such a model is extremely ugly because there is no reason for either m_D or M to be so small, but the double beta decay problem points to it as the most likely alternative to a Dirac mass.

The pure Majorana and non-gauge seesaw models allow the option of spontaneous L violation. These versions imply the existence of Majorons, which are Goldstone bosons associated with the spontaneous L breaking.

The charged Higgs models[9] refer to models involving a new charged Higgs

boson with L violating couplings. Viable versions often lead to Dirac neutrinos (in the generalized sense described above).

The Double Beta Decay Problem

The ITEP tritium beta decay experiment[2] has reported evidence that m_{ν_e} is in the range 17-40 eV. This experiment has not been confirmed or definitively refuted by other experiments*, and it has been strongly criticized by Bergkvist.[14]

The results of other experiments are anxiously awaited. In this talk I will discuss the implications of the ITEP result if it is eventually confirmed.

Many laboratory and geochemical experiments[15] have searched for neutrinoless double beta decay ($\beta\beta_{0\nu}$), which could be driven by a Majorana neutrino mass. No evidence for $\beta\beta_{0\nu}$ has been observed, and although there are many theoretical uncertainties it is clear that $\langle m_{\nu_e} \rangle < (2\text{-}10)$ eV, where $\langle m_{\nu_e} \rangle$ is the effective $|\Delta L| = 2$ mass that enters the $\beta\beta_{0\nu}$ amplitude. One has

$$\langle m_{\nu_e} \rangle = \begin{cases} 0, & \text{Dirac neutrino} \\ m_{\nu_e}, & \text{unmixed Majorana neutrino} \\ \sum_i m_i \xi_i U_{ei}^2 F(m_i,A), & \text{mixture} \end{cases} \tag{7}$$

where the last expression is valid of the ν_e is a mixture[16]

$$\nu_e = \sum_i U_{ei} \nu_i \tag{8}$$

of Majorana mass eigenstates ν_i with masses m_i and relative CP parities $\xi_i = \pm 1$. Since ξ_i can be negative there is a possibility of cancellation between the various ν_i exchanges.** $F(m_1,A)$, defined as

$$F(m_i,A) = \frac{\langle e^{-m_i r}/r \rangle}{\langle 1/r \rangle} \tag{9}$$

is a nucleus dependent propagator correction[17]. It is ~ 1 for $m_i \ll 10$ MeV and $\ll 1$ for $m_i \gg 10$ MeV, and it allows the possibility[17] of A dependence for $\langle m_{\nu_e} \rangle$.

*At this conference Petersen[11] presented results from the Zurich experiment at SIN that are on the verge of contradicting the ITEP results. They find $m_{\nu_e} < 8.8$ eV (statistical errors only, 95%), and $m_{\nu_e} < 21.7$ eV when a conservative estimate of systematic effects is included. Preliminary results from LANL[12] and INS[13] are not yet at the necessary level of sensitivity.

**The negative contributions may be traced back to the fact that fermion masses are often negative before an appropriate γ_5 transformation is performed.

The double beta decay problem is the fact that $\langle m_{\nu_e} \rangle \ll m_{\nu_e}$ if one accepts the ITEP results. Clearly, one solution is that ν_e is a Dirac neutrino. Another is that the ν_e is a mixture of Majorana mass eigenstates which cancel in the $\beta\beta_{0\nu}$ amplitude. This cancellation is not so contrived as it first appears, at least for $m_i \ll 10$ MeV, because in that case $F(m_i,A) \simeq 1$ and $\langle m_{\nu_e} \rangle$ is just the m_{ee} element of the original neutrino mass matrix in the weak basis. This could be zero because of some symmetry. The natural values of $\langle m_{\nu_e} \rangle$ for various classes of models are shown in Table 1. It is seen that $\langle m_{\nu_e} \rangle \simeq 0$ automatically in the light seesaw. $\langle m_{\nu_e} \rangle$ is typically of order m_{ν_e} in the pure Majorana and ordinary seesaw cases, although one could have a cancellation between the light doublet neutrinos due to fine tuning or extra symmetries.

However, I will argue that the cancellation mechanism is most likely ruled out by a variety of laboratory and cosmological constraints on the heavier neutrinos in (8), (except for a few loopholes), so that the most plausible solution to the $\beta\beta_{0\nu}$ problem is that ν_e is a Dirac neutrino.

For definiteness, I will consider only two mass eigenstates, but there are no significant differences if there are more. Then

$$\begin{aligned} \nu_e &= \nu_1 \cos\theta + \nu_2 \sin\theta \\ \eta &= -\nu_1 \sin\theta + \nu_2 \cos\theta \end{aligned} \tag{10}$$

The orthogonal state η may be a new $SU_2 \times U_1$ singlet neutrino (which occurs in the light seesaw model), or an ordinary doublet, such as the ν_μ or ν_τ (this would occur in the ordinary seesaw or pure Majorana case). One has

$$\langle m_{\nu_e} \rangle = m_1 \cos^2\theta \pm m_2 \sin^2\theta \, F(m_2,A) \tag{11}$$

I will assume $m_1 \simeq$ (17-40) eV and $\langle m_{\nu_e} \rangle \equiv 0$ (no essential changes occur for $\langle m_{\nu_e} \rangle \lesssim$ (2-10) eV). Then one must take $\xi_1 \xi_2 = -1$ and

$$\tan^2\theta = \frac{m_1}{m_2 F(m_2,A)} , \tag{12}$$

so that the only unknown is m_2.

Laboratory Limits

The ITEP experiment presumably measures the dominant ν_e component, so we require $\tan^2\theta \leq 1$ and $m_2 \geq m_1$.

Small values of m_2 are excluded by reactor oscillation limits. In particular the Gösgen limits[18] $\Delta m^2 = |m_1^2 - m_2^2| < 0.016$ eV^2 for $\sin^2 2\theta \simeq 1$, and $\sin^2 2\theta < 0.16$ for $\Delta m^2 > 0.1$ eV^2, when combined with (12), allow two possibilities.[19] The first is that $m_2 \simeq m_1$ with $\theta \sim 45^\circ$. This case actually corresponds to a Dirac neutrino (or pseudo-Dirac if the degeneracy is not exact),

because the degenerate Majorana states $\nu_{1,2L} = (\nu_{eL} \pm \eta_L)/\sqrt{2}$ can be combined to form a Dirac ν with $L_{\nu_e} - L_\eta$ conserved. The second possibility is

$$m_2 > 620 \text{ eV } (m_1/27 \text{ eV}) \quad . \tag{13}$$

One can also obtain an upper limit on m_2 because $F(m_2,A) \to 0$ for $m_2 >> 10$ MeV. Hence, no cancellation is possible if m_2 is too large. More precisely, weak universality limits require $\tan^2\theta < 0.05$. The implications of this for m_2 depend on $F(m_2,A)$, which in turn depends sensitively on poorly known nuclear correlations.[17] Under reasonable assumptions, however, one requires[17]

$$m_2 < (500 \text{ MeV} - 3.5 \text{ GeV}) \tag{14}$$

There are a variety of laboratory searches for incoherent heavy admixtures in ν_e from π and K decay and searches for ν_2 decay in beam dumps, wide band beams, and e^+e^- experiments. The excluded regions of $\sin^2\theta$ vs m_2 are shown in Figure 1, along with the relation in (12) needed for a cancellation.

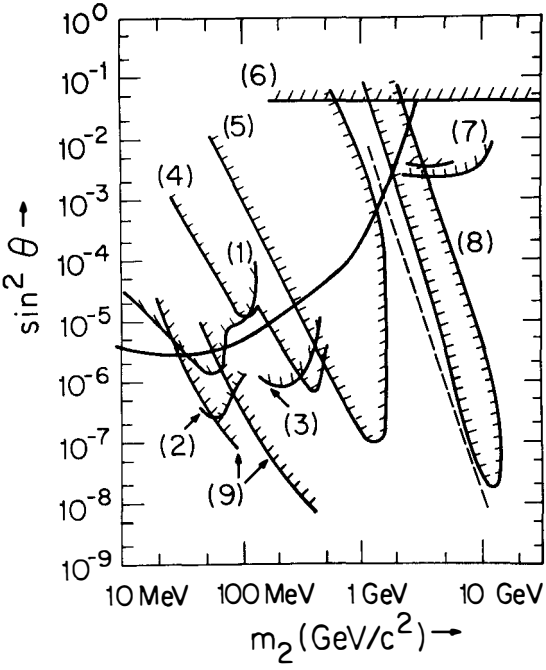


Figure 1. Laboratory constraints on the mass and mixing of a heavy neutrino, adapted from Gilman and Rhie.[20] The limits are from $\pi(1,2)$ and K(3) decay[20], the CHARM wide band beam (4) and beam dump (5) searches for ν_2 decay[20], universality (6), $e^+e^- \to \nu_2\nu_1$ (7, the upper and lower curves are for SU_2

singlets and doublets respectively), $e^+e^- \to \nu_2\nu_2$ (8, SU_2 doublets only), and the new PS-191[21] $\nu_2 \to \nu_1 e^+e^-$ search (9). Also shown is the relation between θ and m_2 needed for a cancellation in $\beta\beta_{0\nu}$ (heavy line).

Note that most of these limits depend very weakly (or not at all) on whether the ν_2 is mainly an $SU_2 \times U_1$ singlet or has normal weak interactions. In both cases the ν_2 production and decay is due to mixing effects. The decay rate for an $SU_1 \times U_1$ singlet is slightly modified because of an off-diagonal neutral current contribution, but the difference is small.

From Figure 1 it is clear that the laboratory limits exclude the range 40 MeV - 0 (10 GeV) for m_2 except for a possible gap from ~(1.7-2) GeV. The relation (12) between $\tan^2\theta$ and m_2 does not occur naturally in any known model for m_2 in this region, but nevertheless it is a possibility. Halprin, Petcov, and Rosen have emphasized[17] that $\langle m_{\nu_e} \rangle$ is A dependent for large m_2. The limits on $\langle m_{\nu_e} \rangle$ from ^{128}Te are now sufficiently stringent[22] (< 1.6 eV) that if $m_1 \sim$ (17-40) eV is cancelled by a ν_2 in the range 150 MeV-3.5 GeV then one expects $\langle m_{\nu_e} \rangle > 6.1$ eV for ^{76}Ge. This is on the verge of being contradicted by several experiments.[15] Given all of the uncertainties in the nuclear physics one cannot claim any discrepancy at present, but in this case $\beta\beta_{0\nu}$ should be observed in ^{76}Ge soon.

In summary, laboratory limits strongly suggest that 620 eV $< m_2 <$ 40 MeV, (with a possible additional window around 2 GeV), independent of whether the η is an SU_2 doublet or singlet.

Cosmological Limits

Let me briefly recall the cosmological limits on a massive neutrino with normal weak interactions (e.g., ν_e, ν_μ, ν_τ).

In the early Universe neutrinos were produced and kept in equilibrium by ordinary weak reactions such as $e^+e^- \leftrightarrow \nu\bar{\nu}$ and $e^-a \leftrightarrow \nu a'$, where a is any target particle. The rate for such reactions is

$$\Gamma_{weak} \sim \langle \sigma v \rangle n_a \sim G_F^2 T^5 \tag{15}$$

where $\langle \sigma v \rangle \sim G_F^2 T^2$ is the thermally averaged cross section (times velocity) and $n_a \sim T^3$ is the number density of target particles*. The neutrinos stayed in equilibrium as long as Γ_{weak} was large compared to the expansion rate of the Universe

$$H \sim T^2/m_p \tag{16}$$

---

*Both Γ_{weak} and H have additional factors involving the number of relativistic particles that are available at temperature T.

where $m_P \sim G_N^{-1/2} \sim 1.2 \times 10^{19}$ GeV is the Planck mass. Clearly $\Gamma_{weak} >> H$ at very early times (large T). However, once the Universe cooled and expanded to the decoupling temperature $T_D \sim (G_F^2 m_P)^{-1/3} \sim 3$ MeV, the neutrino interaction rate became negligible. The neutrinos decoupled and should still be present today, completely analogous to the microwave photons, but relics of a much earlier epoch ~ 1s after the big bang. Due to the expansion of the Universe their momentum has been redshifted so that it is now characterized by an effective temperature ~ 1.9^oK, corresponding to an average number density of $50/cm^3$ for each light ν spin degree of freedom.

Because of the very low neutrino energy, nobody has thought of any practical way to detect the relic neutrinos directly. However, there are so many of them compared to baryons that if they have masses in the 10 eV range they would dominate the energy density of the present Universe. Limits on the energy density require

$$\sum_i m_{\nu_i} < 100 \text{ eV} \quad , \tag{17}$$

where the sum runs of the light, stable (at least compared to the age of the Universe) doublet neutrinos. Conversely, if m_{ν_e} (or m_1) is in the 17-40 eV range the ν_e would dominate the present Universe and provide at least some of the dark matter.*

There are also a variety of constraints on unstable neutrinos[24], provided that they decay via ordinary weak interactions. The dominant modes for a mass eigenstate ν_2 are (assuming $m_2 > m_1$)

$$\begin{aligned} \nu_2 &\to \nu_1 \gamma \quad , \quad m_2 < 2m_e \\ \nu_2 &\to e^+ e^- \nu_1 \quad , \quad 2m_e < m_2 < m_\mu \end{aligned} \tag{18}$$

The first decay occurs at the one loop level and is very slow, while the second occurs at tree level. Both decays are very slow for small m_2 and the decay products are detectable. There are a variety of cosmological and astrophysical limits[24] on m_2 and τ_{ν_2} from the present energy density, the distortions of the background radiation, supernovae, and nucleosynthesis and breakup. For reasonable mixing angles they exclude the range

$$100 \text{ eV} < m_2 < (20\text{-}40) \text{ MeV} \tag{19}$$

for $SU_2 \times U_1$ doublet neutrinos that can decay according to (18). Combined with laboratory limits this implies[25] that the ν_μ and ν_τ (i.e. their dominant mass

*However, detailed estimates of the growth of density perturbations[23] indicate that while ν's in this mass range could easily account for cluster-sized objects, it is very hard to understand how such structures could have fragmented into galaxies in the time available.

eigenstate components) should be lighter than 100 eV.

It should be emphasized that all of these cosmological limits can be evaded if new physics is invoked to allow a fast decay or annihilation of the massive neutrinos into invisible decay products. The most plausible possibilities are $\nu_2 \to \nu_1 F$ or $\nu_2 \to \nu_1 M$, where F and M represent a familon[24] or Majoron[5,8,24] (Goldstone bosons associated with the spontaneous breaking of a family symmetry or lepton number respectively). Another possibility is the annihilation $\nu\nu \to MM$, which occurs at a significant rate for the pure Majorana Model only[5]. This is the only important model in which the present Universe does not have a large density of relic neutrinos.

Let us now return to limits on a heavy ν_2 described by (10) and (12). If the η in (10) is a normal $SU_2 \times U_1$ doublet neutrino such as the ν_μ, ν_τ, or a 4th generation neutrino (this would occur in the pure Majorana and seesaw models) then the ordinary cosmological limits apply and one requires $m_2 > 20$ MeV.

If the η is an $SU_2 \times U_1$ singlet, as in the light seesaw, then ν_2 can be produced in the early Universe by mixing, either by off-diagonal neutral currents such as $e^+e^- \to \nu_2\nu_1$ (which occurs due to the mixing between an SU singlet and doublet) or charged currents $e^-a \to \nu_2 a'$. The production rate is complicated because the mixing angle θ depends on m_1 and m_2 by (12). However, the masses may be generated by spontaneous symmetry breaking and are therefore temperature dependent - i.e. they can be affected by phase transitions in the early Universe. Moreover, for $T \gg m_1$, m_2 one actually produces the coherent mixture $\nu_e = \nu_1 \cos\theta + \nu_2 \sin\theta$ in weak processes. The effects of phase transitions, neutrino oscillations, and rescatterings (which destroy the phase relation between ν_1 and ν_2) have been analyzed in detail[1,26]. The upshot is that for the parameter range of interest the ν_2 are produced in number densities from 1/5 to 1 of those expected for normal doublet neutrinos. Once produced, however, their decay and annihilation rates are slower than for a normal doublet neutrino, so the cosmological limits are actually more stringent. The singlet ν_2 decays via mixing with the ν_1. For $m_2 < 2m_e$ one has $\nu_2 \to \nu_1\nu_1\bar{\nu}_1$ or $\bar{\nu}_1\nu_1\bar{\nu}_1$ via a virtual Z, while for $2m_e < m_2 < m_\mu$ one has the additional decay $\nu_2 \to e^+e^-\overset{(-)}{\nu}_1$ via both W and Z. The result is[1] that for $m_2 < 13$ keV the ν_2 lifetime is longer than the age of the Universe and the ν_2 contribute too much mass to the present Universe. For 13 keV $< m_2 <$ 1 MeV the ν_2 have decayed but there is too much energy density in the $\overset{(-)}{\nu}_1\nu_1\bar{\nu}_1$ decay products. For $m_2 <$ 12 MeV the relativistic decay products would have prevented the growth of galaxies and also distorted the microwave radiation. Finally, for $m_2 <$ (30-40) MeV the ν_2 contributed too much mass during nucleosynthesis and would have led to too

much ^4He, ^3He, and D.

Hence, cosmological arguments exclude doublet ν_2's from very small masses up to ~ 20 MeV and singlets up to ~ (30-40) MeV. All of these limits can be evaded if there is new physics for fast invisible ν_2 decay or annihilation.

Conclusions

The various constraints on m_2 are shown in Figure 2. Basically all values

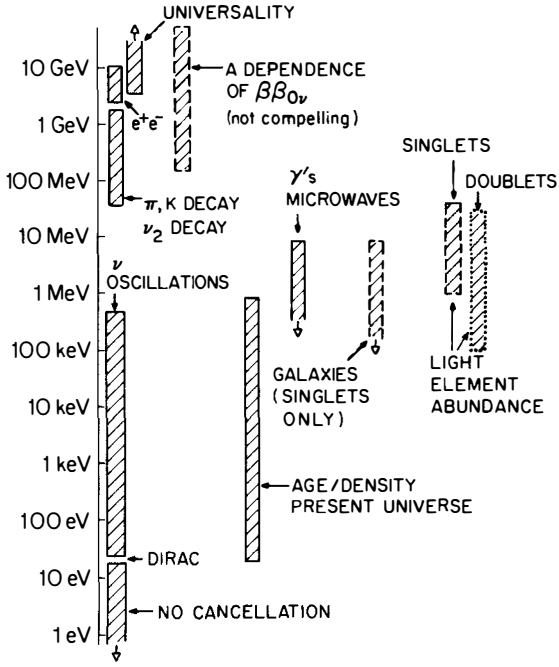


Figure 2. Values of m_2 excluded by laboratory and cosmological limits.

of m_2 are excluded except for $m_2 \sim m_1$, which corresponds to a Dirac neutrino, and for windows around 40 MeV and 2 GeV. It would be very useful to try to push down the laboratory limits to lower masses to close the lower window. The region around 2 GeV is rather unlikely, and can conceivably be excluded by future beam dump experiments. Also m_{ν_e} is strongly A dependent for m_2 ~ 2 GeV and $\beta\beta_{0\nu}$ in ^{76}Ge should show up soon if Nature chose this possibility.

The limits described above are for the standard model with ν_e a mixture of two mass eigenstates. The major change in $SU_{2L} \times SU_{2R} \times U_1$ models is that the ν_2 has additional decay diagrams involving W_R exchange or $W_L - W_R$ mixing.

Assuming $M_{W_R} > 1.7$ TeV from the $K_L - K_S$ mass differences[6] and reasonable W_L-W_R mixing angles, the ν_2 decay rate may be significantly enhanced for $m_2 > 10$ MeV. This weakens the cosmological constraints on m_2 so that the range (10-40) MeV may be allowed. On the other hand, the W_R also leads to new contributions to $\beta\beta_{0\nu}$, which may have enhanced matrix elements[27] and which cannot completely cancel the m_{ν_e} contribution. These new contributions could very well reduce or close the (10-40) MeV window, although there are significant theoretical uncertainties. A more detailed study would be very desirable.

Another possibility is that the ν_e is a combination of more than two mass eigenstates. We have not done an exhaustive study of all of parameter space, but it is unlikely that the constraints on m_2 for the two neutrino case would be significantly modified if there are N heavy neutrinos. This is because the laboratory limits on the heavy neutrinos would be weakened only slightly for reasonable values of N. On the other hand, the cosmological constraints would become tighter because of the existence of several heavy ν's, each of which would contribute to the mass density, etc.

References

1. P. Langacker, B. Sathiapalan, and G. Steigman, Pennsylvania preprint UPR-0285T.
2. V.A. Lubimov, these proceedings.
3. L. Wolfenstein, Nucl. Phys. B186, 147 (1981).
4. E. S. Konopinski and M. Mahmoud, Phys. Rev. 92, 1045 (1953).
5. G. B. Gelmini and M. Roncadelli, Phys. Lett. 99B, 411 (1981); H. Georgi et al., Nucl. Phys. B193, 297 (1983).
6. For a review see P. Langacker, 1985 Int. Symp. on Lepton and Photon Interactions, eds. S. Konuma and K. Takahashi (Nisha, Kyoto, 1985) p.186.
7. M. Gell-Mann et al., in Supergravity, eds. P. von Nieuwenhuizen and D. Z. Freedman (N. Holland, 1979) p. 315; T. Yanagida, Prog. Th. Phys. 64, 1103 (1980); E. Witten, Phys. Lett. 91B, 81 (1980).
8. Y. Chikashige et al., Phys. Lett. 98B, 265 (1981).
9. A. Zee, Phys. Lett. 93B, 389 (1980); Nucl. Phys. B264, 99 (1986).
10. There are variant models with Dirac eigenstates. See Ref. 6.
11. J. Petersen, these proceedings.
12. J. F. Wilkerson, these proceedings.
13. H. Kawakami, these proceedings.
14. K. Bergkvist, Phys. Lett. 154B, 224 (1985); 159B, 408 (1985).
15. See, for example, the summary talk by E. Fiorini, these proceedings.
16. L. Wolfenstein, Phys. Lett. 107B, 77 (1981); M. Doi et al., Phys. Lett. 102B, 323 (1981).
17. A. Halprin, S. T. Petcov, and S. P. Rosen, Phys. Lett. 125B, 335 (1983). See also C. N. Leung and S. T. Petcov, Phys. Lett. 145B, 416 (1984).
18. K. Gabathuler et al., Phys. Lett. 138B, 449 (1984).
19. The Le Bugey reactor group, J. F. Cavaignac et al., Phys. Lett. 148B, 387 (1984), has reported evidence for neutrino oscillations which would be marginally consistent with the Gösgen limits of $\Delta m^2 \sim 0.2$ eV^2, $\sin^2 2\theta \sim 0.25$. These parameters would yield $\langle m_{\nu_e} \rangle \sim 30$ eV.
20. See F. J. Gilman and S. H. Rhie, Phys. Rev. D32, 324 (1985).
21. PS-191: G. Bernardi et al., CERN/EP 85-177.

22. K. Grotz and H. V. Klapdor, Phys. Lett. 153B, 1 (1985). See also the talks by H. V. Klapdor and P. Vogel in these proceedings.
23. See, for example, the talks by G. Steigman and D. Schramm in these proceedings.
24. References may be found in ref. 1.
25. For recent discussions, see S. Sarker and A. M. Cooper, Phys. Lett. B148, 347 (1984); L. Krauss, Phys. Rev. Lett. 53, 1976 (1984); R. Cowsik, Phys. Lett. 151B, 52 (1985).
26. See also M. Yu Khlopov and S. T. Petcov, Phys. Lett. 99B, 117 (1981); 100B, 520(E) (1981).
27. E. Takasugi, these proceedings.

EXPERIMENTAL LIMITS ON COLD DARK MATTER

David N. Spergel
Department of Astronomy
Harvard University
Cambridge, MA 02138, USA

ABSTRACT

The use of an ultralow background germanium spectrometer as a detector of cold dark matter particles that interact with Ge nuclei is discussed. Bounds on dark matter candidates that couple to baryons through Z^0 exchange, like stable massive Dirac neutrinos[1] and scalar neutrinos[2], are presented. These results exclude a halo dominated by particles with scattering cross-section $\sigma_{s.i.} = \sigma_{weak}$ with masses 20 GeV $\leq m \leq$ 5 TeV and apply to s.i. reactions in the range of $\sigma^{s.i.} \simeq 10^{-1}\sigma_{weak}$ to $\sigma^{s.i.} \approx 10^{-28}$ cm^2 (for which the dark matter particles would be stopped in the earth's crust before arriving at our detector) where σ^{weak} is the scattering cross-section between Ge and a heavy standard neutrino that couples to baryons through weak interactions. These limits rule out the existence of technobaryons suggested by Nussinov as a dark matter candidate[3]. The presence in the detector of ^{73}Ge with s=9/2, allows us to obtain some bounds on particles with spin dependent (s.d) interactions, in which case our bounds apply to particles in the range of $\sigma \simeq 10^4\sigma^{s.d.}_{weak}$ to $\sigma \approx 10^{-28}$ cm^2.

If weakly interacting massive particles (WIMPs) comprise the halo of the galaxy, their elastic scatter off of nuclei may produce an observable signal. The measurement of the nuclear recoil due to the WIMPs requires a detector with a low energy threshold and excellent background rejection[4]. In a subsequent talk, I will explore the use of superconducting grains for dark matter detection. In this talk, I will discuss the use of a germanium diode detector to search for dark matter. This project involved collaborators from not only a range of institutions but also from a wide range of fields including radiochemistry, solid-state physics, particle physics, and astronomy. The collaboration consists of Steve Ahlen (BU), Frank Avignone (Univ. of So. Carolina), Ron Brodzinski (PNL), Andy Drukier (Harvard/Smithsonian), Gracielia Gelmini (Harvard) and myself. A more detailed description of this work will soon be submitted to Physics Review Letters.

Because of its low band gap (0.69 eV at 77^{o}K) and high efficiency for converting electronic energy loss to electron-hole (e-h) pairs (2.96 eV per electron-hole at 77^{o}K), germanium detectors are probably the best suited of all existing particle detectors for the detection of low velocity recoil nuclei. In addition, their low level of intrinsic noise (several keV of equivalent electron energy) makes them ideal for the search for rare phenomena, such as considered in this, as well as other exotica such as neutrinoless double beta decay.

In order to interpret the data, the fraction of recoil energy that is converted to electron-hole pairs must be estimated. At low recoil velocities, much of the nucleus' energy is dissipated through nuclear collisions rather than through electronic collisions. For example, a uranium nucleus with energy 6 MeV incident on a silicon diode produces a signal equivalent to a 2 MeV electron. This effect can be parameterized in terms of a relative efficiency factor (R.E.F.), the ratio of the number of electron-hole (e-h) pairs produced by an incident electron to the number of e-h pairs produced by an incident Ge nucleus with same kinetic energy. The optimum R.E.F. value of 1 is achieved only for $E \gg$ MeV.

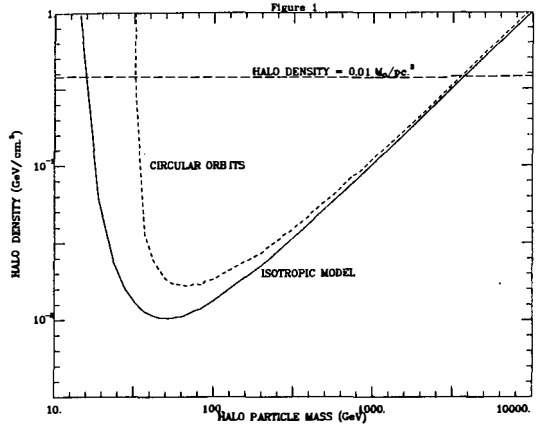
The R.E.F. for Ge detectors has been calculated by evaluating the fraction of the primary Ge recoil energy which is lost in electronic collisions. The electronic energy loss of secondary and higher order recoil nuclei has been accounted for in this calculation, and up to date electronic and nuclear stopping cross-sections[5] have been used. The calculated R.E.F. of ~ 4 for recoil energies of 15 keV is consistent with

experimental data[6].

The USC/PNL group has developed a 135 cm^3 intrinsic Ge detector[7,8] having a background reduced by about three orders of magnitude over conventional low background gamma-ray spectrometers. The detector was placed in the Homestake mine at a depth equivalent to 4000 meters of water in order to eliminate the cosmic ray induced background. The detector was also surrounded by super-pure copper and 11 tons of pure lead to eliminate the radioactive background from the rock. In late 1985, the energy threshold on the detector was reduced to an incident electron energy of 4 keV. This permits the detection of Ge nuclei-WIMP scatterings with recoil energies greater than 15 keV.

The observed count rate can be compared to the rate predicted if the halo was comprised of WIMPs. The particles that comprise the halo are assumed to have a velocity distribution function with an r.m.s. of 250 km/s and a maximum of 550 km/s, while the halo, like the galactic spheroid, slowly rotates with a velocity of 80 km/s[9]. This halo model used in the calculation is conservative. If the maximum halo velocity was closer to the local escape velocity of 750 km/s[10], the lower limit of the excluded mass range would drop to 15 GeV.

Since the predicted count rate depends upon the dark matter halo density, the observed count rate can be used to obtain limits on the density of interacting dark matter particles in the halo. Figure 1 shows these limits for particles with s.i. Z^0 exchange interactions for a standard isotropic halo model and for a model that assumes that all of the particles are on purely circular orbits. Both models include the Sun's motion relative to the galactic halo. Figure 1 can be used for other s.i. vectorial interactions by multiplying the vertical axis by the ratio $(\sigma^{s.i.}_{weak}/\sigma_{s.i.})$. For example, this ratio would be approximately 0.1 for neutral technibaryons.

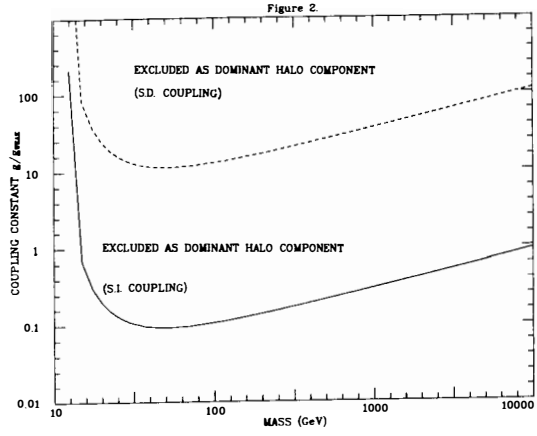


The detector background has a smooth contribution from the Compton-scatter of high energy emitters (e.g. ^{40}K) as well as the narrow line components. The low energy peaks are primarily due to the presence of ^{210}Bi in a solder connection used to make electrical contact with the diode and which "sees" the surface of the detector. The solder will be removed, and the radioactive shield will be upgraded by the use of 448 year old lead in the place of the super-pure copper which has some cosmogenic radioactive contamination. Thus, in spring 1986, the background should be reduced by another factor of ten. The energy threshold was set at 4 keV because of noise at lower energies. The shape of the low energy K absorption edge pairs suggests that E(FWHM) $\approx$ 500 eV. The strong increase of noise below E_{th} = 4 keV is largely due to microphonics engendered by mining operations. Hardware and software are being developed to reduce this noise and permit lowering the energythreshold to 1 keV. By the end of 1986, rejection/detection of the existence of the existence of coherently interacting particles of mass > 8 GeV should be possible.

It will be difficult to reduce the energy threshold below keV, thus the detection of particles of lower mass will require other detectors. The germanium detector is also not sensitive to particles like the photino that couple through s.d. weak interactions. Because of its low energy threshold and its sensitivity to photinos, the superheated superconducting colloid detector[7,8] seems like an attractive candidate for extending the limits derived here.

Our main results are shown in Figure 2, where the range of mass and cross-section of particles excluded as main components of the halo are presented. The ratio g/gw is defined as $(\sigma/\sigma_{weak})^{\frac{1}{2}}$ where σ_{weak} is the cross-section for standard heavy Dirac (s.i.) or Majorana (s.d) neutrinos. The validity of our experimental bound extends to cross-sections on the order of 10^{-28} cm^2.

Figure 2



Particles of larger cross-sections can not reach the detector; however, if they did exist, they would have been detected long ago in germanium and silicon detectors flown in X-ray balloon experiments or in germanium spectrometers on the surface of the Earth.

Acknowledgements

DNS is supported by NSF grant PHY-83-06693. I thank my collaborators for allowing me to describe our results before publication. A special thank you to Ron Brodzinski and Frank Avignone for providing the excellent data that is described in this talk.

References

[1]Bagger, J., Dimopoulus, S., Masso, E., and Reno, J., Phys.Rev.Lett. 54, (1985); Kolb, E. and Olive, K., FERMILAB preprint Pub-85/116-A(1985).

[2]Hagelin, J.S., Kane, G.L., and Raby, S., Nucl.Phys. B241, 648(1984); Ibanez, L.E., Phys.Lett. 137B, 160.

[3]Nussinov, S., Phys.Lett B 165B, 55(1985).

[4]Goodman, M.W. and Witten, E., Phys.Rev. D, 31 3059(1985).

[5]Wilson, W.D., Haggmark, L.G. and Biersack, J.P., Phys.Rev. B 15, 2458(1977).

[6]Chasman, C., Jones, K.W. and Ristinen, R.A., Phys.Rev.Lett. 15, 245(1965).

[7]Brodzinski, R.L., Brown, D.P., Evans, J.C., Jr., Hensley, W.K., Reeves, J.H., Woman, N.A., Avignone, F.T., and Miley, H.S., Nucl.Ins.Methods Phys.Res. A239, 207(1985).

[8]Reeves, J.H., Hensley, W.K. and Brodzinski, R.L., IEEE Transactions on Nuclear Science NS-32, 29(1985).

[9]Bahcall, J. and Casertano, S., "Kinematics and Density of the Galactic Spheroid" IAS preprint 11/85.

[10]Caldwell, J. and Ostriker, J.P., Ap.J. 251, 61(1981).

STATUS REPORT ON THE "GALLEX" SOLAR NEUTRINO PROJECT

Till Kirsten*
Max-Planck-Institut für Kernphysik
Heidelberg
P.O. Box 103 980
D-6900 Heidelberg, F.R.G.



ABSTRACT

The "Gallex"-experiment aims at the radiochemical detection of solar pp-neutrinos via the reaction $^{71}Ga(\nu_e,e^-)^{71}Ge$. The project is now in its implementation phase. A status report of the major aspects of the experiment is given. Acquisition of the full 30 tons of Gallium will last until 9/1989. This marks the beginning of the actual measurements in the Gran Sasso European Underground Laboratory.

---

* GALLEX-COLLABORATION: MPI Heidelberg: W. Hampel, G. Heusser, J. Kiko, T. Kirsten, A. Lenzing, E. Pernicka, B. Povh, S. Richter, K. Schneider, M. Schneller, H. Völk, R. Wink; KFK Karlsruhe; R.v. Ammon, K. Ebert, E. Henrich; TU München: R.L. Mössbauer; CEN Saclay: M. Cribier, M. Dupont (Grenoble), P. Pichard, J. Rich, M. Spiro, D. Vignaud; Nice University: G. Berthomieu, E. Schatzman; Milano University/INFN: E. Bellotti, O. Cremonesi, E. Fiorini, C. Liguori, S. Ragazzi, L. Zanotti; Roma University/INFN: S. d'Angelo, R. Bernabei, L. Paoluzi, R. Santonico; WIS Rehovot: I. Dostrovsky.

Introduction

The Gallex collaboration intends to measure for the first time the pp-neutrino flux from the sun by using a low threshold radiochemical detector based on the reaction $^{71}Ga(\nu_e,e^-)^{71}Ge$. The goals of this experiment are:

- the first experimental verification that nuclear fusion is the principal solar energy source,
- the search for neutrino flavor oscillations down to neutrino mass differences as small as $\Delta m_i^2 \approx 10^{-12}$ eV^2,
- to test the standard solar model[1] (SSM) in view of the solar neutrino problem (^8B neutrino deficit in the chlorine solar neutrino experiment of Davis[2]).

Non-standard solar models have the potential to drastically affect the fluxes of ^8B- and ^7Be-neutrinos. In fact, often they are tailored to reproduce the low neutrino capture rate of the chlorine detector. On the other hand, as long as the sun is presently producing its energy by nuclear fusion, the pp-neutrino flux is hardly altered at all by particularities of solar models but it is fixed by the solar luminosity. If the result of a pp-sensitive detector (Ga-detector) falls short of the SSM-expectation for the pp-neutrino production rate, this would be an unambiguous proof for neutrino flavor oscillations (or decay) and, consequently for non-zero restmass of at least one neutrino mass eigenstate.

Among the potential pp-sensitive neutrino experiments ($E_{threshold}$<420 keV), the radiochemical gallium experiment ($E_{threshold}$=233 keV[3]) is the only one which has been demonstrated to be technically feasible at present. Its feasibility was the major result of the BNL/MPI pilot experiment with 1.3 tons of Ga [4]. Due to funding problems, this collaboration dissolved in 1983. A new collaboration, GALLEX was formed in 1984 (see title page for its members). Major funding, e.g. for the required 30 t of Ga and for the underground laboratory installations, was assured in 1985. Now, the GALLEX project has undergone the crucial transition from hope to reality. Status and plans are described in the following.

Outline of the experiment

Natural Ga contains 39.6% ^{71}Ga and 60.4% ^{69}Ga. The latter is useless for pp-neutrino detection but it can play a role in monitoring interfering (p, n) reactions. The SSM prediction for the total capture rate is approx. 20 times higher for ^{71}Ga than for ^{37}Cl. As an immediate consequence, shielding requirements to reduce interfering (p, n) reactions are less severe for Ga than for the Cl-detector. Table 1 summarizes the expected production rates from the various neutrino sources (a) for the SSM and (b) for a model consistent with the low ^8B-neutrino flux as indicated by the results of the Cl-experiment ($2.0\pm.3$) SNU vs. 6.1 SNU SSM-prediction. Excited state contributions are based on GT strengths deduced from the Indiana (p,n) experiments[6]. The (almost) star model independent contri-

Neutrino source	Standard Solar Model g.s.	exc.s.	total	"Consistent" Model g.s.	exc.s.	total
pp	70.3	-	70.3± .6	71.5	-	71.5± .6
pep	2.5	.7	3.2± .2	2.5	.7	3.2± .2
^{7}Be	28.5	2.1	30.6±1.3	14.2	1.0	15.2± .7
^{8}B	1.2	11.5	12.7±2.0	.3	3.0	3.3± .5
^{13}N	2.5	.2	2.7± .1	.28	.02	.3± .01
^{15}O	3.4	.6	4.0± .2	.68	.12	.8± .04
Total	108.4	15.1	123.5±4.4	89.5	4.8	94.3±2.1

Table 1: ^{71}Ge production rates from ^{71}Ga for ground state and excited state contributions for the SSM and for a "Consistent" model[5]. Unit is 1 SNU=1 capture per 10^{36} target atoms per second.

butions of pp+pep neutrinos to the total production rate are 60% (SSM) and 78% (Consistent model) respectively.

The high costs of Ga force us to choose the smallest target size which is still sufficient to produce a ±10% result within ∿three years of measurements. Monte Carlo calculations based on achieved experimental capabilities lead to a required minimum quantity of 30 tons of natural Ga, corresponding to 1.1 neutrino captures per day for the SSM production rate.

The concept of the experiment is

(i) to expose the target in a chemical form suitable for Ge-extraction for about one half life of ^{71}Ge (11.43 d) in an environment which is sufficiently low of disturbing natural radiations,

(ii) to extract the Ge,

(iii) to detect the extracted ^{71}Ge via its EC decay (back to ^{71}Ga) in extremely background-free counting devices,

(iv) to accumulate sufficient statistics by repeated runs (2-4 years, ∿25 runs per year),

(v) to demonstrate the concerted performance of all experimental components and processes by means of a strong artificially produced low energy neutrino source inserted into the target tank.

Ga target and Ge extraction

Like the pilot experiment, the 30 t experiment will be performed with highly concentrated (∿8m) $GaCl_3$-solution. This chemical form is chosen to benefit from the clear cut kinetics of Ge-extraction from an aqueous solution. As soon as a Ge atom is formed within the $GaCl_3$ solution, it will transform into germanium chloride, $GeCl_4$. This compound is highly volatile and can be swept out from the solution by a circulating stream of air or helium. Due to the generous dimen-

sions and the ideal access logistics of the Gran Sasso Lab (see below), the total solution (∿55 m³) can now be contained in one single large tank (Fig. 1) in which it can be swept in situ. An identical second tank will be installed both, as a safety provision in case of a tank leak and to provide the option to perform Ge-extraction in a mode in which the liquid is physically transferred from tank 1, through the extraction column, into tank 2. At least for the latter mode, there will be no upscaling problems (relative to the pilot experiment). After sweeping, the $GeCl_4$ is taken out by gas scrubbers, extracted with CCl_4, and back extracted with water. Now that all the Ge is confined to a small volume, it is reduced to gaseous germane (GeH_4). After gaschromatographic purification, the germane is admixed to the counting gas of proportional counters described below. These procedures have been successfully tested in more than 30 test runs during the pilot experiment at BNL both, with and without inactive carrier added (.1-3 mg Ge). The main purpose of the carrier is to determine the extraction yield in every individual run.

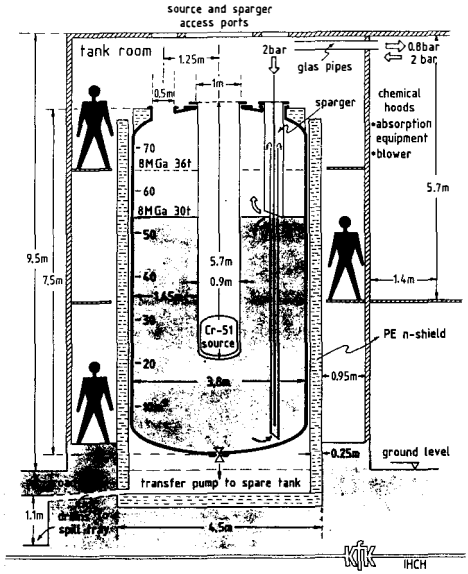


Fig. 1: Sketch of the GALLEX target tank. For acid resistance it is teflon-lined. The insert to accommodate the calibration source will be narrower as shown.

The overall recovery, including conversion into GeH_4, was ∿98%±2% after ∿15 hours of extraction time (pilot experiment). Meanwhile, apparatuses for $GeCl_4$-GeH_4 conversion, GC-purification, and counter filling stations have been set up at MPI. In gaschromatographic purification, the earlier problem of complete separation between GeH_4 and CO_2 has been solved (Fig. 2).

Underground laboratory and side reactions

The critical side reaction for the production of ^{71}Ge in $GaCl_3$ solution is $^{71}Ga(p,n)^{71}Ge$ ($E_{threshold}$=1.02 MeV). The protons may be generated as secondaries by (α,p),(n,p) and cosmic ray muon interactions. This necessitates shielding in an underground laboratory, a radiochemically clean target solution and provisions against fast neutrons from the surroundings (tank walls, rock walls).

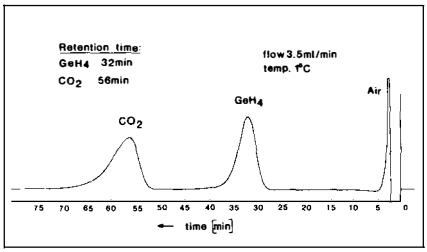


Fig. 2: GeH_4-CO_2 separation after optimalization of operating conditions in the GC-purification procedure.

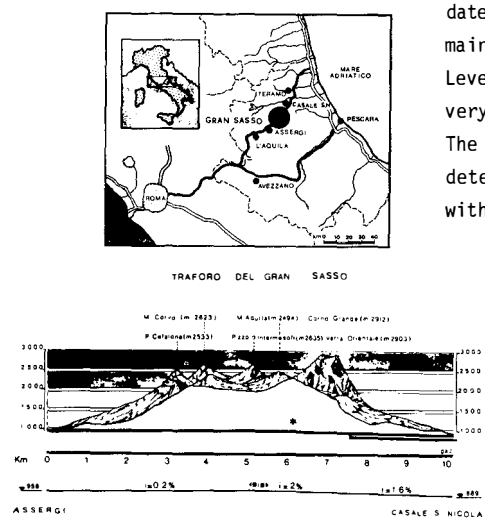


Fig. 3: Situation of the Gran Sasso European Underground Physics Laboratory, the site of the GALLEX experiment (star).

The GALLEX experiment has been approved for installation in hall A of the Gran Sasso European Underground Physics Laboratory. This impressive facility provided by INFN[7] consists of three enormous cavities (approx. 100x18x18 m³ each) which are readily excavated next to a highway under the Gran Sasso massif in the Abruzzese mountains near L'Aquila (Fig. 3). Presently, utilities are being installed, inauguration of the facility is scheduled for January, 1987. The GALLEX experiment will be accommodated in two large buildings: the GALLEX main building (12x10x10 m³) and the Low-Level counting lab (10x10x6 m³), with very convenient access from the highway. The muon flux measured with a hodoscope detector is $\sim 11\mu/m^2$,d in accordance with the estimated effective shielding depth of 3500 m.w.e. The depth dependence of ^{71}Ge production in $GaCl_3$-solution by cosmic ray muons has been derived from measurements and calculations on the same effect for the Cl-detector and from the measured cross section ratio (^{71}Ge from $GaCl_3$)/(^{37}Ar from C_2Cl_4) for 225 GeV muons[8]. Accordingly, the ^{71}Ge production rate in 30 tons of Ga at the GALLEX site is $\lesssim .01$ atoms/day or $\sim 1\%$ of the SSM ν_e induced production rate.

The U/Th concentrations in the dolomitic wall rocks of the cavities are favorably low, neutron activation analyses of various specimens gave results always well below 1 ppm. In a quick look experiment, the integral fast neutron flux in the cavity was found to be $<10^{-6}$ n/cm², s. With the projected 25 cm PE-shield surrounding the tank, this leads to ^{71}Ge production rates below 1% of the SSM ν-signal according to yield determinations with a Pu-Be n-source in the pilot

tank.

Concerning contaminants in the $GaCl_3$ solution itself, it was established in the course of the pilot experiment that the tolerable concentrations are $\leq$2 ppb Th, $\leq$30 ppb U and $\leq$.5 pCi ^{226}Ra/kg solution if each of them is to contribute $\leq$1% of the neutrino-induced SSM production rate. It has also been shown that multi-ton quantities of $GaCl_3$ solutions that meet these specifications can be industrially produced, corresponding specifications are part of the Ga-acquisition contract. For assurance, we routinely analyze relevant test solutions and chemicals for U, Th by neutron activation and for ^{226}Ra by measuring swept out ^{222}Rn using proportional counters.

Low-Level Ge counting

^{71}Ge decays by K (88%), L(10%), and M(2%) electron capture. It is best detected in proportional counters using 1-2 atm GeH_4-Xe mixtures as counting gas. The energy deposition from Auger electrons and X-rays leads to the L-peak at 1.2 keV and the K-peak at 10.4 keV. All provisions typical of low level counting have to be applied to achieve the extremely low background rates required: miniaturization (Fig. 4), use of ultrapure materials for counter construction, anticoincidence shield with NaI and plastic scintillation detectors (Fig. 5), heavy passive shielding with Pb and Fe. Still, the remaining background in the L- and K-peak windows is of the order of 1 cpd. It is mainly caused by (a) beta particles from natural radioactivities of the construction materials; (b) Compton electrons caused by external gamma rays; (c) electronic noise pulses. Fortunately, all these events produce in most cases pulse shapes distinct from those of ^{71}Ge decays (Fig. 6). Our computer-controlled counting system (Fig. 8) is therefore designed to record the whole shape of each PC-pulse by means of a fast transient digitizer. All counting data including the pulse shapes are finally stored on magnetic tapes. Up to 8 counters can be operated simultaneously in the well of the NaI pair spectrometer. Apart from its anticoincidence function, it serves, in the coincidence mode, to identify β^+ decays of $^{69}Ge(T_{1/2}=1.6\ d)$. In this way, one can monitor side reactions in the tank via $^{69}Ga(p,n)^{69}Ge$.

Figure 7 shows the rejection efficiency between ^{71}Ge decays and Compton background simulated by a ^{60}Co source. The pulse form parameter G*I has proved to be particularly discriminating. It is defined as

$$G*I = 100 \left[S(T)/S(t_{max}) \right] \cdot \left[\frac{1}{T} \int_0^T S(t)dt/S(t_{max}) \right]$$

where S(t) is the pulse height at time t after pulse onset, t_{max} is the time at which S(t) is maximal, and T is an empirically selected parameter, here T=160 ns. Overall efficiencies are 70% or better (2/5 L, 3/5 K). The background rates

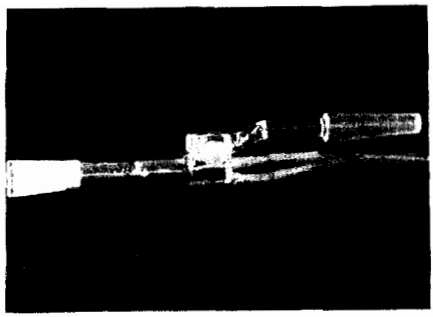


Fig. 4: Miniaturized proportional counter made from suprasile quartz and directly evaporated Al-cathode. The active volume (to the left) is .5cc only. The tungsten anode wire is directly sealed into the quartz ends. Right hand parts serve for gas filling. Wire connections to the preamp are low capacity (<1pF). The dead volume is $\lesssim$5%.

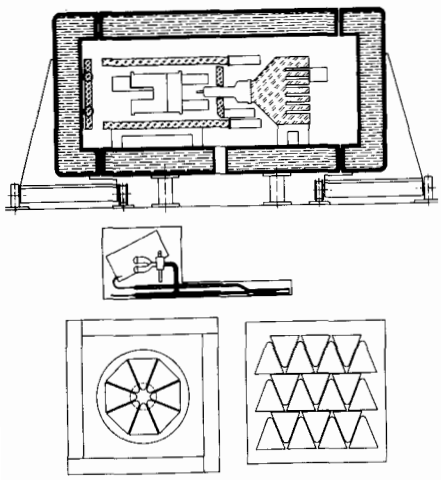


Fig. 5: Scheme of the low-level counting arrangement. A Pb-filled steel tank with movable side ends (top) houses a well type NaI crystal (interior left), a plastic scintillator shield (above and below) and a plastic scintillator block (right). The NaI-well accommodates up to 8 counters encapsulated, together with the preamp, in a Cu-box (middle and bottom left). The scintillator block can accommodate 21 additional counters for operation without NaI crystal (top and bottom right). Plastic scintillators operate in anticoincidence, NaI either in coincidence or anticoincidence. Multipliers are specially selected low potassium mps.

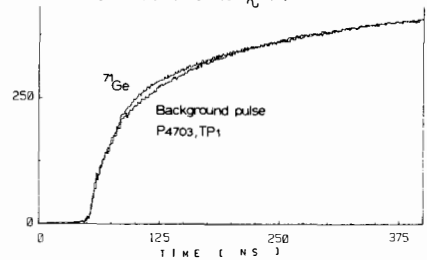


Fig. 6: A ^{71}Ge decay pulse and a background pulse indistinguishable by rise time only but distinguishable by the G*I criterium.

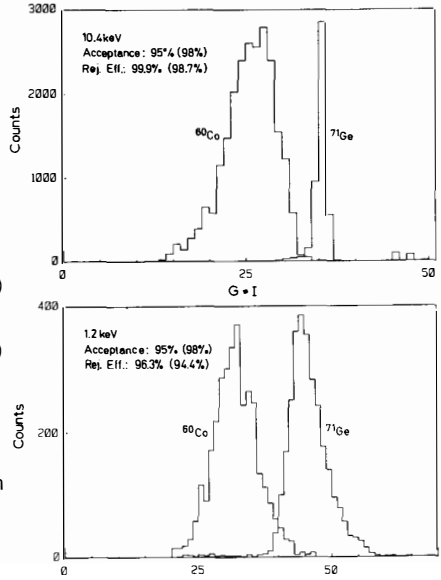


Fig. 7: Rejection efficiencies of Compton background as simulated by a ^{60}Co source in ^{71}Ge counting.

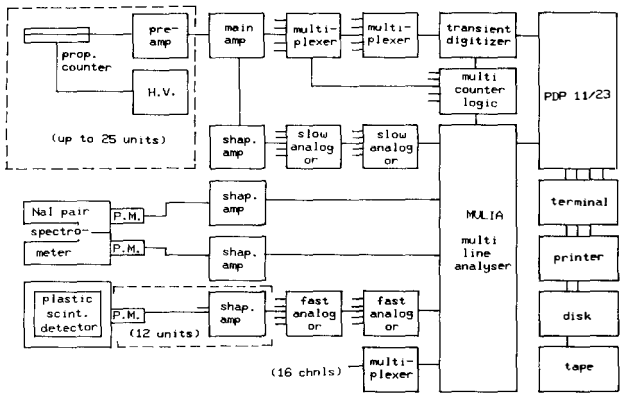


Fig. 8:
Block diagram of the measuring and data acquisition system.

achieved are 0.2 cpd (L-peak), 0.08 cpd (K-peak) for many counters and 0.08 cpd (L-peak), 0.04 cpd and better (K-peak) for a few particularly good counters. A further improvement may result once the low-level spectrometer set-up is transferred in the Gran Sasso underground laboratory. Presently, it is operated in the weakly shielded MPI Heidelberg Low-Level laboratory (∿15 m.w.e. only).

The presently achieved background rates allow to measure 94 SNU (consistent model) during 2 years of operation of the 30 t Ga detector to ±12%.

Calibration source

We consider it as indispensable to demonstrate the concerted performance of all experimental components by means of a strong artificially produced low energy neutrino source. The most favourable choice is the use of ^{51}Cr produced by neutron activation of ^{50}Cr (4.35% natural abundance). ^{51}Cr decays by electron capture ($T_{1/2}$=27.7 d) into ^{51}V. It emits monoenergetic neutrinos of 746 keV (90%) and 426 keV (10%). A source strength of 600-800 kCi is necessary in order to perform a sensible experiment. The feasibility of a 600 kCi source has been recently demonstrated in a test irradiation at the 35 MW Siloe reactor at Grenoble[9]. The test was performed with 12.4 kg Cr powder for 21 days at an undisturbed n-flux of $\sim 9 \times 10^{13}$ n/cm²s. Accurate calibration of the source strength via 320 keV gamma rays (10% of all decays) is facilitated by the use of Cr-powder since it can be homogenized through mixing after irradiation. Among other things, the test irradiation has demonstrated the solution of such practical problems as containments, cooling during irradiation, mixing, and other hot cell operations, definition of shielding and transport requirements. The necessary shielding is entirely determined by the activated impurities. The selected Cr used in the test irradiation was sufficiently pure, the highest remaining γ-activities came from ^{110m}Ag and

from ^{124}Sb. The actual source would consist of 120 kg natural Cr powder in a sealed container of dimensions r≈10 cm, h≈1 m; surrounded by a Pb or W-shield of 10 cm thickness. One source could be used during ∿60 days for 4-6 Ge-extractions. The first extraction would yield ∿3 times more ^{71}Ge produced by the source as by the sun (SSM). With one 600 kCi source, the obtainable accuracy would be ∿20%. The goal of a ±10% result could be achieved with altogether 4 sources.

Time schedule and required accuracy

The time schedule for the GALLEX project is shown in Figure 9. It is largely determined by the Ga-delivery schedule. Our contracts with the supplier define October 1989 as the date at which the full 30 t of Ga will be available to us. The experiment instal lations in the Gran Sasso lab should be completed in early 1988 when the first Ga will be delivered. Test runs of the full scale equipment will be performed in early 1989 using partial Ga quantities already delivered. The actual measurements will start in 1990. After two years of running (50 extractions) we would acquire a result with ±12% statistical error (consistent model) or ± 11% (SSM). However, we must consider the possibility of a signal far below 94 or 123.5 SNU if neutrino flavor oscillations occur (Fig. 10). For maximal mixing of three neutrino flavor oscillations the production rate would be as low as ∿40 SNU. With the MSW matter oscillation effect[10,11] (see Ref.[12] in these Proceedings), even lower production rates are possible. Clearly, an accurate measurement of such low rates would call for much longer measurement times. However, the principal question to be solved is the distinction between deviations from the SSM and neutrino oscillations as the cause of the solar neutrino problem. Provided that there is not a combination of both effects, the Ga experiment can distinguish these two possibilities if the absolute uncertainty is <15 SNU (see Fig. 10). To approach 2σ-significance, we are presently planning to measure for a period of 4 years (100 runs) plus one year for the ^{51}Cr source calibration runs.

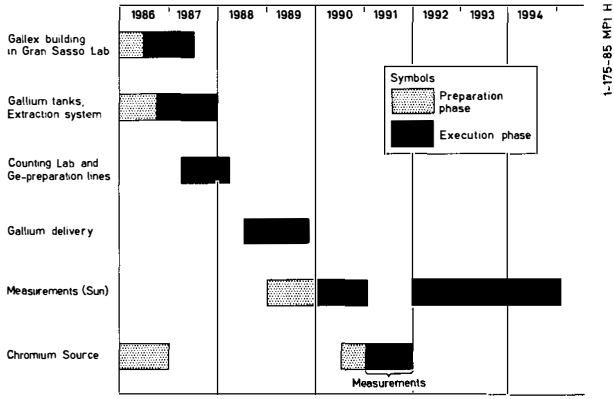


Fig. 9: Projected time schedule for the GALLEX project

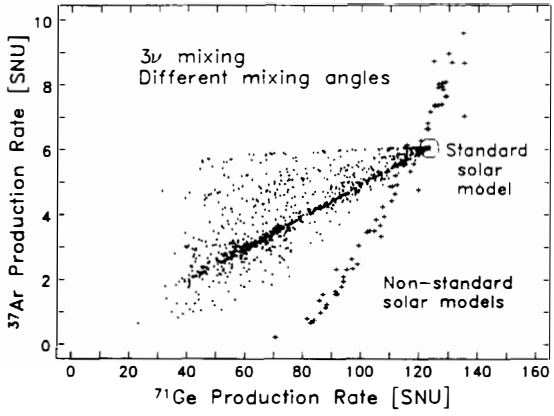


Fig. 10: (from[13]) Expected production rates for the Ga- and Cl-detectors. Crosses apply to all kinds of published non-standard solar models, dots result from Monte Carlo variations of the neutrino mixing parameters Δm_{ij}^2 and Θ_{ij} for vacuum oscillations. The measured ^{37}Ar production rate is 2.0+.3 SNU. Without neutrino mixing, ^{71}Ge production rates below 80 SNU are not possible. Not applicable for $\Delta m^2 \sim 10^{-5}$ eV² (see text).

A final remark concerns the MSW effect. Matter oscillations make the Ga experiment sensitive to neutrino oscillations even for small mixing angles in the range of $10^{-9} < \Delta m^2 < 10^{-5}$ eV². The prize paid for this is an ambiguity, however, in a very narrow mass range at $\sim 10^{-5}$ eV². Here it is possible that the Cl-result is due to neutrino oscillations, yet the Ga-experiment still yields a rate around ~90 SNU.

References

1 J. Bahcall, W. Huebner, S. Lubov, P. Parker, R. Ulrich, Rev.Mod.Phys.54,767 (1982).
2 J.K. Rowley, B.T. Cleveland, R. Davis, AIP Conf.Proc.126,1 (1985).
3 W. Hampel, R. Schlotz, Proc. AMCO-7 (Darmstadt), E. Klepper, ed., GSI Darmstadt 89 (1984).
4 W. Hampel, AIP Conf.Proc.126, 162 (1985).
5 W. Hampel, The cross section for capture of solar neutrinos in ^{71}Ga. MPI Heidelberg Report Feb. 1986, to be published.
6 D. Krofcheck, E. Sugarbaker, J. Rapaport, Phys.Rev.Lett.55, 105 (1985).
7 A. Zichichi, ICOMAN Proc.,Frascati 1983 (ed. E. Bellotti), p. 3.
8 J. Bahcall, B. Cleveland, R. Davis, I. Dostrovsky, J. Evans, W. Frati, G. Friedlander, K. Lande, J. Rowley, R. Stoenner, J. Weneser, Phys.Rev.Lett.40, 1351 (1978).
9 M. Cribier, B. Pichard, J. Rich, M. Spiro, D. Vignaud, A. Besson, A. Bevilacqua, F. Caperan, G. Dupont, J. Gorry, W. Hampel, T. Kirsten, Production of a high intensity 746 keV neutrino source for the calibration of solar neutrino detectors. Subm. to Nucl.Instr.Meth. (1986).
10 S. Mikheyev, A. Smirnov, Jadernaja Fizika 42, 1441 (1985).
11 J. Bouchez, M. Cribier, J. Rich, M. Spiro, D. Vignaud, W. Hampel, Matter effects for solar neutrino oscillations. Subm. to Z. Physik (1986).
12 M. Spiro, these Proceedings.
13 W. Hampel, The impact of neutrino oscillations on the Cl and Ga solar neutrino experiments. MPI Heidelberg Report, Jan. 1986.

Neutrino oscillations in matter and solar neutrino experiments

J.Bouchez , M.Cribier , J.Rich , M.Spiro , D.Vignaud
DPhPE , CEN Saclay

W.Hampel
MPI fur Kernphysik , Heidelberg

presented by M. Spiro

ABSTRACT

Solar neutrino oscillations are reviewed in the two-neutrino case taking into account the effect of coherent forward scattering when neutrinos travel through matter in the sun and earth. As recently pointed out by Mikheyev and Smirnov this effect induces a large suppression of the solar ν_e flux for values of Δm^2 around 10^{-4}-10^{-6} eV^2 even for small values of the mixing angle. The gallium experiment is largely sensitive to this effect. Matter effects also induce important modifications of the shape of the solar neutrino spectrum.

1. Introduction.

Using the formalism of Wolfenstein [1], Mikheyev and Smirnov [2] have shown that the ν_e flux from the sun may be highly suppressed due to coherent forward scattering. Here we give a brief discussion of the physics of this process and then apply the formalism to the solar neutrino case. We show results for the gallium [3] and chlorine [4] experiments. A more complete discussion will be published later [5].

2. The Physics.

We consider the two-neutrino oscillation case with a mixing angle θ (with $0 \leq \theta \leq \pi/4$). The flavour eigenstates ν_e and ν_μ are related to the mass eigenstates ν_1 and ν_2 by the relations :

$$\begin{aligned} |\nu_e\rangle &= \cos\theta\ |\nu_1\rangle + \sin\theta\ |\nu_2\rangle \\ |\nu_\mu\rangle &= -\sin\theta\ |\nu_1\rangle + \cos\theta\ |\nu_2\rangle \end{aligned} \qquad (1)$$

With our angle convention ν_e is "mostly" ν_1

If we consider a superposition $|\nu(t)\rangle$ of ν_e and ν_μ with a momentum p , its time evolution may be written :

$$|\nu(t)\rangle = \nu_e(t)\ |\nu_e\rangle + \nu_\mu(t)\ |\nu_\mu\rangle \qquad (2)$$

and it obeys the equation :

$$i \frac{d}{dt} \begin{pmatrix} \nu_e \\ \nu_\mu \end{pmatrix} = M \begin{pmatrix} \nu_e \\ \nu_\mu \end{pmatrix} \qquad (3$$

with the matrix M given by ($h/2\pi=c=1$)

$$M = \begin{pmatrix} (\Delta m^2/4p)\cos 2\theta & -(\Delta m^2/4p)\sin 2\theta \\ -(\Delta m^2/4p)\sin 2\theta & -(\Delta m^2/4p)\cos 2\theta \end{pmatrix} \qquad (4)$$

We have subtracted from M a multiple of the unit matrix in order to make M traceless. This has no effect on the physics.

Since M is a constant matrix the solution is easy to find and leads to the well-known oscillation pattern for a pure ν_e source. For a wave packet of average momentum p the probability to find a ν_e after a time t (or distance ~L/c) is :

$$P(\nu_e \to \nu_e) = |\langle \nu_e | \nu(t) \rangle|^2 = 1 - \sin^2 2\theta . \sin^2(\pi L / l_v) \qquad (5)$$

$l_v = 4\pi p\ /\ \Delta m^2$ being the vacuum oscillation length with $\Delta m^2 = m_1^2 - m_2^2$. Numerically we have the following relation :

$$l_v = 2.48 \text{ meters } (p/1\text{MeV}/c)\ /\ (\Delta m^2/1\text{eV}^2) \qquad (6)$$

When neutrinos propagate in matter of electron density N the difference in forward elastic scattering for ν_e and ν on electrons changes M to [1]

$$M = \begin{pmatrix} (\Delta m^2/4p)\cos 2\theta + GN/\sqrt{2} & -(\Delta m^2/4p)\sin 2\theta \\ -(\Delta m^2/4p)\sin 2\theta & -(\Delta m^2/4p)\cos 2\theta - GN/\sqrt{2} \end{pmatrix} \quad (7)$$

where G is the Fermi constant.

The matrix depends now on time if the electron density of the traversed matter is not constant and this prevents an analytical solution. Instantaneous eigenstates of propagation , ν_{1m} and ν_{2m} , can be obtained by diagonalizing this matrix. ν_{1m} and ν_{2m} are given as a function of θ_m (mixing angle in matter) which depends on the density :

$$\begin{aligned} |\nu_{1m}\rangle &= \cos\theta_m |\nu_e\rangle - \sin\theta_m |\nu_\mu\rangle \\ |\nu_{2m}\rangle &= \sin\theta_m |\nu_e\rangle + \cos\theta_m |\nu_\mu\rangle \end{aligned} \quad (8)$$

with

$$\tan 2\theta_m = \tan 2\theta . (1 - (l_v/l_o)\sec 2\theta) \quad (9)$$

where : $l_0 = 2\pi / (\sqrt{2}GN) = 1.624\ 10^7$ meters $(6.02\ 10^{23} cm^{-3}/N)$ (10)

This leads to an instantaneous oscillation length in matter given by :

$$l_m = l_v (1 - 2(l_v/l_o)\cos 2\theta + (l_v/l_o)^2)^{-1/2} \quad (11)$$

It is interesting to note the development of ν_{1m} and ν_{2m} as the density varies since , as we show below , in certain cases this determines the propagation of neutrinos in the sun. Two cases must be distinguished (we note here that , due to a sign error , Wolfenstein found the opposite results , as pointed out by Langacker [6]) :

i) $m_1 > m_2$

In that case ν_{1m} goes from ν_1 to ν_e when N(x) goes from zero to infinity , rotating by an angle $\theta < \pi/4$ in the (ν_e, ν_μ) plane.

ii) $m_1 < m_2$

This case is more interesting since ν_{1m} goes from ν_2 to ν_e when N(x) goes from zero to infinity. It thus rotates by an angle $\pi/2-\theta > \pi/4$. There is a value N_R of N(x) for which the diagonal elements of M vanish. This gives a maximal mixing ($\theta_m = \pi/4$) and an oscillation length given by :

$$l_R = l_v / \sin 2\theta$$

This means that in a medium of constant electronic density $N_R = (\sqrt{2}/G)(|\Delta m^2|/4p)\cos 2\theta$ a neutrino produced as a ν_e (or ν_μ) would propagate with maximal oscillation ($\sin^2 2\theta_m = 1$) between ν_e and ν_μ :

$$P(\nu_e \to \nu_e) = 1 - \sin^2 \pi L/l_R$$

This situation is what is called the resonant oscillation. As we shall see below this is not what happens in the sun.

Equation (3) is a Schrodinger equation for a two state system in which the Hamiltonian (M) depends on time (through the density N). As is well known from quantum mechanics if the Hamiltonian changes slowly enough with time, a system that is initially in an eigenstate of the Hamiltonian will remain in a (time dependent) eigenstate. For very high density ($GN/\sqrt{2} >> |\Delta m^2|/4p$) ν_e is an eigenstate corresponding to ν_{2m} if $m_2 > m_1$ or ν_{1m} if $m_1 > m_2$. From the preceeding discussion, if the density falls slowly to zero ν_e will become ν_1 if $m_1 > m_2$ or ν_2 if $m_2 > m_1$. The second case results in a large suppression of ν_e since $|\langle \nu_e | \nu_2 \rangle|^2 = \sin^2\theta < 0.5$.

To get this large suppression we need $m_2 > m_1$ and two other conditions (equations 12 and 13). First, the density at the point of production must be high enough (so that $\nu_e \sim \nu_{2m}$ at the production point):

$$(GN/\sqrt{2})\cos 2\theta > |\Delta m^2|/(4p) \qquad (12)$$

where N is the electron density at the point of origin of the neutrino. Taking N to be the central electron density of the sun (~88) equation (12) becomes

$$\cos 2\theta\, |\Delta m^2|/(1eV^2) < 1.3 \times 10^{-5} (E/1MeV) \qquad (12')$$

The second requirement that the Hamiltonian change "slowly" enough means that the ratio between $d\theta_m/dt$ and the eigenvalues of M be for all time much less than 1. This ratio is at a maximum near the resonant density. This gives the condition:

$$\frac{1}{N}\frac{dN}{dr} < \frac{|\Delta m^2|}{2p}\,\frac{\sin^2 2\theta}{\cos 2\theta} \qquad (13)$$

For the sun ($N^{-1}dN/dr$) is roughly constant ($\sim 1.3 \times 10^{-8}$ meter^{-1}) so we have

$$\frac{\sin^2 2\theta}{\cos 2\theta}\,\frac{|\Delta m^2|}{1eV^2} > 5\ 10^{-9}\,\frac{E}{1MeV} \qquad (13')$$

For a given neutrino energy (12') and (13') define a triangular region in the $\sin^2 2\theta$-Δm^2 plane (log scale). On the other hand, for a given Δm^2 and $\sin^2 2\theta$ (12') and (13') say that the solar neutrino flux will be suppressed for neutrino energies between E_{min} and E_{max}:

$$E_{min} = 7.5\ 10^4\ \text{MeV}\ \cos 2\theta\ |\Delta m^2|/1\text{eV}^2 \tag{14}$$

$$E_{max} = 2\ 10^8\ \text{MeV}\ \sin 2\theta \tan 2\theta\ |\Delta m^2|/1\text{eV}^2 \tag{15}$$

An experiment that could measure the pp [7] or ^{8}B [8] solar neutrino spectra could use (14) and (15) to determine Δm^2 and $\sin^2 2\theta$ if E_{min} or E_{max} fall within the measured part of the spectrum.

Passage of the solar neutrinos through the earth may modify the above results. In the case of maximal ν_e suppression we receive pure ν_2's from the sun. If the propagation eigenstate in the earth makes a large angle ($\simeq\theta-\theta_m$) with ν_1 , ν_2 , we shall mix back this ν_2 beam into a mixture of ν_e and ν_μ if the earth thickness is not much smaller than the corresponding oscillation length. The effects of the earth are small compared with those of the sun.

3. Neutrino amplitude evolution.

The above considerations give a qualitative understanding of the physics. However, since (12') and (13') are not always respected we need a numerical solution to (3) in the sun and earth.

Equation (3) was integrated numerically by expanding the state vector (equation 2) in terms of the eigenvectors (equation 8). The eigenfunctions were then propagated through a small step in the direction of the the neutrino detector taking into account the first order correction due to the variation of the density over the step. This correction is calculated with standard time dependent perturbation theory. This procedure is continued step by step to the neutrino detector. The convergence of this method was verified by diminishing the step size. We note that the step size for each step is calculated so that the perturbative contribution to the amplitude is of order ten percent.

4. Results

The evolution of a 500 keV neutrino produced at the center of the sun is shown in figure 1. The curve gives P(x) where P is the probability that the neutrino is observed as an electron neutrino and x is the ratio between its radial position and the radius of the sun. The curve is calculated for $-\Delta m^2=10^{-7}eV^2$ and $\sin^2 2\theta=0.1$. P reaches 0.5 at the radius where the density equals the resonant density ($x\sim 0.45$). No large oscillations occur here because the neutrino moves adiabatically away from ν_e. The oscillations shown near the surface of the sun are low density (vacuum) oscillations appropriate for a pure ν_2 beam. Averaged over 1 vacuum oscillation period, the value of P at the surface of the sun is equal to $\sin^2\theta$.

Figure 2 shows P at the surface of the sun (averaged over one vacuum oscillation length) as a function of neutrino energy ($\Delta m^2=-10^{-7}eV^2, \sin^2 2\theta=0.1$). The two curves are for neutrinos produced at the center of the sun and for neutrinos produced according to the radial distribution predicted by the standard solar model [9]. Equations (14) and (15) give $E_{min}=7.5$ keV and $E_{max}=2$ MeV and the flux is seen to be suppressed between these limits for neutrinos produced at the center. For neutrinos produced according to the real radial distribution, the effective E_{min} is somewhat higher, as expected.

The remainder of this section presents predictions for the gallium and chlorine neutrino experiments. To calculate these rates we have used the solar spectrum of the standard solar model [9] and the neutrino capture cross sections of [10]. The results are given as the ratio , R, between the predicted capture rate and that predicted assuming no neutrino oscillations. The rates are given as a function of Δm^2 for various mixing angles. The effects of the earth are taken into account and averaged over the day and year. The detector is taken to be placed in the Gran Sasso Laboratory.

Figure 3 shows R for the gallium experiment in the case of $\Delta m^2<0$. Large suppression is observed in this case for a range of Δm^2 that depends on the mixing angles. This range can be determined qualitatively from equations (12') and (13') by taking a neutrino energy of 500 keV which is near the average detected neutrino energy for this experiment according to the standard solar model.

Figure 4 is the same as figure 3 except for the chlorine experiment. In this case a large suppression is observed in the Δm^2 range determined by equations (12') and (13') for $E\sim 5$ MeV.

Figure 5 is the same as figure 1 (with $\sin^2 2\theta=0.4$ however) and 3b except that $\Delta m^2>0$. The observed suppression is ,as expected, near that for vacuum oscillations only .

The information in figures 3 and 4 is summarized in figure 6. It shows the zone of large suppression ($R<0.7$) for the two experiments. As discussed above, the zone is a triangular region determined by the typical energy of the experiment. Also shown are the other published experimental results [12].

Figure 7 shows in more detail the predicted rates for the gallium experiment ($\Delta m^2<0$).

The chlorine experiment [4] has observed R=.65±.10 (2.1±0.3 SNU with the standard solar model giving 5.8 SNU). If one assumes that the observed rate for the chlorine experiment is due to matter oscillations, the chlorine experiment constrains Δm^2 and $\sin^2 2\theta$ to be in the band shown by figure 8. We show in this figure the predicted gallium rate for various points in the band. A result from a gallium experiment could further contrain the values of Δm^2 and $\sin^2 2\theta$. If the observed gallium rate is low (<70SNU) the experiment would show that their are indeed neutrino oscillations since no modification of the solar model could produce such a low rate.

As a conclusion we confirm and extend the results of Mikheyev and Smirnov [2] that a large suppression of the solar ν_e flux may be obtained for values of $m_2^2-m_1^2$ around 10^{-4}-10^{-8} ev^2 even for small mixing angles ($\sin^2 2\theta = 10^{-1}$ to 10^{-3}) . This makes even more interesting the result of the forthcoming gallium experiment since the matter effect makes the detector sensitive to neutrino oscillations in a bigger Δm^2-$\sin^2 2\theta$ region. If we assume the SSM correct , a combination of the gallium results with the chlorine results could allow an almost unambiguous determination of $\sin^2 2\theta$ and Δm^2. Even if we do not assume the validity of the SSM , the future indium [7] or heavy water [8] experiments could be able to determine the same parameters by looking at the shape of the observed solar neutrino spectrum.

We have benefited from fruitful discussions with G.Chardin , T.Kirsten and A.Messiah .

References

[1] L.Wolfenstein , Phys. Rev. D17 (1978) 2369
V.Barger , K.Whisnant and R.J.N.Phillips , Phys. Rev. D24 (1981) 538
V.Barger , K.Whisnant , S.Pakvasa and R.J.N.Phillips
Phys. Rev. D22 (1980) 2718

[2] S.P.Mikheyev and A.Yu Smirnov , talk given at the Int. Workshop on Weak interactions and Neutrinos , Savonlinna (Finland) , June 1985
"Resonant amplification of ν oscillations in matter and solar neutrino spectroscopy" , to be published in Nuovo Cimento (1986)

[3] T.Kirsten , in Proc. of the 1st Symposium on Underground Physics , Saint-Vincent (Aosta , Italy) , 25-28 April 1985
D.Vignaud , in Proc. of the 5th Moriond Astrophysics meeting , Les Arcs (France) , 17-23 March 1985 , edited by J.Audouze

[4] J.K.Rowley , B.T.Cleveland and R.Davis , in "Solar neutrinos and neutrino astronomy" , Homestake (1984) , AIP Conf. Proc. n^{o} 126 , p.1
J.N.Bahcall , B.T.Cleveland , R.Davis and J.K.Rowley
Astrophysical Journal Letters 292 (1985) L79

[5] J. Bouchez et al., to be published.

[6] P.Langacker , private communication (1986)
P.Langacker et al. , Phys. Rev. D27 (1983) 1228

[7] R.S.Raghavan , Phys. Rev. Lett. 37 (1976) 259
M.Cribier , in Proc. of the 11th Int. Conf. on Neutrino Physics and Astrophysics , Dortmund (1984) ,
edited by K.Kleinknecht and E.A.Paschos , p.524
A.K.Drukier and R.Nest , Nucl. Instr. and Meth. A239 (1985) 605

[8] H.C.Chen , Phys. Rev. Lett. 55 (1985) 1534

[9] J.N.Bahcall et al. , Rev. Mod. Phys. 54 (1982) 767

[10] W.Hampel , to be published
D.Krofcheck et al. , Phys. Rev. Lett. 55 (1985) 1051

[11] W.Hampel , "The gallium solar neutrino detector and neutrino oscillations" ,
in Proc. of the 11th Int. Conf. on Neutrino Physics and Astrophysics , Dortmund (1984) ,
edited by K.Kleinknecht and E.A.Paschos , p.530

[12] J.F.Cavaignac et al. , Phys. Lett. 148B (1984) 387 (Bugey)
K.Gabathuler et al. , Phys. Lett. 138B (1984) 449 (Gosgen)
V.Zacek et al. , Phys. Lett. 164B (1985) 193 (Gosgen)
F.Bergsma et al. , Phys. Lett. 142B (1984) 103 (CHARM)
N.J.Baker et al. , Phys. Rev. Lett. 47 (1981) 1576 (FNAL)
F.Dydak et al. , Phys. Lett. 134B (1984) 281 (CDHS)
F.Bobisut , talk given at "III Telemark Conf. on Neutrino Mass and Oscillations" , Telemark (Wisconsin) , Oct. 1984 (BEBC)
J.M.LoSecco et al. , Phys. Rev. Lett. 54 (1985) 2299 (IMB)
L.A.Ahrens et al. , Phys. Rev. D31 (1985) 2732 (BNL)

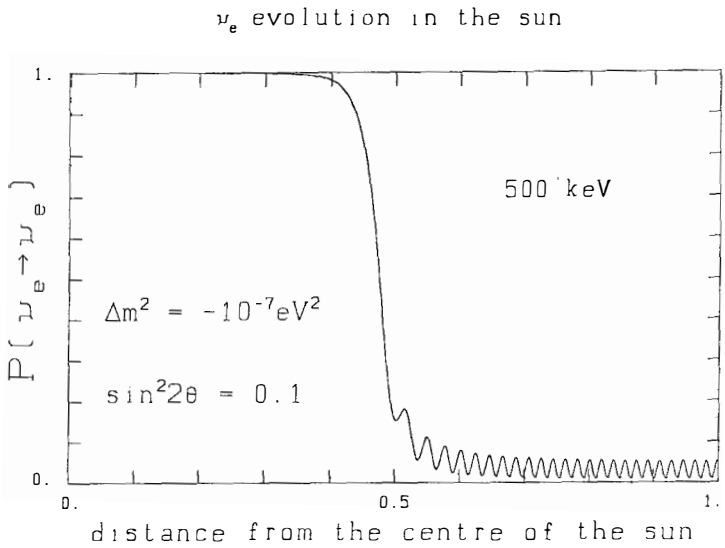


Figure 1 : The propagation of a 500 keV neutrino in the sun. The probability $P(\nu_e \rightarrow \nu_e)$ is plotted as a function of the distance to the centre of the sun where the neutrino is produced . The figure is obtained for $-\Delta m^2 = 10^{-7}$ eV² and $\sin^2 2\theta = 0.1$.

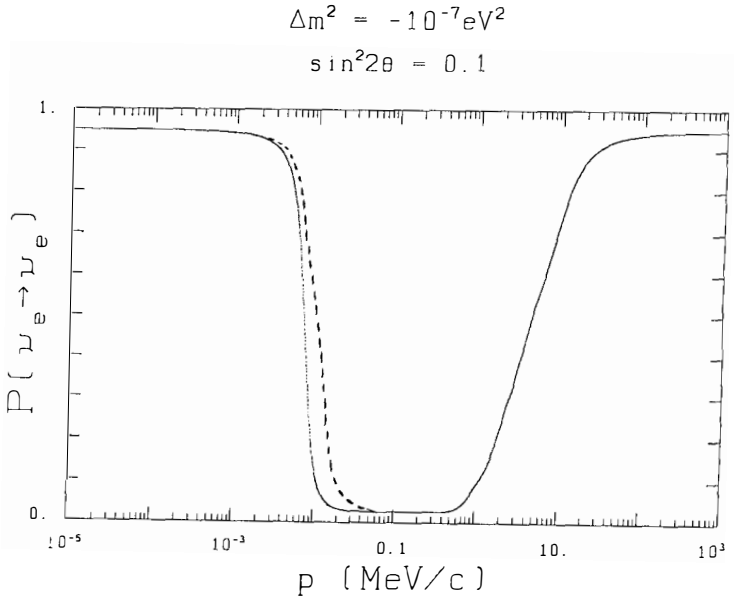


Figure 2 : Probability $P(\nu_e \rightarrow \nu_e)$ as a function of p/(1MeV/c) for $-\Delta m^2 = 10^{-7} eV^2$ and for $\sin^2 2\theta = 0.1$. The result is given for neutrinos at the periphery of the sun and averaged over one vacuum oscillation length. The solid curve is for neutrinos produced at the center of the sun and the dashed curve for neutrinos produced according to the radial distribution of the standard solar model [9].

^{71}Ga

ν_e in the gran sasso

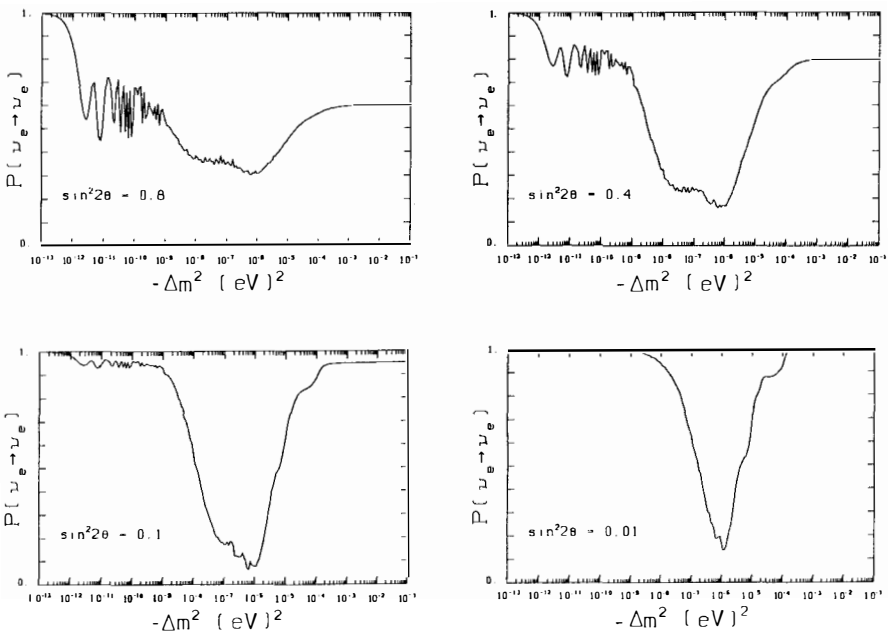


Figure 3 : The ν_e counting rate suppression factor, R, at the earth as a function of $-\Delta m^2$ for solar ν_e, taking into account matter effects in the sun and earth. The figure corresponds to the gallium experiment (neutrino threshold 233 keV) and is plotted for different $\sin^2 2\theta$ values .

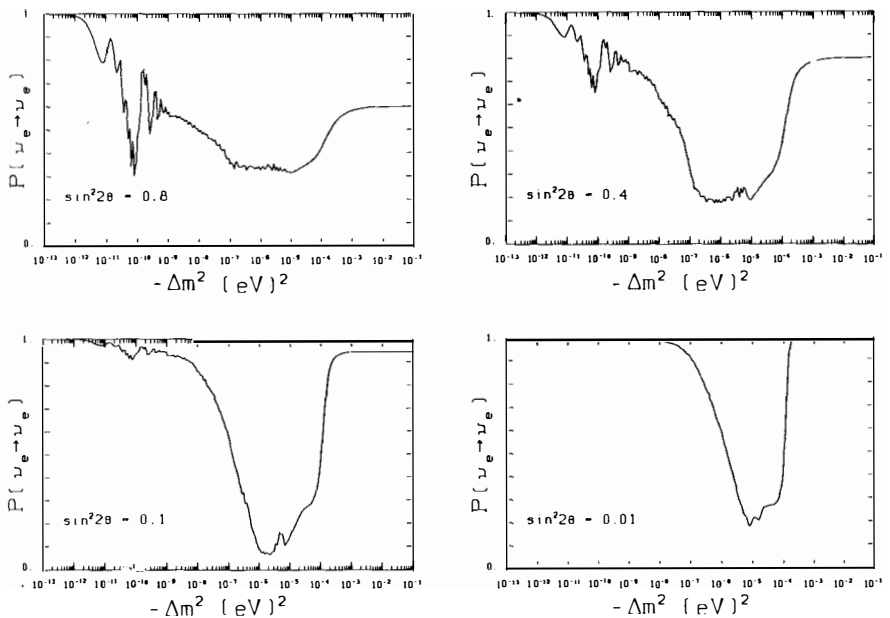
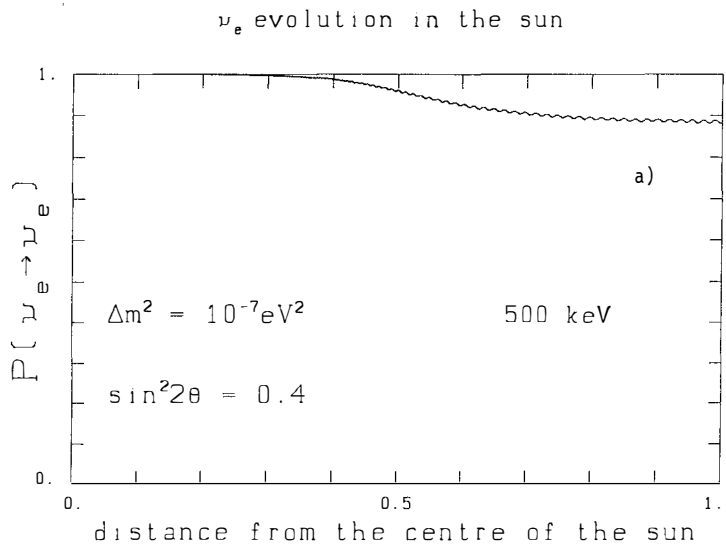


Figure 4 : The ν_e counting rate suppression factor, R, at the earth as a function of $-\Delta m^2$ for solar ν_e, taking into account matter effects in the sun and earth. The figure corresponds to the chlorine experiment (neutrino threshold 814 keV) and is plotted for different $\sin^2 2\theta$ values.



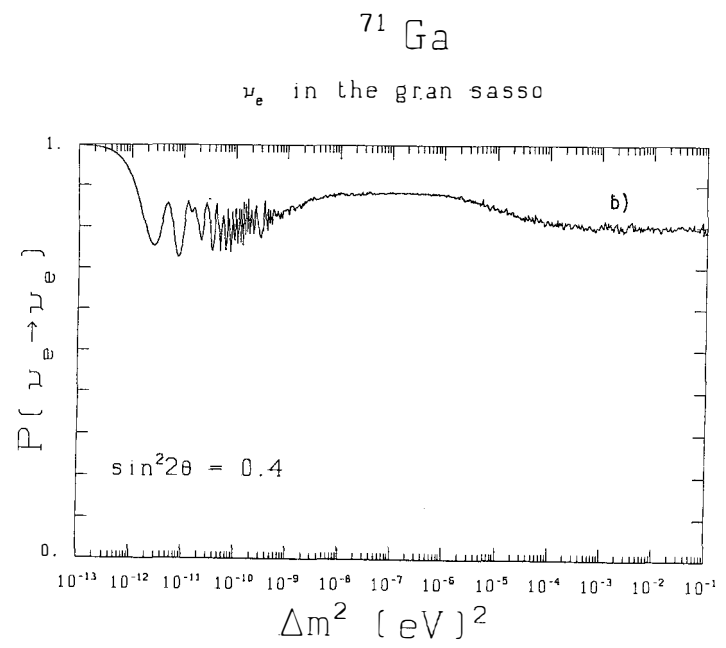


Figure 5 : ν_e evolution in matter if $m_1^2 > m_2^2$, i.e. if $\Delta m^2 > 0$. a) same as figure 1 for $\Delta m^2 = 10^{-7}$ eV^2 and $\sin^2 2\theta = 0.4$. b) same as figure 3b for the gallium experiment.

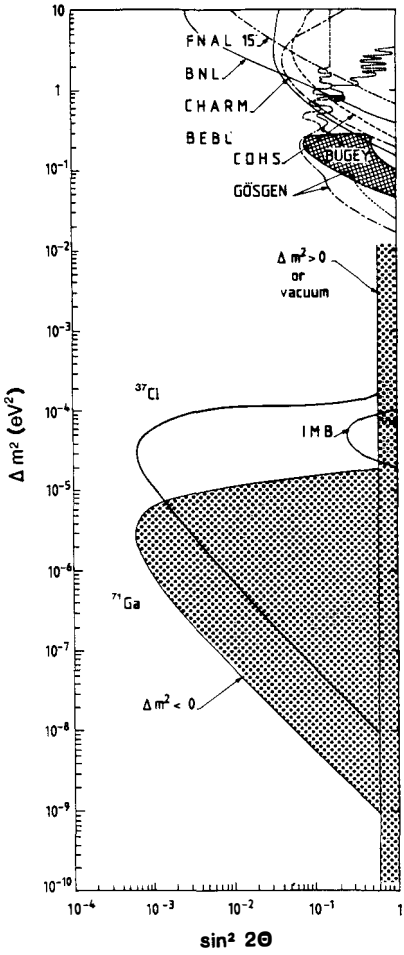


Figure 6 : Sensitivity plot of the solar neutrino experiments to neutrino oscillations . The y and x axis correspond respectively to $|\Delta m^2|$ and $\sin^2 2\theta$. The known results [12] are shown in the upper right corner where the zone excluded by the different experiments is on the right of the corresponding line , except for the Bugey reactor experiment where the hatched area represents the positive oscillation signal observed . Below $\Delta m^2 = 10^{-2}$ eV² the sensitivities of the chlorine and gallium experiments to solar neutrinos oscillations are shown . The dotted areas correspond to a ν_e flux suppression bigger than 30 % .

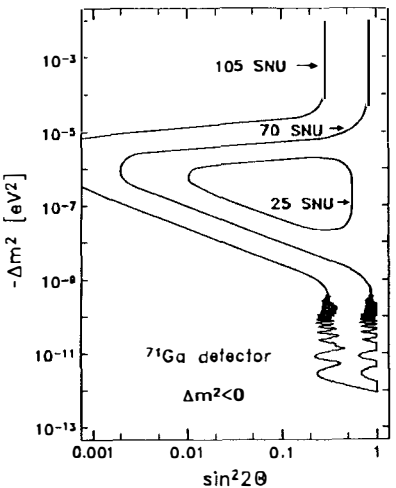


Figure 7 : Sensitivity plot of the gallium experiment to neutrino oscillations. It is similar to what is presented in figure 6 but covers all the Δm^2 range and shows more clearly the two cases with $\Delta m^2 > 0$ and < 0.

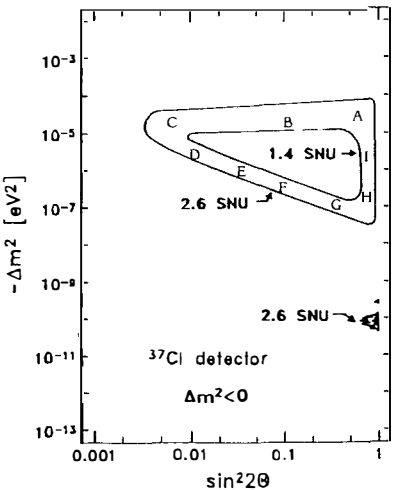


Figure 8 : The dotted band represents the chlorine experiment result [4] on the Δm^2 versus $\sin^2 2\theta$ plot. It assumes that the experimental result corresponds to 35±10 % of the solar neutrino flux. The different letters correspond to different possible results of the gallium experiment: (A=70SNU),(B=105),(C=110),(D=70),(E=25), (F=20),(G=25),(H=40),(I=60) (1 SNU=10^{-36} ν capture/atom/sec).

THE MOLYBDENUM SOLAR NEUTRINO EXPERIMENT

W.C. Haxton
Institute for Nuclear Theory, Department of Physics
University of Washington, Seattle, WA 98195
and
G.A. Cowan, K. Wolfsberg, N.C. Schroeder, D.J. Rokop, J.H. Cappis, and D.B. Curtis
Los Alamos National Laboratory, Los Alamos, New Mexico 87545

Abstract

The present status of the molybdenum solar neutrino experiment is described.

In 1982 a proposal was made to determine the ^{8}B solar neutrino flux, averaged over the past several million years, from the concentrations of ^{97}Tc and ^{98}Tc in a deeply buried molybdenite deposit.[1] Progress on the experiment has been rapid. At this conference I would like to describe both the motivation for and present status of these geochemical measurements.

Davis's ^{37}Cl experiment[2] has established that the flux of ^{8}B neutrinos is less than that predicted by the standard solar model[3] and the standard model of weak interactions. One of the key constraints on solar models is the need to burn hydrogen at a rate consistent with the sun's luminosity. However, as photons require approximately 10^{7} years to migrate from the core to the sun's surface, this constraint is strictly true only in steady-state models. This observation has stimulated a number of nonstandard models in which secular variations in the solar core are postulated to explain the solar neutrino puzzle.[4] Clearly, a test of the standard model assumption of hydrostatic equilibrium and steady-state hydrogen burning is then of fundamental importance. The molybdenum experiment can provide such a test: a measurement of the ^{8}B neutrinos, our most sensitive probe of the sun's central temperature, over a period comparable to the Kelvin time of the solar core.

Over geologic times the ^{8}B neutrinos will produce measurable concentrations of ^{98}Tc ($\tau_{1/2}$ = 4.2 Myr) and ^{97}Tc ($\tau_{1/2}$ = 2.6 Myr) in a deeply-buried molybdenum deposit. As large quantities of ore are needed, one must find a deposit that is worked commercially. In the U.S. only one active deep mine exists, the AMAX Corporation's Henderson Mine in Clear Creek County, Colorado. This deposit extends from 1100 m to 1500 m below the surface[5], and was considerably deeper at the time of formation ($\sim$ 25 million years ago[6]). The present points of minimum overburden are due to glacial scouring that occurred only 10,000 years ago. Throughout most of the ore body the technetium concentration due to cosmic ray backgrounds is estimated to be less than 10% of the standard model solar neutrino signal.

A kiloton sample of this ore will contain approximately five tons of MoS_2 and, assuming standard model fluxes, somewhat in excess of 10^7 atoms each of ^{97}Tc and ^{98}Tc. The task of chemically isolating[7] this trace quantity of technetium for mass spectrometry is greatly simplified by the commercial processing of the ore. Flotation separation at the Henderson mine produces a concentrate that is 90 to 99% molybdenite. The concentrate is shipped to the AMAX roasting plant at Ft. Madison, Iowa, for conversion to MoO_3. The two roasters at this plant have a capacity of 50 tons/day, and thus process concentrate for a typical experimental run (approximately 10 tons) in a fraction of a day. In the roasting process elements such as rhenium and technetium form volatile oxides that pass into the gas stream, largely composed of SO_2, SO_3, and air, with high efficiencies. The gas stream is treated to remove dust, then cooled, scrubbed, and converted to sulfuric

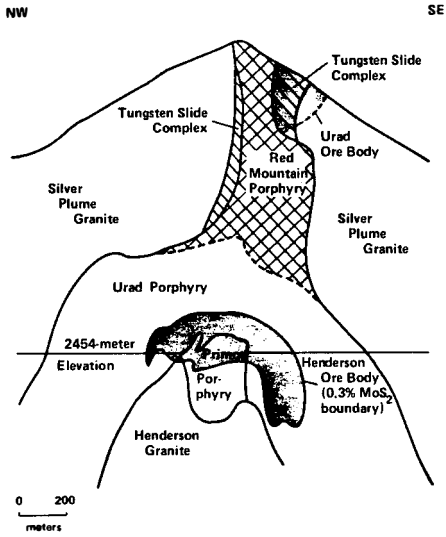


Fig. 1. Geologic section of Red Mountain showing the Henderson ore body (from Ref. 5).

acid. The scrubbing removes rhenium, an element chemically analogous to technetium, and unwanted fluorides, chlorides, and selenium before the gas stream enters the sulfuric acid plant. The initial experimental task is the quantitative recovery of technetium and rhenium from the scrub stream. Ion exchange columns for removing technetium from the scrub stream were first installed in the summer of 1985 and have been tested during runs of concentrate from the Climax mine (Colorado) and from Arizona mines. To improve the absorption of technetium, a pumping system was installed upstream to oxidize the scrub by the addition of NaOCl. These modifications of AMAX procedures cause only minimal disruptions in the commercial operation of the plant.

Pilot experiments monitored the rhenium recovery in these columns. Analysis of column effluents showed a rhenium concentration of 12 ppb, compared to 90 ppm in the scrub upstream of the columns, after four hours of operation. Thus the rhenium concentration in the acid scrub was reduced by a factor of 7500. Because technetium absorbs more strongly than rhenium, quantitative removal of technetium from the scrub stream is assured. These results indicate that four 12-inch columns operating at 7.5 gallons/min should remove ~ 90% of the technetium from the full scrub stream during a 12-hour run.

The experimentalists also established a mass balance for rhenium of 95% relative to the molybdenite feed. Because of uncertainties in flow rates, this value is uncertain to ± 10%. As hoped, it appears that the rhenium does report to the acid scrub stream and is not lost in a sink elsewhere in the plant.

A five-day run of Henderson concentrate is scheduled for February, 1986. Twenty-six ion exchange columns, six drums of NaOCl, and associated supplies have been delivered to the Ft. Madison plant in preparation for this run.

The recovery of technetium from the resin is done at Los Alamos. To remove the kilogram quantities of co-absorbed molybdenum, the resin is washed with a 2 M NaOH/0.5 M NaCl solution. The resin is then ashed in large Pyrex containers. The technetium loss from those procedures is less than 10%. The technetium in the ash is $\geq$ 95% soluble in 6 M HCl.

To separate technetium from 100 g quantities of rhenium, the technetium is precipitated out of HCl solutions containing 0.06 M $KReO_4$, 0.06 M Fe^{2+}, and 0.02 M Na_2SO_3. After the capped solution is permitted to undergo reduction for 90 minutes, 15 M NH_4OH is added to precipitate $Fe(OH)_2$ and TcO_2. The efficiency of the technetium removal depends on the acidity of the solution during reduction. Approximately 2% of the rhenium is carried with the precipitate; however, washing removes most of this contamination. Several precipitation cycles and washes should recover > 99% of the technetium. Work is continuing on the optimization of these procedures.

The final step is the mass spectrometry. When the experimentalists began their studies, state-of-the-art techniques would have required a technetium sample of 10^{12} atoms, rendering the experiment impractical. However, rather spectacular improvements have been made by the Los Alamos team. Currently TcO_4^- beams are being produced that are stable for long periods of time (0.5 to several hours) with no contamination from ubiquitous molybdenum, and with rates in excess of 10,000 cps for a 10^{10} atom technetium sample. These parameters permit one to measure $5 \cdot 10^7$ atoms to $\pm$ 0.5% and 10^6 atoms to $\pm$ 10%. The goal of the Los Alamos team has been quantitative mass spectrometry at the 10^7 - 10^8 atom level.

Thus the major technological hurdles appear to have been overcome. A number of questions, however, remain to be resolved before a claim for detecting solar neutrinos can be made:

1) The cross section for neutrino capture on ^{98}Mo has been determined from forward-angle (p, n) calibrations of the ^{98}Tc Gamow-Teller strength. The standard model cross section, due entirely to the capture of ^{8}B neutrinos, is 18 $\pm$ 5 SNU.[8] The 30% uncertainty in this number exceeds anticipated uncertainties arising from the chemistry and mass spectrometry. In principle, (p, n) calibrations of Gamow-Teller strength distributions can achieve an accuracy of 10 to 15%. An improved measurement is clearly needed.

The ^{97}Mo cross section is not known. The lowest Gamow-Teller transitions have thresholds of 536 keV and 644 keV, and can be excited by ^{7}Be, pep, and CNO-cycle

neutrinos. Of course, ^{8}B neutrinos excite many levels. To disentangle these contributions, high-resolution (p,n) measurements, or some direct calibration, will be necessary. With no present information on Gamow-Teller strengths, it is difficult to anticipate the extent of nuclear structure uncertainties for this isotope.

2) The most difficult aspect of geochemical experiments is the demonstration that natural backgrounds are tolerable. The high uranium content of Henderson ore (11 ppm) produces many neutrons and alpha particles. Although (n,γ) and $(n,2n)$ reactions induced by fission neutrons generally overwhelm solar neutrino signals, these reactions don't occur in the present case because of the absence of stable technetium. (This property also greatly simplifies the mass spectrometry.) Molybdenite occurs as exceptionally pure macroscopic crystals in which the metal-to-sulfur ratio is essentially 1:2. Therefore uranium was assumed to reside only outside these crystals in the original background calculations.[1] This assumption is consistent with subsequent measurements of the uranium content of the Henderson molybdenite concentrate.

The principal background reaction producing ^{98}Tc is believed to be $S(\alpha,p)$Cl followed by ^{98}Mo$(p,n)^{98}$Tc. For the standard model ^{8}B flux the predicted signal-to-background ratio is 40. This reaction also occurs for ^{97}Tc, but other backgrounds producing ^{97}Tc may prove more worrisome. Thermal neutron capture on ^{96}Ru followed by the electron capture transition ^{97}Ru$\dashrightarrow{}^{97}$Tc will produce a 10% background (assuming a 10 SNU solar neutrino capture rate) if the Ru content of the concentrate is 0.4 ppm. It remains unclear whether such efficient separation of ruthenium-bearing minerals occurs in the flotation process. The reaction ^{93}Nb$(\alpha,\gamma)^{97}$Tc may be troublesome if the Nb content of the concentrate exceeds 15 ppm. We are concerned that these backgrounds may make the ^{97}Tc results difficult to interpret.

Long-lived ^{99}Tc ($\tau_{1/2}$ = 0.21 Myr) is produced principally by spontaneous fission of ^{238}U residing in the ore. Thus the ^{99}Tc in the ore concentrate should track the radioactivity backgrounds discussed above. A demonstration that ^{97}Tc and ^{98}Tc are not correlated with ^{99}Tc could be viewed as evidence that uranium-induced backgrounds are not significant.

(Presumably the ^{99}Tc content of the concentrate will be determined by local variations in the uranium content of the ore body and by the efficiency of separation for uranium-bearing minerals in flotation.)

Cosmic ray backgrounds were discussed previously. It would be attractive to establish a correlation between cosmic ray production of ^{98}Tc and depth within the ore body. The Henderson ore may be too deep to make this feasible.

3) The geochemical stability of technetium in the reducing environment of the Henderson ore body must be carefully studied. (Technetium is quite mobile in oxidizing environments.) If technetium is lost on time scales of a million years, the experiment is not credible. A check on migration over $\sim 10^5$ years may be possible by demonstrating that ^{99}Tc is in secular equilibrium with the very small amounts of uranium that may exist in the molybdenite.

4) The roaster may retain a "memory" of previous ore. In particular, ore from shallow mines, with elevated levels of cosmic ray-induced technetium, could contaminate the Ft. Madison plant. Both the extent and duration of such contamination must be studied. The AMAX Corporation is willing to schedule ores from successively deeper molybdenite mines while the experimentalists monitor the technetium in the scrub stream.

In summary, the experimentalists are cautiously optimistic that the major technical roadblocks to this experiment have been removed. Before the end of this year the technetium content of Henderson ore may be known. Clearly, the interpretation of this measurement requires careful attention to questions of chemical mobility, dependence of the background on depth and on the geochemical environment, memory effects in the Ft. Madison plant, and nuclear physics uncertainties in the capture cross sections. As these questions can only be answered by careful experimentation, the program of technetium isolation may continue for some time.

I have not mentioned one very interesting sidelight, the suggestion by Cahn and Glashow[9] that chemical isolation of technetium might provide powerful constraints on the abundance of unknown heavy charged particles. Such a heavy "lepton" could bind to

Ru to form a stable nucleus that would exhibit the chemistry of technetium or rhenium while retaining the isotopic distribution of ruthenium. The principal commercial source of rhenium is molybdenum ore. (ReS_2 is often the primary impurity in molybdenite crystals.) Presumably, stable "technetium" would also concentrate in molybdenite. If 10^7 atoms could be detected in Henderson ore, relative abundances of stable "technetium" to Re of 10^{-17} would be measurable. This implies a sensitivity to an average abundance in the earth's crust of one part in 10^{26}. Of course, without some prior knowledge of the mass of the heavy lepton, the mass spectroscopy is significantly more complicated. Nevertheless one hopes that the availability of powerful techniques for performing the large scale chemistry will motivate clever solutions to the remaining analytical problems.

It is a pleasure to thank the AMAX Corporation for their continued support. This work was supported in part by the U.S. Department of Energy.

References

1) G.A. Cowan and W.C. Haxton, Science 216, 51 (1982) and in *Science Underground*, ed. M.M. Nieto *et al.*, AIP Conf. Proc. 96, p. 105 (New York, 1983).

2) J.K. Rowley, B.T. Cleveland, and R. Davis, Jr., in *Solar Neutrinos and Neutrino Astronomy*, ed. M.L. Cherry, K. Lande, and W.A. Fowler, AIP Conf. Proc. 126, p. 1 (New York, 1985).

3) J.N. Bahcall, W.F. Huebner, S.H. Lubow, P.D. Parker, and R.K. Ulrich, Rev. Mod. Phys. 54, 767 (1982).

4) E.J. Öpik, Contrib. Armagh Obs. No. 9 (1953); W.A. Fowler, Nature (London) 238, 24 (1972); F.W.W. Dilke and D.O. Gough, Nature (London) 240, 262 (1972); C. Dalsgaard, F.W.W. Dilke, and D.O. Gough, Mon. Not. R. Astro. Soc. 169, 429 (1974).

5) D.E. Ranta *et al.*, in *Studies in Field Geology*, ed. R.C. Epis and R.J. Weimer, p. 477 (Colorado School of Mines, 1976).

6) S.R. Wallace, W.B. MacKenzie, R.G. Blair, and N.K. Muncaster, Econ. Geol. 73, 325 (1978).

7) For a more complete description of the chemistry, see K. Wolfsberg *et al.*, in *Solar Neutrinos and Neutrino Astronomy*, ed. M.L. Cherry, K. Lande, and W.A. Fowler, AIP Conf. Proc. 126, p. 196 (New York, 1985).

8) J. Rapaport *et al.*, Phys. Rev. Lett. 54, 2325 (1985); W.C. Haxton, unpublished.

9) R.N. Cahn and S.L. Glashow, Science 213, 607 (1981).

SNO: The Sudbury Neutrino Observatory

SNO Collaboration*
presented by
J.J. Simpson
The Guelph-Waterloo Program for Graduate Work in Physics and
Department of Physics
University of Guelph
Guelph, Ontario N1G 2W1, Canada

Abstract

A proposal to build in Canada at a depth of 6200 m.w.e. a Cherenkov detector sensitive to ^{8}B solar neutrinos is briefly outlined.

Introduction

A proposal has been submitted[1] to the Natural Sciences and Engineering Research Council of Canada, and to funding agencies in the United States and the United Kingdom, to build a neutrino observatory based on a Cherenkov detector filled with heavy water[2], D_2O. The reactions which will be studied with this detector are $\nu + d \rightarrow p + p + e^-$, with a Q-value of -1.44 MeV, ν,e elastic scattering, and the neutral current reaction $\nu + d \rightarrow \nu + p + n$ with a threshold of 2.2 MeV. Because of Q-values and ultimate detector thresholds, only ^8B solar neutrinos are detected. The first two reactions are detected by the Cherenkov light produced by the electron. The advantage of heavy water is that the charged current reaction on the deuteron has a large cross-section so that the event rate with a 7 MeV threshold is about ten times larger than for ν_e scattering. In addition, since the electron gets most of the neutrino energy, the ^8B spectrum from above about 7 MeV may be fairly accurately determined. The neutral current reaction on the deuteron will be detected by the capture of the neutron by another deuteron releasing a 6.25 MeV γ-ray.

The many important reasons for trying to detect solar neutrinos are outlined in other talks at this workshop, as are other methods of detection now commencing or being planned, so they will not be reviewed here.

The Detector

It is proposed to build the detector in the Creighton nickel mine near Sudbury, in central Canada, at a depth of 6800 feet or 6200 metres water equivalent. This would be the second deepest site in the world. The cavern would have a diameter of about 20 m and a height of 25 m. The detector would consist of 1000 tons of heavy water in an acrylic tank suspended in the centre of a metal tank containing about 2300 tons

of light water. There would be 2400 photomultiplier tubes with 20" diameter near the wall of the metal tank, giving 40% coverage for light collection. The light water is necessary to diminish the radioactive background, primarily from the phototubes. The cavity would also be lined with low background concrete to diminish the flux of high energy γ-rays from the surrounding rock. Table 1 presents some of the

TABLE 1

PROPERTIES OF THE SUDBURY NEUTRINO OBSERVATORY
HEAVY/LIGHT WATER DETECTOR

	D_2O	H_2O
DEPTH underground:	6.2 kmwe	
COSMIC RAY rate:	100 /day	
overall CAVITY size:	20 m cylinder	
TOTAL D_2O mass:	1000 tonnes	-- none --
SENSITIVE mass:	3300 tonnes	3200 tonnes
FIDUCIAL mass:	1000 tonnes	910 tonnes
PHOTOELECTRONS per MeV:	8 p.e./MeV	
ENERGY resolution (7 MeV):	14%	
TIME resolution (per PMT):	7.7 ns	
SPATIAL resolution:	1 m	
ANGULAR resolution (7 MeV):	20^o	
ν_e,d directionality (20 evt):	42^o	
ν_e,d directionality (200 evt):	15^o	
ν_e,e directionality (1 evt):		35^o
water TEMPERATURE	10^o C	

properties of the proposed detector. Table 2 gives the reaction rates expected for the various reactions. The experimental threshold for ν,e and the charged current reaction is 7 MeV, and the calculations are

TABLE 2

REACTION RATES
(per kilo-ton D_2O per day)

Reaction	neutrino flux (cm^{-2} sec^{-1})	without expt threshold	with expt threshold
ν_e,e	2. x 10^6	3.5	0.7
ν_e,d (CC)	2. x 10^6	12.	8
ν,d (NC)	4.6 x 10^6	14.	3.5

based on full Monte Carlo simulations. The neutrino flux used is derived from the upper limit of the ^{36}Cl experiment[3]. The neutral current reaction rate is based on detecting the 6.25 MeV γ-ray from n + d capture. The flux used is that from the standard model of the sun[4]. The reason for the small efficiency is that for the latter reaction one-half the neutrinos escape the heavy water and one-half are captured in ordinary water in the heavy water at a concentration of 0.15%. Other techniques, such as doping the heavy water with trace amounts of a substance such as godolinium, could probably improve the neutral current efficiency.

The presently measured uranium and thorium content of the heavy water and acrylic, plus estimates of high energy photon flux from outside, would permit the charged current experiment to be carried out with the present design with a total background of only 2 events per day. The requirements of radio purity of the D_2O and acrylic for the neutral current experiment are much more stringent, because photons above 2.22 MeV can photodisintegrate the deuteron. In particular, the 2.615 MeV γ-ray in the thorium chain is especially problematic. At the moment, we have measured thorium concentrations in acrylic as low as 20 ppt, where 10 ppt would give about 1 background 6.25 MeV event per day. A sample of heavy water has been measured and found to contain

3.7×10^{-2} ppt of thorium where 1×10^{-2} ppt would give one neutral current background event per day. There is thus a reasonable expectation that the necessary reduction in thorium concentration can be achieved and that the neutral current reaction will be studied.

In view of the recent interest in neutrino matter oscillations occurring in the sun (ref. 5 and proceedings of this workshop) a particularly attractive feature of the charged current reaction on the deuteron is that the ^8B neutrino spectrum will be measurable above about 7 MeV (and perhaps lower). If this phenomenon causes the diminished flux of ^8B neutrinos observed in the ^{37}Cl experiment, then the ^8B spectrum shape will be strongly distorted. Depending on the neutrino masses and vacuum mixing angle, either the low energy part of the ^8B spectrum or the high energy part will be considerably diminished. With the high statistics available from the charged current reaction, the shape distortion should be observable.

Table 3 lists the ^8B flux sensitivity (3σ) in a six-month live time run. It is seen that, if no requirement for directionality is imposed on the charged current events, one will be sensitive to between 30 and 100 times lower flux than the upper limit of the ^{37}Cl experiment.

If funding should begin in April 1986, one anticipates that the acrylic tank could be filled first at the beginning of 1990 with light water to test the system (as well, obviously, as looking for ν,e events). After about six months of light water testing, filling with heavy water could commence.

TABLE 3

^8B FLUX SENSITIVITY OF THE SUDBURY NEUTRINO OBSERVATORY
HEAVY/LIGHT WATER DETECTOR
(with 6 mo. live-time)

	D_2O ($/cm^2$ /sec)	H_2O
with NO backgrounds		
ν_e,e (directionality)	1.5×10^5	1.5×10^5
ν_e,d (CC directionality)	4×10^5	------
ν_e,d (CC no directionality)	2.5×10^4	------
ν,d (NC)	6×10^4	------
with ALL backgrounds		
ν_e,e (directionality)	3×10^5	3×10^5
ν_e,d (CC directionality)	4.5×10^5	------
ν_e,d (CC no directionality)	7×10^4	------
ν,d (NC)	4×10^5	------

Conclusions

The proposal for a heavy water Cherenkov detector sensitive to ^8B solar neutrinos has been briefly outlined. The chief distinguishing features of this proposal are its high sensitivity to ^8B neutrinos by the charged current reaction on deuterium, its consequent ability to measure the spectrum of these neutrinos fairly accurately, and the possible ability to measure the neutral current reaction on the deuteron. These features should go a long way to determining the cause of the solar neutrino problem.

* See ref. 1.

References

1. For a full description of the proposal see The Sudbury Neutrino Observatory, SNO-85-3, G.T. Ewan, H.-B. Mak, B.C. Robertson, R.C. Allen, H.H. Chen, P.J. Doe, D. Sinclair, W.F. Davidson, R.S. Storey, E.D. Earle, P. Jagam, J.J. Simpson, E.D. Hallman, A.B. McDonald, A.L. Carter and D. Kessler, July 1985, obtainable from G.T. Ewan, Queen's University, Kingston, Ontario, Canada.

2. H.H. Chen, Solar Neutrinos and Neutrino Astronomy, AIP Conf. Proc. 126, 249 (1985).

3. J.K. Rowley, B.T. Cleveland and R. Davis Jr., Solar Neutrino and Neutrino Astronomy, AIP Conf. Proc. 126, 1 (1985).

4. J.N. Bahcall, Solar Neutrino and Neutrino Astronomy, AIP Conf. Proc. 126, 60 (1985).

5. S.P. Mikheyev and A. Yu. Smirnov, 10th International Workshop, Savonlinna, Finland, June 1985 and to be published.

SOLAR NEUTRINO DETECTION IN ICARUS

Milla Baldo-Ceolin
Dipartimento di Fisica "G.Galilei", Università di Padova, Padova - Italy
Istituto Nazionale di Fisica Nucleare, Sezione di Padova, Padova - Italy

The relevance of the solar neutrino problem has already been discussed several times during this Conference and a number of special purpose solar neutrino experiments have been proposed.

In this context I would like to present and discuss the possibility of direct solar neutrino observation in ICARUS.

ICARUS, (Imaging Cosmic and Rare Underground Signals) is a very large volume (>4500 m^3) continuously sensitive liquid Argon homogeneous detector, proposed for the Gran Sasso Laboratory [1]. This cryogenic image chamber, where the drift-time technique and the continuous read-out permit recording of the complete electron image produced by the ionizing event, is characterized by an excellent spatial and energy resolution. It thus appears particularly suitable for the first direct observation of the solar neutrinos from ^8B decay [2].

The wealth of information that can be provided by the ICARUS detector is due to the fact that the higher energy solar neutrinos from ^8B decay can produce detectable electrons in both neutrino-Argon absorption and neutrino-electron scattering, that is

a) neutrino absorption in Argon

$$\nu_e + {}^{40}Ar \rightarrow {}^{40}K^* + e^- \qquad (1)$$

b) neutrino-electron elastic scattering

$$\nu + e^- \rightarrow \nu + e^- \qquad (2)$$

The possibility of using the same detector for measuring both the neutrino-Argon absorption (process a) which can be produced only by electron-neutrino, and the neutrino-electron elastic scattering (process b), which - with different cross sections - can be produced by both electron-neutrinos and converted neutrinos (ν_μ, ν_τ), allows the complete determination of solar neutrino flux, spectrum shape and flavour composition, providing tests both of the Standard Solar Model and of neutrino oscillations of very low mass difference.

The neutrino-Ar nuclei and neutrino-Ar electrons cross-sections have been evaluated respectively as $7.84 \cdot 10^{-43}$ cm^2 and $10.9 \cdot 10^{-43}$ cm^2 [2]: according to the Standard Solar Model in 6500 Ar tons in one year are expected:

a) a total of $9.5 \cdot 10^3$ neutrino-Argon absorption events of which 4600 with $E_e > 5$ MeV,

b) a total of $2 \cdot 10^4$, elastic scattering events of which 5000 with $E_e > 5$ MeV.

The electron energy spectrum resulting from absorption of neutrinos by ^{40}Ar and from $\nu_e - e^-$ scattering are shown in Fig. 1 and 2.

The signature of solar neutrino elastic scattering events is the forward peaked angular distribution of the recoil electrons.

Absorption events - since the ν_e-Ar absorption will be dominated by the superallowed transition to the isotopic analogue state (T=2, J=0+) at 4.38 MeV excitation in ^{40}K [2] - are unambiguously identified by association with the characteristic gammas of the decay of the 4.38 MeV excited ^{40}K state.

Experimental Resolution and Backgrounds

In order to estimate the sensitivity of the experiment, electrons in the energy range from 5 to 15 MeV in the ICARUS detector have been simulated by computer: their angular and energy spread have been evaluated to be $\Delta E/E = \pm 0.15$ and $\Delta\Theta = 3$ rad/E (MeV). The resulting spread on the energy and angular distributions of the electrons produced in neutrino electron scattering is shown in Fig. 3: 70% of the total sample of produced electrons with $E_e > 5$ MeV are still in the forward 30° respect to the direction of the sun ($\Omega/4\pi < 0.07$).

Furthermore, although the electron energy distribution is already a good representation of the incoming neutrino flux, the neutrino energy spectrum can be reconstructed from these electrons inside $\Theta_{\nu e} < 20°$ and the results are in good agreement with expectations (see Fig. 4).

The distant reactor neutrinos can produce background electrons through the reaction

$$\bar{\nu}_e + e^- \longrightarrow \bar{\nu}_e + e^- \qquad (3)$$

However the ratio

$$P = \frac{P(\nu_e + e^- \longrightarrow \nu_e + e^-)\ E_e > 5\ \text{MeV}}{P(\bar{\nu}_e + e^- \longrightarrow \bar{\nu}_e + e^-)\ E_e > 5\ \text{MeV}} \qquad (4)$$

normalized to the same number of neutrinos and integrated over the whole energy spectra of solar and reactor neutrinos respectively, results $P \sim 70$.

Thus if the reasonable estimate for reactor $\bar{\nu}$ flux $\phi_{react.}/\phi_{sun} < 0.1$ is assumed, the number of electron events from reactor neutrinos with $E_e > 5$ MeV may be evaluated in less than 7 a year in 6500 m^3 of Argon, and the background

appears to be completely negligible: less than one event a year in the angular acceptance region.

Events

$$\nu_e + {}^{40}Ar \rightarrow {}^{40}K^* + e^- \qquad (1)$$

are identified if one or more Compton electrons are detected.

The possibility of identifying the gammas associated to the neutrino Ar absorption events has been investigated by means of event simulation. In $\sim$60% of absorption events there will be at least one Compton electron, from the K decay gammas, with $E_e > 1$ MeV, inside a sphere with R=30 cm, and center on the electron vertex. Thus the probability of wrong gamma-electron association is negligible if the gamma background is less than 10^9 sec^{-1}.

The gamma background expectation seems to be an order of magnitude smaller.

Conclusions

In conclusion in ICARUS experiments:

a) the electron energy distributions and fluxes for events (1) and (2), will provide direct information on solar neutrinos;
b) it will be possible to test the Standard Solar Model predictions for both the frequencies of events (1) and (2);
c) experimental values for the ratio

$$R = \frac{\nu + e^- \rightarrow \nu + e^-}{\nu_e + {}^{40}Ar \rightarrow e^- + {}^{40}K^*}$$

greater than 1.10 will prove that among the solar neutrinos there are neutrinos (ν_μ, ν_τ) converted through neutrino oscillations. In Fig. 5 the expected value for ratio R is plotted against the percentage of converted neutrinos, the experiment being sensitive to neutrino oscillations with very small neutrino masses and oscilaltion amplitudes of a few percent.

If the Davis result [3], the hypothesis of neutrino oscillations, and Standard Solar Model are considered, R will result R = 1.4.

References

1) ICARUS, A Proposal for the Gran Sasso Laboratory, CERN, Harvard, Milano, Padova, Roma, Tokyo, Wisconsin Collaboration - INFN/AE-85/7.

2) M. Baldo-Ceolin, Concerning Solar Neutrino Detection, ICARUS 85/PD1 - May 30, 1985.
J.N. Bahcall et als. to be published.

3) R. Davis, in proceedings Informal Conference on Status and Future of Solar Neutrino Research, edited by G. Friedlander (Brookhaven National Laboratory Report 40879, 1978), Vol. 1, p. 1.

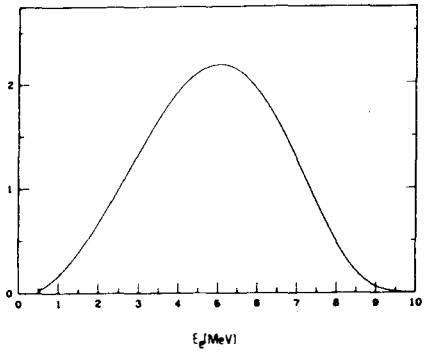


Fig. 1 - Energy spectrum of the recoil electrons from ν-Ar absorption

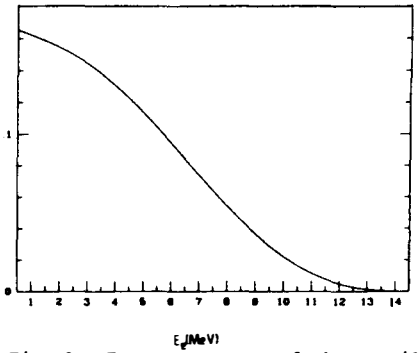


Fig. 2 - Energy spectrum of the recoil electrons from ν_e-e elastic scattering

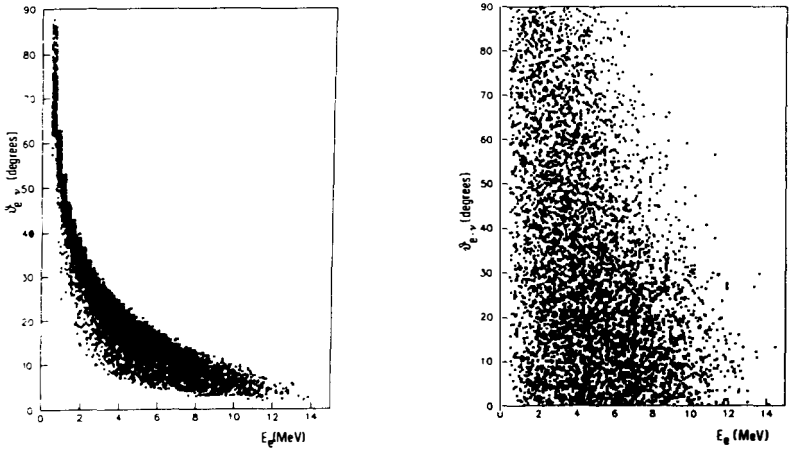


Fig. 3 - Energy-angular correlation of the recoil electrons from ν_e-e elastic scattering without (a) and with (b) experimental errors.

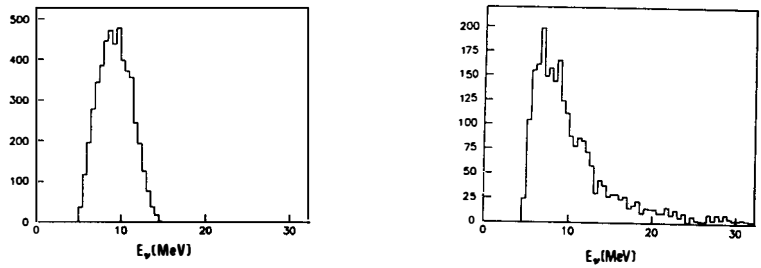


Fig. 4 - Neutrino energy spectrum from recoil electrons from ν_e-e elastic scattering without (a) and with (b) experimental errors.

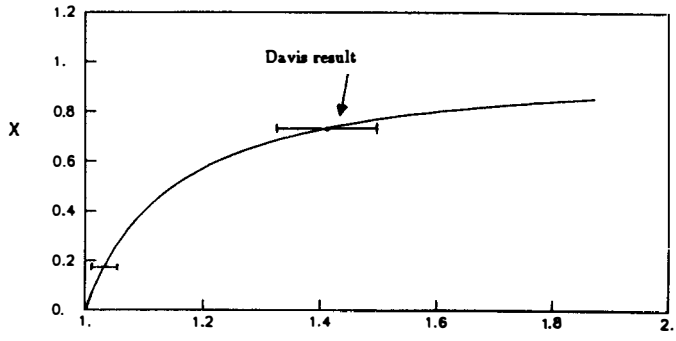


Fig. 5 - The ratio $R = \dfrac{\nu_e + e \to \nu_e + e + (\nu_{\mu,\tau} + e \to \nu_{\mu,\tau} + e)}{\nu_e + Ar \to e^- + K} \cdot \dfrac{\sigma(\nu_\mu e \to \nu_\mu e)}{\sigma(\nu_e e \to \nu_e e)}$ plotted against x, the fraction of solar neutrinos converted by oscillation phenomena.

THE NUSEX EXPERIMENT AT MONT BLANC

presented by E. Bellotti
Dipartimento di Fisica and Sezione INFN - Milano - Italy

LNF - Milan - Turin - CERN Collaboration(+)



ABSTRACT

Data on neutrino induced confined events, nucleon decay candidate and single muons flux are presented. Evidence for a signal from Cygnus X-3 is discussed.

(+)

G. Battistoni, E. Bellotti, C. Bloise, G. Bologna, P. Campana, C. Castagnoli, A. Castellina, V. Chiarella, A. Ciocio, D. Cundy, B. D'Ettorre Piazzoli, E. Fiorini, P. Galeotti, E. Iarocci, C. Liguori, G. Mannocchi, G. Murtas, P. Negri, G. Nicoletti, P. Picchi, M. Price, A. Pullia, S. Ragazzi, M. Rollier, O. Saavedra, L. Satta, S. Vernetto and L. Zanotti.

The NUSEX detector, designed to search for nucleon instability, is installed in the Laboratorio di Cosmogeofisica in the Mont Blanc tunnel. Data collected in more than three years of operation are shortly presented.

SITE AND DETECTOR STRUCTURE

The Laboratory is located in the Mont Blanc tunnel, approximately half way between the two entrances; its geographical position is: latitude 45.8° N (geomagnetic latitude 42.70°); longitude 6.9° E.

The orientation of the detector has been determined using, as a reference, the tunnel axis.

The overburden is greater than 4600 hg/cm^2 of standard rock; a detailed map of slant depth up to 75° from the vertical is available. Mont Blanc rock differs from the standard one having (in brackets the standard rock values): density 2.68 g/cm^3 (2.65 g/cm^3) mean mass number $\langle A \rangle$=20.94 (22) mean atomic number $\langle Z \rangle$=10.34 (11); these differences have been taken into account when computing muons fluxes.

The detector, which is described in detail elsewhere[1], consists of a sandwich of 136 horizonthal iron slabs, 1 cm thick, and layers of limited streamer tubes, 1x1 cm^2 cross section and 3.5 m long. The overall dimension is 3.5 x 3.5 x 3.5 m^3, the total mass is ~ 150 tons. Each layer of detectors consists of 320 tubes equipped with X and Y pick-up strips for two dimensional localization of the streamer.

The minimum trigger conditions to read out the entire set-up are very weak; they are: a) four contiguous planes hit; b) three contiguous planes plus, at least, two other contiguous planes; c) three pairs of contiguous planes.

Localization of a single streamer is of the order of 1 cm; angular resolution for a track crossing 10 layers is better than 1°.

NEUTRINO INDUCED EVENTS AND NUCLEON DECAY CANDIDATES

In about three years of live time, 37 fully contained events (i.e. events whose tracks stop in the detector) have been collected; results on partial samples have been published in past years [2]. These events can be classified as:

26 (24.5) events induced by ν_μ or $\bar{\nu}_\mu$
10 (12.7) events induced by ν_e or $\bar{\nu}_e$
1 event ambigous.

In brackets the expected number of events according the "ν" flux computed by T. Gaisser; it must be remarked that the expected number of neutral current events is ~ 2 events [3]. Energy distribution of these events is shown in Fig. 1, where the predicted rate, corrected for the detector acceptance, is also reported; one could may be notice an excess of high energy events.

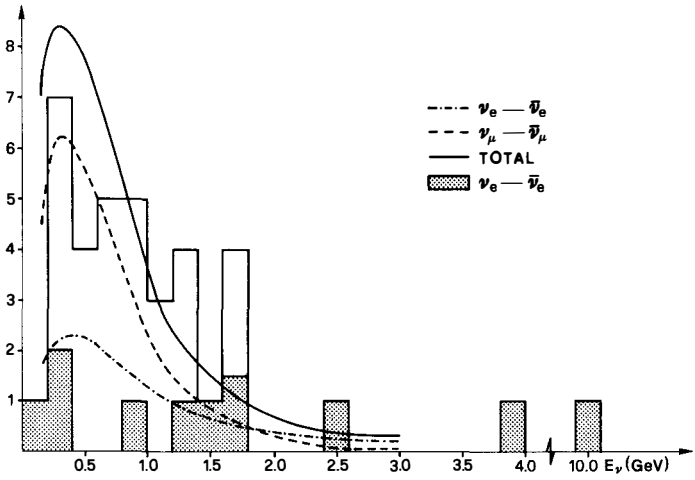


Fig. 1. Energy distribution of confined events.

This sample contains also possible nucleon decay events. The Table reports for a few channels the number of possible candidates, the expected number of background events and the corresponding limits for τ/B, which are of the order of 10^{31} years. The most interesting candidates $p \to \mu^+ K^\circ$, $\mu \to e^+ \pi^\circ$, $n \to \mu\pi$ have been discussed in previous publications [2].

Decay mode	n° of events	background	τ/B (90% C.L.) (10^{31} years)
$p \to e^+\pi^\circ$	1	.25	> .7
$n \to e^+\pi^-$	0		>1.0
$p \to \mu^+\pi^\circ$	0		>1.0
$n \to \mu^+\pi^-$	1	.36	> .3
$p \to \bar{\nu}\pi^+$	8	7	> .2*
$p \to \nu\pi^\circ$	-		>1.3
$n \to \bar{\nu}K^\circ$	0		>1.15
$p \to \mu^+K^\circ$	1	.14	>1.0

* background subtracted

MUON FLUX AND CYGNUS X-3

Rate of muons in the detector is about 1.2 μ's/hour, 1% of them arrive in groups of two or more parallel muons.

The vertical intensity as a function of depth is well described by[4)]

$$I(h) = (7.63 \pm .48)10^{-7}\ e^{-h/(810 \pm .84)}\ cm^2 s^{-1} sr^{-1}\ (h \text{ in } hg/cm^2)$$

as shown in Fig. 2, where data from the present measurement and from a previous measurement by the Torino group in a different garage of the Mont Blanc tunnel, are reported. The good agreement over a wide range of depth is a proof of our good knowledge of all the ingredients (mountain shape, angular dependence, reconstruction programs etc.) which enter in the determination of the vertical intensity.

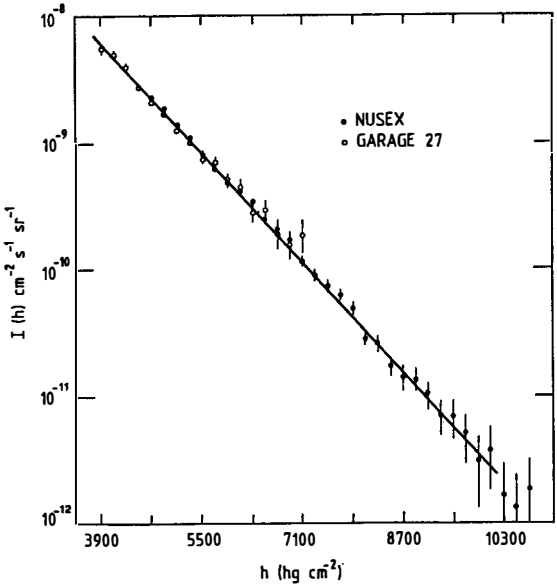


Fig. 2. Muon vertical intensity.

Single muons data have been analyzed to search for localized sources and special attention was dedicated to Cygnus X-3. Properties of this very intense source of radiowaves, x-rays and probably, of very high energy gamma rays are discussed in detail in many papers[5)]. Cygnus X-3, which position in celestial coordinate is 40.9° in declination and 307.9° in right ascension, is a variable source (probably a binary system with a neutron star or a pulsar[5)]) with a period of about 4.8 hours; in the following analysis the ephemeris:

$$T_{\odot} = JD\ 2440949.8986;\ p = .1996830\ d;\ \dot{p} = 1.18\ 10^{-9}$$

as have been determined by Van der Klis and Bonnet-Bidaud[6] from x-rays data, have been used.

Data collected up to Jan. 1985 and from Feb. to Nov. '86 will be discussed separately.

Data up to Jan. '85[7] refer to 21700 single muons with zenith angle less than 75° and crossing at least 10 layers of streamer tubes. With this angular cut, Cygnus X-3 is observed for 64% of the time.

The arrival time of muons with direction in a cone of 4.5° of half aperture in the direction of Cygnus X-3, has been reduced to the barycenter of the Solar system and then folded modulo Cygnus X-3 period. The phase diagram, which is expected essentially flat, is shown in Fig. 3; a clear excess of 20 events over a background of 11 events appears in the phase interval 0.7-0.8; such an effect has a very low probability ($<10^{-4}$) to be due to a statistical fluctuation.

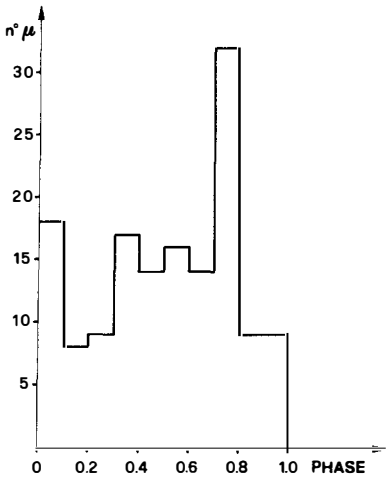


Fig. 3. Phase distribution of "on source" muons.

To check that his effect is not due to some correlation between the phase and shape of the mountain, the exposure of the detector as a function of the depth as well the number of expected muons, has been computed for the different phases. All the phases are equivalent, as expected by the fact that Cygnus precesses 2.1 times/year and the live time was longer than two years. We have also considered 27 other cones (off-source cones) of the same aperture, which cover essentially a declination band centered at the Cygnus declination. The phase of each muon was corrected computing a fake time of

arrival supposing that Cygnus were aligned with its direction of arrival. In this way, the effects of the mountain shape are correctly correlated to phase values. The phase distribution of muons in the off-souce cones (Fig. 4) is flat and in very good agreement with the expected one (χ^2 = 9.8 on 9 n.d.).

Data have been also analyzed varying the period; the maximum excess corresponds to the value as determined by the x-rays data.

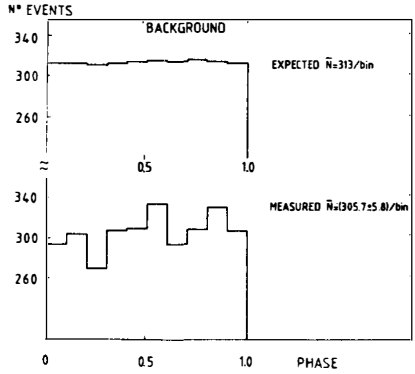


Fig. 4. Phase distribution of "off-source" muons.

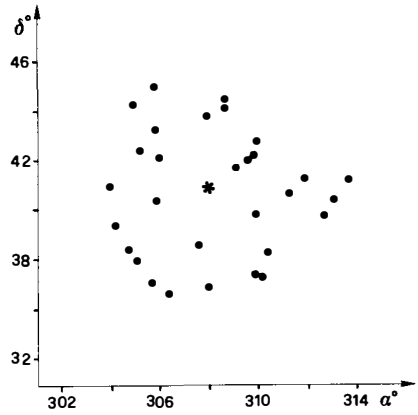


Fig. 5. Angular distribution of "on source" muons.

The half aperture of 4.5° was chosen in order to fully contain the signal; in fact, as shown in Fig. 5, experimental points are spread out around the Cygnus direction. The signal intensity, as a function of half-aperture

angle of the cone centered on Cygnus direction, is shown in Fig. 6; on the same figure the expected curves for different angular resolution are also shown. The computed angular resolution is better than 1°, major contribution coming from multiple scattering in the rock and from geomagnetic deflection. Then, this effect of angular spread, which does not seem to be due to distortions introduced by the detector, must be furtherly investigated.

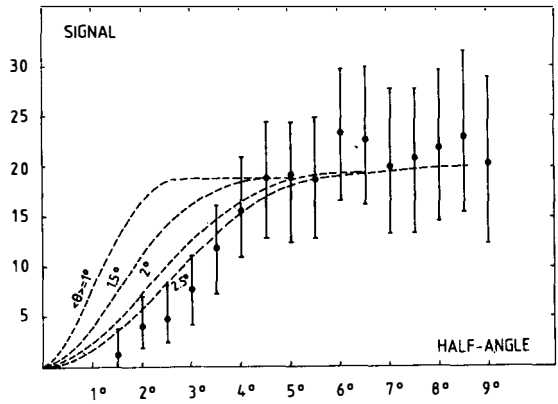


Fig. 6. Signal intensity as a function of angle with Cygnus direction.

The intensity of the observed flux is of the order of 10^{-11} μ's/(cm^2·s) i.e. of the same order of magnitude as the "gamma" ray flux measured at the surface with EAS detectors at the same energy.

Comparison between the depth distribution and the detector exposure to Cygnus allows us to conclude that this muons are not induced by very penetrating particles (i.e. not by standard neutrinos), because, in that case, we would observe muons at very large depth where the exposure is maximum. Then, assuming that this muons are not produced in the rock, their energy is in the range 2-5 TeV.

1985 data. Data collected during 1985 are not yet fully analyzed; in the period from Feb. to Sept. the 26, the detector was operated for 4000 hours.

Data have been analyzed as the previous ones, and no excess in the direction of Cignus is observed; in the .7-.8, phase bin background 1.6 events are expected and 3 more if the signal from Cygnus has the same intensity as in the previous data, while 1 event has been observed (Poisson probability 6%). Due to the limited statistic, no firm conclusion can be drawn; however these data can suggest that there are long term variation also in the high energy emission from Cygnus X-3, as observed by other authors [8].

In the period Sept. 26th - Oct. 10th a radioburst was observed. In this

same period we have been observed 5 events (3.4 were expected) in the on-source cone; they are distributed 1 in the phase bin .3-.4 and 4 in the .8-.9 bin. Again no conclusion can be drawn from these data alone.

CONCLUSIONS

Nusex data show an excess of high energy muons coming from the direction of Cygnus X-3 during year '83-'84, which is not confirmed by data collected in '85; time dependence of this signal will be furtherly investigated.

Angular spread around the source seems not to be due to instrumental effects; this fact and the very high measured flux need a confirmation by future measurements and also a physical interpretation.

REFERENCES

(1) G.Battistoni et al. - The NUSEX detector - LNF 85/48 (P) (Oct. 1985) preprint and submitted to Nucl. Instr. and Methods.
(2) G. Battistoni et al. Phys. Lett. 133B, (1983) 454.
G. Battistoni et al., Proc. HEP 85, Bari, p. 417.
(3) T.Gaisser - private communication
G.Battistoni et al. Nucl. Instr. and Methods 219, (1984) 300.
(4) see f.i. B. D'Ettorre Piazzoli "Cosmic muon results from the nusex experiment" invited talk at the First Symposium on Underground Physics, Saint Vincent, Italy, April 1985.
(5) see f.i. Vladimirskii et al. Sov. Phys. Usp. 28, (1985) 153 and references therein P. M. Chadwich et al. Nature 318 (1985) 642.
(6) M. Van der Klis and J.M. Bonnet-Bidaud - Astron. Astrophys. 95, L5 (1981).
(7) G. Battistoni et al. Phys. Lett. 155B, (1985) 465.
(8) see f.i. C. L. Bhat et al. - Proc. of the XIX ICRC - La Jolla 1985, vol.I, OG 2.1-10 p. 83.

SEARCH FOR HIGH ENERGY MUONS FROM CYGNUS X3 IN THE FREJUS DETECTOR

presented by G. Chardin
DPHPE, SEPh, CEN Saclay

Aachen, Orsay, Polytechnique, Saclay, Wuppertal Collaboration



Abstract : We have analyzed high energy muons in the Fréjus underground nucleon decay detector in the period between February 84 and mid-November 85. No excess of muons is observed in the direction of Cygnus X3, yielding a 90% confidence level upper flux limit of 2.3 10^{-12} $cm^{-2}s^{-1}$ for an average rock overburden of 5000 hg cm^{-2}. Using the 4.79 hour periodicity of Cygnus X3, no signal is found in any phase interval.

Geographical situation:

The laboratory is located in a gallery inside the Fréjus road tunnel, between Modane (France) and Bardonecchia (Italy); the average thickness of rock traversed by muons coming from the atmosphere and crossing the detector is about 1780 m, which corresponds to approximately 4800 hg cm^{-2}. For those muons coming from the direction of Cygnus X3, the average thickness is larger, and is equal to 1835m (approximately 5000 hg cm^{-2}) The corresponding total flux is 4.2 muon/(m^2 x day) (horizontal surface). The longitude of the detector is 6.69° E, and its latitude 45.14° N.

General description of the Frejus detector:

The Fréjus detector is a track visualizing type detector with a very fine grain (5mm*5mm cells) and a fine calorimetric sampling (3mm corresponding to 1/6th of a radiation length of iron) which has been designed to study the nucleon decay. Its granularity makes it well suited for cosmic ray physics through the analysis of the muon events. The detector weighs 900 tons, is 6 meters high and presents a horizontal surface of (6 x 12.3) m^2. The detector is made of 114 vertical modules, each one including eight flash-chamber planes and one Geiger plane. Both flash-chamber and Geiger cells are alternatively horizontal and vertical in order to provide two orthogonal views. The flash chamber read-out is made by external capacitive coupling. The total number of flash cells is about 930,000 and the number of Geiger cells, which act as a trigger for the flash chamber part of the detector, is about 40,000.

What do we know about Cygnus X3?:

It is reasonably inferred from the observations that the Cygnus X3 system is a binary system, with a compact object orbiting around a more massive companion with a period of almost 4.8 h. There is probably accretion of infalling matter from the massive companion on the compact pulsar. Very large radio outbursts from Cygnus X3 have been observed. The modulation curve of the X-ray and infrared emission indicates that the compact object has a rather close orbit around its companion. A lot of experiments[1] have reported the observation of γ rays from Cygnus X3 in the 30 Mev-1 GeV range, in the TeV range, and in extensive air shower observations. More recently, two nucleon-decay dedicated experiments [2, 3a,b] have also claimed evidence for emission from Cygnus X3.

Analysis and results:

The data taking has been continuing since February 19th 1984, when the detector mass was 240 tons. Acquisition of the whole detector started in June 85. The detector was active 78% of the time.

In the present analysis, we have used all the data from February 84 to mid-November 85.

About 165000 muons were reconstructed. After the cuts which require in particular that the track crosses at least 8 planes on each view, we are left with 151000 muons. The loss of events due to the fact that the trigger planes are vertical amounts to 7%.

The orientation of the detector was found using three different methods. First, we have used the measurements available from the construction of the tunnel. Second, we have used the muongraphy of the mountain and the known mountain profile to determine the orientation by a maximum likelihood method. The orientation has finally been determined by gyroscopic measurements(**). These three measurements agree within 0.1°. This indicates that the orientation of the detector is known to an approximate precision of 2 mrad, to be compared with the expected loss of directionality from multiple scattering, Bremstrahlung and interactions in the rock, which is of the order of 15 mrad at our depth. This parameter has been determined using the relative angles in multimuons.

To estimate the importance of the error coming from our automatic reconstruction procedure, we have visualized all the events which are at less than 5° from the Cygnus X3 direction. The mean value of the reconstruction error, mainly due to the influence of the Bremstrahlung, rather common for muons of a few hundred GeV, is 0.4°.

We have also controlled the distribution of rock thickness for the muons coming from the direction of Cygnus X3, and we have compared it with the rock thickness distribution of the muons which fall on the whole road of Cygnus X3, that is with the same distribution of rock thickness as Cygnus X3. We find an excellent agreement between the two distributions (figure 1a,b). In particular, it seems completely excluded in view of these distributions that a significant signal could be due to neutrino interactions since in this case at least 30% of a signal would come from very large thickness of rock (greater than 5 km of rock), and there are no such events. It may be noted that the mean thickness of rock along the road of Cygnus X3 (≈1850m, about 5000 hg cm^{-2}, essentially the same value as for the NUSEX[2] experiment) is larger than the mean thickness for the whole muon sample (≈1780m).

A crucial test is also provided by the scatter plot in equatorial coordinates alpha vs delta for the directions of the incoming events (figure 2). Clearly, there is no accumulation at the angular position of Cygnus X3.

The angular resolution and the accumulated statistics make it possible to consider cones of half angle 2°. We also present data in 5° cones for direct comparison with ref. [2] (Fig. 3 a,b). 341 events are at less than 5° from the Cygnus X3 direction while 333 are expected, and 55 events are at less than 2° from the Cygnus X3 direction while 52.5 are expected. The phase of each event is then calculated from the arrival time t after heliocentric correction, the Cygnus-X3 period P_o at a reference time T_o and its time derivative P according to the formula:

$$\Phi = (t - T_o)/(P_o + P(t - T_o)/2) \text{ modulo } 1$$

with [4]: T_o = Julian Day 2440949.8986 , P_o = 0.1996830 day and $P = 1.18\ 10^{-9}$

The fact that the period of Cygnus X3 is very close to $1/5^{th}$ of a sidereal day induces a strong correlation between the phase and the zenith angle (and the muon rate) if the time distribution of recorded events, modulo 174 days, is not uniform.Special attention has been given to the expected phase distribution, taking into account the increase in time of the active part of the detector, the trigger efficiency, the rock modulation, the effective surface seen along a particular direction. Taking all these factors into account, we get the distribution in dashed lines on figure 3. This expected (background) phase distribution has been estimated using the following method: first, we calculate the number of events as a function of the hour of the sidereal day using all the muons which fall on the road (5° or 2° in radius) followed by Cygnus X3 (Fig. 4). This quantity relies only on data and not on a simulation. When the detector is working, we then calculate the hour of the sidereal day (that is the position along the cone described by Cygnus X3 in terrestrial coordinates) and the corresponding expected flux, and the phase of Cygnus X3. We then histogram this flux as a function of the phase. This expected phase distribution is also calculated for 35 similar windows (every 10 degrees in alpha) on the road of Cygnus X3, which further provide an absolute normalization. This procedure allows to get an unbiased estimate of the phase distribution. Similar fluctuations have been observed in the 35 off-source windows in the path of Cygnus-X3 and yield a uniform probability distribution for a background hypothesis in all 36 windows. We have checked that the angular distribution in $\alpha.\delta$ of events in the most populated phase bins do not show any accumulation near Cygnus-X3. No global excess is observed in these windows, and no evidence from a source can be found.The confidence level for a background hypothesis is 7% for the 5° window and 53% for the 2° window centered on Cygnus X3. If we expect, following an earlier suggestion[2], that the emission of Cygnus X3 occurs in the [0.7, 0.8] bin which has a population of only 27, we get, at a 90% confidence level, a higher limit for an emission which is more than 20 times smaller than that calculated by reference 2. This corresponds, at the level of the detector, to a flux less than 0.1×10^{-12} muon cm^{-2} s^{-1}. The 90% confidence levelflux limits are given in table I forthe 10 phase intervals and for the 5° window.

It has been suggested[5] that there could be a correlation between periods of high radio emission and of high-energy emission from Cygnus X3. A very large radio outburst has been observed during the period between September 26^{th} 1985 and October 19^{th} 1985. No accumulation is seen at the position of Cygnus X3. Furthermore, the phase distribution of events lying in a 5° window which is shown in figure 5 contains a total of 24 events (all of them are single muons) when 21.8 are expected.The background level, estimated along the same method as before, is indicated in dashed lines. It is important to realize that for such a short observation time, the expected background phase distribution is not flat (dashed line in fig. 5). Even with the large Frejus detector, the poor sensitivity in such a short observation period does not allow us to claim any evidence for a signal. The confidence level for the background hypothesis is 38 %.

Conclusion

In conclusion, analysis of the Fréjus data yields new limits on the excess muon flux from the direction of Cygnus-X3 . The positive signals reported in ref. 2 and 3 are not confirmed. It should be noted that, except for the observation period, the conditions (in particular the rock thickness traversed by muons from the direction of Cygnus-X3) were very similar to those in ref. 2.

(**) We are grateful to W.Coosemans and C.Fisher from CERN-LEP for these gyroscopic mesurements.

(1) Watson A.A., Rapporteur talk, 19th Int. Conf. Cosmic Ray Ph., La Jolla, (1985) and references therein.

(2) Battistoni G. et al., Phys. Letters, **155B**, 465-467, (1985)

(3a) Marshak M.L. et al., Phys. Rev. Letters, **54**, 2079-2082, (1985)

(3b) Marshak M.L. et al., Phys. Rev. Letters, **55**, 1965-1968, (1985)

(4) Van der Klis M., Bonnet-Bidaud J.M., Astron. Astroph., **95**, L5-L7, (1981)

(5) Neshpor Yu.I., Stepanian A.A. et al., Astroph. and Space Science, **61**, 349-355, (1979)

Table I.
90% confidence level flux limits for the 5° window in 10 phase bins. The upper limits are calculated by considering that Cygnus-X3 is not visible between 0.37 and 0.73 of siderai day. This arbitrary convention is very similar to the one used in Ref. 2.

Phase	90% C.L. flux limits in units of 10^{-12} cm^{-2} s^{-1} 5° window
0.0-0.1	.76
0.1-0.2	.36
0.2-0.3	1.15
0.3-0.4	.17
0.4-0.5	.42
0.5-0.6	.08
0.6-0.7	1.26
0.7-0.8	< .1
0.8-0.9	< .1
0.9-1.0	1.37
All events, regardless of phase	2.3

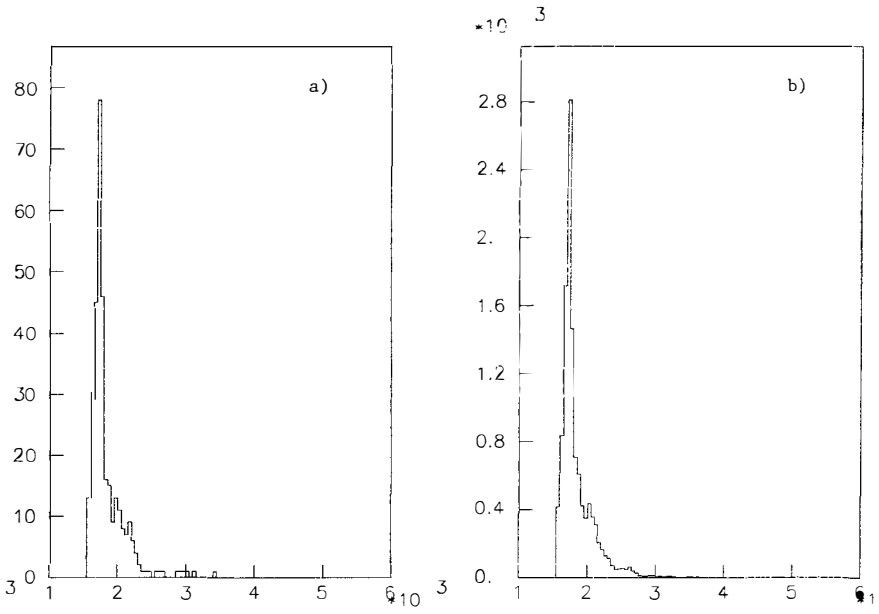


Fig.1 Rock thickness distribution
a/ for events falling in the 5° windo w centered on Cygnus X3
b/ for events falling in the 35 control windows at same declination

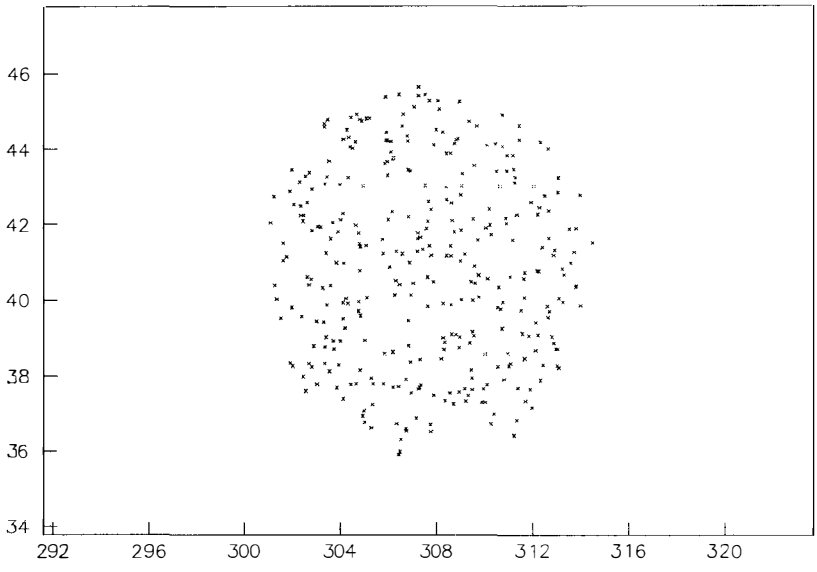


Fig. 2 Scatter plot of detected muons.

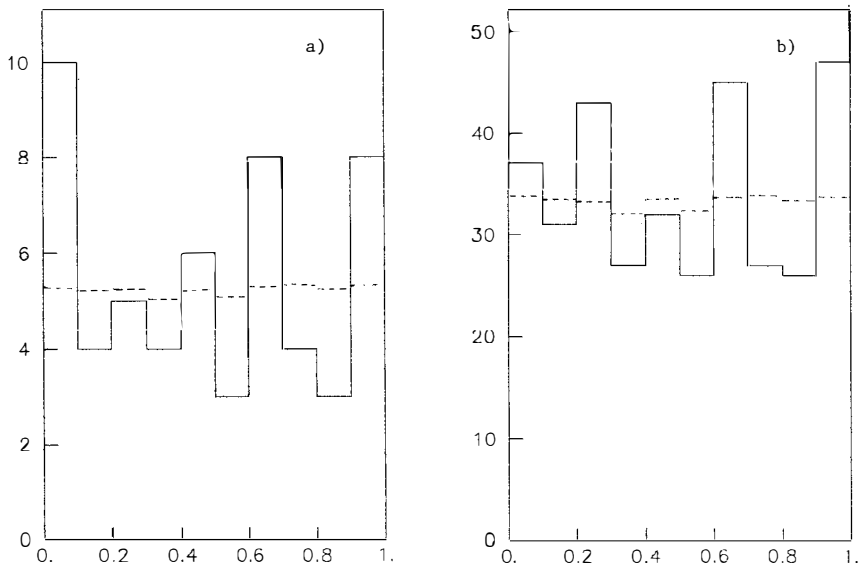


Fig. 3 Phase distribution of muons coming from cones of half angle 2° (a) and 5° (b) centered on Cygnus-X3. The solid line corresponds to the detected muons. The dashed line represents the expected number of atmospheric muons (see text).

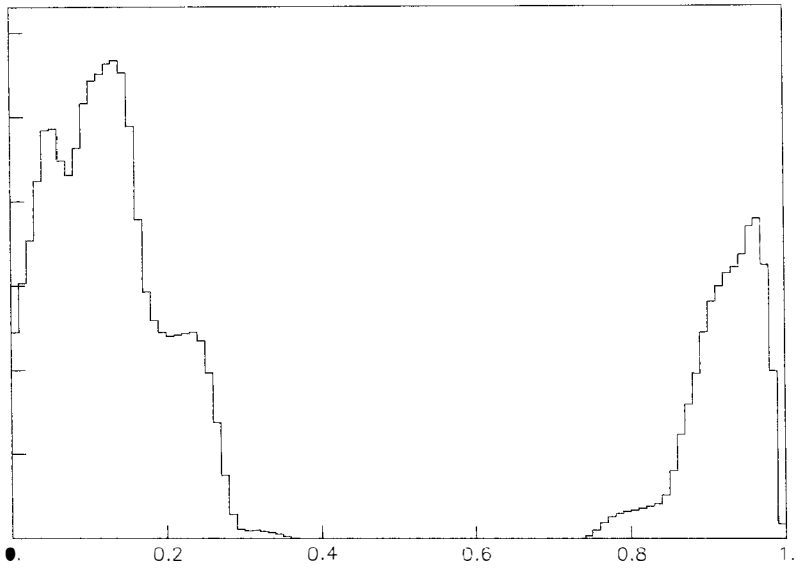


Fig. 4 Cygnus-X3 daily background of atmospheric muons and multimuons. The events are coming from the path of Cygnus-X3: $35.78^{\circ} < \delta < 45.78^{\circ}$.

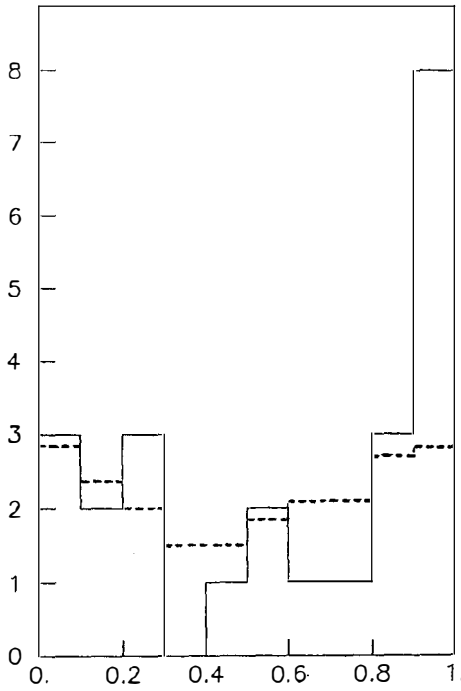


Fig. 5 Phase distribution of muons detected in the 5^{o} window centered on Cygnus-X3 between September 26 and October 19, 1985. The dashed line represents the expected number of atmospheric muons.

BAKSAN UNDERGROUND DATA ON CYGNUS X-3 AT $E_\mu > 200$ GeV AND $E_\mu > 500$ GeV

Yu.M.Andreyev, A.E.Chudakov, I.M.Kogai, V.A.Kozyarivsky
Institute for Nuclear Research, Academy of Sciences of the USSR
60-th October Anniversary Prospect 7a, Moscow 117312, USSR

ABSTRACT

The data accumulated during period of April 1983 through March 1985 do not show any signal from Cygnus X-3. This result is in a strong disagreement with Soudan 1 and NUSEX conclusions if one assumes conventional mechanism of muon production. In NUSEX phase interval 0.7-0.8 the Baksan upper limit at $E_\mu > 500$ GeV is even less than NUSEX flux at $E_\mu > 3000$ GeV.

In 1983 first sensational reports were published on the observation of gamma-rays at energies 10^{14}- 10^{16}eV from known x-ray binary Cygnus X-3[1,2,3]. Most unexpected results came from deep underground experiments, claiming observation of a signal from this source[4,5]. Then investigation of a signal from Cygnus X-3 has been also undertaken at Baksan underground scintillation telescope.

Baksan telescope 16.7 m by 16.7 m horizontally and 11.0 high is located in mountains of North Caucasus at a depth of 850 m.w.e.[6] It consists of six external and two internal layers of scintillation detectors, each layer containing approximately 400 detectors. Angular distribution of single muons is studied with the telescope for several years[7]. Each event representing single muon is required to have hit detectors on two external layers. Hit detectors of the same layer (if number of them is greater then one) must be adjacent, that is to form "spot". Hit detector or "spot" of internal layers, if any, must lie on a straight line with external detectors. The length of muon trajectory inside the telescope is required to be greater than 7 m. This permits angular resolution to be about 2°. Counting rate of such events is 7 s^{-1}. Data are accumulated as a two-dimensional histogram, which represents upper celestial hemisphere divided onto angular bins. They are recorded on magnetic tape every 15 minutes. These data on muon angular distribution were used to form two stripes, covering two intervals in declination: 35.9° - 45.9° and 38.4°- 43.4°. Width of the window in right ascension, defined by 15 min interval and angular resolution, is equal to 5°. Rock profile has allowed to choose two areas of slant depth, corresponding to muon energy $E_\mu > 200$ GeV (hour angle 20°- 101°) and $E_\mu > 500$ GeV (234°- 298°) accordingly. We have analized data from the period of April 1983 through March 1985 with live time of 1.65 yr.

The phase of the middle of each 15 min interval has been obtained with the formula:

$$\Phi = (t - T_o)/P_o - ((t - T_o)/P_o)^2 \cdot \dot{P}/2$$

with T_o = J.D. 2440949.8986, P_o = 0.1996830 d and $\dot{P} = 1.18 \times 10^{-9}$, as obtained by M. van der Klis and J.M.Bonnet-Bidaud[8]. The phase histogram for $\Delta\alpha = 5^o$, $\Delta\delta = 10^o$, $E_\mu > 200$ GeV is shown in Fig.1a. It should be pointed out that background phase distribution, which is considered a priori to be uniform, may prove to be not uniform. It depends on the observation period because averaging time is rather long (174 days since the period of Cygnus X-3 is 0.2002297 sidereal day) and on a rock depth in the direction of the source during sidereal day. The artefact of phase distribution may be obtained by substitution mean values of muon flux for statistical ones in the same time intervals (Fig.1b). To take it into account, it is necessary to divide measured values by expected ones, to obtain final phase histogram shown in Fig.1c.

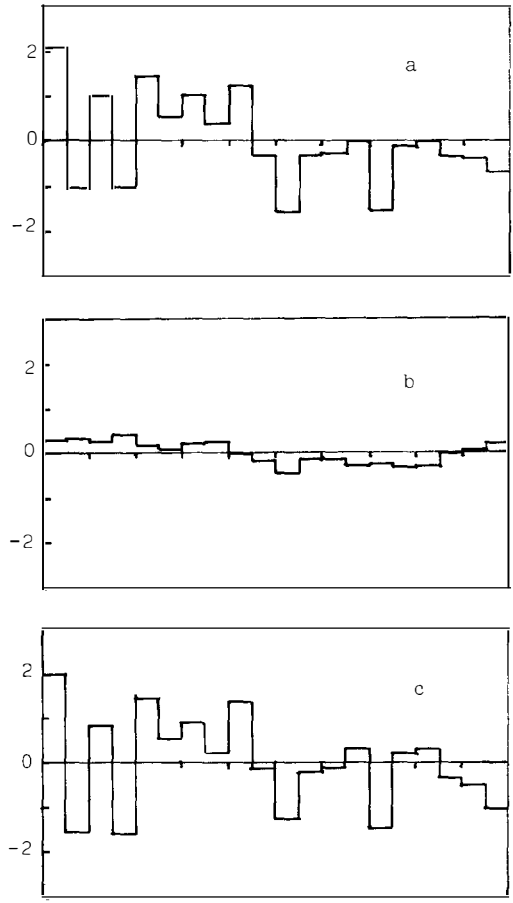


Fig.1: Phase distributions for $\Delta\alpha$=5° $\Delta\delta$ = 10° E_μ > 200 GeV. a - measured, b - artefact, c - with correction.

Comparison of phase distributions obtained at Baksan, NUSEX and Soudan 1 (Fig.2) shows their difference in the phase interval

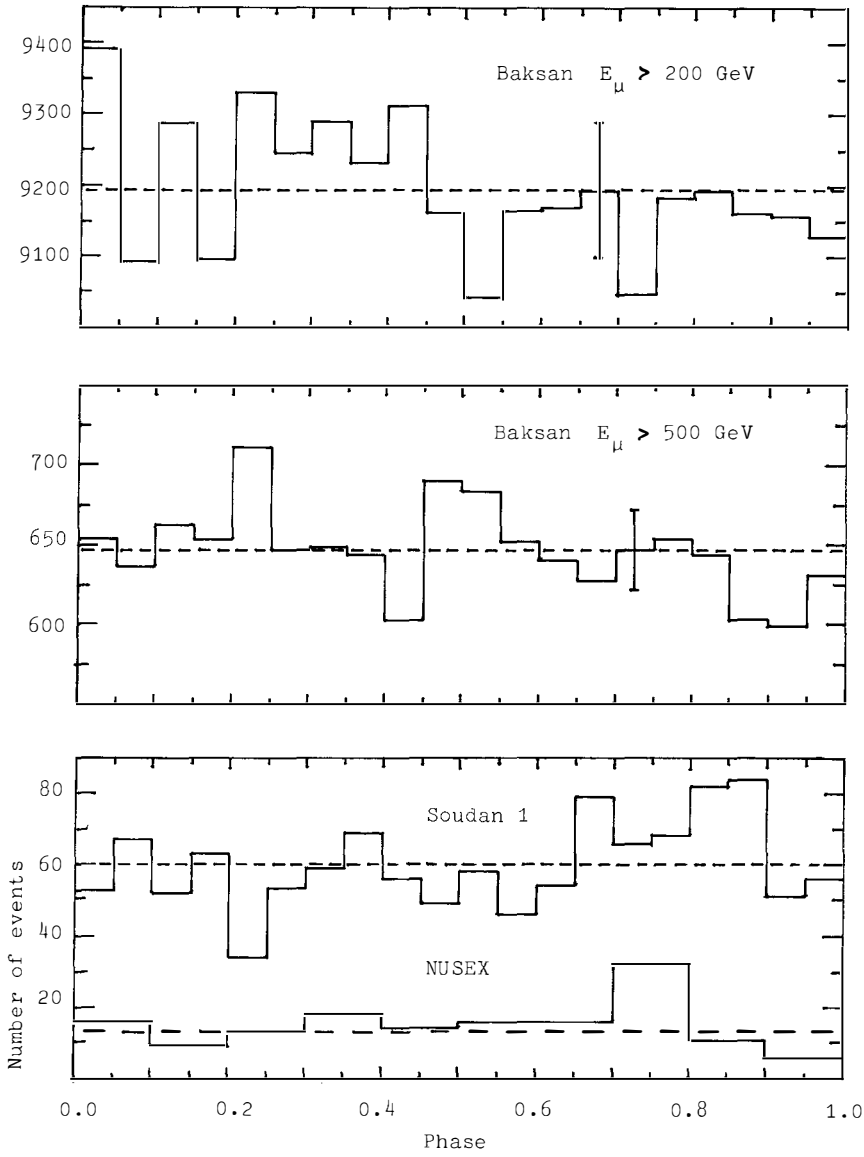


Fig.2: Phase distributions obtained in three experiments.

Ø.6 - Ø.9. When comparing results of these three experiments one should have in mind the following:

	NUSEX	Soudan 1	Baksan
Observation period	Jun'82-Feb'85	Sep'81-Nov'83	Apr'83-Mar'85
Depth, hg/cm^2	55ØØ	18ØØ	85Ø
Threshold muon energy, GeV	3ØØØ	6ØØ	2ØØ
Angular aperture	1Ø°x 1Ø°	radius 3°	5° x 5°

Obtained results enable us to put upper limits for muon flux from Cygnus X-3 at E_μ > 2ØØ GeV and E_μ > 5ØØ GeV in phase interval

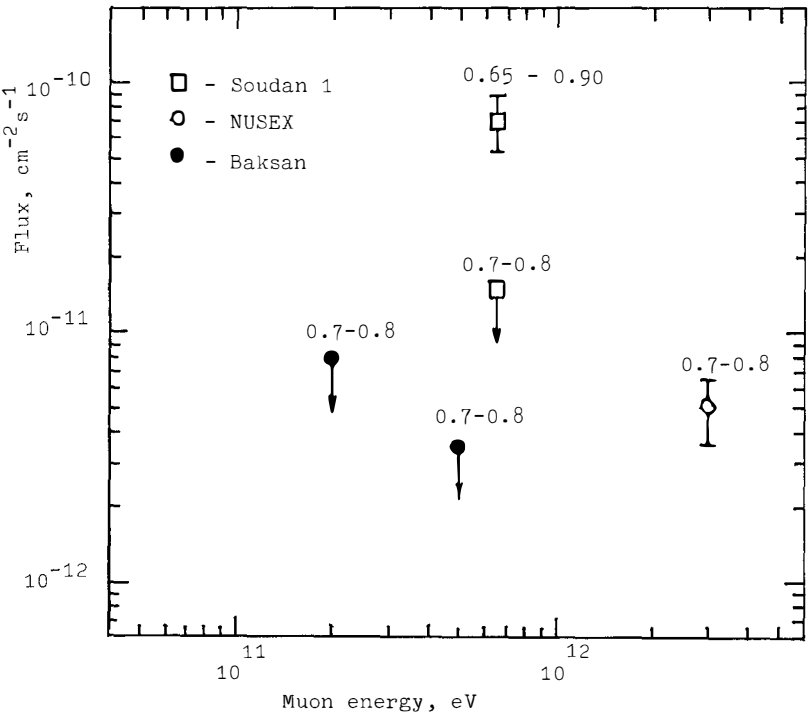


Fig.3: Experimental data on muon fluxes from Cygnus X-3 in shown phase intervals.

Ø.7-ø.8, which are shown in Fig.3. Our results are in a strong disagreement with data, obtained by NUSEX and Soudan 1 groups, if one assumes conventional mechanism of muon production. Our upper limit in the phase interval Ø.7-Ø.8 at E_μ > 5ØØ GeV is even less than NUSEX muon flux at E_μ > 3ØØØ GeV, even taking into account the difference in angular aperture.

References

1. M.Samorski and W.Stamm, Astrophys. J. 268, L17 (1983).
2. J.Lloyd-Evans et al., Nature 3Ø5, 784 (1983).
3. C.Morello et al., Proc. of 18 ICRC, Bangalore, 1, 127 (1983).
4. G.Battistoni et al., Phys. Lett. 155B, 465 (1985).
5. M.Marshak et al., Phys. Rev. Lett. 54, 2Ø79 (1985).
6. E.Alexeyev et al., Proc. of 16 ICRC, Kyoto, 1Ø, 276 (1979).
7. E.Alexeyev et al., Proc. of 16 ICRC, Kyoto, 1Ø, 12 (1979).
8. M.van der Klis,J.M.Bonnet-Bidaud, Astron.Astroph. 95, L5 (1985).

MASSIVE NEUTRINOS AND NEUTRINO MIXING

S.T. Petcov
CERN - Geneva
and
Institute of Nuclear Research and Nuclear Energy
Bulgarian Academy of Sciences
1784 Sofia, Bulgaria

ABSTRACT

The phenomenological theory of neutrino mass generation is reviewed. In particular, examples of schemes with pseudo-Dirac and non-standard Dirac massive neutrinos are considered. Some of the general physical implications of the existence of massive neutrinos and lepton mixing are also briefly discussed.

1. - INTRODUCTION

The problem of neutrino mass is almost as old[1),2)] as the idea of the existence of neutrinos[1)], but no convincing solution has been proposed so far. Neutrinos may well be massless. However, unlike the case of the only known zero mass particle - the photon, whose masslessness is ensured in quantum electrodynamics by a very elegant and powerful principle, namely, the requirement of exact local gauge invariance, no profound principle excluding the possibility of massive neutrinos has been found.

The status of massive neutrinos in the gauge theories of the electroweak interactions is intimately related to the status of the symmetries associated with the conservation of the lepton charges L_e, L_μ, L_τ,... and of the total lepton charge $L = \Sigma_{\ell=e,\mu,\tau,...} L_\ell$ in these theories[3)]. The symmetries which play a fundamental role in the gauge theories - the local gauge symmetries - are dynamical. They fix unambiguously the dynamics governing the basic particle interactions and, apart from the couplings responsible for the mass generation, ensure renormalizability of the theory once the symmetry group and the multiplet content of the theory are specified. It has been known for a long time[4)] that the symmetries associated with the conservation of the lepton charges could not possibly be associated with the existence of exact local symmetries*). Perhaps they may be associated with the existence of exact global symmetries. However, the global symmetries cannot be considered as fundamental in the context of the gauge theories. The gauge theories admit violations of the global symmetries whenever the requirement of local gauge invariance (and renormalizability) and the multiplet content of the theory permit it. As a consequence, massive neutrinos arise quite naturally in the gauge theories of electroweak interactions (including their supersymmetric versions) and especially in the grand unified theories (GUTs).

In the present talk we shall review the phenomenological theory of neutrino mass generation. More specifically, we shall give first a classification of the possible types of neutrino mixing arising in the gauge theories of electroweak interaction. Further, the corresponding neutrino mass terms generating the mixing will be discussed. After that, the properties of the massive Dirac and massive Majorana neutrinos will be compared and examples of schemes with pseudo-Dirac and

---

*) Otherwise the resulting gauge interactions would introduce discrepancy in the Eötvös experiment, unless they were characterized with ultra-small coupling constants.

non-standard Dirac neutrinos will be considered. We shall conclude with a few remarks concerning the relation between the existence of massive Majorana neutrinos and of the neutrinoless double β-decay.

2. - MASSIVE NEUTRINOS AND NEUTRINO MIXING (General analysis)

2.1 The mixing

If the neutrino masses turn out to be non-zero*), it is natural to expect that the neutrinos with definite masses will not coincide with the flavour neutrinos ν_ℓ taking part in the standard weak interaction. In this case neutrino mixing similar to the quark mixing will take place. In general, the following possibilities exist[3].

First, the neutrinos with definite mass can be Dirac[5] or Majorana[6] particles. (We shall denote the former by ν_k and the latter by χ_k.) Second, the number of mass-eigenstate neutrinos m can coincide with or can exceed the number of flavour neutrinos ν_ℓ, which, for generality, we shall assume to be equal to n: m = n, or m > n.

Massive Dirac neutrinos may arise in theories in which at least one additive lepton charge is conserved. In particular, this may be the total lepton charge[7] $L = \Sigma_{\ell=e,\mu,\tau,\ldots} L_\ell$, where L_e is the (additive) electron-lepton charge, etc., or for example, a generalization of the Zeldovich-Konopinsky-Mahmoud (ZKM) lepton charge**),9),10) which, e.g., in the case of three lepton flavours, can have the form[11] $L' = L_e - L_\mu + L_\tau$. The properties of the massive Dirac neutrinos arising in a given theory depend strongly on the type of the lepton charge conserved in the theory.

Massive Majorana neutrinos may arise in theories in which the total lepton charge L is not conserved[12]. Their couplings preserve no lepton charge.

The number of neutrinos with definite masses can exceed the number of left-handed (LH) flavour neutrinos (m > n) only if neutral fermions with non-zero masses which mix (i.e., form mass terms) with the flavour neutrinos ν_ℓ exist[13].

---

*) For a discussion of the experimental status of the neutrino masses, see the contributions, e.g., of V. Liubimov, K. Bergkvist and W. Petersen in the present proceedings. The phenomenology associated with massive neutrinos and neutrino mixing is treated in the contributions of, e.g., E. Fiorini, S.P. Rosen, M. Shaevitz, E. Takasugi and others, and we shall not consider it.

**) The ZKM lepton charge L' was introduced[8] assuming that there exists one four-component (Dirac) neutrino ν associated with both e and μ and that $L'(e^-) = L'(\nu) = L'(\mu^+) = 1$ (i.e., $L' = L_e - L_\mu$). The charge L' was supposed to be conserved by the weak interactions.

Since such fermions have not been observed, they must have a non-standard weak interaction with the charged leptons and quarks. Typical examples of such fermions are the hypothetical right-handed (RH) neutrinos $\nu_{\ell^\circ R}$ (and the LH antineutrino $\bar{\nu}_{\ell^\circ L}$) which are assumed to have a superweak interaction with ordinary matter*). The number of the RH neutrinos $\nu_{\ell^\circ R}(n^\circ)$ may not be equal to the number of the LH neutrinos ν_ℓ.

In such a way, if we leave aside the possibility of coexistence of massive Dirac and massive Majorana neutrinos**), the following cases emerge:

$m = n$:

$$\nu_{\ell L}(x) = \begin{cases} \sum_{k=1}^{n} U^{D}_{\ell k}\, \nu_{kL}(x), \text{ or} & (1) \\ \sum_{k=1}^{n} U^{M}_{\ell k}\, \chi_{kL}(x); & (2) \end{cases}$$

$m > n$:

$$\left.\begin{aligned} \nu_{\ell L}(x) &= \sum_{k=1}^{m} V^{M}_{\ell k}\, \chi_{kL}(x), \\ \nu^{c}_{\ell^\circ L}(x) &= \sum_{k=1}^{m} V^{M}_{\ell^\circ k}\, \chi_{kL}(x) \end{aligned}\right\} \quad (3)$$

or

$$\left.\begin{aligned} \nu_{\ell L}(x) &= \sum_{k=1}^{m} V^{D}_{\ell k}\, \nu_{kL}(x) \\ N_{\ell^\circ L}(x) &= \sum_{k=1}^{m} V^{D}_{\ell^\circ k}\, \nu_{kL}(x) \end{aligned}\right\} \quad (4)$$

Here $\nu_{\ell L}(x)$, $\ell = e,\mu,\tau,...,\sigma$ (n values) are the fields of the flavour neutrinos which enter into the standard weak interaction Lagrangian, $\nu^{c}_{\ell^\circ L}(x)$ and $N_{\ell^\circ L}(x)$ $\ell^\circ = e^\circ,\mu^\circ,\tau^\circ,...$((m-n) values) are LH sterile neutrino fields, $\nu_{kL}(x)$ and $\chi_{kL}(x)$ are, respectively, the LH components of the fields of Dirac and Majorana neutrinos with definite mass. U^D and U^M are n×n unitary lepton mixing matrices and V^D and V^M are m×m unitary lepton mixing matrices. Consequently, the matrices V^D and V^M satisfy the conditions:

$$\sum_k V^{D(M)}_{\ell k} \left(V^{D(M)}\right)^{+}_{k\ell'} = \delta_{\ell\ell'}, \quad (5a)$$

$$\sum_k V^{D(M)}_{\ell^\circ k} \left(V^{D(M)}\right)^{+}_{k\ell^{\circ\prime}} = \delta_{\ell^\circ\ell^{\circ\prime}}, \quad (5b)$$

---

*) They are often called inert or sterile neutrinos[14]. We shall use these terms for any neutral fermions which mix with the ordinary neutrinos ν_ℓ but have a non-standard weak interaction (as a rule, much weaker than that of the neutrinos).

**) For a discussion of this possibility, see, e.g., Ref. 15).

$$\sum_k V^{0(M)}_{\ell k} \left(V^{0(M)}\right)^{+}_{k\ell'} = 0. \qquad (5c)$$

If CP invariance holds in the leptonic sector, the lepton mixing matrix in each of the cases (1)-(4) should be real*)

The fields $\chi_k(x)$ satisfy a Lorentz invariant condition - the Majorana condition:

$$C\bar{\chi}_k^T(x) = \xi_k \chi_k(x), \qquad (6)$$

where ξ_k are arbitrary phase factors. Since the weak interaction is not invariant with respect to the charge conjugation, the phase factors ξ_k have no physical meaning. A convenient choice we shall use further is

$$\xi_k = \begin{cases} 1, & \text{if CP invariance does not hold in the leptonic sector} \\ \pm 1, & \text{if CP invariance holds.} \end{cases} \qquad (7)$$

The Majorana condition (6) reduces the number of the independent components in the four-component complex field $\chi_k(x)$ to two.

All four schemes of neutrino mixing (1)-(4) are possible in the gauge theories of electroweak interactions[3].

In the cases of mixing (1)-(4) the lepton charges L_e, L_μ, L_τ,... are obviously not conserved. Accordingly, the lepton number non-conserving processes $\mu^\pm \to e^\pm\gamma$, $\mu^\pm \to e^\pm e^+e^-$, $K^\pm \to \pi^\pm e^+\mu^-$, etc., are allowed. If Eq. (1) or Eq. (4) take place, the total lepton charge L will be preserved and the $\Delta L \neq 0$ processes such as the neutrinoless double β - ($(\beta\beta)_{0\nu^-}$) decay $(A,Z) \to (A,Z+2) + e^- + e^-$ will be forbidden. In contrast, the $(\beta\beta)_{0\nu}$-decay will be allowed if massive Majorana neutrinos which couple to the electron in the weak charged current exist[17] [as in the cases of Eqs. (2) and (3)].

Further, the mixings (1)-(4) imply the existence of neutrino oscillations[18),14)]. If the number of neutrinos with definite masses coincides with the number of flavour neutrinos [as in the cases (1) and (2)], only oscillations between active neutrinos $\overset{(-)}{\nu}_\ell \rightleftarrows \overset{(-)}{\nu}_{\ell'}$, ($\ell \neq \ell'$, $\ell' = e, \mu, \tau, \ldots$) are possible. The probability conservation implies that the probabilities of the

---

*) More precisely, one can always choose a specific convention for the CP phases of the charged lepton, neutrino and $W^\pm$-boson fields in which the lepton mixing matrix is real [for a detailed discussion of the case of mixing of Majorana neutrinos, see, e.g., Ref. 16)].

transitions $(\bar{\nu})_\ell \to (\bar{\nu})_{\ell'}$, $P(\bar{\nu})_{\ell'};(\bar{\nu})_\ell$ satisfy the conditions*):

$$\sum_{\ell'=e,\mu,\tau,\ldots} P_{(\bar{\nu})_{\ell'};(\bar{\nu})_\ell} = 1 \ , \quad \sum_{\ell=e,\mu,\tau,\ldots} P_{(\bar{\nu})_{\ell'};(\bar{\nu})_\ell} = 1 \ . \tag{8}$$

As is well known, the oscillations $(\bar{\nu})_\ell \to (\bar{\nu})_{\ell'}$ may lead to observable effects in the charged current weak interaction processes induced by the neutrinos (e.g., the reactions $\nu_\ell + N \to \ell' + X$, $\ell' \neq \ell$, may become possible at some distance from the neutrino source). However, as a consequence of (8), the ν_ℓ-N neutral current reactions will not be affected by the existence of the indicated transitions if the standard electroweak theory is correct as, according to it, the weak neutral current ν_ℓ-N interaction is universal for the neutrinos with different flavours.

This conclusion is not valid if in addition to the oscillations between active neutrinos $(\bar{\nu})_\ell \to (\bar{\nu})_{\ell'}$, oscillations between active and sterile neutrinos $\nu_\ell \to N_{\ell^\circ,L}$ $(\bar{\nu}_\ell \to \bar{N}_{\ell^\circ,R})$ or $\nu_\ell \to \bar{\nu}_{\ell^\circ,L}$ $(\bar{\nu}_\ell \to \nu_{\ell^\circ,R})$ take place**),19),20), as in the cases of mixing (3) and (4). The experimentally measured cross-section of the process $\nu_\ell + N \to (\text{neutrino}) + X$, for instance, may exhibit then a characteristic oscillatory dependence on the neutrino energy (or/and on the distance between the neutrino source and the detector). In any case, disappearance of active neutrinos on the way to the target should take place.

The preceding discussion indicates that the physical implications of the four possible types of mixing considered (1)-(4) are quite different. This can be used, in principle, to distinguish between them experimentally.

2.2 The mass terms

The effective source of neutrino mixing in the gauge theories of electroweak interactions is the neutrino mass term. The type of massive neutrinos arising in a given theory is determined by the symmetries the neutrino mass term and the theory as a whole have.

The mixing (1) can take place if RH neutrinos $\nu_{\ell^\circ R}$ (and LH antineutrinos $\bar{\nu}_{\ell^\circ L}$) exist and they are as many as the LH flavour neutrinos ν_ℓ: $\ell^\circ = \ell = e,\mu,\tau,\ldots,\sigma$. Then RH neutrino fields $\nu_{\ell R}(x)$ should be present in the theory describing the electroweak interactions. The neutrino mass term leading to (1) has the form[7] (Dirac mass term):

---

*) These can be shown to follow from the unitarity of the mixing matrices U^D and U^M.

**) The oscillations between active neutrinos are often referred to in the literature[19),20)] as oscillations of the first class, while those between active and sterile neutrinos are called second class oscillations.

$$\mathcal{L}_{\nu}^{D} = - \bar{\nu}_{\ell L}(x) M^{D}_{\ell\ell'} \nu_{\ell' R}(x) + h.c., \tag{9}$$

where M^D is a n×n matrix (M^D is complex if CP is not conserved in the leptonic sector and real, if CP is conserved). Obviously, $\mathcal{L}_{\nu}^{D}$ conserves the total lepton charge L. It is diagonalized in the same way as the quark mass terms appearing (in the weak eigenstate bases) in the standard theory and the matrix U^D is the leptonic analogue of the Cabibbo-Kobayashi-Maskawa mixing matrix.

The neutrinos with definite masses may be Majorana particles and the mixing (2) may take place, if the neutrino mass term is formed only by the fields of the ordinary LH flavour neutrinos[2] $\nu_{\ell L}(x)$ (Majorana mass term):

$$\begin{aligned}\mathcal{L}_{\nu}^{M} &= - \frac{1}{2} \left(C^{-1} \nu_{\ell L}(x)\right)^{T} M_{\ell\ell'} \nu_{\ell' L}(x) + h.c. = \\ &= - \frac{1}{2} \overline{\nu^{c}_{\ell R}}(x) M_{\ell\ell'} \nu_{\ell' L}(x) + h.c.,\end{aligned} \tag{10}$$

where C is the charge conjugation matrix ($C^{-1}\gamma_\mu C = -\gamma_\mu^T$, $C^T = -C$, $C^+ = C^{-1}$), M is n×n, in general, complex matrix and $\nu^{C}_{\ell R}(x) \equiv C\bar{\nu}^{T}_{\ell L}(x)$ is a RH field [transforming as $\nu_{\ell L}(x)$ under the proper Lorentz transformations). Since $C^T = -C$ and the fields $\nu_{\ell L}(x)$ obey the Fermi statistics, we have: $M^T = M$. Evidently, if M has the most general form possible, $\mathcal{L}_{\nu}^{M}$ will not conserve neither the lepton charges $L_e, L_\mu, L_\tau, \ldots$ nor the total lepton charge L. In particular, transition of a LH electron neutrino ν_e into a RH electron antineutrino $\bar{\nu}_e$ in one space-time point is possible due to $\mathcal{L}_{\nu}^{M}$ if $M_{ee} \neq 0$.

A complex symmetric matrix can be cast in a diagonal form with the help of the congruent transformation:

$$(U^{M})^{T} M U^{M} = m, \quad m_{ik} = \delta_{ik} m_k, \quad m_k \geq 0, \tag{11}$$

where U^M is a n×n unitary matrix, the lepton mixing matrix. Correspondingly, the mass term (10) can be diagonalized by introducing the fields:

$$\chi_k(x) = (U^{M})^{+}_{k\ell} \nu_{\ell L}(x) + (U^{M})^{T}_{k\ell} \nu^{c}_{\ell R}(x), \quad k = 1, 2, \ldots, n. \tag{12}$$

As follows from (12), the field $\chi_k(x)$ with mass m_k satisfies the Majorana condition:

$$C\bar{\chi}_k^{T}(x) = \chi_k(x). \tag{13}$$

Consequently, the neutrinos with definite mass χ_k in the case under consideration are Majorana particles. Inverting the relations (12) for the LH components of the fields $\chi_k(x)$, we arrive at (2).

Suppose next that CP is conserved in the leptonic sector[16),21)]. Under the

CP transformation we have:

$$\nu_{\ell L}(x) \xrightarrow{CP} \eta_{CP}(\nu_{\ell L})\gamma_4 C\bar{\nu}^T_{\ell L}(x'),\quad x' = (-\vec{x}, ix_0),\quad \ell = e,\mu,\tau,\ldots,\sigma, \tag{14}$$

where $\eta_{CP}(\nu_{\ell L})$ are unphysical phase factors. A convenient choice of the latter for our considerations is

$$\eta_{CP}(\nu_{\ell L}) = i,\quad \ell = e,\mu,\tau,\ldots,\sigma. \tag{15}$$

Using (14) and (15) it is not difficult to show that the neutrino mass Lagrangian (10) would be CP invariant if M is a real matrix:

$$M = M^*. \tag{16}$$

A real symmetric matrix can be diagonalized by means of the orthogonality transformation:

$$(U^M)^T M U^M = m',\ (U^M)^* = U^M,\ (U^M)^T = U^{M-1}$$
$$m'_{ik} = \delta_{ik} m'_k,\quad i,k = 1,2,\ldots,n. \tag{17}$$

The non-zero eigenvalues of a real symmetric matrix can be positive or negative:

$$m'_k = \rho_k m_k,\quad m_k > 0,\quad \rho_k = \pm 1. \tag{18}$$

It follows from (17) and (18) that the mass Lagrangian (10) can be reduced to a diagonal form by introducing the fields

$$\chi_k(x) = (U^M)^T_{k\ell}\left(\nu_{\ell L}(x) + \rho_k \nu^c_{\ell R}(x)\right),\quad k = 1,2,\ldots,n. \tag{19}$$

The field $\chi_k(x)$ possesses a mass m_k ($m_k > 0$) and satisfies the Majorana condition:

$$C\bar{\chi}^T_k(x) = \rho_k \chi_k(x)\quad (\rho_k = \rho_k). \tag{20}$$

Using (14), (15), (19) and (20) it is not difficult to show that under the CP transformation

$$\chi_k(x) \xrightarrow{CP} \eta_{CP}(\chi_k)\gamma_4 \chi_k(x'), \tag{21}$$

where

$$\eta_{CP}(\chi_k) = i\rho_k \tag{22}$$

is the CP parity of the field $\chi_k(x)$. To summarize, if CP invariance holds in the leptonic sector and the neutrinos possess a Majorana mass term, then[22),16),21)]:

(i) the neutrinos with definite mass are Majorana particles which have a definite CP parity;

(ii) the CP parity of a massive Majorana neutrino (particle) can take the values (+i) or (-i); correspondingly, two types of massive Majorana neutrinos differing by their CP parities may exist[14)];

(iii) the CP parity of the Majorana neutrinos is determined by the signs of the corresponding eigenvalues of the neutrino mass matrix*).

Finally, let us note that in the simple case of two lepton flavours (ℓ=e,μ), the eigenvalues $m'_{1,2}$ of the neutrino mass matrix M and the mixing angle θ appearing in the mixing matrix

$$U^M = \begin{pmatrix} \sin\theta & -\cos\theta \\ \cos\theta & \sin\theta \end{pmatrix} \tag{23}$$

are determined by the elements of M as follows[12]:

$$m'_{1,2} = \frac{1}{2}\left\{ M_{ee} + M_{\mu\mu} \pm \sqrt{(M_{ee} - M_{\mu\mu})^2 + 4M_{\mu e}^2} \right\}, \tag{24}$$

$$tg\,2\theta = \frac{2M_{\mu e}}{M_{\mu\mu} - M_{ee}}, \quad \sin 2\theta = \frac{2M_{\mu e}}{\sqrt{(M_{ee} - M_{\mu\mu})^2 + 4M_{\mu e}^2}}. \tag{25}$$

We shall give next an example of a neutrino mass term leading to the case of mixing in which the number of neutrinos with definite mass exceeds the number of lepton flavours. If RH neutrinos $\nu_{\ell R}$ (ℓ=e,μ,τ,...,σ) exist as counterparts of the LH flavour neutrinos ν_ℓ (i.e., they are as many as the LH neutrinos), the most general neutrino mass Lagrangian has the form[13] (Dirac + Majorana mass term):

$$\mathcal{L}_\nu^{D+M} = -\frac{1}{2}\left\{ \overline{\nu^c_{eR}}(x) M^L_{ee'} \nu_{e'L}(x) + 2\,\overline{\nu_{eR}}(x) M^D_{ee'} \nu_{e'L}(x) + \right.$$
$$\left. + \overline{\nu_{eR}}(x) M^R_{ee'} \nu^c_{e'L}(x) \right\} + h.c., \tag{26}$$

where M^L, M^D and M^R are n×n complex matrices and $\nu^C_{\ell L}(x) \equiv C\,\bar{\nu}^T_{\ell R}(x)$ is a LH field [transforming as $\nu_{\ell R}(x)$ under the proper Lorentz transformation]. As like the mass matrix in the case of Majorana mass term (10), the matrices M^L and M^R are symmetric: $(M^{L,R})^T = M^{L,R}$. Obviously, $\mathcal{L}_\nu^{D+M}$ in its most general form does not conserve the lepton charges $L_e, L_\mu, L_\tau, \ldots$ and L.

The diagonalization of $\mathcal{L}_\nu^{D+M}$ is performed in the same way as the diagonalization of $\mathcal{L}_\nu^M$ [13]. The neutrinos with definite mass χ_k are Majorana particles. They are twice as many as the number of lepton flavours: k = 1,2,...,2n. The Majorana neutrino fields χ_k are given by:

$$\chi_k(x) = (V^M)^+_{k\ell}\,\nu_{eL}(x) + (V^M)^T_{k\ell}\,\nu^c_{eR}(x) +$$
$$+ (V^M)^+_{k\bar{\ell}}\,\nu^c_{eL}(x) + (V^M)^T_{k\bar{\ell}}\,\nu_{eR}(x) = C\,\bar{\chi}^T_k(x), \tag{27}$$

---

*) It can be shown that these results are general and do not depend on the CP phase convention used.

where V^M is 2n×2n unitary mixing matrix*). Using the unitarity of V^M one can express $\nu_{\ell L}(x)$ and $\nu^C_{\ell R}$ as linear combinations of the LH components of the fields $\chi_k(x)$, which leads to Eq. (3).

The implications of CP invariance in the leptonic sector in the case of the (Dirac+Majorana) neutrino mass term are very similar to those obtained in the case of the Majorana mass term. The matrix V^M can be considered to be real, sign factors ρ_k associated with the CP parity $\eta_{CP}(\chi_k)$ appear in the decomposition (27) multiplying the terms with the RH fields $[\nu^C_{\ell R}(x)$ and $\nu_{\ell R}(x)]$ as well as in the Majorana condition for the fields $\chi_k(x)$ [see Eqs. (19) and (20)].

Let us note finally that the mixing (4) may arise in theories with mirror fermions[23].

2.3 Massive Dirac and massive Majorana neutrinos: comparison of the properties

Let us consider now in more detail the properties of a Majorana neutrino having a field $\chi(x)$,

$$C\bar{\chi}_k^T(x) = \xi\chi(x), \quad \xi = \begin{cases} 1, & \text{if CP invariance does not hold} \\ & \text{in the leptonic sector} \\ \pm 1, & \text{if CP invariance holds} \end{cases} \tag{28}$$

and compare them with the properties of a Dirac neutrino ν [whose field we shall denote by $\nu(x)$].

First, it is not difficult to show using Eq. (28) that the particle and the antiparticle creation and annihilation operators in $\chi(x)$ coincide. Therefore, $\chi(x)$ is the field of a particle identical with its antiparticle, i.e., a truly neutral spin-$\frac{1}{2}$ object which cannot carry additive quantum numbers as lepton charge, fermion number, weak hypercharge, etc. Hence, in contrast to the Dirac neutrino fields, the Majorana fields cannot be subject to continuous global phase transformations $\chi(x) \to e^{i\alpha}\chi(x)$ (they cannot "absorb" phases). Such transformations are incompatible with the Majorana condition (28).

Second, besides the standard lepton (fermion) number conserving propagator $\overbrace{\chi_\alpha(x)\,\bar{\chi}_\beta(y)}$ the Majorana neutrino has a non-trivial lepton (fermion) number non-conserving propagator:

$$\overbrace{\chi_\alpha(x)\,\bar{\chi}^T_\beta(y)} = \xi C_{\beta\delta}\overbrace{\chi_\alpha(x)\,\bar{\chi}_\delta(y)} \neq 0 \,. \tag{29}$$

Obviously, $\overbrace{\nu_\alpha(x)\nu_\beta(y)} = 0$.

---

*) The first n rows in V^M are formed by the elements $V_{\ell k}$ and the second n rows are formed by $V^M_{\bar{\ell}k}$ ($\ell,\bar{\ell} = e,\mu,\tau,\ldots,\sigma$; $k = 1,2,\ldots,2n$).

Third, it is easy to show, using Eq. (28), that

$$\bar{\chi}(x)\sigma_{\mu\nu}\chi(x) = 0, \quad \bar{\chi}(x)\sigma_{\mu\nu}\gamma_5\chi(x) = 0, \quad \bar{\chi}(x)\gamma_\mu\chi(x) = 0. \tag{30}$$

The first two equations in (30) imply that the massive Majorana neutrinos cannot possess intrinsic magnetic or electric dipole moments, which is not valid, in general, for the massive Dirac neutrinos.

Finally, the CPT and CP transformation properties of the massive Dirac and the massive Majorana neutrinos are very different. Since Majorana particles have no distinctive antiparticles, the CPT and the CP transformations leave Majorana particle states essentially unchanged*). In contrast, they transform a state of a Dirac neutrino into a state of a different particle - its antiparticle. Furthermore, in the case of CP conservation, Majorana neutrinos possess a definite CP parity [see Eq. (21)]:

$$|\chi(r,p)\rangle \xrightarrow{CP} \eta^*_{CP}(\chi)\,|\chi(-r,p_P)\rangle, \quad \eta^*_{CP}(\chi) = \pm i, \quad p_P = (-\vec{p}, ip_0), \tag{31}$$

where $|\chi(r,p\rangle$ denotes a state of χ with definite four-momentum $p = (\vec{p}, ip_0)$ and projection r of the spin on the momentum $\vec{p}$. As was noticed first by Wolfenstein[22], the relative CP parity of Majorana neutrinos is an observable quantity and may play a fundamental role in the processes involving real or virtual neutrinos such as the $(\beta\beta)_{0\nu}$-decay, neutrino radiative decays, etc. Obviously, massive Dirac neutrinos have no such a characteristic.

2.4 Some specific examples

We have seen that the neutrinos with definite mass in the case of the Majorana mass term which does not conserve any lepton charge are Majorana particles. Let us consider next two specific examples of Majorana mass terms which have Dirac mass eigenstates. To simplify the discussion, we shall assume that CP is conserved in the leptonic sector [i.e., that the neutrino mass matrix M in Eq. (10) is real] and that only two lepton families, those of the electron and of the muon, exist. In this case, in Eqs. (17)-(22) n = 2 and U^M and $m'_{1,2}$ are given by Eqs. (23)-(25).

(i) Pseudo-Dirac neutrino

Suppose that the diagonal elements in the neutrino mass matrix satisfy

$$M_{ee} + M_{\mu\mu} = 0. \tag{32}$$

---

*) The indicated specific CPT and CP transformation properties of the Majorana particle states have interesting implications for, e.g., the production of Majorana fermions in e^+-e^- annihilation and p-$\bar{p}$ collisions[24),25)].

From (24) and (18), we obtain in this case, for the masses of the Majorana neutrinos χ_1 and χ_2:

$$m_1 = m_2 = \sqrt{M_{\mu\mu}^2 + M_{\mu e}^2} = m, \qquad \eta_1 = 1, \quad \eta_2 = -1. \tag{33}$$

The mass Lagrangian has the form

$$\mathcal{L}_D^M = -\frac{1}{2} m \left(\bar{\chi}_1(x)\chi_1(x) + \bar{\chi}_2(x)\chi_2(x)\right). \tag{34}$$

Instead of $\chi_1(x)$ and $\chi_2(x)$, let us introduce the field

$$\psi(x) = \frac{1}{\sqrt{2}}\left(\chi_1(x) - i\chi_2(x)\right). \tag{35}$$

Since $C\bar{\chi}_1^T(x) = \chi_1(x)$ and $C\bar{\chi}_2^T(x) = -\chi_2(x)$, one has:

$$C\bar{\psi}^T(x) = \frac{1}{\sqrt{2}}\left(\chi_1(x) + i\chi_2(x)\right). \tag{36}$$

Using (34), (35) and (36) we get:

$$\mathcal{L}_D^M = -m\bar{\psi}(x)\psi(x). \tag{37}$$

It follows from (35)-(37) that $\psi(x)$ is a complex four-component $[C\bar{\psi}^T(x) \neq \psi(x)]$ field of a neutrino with mass m. Thus, we have shown that the fields of two Majorana particles possessing equal masses and opposite CP parities are equivalent to the field of one Dirac particle having the same mass. It follows from (19), (23), (25), (35) and (36) that the LH flavour neutrino fields $\nu_{eL}(x)$ and $\nu_{\mu L}(x)$ are connected with $\psi_L(x)$ and $\psi_L^C(x)$ $[\psi_L^C(x) = \frac{1}{2}(1+\gamma_5)\psi^C(x)$, $\psi^C(x) = C\bar{\psi}^T(x)]$ as follows:

$$\nu_{eL}(x) = \psi_L(x)\cos\theta' - \psi_L^c(x)\sin\theta', \qquad \nu_{\mu L}(x) = \psi_L(x)\sin\theta' + \psi_L^c(x)\cos\theta', \tag{38}$$

where

$$\theta' = \frac{\pi}{4} - \theta, \quad \operatorname{tg} 2\theta' = \frac{M_{\mu\mu}}{M_{\mu e}}, \quad \sin 2\theta' = \frac{M_{\mu\mu}}{\sqrt{M_{\mu\mu}^2 + M_{\mu e}^2}}. \tag{39}$$

The mass term (37) is invariant with respect to a global gauge transformation of the complex field $\psi(x)$. However, the lepton charge associated with this invariance (in the general case of $\theta' \neq 0$) is not conserved by the standard weak interaction. This is evident from the expression (38) for the neutrino fields entering into the weak charged lepton current. As a consequence, the weak interaction generates a Majorana mass for ψ which is much smaller than its Dirac mass. Effectively, it lifts the mass degeneracy between χ_1 and χ_2 splitting the Dirac neutrino ψ into two Majorana neutrinos with very close but different masses. In view of this the neutrino ψ is called pseudo-Dirac[10].

Both oscillations of neutrinos and processes like $\mu^{\pm} \to e^{\pm}+\gamma$ and $(\beta\beta)_{o\nu}^-$

decays are allowed in the case of pseudo-Dirac neutrinos. In fact, all processes typically associated with the existence of massive Majorana neutrinos are allowed even in the limit of zero Majorana mass corrections to the mass of the pseudo-Dirac neutrino[11),26)]. Finally, it should be noted that a weak β-decay Lagrangian which implies, in essence, a pseudo-Dirac neutrino was discussed a long time ago by Pauli[27)].

(ii) Non-standard Dirac neutrino

Let us assume that in the Majorana mass matrix

$$M_{ee} = M_{\mu\mu} = 0, \quad M_{\mu e} > 0. \tag{40}$$

As follows from (24), the masses of the Majorana neutrinos χ_1 and χ_2 coincide in this case

$$m_1 = m_2 = M_{\mu e} = m, \tag{41}$$

while their CP parities are opposite

$$\eta_{CP}(\chi_1) = i, \quad \eta_{CP}(\chi_2) = -i. \tag{42}$$

We have just shown that if the conditions (41) and (42) are fulfilled, the Majorana mass term is reduced to a Dirac mass term. In the case under consideration, the neutrino mass term has the form:

$$\begin{aligned} \mathcal{L}_\nu^M &= -\frac{1}{2} m \left(\overline{\nu^c_{\mu R}}(x) \nu_{eL}(x) + \overline{\nu^c_{eR}}(x) \nu_{\mu L}(x) \right) + h.c. = \\ &= -\frac{1}{2} m \left(\left(C^{-1}\nu_{\mu L}(x)\right)^T \nu_{eL}(x) + \left(C^{-1}\nu_{eL}(x)\right)^T \nu_{\mu L}(x) \right) + h.c. \end{aligned} \tag{43}$$

Obviously, the Lagrangian (43) conserves the ZKM lepton charge[8)] $L' = L_e - L_\mu$. This implies that the neutrino with definite mass is a Dirac particle. Indeed, $\mathcal{L}_\nu^M$ given by (43) is diagonalized by introducing the four-component complex (i.e., Dirac) field $\nu(x)$ so that

$$\nu_L(x) = \nu_{eL}(x), \quad \nu_R(x) = \nu^c_{\mu R}(x) \quad \left(C\bar{\nu}^T(x) \neq \nu(x)\right). \tag{44}$$

The weak lepton charged and neutral neutrino currents have then the form:

$$\begin{aligned} j_\alpha^-(x) &= 2\left\{ \bar{e}_L(x)\gamma_\alpha \nu_L(x) + \bar{\mu}_L(x)\gamma_\alpha \nu_L^c(x) \right\} \\ j_\alpha^{0\nu}(x) &= \bar{\nu}_L(x)\gamma_\alpha \nu_L(x) + \bar{\nu}_L^c(x)\gamma_\alpha \nu_L^c(x), \quad \nu_L^c(x) = C\bar{\nu}_R^T(x) \end{aligned} \tag{45}$$

It follows from (45) that the charge L' conserved by the neutrino mass term is conserved also by the weak interactions. This constitutes the basic difference with the case of pseudo-Dirac neutrino. The mass of the neutrino ν does not receive weak Majorana corrections and, consequently, ν is a true Dirac neutrino.

Let us note that the physical properties of the massive Dirac neutrinos

arising in a theory with Majorana mass term (10) [i.e., no sterile neutrinos], in which the ZKM lepton charge (or some generalization of it) L' is conserved, are very different from the properties of the massive Dirac neutrinos arising as eigenstates of the Dirac mass term (9) when the total lepton charge L is conserved*),10),28). This difference stems from the fact that whereas only the LH components of the standard Dirac neutrino fields are "active" [see Eqs. (1) and (9)], both the LH and the RH components of the non-standard Dirac neutrino fields enter, as is indicated by Eq. (45), into the weak lepton currents.

We shall formulate next some general results concerning the relation between the neutrino mass spectrum as well as the varieties of massive neutrinos generated by a Majorana mass term $\mathcal{L}_{\nu}^{M}$ [Eq. (10)] and the symmetries it has in the case of n types (flavours) of neutrinos ν_{ℓ}. The necessary and sufficient condition for the appearance of massive Dirac neutrinos in a theory with neutrino mass term of Majorana type $\mathcal{L}_{\nu}^{M}$ is the existence of at least one conserve lepton charge9),10),15),29). Let us consider for simplicity the case of one conserved lepton charge L'. The structure of the Majorana mass term [see Eq. (10)] implies that any conserved lepton charge should be, in general, a non-standard linear combination of the ordinary lepton charges L_{ℓ}:

$$L' = \sum_{\ell = e,\mu,\tau,\ldots} n_{\ell} L_{\ell} \ , \quad n_{\ell} = \pm 1, 0 \ , \quad \ell = e,\mu,\tau,\ldots\sigma . \tag{46}$$

($n_{\ell} \neq 0$ at least for one ℓ). The number of massive Dirac neutrinos N_D as well as the number of massless neutrinos N_o are determined by the explicit form of this combination15),29):

$$N_D = \min\left(n_+(L'), n_-(L')\right)$$
$$N_0 = \left|n_+(L') - n_-(L')\right| , \tag{47}$$

where $n_+(L')(n_-(L'))$ is the number of ordinary lepton charges L_{ℓ} which enter into the expression for L' with plus (minus) sign**). For $\min(n_+(L'),n_-(L')) \neq 0$, the lepton charge L' given by (46) is, obviously, a generalization of the ZKM lepton

---

*) The latter are sometimes referred to as standard Dirac neutrinos, while the former are called non-standard Dirac neutrinos.

**) The diagonalization of the neutrino mass term $\mathcal{L}_{\nu}^{M}$ may reveal that some of these $(\min(n_+(L'),n_-(L'))$ Dirac neutrinos are massless. It can be shown, however, that they acquire radiatively induced Dirac mass terms at two-loop level [the diagrams, generating these Dirac mass corrections are similar to the two-loop diagrams discussed in Ref. 30)]. Let us add also that if several lepton charges are separately conserved, the total numbers of massive Dirac and massless neutrinos are given, respectively, by the sums of the numbers of massive Dirac and massless neutrinos associated with each of the conserved lepton charges via the formulae given above.

charge. As a consequence, the properties of the Dirac neutrinos arising as a result of the conservation of the charge L' are analogous to the properties of the ZKM (i.e., non-standard) Dirac neutrino.

Consider, for illustration, the case of three flavour neutrinos ν_e, ν_μ and ν_τ, possessing a Majorana mass term which conserves the charge $L' = L_e - L_\mu + L_\tau$, conserved also by the weak interactions[11),31)]

$$\mathcal{L}_\nu^{'M} = -\frac{1}{2}\left(\bar{\nu}^c_{eR}\ \bar{\nu}^c_{\mu R}\ \bar{\nu}^c_{\tau R}\right)\begin{pmatrix} 0 & M_{e\mu} & 0 \\ M_{e\mu} & 0 & M_{\mu\tau} \\ 0 & M_{\mu\tau} & 0 \end{pmatrix}\begin{pmatrix} \nu_{eL} \\ \nu_{\mu L} \\ \nu_{\tau L} \end{pmatrix} + h.c.$$

It is not difficult to show that this mass term conserves CP and therefore $M_{e\mu}$ and $M_{\mu\tau}$ should be real parameters. The diagonalization of $\mathcal{L}_\nu^{'M}$ leads to one massless Majorana neutrino χ_1 and two massive Majorana neutrinos χ_2 and χ_3, which are degenerate-in-mass, possess opposite CP parities and are equivalent to a massive Dirac neutrino ν:

$$\begin{pmatrix} \nu_{eL} + \nu^c_{eR} \\ \nu_{\mu L} + \nu^c_{\mu R} \\ \nu_{\tau L} + \nu^c_{\tau R} \end{pmatrix} = \begin{pmatrix} \chi_1 \cos\theta + \frac{1}{\sqrt{2}}(\chi_2 + \gamma_5\chi_3)\sin\theta \\ \frac{1}{\sqrt{2}}(-\chi_2 + \gamma_5\chi_3) \\ -\chi_1 \sin\theta + \frac{1}{\sqrt{2}}(\chi_2 + \gamma_5\chi_3)\cos\theta \end{pmatrix} = \begin{pmatrix} \chi_1 \cos\theta + (\nu_L + C\bar{\nu}_L^T)\sin\theta \\ -\nu_R + C\bar{\nu}_R^T \\ -\chi_1 \sin\theta + (\nu_L + C\bar{\nu}_L^T)\cos\theta \end{pmatrix}.$$

Here $tg\theta = (M_{e\mu}/M_{\mu\tau})$, $\nu(x) = 1/\sqrt{2}(\chi_2(x)+\chi_3(x))$ and $\eta_{CP}(\chi_1) = \eta_{CP}(\chi_2) = i$, $\eta_{CP}(\chi_3) = -i$.

The mass of χ_2 and χ_3, and consequently of ν is given by $m = \sqrt{M^2_{e\mu} + M^2_{\mu\tau}}$. As a consequence of the conservation of the lepton charge $L' = L_e - L_\mu + L_\tau$, $(-)$ $(-)$ oscillations are allowed, while $\nu_e \leftrightarrow \nu_\tau$ $(-)$ cannot take part in the oscillations. ν_μ Obviously, the $(\beta\beta)_{o\nu}^-$ decay is forbidden but the processes $\mu^- + (A,Z) \to e^+ + (A,Z-2)$, $\tau^- \to e^- + \gamma$, $\tau^- \to e^- + e^+ + e^-$, $\tau^- \to e^- + \mu^+ + \mu^-$, etc., are not. However, the predicted cross-section for the $\mu^- - e^+$ conversion and the rates for the indicated τ decays are unobservably small if the Dirac neutrino mass m does exceed a few MeV[32),31)].

Let us note finally that pseudo-Dirac neutrinos can appear in a scheme with Majorana mass term $\mathcal{L}_\nu^M$ if $\mathcal{L}_\nu^M$ possesses global symmetries which are not symmetries, e.g., of the weak interaction[10),15)].

3. - MAJORANA NEUTRINOS, NEUTRINO OSCILLATIONS AND $(\beta\beta)_{o\nu}^-$ DECAY: A FEW REMARKS

If neutrinos turn out to be massive, the question about the type of massive neutrinos (Dirac or Majorana) will inevitably arise. This will be a fundamental question to answer as it will concern the very nature of the neutrinos as well as

the basic symmetries and the structure of the theory of electroweak interactions. As was shown in Refs. 33) and 34), it is impossible to determine the type of massive neutrinos in experiments by studying neutrino oscillations. In fact, it is possible to conclude on the basis of the existing large number of studies[3] that the effects associated only with the existence of massive Majorana neutrinos are very subtle, being of the order of $(m_k/E)^2$, where E is some characteristic energy scale typical for the given process involving real or virtual neutrinos. If neutrinos have masses smaller than 100 eV, most sensitive to such effects seem at present the experiments searching for $(\beta\beta)_{0\nu}^-$ decay. We would like to conclude with a few remarks concerning the elementary particle aspects of the $(\beta\beta)_{0\nu}^-$ decay theory.

We shall assume that the $(\beta\beta)_{0\nu}^-$ decay proceeds via the exchange of Majorana neutrinos coupled to the electron in the weak charged current. If weak RH currents exist, three types of contributions in the $(\beta\beta)_{0\nu}^-$ decay amplitude $A_{(\beta\beta)_{0\nu}}$ are possible[35]: (to leading order in the perturbation theory in the Fermi coupling constant G_F):

$$A_{(\beta\beta)_{0\nu}} = A^{LL}_{(\beta\beta)_{0\nu}} + A^{LR}_{(\beta\beta)_{0\nu}} + A^{RR}_{(\beta\beta)_{0\nu}} \qquad (48)$$

where $A^{LL(RR)}_{(\beta\beta)_{0\nu}}$ denotes the contribution generated by the operator in the S-matrix containing the product of two LH (RH) charged lepton currents, while $A^{LR}_{(\beta\beta)_{0\nu}}$ denotes the contribution generated by the operator containing the product of LH and RH charged lepton currents. We shall be interested in the dependence of $A^{LL}_{(\beta\beta)_{0\nu}}$, $A^{LR}_{(\beta\beta)_{0\nu}}$ and $A^{RR}_{(\beta\beta)_{0\nu}}$ on the neutrino masses.

Assuming that the weak eigenstate neutrino fields $\nu_{eL}(x)$ and $\nu_{eR}(x)$ coupled to the electron field in the LH and RH charged lepton currents are given by

$$\nu_{eL}(x) = \sum_k U^L_{ek}\,\chi_{kL}(x), \quad \nu_{eR}(x) = \sum_k U^R_{ek}\,\chi_{kR}(x) \qquad (49)$$

where U^L and U^R are mixing matrices, and that the masses of the Majorana neutrinos χ_k ($m_k > 0$) do not exceed a few MeV, one has[22),16),21),35)]:

$$A^{LL(RR)}_{(\beta\beta)_{0\nu}} \sim \langle m\rangle^{L(R)} = \begin{cases} \sum_k m_k \left(U^{L(R)}_{ek}\right)^2, & \text{if CP is not conserved} \\ \sum_k m_k \frac{1}{i}\eta_{CP}(\chi_k)\left|U^{L(R)}_{ek}\right|^2, & \text{if CP is conserved} \end{cases} \qquad (50)$$

All the dependence of $A^{LL(RR)}_{(\beta\beta)_{0\nu}}$ on the neutrino masses m_k, is confined in the parameter $\langle m\rangle^{L(R)}$, information about whose value is extracted from the data. The dependence of $A^{LR}_{(\beta\beta)_{0\nu}}$ on m_k is determined by a factor in the corresponding matrix element which has the form:

$$A^{LR}_{(\beta\beta)_{0\nu}} \simeq \sum_k \int q^2 \frac{U^L_{ek} U^R_{ek}}{q^2 + m^2_k} \xi_k \qquad (51)$$

where q is the momentum of the virtual neutrino χ_k, $(q^2+m_k^2)^{-1}$ is the neutrino propagator and ξ_k is the sign factor in the Majorana condition for $\chi_k(x)$ [see Eqs. (6) and (7)]. Obviously, in the limit of zero neutrino masses $A^{LL(RR)}_{(\beta\beta)_{0\nu}} = 0$. Let us consider briefly the behaviour of $A^{LR}_{(\beta\beta)_{0\nu}}$ in this limit.

If the neutrino mixing is introduced phenomenologically[27], the mixing matrices U^L and U^R need not be related. It follows then from Eq. (51) that even if $m_k = 0$, $A^{LR}_{(\beta\beta)_{0\nu}}$ may be different from zero. Thus one arrives at the well-known conclusion[36),37)] that if RH currents exist, the $(\beta\beta)_{0\nu}$-decay can take place even in the case of massless Majorana neutrinos. Although true in the framework of the phenomenological approach, this conclusion is not valid in the gauge theories of electroweak interactions and we are going to show that next. Indeed, the neutrino mixing results in the gauge theories from the diagonalization of the neutrino mass term. Since RH neutrino fields ($\nu_{eR}(x)$,...) are assumed to be present in the theory, the mixing (49) can be generated only by a mass term of Dirac+Majorana type. As it follows from Eq. (27) and the discussion after it, the matrices U^L and U^R are not independent in this case: $U^L_{\ell k} = V^M_{\ell k}$, $U^R_{\ell k} = (V^M_{\ell k})^* \xi_k$ ($\xi_k = \rho_k$) where V^M is the unitary matrix diagonalizing the neutrino mass matrix. This implies that

$$\sum_k U^L_{ek} U^R_{ek} \xi_k = \sum_k V^M_{ek} (V^M)^+_{k\bar{e}} \xi^2_k = 0, \qquad (52)$$

the last equality being a consequence of Eq. (5c) ($\xi_k^2 = 1$). From Eqs. (51) and (52), we arrive at the conclusion that in the gauge theories with RH currents and neutrino mixing (51): (i) $A^{LR}_{(\beta\beta)_{0\nu}} = 0$ if $m_k = 0$, and (ii) for $m_k \neq 0$ the amplitude $A^{LR}_{(\beta\beta)_{0\nu}}$ is suppressed by a mechanism analogous to the GIM mechanism. Our considerations show that if the electroweak interaction is described by a gauge theory and the $(\beta\beta)_{0\nu}$-decay can be generated by the mechanism discussed, the observation of the $(\beta\beta)_{0\nu}$-decay would imply the existence of massive Majorana neutrinos irrespective of whether RH currents exist or not[38),*)].

Finally, let us note that contrary to what is often stated in the literature on the subject[40)], the $(\beta\beta)_{0\nu}$-decay rate is not bounded to be particularly suppressed in a theory with pseudo-Dirac neutrinos coupled to the electron[11)]. For example, in the scheme with pseudo-Dirac neutrino discussed (no RH currents) from (33), (35), (38), (39) and (50), we get

---

*) For a different analysis of the relation between the existence of the $(\beta\beta)_{0\nu}$-decay and the existence of massive Majorana neutrinos, see Ref. 39).

$$A_{(\beta\beta)_{0\nu}} \sim \langle m \rangle_{PD} = m \sin 2\theta',$$

where m is the mass of the pseudo-Dirac neutrino and θ' is the mixing angle. Note that $A_{(\beta\beta)_{0\nu}}$ is proportional to the mass of the pseudo-Dirac neutrino and not to the Majorana correction to the mass[11].

4. - CONCLUSION

We have seen that the existence of non-zero neutrino masses and neutrino mixing implies an extremely rich spectrum of possible neutrino properties. All schemes of mixing considered by us can be realized in the gauge theories of electroweak interactions[3]. It is our hope that one of them is relevant to the reality.

REFERENCES

1) W. Pauli - Letter (December 1, 1930) to a meeting of physicists in Tübingen [see, for example, Brown, Physics Today, September 1978].
2) F. Perrin - Comptes Rendus 197 (1933) 1625;
   E. Fermi - Nuovo Cimento 11 (1934) 1.
3) For a more extensive discussion, see, e.g., the review articles:
   G. Costa and F. Zwirner - Univ. of Padova Preprint DFPP 10/85 (April 1985), to appear in Rivista del Nuovo Cimento;
   J.D. Vergados - Physics Reports 133 (1986) Vol. 1,2;
   S.T. Petcov - Lecture Notes in Physics, Vol. 181, eds. J. Lindfors and R. Raitio, Springer Verlag (1983), p. 392.
4) T.D. Lee and C.N. Yang - Phys.Rev. 98 (1955) 101.
5) P.A.M. Dirac - Proc.Roy.Soc. A117 (1928) 610; ibid. A118 (1928) 351; ibid. A126 (1930) 360.
6) E. Majorana - Nuovo Cimento 14 (1937) 170.
7) S.M. Bilenky and B. Pontecorvo - Phys.Lett. 61B (1976) 248;
   S.E. Eliezer and D.A. Ross - Phys.Rev. D10 (1974) 3088;
   H. Fritzsch and P. Minkowski - Phys.Lett. 62B (1976) 72.
8) Ya.B. Zeldovich - DAN SSSR 86 (1952) 505;
   E.J. Konopinsky and H. Mahmoud - Phys.Rev. 92 (1953) 1045.
9) S.M. Bilenky and B. Pontecorvo - Phys.Lett. 102B (1981) 32.
10) L. Wolfenstein - Nucl.Phys. B186 (1981) 147.
11) S.T. Petcov - Phys.Lett. 110B (1982) 245.
12) V. Gribov and P. Pontecorvo - Phys.Lett. 28B (1969) 463.
13) S.M. Bilenky and B. Pontecorvo - Lett.Nuovo Cimento 17 (1976) 569.
14) B. Pontecorvo - Zh.Eksp. Teor.Fiz. 34 (1958) 247.
15) C.N. Leung and S.T. Petcov - Phys.Lett. 125B (1983).
16) S.M. Bilenky, N.P. Nedelcheva and S.T. Petcov - Nucl.Phys. B247 (1984) 61.
17) G. Racah - Nuovo Cimento 14 (1937) 322.
18) B. Pontecorvo - Zh.Eksper.Teor.Fiz. 33 (1957) 549.
19) V. Barger et al. - Phys.Rev.Lett. 45 (1980) 692.
20) J. Schechter and J.W.F. Valle - Phys.Rev. D22 (1980) 2227.
21) B. Kayser - Phys.Rev. D30 (1984) 1023.
22) L. Wolfenstein - Phys.Lett. 107B (1981) 77.
23) J. Maalampi and M. Roos - Phys.Lett. 146B (1984) 333.
24) S.T. Petcov - Phys.Lett. 139B (1984) 421.
25) S.M. Bilenky, E.Ch. Christova and N.P. Nedelcheva - Phys.Lett.161B(1985)397.
26) J.W.F. Valle - Phys.Rev. D27 (1983) 1672.

27) W. Pauli - Nuovo Cimento 6 (1957) 204.
28) S.T. Petcov - Phys.Lett. 115B (1982) 401.
29) D. Wyler and L. Wolfenstein - Nucl.Phys. B218 (1983) 205.
30) S.T. Petcov and S. Toshev - Phys.Lett. 143B (1984) 175.

31) M.J. Dugan et al. - Phys.Rev.Lett. 54 (1985) 2302.
J.W.F. Valle - Phys.Lett. 159B (1985) 49.
32) S.T. Petcov - Soviet J.Nucl.Phys. 25 (1977) 340, errata ibid. p. 698.
33) S.M. Bilenky, J. Hošek and S.T. Petcov - Phys.Lett. 94B (1980) 495.
34) M. Doi et al. - Phys.Lett. 102B (1981) 323.
35) For a review of the theory of $(\beta\beta)_{0\nu}$-decay, see, e.g.:
W.C. Haxton et al. - Progr. in Part. and Nucl.Phys. 12 (1984) 409;
M. Doi et al. - Osaka University Preprint OS-GE-85-03.
36) C.D. Enz - Nuovo Cimento 6 (1957) 250.
37) H. Primakoff and S.P. Rosen - Phys.Rev. 184 (1969) 1925.
38) B. Kayser, S.T. Petcov and S.P. Rosen - in preparation.
39) J. Schechter and J.W.F. Valle - Phys.Rev. D25 (1982) 2951;
J.F. Nieves - Phys.Lett. 147B (1984) 1375;
E. Takasugi - Phys.Lett. 149B (1984) 372.
40) See, e.g.: M. Doi et al. - Ref. 35).

SNEUTRINOS IN RARE KAON DECAY

A. HALPRIN
PHYSICS DEPARTMENT
UNIVERSITY OF DELAWARE
NEWARK, DE 19716
USA



Abstract

We consider in detail the impact of light (a few MeV or less) scalar neutrinos on the rare decay $K^+ \to \pi^+$ invisible. We argue that such SUSY particles, if they exist, should be produced at least as copiously as ordinary neutrino pairs and that the contributions of the neutrino and sneutrino channels to the pion energy spectrum are distinguishable.

One premise of this meeting is surely that neutrinos are nearly perfect. However, they might be even more engaging if they stopped their incessant spinning. This possibility was held out in the early seventies by the pioneers of supersymmetry (SUSY) in the form of, $\tilde{\nu}$, a spinless superpartner for the neutrino, which, in the limit of exact SUSY, should have a mass equal to that of ν.[1,2] Most, but not all,[3] realistic models prefer a SUSY mass splitting in the GeV range. Indeed, there are even experimental constraints on the scalar superpartners of electrons and quarks that support such models. However, no such direct experimental evidence exists for the scale of SUSY breaking between a neutrino and its scalar superpartner in any generation. Moreover, since neutrinos are so nearly perfect, it would be most appropriate for nature to leave neutrino SUSY sufficiently unbroken that it is recognizeable. We shall therefore consider the possibility that sneutrino-neutrino mass splitting is no more than a few MeV in at least one generation.

The consequences of light sneutrino emission in muon decay have recently been considered by Buchmuller and Scheck.[4] More specifically, they have calculated the modification of the electron energy spectrum in $\mu \to e$+invisible arising from the decay channel $\mu \to e\tilde{\nu}_\mu\tilde{\nu}_e$ proceeding through the diagram of Fig. 1. For sneutrino masses less than a few MeV they obtained a lower limit on the wino (the spin 1/2 partner of the the W gauge boson) mass of 320 GeV. However, the scalar neutrino channel rate vanishes if either one of the sneutrinos is too heavy. It is therefore essential to examine a reaction of the type $A \to B + \tilde{\nu}\tilde{\nu}$, where $\tilde{\nu}$ is the lightest sneutrino.

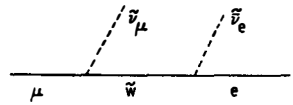


Figure 1

An interesting candidate reaction of this type is sneutrino pair production in the rare decay $K^+ \to \pi^+$ +invisible. An initial motivation for such experiments, which are now underway,[5] came from the observation by Deshpande and Eilam[6] that one could improve the experimental limit on

the τ neutrino mass by determining the location of a characteristic kink in the pion energy spectrum. The location of the kink is essentially the mass of the heavy neutrino in the standard decays $K^+ \to \pi^+ \nu_\mu \bar{\nu}_\mu$. It is therefore of some interest to compare the pion energy spectrum arising from the sneutrino channel with that due to the standard neutrino channel and identify, if possible, a SUSY signature. An analysis has been carried out together with Jose Nieves and Palash Pal[7] which I shall summarize below.

The elemental process which gives rise to the decay $K \to \pi \tilde{\nu} \tilde{\bar{\nu}}$ is $s \to d \tilde{\nu} \tilde{\bar{\nu}}$, and the Feynman diagrams for this process are given in Figures 2 and 3. Figure 2 contains all the neutral current mediated processes while Figure 3 displays the characteristic charged current box diagrams.

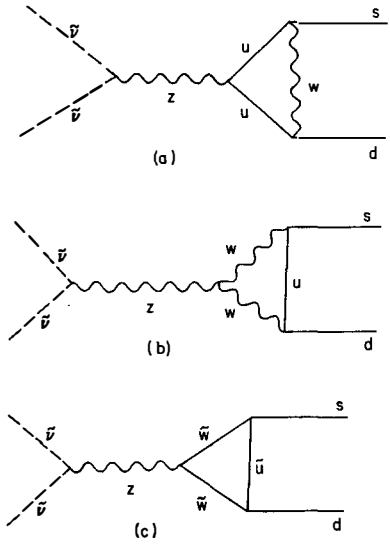


Figure 2

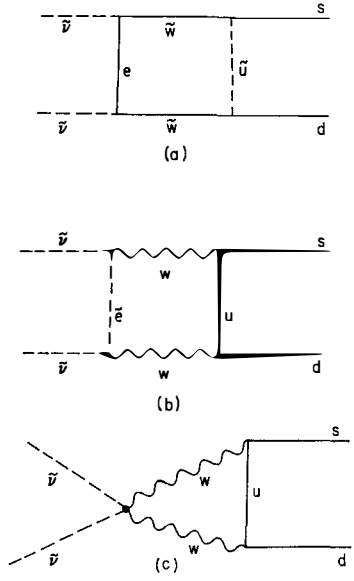


Figure 3

The transition amplitude that results can (at least for $m_s >> m_d$) be written as

$$t = C\ \bar{d}\ \gamma^{\mu}(1-\gamma_5)s\ \left[\ a(q_1-q_2)_{\mu} + b(q_1+q_2)_{\mu}\right] \tag{1}$$

where

$$C = \frac{G_F\alpha}{\sqrt{2}\ \pi\ \sin^2\theta_w} \tag{2}$$

q_1 and q_2 are, respectively, the momenta of $\tilde{\nu}$ and $\tilde{\bar{\nu}}$, and the factors a and b depend on details of the diagrams, including the plethora of unknown mass parameters. The physical $K^+ \to \pi^+\tilde{\nu}\tilde{\bar{\nu}}$ amplitude is then

$$T = C\left[\ f_+\ (q^2)(k+p)^{\mu} + f_-(q^2)\ (k-p)^{\mu}\ \right]$$

$$X\left[\ a\ (q_1-q_2)_{\mu} + b\ (q_1+q_2)_{\mu}\ \right] \tag{3}$$

where

$$q = q_1 + q_2 = k-p \tag{4}$$

k and p are the momenta of K^+ and π^+, respectively, and the form factors, f_+ and f_-, are known from K-$\pi\mu\nu$ decay. The pion energy spectrum arising from the sneutrino mode is then given by

$$\frac{d\Gamma(\nu\nu)}{dE} = \frac{1}{(2\pi)^5}\left(\frac{G_F\alpha}{\sin^2\theta_w}\right)^2 \frac{|\vec{p}|}{4m_K}\ \rho\ J \tag{5}$$

where

$$\rho = \left(1 - \frac{4m^2_{\tilde{\nu}}}{q^2}\right)^{\frac{1}{2}} \quad \text{and} \quad J = J(a,b) \tag{6}$$

It should be emphasized that the ratio a/b determines the shape of this spectrum. We find: the neutral current graphs of Fig. 2 do not contribute to b, Fig. 3c does not contribute to a, and Fig. 3a gives the ratio

$$\frac{a}{b} = \frac{-2(1-\chi)}{1+\chi} \quad \frac{1 + \frac{\chi}{1-\chi}\ln\chi}{1 + \frac{2\chi}{1-\chi^2}\ln\chi} \tag{7}$$

where

$$\chi = (m_{\tilde{u}}^2/m_{\tilde{w}}^2) \tag{8}$$

For the popular choice $m_{\tilde{w}}$=50 GeV and $m_{\tilde{u}}$=20 GeV, Eq. 8 yields a/b≃1. We therefore conclude that a/b is likely of order unity independent of details of the diagrams, and it is instructive to examine the spectrum in this case.

In Fig.4 we plot J for a/b=1 together with the analogous quantity for the $\nu\bar{\nu}$ channel. The curves are given for vanishing neutrino and sneutrino masses and each J is plotted relative to its maximum. The branching ratios for the two channels will be discussed later. The neutrino channel J vanishes at p=0 due to helicity suppression, in marked contrast to the sneutrino mode. For nonvanishing neutrino mass, $(J_\nu/J_{\nu max})/(J_{\tilde{\nu}}/J_{\tilde{\nu}max}) \sim m_\nu^2$ for p=0.

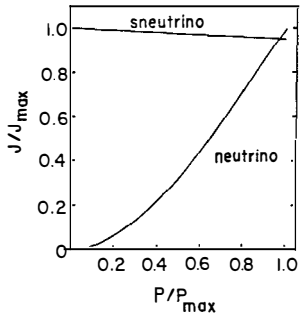


Figure 4

When comparing the branching ratios for the two channels, two special cases can be distinguished: (i) $m_{\tilde{w}}/m_w < 1$, $m_{\tilde{u}}/m_{\tilde{w}} < 1$, $m_{\tilde{e}}/m_{\tilde{w}} > 1$ and (ii) All superpartners except $\tilde{\nu}$ have masses $\gg m_w$. In the first

case, comparison of Fig.2 and 3 with the analogous graphs for the $\nu\bar{\nu}$ mode shows that the sneutrino channel is dominant. In the second case,Fig. (2a), (2b) and (3c) still survive and are the same order of magnitude as the $\nu\bar{\nu}$ amplitude.

We are led to conclude:(i) If light sneutrinos exist, they will be produced at least as copiously as neutrinos in $K^+ \to \pi^+$ invisible. (ii) The ν and $\tilde{\nu}$ channel contributions to the π^+ energy spectrum differ markedly at low energies and present an interesting observational challenge.

I wish to thank the particle theory group at the Israel Institute of Technology (Technion) for their hospitality while this talk was being prepared.

References

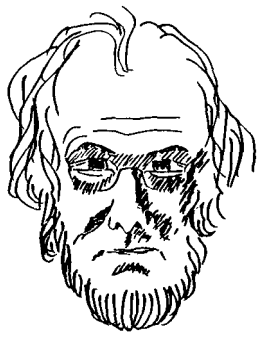
1) J. Wess and B. Zumino, Nucl. Phys. B70,39 (1974)
2) For a recent survey of SUSY see for example J. Ellis, Proceedings of the International Symposium on Lepton and Photon Physics, Ithica, New York, USA (1983)
3) For example,see L. Ibañez, Phys. Lett. 137B, 60 (1984)
4) W. Buchmuller and F. Scheck, Phys. Lett. 145B, 421 (1984)
5) Brookhaven experiment--Also see Kaon Factory Proposal, TRIUMF, September 1985
6) N.G. Deshpande and G. Eilam, Phys. Rev. Lett. 53, 2289 (1984). For extension to Majorana neutrinos see J.F. Nieves and P.B. Pal, Phys. Rev. D32, 1849 (1985)
7) A. Halprin, J.F. Nieves and P.B. Pal, University of Maryland preprint, 1986.

ON THE POSSIBLE ASTROPHYSICAL EVIDENCE FOR A RADIATIVELY DECAYING NEUTRINO

J. Maalampi
Research Institute for Theoretical Physics
University of Helsinki, Helsinki, Finland

K. Mursula
NORDITA, Copenhagen, Denmark

M. Roos
Department of High Energy Physics
University of Helsinki, Helsinki, Finland



ABSTRACT

We consider the possibility that the step-like structure observed in the cosmic background radiation at $\lambda = 1667 \pm 10$ Å would indicate radiative decays of massive cosmic neutrinos. In the standard electroweak theory the corresponding radiative lifetime is several orders of magnitude longer than observed, due to the purely left-handed structure of the charged weak currents. We point out that in models which include also right-handed currents, the lifetime can naturally be short enough to account for the astrophysical observations.

The cosmic ultraviolet background radiation may contain information on the decay of a big bang relic massive neutrino[1-4]. For a neutrino ν_2 with mass m_2 in the eV region, the radiative decay into a lighter neutrino ν_1

$$\nu_2 \to \nu_1 + \gamma , \tag{1}$$

would manifest itself as a monochromatic line at E_0 in the far UV spectrum. Decays during the distant past would redshift this line, producing a step-like increase at $E \leq E_0$.

A first hint of such a step reported[5] an increase in the intensity of the diffuse high-latitude spectrum from 260 ± 40 (in photons/s·cm^2·sr·Å units) in the range 1300 - 1525 Å, to $\sim$ 600 in the range 1680 - 1800 Å. However, since different detectors were used in the two wavelength bands, systematic errors could have caused the step.

Subsequently, rocket observations[6] with three UV broad band photometers covering the bandpasses 1450 - 1780 Å (peak sensitivity at 1590 Å), 1610 - 1950 Å (peak 1720 Å), and 1700 - 2420 Å (peak 2125 Å) indicated extragalactic diffuse radiation intensities of 550 ± 150, 900 ± 150, and $\lesssim$ 1300, respectively.

Recently, a compilation[7] of exposures at high galactic latitudes with the International Ultraviolet Explorer claims a step-like signal of 5σ significance at λ_0 = (1667 ± 10) Å in the otherwise flat continuum. This corresponds to a photon energy E_0 = 7.4 eV or, due to the relation $m_1^2 = m_2\,(m_2 - 2E_0)$, a neutrino mass of m_2 = 14.9 eV, assuming m_1 = 0 eV. Note that photons of this energy propagate freely through the intergalactic medium as well as through the interstellar medium and are consistent with the existence of neutral hydrogen clouds in galactic haloes[8].

The intensity change ΔI_0 at the step is[7] 454 ± 274, or within errors the same as in the previous observations[5,6]. One then deduces the lifetime of a hypothetical ν_2 from[1,2]

$$\tau_{obs} = \frac{c\, n(\nu_2)}{4\pi\, \Delta I_0\, H_0\, \lambda_0} , \tag{2}$$

where $n(\nu_2)$ is the number density of ν_2's in the Universe today. Assuming $n(\nu_2) \simeq 100$ cm^{-3} for the decaying neutrinos, one finds

$$2 \cdot 10^{15} \text{ yr} \lesssim \tau \lesssim 16 \cdot 10^{15} \text{ yr}. \tag{3}$$

Note that this result does not contradict the lower bound, $\tau \geq 3 \cdot 10^{15}$ yr, derived[2,3] from other astrophysical data. It is remarkable that the upper limit is several orders of magnitude smaller than the lifetime one would expect[9] within the standard $SU(2)_L \times U(1)_Y$ theory of electroweak interactions.

The effective matrix element for the decay (1) compatible with gauge invariance is of the general form[10]

$$\mathcal{M} = \varepsilon^{\mu}\, q^{\nu}\, \bar{\nu}_1(p_1)\sigma_{\mu\nu}(a + b\gamma_5)\nu_2(p_2), \tag{4}$$

where ε^{μ} and $q^{\nu} = (p_2 - p_1)^{\nu}$ are the polarization vector and the momentum of the photon, respectively. From (4) one derives

$$\frac{1}{\tau} = \Gamma(\nu_2 \to \nu_1\gamma) = \frac{1}{8\pi}\left(\frac{m_2^2 - m_1^2}{m_2}\right)^3 (|a|^2 + |b|^2) = E_0^3\,(|a|^2 + |b|^2)/\pi \tag{5}$$

The decay (1) in the standard model proceeds (in the unitary gauge) through the two one-loop diagrams shown in Fig. 1.

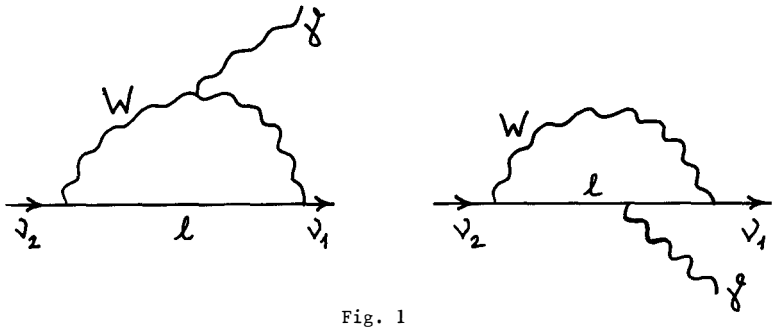


Fig. 1

A full standard model calculation[9] with $m_2 = 15$ eV and $m_1 = 0$ gives

$$\tau^{-1}_{\text{Stand.}} = \Gamma(\nu_2 \to \nu_1\gamma) = \frac{K\alpha G_F^2}{128\pi^4}\, m_2^5\, |\Sigma_{\ell} U_{1\ell} U_{2\ell} F(r_\ell)|^2 \simeq K(3\cdot 10^{23}\,\text{yr})^{-1}\, |\Sigma_{\ell} U_{1\ell} U_{2\ell} F(r_\ell)|^2 \tag{6}$$

where $K = 1$ (or 2) for Dirac (or Majorana) neutrinos, U is the leptonic mixing matrix and $F(r_\ell) = O(1)$ is a smooth function of $r_\ell = m_\ell/M_W$. With three light charged leptons ($r_\ell \ll 1$), the leading term in the sum is cancelled due to the unitarity of U, and the rate is thus additionally suppressed by the factor r_ℓ^2. Nevertheless, even if this GIM cancellation were avoided by adding new heavy generations[9] or by making the unitarity sum incomplete (e.g. with an extra singlet ν), the natural lower bound is $\tau \geq 10^{23}$ yr for a 15 eV neutrino in the $SU(2)_L \otimes U(1)_Y$ gauge theory.

The essential feature of Eq. (6) is that the scale is (apart from G_F) set solely by the mass of the neutrino as a consequence of the pure left-handed structure of $W^{\pm}$-lepton interactions in the standard model. Indeed, if the two $W\ell\nu_i$ vertices in the decay amplitude (see Fig. 1) are both of the same chirality, only the momentum part of the internal charged lepton propagator $(\not{p}_\ell - m_\ell)^{-1}$ contributes to the matrix element. All terms of the gauge invariant form (4) are then proportional to the neutrino mass, thus $\Gamma \sim m_2^5$. However, if the $W\ell\nu$

vertex would contain a right-handed piece, also the mass part of the lepton propagator would contribute to the amplitude.

In the first model based on the $SU(2)_L \times SU(2)_R \times U(1)$ gauge group, a RH neutrino $\nu_R(1,2,-1)$ can decay radiatively to an LH neutrino $\nu_L(2,1,-1)$, provided the vector bosons $W_R^{\pm}$ and $W_L^{\pm}$ mix (see Fig. 2). The lighter of the

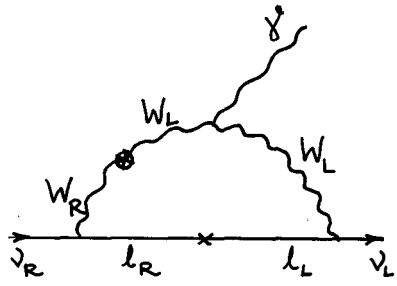


Fig. 2

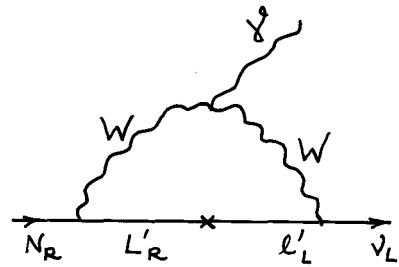


Fig. 3

two vector boson mass eigenstates, $W_1 \equiv \cos\zeta W_L + \sin\zeta W_R$, couples to leptons according to

$$\mathcal{L} = -W_1^{\mu} \frac{g}{\sqrt{2}} (\cos\zeta\, \bar{\nu}_L \gamma\, \ell_L + \sin\zeta\, \bar{\nu}_R \gamma_{\mu}\, \ell_R) + \text{h.c.}, \tag{7}$$

where ζ is the bosonic mixing angle. We neglect here the possible intergenerational mixing and the mixing between ν_L and ν_R, which are inessential to our argument. The contribution of the diagrams mediated by the heavier vector boson W_2 can be neglected since $M_{W_2} \geq 20\, M_{W_1} \simeq 1.6$ TeV from the $K_L - K_S$ mass difference and other low-energy constraints[14]. The decay width for $\nu_R \to \nu_L \gamma$ (or $\nu_L \to \nu_R \gamma$) is given by

$$\tau_{LR}^{-1} = \Gamma(\nu_R \to \nu_L \gamma) \simeq (4 \cdot 10^{13}\ \text{yr})^{-1} \left(\frac{E_0}{7.4\ \text{eV}}\right)^3 \left(\frac{m_\ell}{\text{MeV}}\right)^2 \sin^2 2\zeta \tag{8}$$

independently of the neutrino masses for fixed E_0.

The lifetime one deduces from astrophysics depends on the present cosmological density $n(\nu_R)$ of the ν_R. This may be smaller than the density of the standard LH neutrinos, $n(\nu_L) \simeq 100\ \text{cm}^{-3}$, since the more weakly interacting RH neutrinos decouple from the thermal equilibrium earlier[15]. If they decoupled after the muons were annihilated they would today be as abundant as the ν_L. This corresponds to the situation when $M_{Z_R} \gtrsim 3$ TeV. In this case we obtain, by comparing Eqs. (3) and (8), the condition

$$0.05 \leq \frac{m_\ell}{\text{MeV}} \sin 2\zeta \leq 0.14\,. \tag{9}$$

If ν_R belongs to the electron family, Eq. (9) requires $\zeta \gtrsim 0.05$. This possibility is clearly excluded since the experimental upper bound from the $K_L - K_S$ mass difference is $\zeta_{exp} \lesssim 0.004$[14]. On the other hand, the ν_R could still be a member of the μ or τ families: then Eq. (9) predicts $\zeta = (2\text{-}7)\cdot 10^{-4}$ or $\zeta = (1\text{-}4)\cdot 10^{-5}$, respectively.

If the ν_R density $n(\nu_R)$ is less than the standard neutrino density $n(\nu_L)$, the value of τ_{obs} in Eq. (3) is reduced by a factor $n(\nu_R)/n(\nu_L)$ and correspondingly larger values of the angle ζ are required.

In the mirror model[12] the situation is favourable in two respects. Firstly, the cosmological density of mirror neutrinos N_R is never suppressed since their neutral current interactions have the same strength as those of the standard LH neutrinos. Secondly, charged mirror leptons, L, must be heavy, $20 \lesssim m_L \lesssim 250$ GeV, and therefore the radiative width increases. The relevant part of the weak Lagrangian is given by[16]

$$\mathcal{L} = -W^\mu \frac{g}{\sqrt{2}} (-\sin\theta_\ell \bar{\nu}_L \gamma^\mu L_L + \cos\theta_\ell \bar{N}_R \gamma^\mu L_R) + \text{h.c.}, \tag{10}$$

where θ_ℓ is the ℓL mixing angle parametrizing the mixing between the weak eigenstates of the charged lepton ℓ and its mirror partner L. One typical diagram contributing to the decay $N_R \to \nu_L \gamma$ is shown in Fig. 3. The width is, independently of the neutrino masses for fixed E_0, given by

$$\tau^{-1}_{Mirror} = \Gamma(N_R \to \nu_L \gamma) \simeq K(2\cdot 10^5 \text{ yr})^{-1} \left(\frac{E_0}{7.4 \text{ eV}}\right) \left(\frac{m_L}{20 \text{ GeV}}\right) \sin^2 2\theta_\ell. \tag{11}$$

Comparing this to τ_{obs} of Eq. (3), we find for $20 \leq m_L \leq 250$ GeV

$$2\cdot 10^{-7} \lesssim \theta_\ell \lesssim 1\cdot 10^{-5} \tag{12}$$

which is far below the present experimental upper limit[16], $\theta_\ell \lesssim 0.1$. Let us note that values of the mixing angle in this range are suggested by some specific mirror models[17].

We conclude that the standard electroweak model cannot account for the short radiative lifetime, $\tau_{obs} \lesssim 10^{16}$ yr, of a massive neutrino, as suggested by astrophysical observations[5-7]. This is due to the purely LH structure of the weak interactions which makes the radiative width $\Gamma_{rad}(\nu_2 \to \nu_1 \gamma)$ proportional to $E_0^3 m_2^2$, where $E_0 = 7.4$ eV is the observed photon energy and m_2 is the mass of ν_2. Accordingly, in the standard model the radiative lifetime for neutrinos in the allowed range ($m_i \lesssim 50$ eV) is always larger than 10^{22} yr.

In non-standard electroweak models which encompass also RH currents, Γ_{rad} is proportional to $E_0^3 m_\ell^2$, where ℓ is a charged lepton. Consequently, the lifetime is shortened by the enormous factor $(m_\ell/m_2)^2$ compared to the standard model.

This enables RH models to explain the astrophysical observation[18]. The predictions for the model parameters are given in Eqs. (9) and (12), respectively. The implied small mixing angles would make it very hard to see the effects of RH interactions of known particles in laboratory experiments. However, N_R would contribute to the total width of Z^0 by an equal amount as the standard neutrino.

We note that ν_R or N_R will together with ν_{eL}, $\nu_{\mu L}$ and $\nu_{\tau L}$ saturate the famous cosmological bound of at most 4 light neutrinos, derived from the present helium abundance in the Universe. If this limit is taken seriously, the RH or mirror neutrinos of the other families should be much heavier or much more unstable than the one discussed here.

Although the astrophysical information used is controversial[5], or scanty[6], or preliminary[7], there is hope for very precise data in the near future, when the Berkeley Extreme Ultraviolet/Far Ultraviolet Shuttle telescope will be launched on the Space Shuttle[19].

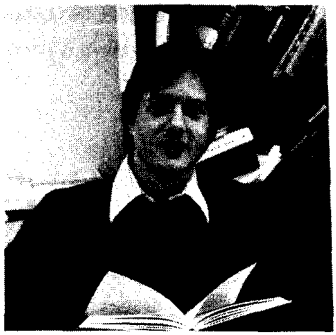
It is a pleasure to acknowledge the useful and stimulating discussion we have had (K.M. and M.R.) with D. Fargion, Rome, and (M.R.) with S. Bowyer and C. Martin, Berkeley. J.M. has been supported by Bundesministerium für Forschung und Technologie, Bonn, F.R. Germany.

REFERENCES

1. R. Cowsik, Phys. Rev. Lett. 39, 784 (1977);
D. Dicus, E. Kolb and V. Teplitz, Astrophys. J. 221, 327 (1978);
A. de Rujula and S. Glashow, Phys. Rev. Lett. 45, 942 (1980).
2. F.W. Stecker, Phys. Rev. Lett. 45, 1460 (1980);
F.W. Stecker, and R.W. Brown, Astrophys. J. 257, 1 (1982).
3. R. Kimble, S. Bowyer and P. Jacobsen, Phys. Rev. Lett. 46, 80 (1981).
4. D. Fargion and M. Roos, Phys. Lett. 147B, 34 (1984).
5. M. Maucherat-Joubert, P. Cruvellier and J.M. Deharveng, Astron. Astrophys. 70, 467 (1978); R.C. Anderson et al., Astrophys. J. 234, 415 (1979).
6. P. Jakobsen et al., Astron. Astrophys. 139, 481 (1984).
7. G. Auriemma et al., INFN-Rome preprint 447 (1985, unpublished).
8. A. Melott and D. Sciama, Phys. Rev. Lett. 46, 1369 (1981);
Y. Rephaeli and A. Szalay, Phys. Lett. 106B, 73 (1981).
9. P.B. Pal and L. Wolfenstein, Phys. Rev. D25, 766 (1982), and references quoted therein.
10. W. Marciano and A. Sanda, Phys. Lett. 67B, 303 (1977);
S. Petcov, Sov. Nucl. Phys. 25, 340 (1977); E 25, 698 (1977).
11. J.C. Pati and A. Salam, Phys. Rev. D10, 275 (1974);
R.N. Mohapatra and J.C. Pati, Phys. Rev. D11, 566 (1975); ibid. 2558;
G. Senjanovic and R.N. Mohapatra, Phys. Rev. D12, 1502 (1975).
12. See e.g., J.C. Pati and A. Salam, Phys. Lett. 58B, 333 (1975);
J. Maalampi and K. Enqvist, Phys. Lett. 97B, 217 (1980);
F. Wilczek and A. Zee, Phys. Rev. D25, 553 (1982).
13. K. Enqvist, K. Mursula and M. Roos, Nucl. Phys. B226, 121 (1983).
14. See e.g., L. Wolfenstein, Phys. Rev. D29, 2130 (1984).
15. G. Steigman, K.A. Olive and D.N. Schramm, Phys. Rev. Lett. 43, 239 (1979).
16. J. Maalampi, K. Mursula and M. Roos, Nucl. Phys. B207, 333 (1982).
17. K. Enqvist and J. Maalampi, Z. Phys. C21, 345 (1984).
18. See also J. Maalampi, K. Mursula and M. Roos, Phys. Rev. Lett. 56 (1986).
19. S. Bowyer, private communications.

LIMITS ON THE TAU NEUTRINO MASS

David S. Koltick
Department of Physics
Purdue University
West Lafayette, Indiana 47907



ABSTRACT

The methods used to place experimental limits on the mass of the tau neutrino are reviewed and the most recent upper limits are presented. Results are reported for the PEP experiments at SLAC, HRS, Mark II, and DELCO and from the DORIS experiment ARGUS at DESY. There is agreement that the tau neutrino mass is below the mass of the muon. The best upper limit is $M_{\nu_\tau} < 70$ MeV/c^2.

There are many reasons why the search for a massive tau neutrino might be successful.[1-7] If neutrinos are massive, a mass hierarchy by generation is expected, as is the case for the quarks and charged leptons. If true, the mass of the τ neutrino would be the largest and thus, possibly easier to measure. In some theories a mass hierarchy is confirmed. Gell-Mann, Ramond and Slansky[8] as well as others have derived a mass relationship between generations

$$M_{\nu_\tau} = \frac{M_\tau^2}{M_e^2} M_{\nu_e} \quad . \tag{1}$$

If this relationship is used with the reported ITEP result, a tau neutrino mass larger than the mass of the muon is expected.

In this paper the techniques used to place limits on the mass of the tau neutrino are reviewed and the best upper limits found using each technique are presented.

BETA DECAY

The first method used to test for a massive τ neutrino was to study the end point of the "beta" decay spectrum,[9] $\tau \to e\nu_e\nu_\tau$ and $\tau \to \mu\nu_\mu\nu_\tau$. The main limitation of this technique is that it requires a measurement of tracks having a momentum equal to that of the beam. Since the momentum resolution of a spectrometer for fast tracks goes like,

$$\delta P \sim P^2 \quad , \tag{2}$$

the measurement of the neutrino mass depends on the poorest measured momentum values in the experiment. The measurement also requires a knowledge of the beam energy and width since a Lorentz boost must be performed to place the observed decay products in the lab frame. Further radiative correction must be applied and an underlying decay mechanism must be assumed.

This method becomes more difficult as the beam energies are increased. There ΔE_{beam} tends to increase, making the Lorentz boost more uncertain, and the radiative effects become more important. When the beam energy is increased by a factor of 10 in going from SPEAR to PEP, then either the momentum resolution of the detector must be greatly improved or a much larger data set is required. But since large spectrometers tend to have similar resolutions and data set sizes decrease as a function of energy, the best results using the beta decay technique are obtained at low center of mass energies. Even so, SPEAR produced data sets with as many as ~ 50,000 tau pairs resulting in a τ neutrino mass limit[9] of only 250 MeV/c^2. The problem at low energies is that τ events are hard to separate from the hadronic background, especially charm which has a similar mass.

SINGLE PARTICLE HADRONIC DECAY

Another technique is to look at two body decays such as $\tau \to \pi\nu_\tau$ or $\tau \to K\nu_\tau$. In the τ rest frame the momentum spectrum of the neutrino and hadron are just a delta function. In momentum space this can be represented as a spherical shell. When the shell is viewed in the laboratory frame it is elongated in the direction of the boost. For a massive neutrino, if the boost is large enough, a gap will develop between the origin and the lowest momentum values. If the neutrino is massless, no matter how large the boost, a gap will not develop. Since the neutrino is unobservable the hadron must be studied and the neutrino spectrum inferred. It is found by subtracting E_{hadron} from E_{beam}. This method suffers from the same problems as the beta decay approach except that an underlying decay mechanism is not required. The best limit of $M_{\nu_\tau} \leq 250$ MeV/c^2 again comes from SPEAR.[10]

HADRONIC MASS SPECTRUM

The technique most likely to further improve the τ neutrino mass limit is the study of the hadronic mass spectrum in high multiplicity τ decays. These decays tend to have masses approaching that of the tau. At the end point of the hadronic mass spectrum a very simple relationship between M_{ν_τ} and $M_{hadrons}$ holds:

$$M_{\nu_\tau} = M_\tau - M_{hadrons} \quad . \tag{3}$$

This technique has many advantages: 1) The invariant mass of the τ is well measured, being known to ± 3 MeV/c^2. 2) The reconstruction of a high multiplicity mass involves the full momentum range of the detector and can include the measurement of neutral energy. A good detector can achieve a mass resolution of ~ 10 MeV/c^2 and better resolution is obtainable. 3) High energies become an advantage because rare decay modes of the τ can then be easily separated from the hadronic background. 4) Working with mass as a variable means the beam energy and width do not enter into the neutrino mass calculation. 5) Radiative corrections are greatly reduced and affect the calculation only to the extent that a hard photon might be included in the mass calculation, a very rare occurrence. 6) The decay is two body, $\tau \to \nu_\tau H$, where H is the entire hadronic system.

The Mark II group at PEP was the first to take advantage of this technique[11] by using the decay $\tau \to 3\pi^{\pm}\pi^{o}\nu_\tau$. The shape of the mass spectrum, shown in Fig. 1, is in good agreement with the two body decay $\tau \to \rho'\nu_\tau$. Only the 22 events with masses above 1.5 GeV/c^2 are used to set the limit. The limit is independent of whether or not the ρ' or a phase space shape is used for the hadronic mass spectrum. This is reasonable because the high end of the mass spectrum is dominated by phase space and the weak interaction matrix element

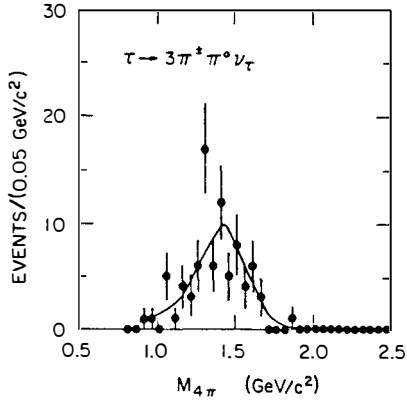


Fig. 1 The Mark II $3\pi^{\pm}\pi^{\circ}$ invariant mass distribution from selected τ decays. The curve is for $m_{\nu_\tau} = 0$.

for the decay. Using a data set only 1/3 as large as those at SPEAR, an improved limit of 142 MeV/c^2 at 95% confidence level was found.

The DELCO group[12] has applied the same technique to the rare decay $\tau \to K^+K^-\pi^{\pm}\nu_{\tau}$, which has a branching ratio of only 0.22%. To fit the data, a $K^+K^-\pi^{\pm}$ phase space model of the decay has been used as well as the predictions of the conserved vector current (CVC) hypothesis. The CVC hypothesis relates the isospin, I=1, part of the e^+e^- scattering amplitude to the weak isovector decay amplitude in τ decay. The cross section data, $e^+e^- \to K^*K$, for the I=1 channel at a center of mass energy below the τ mass, were obtained from an experiment performed at ORSAY.[13] To the precision of the four events observed, the ORSAY data are adequate. However if a large number of these rare τ decays were to become available the uncertainty in the K^*K cross section would dominate the mass limit requiring better measurements. The DELCO group finds an upper limit at 95% confidence level of $M_{\nu_\tau} < 157$ MeV/c^2.

The HRS group at PEP has measured the mass spectrum of the rare decays $\tau \to 5\pi^{\pm}\nu_{\tau}$ and $\tau \to 5\pi^{\pm}\pi^{\circ}\nu_{\tau}$, each having a branching ratio[14] of $\sim 7 \times 10^{-4}$. The HRS group has observed 5 events of each type. The Mark II has confirmed these observations by observing 2 events of each type.[15] To separate the τ signal from the hadronic background, advantage was taken of the fact that in the limit of first-order QED, τ-pair production leads to a unique momentum for each lepton. The thrust axis of these events is taken to be the direction of the produced τ pairs. By performing a Lorentz boost on the hadronic decay products of the τ, P^* can be measured. P^* is the momentum of the τ neutrino in the rest frame of the τ. As can be seen in Fig. 2 the hadronic background appears at high values of P^*, whereas the high mass τ decays appear near $P^* \sim 0$. Monte Carlo calculations show that radiative effects in τ pair production cause less than a 10% loss of signal when separating τ events from hadronic events in this manner.

It is interesting to note that both groups observe equal numbers of 5π and 6π events. This is understandable considering that the weak amplitude is composed of equal amounts of vector and axial vector currents and that the phase

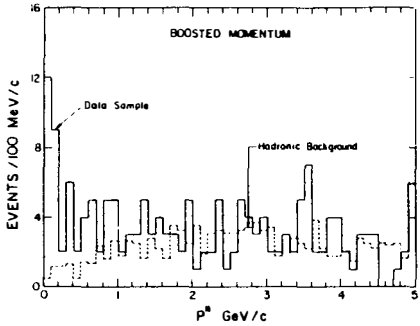


Fig. 2. The measured momentum, P*, in the τ rest frame for τ candidate events (solid line) and the hadronic background (dashed line).

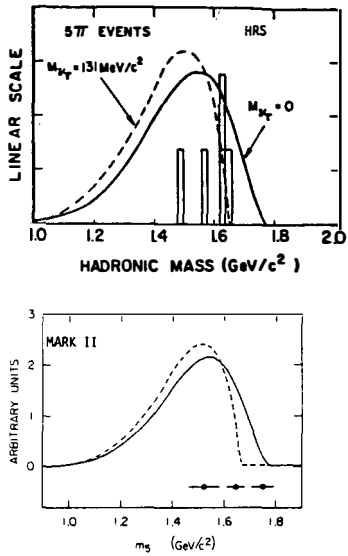


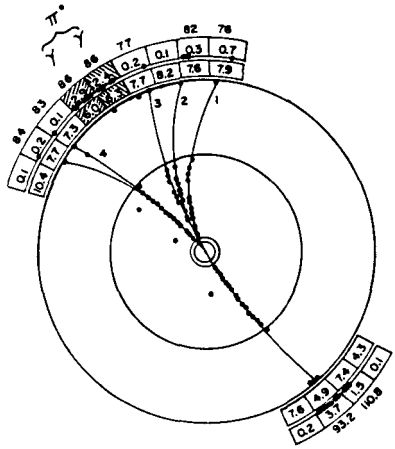
Fig. 3. The hadronic invariant mass of the events $\tau \to 5\pi^{\pm}\nu_\tau$. The solid lines are phase space times the weak matrix element for the best fit $M_{\nu_\tau} = 0$. The dashed lines are the 95% confidence level upper limit fits from a.) the HRS group. b.) the Mark II group.

spaces for the decays are similar. The 5π decays proceed through the axial vector current and the 6π decays through the vector current.

Both the Mark II and HRS group have reported upper limits using the $\tau \to 5\pi^{\pm}\nu_\tau$ events. The data are fit to a Monte Carlo generated $5\pi^{\pm}\nu_\tau$ phase space times the weak matrix element for the decay[16] as shown in Fig. 3. Using 3 events, the Mark II group finds an upper limit of 125 MeV/c^2, while the HRS group, using 5 events, finds an upper limit of 133 MeV/c^2. Both limits are at the 95% confidence level.

The phase space model predicts that half the $\tau \to 5\pi^{\pm}\nu_\tau$ decays should have a hadronic mass below 1.5 GeV/c^2. Yet the events reported by both groups are at the upper end of phase space. This may indicate τ decay to a state narrower than is expected for hadrons in this mass region. More data is needed to check this possibility. Again, because of the small number of events, the limits are not affected by how the τ lepton is decaying, but to improve the limit once a larger data set becomes available requires a better understanding of the mass spectrum.

The best limit to date using the mass spectrum technique has been obtained by the HRS group[17] measuring the end point of the decay $\tau \to 5\pi^{\pm}\pi^{0}\nu_\tau$. An example of such an event is shown in Fig. 4. The shape of the mass spectrum is predicted by the weak interaction matrix element,



$$\tau \longrightarrow 5\pi^{\pm}\,\pi^{\circ}\,\nu_{\tau}$$

Fig. 4. An event from the HRS group of $\tau \to 5\pi^{\pm}\pi^{\circ}\nu_{\tau}$.

phase space and the conserved vector current (CVC) hypothesis. The shape is given by[15]

$$\frac{d\,\Gamma}{d\,M_{had}} \sim M_{had}\left[(M_{\tau}^2-M_{had}^2)^2 - M_{\nu}^2(2M_{\tau}^2+2M_{had}^2-M_{\nu}^2)\right]^{1/2} \left[(M_{\tau}^2-M_{had}^2)(M_{\tau}^2+2M_{had}^2) - M_{\nu}^2(2M_{\tau}^2-M_{had}^2-M_{\nu}^2)\right] \frac{\sigma^{1}_{e^+e^-}(M_{had})}{\sigma_{pt}(M_{had})} \qquad (3)$$

where $\sigma_{e^+e^-}$ is the isospin one part of the cross section and $\sigma_{pt}(M_{had})$ is the point cross section which varies as $1/M_{had}^2$.

Measurements of the $e^+e^- \to 6\pi$ annihilation cross section for center of mass energies in the τ mass region have been reported by Cosme et al.[18] In this data there is a threshold-like behavior near 1.5 GeV/c^2. Using a linear fit to the measured 6π cross section in the τ mass region, a 95% confidence level upper limit of 86 MeV/c^2 is found for M_{ν_τ}. This is shown as the dashed line in Fig. 5. If the cross section "threshold" is varied by $\pm$50 MeV/c^2, the limit changes by less than 1.5 MeV/c^2.

Combining the $5\pi^{\pm}$ and $5\pi^{\pm}\pi^{\circ}$ data, the HRS group finds a 95% confidence level upper limit of $M_{\nu_\tau} < 84$ MeV/c .

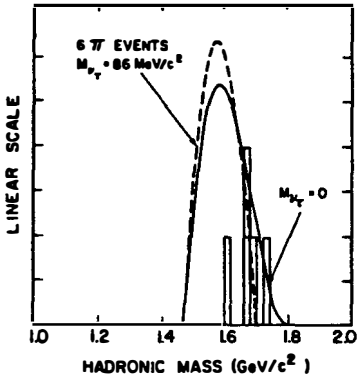


Fig. 5. The invarient mass of the HRS events $\tau \to 5\pi^{\pm}\pi^{\circ}\nu_{\tau}$. The solid line is based on equation 3, with the best fit $M_{\nu_\tau} = 0$. The dashed line is the 95% confidence level upper limit fit.

COMBINATION METHOD

The problems of setting a neutrino mass limit using a single hadron in the final state were discussed earlier. This same technique can be applied to the higher multiplicity τ-decays. The ARGUS group running in the e^+e^- storage ring DORIS II at DESY have used the decay $\tau \to 3\pi^{\pm}\nu_{\tau}$ in this manner.[19]

Because the beams at DORIS have an energy width of only a few MeV, and to first order in QED, produced τ pairs have a unique energy, $E_{\tau} = E_{beam}$, a good approximation to the neutrino energy can be found using

$$E_{\nu_\tau} = E_{beam} - \sum_{hadrons} E_i \quad . \qquad (4)$$

The sum is over the 3 observed hadrons.

If the hadronic system were to have a unique mass the lower end point of the neutrino energy spectrum would be shifted by an amount

$$\Delta E = \frac{\gamma}{2E^*} M^2_{\nu_\tau} \qquad (5)$$

where $\gamma = E_{\tau}/M_{\tau}$ and $E^*(M_{hadron})$ is the rest frame neutrino energy, a function of the hadronic mass. But because the hadronic system has a variable mass, the end point region becomes smeared, having a shape dependent on the hadronic mass spectrum.

The exact shape of the energy spectrum depends on many factors which include: (1) Radiative corrections, which tend to deplete the low energy region of the spectrum. If neglected, they would mimic a massive neutrino. (2) The beam energy, since E_{beam} enters directly into the calculation of E_{ν}. An uncertainty in the energy causes a shift of the entire spectrum. (3) The energy width of the beam. While this number is negligible at DORIS, at PEP it is between ~ 15 - 20 MeV and at Tristan it will be as large as ~ 60 MeV. Its effect is to smear the spectrum. (4) The hadronic mass spectrum. The shape of the hadronic mass distribution is uncertain in the tails of the distribution and is not predicted theoretically. Therefore the exact shape of the energy spectrum cannot be calculated. But the shape is known well enough not to have

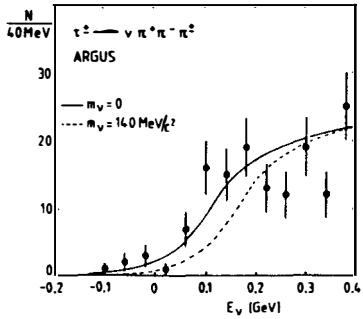


Fig. 6. The experimental data and Monte Carlo expectations for $M_{\nu_\tau} = 0$ (solid line) and $M_{\nu_\tau} = 140\ MeV/c^2$ (dashed line).

an important effect on the neutrino mass limit. (5) Lastly, the effects of the momentum calibration, momentum resolution, detector acceptance and backgrounds are most important.

Combining all these effects into a Monte Carlo, the ARGUS group has calculated the shape of neutrino energy spectrum shown in Fig. 6. They report the world's best limit of $M_{\nu_\tau} < 70\ MeV/c^2$ at 95% confidence level.

CONCLUSIONS

The HRS and ARGUS groups agree that the mass of the τ neutrino mass is below the mass of the muon. These results forbid τ neutrino decay with a muon in the final state. This conclusion is important considering that astrophysical arguments restrict stable neutrinos to have masses less than 100 eV/c^2 or greater than 2 GeV/c^2. Excluding the decay involving the muon together with arguments concerning the survival of primordial deuterium[20] may exclude an unstable τ neutrino heavier than ~ 1 MeV/c^2.

Both the HRS and ARGUS groups are in disagreement with the results of the ITEP group if massive neutrino generations are related by equation 1. In this case both groups predict an electron neutrino mass less than 7 eV/c^2.

REFERENCES

1. V.A. Lubimuv et al., Phys. Lett. 94B, 266 (1980); S. Boris et al., Phys. Lett. 159B, 1217 (1985).

2. The question is reviewed by S.M. Faber and J.S. Gallagher in Ann. Rev. Astron. Astrophys. 17, 135 (1979).

3. R. Davis et al., BNL Nu. Workshop, 1981.

4. A. Bosma, The Distribution and Kinematics of Neutral Hydrogen in Spiral Galaxies, Ph.D. Thesis (1978), Groningen Univ. Groningen.

5. E.L. Turner, Ap. J. 208, 304 (1976).

6. J. Zwicky, Helv. Phys. Acta. 6, 110 (1933); S. Smith, Ap. J. 83, 23 (1936).

7. J.E. Gunn et al., Ap. J. 223, 1015 (1978).

8. M. Gell-Mann, P. Ramond and R. Slansky, in: Supergravity, eds. P. van Nieuwenhuizen and D. Z. Freedman (North-Holland, Amsterdam, 1979); T. Yanagida, in: Proc. Workshop on the Unified Theory and the Baryon Number in the Universe (KEK, Japan, 1979); Prog. Theor. Phys. 64, 1103 (1980); R.N. Mohapatra and G. Senjanovic, Phys. Rev. Lett. 44, 912 (1980).

9. C.A. Blocker et al., Phys. Lett. 109B, 119 (1982); W. Bacino et al., Phys. Lett. 41, 13 (1978).

10. C.A. Blocker, Phys. Lett. 109B, 119 (1982).

11. C. Mateuzzi et al., Phys. Rev. D 32, 800 (1985).

12. G. B. Mills et al., Phys. Rev. Lett. 54, 624 (1985).

13. B. Delcourt et al., Proceedings of the Lepton-Photon Symposium, Bonn, p. 205, 1981.

14. I. Beltrami et al., Phys. Rev. Lett. 54, 1775 (1985).

15. P.R. Burchat et al., Phys. Rev. Lett. 54, 2489 (1985).

16. Y.S. Tsai, Phys. Rev. D 4, 2821 (1971); F.J. Gilman and D.H. Miller, Phys. Rev. D 17, 1846 (1978).

17. S. Abachi et al., Purdue University preprint Pu-85-541, Oct. 1985 (Submitted to Phys. Rev. Lett.).

18. G. Cosme et al., Nucl. Phys. B152, 215 (1979).

19. H. Albrecht et al., DESY Preprint 85-054, June 1985 (submitted to Phys. Lett. B).

20. L.M. Krauss, Phys. Rev. Lett. 53, 1976 (1984); S. Sarker and A.M. Cooper, Phys. Lett. 148B, 347 (1984).

SEARCHES FOR DECAYS OF HEAVY NEUTRINOS IN THE CHARM EXPERIMENT

The CHARM Collaboration

J. Dorenbosch
NIKHEF, Amsterdam, The Netherlands

J.V. Allaby, U. Amaldi, G. Barbiellini, C. Berger, F. Bergsma, A. Capone, W. Flegel, L. Lanceri, M. Metcalf, C. Nieuwenhuis, J. Panman and K. Winter
CERN, Geneva, Switzerland

I. Abt, J. Aspiazu, F.W. Büsser, H. Daumann, P.D. Gall, T. Hebbeker, F. Niebergall, P. Schütt and P. Stähelin
II. Institut für Experimentalphysik, Universität Hamburg, Hamburg, Fed. Rep. Germany

P. Gorbunov, E. Grigoriev, V. Kaftanov, V. Khovansky and A. Rosanov
Institute for Theoretical and Experimental Physics, Moscow, USSR

A. Baroncelli, L. Barone, B. Borgia, C. Bosio, M. Diemoz, U. Dore, F. Ferroni, E. Longo, L. Luminari, P. Monacelli, F. de Notaristefani, P. Pistilli, R. Santacesaria, C. Santoni, L. Tortora and V. Valente
Istituto Nazionale di Fisica Nucleare, Rome, Italy

Presented by C. Santoni

ABSTRACT

Searches for decays of heavy neutrinos produced in meson decay and in light neutrino interactions were conducted at CERN by the CHARM Collaboration in the wide-band neutrino beam produced by 400 GeV primary protons and in a prompt neutrino beam produced by dumping 400 GeV protons in a Cu target. No evidence for these decays was found. The experiments were sensitive to neutrinos with mass in the range 0.01-2.8 GeV. The limits on the square of the neutrino mixing angle obtained are $\approx 10^{-3}$-10^{-7} depending on the neutrino mass.

Searches for decays of heavy neutrinos produced in meson decay and in neutrino interactions were performed at CERN by the CHARM Collaboration in the 400 GeV wide-band neutrino beam (WBB) and in the neutrino beam produced by dumping 400 GeV protons in a Cu target (BDB).

If neutrinos are massive, their weak (flavour) eigenstates are linear combinations of the mass eigenstates [1]:

$$\nu_\ell = \Sigma\, U_{\ell i}\, \nu_i \quad (\ell = e, \mu, \tau, ..., i = 1, 2, 3, ...) \tag{1}$$

A neutrino beam can contain, in addition to its major part of light neutrinos, a minor component of heavy ones. Such neutrinos may be originated in the decay of pseudoscalar mesons M (π, K, D, F, ...), produced by the interaction of protons with the target, and then decay in the detector.

The number of heavy neutrino decay events expected in the detector is given by:

$$N_{ev} = \Phi\, P_{dec} \approx |U_{\ell' i} U_{\ell i}|^2 , \tag{2}$$

where Φ is the heavy neutrino flux and P_{dec} is the probability for the neutrino to decay in the detector; $U_{\ell' i}$ and $U_{\ell i}$ are the neutrino mixing angles entering respectively into the meson and the heavy neutrino decay probability.

In the WBB, heavy neutrinos should come from π's and K's. We searched for them in the decay [2]

$$\nu_i \rightarrow e^+ e^- \nu_e . \tag{3}$$

This search was a byproduct of the measurement of the neutrino- and antineutrino-electron cross-sections [3]. The events induced by reaction (3) would appear in the calorimeter detector [4] as muonless narrow showers, which are a characteristic of electromagnetic showers [5]; the angle θ between the shower axis and the direction of the incoming neutrino beam would be small, and more than two minimum ionizing particles would be at the shower origin. The background was due to the elastic and quasi-elastic charged-current events induced by the electron-neutrino contamination of the beam; to the scattering of neutrinos on electrons; and to neutral-current events with a γ or a π^0 in the final state, produced by coherent scattering of muon neutrinos on nuclei [6]. The number of events attributed to heavy neutrino decay is compatible with zero.

The limits at 90% c.l. on the square of the mixing angle $|U_{ei}|$ are shown in Fig. 1, curve f), together with limits obtained in other experiments: a) limits obtained in the BDB experiment by the CHARM Collaboration assuming that heavy neutrinos are produced in D decay [7]; b) limits from solar neutrinos [8]; c) limits obtained studying the decay $\pi \rightarrow \nu e$ [9]; d) limits obtained by the CHARM Collaboration in a beam dump experiment [2,7] assuming that heavy neutrinos are produced in the chain $F \rightarrow \tau \nu_3$, $\tau \rightarrow \nu_3 X$; e) limits from the measurement of the branching ratio $K \rightarrow \nu e$ [10]; g) limits from the study of the decay $K \rightarrow \nu e$ at

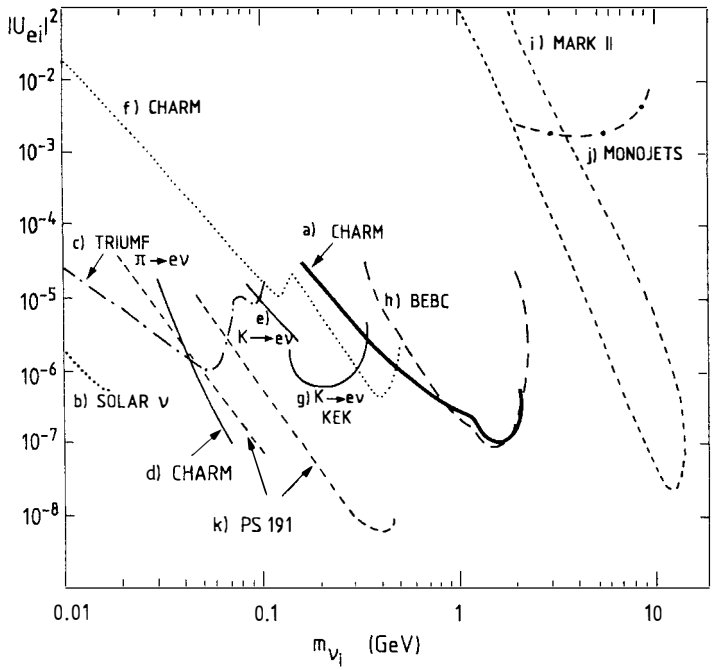


Fig. 1

KEK [11]; h) limits obtained in the beam-dump experiment by the BEBC Collaboration [12]; i) limits obtained from a search for secondary vertices in the MARK II experiment assuming that the heavy neutrinos are produced by the reaction $e^+e^- \rightarrow \nu_i\bar{\nu}_i$ [13]; j) limits obtained in a search for monojet events due to the reaction $e^+e^- \rightarrow \nu_e\bar{\nu}_i$ [14]; k) limits obtained in a neutrino decay experiment performed at the CERN PS neutrino beam [15]. The WBB experiment is not sensitive to values of $|U_{ei}|^2 > 0.1$ for neutrino masses larger than 350 MeV. The sensitivity was limited by the huge amount of neutrino interaction background.

The detector of the BDB experiment [2,7] consists of a nearly empty decay region (to minimize the neutrino interactions) followed by one module of the CHARM calorimeter [4] to measure the energy of the decay products. In the decay region packs of proportional chambers were placed to identify the decay point and to improve the measurement of the angle of the decay particles. Since the protons are dumped in a thin target, in the BDB almost half of the neutrinos comes from short-living particles such as D's and F's. This allowed to search for heavy neutrinos with a mass up to 1.5 GeV.

The neutrino decays [1]:

$$\nu_i \to e^+e^-\nu_e\,, \tag{4a}$$

$$\nu_i \to \mu^+\mu^-\nu_\mu\,, \tag{4b}$$

$$\nu_i \to e^+\mu^-\nu_e,\ \mu^+e^-\nu_\mu\,. \tag{4c}$$

and the corresponding channels of antineutrinos, were searched for. The signature of reactions (4) would be events originating in the decay region at a small angle with respect to the neutrino beam axis, with one or two separate electromagnetic showers [decay (4a)], two tracks [decay (4b)], and one electromagnetic shower and one track in the case of the decay (4c). The event selection was done by computer and no candidate was found.

From these negative results, limits on the square of the mixing angles $|U_{ei}|$ and $|U_{\mu i}|$ were obtained, assuming that heavy neutrinos come from D and F decays:

$$\begin{aligned} &D \to \ell\nu_i X, \quad \nu_i \to \ell\ell'\nu \\ &\\ &F \to \nu_3\tau\ (\tau \to \nu_3 X), \quad \nu_3 \to ee\nu\,. \end{aligned} \tag{5}$$

In the case of the F hypothesis we assumed $\sigma(pp \to FFX)/\sigma(pp \to DDX) = 0.2$ and the branching ratio for the F to decay into a zero mass neutrino = 0.03. Since the limit on the mass of the ν_τ is 70 MeV [16], the heavy neutrino was identified with the tau neutrino. This means that we take $|U_{\ell'i}| = 1$ in Eq. (2). The normalization was done using the "prompt" ν_μ interaction observed in the calorimeter during the exposure. The limits at 90% c.l. on $|U_{ei}|^2$ are shown in Fig. 1 [curves a) and d)]. Limits on $|U_{\mu i}|^2$ are shown in Fig. 2, curve a). In the same figure are shown also the limits obtained in other experiments: b) limits obtained in a search for heavy neutrino produced in neutrino interactions by the CHARM Collaboration [7]; c) limits obtained studying the decay $\pi \to \nu\mu$ at SIN [17]; d) limits from the study of the decay $K \to \nu\mu$ at KEK [11]; e) limits from the study of the decay $K \to \nu\bar{\nu}\nu\mu$ at LBL [18]; f) limits obtained by the BEBC Collaboration in the beam-dump experiment [12]; g) limits obtained from a search for secondary vertices in the MARK II experiment assuming that the heavy neutrinos are produced by the reaction $e^+e^- \to \nu_i\bar{\nu}_i$ [13]; h) limits obtained in a neutrino decay experiment performed at the CERN PS neutrino beam [15]. For large mixing angles the sensitivity of the BDB experiment is limited to small masses (i.e. for $|U_{\ell i}|^2 > 10^{-1}$ it is sensitive to $m_{\nu_i} < 1000$ MeV and for $|U_{\ell i}|^2 > 10^{-4}$ to $m_{\nu_i} < 1500$ MeV) because the beam of heavy neutrinos is attenuated by decay before reaching the detector, which is located at a distance of 480 m from the target.

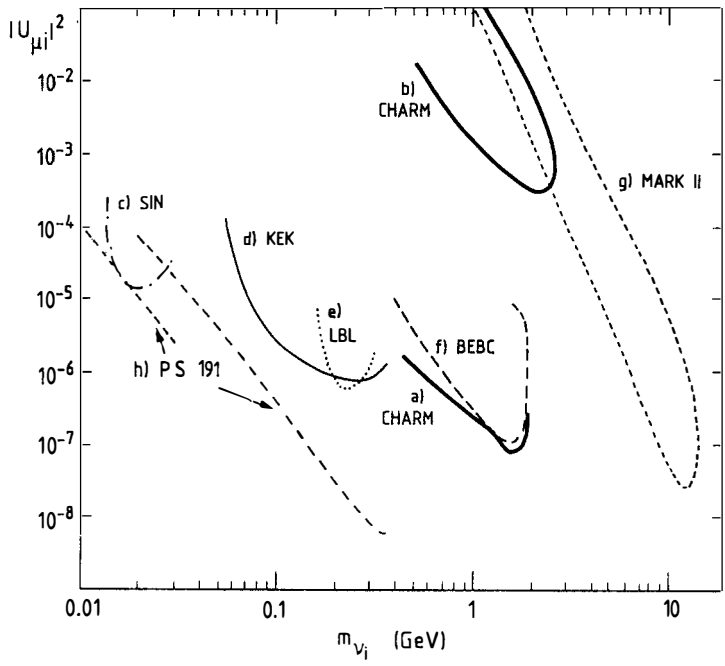


Fig. 2

In a third search, heavy neutrinos were assumed to be produced in the CHARM calorimeter [7] by muon neutrinos via a neutral-current interaction:

$$\nu_\mu N \rightarrow \nu_i X \,. \tag{6}$$

The subsequent decays into a muon and hadrons [1]:

$$\nu_i \rightarrow \mu X \tag{7}$$

were searched for in the calorimeter itself [4]. This is a flavour changing neutral-current interaction. In this case there may be other contributions to the mixing than $U_{\ell i}$ [19]; however this possibility was neglected in the present analysis. The topology of events induced by the production of heavy neutrinos according to reaction (6), and their subsequent decay in the calorimeter by reaction (7), would show two showers separated by a gap along the beam direction, with a muon pointing to the vertex of the second one. One

candidate event was found, whilst the expected background due to the random superposition of the events in the gate timing of the detector is 1.9 ± 0.4 events. The limits obtained from this search are shown in Fig. 2, curve b). In conclusion, there is no evidence for the decay of heavy neutrinos with mass in the range up to 2.8 GeV. In these searches, the limits on inter-family mixing of neutrinos obtained are $|U_{ei}|^2 < 5 \times 10^{-7}$ for $m_{\nu_i} \approx 400$ MeV (WBB neutrino decay experiment), $|U_{ei}|^2$, $|U_{\mu i}|^2 < 10^{-7}$ for $m_{\nu_i} \approx 1.5$ GeV (BDB experiment, D decay hypothesis), $|U_{ei}|^2 < 10^{-7}$ for $m_{\nu_i} \approx 70$ MeV (BDB experiment, F hypothesis), and $|U_{\mu i}|^2 < 3 \times 10^{-4}$ for $m_{\nu_i} \approx 2.5$ GeV (WBB neutrino interaction experiment).

References

1. R. E. Shrock, Phys. Rev. D24 (1981) 1232.
   M. Gronau, Phys. Rev. D28 (1983) 2762.
2. F. Bergsma et al. (CHARM Collab.), Phys. Lett. 128B (1983) 361.
3. F. Bergsma et al. (CHARM Collab.), Phys. Lett. 147B (1984) 481.
4. A. N. Diddens et al. (CHARM Collab.), Nucl. Instrum. Methods 178 (1980) 27.
5. M. Jonker et al. (CHARM Collab.), Nucl. Instrum. Methods 200 (1982) 183.
6. F. Bergsma et al. (CHARM Collab.), Phys. Lett. 157B (1985) 469.
7. J. Dorenbosch et al. (CHARM Collab.), Phys. Lett. 166B (1986) 473.
8. See D. Toussaint and F. Wilczek, Nature 289 (1981) 777.
9. D.A. Bryman et al., Phys. Rev. Lett. 50 (1983) 1546.
10. See D. Berghofer et al., Proc. Int. Conf. on Neutrino Physics and Astrophysics, Maui, Hawaii, 1981, eds R.J. Cence, E. Ma and A. Roberts (Univ. of Hawaii, Honolulu, 1981), Vol. II, p. 67.
11. T. Yamazaki, Proc. 22nd Int. Conf. on High-Energy Physics, Leipzig, 1984, eds. A. Meyer and E. Wieczorek (Akad. Wissensch. DDR, Leipzig, 1984), Vol. I, p. 262.
12. A.M. Cooper-Sarkar et al., Phys. Lett. 160B (1985) 207.
13. G.J. Feldman, talk on MARK II results at the 20th Rencontre de Moriond, Les Arcs, France, 1985, to be published.
14. See F.J. Gilman and S.H. Rhie, Phys. Rev. D 32 (1985) 324.
15. G. Bernardi et al., Phys. Lett. 166B (1986) 473.
16. H. Albrecht et al., peprint DESY 85-054 (1985), to be published in Physics Letters B.
17. R. Abela et al., Phys. Lett. 105B (1981) 263.
18. C.Y. Pang et al., Phys. Rev. D8 (1973) 1989.
19. M. Gronau, C.N. Leung and J.L. Rosner, Phys. Rev. D29 (1984) 2359.

LIMITS ON NEUTRINOS MIXING PARAMETERS FROM A HEAVY NEUTRINO DECAY SEARCH

J.M.Lévy
L.P.N.H.E.-Université Paris VI and VII

ABSTRACT

Results of a neutrino decay search are used to put limits on the elements of the leptonic mixing matrix.

If neutrinos are massive, they may mix both between and among generations. Even if one discards Majorana mass terms, there still remains the possibility of inter-generation mixing, as is the case for quarks. If some mass eigenvalues are sufficiently high, the corresponding states would then decay into leptons and lighter neutrinos or even charged pseudo-scalars and leptons.

On the other hand, due to mixing, a standard neutrino beam would embody a certain fraction of such massive states and therefore, would exhibit the phenomenon of neutrino decay[1].

A dedicated experiment was performed to look for such decays and in the following we give the limits that its results entail for the heavy neutrino couplingsto ν_μ and ν_e.

The CERN PS191 experiment was run in July - August 1984. The set up has been described elsewhere[2], so we only give the basic facts here; the apparatus consisted of a ~ 12 m long decay volume followed by a ~ 7 X_o electromagnetic calorimeter (EMC). Eight pairs of flash chambers were placed in the decay volume to allow identification and reconstruction of charged tracks, and the intervening space was filled with helium bags. A scintillation hodoscope made of 20 vertical slates viewed at both ends by photo multipliers was placed at a depth of ~ 1.8 X_o inside the calorimeter (fig. 1).

A neutrino decaying to $e^-e^+\nu$ or πe would have been recognized as a pair of tracks originating from a point inside helium and giving rise to (at least) one shower in the EMC. Hence the trigger conditions required to apply the high voltage on the chambers and start the acquisition process were the following: either two P.M. from two different scintilator slabs gave a signal in coincidence above a low threshold (corresponding to a minimum ionizing particle) or two P.M. from the same slab both gave a signal above the low threshold, one of them being above a high threshold which corresponded more or less to two minimum ionizing tracks, making allowance for attenuation.

The recorded events were scanned off line and the following demands were applied to select decay candidates: two tracks originating from a point inside helium, one of which, at least, had to produce a shower in the calorimeter and to fire two or more decay volume FC's; the other track had

to fire at least 3 FC's if out of EMC, or at least two if in the EMC; in the latter case, it was demanded that the projected distance between impacts be at least 5 cm. No event fulfilling these criteria was found.

In order to exploit this result, we used the following procedure: a standard neutrino beam simulation program (VENUS)[3] was modified by implementing the correct two-body kinematics for decays of charged pseudo-scalar mesons into lepton+massive neutrino and replacing the partial decay widths by their values for a non-zero neutrino mass computed as if the mixing matrix element were equal to 1. A second program, fed with the flux from the latter, simulated neutrino decay in the fiducial volume, detection by the apparatus and applied the above mentioned cuts.

Baring very fast neutrino decay which would render the experiment insensitive, the probability of seeing no decay in a fiducial length L is

$$\prod_{\nu} \exp\left(\frac{-mL}{p_\nu c\tau}\right)$$

where the product runs over all neutrinos in the beam, the decay of which would be detected and recognized as such. Imposing a given confidence level β on thus finds:

$$\frac{mL}{c\tau} \sum_{\nu} \frac{1}{p_\nu} < -\mathrm{Log}\beta$$

The sum in this last inequality is estimated, up to the squared production mixing matrix element which enters as a multiplicative factor, by using the two programs which we have just described.

If one assumes that the width is dominated by the U_{eh} mixing matrix element, the lifetime can be computed as

$$\tau^{-1} \simeq m^5 \frac{G_F^2}{192\pi^3} |U_{eh}|^{2(*)}$$

for m above a few MeV; above 140 MeV the partial width for $\nu \to e^- \pi^+$ which embodies the same unknown factor must be added to the above. On the other hand, since no decays were found, it is legitimate when computing

---

(*) We use the notation $U_{\beta k}$, β = e, μ, τ for the mixing matrix element relating a mass eigenstate k with the neutrino produced by charge current reactions together with an electron, a muon or a τ. We shall use k = h for "heavy" and k = ℓ for "light".

limits on $U_{\mu h}$ to assume the width to be dominated by this last quantity; in the purely leptonic decay modes, we further assume that the final neutrino is essentially massless and electron-like, so that the approximation $|U_{e\ell}|^2 \simeq 1$ is made.

If, as frequently hypothesized, Majorana and Dirac mass terms co-exist, the mass eigenstates are quite generally Majorana particles[4]. This changes the width to the channels considered here and allows decay through neutral currents. Making the same assumption as above about the final ν, the modifications to apply to the results given here are essentially[5]:

(a) The limits from channels where neutral currents can play a role (here, $e^-e^+\nu$ only) should be lowered by a factor $\sqrt{5}/2$.

(b) The limits from purely charged current channels should be lowered by $\sqrt{2}$.

Our results are given in figs 2, 3, 4 where they are compared to limits coming from other experiments. The advantage of a dedicated search using a high granularity apparatus is obvious.

We have roughly estimated the values of the mixing matrix elements above which an experiment like this would be insensitive due to nearly total decay of the massive component before reaching the apparatus. These are far above the limits already found by secondary peak searches (see plots) which do not suffer from the same problem; so we feel fairly sure that this is not the cause of one not having found decays and that our limits are reliable.

REFERENCES

1) M. Gronau, Searching for heavy unstable neutrinos, SLAC PUB 2976 (1982); R.E. Schrock, Phys. Rev. D24 (1981) 1232.

2) G. Bernardi et al., Phys. Lett. 166B (1986) 479.

3) W. Venus, Rutherford Appleton Lab., private communication.

4) See eg. T.P. and L.F. Li, Phys. Rev. D22 (1980) 2860; J. Schechter and J.W.F. Valle, Phys. Rev. D22 (1980) 2227.

5) J.M. Levy, to appear.

6) F. Bergsma et al., Phys. Lett. 128B (1982) 33.

7) D.A. Bryman et al., Phys. Rev. Lett. 50 (1983) 20.

8) T. Yamazaki et al., in "Neutrino 84" Dortmund.

9) R. Abela et al., Phys. Lett. 105B (1981) 263.

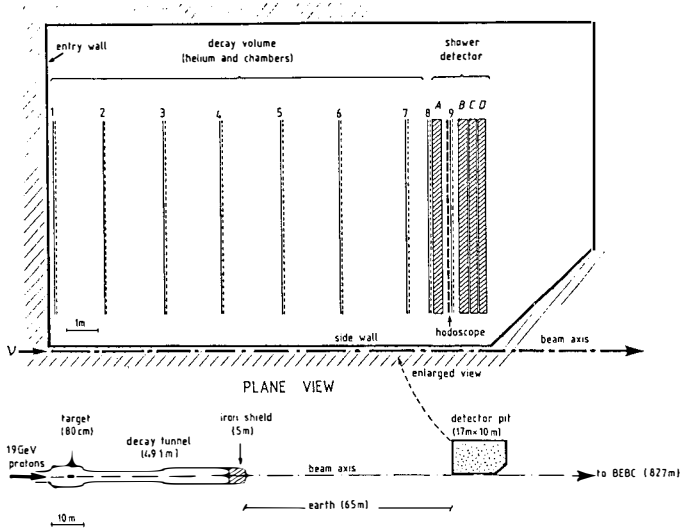


Fig. 1

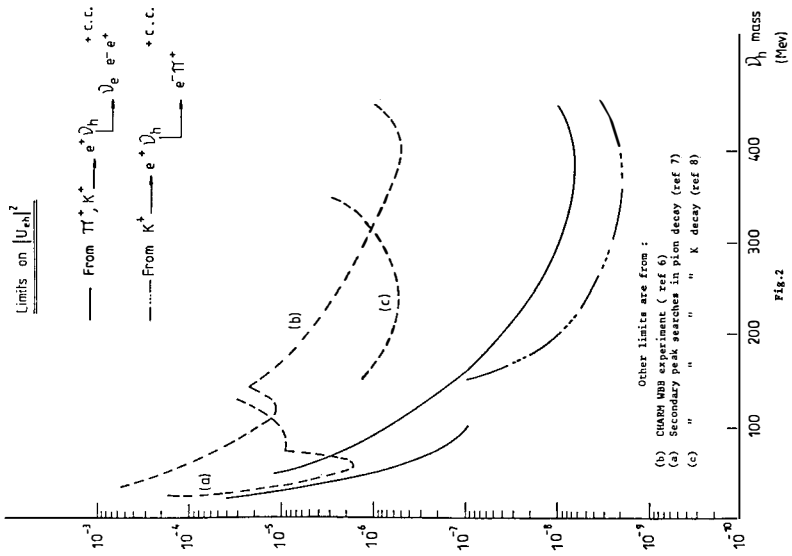


Fig.2

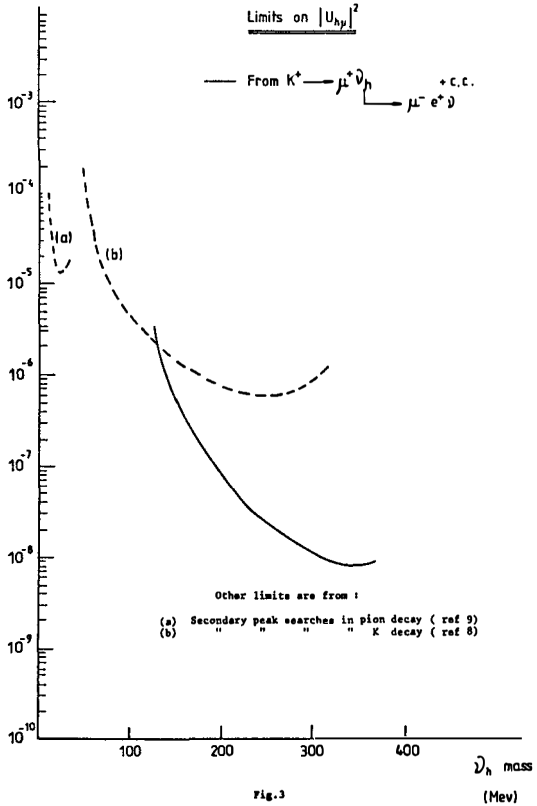

Limits on $|U_{h\mu}|^2$
From $K^+ \to \mu^+ \nu_h$ $\to \mu^- e^+ \nu$ + c.c.
(a)
(b)
10^{-3}
10^{-4}
10^{-5}
10^{-6}
10^{-7}
10^{-8}
10^{-9}
10^{-10}
100
200
300
400
ν_h mass
(Mev)
Other limits are from :
(a) Secondary peak searches in pion decay (ref 9)
(b) " " " " K decay (ref 8)

Fig.3

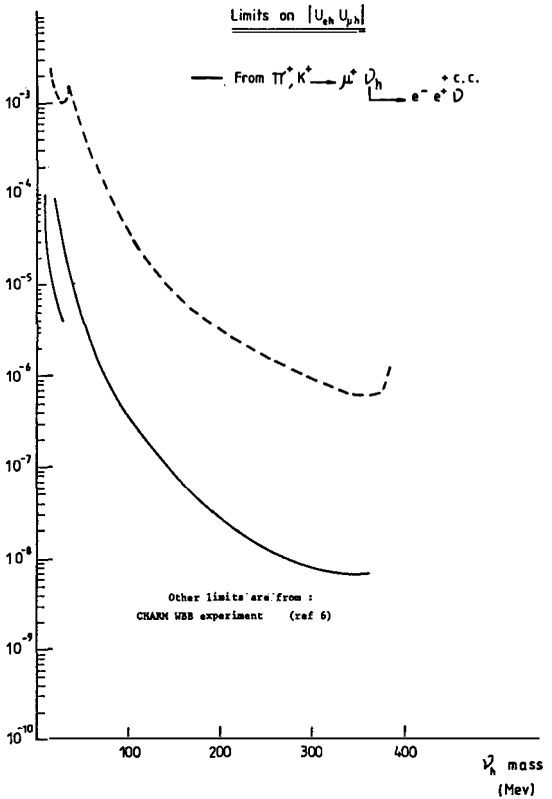

Limits on $|U_{eh} U_{\mu h}|$
From $\pi^+, K^+ \to \mu^+ \nu_h$ $\to e^- e^+ \nu$ + c.c.
10^{-3}
10^{-4}
10^{-5}
10^{-6}
10^{-7}
10^{-8}
10^{-9}
10^{-10}
100
200
300
400
ν_h mass
(Mev)
Other limits are from :
CHARM WBB experiment (ref 6)

Fig.4

SEARCH FOR HEAVY NEUTRAL LEPTONS AT CELLO

R. ALEKSAN
Département de Physique des Particules Elémentaires, CEN-Saclay,
91191 Gif-sur-Yvette Cedex, France.

ABSTRACT

A search for heavy neutral leptons in e^+e^- collisions at an average c.m. energy of 44.2 GeV has been carried out with the CELLO detector at PETRA. No evidence for such new particles has been observed. We exclude their pair-production at 95% CL if their mass is in the range 3.1 to 18.0 GeV/c^2 . The possibility to produce a single heavy neutrino together with a standard neutrino has also been studied. We are excluding such an electron-like heavy neutral lepton with a mass between 0.6 to 34.6 GeV/c^2 if its coupling to the W boson is V-A and between 0.4 to 37.4 GeV/c^2 for V+A.

Introduction

The e^+e^- interactions are a very appropriate tool for the search of heavy neutral leptons provided their lifetime is not too large.

Data and experimental set up.

The data were taken in 1983 and 1984 with the CELLO detector at PETRA. During this period, part of the data were accumulated at a fixed energy of the center of mass while part of it came from an energy scan between 39.8 and 46.8 GeV. The overall accumulated luminosity was 21.4 pb^{-1} at an average energy of 44.2 GeV.

CELLO [1] is a general purpose detector for e^+e^- physics and was particularly well optimized for lepton identification. Interleaved cylindrical drift and proportional chambers, in a 13 kΓ magnetic field produced by a thin superconducting solenoid, measure charged particle momenta over 92% of the solid angle with a resolution of $0.013\sqrt{1+P_T^2}$. P_T (p_T in GeV/c). A lead-liquid argon calorimeter covering a solid angle of 86% of 4π steradians gives an energy resolution of $\sigma(E)/E = 0.13/\sqrt{E}$ for electromagnetic showers. Large planar drift chambers mounted on a hadron absorber of 80 cm thick iron ensure muon identification over 92% of 4π steradians.

Production mechanisms

The two possible mechanisms are the $N\bar{N}$ pair production through the Z^0 annihilation (fig. 1) or the production of a single heavy neutrino together with a light neutrino through a W exchange (fig. 2).

The cross section of the annihilation mechanism is given by :

$$\sigma = \frac{G^2 s}{96\pi}\left[\frac{M_Z^2}{s-M_Z^2}\right]^2 \beta\,(3+\beta^2)\,(1-4\sin^2\theta_W + 8\sin^4\theta_W)$$

with G the Fermi constant,

$$\beta = \left[1 - \frac{4M_\nu^2}{s}\right]^{1/2}$$

and $\sin^2\theta_W$ the Weinberg mixing angle.

Taking $\sin^2\theta_W = 0.25$ and $M_Z >> s$ one gets :

$$\sigma = 8.5\ 10^{-5} \left[\frac{M_Z^2}{s-M_Z^2}\right]^2 \beta\ (3+\beta^2)\ s\ (GeV^2)\ pb \quad \text{(fig. 3)}$$

The cross section for the production of a single heavy neutral lepton can be calculated using a V-A or a V+A current at the vertex eWN (fig. 3).

$$\sigma_{(V-A)} = \frac{G^2}{4\pi}\left(1-\frac{M_N^2}{s}\right)^2 (a-1)^2 \left[\frac{s}{a-1} + (s-M_N^2) + \frac{1}{2}\left[s+a\ (s-M_N^2)\right] \log\frac{a-1}{a+1}\right]$$

$$\sigma_{(V+A)} = \frac{G^2}{4\pi}\left(1-\frac{M_N^2}{s}\right)^2 2s\ \left(\frac{M_W^2}{M_W^2 + s - M_N^2}\right)$$

$$\text{where}\quad a = \frac{s + 2M_W^2 - M_N^2}{(s - M_N^2)}$$

It is obvious that with this mechanism, one is sensitive to heavier neutral leptons. This is why we have discarded the pair-production in the t channel with a W exchange. One should however note that in the cross section, the e-N mixing has been set to 1 . If $|U_{eN}|^2 << 1.$, the cross section is scaled down and becomes too small to be measured.

Decay

It is commonly assumed that a heavy neutral lepton decays in the same way as a charged lepton through a W boson (fig. 4) and has the following width :

$$\Gamma(N^\circ \to \ell X) = \frac{G^2 M_{N^\circ}^5}{3(4\pi)^3} \frac{\Sigma_\ell |U_{N^\circ\ell}|^2}{B(N^\circ \to \ell\ \nu_e e)}$$

leading to a lifetime of :

$$\tau_N = \frac{M_\mu^5}{M_N^5}\ \tau_\mu \frac{B(N^\circ \to \ell\nu_e e)}{\Sigma\ |U_{N^\circ\ell}|^2}$$

It is clear from this expression that in order to observe the neutrino decay in our detector, the value $M_N^5 \Sigma |U_{N\ell}|^2$ has to be large enough.

Depending upon the mass of the heavy neutrino, the decay channels are different. The semi-leptonic decays of a light neutrino ($\sim$ 2 GeV/c²) are proceding through the hadronic resonances in the same way than for the tau lepton [2] while a heavy one will decay into the $q\bar{q}$ continuum [3]. Since the coupling of the W to quarks and leptons is identical, a naive estimation of the branching ratios gives :

$B(\ell \nu_e e) : B(\ell \nu_\mu \mu) : B(\ell \nu_\tau \tau) : B(\ell ud) : B(\ell cs) = 1:1:1:3:3$

The QCD radiative corrections are slightly modifying this to :

$B(\ell \nu_\mu \mu) \simeq B(\ell \nu_e e) \simeq 10.7$ %.

$B(\ell \nu_\tau \tau) \simeq 10.1$ %.

$B(\ell u\bar{d}) \simeq B(\ell c\bar{s}) \simeq 32$ %.

$B(\ell u\bar{s}) \simeq B(\ell c\bar{d}) \simeq 2$ %.

ℓ stands for the charged lepton which is preferentially coupled to the heavy neutral lepton.

Data preselection

Taking advantage of the good ability of our detector to identify electrons and muons, we have searched for a heavy neutral lepton coupled to one of these leptons. All the data have been therefore filtered by requiring the following cuts :

- 1 identified lepton with $P \geq 4$ GeV/c and $|\cos\theta| \leq 0.87$
- ≥ 2 tracks in the central detector

The events satisfying these cuts have then been reprocessed through our general reconstruction programme optimized for tracks having an impact parameter as large as 35 cm.

Search for heavy neutral leptons produced in pairs

Since in this case at least 2 leptons are produced, our selection criteria are :

- ≥ 4 charged particles with $|\cos\theta| < 0.92$
- ≥ 1 isolated particle identified as a lepton with $p > 2$ GeV/c
  The isolation criteria is : no charged particle in a cone 18° angle ($\cos\theta_{min} < 0.95$) around the direction of the lepton.
- ≥ 2 identified leptons of the same type and opposite charge.

According to the event multiplicity, we have distinguished 2 cases.

a) 4 particles in the final state.

- The total charge of the event should be 0
- The invariant mass of any pair of opposite charge particle should be greater than 1 GeV/c^2

The last cut is very efficient for rejecting radiative events where the photon is converted in the beam pipe, or off momentum particles interacting in the beam pipe or α^4 QED processes. The events satisfying these cuts were then fitted with 3 or 4 constraints (3C allows for the radiation of a photon in the beam pipe). Since the purely leptonic decay of a heavy neutral lepton always produced at least one neutrino, only those of the 4 prong events which do not have a good fit are kept.

b) $\geq$ 5 charged particles in the final state.

- The momenta of the leptons have to be larger than 4 GeV/c. This rejects deep inelastic scattering and inelastic Compton interactions.
- The invariant mass of the electron and its nearest charged particle has to be greater than 200 MeV/c^2. This rejects the events with an electron interacting in the beam pipe or with the conversion of a photon.

The overall efficiency of these cuts depends on the mass of the searched particles and varies from 3.6% for a mass of 2 GeV/c^2 to 51.5% for 20 GeV/c^2.

Results

We are finally left with 2 events. One 4 prong events having 3 identified electrons and a high multiplicity events with 2 identified muons. If we assume that these events are coming from $e^+e^- \rightarrow N\bar{N}$, it is possible by assigning the observed particles to one or the other heavy neutral lepton to define the smallest possible mass for N. We find respectively 8. and 13. GeV/c^2 for this smallest mass in order for these events to be acceptable candidates.

Background

There are 2 sources of background. The most important contamination comes from the processes with 2 intermediate photons (α^4). Among those, we have considered the case where an electron from the initial line is scattered at a large angle. The second lepton is created in the $q\bar{q}$ system. The other possibility which has been studied is the case were the two initial electrons are scattered at large angles. The background for the event with 2 muons comes from the conversion of a virtual photon into a mu-pair. The second source of contamination is due to the single photon annihilation into $q\bar{q}$. Since

the leptons are produced in the jets, it can be easily understood that this background is negligible in our cuts.

We have summarized in table 1 the different types of candidates found and the expected background.

Signatures	Number of events seen	Expected background
4 charged particles with 2 leptons	1	0.74 ± 0.07
≥ 5 charged particles with 2 electrons.	0	1.4 ± 0.3
≥ 5 charged particles with 2 muons.	1	0.13 ± 0.03

Table 1

Limits

In a first step, let us supose that the mixing matrix element U_{Ne} or $U_{N\mu}$ is large enough such that the decay occurs close to the interaction region (≤ 2 cm). Knowing our detection efficiencies it is simple to extract a 95% CL limit. These limits are shown in fig. 5 a and b . We exclude heavy neutral leptons pair-produced in the range from 3.2 GeV/c² to 17.4 GeV/c² if the N-μ coupling is dominant and in the range from 3.1 GeV/c² to 18.0 GeV/c² if the N-e coupling is the largest.

Let us now concentrate on the mixing matrix elements and see for which values of $|U_{N\mu}|^2$ or $|U_{Ne}|^2$ our result holds. Since we have made a 2 step selection, we have a good efficiency for events where the neutral leptons have decayed away from the interaction point. The efficiency of the pre-selection has been studied by generating MC events where the heavy neutrinos are decaying at different distances from the interaction point. These efficiencies are continuously decreasing for vertices at 5 cm to 20 cm from the interaction point. As an example, our acceptance for an event with 2 heavy neutral leptons of 15 GeV/c² both decaying at 5 cm is 55% and goes down to 19% at 20 cm. It is interesting to note that we still are reasonnably efficient up to 20 cm. Going back to the preselected data, we have made the following cuts in order to search for events with a secondary vertex.

- ≥ 4 charged particles
- The average impact parameter of the event ≥ 1 cm
- ≥ 50% of the tracks should have an impact parameter ≥ 1 cm

The events which are not accepted by these cuts will have to satisfy our previous selection criteria. All the events which fulfill the secondary vertex cuts have been visually scanned to search for candidates having 2 separated vertex. (To avoid events with interaction in the beam pipe, vertices in a region of ± 1 cm around the vacuum tube have been discarded).

No new candidate was found.

By folding the detection efficiencies $\varepsilon(X_1, X_2)$ with the decay probability,

$$E = \int_0^{25} dX_1 \int_0^{25} dX_2 \varepsilon(X_1, X_2) \left[1-\exp\left[-1.15\, X_1 \frac{M_N^6 \, |U_{N\ell}|^2}{P_N \mathrm{Br}(N\to l\nu_e e)}\right]\right]\left[1-\exp\left[-1.15\, X_2 \frac{M_N^6 \, |U_{N\ell}|^2}{P_N \mathrm{Br}(N\to l\nu_e e)}\right]\right]$$

where X_1 and X_2 are the distances (in cm) at which the decays occur, we calculate the expected number of events with the two heavy neutrinos decaying in our detector and we determine a 95% exclusion contour in the plane define by the mixing matrix element and the mass of the heavy neutrino (fig. 6). It should be noted that we have slightly better limits for heavy neutral leptons decaying away from the interaction point (≥ 2 cm). This is mainly due to the fact that no event of this type has been found. Our analysis improves the existing limits in the high mass region [4].

Single heavy neutral lepton production

It is clear from fig. 2 that this production mechanism leads to unbalanced events since one neutrino is produced back to back to the heavy neutral lepton. As an example, a 25 GeV/c² massive neutrino implies a momentum of 14.9 GeV/c for the ν_e opposite to it at an energy of 44. GeV center of mass.

Selection criteria

We have studied 2 signatures

a) For e-μ events
- 2 charged particles with $|\cos\theta| \leq 0.85$ and $P > 2$ GeV/c where 1 particle is identified as an electron and the other one as a muon.
- Acoplanarity ≥ 0.35
- $|P_1| + |P_2| \geq \frac{\sqrt{s}}{8}$

- Invariant mass of the 2 particles ≥ 0.2 GeV/c^2
- No electromagnetic neutral shower with E_{cal} 500 MeV detected.

b) Multihadronic events

- ≥ 5 charged particles with $|\cos\theta| \leq 0.92$
  where 1 charged particle identified as an electron with $P \geq 4$ GeV/c
- $\Sigma P_i \geq 10$ GeV/c.
- No charged tracks within a cone of half-angle of 18° ($\cos\theta$=0.95) around the thrust axis of the events

Results

a) e-μ events.

Within our cuts, 0.13 event is expected when 1 candidate is found. In order to check that the background is well understood, we have reduced the acoplanarity cut to 100 mrad. 12 events are observed for a background estimation of 10.8 . This allows us to conclude that there is no evidence for an anomalous production of e-μ events. Using the 1 candidate for an expected background of 0.13, we can exclude at 95% CL the existence of such objects above 600 MeV/c^2 for a V-A coupling and 400 MeV/c^2 for V+A coupling in the low mass region (fig. 7).

b) e + hadrons events.

4 candidates are found from the event selection, with an estimated background of 6.8 ± 1.1 . The main source comes from the deep inelastic scattering. We give in the table 2 the expected number of events of this reaction together with the inelastic Compton and $q\bar{q}$ annihilation. According to these numbers we can exclude a neutral lepton at 95% CL with a mass lower that 34.6 GeV/c^2 using V-A coupling and 37.4 GeV/c^2 using V+A (fig. 8).

Reactions	Number of expected events
DIS	4.9 ± 0.9
IC	1.2 ± 0.5
Annihilation	0.7 ± 0.1
Total	6.8 ± 1.1

Table 2

It is very important to note that this last search only applies for an electron like heavy neutral lepton. This implies that $|U_{Ne}|^2$ is of the order of 1. Since the cross section has to be multiplied by this parameter, we would not have been sensitive for

values smaller than 0.2 . Therefore looking for such large e-N coupling implies that the heavy neutrino will decay at the interaction point. The present result improves the earlier limits from PETRA [5].

CONCLUSION

We have searched for a heavy neutral lepton pair-produced through the Z^0 boson or produced together with a usual neutrino in the t channel. No evidence has been found in both cases. We have set 95% CL limits in a range going from 3.1 to 18.0 GeV/c^2 in the first mode while in the second mode we exclude the region between 0.6 to 34.6 GeV/c^2 with a V-A current at the eWN vertex and between 0.4 to 37.4 GeV/c^2 with V+A .

REFERENCES

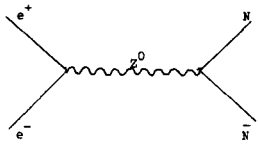
[1] : CELLO Collaboration, H.J. Behrend et al., Physica Scripta 23 (1981) 61

[2] : Y.S.Tsai, Phys. Rev. D4 (1971) 2821.

[3] : Y.S.Tsai, SLAC PUB 2450 (1979).

[4] : G.Feldman, Proceedings of the Leptonic session of the XXth Rencontre de Moriond, Les Arcs, March 17-23 1985 , edited by J.Tran Thanh Van (Editions Frontières), p.323.

[5] : Jade collaboration, W.Bartel et al., Phys. Lett. 123B (1983) 353.



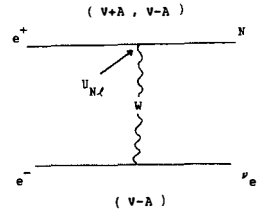


Fig. 1 : Feynman diagram for $e^+e^- \rightarrow N\bar{N}$

Fig. 2 : Feynman diagram for $e^+e^- \rightarrow N\nu_e$

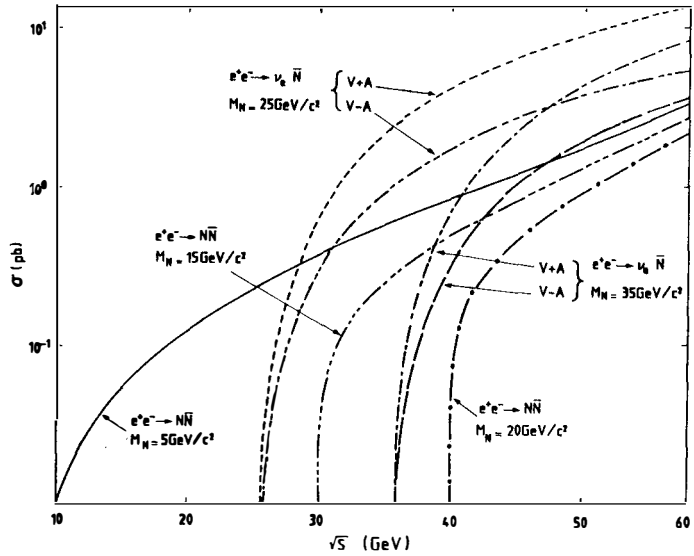


Fig. 3 : Total cross section versus the center of mass energy for several mass of heavy neutral lepton for the reaction of fig. 1 and fig. 2 .

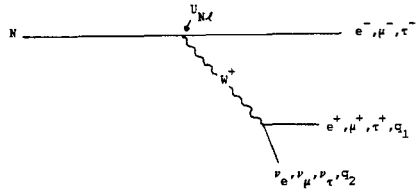


Fig. 4 : Decay mechanism of a heavy neutral lepton

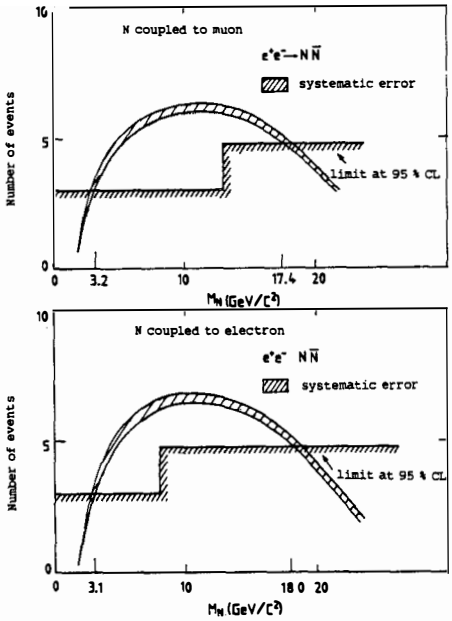


Fig. 5 : Expected number of events versus the mass of the heavy lepton pair produced
a) with a dominant coupling to muons
b) with a dominant coupling to electrons

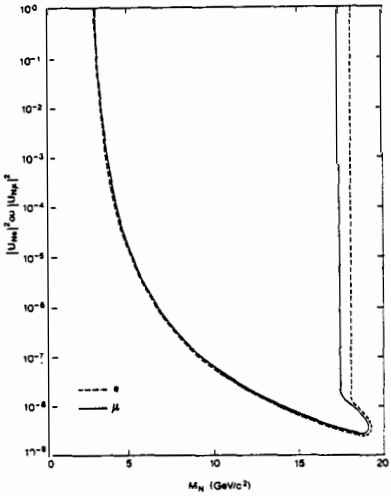


Fig. 6 : 95% CL exclusion contour of heavy neutral leptons versus the $|U_{N\ell}|^2$.
The solid line is for $|U_{N\mu}|^2$ and the dashed line for $|U_{Ne}|^2$.

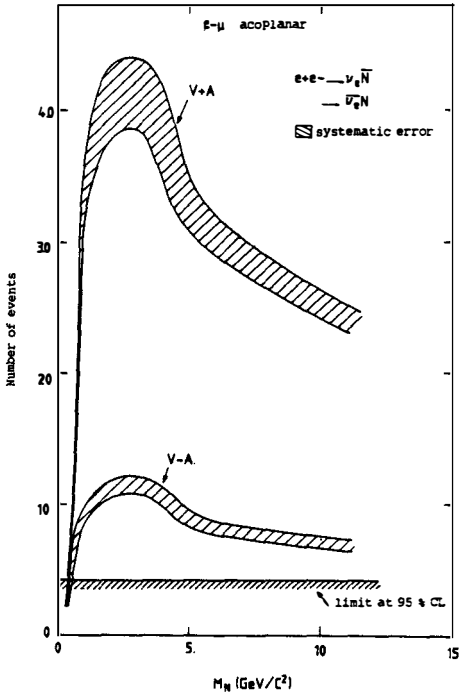


Fig. 7

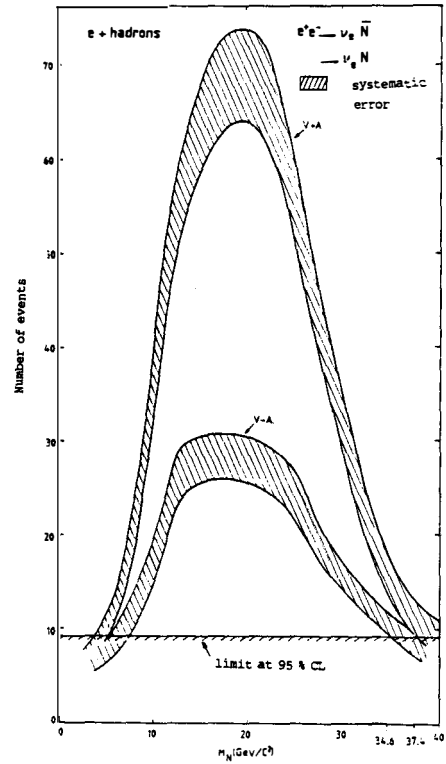


Fig. 8

Fig. 7 : Expected number of events versus the mass of the heavy lepton produced by the mechanism of fig. 2 and with an e-μ final state.

Fig. 8 : Expected number of events versus the mass of the heavy lepton produced by the mechanism of fig. 2 and with an e+hadrons final state.

A SEARCH FOR HEAVY NEUTRAL LEPTONS IN ν_μ-N INTERACTIONS

S. Mishra, P. Auchincloss, R. Blair, C. Haber, W.C. Leung, E. Oltman, M. Ruiz, F.J. Sciulli, M. Shaevitz, W.H. Smith
R. Zhu, Columbia University, New York, NY 10027
Y.K. Chu, D.B.MacFarlane, R.L. Messner, D.B. Novikoff, M.V. Purohit, California Institute of Technology, Pasadena, CA 91125
D. Garfinkle, F.S. Merritt, M. Oreglia, P. Reutens
University of Chicago, Chicago, IL 60637
R. Coleman, H.E. Fisk, Y. Fukushima, Q. Kerns, B. Jin, D. Levinthal, T. Kondo, W. Marsh, P.A. Rapidis, S. Segler, R. Stefanski, D. Theriot, H.B. White, D. Yovanovitch
Fermi National Accelerator Laboratory, Batavia, IL 60510
A. Bodek, F. Borcherding, N. Giokaris, K. Land, I. Stockdale,
University of Rochester, Rochester, NY 14627
O. Fackler, K. Jenkins, Rockefeller University, NY, NY 10021

Talk presented by M. Shaevitz.

ABSTRACT

Preliminary results from a search for heavy neutral lepton production in high energy, neutrino interactions are presented. No evidence for heavy lepton production is observed and heavy leptons with masses between 1-14 GeV are excluded for couplings to muons below 1 to 10^{-3} of Fermi strength, depending on the lepton mass.

Neutral heavy leptons have been proposed in many theoretical models. These models include many grand unified theories,[1,2] models[3] with a fourth generation of fermions (L^o,L^-), and postulates[4] of recurrences of the known lepton flavors including ν_e, ν_μ and ν_τ. Past searches using particle decays (π, K and D-mesons) have probed heavy lepton masses below $\sim$ 2 GeV. Higher energy e^+e^- experiments at PEP and Petra have extended the mass range up to 22.5 GeV mainly for heavy leptons coupled to electrons. We present preliminary results of a search for neutral heavy leptons produced in a high energy muon neutrino scattering experiment probing lepton masses up to 14 GeV.

The experiment uses the Fermilab dichromatic neutrino beam[5] and the CCFRR detector.[6] For the experiment, 5.64 x 10^{18} protons accumulated during two running periods[7] produced momentum and sign-selected secondary pions and kaons. These secondaries traverse a 350m long evacuated decay pipe, and produce neutrinos at the detector ($\sim$ 1 km downstream) with energies between 30 and 250 GeV. The detector consists of a 640 ton target calorimeter with liquid scintillation counters and muon tracking spark chambers followed by a 340 ton muon spectrometer also instrumented with spark chambers. The fractional resolution is $0.89/\sqrt{E}$ and 0.11 for the hadron shower energy and the muon momentum respectively. For this study, 164,000 neutrino-nucleon charged and 50,000 neutral-current interactions were recorded with a measured anti-neutrino contamination of 10^{-3}.

Heavy neutral leptons can be produced in neutrino scattering reactions via the neutral current interaction. If U^2 represents the coupling relative to Fermi strength, then the production of a heavy neutral lepton, L^o, with mass M_{L^o} has a production cross section of

$$\frac{\sigma(\nu_\mu N \to L^o X)}{\sigma(\nu_\mu N \to \nu_\mu X)} = U^2 \cdot \left(1 - \frac{M_{L^o}^2}{sx_{BJ}}\right) ,$$ where s = square of the c.m. energy .

After production, the L^o can then decay either by the charged or neutral-current interaction to leptons and hadrons. We have used two methods to search for a neutral heavy lepton

signature: 1) the anomalous production of dimuon events with kinematics different from charm production or pion/kaon decay; 2) heavy leptons with lifetimes such that a secondary vertex will appear downstream of the primary production vertex.

In the first method, 658 dimuon events inside the fiducial region of the detector with $P_{\mu+}$ and $P_{\mu-}$ greater than 4.5 GeV were considered. These events have been separated from the total data sample by using loose analysis requirements to isolate candidates followed by visual scanning by physicists. The efficiency for a true dimuon event to reach this sample is greater than 99%. (The event selection and efficiency is discussed more fully in Ref. 7.) These dimuon events are then subjected to further requirements that eliminate the common sources of dimuons, charm production and pion/kaon decays in the hadronic shower. Those specialized cuts are:

ϕ_{-+} (azimuthal angle between the two muons) $< 120^{o}$

$P^{T}_{\mu+}$ (transverse momentum of the μ^{+} with respect to the beam direction) > 1.2 GeV

$P_{\mu+}/P_{\mu-}$ (momentum ratio of the two muons) > 0.1 .

With these cuts, all observed dimuons are eliminated. On the other hand, a large fraction of dimuons from heavy lepton decay would pass these cuts (the efficiency for a L^{o} with $M_{Lo} = 5$ GeV is 53%). Figure 1 shows the ϕ_{-+} and $P^{T}_{\mu+}$ distributions of the data (solid line) and a Monte Carlo simulation of a 5 GeV heavy lepton (dashed line). The null result of the experiment combined with Monte Carlo efficiency calculations for different mass heavy lepton, then, yields the 90% C.L. limits shown in Fig. 2 (curve a).

The second method seeks to isolate long-lived heavy leptons that decay in the apparatus. Each observed neutral-current event is searched starting 1 meter downstream of the primary production vertex for an indication of a secondary decay vertex. The secondary vertex must have two consecutive scintillation counters with pulse height corresponding to greater than ten minimum ionizing particles. (The target has scintillation counters every 10 cm of steel and has an average density of 4.25 g/cm^{3}.) With the additional requirement that the average pulse height in the counters between the end of

the primary vertex and start of the secondary vertex be less than 0.5 minimum ionizing per counter, no events in the data sample survive. To obtain a limit on neutral lepton production, a Monte Carlo calculation incorporating the lifetime of the L^o, geometrical acceptance, and losses in the primary hadron shower gives the sensitivity versus lepton mass. For this calculation, the heavy lepton lifetime is assumed to follow the standard V-A calculation with corrections for the effective number of charged current channels available in the decay, $\Phi(M_{L^o})$:[1)]

$$\Gamma_{L^o} = |U|^2 \Phi(M_{L^o}) \left(\frac{M_{L^o}}{M_\mu}\right)^5 \Gamma_\mu \quad .$$

Combining the Monte Carlo with the absence of double vertex events in the data leads to the 90% C.L. limits shown in Fig. 2 (curve b).

In summary, we observe no evidence for neutral heavy lepton production by incident muon neutrinos and exclude heavy leptons in the mass range of 1-14 GeV with couplings to muons below 1 to 10^{-3} of Fermi strength depending on the lepton mass. These results are preliminary; final results will be published in the near future.

References

1) M. Gronau et al, Phys. Rev. D29, 2539 (1984).
2) R.N. Mohapatra, G. Senjanovic, Phys. Rev. D23, 165 (1981).
3) M. Perl, Proc. Santa Fe DPF Mtg., p. 159 (1984).
4) J.D. Bjorken, C.H. Llewellyn-Smith, Phys. Rev. D7, 887 (1973).
5) R. Blair et al, NIM 226, 281 (1984).
6) D. MacFarlane et al, Z. Phys. C26, 1 (1984).
7) K. Lang et al, submitted to Z. fur Phys. C.

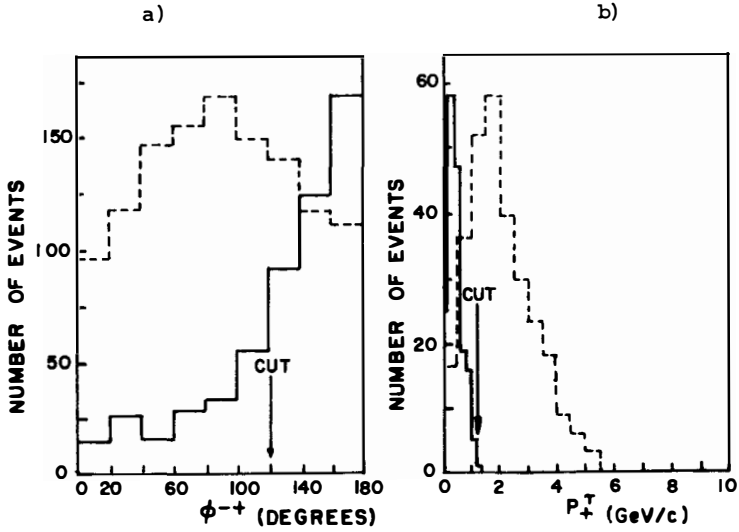


Fig. 1a) The distribution of the azimuthal angle between the μ^+ and μ^-. (The solid line is the data and the dashed line is from the Monte Carlo calculation with M_{LO} = 5 GeV.)
Fig. 1b) The distribution of the transverse momentum of the μ^+ with respect to the beam direction (curves as in Fig. 1a)

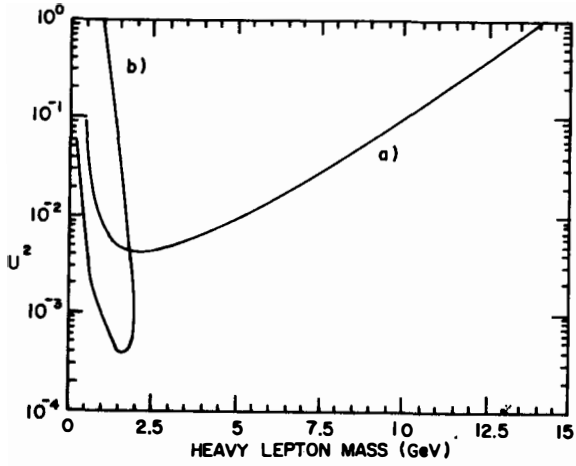


Fig. 2) The correlated 90% C.L. limit between the heavy lepton mass, M_{LO}, and the coupling to muons, U^2. The dimuon search gives curve a) and the double vertex search curve b). (The region above the curves is excluded.)

NEUTRINO OSCILLATION EXPERIMENTS AT ACCELERATORS

Michael H. Shaevitz

Columbia University
New York, NY 10027 USA



ABSTRACT

A review of the current and future neutrino oscillation experiments at accelerators is presented.

Over the past two decades, the neutrino has been one of the main probes used to study weak interactions. These studies have been in excellent agreement with the standard electro-weak model. In this model, the neutrino is a weakly interacting, spin 1/2 particle which is assumed to have zero mass and definite lepton number. In general, there is no inherent reason for neutrinos to be massless and, further, if they are massive, the mass matrix need not be diagonal. If the mass matrix is non-diagonal and at least one neutrino flavor has a finite mass, then neutrino oscillation can occur. Neutrino oscillations provide the only possible tool to study muon and tau neutrino masses in the keV and below mass range. In addition, oscillation studies can also show the effects of a massive fourth generation neutrino or a wrong-handed neutrino.

Neutrino oscillations will occur if two conditions are satisfied: 1) The weak eigenstates are quantum mechanical mixtures of mass eigenstates,

$$\nu_\alpha = \Sigma U_{\alpha j}\nu_j \ , \text{ with } \alpha = e,\mu,\tau,\ldots \text{ and } j = 1,2,3 \ldots$$

2) At least one mass eigenstate has a finite mass with,

$$\Delta m_{ij}^2 = m_{\nu_i}^2 - m_{\nu_j}^2 \neq 0 \ .$$

For the case of two component mixing, the initial weak eigenstate is given by

$$|\nu_\alpha\rangle = \cos\theta|\nu_1\rangle + \sin\theta|\nu_2\rangle \ ,$$

where $|\nu_1\rangle$ and $|\nu_2\rangle$ are the mass eigenstates and $\sin\theta = U_{\alpha 2} = U_{\beta 1}$ describes the two component mixing. From these equations, one can then derive the following probability distributions for the transitions of a weak eigenstate $|\nu_\alpha\rangle$:

i) $$\text{Prob}(\nu_\alpha \rightarrow \nu_\alpha) = 1 - \sin^2(2\theta)\sin^2\left(\frac{1.27\ \Delta m^2 L}{E}\right) \ ,$$

and

ii) $$\text{Prob}(\nu_\alpha \rightarrow \nu_\beta) = \sin^2(2\theta)\sin^2\left(\frac{1.27\ \Delta m^2 L}{E}\right) \ ,$$

where L is the distance from the ν source to the detector in km, E is the energy of the ν in GeV, and Δm^2 is in eV^2. An extension to more than one active oscillation channel can easily be made but the number of parameters to be experimentally determined increases. For this reason, most experimental papers present results only for the one channel

assumption. Kleinknecht[1] at this conference has investigated the restrictions on mixings and masses for three component oscillations that can be obtained by combining the results of many experiments on different channels.

Inclusive Oscillation Experiments

Two types of oscillation experiments, inclusive (or disappearance) and exclusive (or appearance) experiments, are possible corresponding to Eq. i) or ii), respectively. An inclusive (or disappearance) oscillation study is made by measuring the change in the number of a given type of neutrino, ν_α, with distance or energy. These experiments are sensitive to all the oscillation channels probed by exclusive experiments and, in addition, to oscillation in which the final state neutrino does not interact with the usual strength. Examples of the latter are: 1) a ν_x associated with a new heavy lepton with mass too heavy to be produced in present neutrino experiments; and 2) wrong-handed neutrinos (i.e. $\bar{\nu}_\mu$ left-handed) with suppressed weak interaction couplings.

The small Δm^2 sensitivity of an inclusive experiment is dependent on the statistical and systematic errors present for the comparison to Eq. i). Measurements of the ν interaction rate at two distances minimizes the dependence of the measurement on knowledge of the energy spectrum and absolute flux at the source. Further, if the data at the two distances are taken simultaneously by using two detectors, any systematic time dependence errors are also eliminated. For an oscillation measurement using data at two distances, there is a high Δm^2 limit to the sensitivity of the experiment. This limit corresponds to the point at which both detectors are many oscillation lengths from the source. At this point, the finite neutrino source size and detector energy resolution reduce the oscillatory behavior of Eq. i).

The high Δm^2 limit is absent if the neutrino intensity as a function of E_ν at the source is known. This knowledge is typically model dependent and therefore introduces some additional systematic uncertainties.

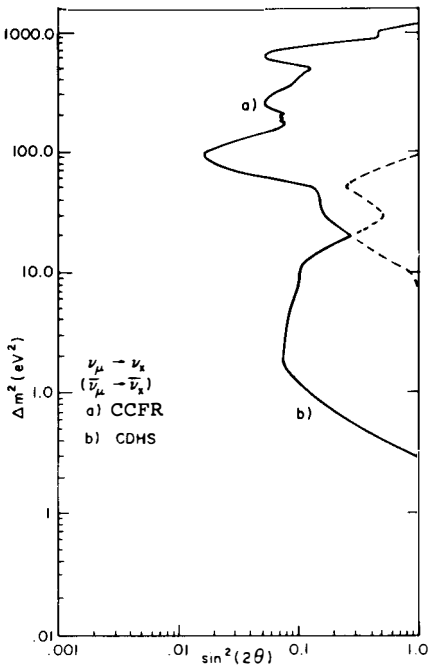
Inclusive oscillation measurements have been made in

muon and electron neutrino beams. Table I and Fig. 1 give a summary of the current situation assuming only two component mixing. The electron neutrino measurements have been made primarily with anti-electron neutrinos from reactors. The details of these measurements are discussed more fully in other parts of these proceedings but the results of the two major experiments, Bugey[6] and Goesgen,[5] are in some disagreement.

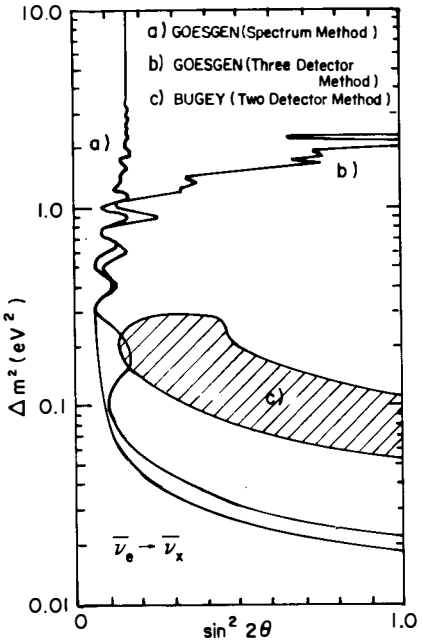
Table I: Present Inclusive Limits

	Lower Limit Δm^2 for $\sin^2(2\theta)=1$	Best Limit $\sin^2(2\theta)$	Experiment
$\nu_\mu \rightarrow \nu_x$	.3 eV^2	.06/Δm^2=3eV^2	CDHS-PS[2]
	15 eV^2	.02/Δm^2=120eV^2	CCFR(NBB)[3]
$\bar{\nu}_\mu \rightarrow \bar{\nu}_x$	15 eV^2	.02/Δm^2=200eV^2	CCFR(NBB)[3]
$\nu_e \rightarrow \nu_x$	10 eV^2	.34/Δm^2 large	BEBC(WBB)[4]
$\bar{\nu}_e \rightarrow \bar{\nu}_x$	.015 eV^2	.17/Δm^2 large	Goesgen(reactor)[5] (spectrum analysis)
	.12 eV^2	.2/Δm^2=1eV^2	Bugey (reactor)6) (two detector analysis)
	[positive signal(3.2σ) Δm^2=.2eV^2 $\sin^2 2\theta$=.25]		

Searches for inclusive muon neutrino oscillation have been performed by the CCFR[3] and CDHS[2] collaborations using two detectors in a high energy ($<E_\nu>$ = 80 GeV) and low energy ($<E_\nu>$ = 1.2 GeV) muon neutrino beam respectively. The CCFR experiment, in the Fermilab high energy, dichromatic beam, collected 150 k charged current events in two detectors at 715 m and 1115 m from the decay pipe or neutrino source (Fig. 2). Analysis requirements were imposed to equalize the acceptance of the detectors and to ensure that all accepted events would trigger and be fully reconstructed in both detectors. The oscillation measurement was performed by comparing the number of events in the two detectors as a function of neutrino energy (Fig. 3). A comparison of the data with the hypothesis of no oscillations gave an acceptable χ^2 and, therefore, was consistent with a null



a)



b)

Fig. 1. Inclusive oscillation limits for a) $\nu_\mu \rightarrow \nu_x$, and b) $\bar{\nu}_e \rightarrow \bar{\nu}_x$ (90% C.L.).

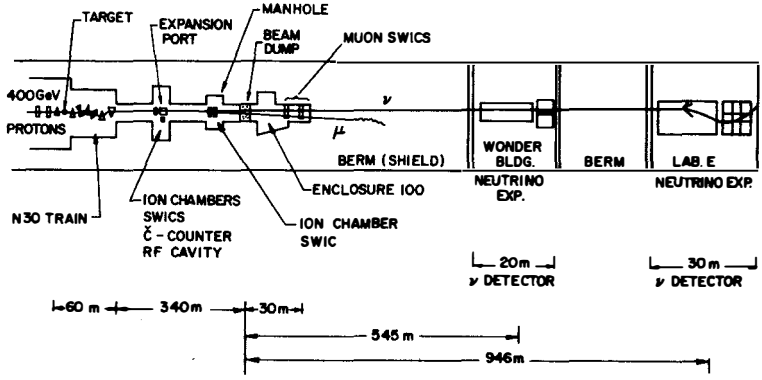


Fig. 2. Narrow band beam configuration for the CCFR Expt.

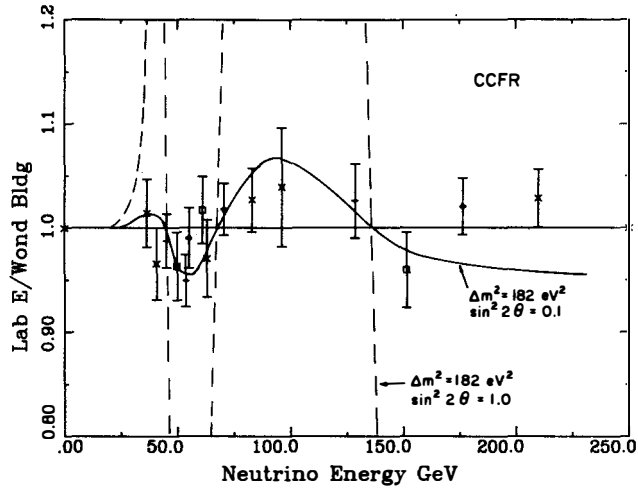


Fig. 3. Ratio of events in two detectors from the CCFR experiment. A curve (solid) for a typical Δm^2 value and 10% mixing is shown. The curve for maximal mixing (dashed) at the same Δm^2 is largely off-scale.

signal. Statistical comparisons of the data with various Δm^2 and $\sin^2(2\theta)$ hypotheses were then used to produce the 90% C.L. limits shown in Fig. 1. The CDHS experiment used a low energy bare target beam from the CERN-PS with two detectors at 130 m and 880 m from the source. Comparing the event rates in the two detectors with the expected $1/L^2$ behavior yielded the limits shown in Fig. 1. The combination of the CCFR and CDHS limits excludes $\nu_\mu \rightarrow \nu_x$ oscillations in the region between $1 < \Delta m^2 < 800$ eV^2 for mixings with $\sin^2(2\theta) > 0.1$.

Exclusive Oscillation Experiments

In an exclusive (or appearance) search, an experiment must isolate the anomalous appearance of some neutrino type, ν_β, in a relatively pure beam of another type, ν_α. If no statistically significant signal of ν_β's are observed, the experiment can then set limits on the probability for ν_α to change into ν_β, $P(\nu_\alpha \rightarrow \nu_\beta)$. The limit of $P(\nu_\alpha \rightarrow \nu_\beta)$ can then be turned into a correlated limit on $\sin^2(2\theta)$ and Δm^2 using Eq. ii). The region covered by a given experiment is bracketed by the following limits:

Large $\sin^2(2\theta) \approx 1$ Region	Large $\Delta m^2 (L \gg L_{osc} = \frac{2.5E_\nu}{\Delta m^2})$ Region
$\Delta m^2 > [P(\nu_\alpha \rightarrow \nu_\beta)]^{\frac{1}{2}} / 1.27 (\frac{L}{E_\nu})$	$\sin^2(2\theta) > 2P(\nu_\alpha \rightarrow \nu_\beta)$

The sensitivity of an experiment is determined by the background rate of ν_β's, the measured rate of ν_α's, and the value of L/E_ν. Large L/E_ν values give the smallest Δm^2 limits but may decrease the $\sin^2(2\theta)$ sensitivity because the observed ν_α event rate falls with increasing L or decreasing E_ν. To make a convincing case for a positive signal, the properties of the ν_β's (i.e. the energy distribution) should resemble the ν_α's, and the appearance of the ν_β's should follow the energy/distance relation of Eq. ii).

The current best exclusive limits are given in Fig. 4 and Table II. (A more complete discussion of exclusive limits is given in Ref. 7.) All experiments assume two component mixing in the analysis and the limits are at the 90% C.L.

Table II: Present Exclusive Limits for Neutrino Oscillations

	Δm^2 at $\sin^2(2\theta)=1$	Large Δm^2 $\sin^2(2\theta)$ Limit	Experiment
$\nu_\mu \rightarrow \nu_e$	0.6 eV^2	6×10^{-3}	Col-BNL [8]
	1.16 eV^2	0.038	BEBC/PS [9]
	0.43 eV^2	3.4×10^{-3}	BNL-E734 [10]
	Positive Result	$\sin^2(2\theta)=0.03\pm .01$ @ $\Delta m^2=5 eV^2$	PS-191 [11]
$\bar{\nu}_\mu \rightarrow \bar{\nu}_e$	2.4 eV^2	0.013	FNAL/15' [15]
	0.49 eV^2	0.028	LAMPF-UCI [13]
$\nu_\mu \rightarrow \nu_\tau$	3 eV^2	0.013	FNAL-E531 [14]
$\bar{\nu}_\mu \rightarrow \bar{\nu}_\tau$	2.2 eV^2	0.044	FNAL/15' [12]
	7.4 eV^2	0.088	FNAL/15' [15]
$\nu_e \rightarrow \nu_\tau$	8.0 eV^2	0.6	Col-BNL [8]
$\bar{\nu}_e \rightarrow \bar{\nu}_\tau$	None	None	None

The BEBC-PS experiment[9] uses a high intensity, low energy ($\langle E_\nu \rangle \approx 1.5$ GeV) horn neutrino beam from the CERN PS which was designed to have a small ν_e contamination. The decay tunnel is 45m long and the BEBC bubble chamber is located 825m from the source. Four electron neutrino events have been found for a sample of 418 muon neutrino events leading to the limits shown above.

For the BNL 734 experiment,[10] the detector was located 96m from the neutrino source, a wide-band horn beam with $\langle E_\nu \rangle \approx 1.2$ GeV. The experiment detected 418 ν_e quasi-elastic and 1370 ν_μ quasi-elastic events. After correcting for the difference in the number of protons on target in these samples (a factor of 6.29) and the difference in acceptance due to the high $Q^2 > 0.35$ GeV^2 cut for the ν_μ events (a factor of ~ 10), the measured ν_e/ν_μ flux ratio is given as $\sim 0.5 \times 10^{-2}$. Subtracting the calculated ν_e flux from kaon and muon decay thus gives the limits shown in Fig. 1 and Table I.

The PS 191 experiment[11] uses an electromagnetic calorimeter detector at 130m from the neutrino source. The

source is the bare target beam at CERN with an average neutrino energy of 600 MeV. The detector is a fine sampling (.7 χ_o samples) calorimeter using flash tube chambers and 3mm iron sheets. The fine sampling allows the experiment to study the backgrounds to ν_e events from π^o production by muon neutrinos. The experiment detects 27 ν_e candidates in a sample of $\sim$ 600 ν_μ events. The expected number is 8.2 ± 1.6 from ν_e's in the beam and π^o background and leads to an excess of 18.8 ± 5.4 events or $2.9\pm0.9\%$ of the ν_μ flux. If this excess is interpreted as neutrino oscillation, the positive signal results in the allowed region shown in Fig. 4. This result is compatible with the BEBC-PS result if $\sin^2(2\theta) < 0.025$ but is in conflict with the BNL 734 measurement. If the PS-191 signal is taken to be $\Delta m^2 = 5$ eV^2 and $\sin^2(2\theta) = 0.03\pm0.009$, then the predicted rate for the BNL experiment is $\nu_e/\nu_\mu = 0.7\pm0.2\%$. The BNL experiment observes $0.4\pm0.08\%$ with no beam ν_e subtraction and $0.0\pm0.10\%$ with a subtraction.

Several $\nu_\mu \rightarrow \nu_e$ experiments will have results shortly covering an even larger sensitive region. The PS 191 detector is being brought to Brookhaven and will take data in Spring/Summer of 1986. In addition, two experiments are presently underway at Brookhaven (E776-Columbia/Illinois/Johns Hopkins) and LAMPF (E645-Ohio St/Argonne/LAMPF). These experiments should have good sensitivity (E776 should cover $\sin^2 2\theta > 10^{-3}$ for $\Delta m^2 > 0.7$ eV^2) in the region of the PS 191 result and results are expected in the next year.

Several searches have been made for $\nu_\mu \rightarrow \nu_\tau$ oscillations using bubble chamber and counter detectors. The most sensitive search was performed by the E531 hybrid emulsion spectrometer in the Fermilab wideband horn beam. The experiment used an emulsion target of necessarily small size (23 ℓ), 700m from the neutrino source and searched for τ-leptons with finite decay length. The total ν_μ interactions recorded in the emulsion was 1241 and when combined with a threshold factor for the τ-lepton mass leads to the limits shown in Fig. 4. In principle, a better $\sin^2(2\theta)$ sensitivity could be achieved with a larger detector if at the same time τ-leptons could be isolated with little background. Better sensitivity

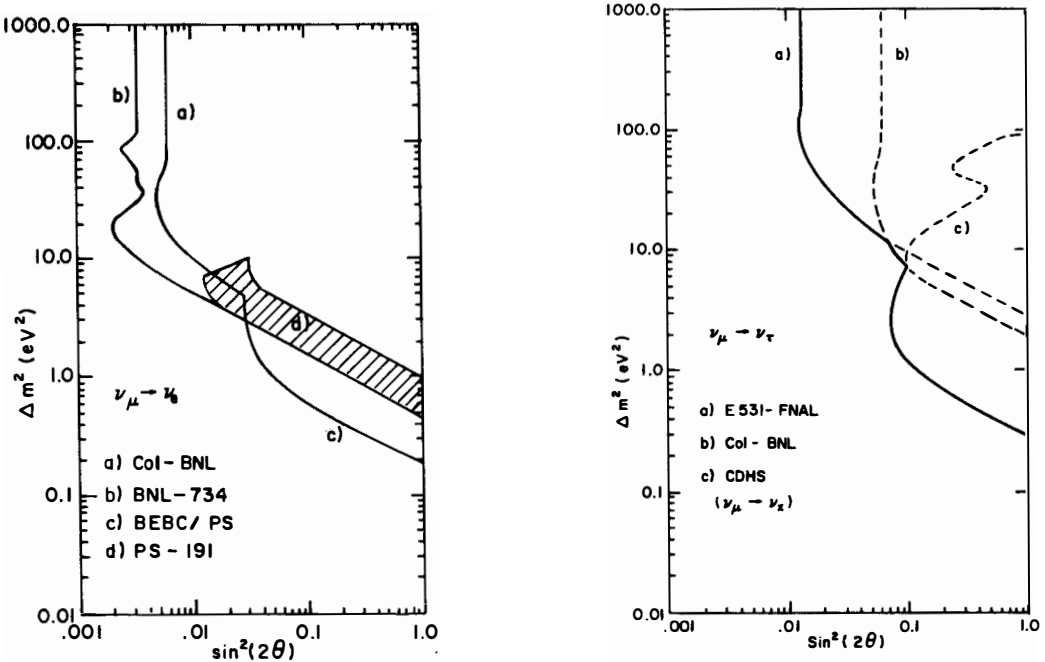


Fig. 4. Exclusive oscillation limits for a) $\nu_\mu \rightarrow \nu_e$, and b) $\nu_\mu \rightarrow \nu_\tau$ (90% C.L.).

at lower Δm^2 could be achieved by placing the detector farther from the neutrino source but, then, will result in less $\sin^2(2\theta)$ sensitivity. At present, no new $\nu_\mu \rightarrow \nu_\tau$ searches are planned.

Conclusions

The search for neutrino oscillations has covered most of the possible channels but certainly not most of the allowed parameter space. The majority of experiments has obtained negative results setting limits on the allowed oscillation parameters. Two experiments have reported positive signals. These experiments along with others will continue running in this region with better statistics and control of systematic uncertainties, and should either confirm or refute the positive result.

At present there is no strong theoretical argument why neutrinos should be massless; in fact, it is natural to assume that they are massive with mixing between generations of weak eigenstates. Setting the scale of these masses and mixings is another problem with little theoretical guidance. For these reasons, experimentalists will continue to probe the unexplored regions of small masses and mixings as experimental techniques and opportunities are improved.

This research was supported in part by the National Science Foundation.

References

1) K. Kleinknecht, "Oscillations between Three Neutrino Flavors", these Proceedings.
2) F. Dydak et al, Phys. Lett. 134B, 34 (1984).
3) I.E. Stockdale et al, Phys. Rev. Lett. 52, 1384 (1984); C. Haber et al, Fourth Moriond Workshop, France (1984). I.E. Stockdale et al, Z. Phys. C27, 53 (1985).
4) O. Erriquez et al, Phys. Lett. 102B, 73 (1981).
5) K. Gabathuler et al, Phys. Lett. 138B, 449 (1984). V. Zacek et al, Phys. Lett. 164B, 193 (1985).
6) J.-F. Cavaignac et al, Phys. Lett. 148B, 387 (1984).
7) C. Baltay, Neutrino 81, Maui, Hawaii (1981); A. Bodek, ICOBAN 84, Park City, Utah (1984); M. Shaevitz, Proc. Lepton-Photon Symposium, Cornell Univ. (1983).
8) N.J. Baker et al, Phys. Rev. D28, 2705 (1984).
9) R.J. Loveless et al, Proc. DPF Mtg. U of Oregon (1985).
10) L.A. Ahrens et al, Phys. Rev. D31, 2732 (1985).
11) F. Vannucci, Proc. EPS-HEP 85 Conf., Bari, Italy (1985).
12) A.E. Asratyan et al, Phys. Lett. 105B, 301 (1981).
13) H. Chen et al, Irvine-Los Alamos-Maryland experiment E225 at LAMPF. See J. Wotschack review talk at Neutrino 84, Dortmund, Germany.
14) N. Ushida et al, Phys. Rev. Lett. 47, 1694 (1981).
15) G.N. Taylor et al, Phys. Rev. D28, 2705 (1984).

EXPERIMENTAL CONSTRAINTS ON LEPTON MIXING ANGLES AND NEUTRINO MASS DIFFERENCES FOR THREE SIMULTANEOUSLY OSCILLATING NEUTRINO FLAVOURS

K. Kleinknecht
Institut für Physik der Universität Mainz
Mainz, Fed. Rep. Germany

Abstract

An analysis of experimental results in the framework of simultaneous oscillations of three neutrino flavours is used, in a combined fit, to constrain the elements of the 3 x 3 unitary lepton mixing matrix and to obtain limits on the three lepton mixing angles $\alpha_{e\mu}$, $\alpha_{e\tau}$ and $\alpha_{\mu\tau}$.

Lepton mixing can be described by a 3 x 3 unitary matrix. In fact, the weak eigenstates ν_e, ν_μ and ν_τ are related to the mass eigenstates ν_1, ν_2 and ν_3 by a unitary matrix U_{ik} [1]:

$$|\nu_\ell> = \Sigma_k U_{\ell k} |\nu_k> \qquad (\ell = e,\mu,\tau;\ k = 1,2,3) \qquad (1)$$

and this matrix $U_{\ell k}$ can be parametrized in analogy to the quark mixing matrix. We use the parametrization of Maiani [2], given in table 1.

Table 1

Maiani parametrization of lepton mixing matrix

$$U = \begin{pmatrix} C_\beta C_\theta & C_\beta S_\theta & S_\beta \\ -S_\gamma C_\theta S_\beta e^{i\delta'} - S_\theta C_\gamma & C_\gamma C_\theta - S_\gamma S_\beta S_\theta e^{i\delta'} & S\gamma C\beta e^{i\delta'} \\ -S_\beta C_\gamma C_\theta + S_\gamma S_\theta e^{i\delta'} & -C_\gamma S_\beta S_\theta - S_\gamma C_\theta e^{-i\delta'} & C_\gamma C_\beta \end{pmatrix}$$

Up to now, the scarcity of data and the complexity of the problem have prevented a general analysis of experimental data without restrictive assumptions, i.e. with three free angles and neutrino masses. Instead, experimentalists searching for neutrino oscillations have usually made the ad hoc assumption that only one angle and one neutrino mass difference is different from zero, and have given their results in terms of these two quantities.

We present here a general analysis of available experimental data with five free parameters, i.e. three angles and two neutrino mass differences [3].

The time evolution of an initially pure ν_ℓ state can be expressed in terms of mass differences and the neutrino energy E. If this energy is large compared to the neutrino mass, the probability to find a $\nu_{\ell'}$, after a distance L(m) from the production point of an initially pure ν_ℓ state of energy E(MeV) is [4]:

$$P_{\ell\ell'} = \sum_{k,k'=1} U_{\ell k} U_{\ell k'} U_{\ell' k} U_{\ell' k'} \cos (2.54\ \Delta m^2_{k'k} L/E) \qquad (2)$$

where $\Delta m^2_{k'k} = |m^2(\nu_{k'}) - m^2(\nu_k)|$ is measured in (eV^2).

As a simplification, the elements $U_{\ell k}$ are assumed to be real. This leaves us with five free parameters to be determined, because for thee neutrino masses only two Δm^2 values are independent.

For the Maiani parametrization, in the limiting case of only one angle being finite, this angle can be directly related to oscillations between two flavours of neutrinos. The Maiani angles θ, β and γ are thus uniquely related to the oscillations channels $\nu_e \leftrightarrow \nu_\mu$, $\nu_e \leftrightarrow \nu_\tau$ and $\nu_\mu \leftrightarrow \nu_\tau$ respectively. We call these angles $\theta = \alpha_{e\mu}$, $\beta = \alpha_{e\tau}$ and $\gamma = \alpha_{\mu\tau}$. We note that this decoupling of angles does

not occur in the Kobayashi-Maskawa notation.

The experimental data on neutrino oscillations can be divided into two classes: 1. Disappearance experiments, where the flux of neutrinos of one flavour is measured at two distances from their production point. 2. Appearance experiments, where neutrinos of flavour ℓ are searched for in a beam of neutrinos of flavour $k \neq \ell$.

For the simultaneous fit of oscillation experiments of different kinds, we have used all data from reactor and accelerator experiments available at this time. They are listed in table 2 [4]. For each experiment, the original data were used, such that for a given neutrino energy each experiment gives a contribution to the global χ^2 in the fit. For each experiment we checked that, making the restrictive assumptions of the authors, the procedure used here gave back the quoted result of the authors in the two-parameter model with only one θ and one Δm^2.

Table 2

Oscillation experiments included in the fit [4]. The last column is the χ^2 contribution of the experiment for the hypothesis of no oscillation.

Experiment	Measured quantity	Δm^2 range [eV^2]	$\chi^2_{\text{no osc.}}$ / NDF
(1) CCFRR	$P_{\mu\mu}$ ratio	30. - 1000.	15.5/14
(2) CDHS	$P_{\mu\mu}$ ratio	0.24 - 90.	15.3/14
(3) CHARM	$P_{\mu\mu}$ ratio	0.60 - 20.	1.8/3
	$P_{e\mu}$ difference	1. - 10.	0/0
(4) GOESGEN	P_{ee} absolute	> 0.01	15.5/15
(5) GOESGEN	P_{ee} ratio	0.03 - 3.	7.4/15
(6) BUGEY	P_{ee} ratio	0.02 - 5.	20.9/8
(7) ν_τ Exp.'s	$P_{\mu\tau}/P_{\mu\mu}$	> 0.2	6.3/5
(8) BNL	$P_{\mu e}$ absolute	> 0.43	2.4/6

A total chisquare function was constructed from the measured quantities Q^m (ratios of oscillation probabilities at different L/E or absolute probabilities from a comparison to calculated initial fluxes) and the corrsponding computed values Q^c. The data points of each experiment i are allowed to vary together by a scale factor N_i within the quoted normalization uncertainty $\sigma(N_i)$. The expression

$$\chi^2 = \sum_{i=1} \left[\sum_j \left(\frac{N_i\, Q^m_{ij} - Q^c_{ij}}{\sigma(Q^m_{ij})} \right)^2 + \left(\frac{N_i - 1}{\sigma(N_i)} \right)^2 \right] \qquad (3)$$

is minimized by fitting the mixing angles and mass differences, where the index i labels the experiments, and the index j gives the bin in L/E for a specific experiment.

The results of the best fit are listed in table 3. Limits on the oscillation parameters can be derived from (3) in three parameter planes ($\sin^2 2\alpha_{e\mu}$, Δm^2_{12}), ($\sin^2 2\alpha_{e\tau}$, Δm^2_{13}), and ($\sin^2 2\alpha_{\mu\tau}$, Δm^2_{23}). The curves in Fig.1 give the largest allowed $\sin^2 2\alpha$ values (for 90%C.L.) as a function of the corresponding Δm^2. Each such point has been obtained under the condition that in the other two planes all combinations ($0. < \sin^2 2\alpha < 1.$, $0.01 < \Delta m^2 < 1000\ eV^2$) are possible.

There are two best fit solutions with a $\chi^2_{min} = 78$ for 84 D.F. One of them is (solution a) reached for the parameters $\Delta m^2_{21} = 34\ eV^2$ and $\Delta m^2_{31} = 0.2\ eV^2$. For this solution, the angles are constrained to be $\sin^2 2\alpha_{e\mu} < 4 \times 10^{-3}$, $\sin^2 2\alpha_{e\tau} < 0.13$ and $\sin^2 2\alpha_{\mu\tau} < 0.02$, and the mixing matrix is given in Table 3a, with 90%C.L. limits. The values for Δm^2 are different from zero only at the 1.5 standard deviation level, i.e. the finite values are not significant.

Table 3a

90%C.L. limits on mixing matrix elements for best fit values $\Delta m^2_{12} = 34\ eV^2$ and $\Delta m^2_{13} = 0.2\ eV^2$

$$U = \begin{pmatrix} 1.00 - 0.98 & 0. - 0.03 & 0. - 0.18 \\ -0.04 - 0. & 1.00 - 0.99 & 0. - 0.07 \\ -0.18 - 0. & -0.07 - 0. & 1.00 - 0.98 \end{pmatrix}$$

$\sin^2 2\alpha_{e\mu} < 0.004$; $\sin^2 2\alpha_{e\tau} < 0.13$; $\sin^2 2\alpha_{\mu\tau} < 0.02$.

Table 3b

90%C.L. limits on mixing matrix elements for fit values $\Delta m^2_{12} = 0.2\ eV^2$ and $\Delta m^2_{13} = 38\ eV^2$

$$U = \begin{pmatrix} 1.00 - 0.97 & 0. - 0.19 & 0. - 0.15 \\ -0.21 - 0. & 1.00 - 0.98 & 0. - 0.07 \\ -0.14 - 0. & -0.10 - 0. & 1.00 - 0.98 \end{pmatrix}$$

$\sin^2 2\alpha_{e\mu} < 0.15$; $\sin^2 2\alpha_{e\tau} < 0.09$; $\sin^2 2\alpha_{\mu\tau} < 0.02$

A second local minimum of χ^2 is found at $\Delta m^2_{21} = 0.2\ eV^2$ and $\Delta m^2_{31} = 38\ eV^2$, i.e. interchanging the two values from solution a. Here also $\chi^2_{min} = 78$, the 90%C.L. limits on the angles are $\sin^2 2\alpha_{e\mu} < 0.15$, $\sin^2 2\alpha_{e\tau} < 0.09$ and $\sin^2 2\alpha_{\mu\tau} < 0.02$, and the range of matrix elements is given in Table 3b.

Since there is no way of dicriminating between the two solutions, global limits on angles for mass differences in the range $\Delta m^2_{12} > 0.06\ eV^2$, $\Delta m^2_{13} > 0.04\ eV^2$ and $\Delta m^2_{23} > 2\ eV^2$ are $\sin^2 2\alpha_{e\mu} < 0.15$, $\sin^2 2\alpha_{e\tau} < 0.13$ and $\sin^2 2\alpha_{\mu\tau} < 0.02$ while for

any specific mass difference $\Delta m_{k'k}$. the 90%C.L. limit on the correponsing $\sin^2 2\alpha_{\ell\ell'}$, is given in Figs. 1a through 1c. For the hypothesis of no oscillation, i.e. all mixing angles fixed to zero, a χ^2 of 85 for 87 D.F. is obtained, i.e. the data are consistent with this hypothesis.

In conclusion, we have shown that an analysis of existing data on oscillations of three neutrino flavours yields limits on the mixing matrix and on the three mixing angles each corresponding to one channel of oscillations. While this method does not in general allow stringent constraints on the mixing parameters to be extracted from one experiment, the combination of the different experimental data gives limits on angles and the mixing matrix elements which are about as restrictive as earlier two-neutrino analyses in separate oscillation channels. The ensemble of data is consistent with no oscillation occuring.

If neutrino masses are finite [5], then mixing angles of the order of $\sqrt{(m_e/m_\mu)}$ or $\sqrt{(m_\mu/m_\tau)}$ are expected in some models invoking family symmetries [6]. Experiments have nearly reached the level of sensitivity needed for testing such models. As in the case of quark mixing, the problem of family mixing is still waiting for a solution.

REFERENCES

[1] S.M.Bilenky and B.Pontecorvo, Phys.Rep. 41C (1978) 225
A.deRujula et al., Nucl.Phys. B168 (1980) 54
S.P.Rosen, Preprint Los Alamos LA-UR-84-1789 (1984)

[2] L.Maiani, Proc.Intern.Symp. on Lepton and Photon Interactions at High Energies (Hamburg 1977), p.877

[3] H.Blümer and K.Kleinknecht, Phys.Lett. 161B (1975) 407 and references quoted therein

[4] Experimental results are taken from the following references:

CCFRR	(1)	C.Haber et al., Phys.Rev.Lett 52 (1984) 1384
CDHS	(2)	F.Dydak et al., Phys.Lett. 134B (1984) 281
CHARM	(3)	F.Bergsma et al., Phys.Lett. 142B (1984) 103
Goesgen	(4)	J.L.Vuilleumier et al., Phys.Lett. 114B (1982) 298
Goesgen	(5)	K.Gabathuler et al., Phys.Lett. 138B (1984) 449
Bugey	(6)	J.F.Cavaignac et al., Phys.Lett. 148B (1984) 387
ν_τ search	(7)	N.J.Baker et al., Phys.Rev.Lett. 47 (1981) 1576
		N.Armenise et al., Phys.Lett. 100B (1981) 182
		O.Errique et al., Phys.Lett. 102B (1981) 73
		N.Ushida et al., Phys.Rev.Lett. 47 (1981) 1694
		G.N.Taylor et al., Phys.Rev. D28 (1983) 2705
		H.C.Ballagh et al., Phys.Rev. D30 (1984) 2271
BNL	(8)	L.A.Ahrens et al., Phys.Rev. D31 (1985) 2732

[5] V.A.Lubimov et al., Phys.Lett. 94B (1980) 266; Proc. EPS Conf. on High Energy Phys., Brighton (1984) p.386
K.E.Bergkvist, Phys.Lett. 154B (1985) 224
J.J.Simpson, Phys.Rev.Lett. 54 (1985) 1891
F.Calaprice et al., submitted to Phys.Rev.Lett. (June 1985)

[6] Z.G.Berezhiani, Phys.Lett. 150B (1984) 177
H.Fritzsch and P.Minkowski, Phys.Rep. 73 (1981) 67
H.Fritzsch, Nucl.Phys. B155 (1979) 189
B.Stech, Phys.Lett 130B (1983) 89
M.Shin, Phys.Lett. 145B (1984) 285

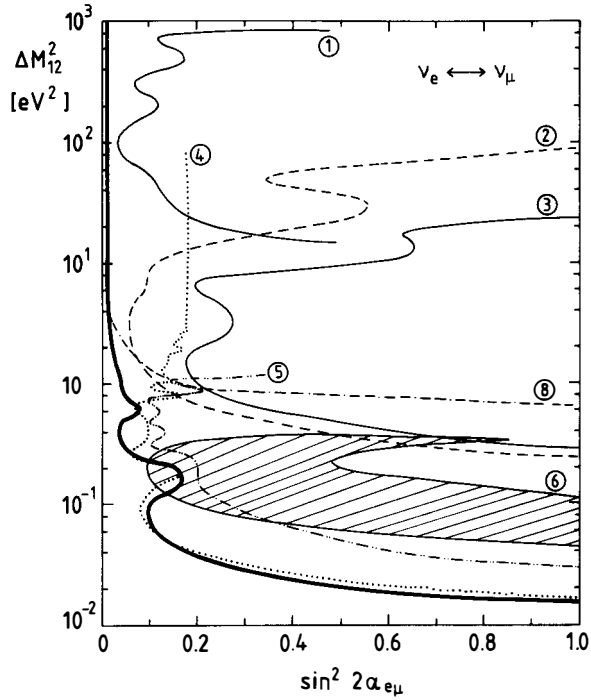


Fig.1a: Limits on mixing parameter $\sin^2 2\alpha_{e\mu}$ vs. neutrino mass difference ΔM^2_{12}. The thin lines are 90%C.L. upper limits on $\sin^2 2\alpha_{e\mu}$ from individual experiments 1) 2) 3) 4) 5) and 7) in ref. [4] assuming $\alpha_{e\tau} = \alpha_{\mu\tau} = 0$, the shaded arae is the allowed range from the Bugey experiment (6) in ref. [4]. The broad line is the 90%C.L. upper limit on $\sin^2 2\alpha_{e\mu}$ from the three-flavour oscillation analysis, allowing the other two mixing angles to vary over the whole range $0 \leq \sin^2 \alpha_{e\tau} \leq 1$ and $0 \leq \sin^2 2\alpha_{\mu\tau} \leq 1$.

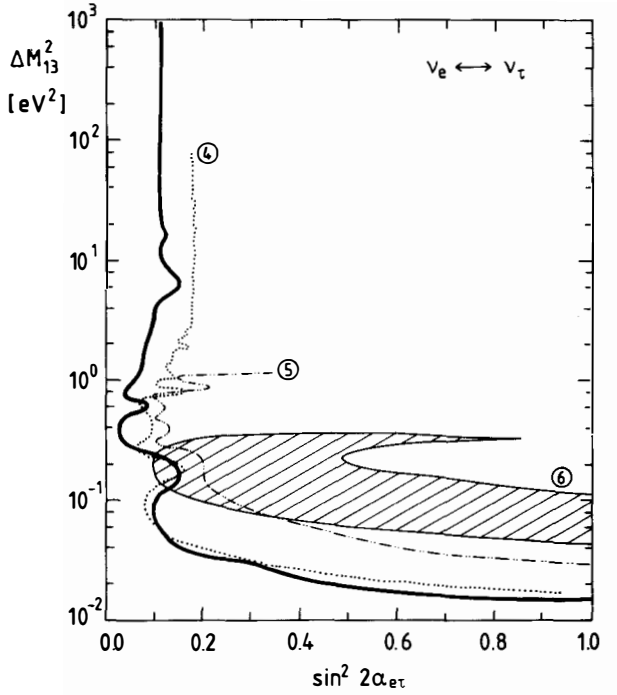


Fig.1 b:Limits on mixing parameter $\sin^2 2\alpha_{e\tau}$ vs. ΔM^2_{13}. Thin lines are 90% C.L. upper limits from individual experiments assuming $\alpha_{e\mu}=\alpha_{\mu\tau}=0$. Broad line from three-flavour analysis

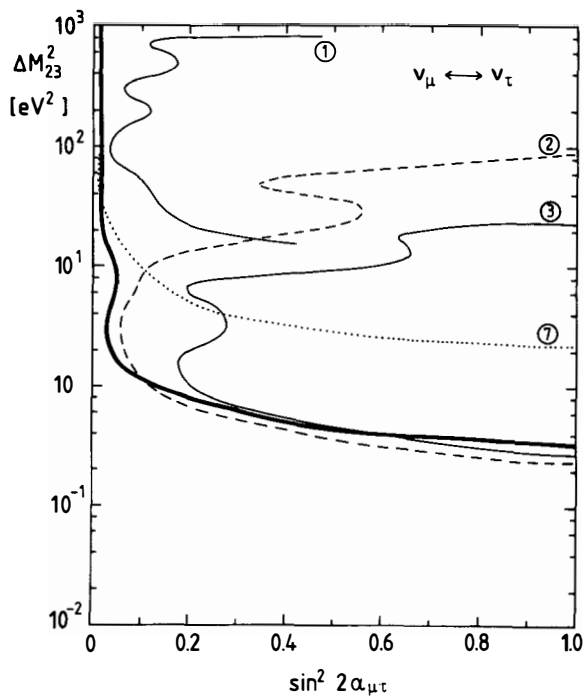


Fig.1c:Limits on mixing parameter $\sin^2 2\alpha_{\mu\tau}$ vs. ΔM^2_{23}.

RESULTS ON NEUTRINO OSCILLATIONS FROM AN APPEARANCE EXPERIMENT IN BEBC

S. Katsanevas(*)
CERN, Geneva, Switzerland



ABSTRACT

We have searched in the heavy liquid BEBC bubble chamber for ν_e events which could arise from oscillations of a ν_μ beam obtained from a 19.2 GeV proton beam at the CERN PS targeted 825 m upstream from BEBC. The appearance of ν_e CC interactions provides a sensitive indication of $\nu_\mu \rightarrow \nu_e$ oscillations. We observe 472 ν_μ CC events and 4 ν_e events, with an estimated background of 3.5 ν_e CC events. We find no evidence for $\nu_\mu \rightarrow \nu_e$ oscillations and set the limits on the oscillation parameters: $\delta m^2 \leq 0.10$ eV^2 (for maximal mixing) and $\sin^2 2\theta \leq 0.016$ for $\delta m^2 = 2.5$ eV^2 at 90% confidence level.

(*) On leave of absence from University of Athens, Athens, Greece.

1. INTRODUCTION

Following the original suggestion by B. Pontecorvo [2] for a possible lepton-number violation and a non-zero neutrino mass, leading to neutrino mixing and oscillations, a number of experiments have looked for such an effect [3]. Neutrino mixing occurs when the weak-interaction eigenstates ν_α (α = e, μ, τ) are linear combinations of the mass eigenstates ν_i (i = 1, 2 ,3). In this scheme, assuming mixing between two neutrino flavours only, the probability to observe a ν_e, starting with a ν_μ at an energy E, is

$$P(\nu_\mu \rightarrow \nu_e) = \sin^2(2\theta)\sin^2(1.27\ \delta m^2\ L/E) \qquad (1)$$

where L is the neutrino propagation length in meters and E is expressed in MeV. The two parameters $\sin^2(2\theta)$ and $\delta m^2 = (m_2^2 - m_1^2)$ determine the probability that a ν_μ of energy E will oscillate into a ν_e after a length L.

This experiment, performed at the CERN PS [1], used a neutrino beam generated by 19.2 GeV/c protons hitting a cylindrical beryllium-oxide target. A magnetic horn focussed the π^+ and K^+ produced in the target, while defocussing the negative component. The horn was followed by a 45 m decay tunnel and a concrete iron shielding. The average energy of the ν_μ incident on the detector was 1.5 GeV. The major sources of ν_e background are μ^+ decays (which produced low energy ν_e) and $K_{\ell 3}$ decays (which produce higher energy ν_e). From existing measurements of the π and K production rates at this energy within our angular acceptance and from the known geometry of the beam, we estimate the background ν_e event rate to be 0.7% of the ν_μ rate. The energy dependence of this background is shown in fig. 1, together with the spectrum of events induced by ν_μ.

Our detector was the BEBC bubble chamber, filed with a Ne/H_2 mixture. It was located at a distance of 825 m from the target. A cylindrically symmetric set of proportional wire chambers (the Internal Picket Fence - IPF) outside the 7 cm steel containment vessel of the chamber provides timing information on leaving tracks.

Two data sets were obtained: the first one in 1983 yielded 228 000 pictures, corresponding to 2.7 10^{18} protons on target; the second one, in 1984 yielded 566 000 pictures, corresponding to 6.4 10^{18} protons on target. During the first of these two runs the Ne/H_2 mixture used had 70 molar% Ne (density ρ = 0.63 g/cm^3, radiation length X_o = 47 cm); during the second run it had 73 molar% Ne (ρ = 0.68 g/cm^3, X_o = 43 cm). The fiducial mass used for the present analysis was 14 tons. 71 000 Cosmic Ray (CR) pictures were taken and analyzed. All the pictures were visually scanned for events induced by neutrals, with the exception of bare one-prong events without V^o's

or gammas, and isolated gammas or electrons having momentum larger than 120 MeV/c. Approximately 60% of the pictures were scanned twice and, in addition, a special scan was performed on the entire film for those frames flagged by a track that gave a hit in the IPF during the 2.2 μs beam gate. 4017 (207) interactions and 589 (27) isolated gammas or electrons were found and measured in the neutrino (CR) film.

2. DATA ANALYSIS

2.1 ν_μ events

The identification of the ν_μ charged current (CC) events rests primarily on the identification of the μ^- produced in the interaction. We considered as muon candidates the negative tracks that left the chamber (through the walls or the bottom) after a track length of at least 20 cm, or came to rest with or without a visible decay and a range compatible with that of a muon. To allow a good π/μ discrimination, muons stopping without a visible decay were required to have a momentum at production greater than 150 MeV/c.

In fig. 2 the angular distribution of the visible event momentum with respect to the incident neutrino direction is shown for ν_μ CC candidates. Events with $\cos\theta \sim +1$ are produced by the ν_μ beam; cosmic ray interactions produce most of the remainder. The requirement that $\cos\theta > 0.8$ selects 472 ν_μ CC candidates, with a loss of 6% according to Monte-Carlo studies. A further loss of 2% is estimated to derive from the fact that bare one-prong events are not scanned for. The number of events corrected for scanning efficiency is 529. We stress however that the results quoted below do not depend on the absolute scanning efficiency, provided that it is the same for the ν_e and the ν_μ induced CC interactions. The result will depend however on the relative efficiency to identify muons and electrons. In table 1 we give the percentages of ν_μ CC events according to the identification of the μ^- track. The corresponding Monte-Carlo predictions are also given in the same table. The agreement is excellent.

TABLE 1

ν_μ CC events	Leaving with IPF hit	Leaving without IPF hit	Stop
Experiment	40% ± 2%	35% ± 2%	25% ± 2%
Monte-Carlo	39%	35%	26%

For small values of δm^2 the oscillation amplitude is proportional to (L/E). Therefore it is important that the energy of the events be estimated correctly. We approximate it by the visible energy, defined as the sum of the energies of the muon and mesons in the final state plus the kinetic energy of baryons. The π/p ambiguity can therefore introduce significant bias in this determination. In a heavy liquid chamber, however, most of the final state protons come from the breakup of the neon nucleus and hence get only kinetic energy from the interaction. Therefore, by matching the total visible energy and the longitudinal momentum, $p_{//}$, for each event, π^+ can be distinguished from protons. To this purpose, we make use of the variable

$$\eta = \sum_{i=1}^{N} (E^i - P^i_{//}) \qquad (2)$$

where N is the number of particles in the final state, $P^i_{//}$ is the component of the momentum of the i-th particle along the beam direction and E^i its energy or, if identified as a baryon, its kinetic energy. The kinematics of νN interactions is such that η would be zero if all the particles in the final state are detected and their masses correctly assigned, loss of neutrons, γ's shift the average to positive values. This η distribution is shown in fig. 3(b) and the energy spectrum of ν_μ events in fig. 3(a).

The distributions of μ, π^-, p, π^+ are shown in figs 4(a-d). The solid line accompanying the plots is the Monte-Carlo prediction normalised to the total number of events. The agreement between the Monte-Carlo [4] (containing quasi-elastic production, Δ resonance production, and multipion kinematics and taking into account nuclear effects) and the data is very good, corroborating both particle identification and the scanning and measuring procedure.

Our background consists of cosmic ray particles, neutrino neutral current interactions and neutrons produced upstream the chamber volume giving rise to a negative pion simulating a muon. We studied this background using Monte-Carlo, simulation of the NC interactions, the CR events and the π^+ simulating a μ^+ in our data, and have found it to be of the order of 7%.

2.2 ν_e events

We identified the ν_e CC events through the identification of the e^-. To be accepted as an electron, a track should satisfy one of the following criteria: (a) There should be an e^+e^- pair, of total momentum greater than 30 MeV/c pointing tangentially to the track. (b) There should be a γ-ray, carrying at least 20% of the initial energy. (c)There should be an e^+e^- pair lying on the track (direct pair production). (d) Should spiralize to the end, so that the range is incompatible with that of a muon.

Four events have been identified as ν_e CC events with energies E_ν = 1.26, 2.44, 2.78 and 6.50 GeV respectively. Monte-Carlo studies indicate that from 472 ν_μ CC events we should expect a ν_e CC background of 3.5 events, which is compatible with what we observe. We notice that the energies of the ν_e events are somewhat higher than those of the ν_μ events, as expected from the ν_e contamination in the beam.

To obtain now from our data limits on possible $\nu_\mu \to \nu_e$ oscillations we make the usual assumption of only two neutrino flavours. The detection efficiency, as a function of the energy of the electron, was estimated using two independent Monte-Carlo programs. We accepted an event as effectively tagged if at least two occurrences of conditions α–d were fulfilled. The number of expected e^- events, assuming ν oscillations, is given by the number of ν_μ CC events (after subtraction of the hadronic background) multiplied by the probability of oscillation (1) and a weighting factor taking into account the effects of the difference in cross section between ν_e and ν_μ near the μ^- threshold and the difference in acceptance for ν_e and ν_μ due to the different tagging procedure. The expected number of background e^- has also been included in the statistical analysis.

Fig. 5 shows the preliminary 90% confidence levels in the Δm^2 vs $\sin^2 2\Theta$ plot, compared to previous experiments [5]. The limits thus obtained for maximum mixing are $\delta m^2 \lesssim 0.10\ eV^2$ and $\sin^2 2\Theta \lesssim 0.016$ for $\delta m^2 \sim 2.5\ eV^2$.

REFERENCES

[1] Experiment PS180, Athens[1]–Padova[2]–Pisa[3]–Wisconsin[4] Collaboration:
C. Angelini[3], A. Apostolakis[1], A. Baldini[3], M. Baldo-Ceolin[2], L. Bertanza[3], F. Bobisut[2], E. Calimani[2], U. Camerini[4], S. Ciampolillo[2], R. Fantecchi[3], V. Flaminio[3], W.J. Fry[4], H. Huzita[2], P. Ioannou[1], S. Katsanevas[1], J. Koutentakis[1], C. Kourkoumelis[1], M. Loreti[2], R. Loveless[4], G. Miari[2], R. Pazzi[3], P. Pramantiotis[1], M. Procario[4], G. Puglierin[2], D.D. Reeder[4], L.K. Resvanis[1], B. Saitta[3] and M. Vassiliou[1].

[2] B. Pontecorvo, JETP 34 (1958) 247 and 7 (1958) 172; Zh. Eksp. Teor. Fiz. 53 (1967) 53 [JETP 26 (1968) 984];
S.M. Bilenky and B. Pontecorvo, Phys. Rep. 41 (1978) 225.

[3] For a complete review of neutrino oscillation experiments, see V. Flaminio and B. Saitta, Neutrino oscillation experiments, INFN PI/AE 85/6, to be published on Rivista del Nuovo Cimento.

[4] S. Katsanevas and M. Vassiliou, PS180, internal report.

[5] F. Bergsma et al., Phys. Lett. 142B (1984) 103;
L.A. Ahrens et al., Phys. Rev. D31 (1985) 2732.

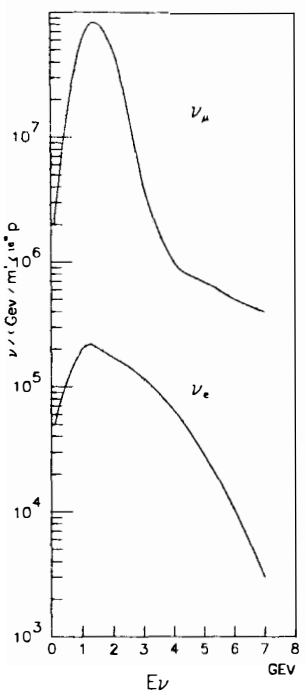


Fig. 1 Expected ν_μ and ν_e fluxes

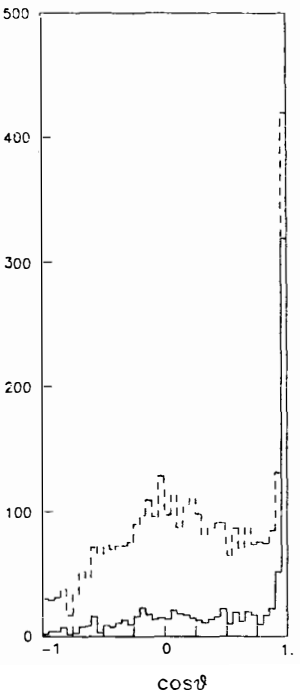


Fig.2 Anguiar distribution o f events with μ- candidates (---- all events)

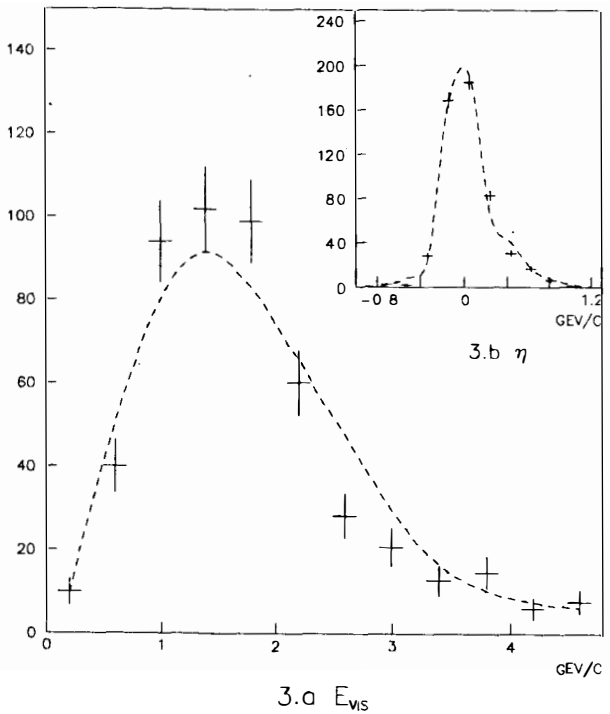


Fig.3 Visible energy and η distribution for CC events. The curve shows the MC prediction

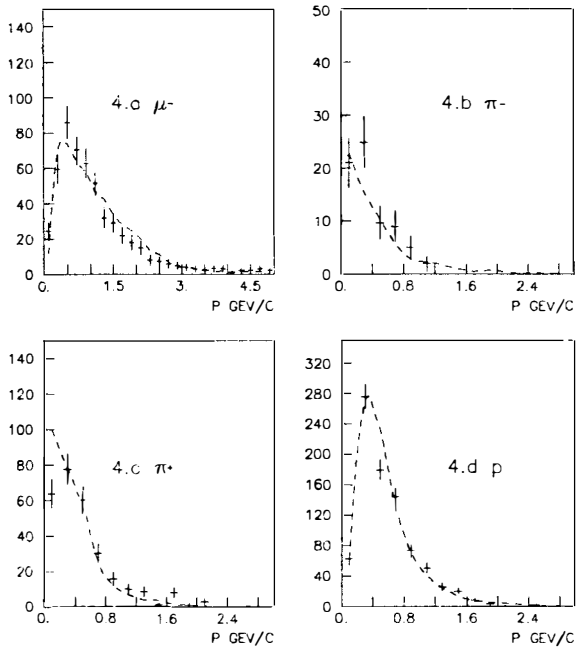


Fig.4 Momentum distributions of μ,π and p

The curve shows the MC prediction

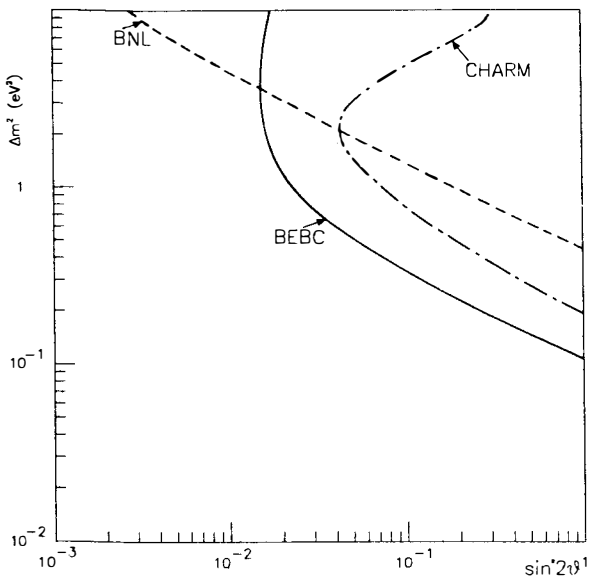


Fig.5 Preliminary results of this experiment

compared with other $\nu_\mu \rightarrow \nu_e$ experiments

BNL is Ahrens et al CHARM is Bergsma et al ref 5

The regions to the right are excluded with 90% CL

SEARCH FOR NEUTRINO OSCILLATIONS AT LAMPF

R.W. Harper, T.Y. Ling, J.W. Mitchell, T.A. Romanowski,
E.S. Smith, M. Timko
Ohio State University, Columbus, OH 43210

S.J. Freedman, J. Napolitano
Argonne National Laboratory, Argonne, IL 60439

B.K. Fujikawa, R.D. McKeown
California Institute of Technology, Pasadena, CA 91125

K.T. Lesko, E.B. Norman
Lawrence Berkeley Laboratory, Berkeley, CA 94720

R.D. Carlini, J.B. Donahue, G.T. Garvey, V.D. Sandberg
Los Alamos National Laboratory, Los Alamos, NM 87545

W.C. Choi, A. Fazely, R.L. Imlay, W.J. Metcalf
Lousiana State, University, Baton Rouge, LA 70803

Presented by Elton S. Smith



ABSTRACT

The decays of stopped pions in the LAMPF beam stop present a unique opportunity to probe neutrino oscillations in the mass region of $\delta m^2 \sim 0.1 eV^2$ and mixing parameters as low as $\sin^2 2\theta \sim 10^{-3}$. The appearance of $\bar{\nu}_e$ will be measured with high sensitivity by Experiment 645 during the run cycle that begins in the summer of 1986.

Intermediate-energy proton accelerators provide neutrino sources in the energy range 10-50 MeV, which are ideal for oscillation searches in the mass region $\delta m^2 \sim .1 eV^2$. In addition, the available beams are very intense, allowing the experiments to be sensitive to mixing parameters as low as $\sin^2 2\theta \sim 10^{-3}$. The distance of the detector from the beam stop (L) and neutrino energy (E_ν) set a typical oscillation scale of $L/E_\nu \sim .6$ m/MeV, a value intermediate to that which can be obtained in reactors and high energy experiments.

The Los Alamos Meson Physics Facility (LAMPF) provides a 670 μA proton beam with a kinetic energy of 800 MeV. The beam is absorbed in a copper beam stop, producing on the average 0.09 pions for every proton.[1] Although both positive and negative pions are produced, π^- quickly fall into atomic orbitals and are absorbed into the nucleus by strong processes. The π^+ come to rest and decay, producing the beam-stop neutrino spectra via the decay sequence $\pi^+ \to \mu^+\nu_\mu$, $\mu^+ \to e^+\nu_e\bar{\nu}_\mu$. These decays provide a clean point source of ν_e, $\bar{\nu}_\mu$ and ν_μ.

The LAMPF experiment E-645 is located 24 m from the beam stop at a polar angle of 17° from the main proton beam. The liquid scintillator detector is the target for the inverse beta decay reaction $\bar{\nu}_e p \to e^+ n$ which, if seen, would provide a signature for the appearance of $\bar{\nu}_e$. The construction phase of the experiment is complete. Calibration and cosmic-ray background studies are currently under way. The first data run is expected to begin in July of 1986.

The design and construction of the experiment is dictated by the expected backgrounds rather than by the signal of a single isolated positron. Due to the long accelerator duty cycle (~9%), cosmic rays constitute a serious background, since Los Alamos is 2100 m above sea level. The detector will operate inside a tunnel with an overburden of 3000 g/cm^2, enough passive material to eliminate the hadronic component in the cosmic-ray flux (see Figure 1). The estimated integrated muon flux inside the tunnel is 8 kHz. In addition, the central detector is covered by a 4π cylindrical cosmic-ray shield,[2] which contains a 15.2 cm outer layer of liquid scintillator and an inner layer of lead (12.7 cm) and iron (5.1 cm). The outer layer is used to veto charged particles. The passive layer is designed, in particular, to eliminate the background of muons stopping outside the active layer, where an electron from the decay radiates a photon that can pass through the scintillator undetected before it converts inside the shield. To minimize inefficiencies in the

shield, the scintillator fills only three optically isolated sections: the cylinder and one endcap, the bottom and the other endcap. The scintillator is viewed by 360 photomultiplier tubes (EMI 4870-B) to provide ample redundancy.

The central detector has forty layers, each one consisting of a scintillator plane followed by vertical and horizontal proportional drift-chambers (see Figure 2). The liquid scintillator is contained in horizontal lucite tanks (366 30 3 cm^3) and viewed at both ends by Hamamatsu R878 phototubes. Particles lose 75% of their energy in the scintillator, the rest is deposited in the lucite and drift tube walls. The drift-chamber planes consist of 45 wires assembled 8.1 cm apart. Drift-time and pulse-height information are recorded for every wire. Nuclei with loosely bound neutrons, e.g. ^{27}Al and ^{13}C, provide a target for ν_e interactions and are a source of background since we are not able to distinguish between electrons and positrons (see Table I). Thus, the drift tubes are constructed of laminated Kraft paper with only a 25-μm aluminum inner layer to shape the electric field.[3] The detector weight is 20 metric tons, of which 2.3 tons is hydrogen.

We must be able to distinguish protons from electrons with high efficiency in order to eliminate knock-on protons produced in fast neutron interactions. The granularity of the detector permits such identification to be made by comparing the particle range to the energy loss measured in the scintillator. An additional selection can be made based on the dE/dx measurement in a single scintillator plane. Using these criteria, protons have been rejected by a factor of 3×10^{-4} in a prototype detector studied in the LAMPF test beam channel. Given the present estimates of neutron backgrounds (~1000/day) in our detector, this rejection is adequate to eliminate knock-on protons with kinetic energies greater than 100 MeV.

The signals from the detector and the shield are digitized with flash ADC's and stored in cyclic memories containing 150 μsec of data. The positron trigger is flagged by hits in three consecutive planes. At this point, data are continued to be read into the memories for 100 μsec, so that when the data are eventually transferred to the computer, only 50 μsec of information is recorded before the event trigger. The history is used to tag any signals that might be associated with the trigger, e.g. a stopping muon. The data recorded after the trigger is needed to help identify the neutron, which would be present if the event was in fact a

$\bar{\nu}_e$ interaction. Mylar sheets painted with natural Gd_2O_3 are located between all scintillator planes. Neutrons from the interaction may thermalize in the scintillator and capture on Gd, which deexcites by emitting 4.5 gamma rays on the average. The detection of these gammas (total energy is 7.9 MeV) provides a neutron signature. The detection efficiency of the neutrons is expected to be about 25%, but depends on requirements imposed on the detection of the resulting gammas.

In Figure 3 we show the expected sensitivity of E-645 to neutrino oscillations. The $\bar{\nu}_e p$ interaction cross section is 11×10^{-41} cm^2.[4] Assuming a positron detection efficiency of 50%, the event rate for maximum oscillation is 47 events/day. Background rates, which limit the sensitivity of the experiment, are hoped to be kept to less than .1 events/day. For comparison, the best published limits are also shown in the figure.[5]

Table I. Backgrounds due to ν_e interactions in the detector.

Target	Mass (tons)	$\sigma(10^{-41} cm^2)$	Rate/day in Detector (E_ν>35MeV)
^{12}C	15	1.5	<0.01
^{13}C	0.15	< 5	<0.05
^{27}Al	0.2	< 5	<0.03

References

1. R.C. Allen et al., Phys. Rev. Lett. 55, 2401 (1985) and H.H. Chen et al., Nucl. Instrum. Meth. 160, 393 (1979).
2. S.J. Freedman et al., Nucl. Instrum. Meth. 215, 71 (1983).
3. J. Fitch et al., Nucl. Instrum. Meth. 226, 373 (1984).
4. S.E. Willis et al., Phys. Rev. Lett. 44, 522 (1980) and S.E. Willis et al., Phys. Rev. Lett. 45, 1370 (1980).
5. L.A. Ahrens et al., Phys. Rev. D 31, 2732 (1985); F. Bergsma et al., Phys. Lett. 142, 103 (1984); G.N. Taylor et al., Phys. Rev. D 28, 2705 (1983).

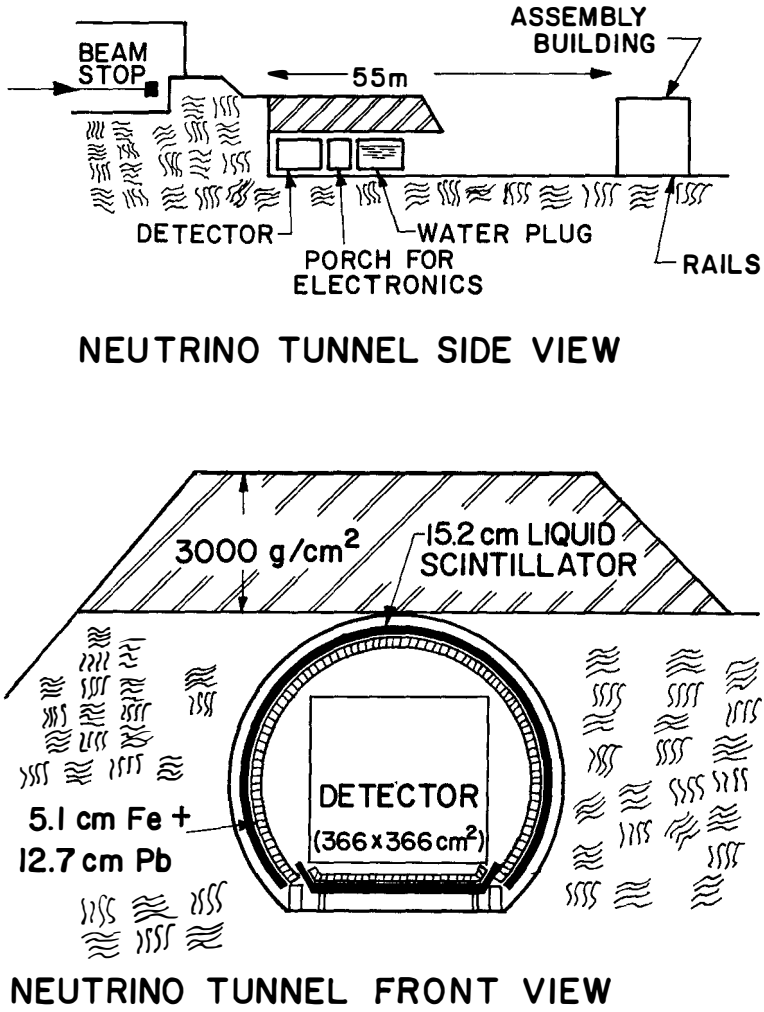


Figure 1. Cosmic-ray shielding which includes 3000 g/cm^2 of overburden, an active charged particle veto, and an inner layer of lead and iron.

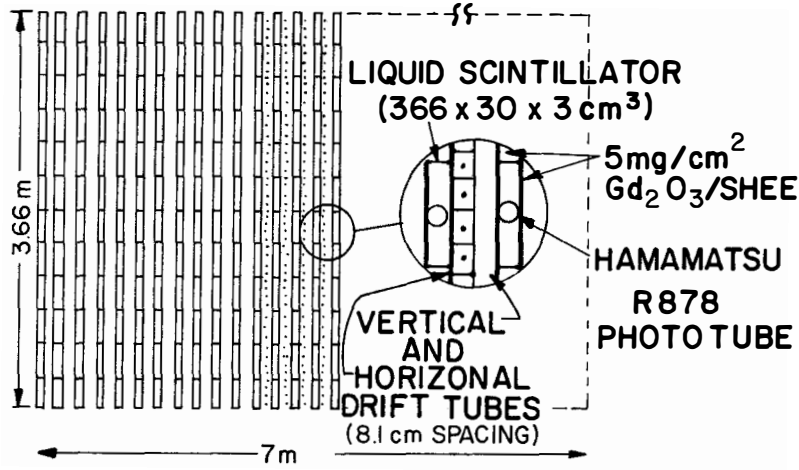


Figure 2. E-645 detector sandwich consisting of forty scintillator and drift-chamber planes.

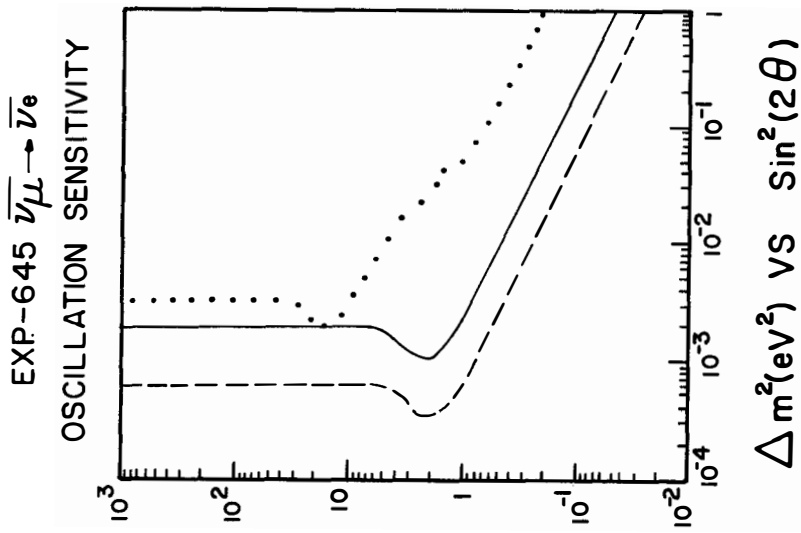


Figure 3. Expected sensitivity of E-645 to neutrino oscillations. The dashed curve assumes the experiment is free of background. The full curve assumes a background rate of .1 events/day. The dotted curve shows current oscillation limits.

SEARCH FOR NEUTRINO OSCILLATIONS WITH KARMEN*

Reinhard Maschuw
Kernforschungszentrum Karlsruhe
Institut für Kernphysik I
D-7500 Karlsruhe, W.-Germany



Abstract

Beam dump neutrinos ν_μ, $\bar{\nu}_\mu$ and ν_e from the spallation neutron source ISIS of the Rutherford Appleton Laboratory are used for a series of ν-experiments in the energy range between 5 and 50 MeV. One of the major topics is the search for ν-oscillations in three different oscillation modes simultaneously, i.e. $\nu_\mu \rightarrow \nu_e$ appearance, $\nu_e \rightarrow x$ disappearance and $\bar{\nu}_\mu \rightarrow \bar{\nu}_e$ appearance. The status of the project is described.

*Members of the KARMEN collaboration:
G.Drexlin, H.Gemmeke, G.Giorginis, W.Grandegger, A.Grimm, J.Hesselbarth, K.Kleinfeller, D.Mann, R.Maschuw, M.Momayezi, K.-H.Ottmann, P.Plischke, F.Raupp, M.Reuscher, F.K.Schmidt, P.Wild, J.Wochele, S.Wölfle, B.Zeitnitz: Kernforschungszentrum and Universität Karlsruhe; J.Böttcher, E.Finckh, W.Kretschmer, K.Stauber, R.Stegen, D.Vötisch, E.Zell: Universität Erlangen; J.A.Edgington, J.M.Fontaine, G.Marinos, A.M.Ryan: Queen Mary College London; N.E.Booth: Oxford University; A.Dodd: Rutherford Appleton Laboratory.

KARMEN which stands for "Karlsruhe Rutherford Medium Energy Neutrino Experiment" denotes an experimental programme of neutrino physics[1,2] to be performed at the recently inaugurated spallation neutron source ISIS of the Rutherford Appleton Laboratory. The Uranium-Heavy-Water spallation target bombarded with a 200 μA, 800 MeV proton beam from a rapid cycling synchrotron, for our purposes serves as "beam dump" neutrino source. It provides monoenergetic ν_μ with E_{ν_μ} = 29.8 MeV emerging from π^+ decay at rest whereas the subsequent μ^+ decay provides $\bar{\nu}_\mu$ and ν_e with continous energy spectra up to 52.8 MeV (see fig.1). At a distance of 17 m from the target station where the neutrino detector will be located the average flux for each kind of neutrinos will be 1.3×10^6 cm^{-2} sec^{-1}.

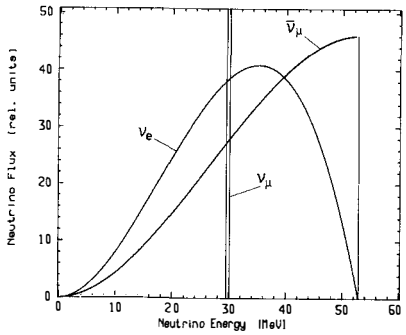


Fig.1: Energy spectrum of the ISIS beam dump neutrino source. The total number of neutrinos is equal for ν_μ, $\bar{\nu}_\mu$ and ν_e.

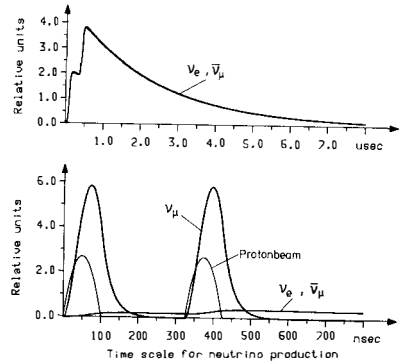


Fig.2: Time structure of the ISIS neutrino source. Repitition frequency 50 Hz.

Apart from this characteristic energy spectrum the most important feature of the ISIS beam dump neutrino source is its time structure which is closely related to that of the proton beam (see fig.2). There are two proton pulses of 100 nsec width separated in time by 230 nsec, having a repetition rate of 50 Hz. According to the lifetime of the π^+ (26 nsec) the ν_μ more or less completely follow the time structure of the protons which means that ν_μ-induced reactions will be looked for only in a time win-

dow of 0 - 150 nsec and 330 - 480 nsec respectively. On the other hand reactions induced by $\bar{\nu}_\mu$ and ν_e from the much slower decay of the μ^+ will be searched for in the time window between 0.5 and 9 μsec where the ν_μ are no longer present. Thus ν_e and $\bar{\nu}_\mu$ are well separated in time from the monoenergetic ν_μ. In terms of a duty factor this time structure would mean $D(\nu_\mu) = 1.5 \times 10^{-5}$ and $D(\bar{\nu}_\mu, \nu_e) = 4.25 \times 10^{-4}$ respectively. These numbers reflect the big advantage of such a pulsed ν-source as they represent the suppression factors of any randomly distributed background, e.g. cosmic radiation. Moreover this background can be measured with high precision during the beam pause and be subtracted from the event rate in the relevant time windows. In addition the time structure, as will be shown below, provides nice and stringent signatures for various ν-induced reactions.

Once having these neutrinos a suitable ν-detector should be completely active as it has to detect e, γ, n and μ in the energy range between 5 and 50 MeV with high precision. Thus any inactive material which could absorb even a small portion of this energy has to be avoided as not to deteriorate the resolution. Moreover, the detector has to be very massive due to the low cross sections in this energy range. But even a detector of 50 t mass will not see more than 1 to 10 neutrino events per day. To unambiguously detect these rare events with significant evidence any background has to be suppressed far below this rate. As the low neutrino duty cycle only affects the uncorrelated background the beam associated background of neutrons and gammas from the spallation target requires effective shielding.

During the past two years we therefore set up a neutrino area at ISIS where a 6000 t neutrino blockhouse is the most prominent part of. Steel walls of 2 m thickness and a 3 m thick steel roof enclose the detector area with dimensions 10x4.2x7 m, which can be closed by a handdriven steel door of 520 t weight. This massive amount of shielding together with the biological shield of 5 m of steel around the target station, plus additional shielding along the adjacent neutron beam lines, plus the use of

an active anticounter system, plus making use of the time structure of the ν-source will reduce the background to the low level required.

The neutrino facility described above is going to be used for a series of neutrino experiments. Referring to the item of this session the discussion of the physical aims of KARMEN will be restricted to the problem of ν-oscillations only. During 1986 a 60 t organic scintillation detector will be installed. It will be used to look for three different oscillation modes simultaneously i.e. $\nu_\mu \rightarrow \nu_e$ appearance, $\bar{\nu}_\mu \rightarrow \bar{\nu}_e$ appearance and $\nu_e \rightarrow x$ disappearance which requires detection of ν_e and $\bar{\nu}_e$ respectively. Making use of the high abundance of ^{12}C nuclei in the organic scintillator, ν_e will be detected via the reaction:

$$\nu_e + {}^{12}C \rightarrow {}^{12}N + e^- \; -17.3 \text{ MeV};$$

$$16 \text{ msec} \downarrow$$

$${}^{12}C + e^+ \; (16.3 \text{ MeV}) + \nu_e$$

This gives rise to a delayed coincidence between an e^- from the first part of the reaction and an e^+ from the ^{12}N-decay at the same location in the detector. The coincidence therefore means another suppression factor of almost 10^{-4} for any background as it reduces the detector volume from 5×10^7 cm^3 to about 6×10^3 cm^3 only. One thus has a very stringent and almost background free signature for ν_e. With respect to $\nu_\mu \rightarrow \nu_e$ oscillations one has to have in mind that the ν_μ are monoenergetic and only present in two short time windows of 0 - 150 nsec and 330 - 480 nsec. Thus one looks for monoenergetic e^- of 12.7 MeV in the ν_μ-time window followed by an e^+ with average energy of about 10 MeV in a time window of .5 to 20 msec, where all other neutrinos have vanished already. The same signature applies for a $\nu_e \rightarrow x$ disappearance oscillation except for the first part of the coincidence where one now looks for e^- up to 35 MeV energy in the time window of the original ν_e, i.e. 0.5 to 9 μsec. With respect to an oscillation signal one would run into the common calibration problems of all disappearance experiments. But suitably combining the "$\nu_\mu \rightarrow \nu_e$"- and "$\nu_e \rightarrow x$"-events one gets a rather flux independant measure of the oscillation probability $P(\nu_\mu \rightarrow \nu_e)$ in terms of a two component neutrino composition.

A similar delayed coincidence signature will exist also for a possible $\bar{\nu}_\mu \rightarrow \bar{\nu}_e$ appearance oscillation. The large content of ^1H-nuclei in the scintillator will be used for the inverse ß-decay reaction

$$\bar{\nu}_e + {}^1H \rightarrow n + e^+ - 1.8 \text{ MeV}$$
$$\text{therm.} \rightarrow Gd(n,\gamma)\ 8 \text{ MeV}.$$

In a first step a positron which carries almost the entire $\bar{\nu}_e$ energy up to 51 MeV will be detected. The neutrons being thermalized in the scintillator very soon will be captured by a small amount of Gd brought into the detector in a sophisticated way. The capture would give rise to on average three gamma quanta with sum energy of 8 MeV, which will be detected in delayed coincidence with the positron within a sphere of 1 m diameter.

The delayed coincidence signatures for all three ν-oscillation modes very clearly demonstrate the big advantage of the time structure of the ISIS beamdump ν-source in combination with a high resolution scintillation calorimeter.

Fig.3 shows the sensitivities of the ν-oscillation experiments for two years of measuring at full ISIS intensity (appr. 4 years actual time). The higher sensitivity to the $\bar{\nu}_\mu \rightarrow \bar{\nu}_e$ oscillation is barely due to the larger cross section of the $\bar{\nu}_e$-p process and the higher $\bar{\nu}_\mu$ energies compared to the ν_e-^{12}C reaction at 30 MeV energy. However, these sensitivity plots should not be over-interpreted as long as no real data have been measured. But we think that

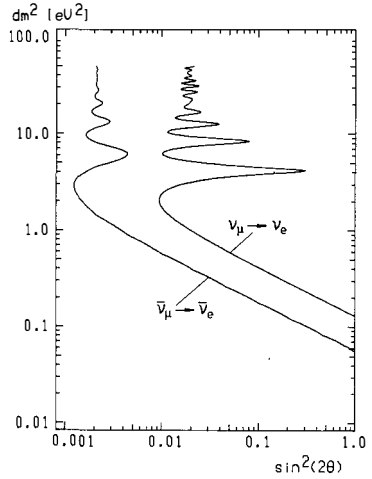


Fig.3: Sensitivities for neutrino oscillations at KARMEN

it is a fair and realistic statement to be sensitive to the mixing angle $\sin^2 2\theta$ slightly below 10^{-2} and to Δm^2 slightly below 10^{-1} eV^2 even with less statistics and assuming a background rate up to 1 per day. Within these limits we believe that any result would have minimum systematic errors due to the very stringent signatures and the comparison possibility for different oscillations in the same experiment.

Finally the 60 t scintillator calorimeter shall be described (see fig.4). A large steel vessel 6 m high, 3.2 m wide and 3.5 m long is filled with 65 000 l mineral oil based liquid scintillator (KfK/MERCK). The 150 mm thick head walls contain 1120 bores each, to keep the overall 2240 phototubes looking into the scintillator. The central detector consists of 512 optically separated modules of 18x18 cm cross section and 350 cm length. Each module is viewed by two 3" phototubes XP 3462 from either end. The optical segmentation consists of very thin (2x1.5 mm) double lucite sheets glued together at its rim containing Gd-coated paper in between (70 g/cm^2 Gd $\hat{=}$ 0.1 weight %). The thin air gap between the lucite sheets provides total internal reflection to guide the light towards the phototubes whereas the Gd_2O_3 paper serves for the neutron detection. The central detector is surrounded by a layer of half width modules serving as active inner anticounter to define a "contained event". 20 cm thick steel slabs providing the mechanical strength of the detector are used as passive inner shield followed by a 3 cm NE110 scintillator active outer anticounter. This sandwich anticounter system predominantly is designed to suppress neutrals entering the detector from the last 20 cm of passive shielding by a factor of 10^{-2}.

The detector is self triggering from each of the 512 modules with a fast (< 400 nsec) "valid event" decision from a timing logic and a trigger processor. A 30 µsec pretrigger activates the detector for stopped muons which when decaying could fake a ν-induced event during the relevant time windows. The mechanical, chemical as well as the physical properties of the detector system have been tested in various prototypes of 200 l (1 module), 1000 l (9 modules) and 8000 l (35 central + 24 outer modules) size. The position dependant light output has been

measured with triggered cosmics and can completely be reproduced by Monte Carlo. As expected any light output is linearly correlated to the energy deposit in the detector. The same linear correlation holds for the time difference measured between the ends of a module and the actual position of light emission. From cosmic ray measurements as well as with the UV-laser calibration system the energy resolution was determined to be $\sigma = .12/\sqrt{E(MeV)}$. Finally a neutron detection efficiency of 30% could be deduced from a mock up experiment with tagged neutrons in the 1000 l detector.

As now almost all detector components are ready or just being manufactured detector assembly will go ahead as soon as the detector vessel will be delivered in April 1986. Data taking is scheduled to start at the end of 1986 when also ISIS is expected to operate close to its design values.

REFERENCES

1) R.Maschuw, B.Zeitnitz
Neutrino Physics at the Pulsed Spallation Neutron Source SNS,
KfK-Report 3362, June 1982

2) B.Zeitnitz
Low Energy Neutrino Physics at High Intensity Pulsed Proton Accelerators
Progress in Particle and Nuclear Physics, Vol.13, 1985,

NEUTRINO PHYSICS WITH A MASSIVE UNDERGROUND DETECTOR

John M. LoSecco
Physics Department
University of Notre Dame
Notre Dame, Indiana 46556
U.S.A.



R. M. Bionta, G. Blewitt, C. B. Bratton
D. Casper, P. Chrysicopoulou, R. Claus
B. Cortez,S. Errede, G. Foster, W. Gajewski,
K.S. Ganezer, M. Goldhaber, T. J. Haines, T. W. Jones,
D. Kielczewska, W. R. Kropp, J. G. Learned,
E. Lehmann, H. S. Park, F. Reines, J. Schultz, S. Seidel,
E. Shumard, D. Sinclair, H. W. Sobel, J. L. Stone,
L. Sulak, R. Svoboda, G. Thornton, J. C. Van Der Velde

University of California, Irvine, CA 92717
University of Michigan, Ann Arbor, MI 48109
Brookhaven National Laboratory, Upton, NY 11973
California Institute of Technology, Pasadena, CA 91125
Cleveland State University, Cleveland, OH 44115
University of Hawaii, Honolulu, HI 96822
University College, London WC1E 8BT, United Kingdom
Warsaw University, Warsaw PL-00-681, Poland

ABSTRACT

401 contained neutrino interactions occuring in a massive underground detector are used to study neutrino oscillations, geomagnetic effects and to search for point sources. An additional 187 events from neutrino interactions in the surrounding rock are used to search for energetic extraterrestrial neutrino sources. A search for an energetic muon signal from Cygnus X3 has failed to give positive results.

Introduction

Massive underground experiments initially designed to study proton decay have also yielded some unique information about neutrinos. The sole source of signals in these detectors are penetrating muons, with initial energies > 400 GeV, coming from the surface and neutrino interactions in the detector itself or in the surrounding rock. The primary source of neutrinos is believed to be from pion, kaon and muon decay of particles produced by cosmic ray interactions in the atmosphere. The flux will produce about 120 $\pm$ 24 events per year in a kiloton of matter.

The IMB detector[1], an imaging water Cherenkov detector has a sensitive region of 8000 metric tons and a fiducial volume starting 2.5 meters in from all walls, of 3300 metric tons. The initial operation of the detector yielded 401 contained events[2] in 417 days of livetime. 187 events, upward muons believed to be neutrino interactions were observed[3] in a period of 396 live days. To avoid contamination from surface muons the upward muon sample was restricted to events with local zenith angles greater than 90° from above, i.e. below the horizon.

In addition to these data samples, approximately 800 hours of live time have been examined in an attempt to confirm reports of signals associated with the extraterrestrial source Cygnus X3. The livetime has been taken when the potential source was above the horizon.

Contained Event Sample[4]

For the contained events we have measured the position of the interaction and the direction and visible energy of the tracks. We have also recorded the time of occurance of the event and the number of muon decays occuring with a 7.5 μ sec window following the trigger. 105 of the events have

at least one muon decay signature. 310 events have a clear single prong topology.

For nucleon decay[2] we have concentrated our attention on wide angle multitrack events[6] typical of low momentum nucleon decays. For neutrino physics we have made use of the 310 event single prong sample.[1] These events have a visible energy that runs from 175 MeV to 2 GeV. The corresponding neutrino energy is somewhat higher due to the energy lost to particle masses and to kinetic energy below the Cherenkov threshold (1.52 mc^2). In general the neutrino energy is in excess of 400 MeV.

Neutrinos interacting in the detector come from all directions. They originate in the atmosphere. Except for small geomagnetic effects the neutrino spectrum is independent of direction. The distance the neutrinos have traveled varies from 8 km for those coming from directly above the detector to 13,000 km for those coming up from the other side of the earth. This broad range of distances could provide 3 decades of sensitivity to Δm^2 for neutrino oscillations. In fact a smaller region is accessible due to the rapid change of distance with neutrino direction near the horizon and hence the rather low exposure for this range of distances. Neutrino oscillations could manifest themselves as a distance dependent effect in the neutrino spectrum. For two component mixing the probability of finding a neutrino of a given type, with energy E after travelling a distance L is:

$$1) \qquad P(\nu \rightarrow \nu) = 1. - \sin^2 2\eta \cos^2 \left(1.27 \frac{E}{L} \Delta m^2\right)$$

We have carried out a search[1),7)] for neutrino oscillations using two data samples. All of the single prong events have been used in a search for oscillations of

νe and $\nu\mu$ into non interacting states. In addition, if we restrict our sample to those events with a clear muon decay signature we can study the oscillations of $\nu\mu$ into any other state.

The search compares the energy spectrum measured for a neutrino sample coming from great distances to those directly above. Distortions expected from oscillations are introduced into the measured downward spectrum and the modified spectrum is compared with the observed one from a long distance. When the two samples differ by a statistically significant amount (90% c.l.) we can exclude the set of oscillation parameters used to distort the downward spectrum.

The regions excluded by this analysis are illustrated in figures 1 and 2. Figure 2 shows the excluded region for $\nu\mu$ oscillations.

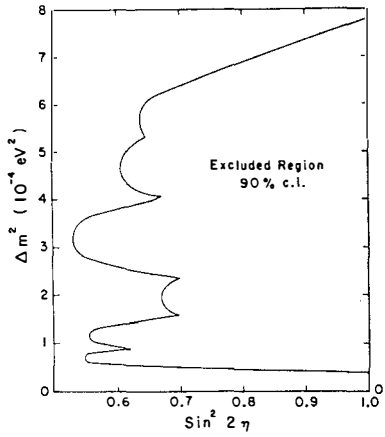


Figure 1

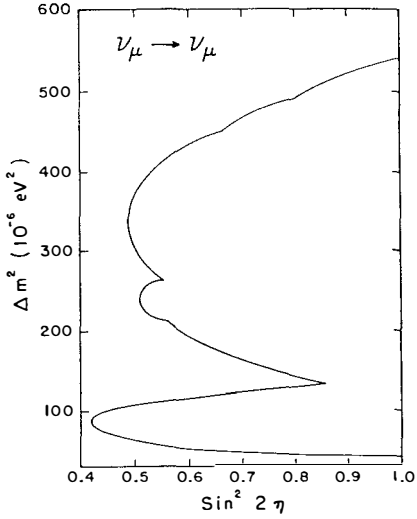


Figure 2

These plots have an irregular shape coming from the use of 13 overlapping annular regions about the vertical. Each region contains 1/5 of the total solid angle to have enough events to be sensitive. Scattering confuses the direction such that smaller angular regions would not increase the significance of the result.

These data may also be used for a point source search of neutrinos in the range 400 MeV to 2 GeV. There are possible extraterrestrial and local sources. The search has been carried out in both coordinates. A cone with half opening angle of 30° has been used to sweep through the sample[8] on a grid of 51200 points equally spaced in solid angle. The number of events within the cone was measured for each direction. On the average one would expect 21 events in the cone if they were uniformly distributed. Fluctuations are, of course, to be expected. Since a 30° cone contains 6.7% of the solid angle many of the regions overlapped. The number of events in the cone is histogrammed in figure 3. The maximum found was 38 events in both cases. Neither of these results are significant.

In our searches we have overlooked the effects of geomagnetic modulation on the neutrino flux. In particular, due to the northern location of our detector, 54° N geomagnetic lattitude, the downward neutrino flux is enhanced at low energies. This occurs because the magnetic field cut off is weaker than for the earth at

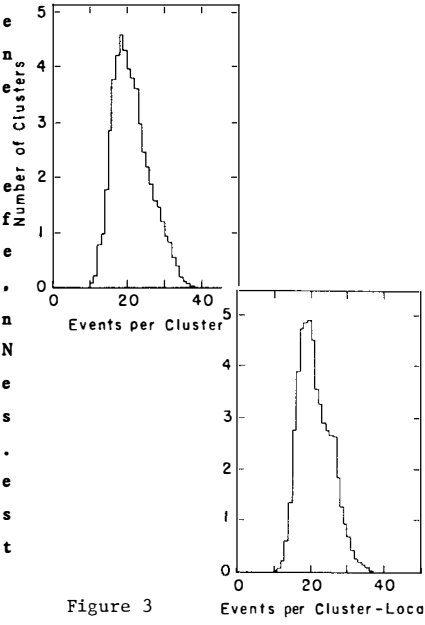


Figure 3

large. This effect looks similar to the effect of neutrino oscillations and so failing to take it into account gives us a more conservative limit.

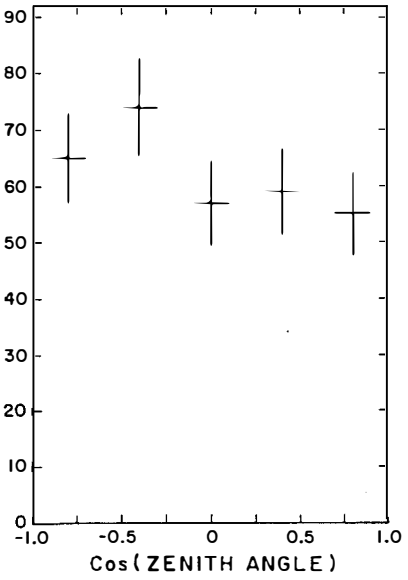


Figure 4

We have also not included the possible effects that matter[9] may have on neutrino oscillations. These effects are difficult to include since our neutrinos span cords of the earth and travel through different density domains. The lack of reasonable knowledge about the density distribution in the earth will reduce our confidence in our conclusions. Perhaps when more is known about neutrino oscillatons these can be used to study the density distribution itself.

Geomagnetic effects are manifest in our data sample. The log (E/L) distribution has the characteristic shape expected from an energy dependent direction modulated flux. Figure 4 shows our zenith angle distribution. Events coming down from above are on the left. Those from below are on the right. One anticipates ~20% variation on this plot with peaking to the left of center.

We also have some evidence for an east west effect.[7] The effect is most pronounced for events lying near the horizon. for the band 78.5° to 101.5° away from the vertical we find 17 events from the east and 8 events from the west.

Upward Muons[3)]

We have recovered 187 upward going muons from an exposure of 396 days livetime. the detector has an effective area of 390 m^2. The efficiency for recovering these events is 83%. The measured flux is 2.50 $\pm$ .19μ's/cm^2/sec./sr. This is in good agreement with expected rate of 2.36 x $10^{-13}$$\mu$'s/$cm^2$/sec./sr. An upper limit on excess flux of 4.0 x $10^{-14}$$\mu$'s/$cm^2$/sec./sr. is found when averaged over the entire hemisphere.

These upward muon events provide less information than the contained events. They come from neutrino interactions in the rock surrounding the detector. Because of the range of muons in rock the effective detector mass, and cross sections are a function of neutrino energy. On the other hand, since these events are significantly more energetic than the contained event sample, the angle of the muon is closer to that of the true neutrino direction. In searching for astrophysical point sources some care is needed. Only events below the local horizon have been collected. The detector is at 42° N lattitude. Some portions of the northern sky never drop below the horizon and many only spend a small percentage of time in a region where we can observe them. Cygnus X3, for example, only spends 16% of the time below our local horizon. Some likely southern sources, such as LMC X 4, never rise in the northern hemisphere and are ideal for study with this method.

To carry out a neutrino source search requires some features of the source to be known or assumed. The scattering angle and muon range in rock are functions of the neutrino energy. The search was carried out with two different spectral indices assumed. The spectral indices 2.3 and 3.0 had corresponding angular cuts of 7.0° or 9.5° about the assumed source direction. Detector resolution is significant for events coming from an $E^{-2.3}$ source, but the detector is essentially scattering limited if the flux is softened to E^{-3}.

Limits for both indices are given in table 1. The sample shows no evidence for any sources. Flux limits on the order of 10^{-4} - 10^{-3} $\nu/cm^2/sec.$ are set for high energy neutrinos.

Underground Muons from Cygnus X3

Reports of energetic muons associated with Cygnus X3 have come from two sources. The Soudan group[11] at a depth of 1800 mwe has reported a flux of $7 \times 10^{-11} \mu/cm^2/sec.$ The Nusex group[12] at a depth of 6200 mwe has reported a flux of $2.5 \pm 0.5 \times 10^{-12} \mu/cm^2/sec.$

The I.M.B. detector is not optimized to study this effect. It is fairly shallow (1570 mwe) and the high muon flux has often been discarded without being carefully examined. In the region above the horizon (70° - 80° from the zenith) the surface muon flux has dropped to a manageable level and the muons can be tagged and studied[4]. This angle corresponds to a depth of 4500-9000 mwe and is roughly comparable to the Nusex depth. A search carried out in 538 hours of livetime in the period Feb., 1983 to July, 1984 has failed to confirm their result. A 95% c.l. on the flux of $4.0 \times 10^{-12} \mu/cm^2/sec$ is set for the .7 - .8 phase bin of reference 12. The rate for all muons in the angular region 70° - 80° was six times higher than reported by Nusex and may indicate that the effective depth of this search is much shallower.

An attempt to confirm the Soudan result was based on a search of 300 hours of data when Cygnus was within 25° of the zenith.[5] This gives an effective depth of about 1750 mwe. A 95% c.l. flux bound of $1.3 \times 10^{-10} \mu/cm^2/sec$ was set with a threshold of 550 GeV.

We have failed to confirm the existence of either effect.

Table 1

Muon Induced Flux Limits from Upward Muons

Source	Spectral Index	90% c.l. flux limit $\nu/cm^2/sec \times 10^4$	90% c.l. flux limit $\mu/cm^2/sec \times 10^{14}$
LMC X-4	2.3	.51	3.5
	3.0	13	3.7
Centaurus A	2.3	.77	5.4
	3.0	10	2.9
Vela X-1	2.3	.51	3.5
	3.0	15	4.1
Crab	2.3	1.3	8.8
	3.0	43	12
Hercules X-1	2.3	.99	6.9
	3.0	73	20
Cygnus X-3	2.3	3.1	21
	3.0	60	17
M31	2.3	3.1	21
	3.0	60	17
Geminga	2.3	1.0	7.0
	3.0	31	8.6
SS433	2.3	.82	5.7
	3.0	32	9.0
3C273	2.3	.55	3.8
	3.0	14	3.8
Galactic Center	2.3	.55	3.8
	3.0	12	3.5

Summary

The I.M.B. detector has proved to be a major new tool for neutrino physics. A broad range of energies and distances have been studied. Since the neutrinos come from natural sources we have studied geomagnetic effects and searched for additional possibly point sources. While none have been found, the detector sensitivity is below that needed for many potential souces and the search continues.

The detector has failed to confirm reports of a muon flux underground associated with the source Cygnus X3.

Acknowledgements

We would like to thank the Morton-Thiokol company for hospitality at their Fairport Mine. This work was supported by the U.S. Department of Energy and the National Science Foundation.

References

1) J. LoSecco, et al., Phys. Rev. Lett. 54, 2299 (1985) and reference quoted therein.

2) G. Blewitt, et al., Phys. Rev. Lett. 55, 2114 (1985)

3) R. Svoboda, "A Search for Astrophysical Point Sources of Neutrinos Using a Large Underground Water Cerenkov Detector" Ph.D. thesis, University of Hawaii, 1985

4) J. Van der Velde, I.M.B. internal reports 85-16, 85-17, 85-18 "Search for the Soudan/Nusex Effect in our 70°-80° Muon Sample", 1985 Presented at the 19th ICRC, La Jolla, Calif. (1985)

5) G. Thornton, I.M.B. internal report PDK 85-19 "Vertical Muons from Cygnus X3", 1985, presented at the 19th ICRC, La Jolla, Calif. (1985)

6) G. Blewitt, et al., "Search for Two Prong Proton Decays", Caltech Report, CALT 68-1265
G. Blewitt "A Search for Free Proton Decay and Nucleon Decay in O^{16} Using the Invariant Mass and Momentum of Exclusive Final States" Ph.D. thesis, California Institute of Technology (1986)

7) J. LoSecco, et al., "Contained Neutrino Interactions in an Underground Water Detector" UND-PDK-86-1 (to be published)

8) H. D. Politzer and J. P. Preskill, Phys. Rev. Lett. 56, 99 (1986)

9) L. Wolfenstein, Phys. Rev. D17, 2369 (1978)

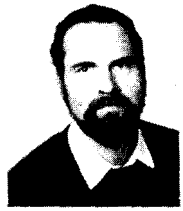
10) J. LoSecco, et al., Proceedings of the 19th Cosmic Ray Conference, La Jolla, Calif. (1985) Volume 8, page 116

11) M. L. Marshak, et al., Phys. Rev. Lett. 54, 2079 (1985) and Phys. Rev. Lett 55, 1965 (1985)

12) G. Battisoni, et al., Phys. Lett. 155B, 263 (1985)

EXPERIMENTAL METHODS FOR THE DETERMINATION OF THE NEUTRON LIFETIME

K. Schreckenbach
Institut Laue-Langevin
F-38042 Grenoble, France



ABSTRACT

The half life of the neutron is an important entity in neutrino physics, since it provides information on the weak interaction coupling constants. Possible experimental techniques include neutron bottles, decay products out of a continuous or chopped neutron beam and the $\bar{\nu}_e$ + p reaction with reactor $\bar{\nu}_e$. The various experimental approaches and the present experimental neutron lifetime values are discussed.

1. Introduction

The lifetime τ_n of the free neutron is an important entity in neutrino physics since it defines the cross section of reactions such as $\bar{\nu}_e p \rightarrow n\ e^+$ and, more generally, is related to the weak interaction coupling constants g_V and g_A. Thus the normalization of the recent $\bar{\nu}_e p \rightarrow n\ e^+$ data in neutrino oscillation experiments at nuclear reactors[1,2] as well as the calculation of the solar neutrino rate from the pp and pe reactions depend on the knowledge of τ_n.

Governed by the baryon and lepton conservation laws the neutron decays by

$$n \rightarrow p + \bar{e} + \bar{\nu}_e + 782\ \text{keV}$$

i.e. by weak interaction in form of a semi-leptonic decay and with a lifetime of about 15 minutes.

Several experimental approaches are possible to measure or deduce the neutron lifetime :

a) Containment of neutrons in a material or magnetic bottle.
b) Rate of decay products out of a neutron beam.
c) Measurement of the beta asymmetry in the free neutron decay.
d) Cross section measurements of inverse reactions such as $\bar{\nu}_e + p \rightarrow n + e^+$.
e) Properties of the intermediate vector boson W .

In the following some comments will be given on the different methods and the present experimental values for τ_n will be summarized.

2. Principles of neutron lifetime measurements

2.1. Neutron storage experiments

In neutron storage experiments the number of neutrons N_n is measured as a function of the storage time t_s :

$$N_n\ (t_s)/N_n\ (0) = \exp - (t_s/(\tau_n + \tau_{loss})),$$

where τ_{loss} denotes the losses of neutrons in the system by other effects than decay. Fig. 1 shows a schematic lay-out of such an experiment.

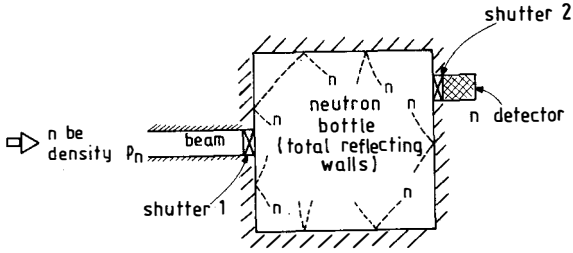


Fig. 1 : Schematic view of a neutron bottle experiment

The "neutron bottle" is filled (shutter 1 open) until the neutron density in the bottle is equal to that in the beam. After a storage time t_s (shutters 1 and 2 closed) the shutter 2 is opened and the remaining neutrons counted and absorbed in the neutron detector. The cycle is repeated for different t_s but the same initial ρ_n.

Such bottle experiments have the advantage that the absolute number $N_n(0)$ must not be known, but suffers from low neutron fluxes and additional losses of neutrons. In fact, only ultra cold neutrons (UCN, $v_n \lesssim 5$m/s) can be contained in material bottles, since repulsive wall potentials are not larger than $\sim 10^{-7}$ eV.

Until recently UCN densities of only ~ 1 n/cm^3 were available. New devices promise a gain of two orders of magnitude[3]. Mampe et al.[4] achieved a storage time of 553 s using a fluid surface for the walls. A variation of the bottle size and hence mean free path length for the neutrons allowed an estimation of τ_{loss}, resulting in τ_n = 850 (60) s. By a similar method Kosvintsev et al.[5] obtained τ_n = 875 (95) s.

Kügler et al.[6] succeeded in a magnetic storage of neutrons. A superconducting sextupole torus was used to contain neutrons by the force on the neutron magnetic moment μ_n in a magnetic field gradient :

$$F = \mu_n \text{ grad } B$$
$$\mu_n = 6.10^{-8} \text{ eV/Teslar}$$

Again only UCN could be stored and resonance losses occurred in the storage ring. A value of τ_n (>) 907(70)s was deduced.

2.2. In-beam measurements of decay products

The most precise values for direct neutron life time measurements were obtained up to now by counting neutron decay products in a continuous neutron beam[7,8,9]. Several new experiments are in progress using a chopped beam mode. This new generation of experiments is now possible due to the availability of intense beams of slow neutrons. As an example the guides for cold neutrons at the ILL High Flux Reactor provide fluxes of $\phi_n = 2 \times 10^9$ n cm^{-2} s^{-1} with a mean velocity of 800 m/s, $\rho_n = 25000$ n cm^{-3} and thus a decay rate of ~ 30 neutrons per cm^3 of the beam.

Fig. 2 shows schematically the experimental set-up of a neutron life time experiment with a continuous neutron beam. The charged decay products proton or/and electron are guided by a electric or magnetic field to the detectors. Thus they are detected over an effective length l_{eff} of the beam in 4π geometry. The neutron density is measured in a thin neutron counter (weakly absorbing, surface density m) via a neutron capture reaction with known cross section

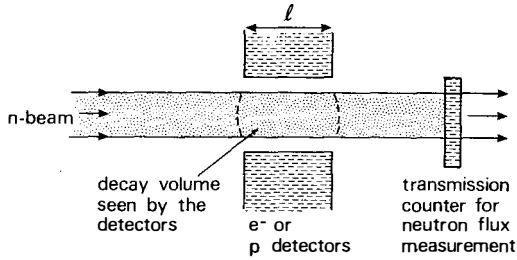


Fig. 2: Experimental set-up for a neutron life time experiment by decay products in a continuous beam.

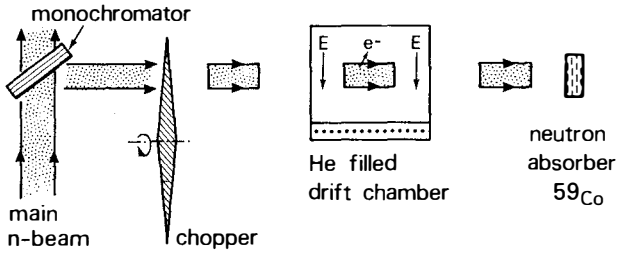


Fig. 3: Same as Fig. 2 but with a chopped beam[11].

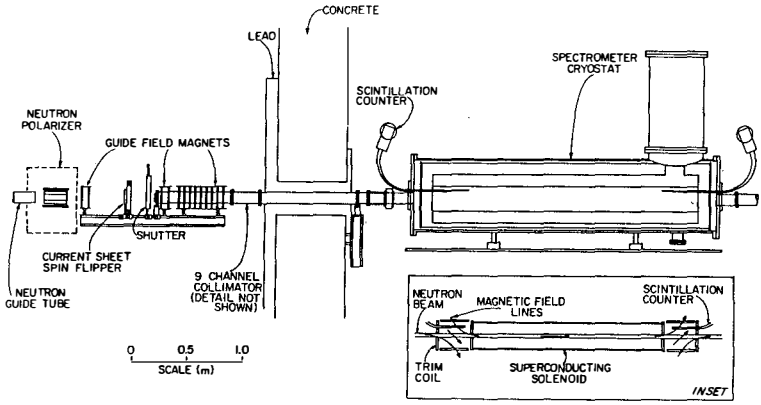


Fig. 4:Arrangement for a beta asymmetry measurement with the spectrometer PERKEO. Decay electrons from longitudinally polarized neutrons are guided by the magnetic field of the solenoid to the scintillation counters[10]

$\sigma_o(v_o)$ and $\sigma = \sigma_o\, v_o/v_n$, v_n neutron velocity. The neutron life time is given then by

$$\tau_n = \frac{l_{eff}}{m\, v_o\, \sigma(v_o)} \quad \frac{d\, N_R/dt}{d\, N_d/dt}$$

The number of decay products N_d and reactions N_R in the neutron counter as well as l_{eff} must be determined absolutely. The best measurements of this kind obtained a precision of 1 to 2%, but deviate from each other by as much as 7% (see Fig. 6).

A typical experimental arrangement for the chopped beam mode is shown in Fig. 3. The neutron life time is given by :

$$\tau_n = N_n/(\Delta N_{e^-}/\Delta t)$$

N_n denotes the neutrons per burst, ΔN_{e^-} the decay electrons emitted during the time interval Δt where the burst moves inside of the detection volume. At present a superconducting solenoid ("PERKEO")[10] and an in-beam ^{4}He drift chamber[11] are used as 4π electron detectors. The background is measured when the neutron burst is well outside the detector volume. The neutron number N_n can be determined by activation analysis of a beam absorber, for instance ^{59}Co. For the case of the He drift chamber $N_n/\Delta t$ can be measured by adding a well defined amount of ^{3}He, which undergoes the reaction ^{3}He (n,p)t. Thus only the ratio of the decay electrons to the (n,p) events must be determined. The events can be discriminated in the drift chamber working in a time projection (TPC) mode.

2.3. Beta decay asymmetry

The neutron life time can be deduced from measurements of the beta decay asymmetry of polarized neutrons, assuming the validity of the CVC and V-A theory.

$$W(\theta) \sim (1 + A \cdot \cos\theta \cdot v/c)$$

$$A = -2\lambda\, \left(\frac{\lambda - 1}{1 + 3\lambda^2}\right)$$

$$\lambda = g_A/g_V$$

$$\tau_n = \frac{1.0354 \cdot 10^{-94}\ \mathrm{erg^2\,cm^6}}{g_V^2\,(1 + 3\,\lambda^2)}$$

g_V from $0^+ \rightarrow 0^+$ nuclear beta decays[12]

Recently a precise measurement of A was carried out with the spectrometer PERKEO (Fig. 4) at the ILL High Flux Reactor. A value of τ_n = 898(6)s was deduced from λ = -1.262(5)[10]. Prior to this result the particle data group recommended 1984 a value λ = - 1.254(6)[15] as an average of several less precise measurements.

2.4. τ_n and neutrino induced reactions

The inverse neutron beta decay reaction $\bar{\nu}_e + p \rightarrow n+e^+$ has a cross-section which is proportional to $(E_\nu - Q)^2/\tau_n$, Q = 1.8 MeV[13]. Thus a comparison of the recent precise $\bar{\nu}_e$ detector ($\bar{\nu}_e p \rightarrow ne^+$) data[1,2] at nuclear reactors with the $\bar{\nu}_e$ flux of the reactor provides a value for the neutron life time, or a limit for τ_n including the possibility of neutrino oscillations. The $\bar{\nu}_e$ source flux and spectrum of a reactor can be deduced from experimental beta spectra of fission product, converted into the correlated $\bar{\nu}_e$ spectra[14]. A recent measurement is illustrated in Fig. 5.

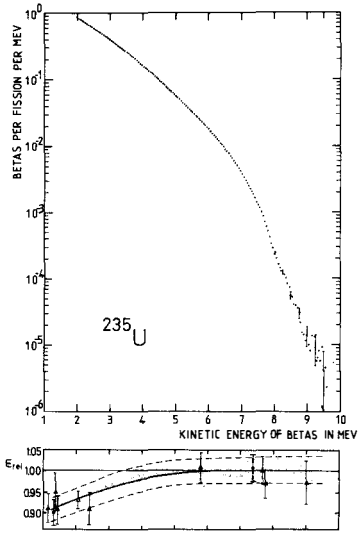


Fig. 5 :
Experimental beta spectrum of ^{235}U fission products recorded at the magnetic beta spectrometer BILL. In the lower part the efficiency curve of the spectrometer with the absolute uncertainty range (shadowed area) is shown[14].

Those measurements provide normalized $\bar{\nu}_e$ spectra (per fission) for fissile isotopes contributing to the reactor power. The $\bar{\nu}_e$ flux of the reactor can finally be composed knowing the number of fissions per second which take place for each fissile isotope in the reactor core. From the recent evaluation of the $\bar{\nu}_e$ detector data taken at the Gösgen power reactor[1] a value of τ_n = 866(57)s can be deduced under the hypothesis of no neutrino oscillations.

3. Conclusion

Fig. 6 summarizes the available data on neutron life time measurements. The most precise direct measurements are not fully consistent among each other. The recent measurement of λ[10] supports the recommended value of the particle

data group for τ_n with the drawback that λ and τ_n are linked by theoretical assumptions. Obviously improved direct measurements of the free neutron life time are demanded.

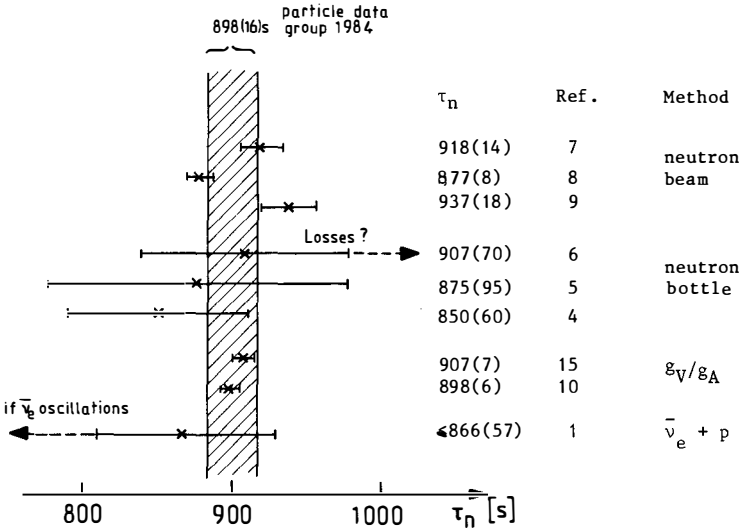


Fig. 6 Available experimental values on the neutron life time.

References :

1) V. Zacek et al. Phys. Lett. 164 B, 193 (1985)
2) J.F. Cavaignac et al., Phys. Lett. 148 B, 387 (1984)
3) P. Ageron and W. Mampe, in NBS Special Publication 711 (ed. G.L. Greene) pp. 16 (1986)
4) W. Mampe, in NBS Special Publication 711 (ed. G.L. Greene) 59 (1986)
5) Yu.Yu. Kosvintsev et al. JETP Lett. 31, 236 (1980)
6) K.J. Kügler et al. NIM 228, 240 (1985)
7) C.J. Christensen et al. Phys. Rev. D5, 1628 (1972)
8) L.N. Bondarenko et al. JETP Lett. 28, 303 (1978)
9) J. Byrne et al. Phys. Lett. 92 B, 274 (1980)
10) P. Bopp et al., Phys. Rev. Lett. 56, 919 (1986)
11) P. Liaud et al., J. de Physique 45, Colloque 3, 37 (1984)
12) D.H. Wilkinson, Nucl. Phys. A 377, 474 (1982)
13) P. Vogel, Phys. Rev. D 29, 1918 (1984)
14) K. Schreckenbach et al. Phys. Lett. 160 B, 325 (1985) and ref. cited therein.
15) Particle Data Group, Rev. Mod. Phys. 56, 51 (1984)

THE OSCILLATION EXPERIMENT AT THE GOESGEN REACTOR

J.-L. Vuilleumier
Institut de Physique de l'Universite de Neuchatel
A. L. Breguet 1
CH-2000 Neuchatel, Switzerland



ABSTRACT

The spectrum of positrons from the reaction $\bar{\nu}_e + p \rightarrow e^+ + n$ was measured at three distances, 37.9, 45.9 and 64.7, from the core of the Goesgen reactor. These data were analyzed in terms of neutrino oscillations of the type $\bar{\nu}_e \leftrightarrow x$. No evidence for neutrino oscillations was found. In particular the oscillation parameter region favored by an experiment at the Bugey reactor is not supported by the data presented here.

Nuclear reactors are powerful sources of $\bar{\nu}_e$ with energies up to 8 MeV from the beta decay of the fission products. They are well suited to study oscillations of the type $\bar{\nu}_e \leftrightarrow x$ ($\bar{\nu}_e$ dissappearance). In the two neutrino model the probability for a neutrino to be a $\bar{\nu}_e$ at distance L is given by:

$$P(L,E,\Delta^2,\theta) = 1-\frac{1}{2}\sin^2 2\theta\left(1-\cos\frac{2.53\Delta^2(eV^2)L(m)}{E_\nu(MeV)}\right) \quad (1)$$

with $\Delta^2=|m_1^2-m_2^2|$ (m_1 and m_2 are the eigenmasses) and θ the mixing angle.

Two dedicated experiments have been performed recently, at the Goesgen (Switzerland) and Bugey (France) reactors. Both of them use one single detector which successively measures the flux at various distances from the reactor core. Data have also been obtained at the Rovenskaia (USSR) reactor, but only at one distance so far.

The Goesgen experiment, conducted by a Caltech-SIN-TU Munich collaboration, has now been completed. The Goesgen reactor is a 2800 MWth pressurized water reactor. The detector was located outside the containment building, which provides 8 m of concrete shielding from the core. The flux was measured first at L=37.9 m from the core [1]), the shortest possible distance, then at 45.9 m [2]) and finally at 64.7 m [3]).

The Goesgen reactor has a cylindrical core of 3.2 m diameter and 3.4 m height. It produces energy essentially from the fission of ^{235}U, ^{239}Pu, ^{238}U, and ^{241}Pu. The averaged contributions for the measurements at 37.9, 45.9 and 64.7 m, (which are slightly different), are shown in

table 1. The fission rates can be calculated from the energy released per fission. The total neutrino flux is then obtained by combining the fission rates with the neutrino yields per fission. For the dominant isotopes ^{235}U and ^{239}Pu reliable neutrino yields have been derived from the measured beta spectra of the fission products [4]. The relatively small contributions of the remaining isotopes ^{238}U and ^{241}Pu was determined from the calculated spectra of ref. 5. The uncertainty on the neutrino flux amounts to 3% in the relevant energy range.

Table 1. Averaged isotopic contribution to the reactor power for the Goesgen experiment

Distance	^{235}U	^{239}Pu	^{238}U	^{241}Pu
37.9 m	61.9%	27.2%	6.7%	4.2%
45.9 m	58.4%	29.8%	6.8%	5.0%
64.7 m	54.3%	32.9%	7.0%	5.8%

The detector used the reaction

$$\bar{\nu}_e + p \rightarrow e^+ + n \,. \qquad (2)$$

A time coincidence between positron and neutron is required as the signature for a neutrino event. The detector system (fig. 1) consists of five planes of six target cells filled with liquid scintillator (377 l total volume) serving as proton target, positron detector and neutron moderator, alternated with four ^3He wire chambers (thermal neutron

detectors). The neutrino energy is determined from the measured positron kinetic energy E_{e^+} (the neutron only has a few tens of keV's) using the relation:

$$E_{e^+} \cong E_{\nu} - 1.8 \text{ MeV}. \quad (3)$$

Pulse shape discrimination was used to suppress fast neutron background in the target cells. The position of an event along the length of a target cell was obtained from the time difference of the photomultiplier pulses at either end. Each ^{3}He chamber has 16 groups of resistive wires arranged in one plane. The position along a wire was determined by charge division. In spite of the complexity of the design it was possible to achieve a very low level of natural radioactivity. The requirement of a position correlation between target cell and neutron counter events reduces the accidental background by a factor of 7, at the modest cost of an 8% loss in detection efficiency. The detector is completely surrounded by veto counters followed by various shielding layers, including 2 m of concrete on the sides and 4 m on top to suppress the cosmics background.

The measured spectra are somewhat washed out by several instrumental effects. The energy response function was calculated by Monte Carlo taking into account the energy resolution of the detector (18% FWHM at 1 MeV), annihilation in flight and at rest, positron bremsstrahlung and the wall effect. The probability to detect a neutron created in a target cell was measured with a Sb(Be) neutron source and is 21.7 ± 0.006 %.

At each of the three positions the reactor off spectrum was measured

during the one month long annual shutdown of the reactor. After background subtraction a total of 10930 ± 220 events with 0.7 MeV < E_{e^+} < 5.6 MeV were seen at 37.9 m in 3441 h of data aquisition, 10590 ± 190 at 45.9 m in 4893 h and 8787 ± 325 at 64.7 m in 8608 h (fig. 2).

The simplest way to analyze the data is to compare the three spectra looking for differences in shape and normalization resulting from oscillations (eq. 1), after correcting for the different solid angles and the small changes (<2%) due to slightly different mix of fissile isotopes and taking into account the finite energy and spatial resolution. This analysis is free of uncertainties affecting the cross section of the detection reaction (eq. 2), the absolute reactor neutrino flux, and the acceptance of the detector. As it turns out, the three spectra are in good agreement and there is no evidence for oscillations of the type $\bar{\nu}_e \leftrightarrow x$. Oscillations with small mixings, long (compared with the distances) or short (compared with the core size) lengths are also allowed. But, performing a maximum likelihood ratio test in the frame of the two neutrino model, a large area in the Δ^2 vs $\sin^2 2\theta$ plane is excluded as shown in fig. 3 for $0.02 < \Delta^2 < 2\ eV^2$.

These findings can be compared with those of the Annecy-ISN Grenoble collaboration at Bugey [6]. The Bugey reactor is very similar to the Goesgen reactor. The Bugey detector is a simplified version of the Goesgen detector, with poorer background suppression. The major difference is that the Bugey detector is located inside the containement building, in the subbasement, much closer to the core. The spectrum was measured at 13.6 m (39881 ± 262 events) and 18.3 m (23345 ± 310). And here comes a second difference with Goesgen: the two Bugey spectra do

not scale with the solid angle. The shape does not change significantly but the ratio of the integrated rates after correcting for the solid angle and changes in fuel composition becomes Y(13.6 m)/Y(18.3 m) = 1.102 ± 0.014 (stat.) ± 0.028 (sys.). This 3σ discrepancy was tentatively explained by oscillations of the type $\bar{\nu}_e \leftrightarrow x$, with the parameters Δ^2 and $\sin^2 2\theta$ inside the area shown in fig. 3. The preferred values are $\Delta^2 = 0.2\ eV^2$ and $\sin^2 2\theta = 0.3$. The area allowed by Bugey, however, is excluded with a high degree of confidence by the Goesgen data. It appears very difficult to reconcile the two experiments.

As a consistency check, and to be sensitive to large values of Δ^2, the three Goesgen positron spectra were compared to the expected spectra determined from the neutrino yield and the cross section of the detection reaction (eq. 2). The error on the normalization of 6% must then be taken into account. It results essentially from the uncertainties in the acceptance of the detector and the expected neutrino yield. Anyway, the expected spectra assuming no oscillations are in good agreement with the measured ones (fig. 2), in shape and normalization (the ratio of the measured to expected integrated rates is 1.04 ± 0.06). Improved limits on the parameters Δ^2 and $\sin^2 2\theta$ are derived (fig. 3). For $\Delta^2 > 2\ eV^2$ one gets $\sin^2 2\theta < 0.18$ (90%CL). Similarly the Bugey spectra were compared to expectations assuming no oscillations. While the 13.6 m spectrum is in agreement, the 18.3 m one is lower at all energies by about 12 %. It appears difficult to explain this behaviour by oscillations. Oscillations leading to a noticeable difference between the spectra at 13.6 and 18.3 m will distort both spectra in a significant way, not just the one at 18.3 m (eq. 1).

Further, the Goesgen spectra were compared with the spectrum previously obtained with essentially the same detector at 8.8 m from the core of the 57 MW ILL reactor [7]. The fuel elements consist of pure ^{235}U, so that a correction has to be applied (5% at 3 MeV neutrino energy, 13% at 6 MeV). Again good agreement is found, confirming the evidence against oscillations with parameters as large as those suggested by the Bugey experiment [2].

In this context the data obtained by a group of the Kurtchatov institute at the Rovenskaia reactor [8]) is worth mentioning. The Rovenskaia reactor has about the same fuel composition as in Goesgen or Bugey. The thermal power is 1375 MW. The reactor is under ground and the detector is located in a cave underneath the core, at a distance of 18.06 m. The cosmics background is thus quite low.

The apparatus also makes use of reaction (2) and consists of a large tank filled with 240 ℓ of Gd loaded scintillator in which the positrons as well as the neutrons, after thermalization, are detected. The detection efficiency is 32.1 ± 1.8 %. Reactor on data have been accumulated during a 57.2 days period (live time). The background was measured in a 20.1 days reactor off period. In total some 30000 neutrino events were observed. The integral rate agrees well with the prediction based on the measured beta spectra of the fission products [4]). This contradicts the low rate measured at 18.3 m, almost the same distance, at the Bugey reactor (18.3 m). The limits on the oscillation parameters derived by Afonin et al. however are not as restrictive as the Goesgen limits.

We thus conclude that reactor experiments at present give no evidence for oscillations. The positive result from Bugey is in serious conflict with the Goesgen data. Clarification of this discrepancy may come soon. The Bugey experiment is being repeated, and it is foreseen to move the Rovenskaia detector to a larger distance. In addition a new experiment at the 2200 MWth Savannah River reactor has started producing data [9]).

REFERENCES

[1]) J.-L. Vuilleumier, Phys. Lett. 114B, 298(1982)

[2]) K. Gabathuler et al., Phys. Lett. 138B, 449(1984)

[3]) V. Zacek et al., Phys. Lett. 164B, 193(1985)

[4]) K. Schreckenbach et al., Phys. Lett. 160B, 325(1985); K. Schreckenbach, these proceedings.

[5]) P. Vogel et al., Phys. Rev. C24, 1543(1981)

[6]) J.-F. Cavaignac et al., Phys. Lett. 148B, 387(1984); Bouchez, these proceedings

[7]) H.M. Kwon et al., Phys. Rev. D24, 1097(1981)

[8]) A.I. Afonin et al., Pis'ma v ZhETF 42, 230(1985)

[9]) H. Sobel, these proceedings

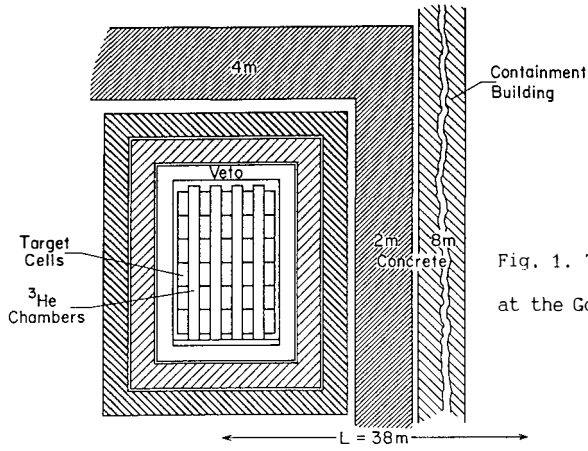


Fig. 1. The neutrino detector at the Goesgen reactor.

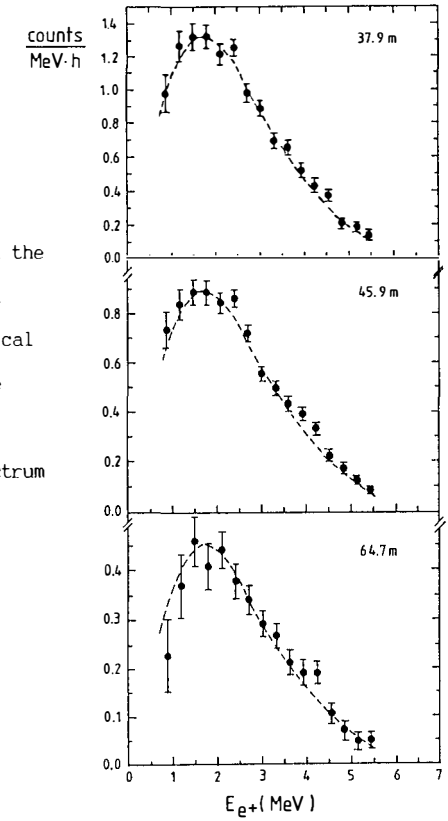


Fig. 2. The positron spectra from the reaction $\nu_e + p \rightarrow e^+ + n$ measured at the Goesgen reactor. The vertical scales have been adjusted for the differences in solid angle. The dashed curve is the expected spectrum assuming no oscillations.

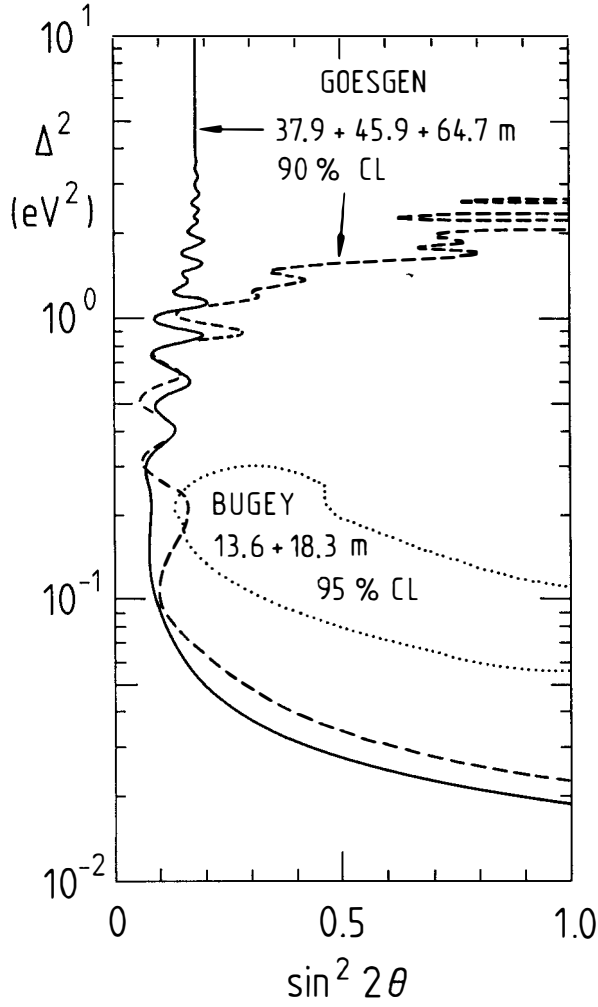


Fig. 3. Limits on $\nu_e \leftrightarrow x$ oscillations from reactor experiments. For Goesgen [3]) the allowed areas are to the left of the curves; dashed curve: from a direct comparison of the spectra at 37.9, 45.9 and 64.7 m; solid curve: including the information on the expected spectrum. For Bugey [6]) the allowed area is inside the dotted curve and was obtained from a comparison of the spectra measured at 13.6 and 18.3 m.

BUGEY COLLABORATION

J. BOUCHEZ
Département de Physique des Particules élémentaires,
CEN-Saclay, 91191 Gif-sur Yvette Cedex France.

ABSTRACT

We show that comparisons between different reactor experiments do not presently allow to unambiguously prove or disprove neutrino oscillations. Requirements for new generation experiments are deduced from Monte Carlo studies. Finally, the present status and prospects of the Bugey experiment are given.

I - Comparison of reactor experiments

We have used in this study the 3 experiments for which the relevant information was available :

The ILL [1], Gosgen [2] and Bugey [3] experiments. The results are summarized in table 1. We shall focuss first on integral event rates, then on the shape of the measured energy spectra.

Table 1

Expt	ILL	BUGEY		GOSGEN		
Distance (meters)	8.8	13.6	18.3	37.9	45.9	64.7
R	0.95±0.035	0.98±0.006	0.89±0.013	1.03±0.02	1.055±0.02	0.99±0.04

R is the ratio of measured rates to Monte Carlo predictions assuming no oscillation. Quoted errors are only statistical. See text for systematics.

A - Integral rates

Apart from statistical errors, systematic uncertainties have to be taken into account when comparing the different results. These systematics can be classified as follows :

1) Uncertainties common to all experiments

These come from the lack of exact knowledge of the $\bar{\nu}$ flux coming from the reactor. Measurements exist for U^{235} and Pu^{239} isotopes, with a 5% statistical accuracy and 5% systematic uncertainty on normalisation and on corrections to be applied to get the $\bar{\nu}$ spectrum from the measured electron spectrum. The same uncertainty exists on computations for U^{238} and Pu^{241} isotopes, for which no measurements are available.

A 2% uncertainty on the neutron lifetime (i.e. on the $\bar{\nu}$ p cross section) adds up when deducing the event rate from the flux.

As an example, figure 1 illustrates the discrepancies existing between different measurements and computations for U^{235} : above 3 MeV neutrino energy (that is 1.2 MeV positron energy), one sees spreads well above 20%, increasing with energy.

In conclusion, an uncertainty of at least 7% on the absolute rate, common to all experiments, has to be taken into account.

2) Uncertainties common to different positions of a given experiment.

These uncertainties are experiment dependant. The main contributions come from the knowledge of the absolute neutrino detection efficiency of the detector and the number of free protons in the target, and amount typically to 4%.

Furthermore, an energy shift of 100 keV on the low energy cut of the position spectrum gives rise to a 3% systematic effect. A shift of 200 keV is actually seen when comparing Bugey and Gosgen Monte Carlos (see figure 2), two experiments having quasi identical detectors : a possible explanation could be a different handling of the broadening and shift of the energy response due to the 2 gammas originating from the positron annihilation.

In conclusion, each experiment has its own 5% normalisation uncertainty on integral rates, common to the measurements done at different positions.

3) Position dependant uncertainties.

These uncertainties come from the knowledge of the solid angle, the reactor power, the dead time and the neutron efficiency variations during measurements at a given position, and amount typically to about 2%.

4) Consequences

In table 2, we show the predictions for R, ratio of measurements to predictions, assuming a 2 neutrino oscillation with $\delta m^2 = 0.2\ ev^2$ and $\sin^2 2\theta = 0.2$. We can get a good descriptions of the measured rates if we increase the predictions by 7% for all experiments, plus 4% for the 3 Gosgen positions and minus 4% for ILL. We can even improve the agreement by using the 2% normalisation uncertainty on each point. All these shifts are equal or smaller to the above mentionned systematics, so that measured integral rates cannot, in our opinion, disprove the existence of such an oscillation. The no oscillation case is of course not excluded, except for a 3σ difference between the two Bugey positions (Bugey1/Bugey2 = 1.10 ± 0.014 (stat) ± 0.028 (syst)).

Table 2

	R(measured)	R(0.2,0.2)	+7% all	{ +4% Gosgen −4% ILL
ILL	0.95±0.035	0.94	1.01	0.97
Bugey1	0.98±0.006	0.88	0.95	0.95
Bugey2	0.89±0.013	0.84	0.91	0.91
Gosgen1	1.03±0.02	0.89	0.96	1.00
Gosgen2	1.055±0.02	0.91	0.98	1.02
Gosgen3	0.99±0.04	0.91	0.98	1.02

B - Shape analyses

The shape of the spectra is certainly less dependant on systematics, since it only depends on the positron energy calibration and its good monitoring throughout the experiment. The only problem comes from the different fuel composition (burn up effect) which distorts the spectrum. This can be corrected using Monte Carlo to bring all data to the same fuel composition. The correction is a few percent, so that systematic uncertainties on each isotope contribution are of no consequence.

A more severe problem when comparing different experiments comes from a possible difference in energy scale (mainly a shift, as previously explained). We didn't try to take this effect into account in our shape comparisons.

We have compared ratios of experimental spectra (corrected for burn up) to the corresponding predicted ratios using a given Monte Carlo (the Bugey one), both for the no oscillation case and for an oscillation with $\delta m^2 = 0.2\ eV^2$, $\sin^2 2\theta = 0.2$. The fit contains only a free normalisation parameter A rescaling the Monte Carlo ratio. The main results are summarized in table 3.

Table 3

	$\frac{\text{Bugey1}}{\text{Bugey2}}$	$\frac{\text{Gosgen1}}{\text{Gosgen2}}$	$\frac{\text{Bugey1}}{\text{Gosgen1}}$
No osc [A	1.09±0.01	0.978±0.016	0.984±0.013
No osc [χ^2/N	11.8/15	7.4/15	19.0/15
(0.2,0.2) [A	1.03±0.01	1.015±0.017	0.957±0.013
(0.2,0.2) [χ^2/N	10.6/15	11.1/15	25.8/15

A few remarks are of order :

First, good fits are obtained both for oscillation and no oscillation when comparing 2 positions of a given experiment. In particular, a $X^2/N = 11.1/15$ is obtained for Gosgen1/Gosgen2 with oscillation, giving a probability of 75%, whereas the Gosgen publication [2b] gives only a 10% probability for the same solution using a maximum of likelihood method. We have no clear explanation for this discrepancy.

Second, the comparison betwen Bugey1 and Gosgen1 gives bad probabilities both for oscillation and no oscillation. Taken litterally, it would exclude both ! As already mentionned, this could actually be explained by systematic differences in energy calibration between the two experiments. The result of both fits is shown on figure 3.

Our conclusion is that by no means, present experiments can prove or disprove oscillation by looking only at the shape of their spectra, and that comparisons between experiments is made difficult due to systematic effects.

II - New generation experiments ?

A way out of the present unsatisfactory situation is to design a new experiment with 2 detectors running together, and having enough sensitivity to be able to unambiguously prove/disprove an oscillation with parameters around $\delta m^2 = 0.2\ eV^2$, and $\sin^2 2\theta \geq 0.1$, by looking only at the shape of the spectra. That's the only way to get rid of most systematic errors, as long as a good energy calibration monitoring is assumed.

Taking the present Bugey detector as reference, we have defined an improvement factor in sensitivity M to achieve such a programm within one year data taking. The background rate was taken equal to the present Gosgen rate (Bugey rate was higher due to shielding problems and the lack of localisation of the neutron in the Helium chambers).

The effect of the other reactors present on the Bugey site was taken into account.

We fixed M = 3 at the 13.6 m location, and varied the distance L and the improvement factor M for the far detector.

The result of this study shows that the optimal distance lies between 30 and 40 meters and that an improvement factor of 9 is necessary. The figure 4 shows which sensitivity to $\sin^2 2\theta$ is obtained in these conditions, looking only at the shape of the spectra.

III - Status of the Bugey experiment

The Bugey collaboration has increased to 5 french laboratories (LAPP Annecy, ISN Grenoble, CPPM Marseille, CdF Paris and DPhPE Saclay) and is preparing a new detector using cells of liquid scintillator charged with neutron capturing salts (see J.F. Cavaignac's talk in the same proceedings) which could achieve the above mentionned goals.

In the meantime, we have started a remeasurement at 13.6 and 18.3 meters with the same detector and a few improvements :

- Active shielding against cosmics by use of 2 planes of plastic scintillators on top of the shield containing the detector.

- Differential passive shielding at the 13.6 m location to study the possible presence of a reactor correlated background.

- Removal of internal lead in the shielding between detector and borated water.

- More permutations of the detector between the 2 locations (better handle of burn up effects)

- Improvements in electronics and data acquisition.

Data have been collected with reactor ON at the two locations, and with different shielding conditions at 13.6 meters. Reactor OFF data exist at 18.3 meters. We have to wait for the next reactor shut down in June 86 to collect reactor off data at 13.6 meters. We also need a new absolute calibration of the neutron efficiency of the detector to compare new data to the previous experiment.

The first results should be available around summer'86, and a module of the new detector should be operational in spring'87.

References

[1] H. Kwon et al., Phys. Rev. D24 (1981) 24

[2] a) J.L. Vuilleumier et al., Phys. Letters 114B (1982) 298
b) K. Gabathuler et al., Phys. Letters 138B, (1984) 449
c) V. Zacek et al., Phys. Letters 164B (1985) 193

[3] J.F. Cavaignac et al., Phys. Letters 148B, (1984) 387

[4] M.V. Klapdor et al., Phys. Rev. Letters 48 (1982) 127

[5] F.T. Avignone et al., Phys. Rev. C22 (1980) 594

[6] A.A. Borovoi et al., Yad. Fiz. 37 (1983) 1345

[7] P. Vogel et al., Phys. Rev. C24 (1981) 1543

[8] K. Schreckenbach et al., Phys. Letters 99B (1981) 251

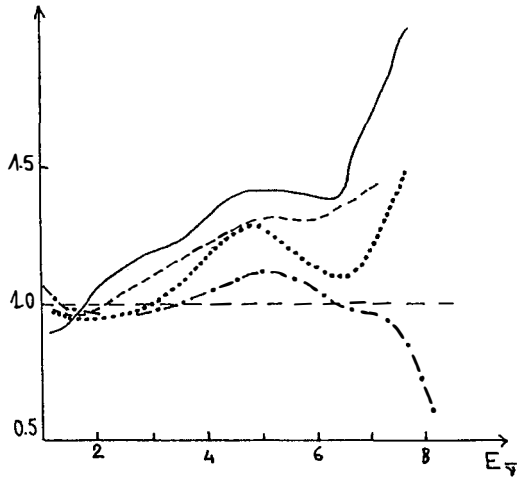


Figure 1
Comparison of $\bar{\nu}$ flux (rate) coming for U^{235} from different measurements and computations, with respect to Klapdor [4] : — Avignone [5], --- Borovoi [6], ... Vogel [7], -.- Schreckenbach [8].

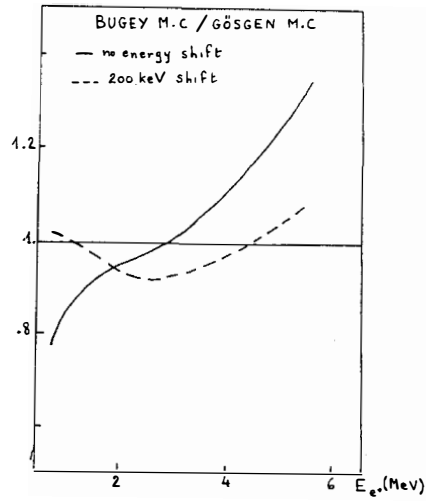


Figure 2
Ratio of Bugey and Gosgen Monte Carlo positron spectra, with and without a 200 keV shift in the energy scale.

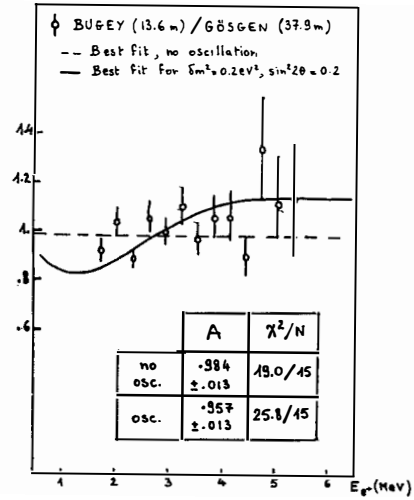


Figure 3
Shape fit of the ratio of measurements Bugey1/Gosgen1 (see text for details).

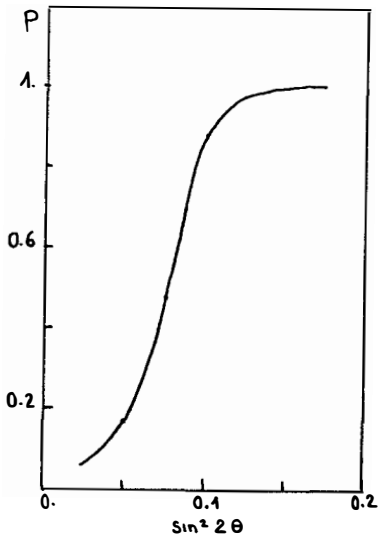


Figure 4
Probability of excluding the no-oscillation case at 95% C.L. by shape analysis after one year measurements at 13.6 and 30 meters with 2 detectors of sensitivity respectively 3 and 9 times that of the present detector, as a fonction of $\sin^2 2\theta$ and for $\delta m^2 = 0.2\ eV^2$.

TWO POSITION RESULTS FROM THE IRVINE MOBILE NEUTRINO OSCILLATION DETECTOR

Henry W. Sobel
Physics Department
University of California, Irvine
Irvine, California 92717
U.S.A.

N. Baumann,(1) Z. Greenwood, H. Gurr,(2) W. Kropp,
M. Mandelkern, L. Price, F. Reines, H. Sobel

(1) The Savannah River Plant, Aiken, S.C.
(2) The University of South Carolina, Aiken, S.C.



Abstract

We report preliminary two position data from the Irvine Neutrino Oscillation Experiment. A three standard deviation exclusion region is obtained for the parameters $\sin^2 2\theta$ and δm^2.

1. Introduction

This report gives preliminary results from the University of California, Irvine (UCI) Neutrino Oscillations Experiment. We have constructed and installed a detector in our Savannah River Plant (SRP) Neutrino Laboratory. The detector is designed to be movable, and can, with relative ease, be positioned at any distance from the reactor core between about 18 and 50 meters. The neutrino flux at the closest position is approximately $10^{13}/cm^2/sec$.

2. The SRP Reactor as a Neutrino Source

Power reactors, used in most other (reactor) neutrino oscillation experiments, produce neutrinos from the fission of significant fractions of each of the isotopes ^{235}U, ^{238}U and ^{239}Pu. The neutrino spectrum of each component is different. At the SRP production reactor, ^{239}Pu produces less than 8% of the fissions, and ^{238}U less than 4%. As a result, for energies between 2 and 8 MeV, the difference from a pure ^{235}U neutrino spectrum is less than 1.5%.

3. A Disappearance Experiment

The detector is designed to observe neutrinos via the inverse beta reaction:

$$\bar{\nu}_e + p \rightarrow e^+ + n$$

Since the neutrino energy is less than 10 MeV, the reaction is nonrelativistic, and the positron kinetic energy is:

$$E_{e^+} = E_\nu - (m_n - m_p + m_e) = E_\nu - 1.8 \text{ MeV}$$

A measurement of the positron spectrum is thus a measurement of the neutrino spectrum.

If the $\bar{\nu}_e$ changes to another neutrino type, the new neutrino will be below its inverse beta threshold, and thus be unobservable. A reactor experiment is therefore, a disappearance experiment: a deficiency in the $\bar{\nu}_e$ signal is expected if oscillations occur.

4. The Detector

A schematic of the detector is shown in figure 1. The target is 300 liters of NE313, a xylene based scintillator loaded with 0.5% gadolinium. This scintillator provides pulse shape information, allowing us to distinguish between lightly and heavily ionizing particles (positrons and protons). The gadolinium provides fast, high efficiency neutron detection. The target is surrounded by 1100 liters

of a mineral oil based scintillator, divided into two volumes (the blanket region). Each volume is viewed by 30 five inch photomultiplier tubes (PMT's). The detector is surrounded by two inches of low background lead, a three inch thick plastic scintillator anticoincidence, and finally, eight inches of additional lead. Room is provided for additional neutron shielding (B or Cd).

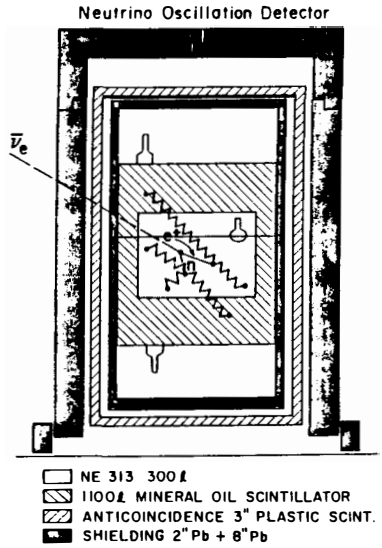


Fig. 1 Schematic of the detector.

An electron antineutrino from the reactor can interact with a target proton. The resultant positron stops and promptly annihilates. Each 0.5 MeV annihilation gamma ray has a high probability of depositing its energy in the liquid scintillator. The neutron, with kinetic energy of tens of KeV, quickly thermalizes and is captured with a characteristic time of 10 us, by a Gd nucleus. The resultant ~ 8 MeV of gamma rays are detected with high efficiency.

5. Detector Characteristics

a. Energy Resolution:

We have measured the energy resolution of the Target and Blanket detectors using various sources. The results can be expressed as follows:

$$\sigma_{Target} = .12 \sqrt{E(MeV)}$$

and

$$\sigma_{Blanket} = .20 \sqrt{E(MeV)}$$

b. Detector Efficiencies:

Monte Carlo simulation of the detector properties have been made and give the positron and neutron detection efficiencies. When we integrate over the expected energy spectrum, the positron detection efficiency, is found to be ~ 0.7 using a threshold energy of 1.8 MeV.

The delayed neutron efficiency with a gamma threshold of 4 MeV is found to also be ~ 0.7. Experimental measurements of these quantities to verify the results of the Monte Carlo are still in a preliminary stage.

c. Neutron Capture Time:

The neutron capture time also enters into the overall detection efficiency. This is measured with various neutron sources and is found to be ~ 10 us, in agreement with the Monte Carlo, and with direct calculations.

d. Hardware and Triggering

The signature of an inverse beta event is (Fig. 1.) a prompt pulse in the target due to the positron plus its annihilation gamma rays, followed by a second pulse in the target and the blankets characteristic of the capture gamma rays. A Master trigger event is recorded if the prompt pulse is greater than or equal to 0.5 MeV with nothing greater than 1.0 MeV in the blankets and if the delayed pulse falls within 30 micro seconds and exceeds 4.0 MeV. The prompt pulse has a hardware block of 250 microseconds generated by a muon penetration of the anticoincidence. The delayed pulse is also blocked by a simultaneous event in the anticoincidence. A similar trigger called the Accidental trigger is generated with identical requirements, with the exception that the window for the delayed pulse is taken asynchronously, using a 30 microsecond window 2 milliseconds before the prompt pulse.

Pulse height and timing information are recorded for the target, two blanket regions and the anticoincidence, using waveform digitizers, ADC's, and TDC's. This information is used to make further cuts off line.

With these requirements we obtain the following trigger rates:

i. Reactor On - Power 2300 MW - 18.2 Meters

Prompt rate	40 $sec.^{-1}$
Delayed rate	25 $sec.^{-1}$
Master trigger rate	2.7 $min.^{-1}$
Accidental trigger rate	1.5 $min.^{-1}$

ii. Reactor Off

Prompt rate	29 $sec.^{-1}$
Delayed rate	5 $sec.^{-1}$
Master trigger rate	.6 $min.^{-1}$
Accidental trigger rate	.2 $min.^{-1}$

e. Software Cuts

Further cuts are applied to the data to increase the signal to background ratio.

i. We eliminate any delayed pulse greater than 10.0 MeV.

ii. We eliminate any event which has greater than 2 pulses in the target region within plus or minus 30 microseconds of the master trigger.

iii. We only accept delayed events within 15 microseconds of the prompt pulse.

iv. If either of the blanket regions have more than 1.0 MeV at the time of the prompt pulse we reject the event.

v. We accept only those events where the prompt target pulse is greater than 1.8 MeV.

vi. We use the pulse shape discrimination properties of the target scintillator and accept only electron like pulse shapes.

As a result of the above cuts, we achieve a signal to background ratio of about sixteen to one in the 18.2 meter position (Fig. 2) and about a factor of two worse than that at the 23.7 meter position.

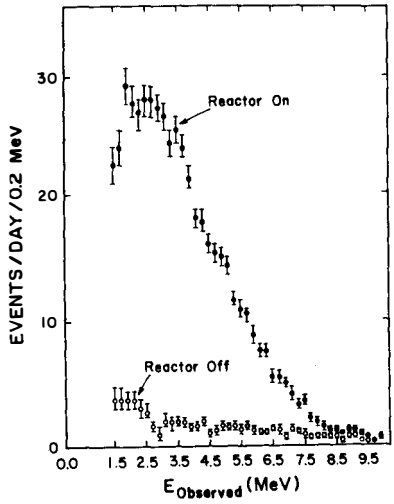


Fig. 2 A sample of the 18.2 meter data set, illustrating a signal to background of about 16 to 1.

6. Data

The results of 104 days of reactor "on" live time and 41 days of reactor "off" live time is given in figure 3

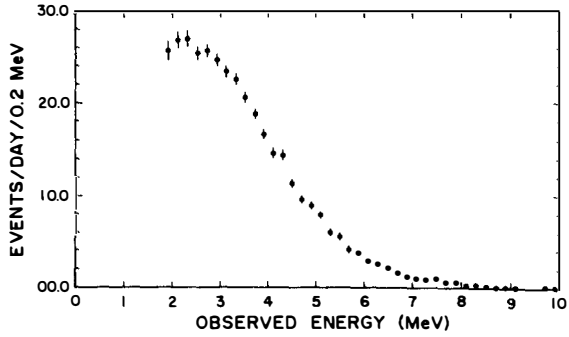


Fig. 3 The positron spectrum from 18.2 meters.

for the 18.2 meter position. The data represents an equivalent of about 38,000 neutrino interactions in the target. The abscissa is the observed energy deposited as the prompt pulse, and represents the sum of the positron kinetic energy and the fraction of the resultant annihilation gamma ray energy which is contained in the target region. A monte carlo calculation gives 0.75 MeV for this additional energy. This energy boost is helpful in that it allows us to be sensitive to a lower positron energy for a given discriminator setting.

Preliminary data from position 2 (23.7 meters) is given in figure 4. This is about one half of the expected total in this location and consists of 87 days with the reactor on and 50 days off. This represents about 19,000 events.

The unnormalized data sets are shown together in figure 5 for comparison of relative shape.

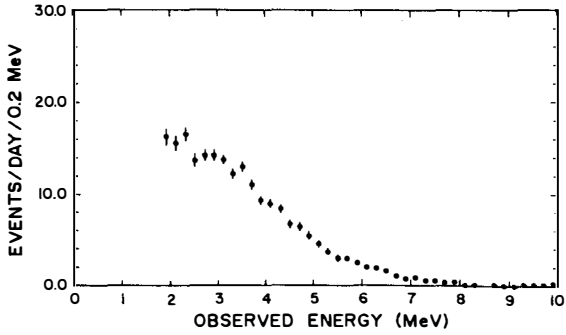


Fig. 4 Preliminary positron spectrum from 23.7 meters.

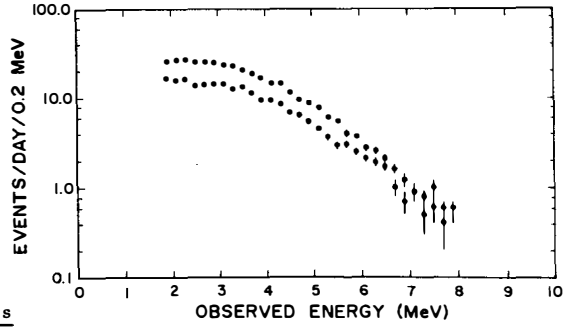


Fig. 5 A comparison of position 1 and position 2 data.

7. Preliminary Results

i. Integrated rates:

In order to compare the rates in the two locations we must correct

for reactor power differences and distance. A ratio of unity is expected in the absence of oscillations. We observe a ratio of position 1 /position 2 = 1.038 ± 0.0137. The error is statistical only.

ii. Differential comparison:

Figure 6 shows the ratio of the data for the two positions as a function of observed energy. The data has been normalized for power and distance. Superimposed on this data is the predicted ratio for this experiment using the values of $\sin^2 2\theta$ and δm^2 favored by the results of the Bugey experiment.[1)]

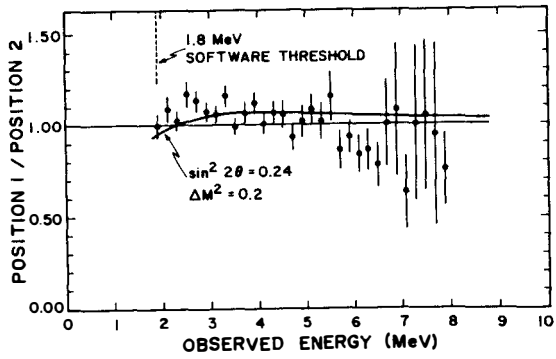


Fig. 6 The ratio of position 1 to position 2 as a function of observed energy. Also shown is the predicted ratio for the parameters favored by the Bugey experiment.

8. Systematic Errors

The conclusions of our experiment can also be presented as an exclusion region in the parameter space of $\sin^2 2\theta$ and δm^2. In order to use our data to set these limits, we must first assess our systematic errors. In this analysis, we are comparing data taken in one position to that taken in another. In this case, many of the systematic errors, such as the uncertainty in determining detector efficiencies, do not play a role in the final result.

The systematic errors effecting the ratio of position 1 to position 2 are as follows:

i. The error due to uncertainties in reproducing the same pulse shape discrimination level is estimated to be less than .5%.

ii. The error introduced by uncertainties in the absolute distance of each position from the reactor core center is estimated to be less than .4%.

iii. The flux distribution in the reactor core may not be symmetric. This would introduce an equivalent shift in the core

center. The uncertainty introduced by this effect is less than .5%.

iv. The isotopic composition of the core during the exposure of each of the two data sets is different. In our case the overwhelming contribution to the neutrino flux comes from Uranium 235. The resultant uncertainty in the neutrino flux is less than .5%.

v. The absolute reactor power is claimed to be known to ± 1% by the reactor personnel. For this analysis, the absolute error is not relevant, only the relative power from one period to the next enters. We record the power as given by the reactor facility with each event. The error introduced into the ratio is much less than .5%.

vi. We monitor the calibration weekly with the introduction of radioactive sources. The error due to this uncertainty in comparing two data sets is less than .5%.

Currently we have an uncertainty of about 10% in our absolute calibration. The results of the following analysis were done for extremes of the calibration and the most conservative limits were taken. The calibration uncertainties will be studied this summer after completing the position 2 measurement and another position 1 normalization.

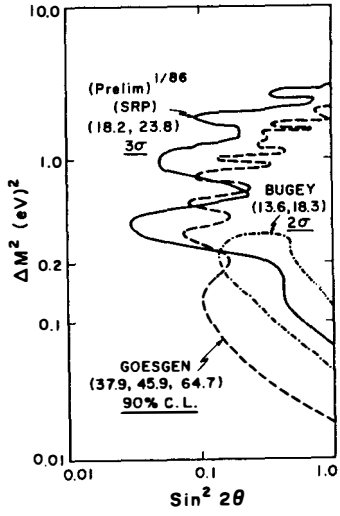


Fig. 7 Preliminary exclusion region arrived at from the data presented here. Also shown is the Goesgen exclusion region and the Bugey allowed region.

Based on the above description, we use a conservative ± 2% systematic error in the following analysis. The results are shown in figure 7. The region to the right of the UCI curve is excluded at the 99.7% confidence level (3 σ). With the larger event sample now being collected, we can expect the exclusion region to grow to include smaller values on $\sin^2 2\theta$.

Also shown in figure 7 are the regions of parameter space allowed

by the Bugey experiment,[1] and the region excluded by the Goesgen experiment.[2] Note that this latter group expresses their result as a 90% confidence limit.

7. The Future

We will finish data taking at position 2 in April 1986, and then return to position 1 to complete this two position comparison. The next sequence will involve the original 18.2 meter position and a third location currently expected to be at about 52 meters. The predicted ratio of the 23.7 meter position to the 52 meter position for a region of interest of $\sin^2 2\theta = 0.25$ and $\delta m^2 = 0.1$ is shown in figure 8. The large differences shown in this comparison will allow a definitive test.

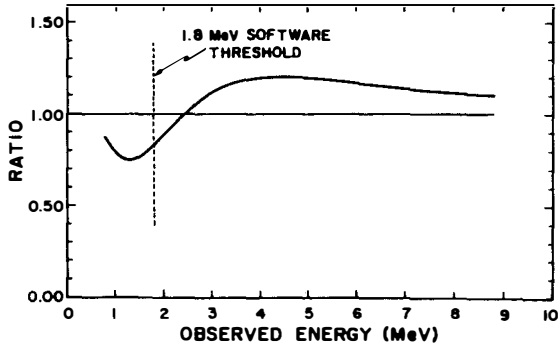


Fig. 8 The predicted ratio of the 23.7 meter position to the 52 meter position.

This work is supported in part by the U.S. Department of Energy.

References:

1. Cavaignac, J.F., et al, Physics Letters, 148B, 387, Nov. (1984).
2. Kwon, H., et al, Phys. Rev. D, 24, 1097, Sept. (1981) Vuilleumier, J.L., et al, Physics Letters, 114B, 298, Nov. (1984). Gabathuler, et al, Physics Letters, 138B, 449, April (1984).

STUDYING REACTOR ANTINEUTRINO OSCILLATIONS WITH LARGE UNDERGROUND DETECTORS ?

P.O. Lagage
Service d'Astrophysique
Centre d'Etudes Nucléaires de Saclay
91191 Gif-sur-Yvette Cédex - FRANCE



ABSTRACT

The various nuclear reactors on the planet induce a sizeable antineutrino background in most underground laboratories. In this paper, I discuss the possibility of studying neutrino oscillations on relatively large distances by detecting these antineutrinos in large underground detectors, like those currently proposed.

1. Introduction

On one hand, small (0.3 ton) liquid scintillator detectors are located near (10-65 m) powerful nuclear reactors to study neutrino oscillations ([1]), references therein and these proceedings).

On the other hand, large ($> 10^3$ tons) liquid scintillator, liquid argon, heavy water detectors are proposed in underground laboratories with various objectives both in astrophysics and in particle physics. (For more details on these detectors see, for example, the proceedings of the UP85 conference, St Vincent (Italy), to appear in Nuovo Cimento).

These detectors are, at least in principle, also able to detect reactor antineutrinos and have the advantage of a large volume of detection [a]. Then the question which arises immediately is the following: is it possible to study reactor $\bar{\nu}_e$ oscillations on large distances with such detectors? Since these detectors have to be settled underground in order to be shielded against cosmic rays, we have first to wonder whether there exists a sizeable flux of $\bar{\nu}_e$ in underground laboratories; and then, if these $\bar{\nu}_e$ are indeed detectable by the underground detectors considered. These questions are addressed in the next sections by considering successively different sources of $\bar{\nu}_e$. In section 2, the nuclear power stations in operation are considered. Section 3 is devoted to the nuclear power stations under construction and contains some general considerations about various backgrounds in large underground detectors. Section 4 deals with the smaller reactors which equip the fleet with nuclear propulsion. A brief discussion follows in Section 5.

2. Nuclear power stations in operation

When we examine the geographic distribution of the nuclear power stations in operation, we can see that there exists no nuclear power station close to an underground laboratory. But, there are a lot of them far away (345 in 1984). The mean fluxes of $\bar{\nu}_e$ induced in 1984 by these reactors in various underground laboratories are indicated in table I, as well as the mean distance traversed by these $\bar{\nu}_e$. According to the location of the laboratory, the $\bar{\nu}_e$ flux varies from $2\ 10^4\ \bar{\nu}_e\ cm^{-2}s^{-1}$ to $2\ 10^6\ \bar{\nu}_e\ cm^{-2}s^{-1}$.

a) The existing large detectors have an energy threshold too high to be able to detect reactor $\bar{\nu}_e$.

Table 1: Mean antineutrino fluxes induced in various underground laboratories by the nuclear power stations in operation during 1984; the coefficient of availability of each reactor has been taken into account. The mean distance covered by these $\bar{\nu}_e$ from their source to the laboratory is also indicated. The symbols ●(o), ■(□), ▲(△) indicate the main purpose of the experiments placed in the laboratories: respectively proton decays, supernova explosions, solar neutrinos; full symbol: in operation, open symbol: proposed or planned. The data concerning nuclear power stations have been extracted from the ELECNUC data Bank (CEA, DPg, France).

Location of laboratories	Mean $\bar{\nu}_e$ fluxes ($cm^{-2}s^{-1}$) during 1984	Mean distance covered by these $\bar{\nu}_e$
Mont-Blanc (France) ●,■	$2.1\ 10^6$	290 km
Fréjus (France) ●	$2.0\ 10^6$	300 km
Kamioka (Japan) ●,o	$1.0\ 10^6$	280 km
Fairport-Harbor (Ohio, USA) ●	$7.8\ 10^5$	470 km
Sudbury (Canada) △	$5.0\ 10^5$	600 km
Gran Sasso (Italy) o,□,△	$3.1\ 10^5$	1000 km
Artemosk (USSR) ■	$2.5\ 10^5$	990 km
Soudan (Minesota, USA) ●,o	$1.7\ 10^5$	1230 km
Baksan (USSR) ■,△	$9.4\ 10^4$	1890 km
Lead (Dakota, USA) ■,▲	$7.4\ 10^4$	2140 km
Park City (Utah, USA) ●	$5.1\ 10^4$	2620 km
Kolar Gold Field (India) ●	$2.4\ 10^4$	3360 km

The consequences of such a background for the detection of various sources of low energy $\bar{\nu}_e$ have already been discussed [2] (see also Fig. 1). Here, I just would like to remind that below a certain energy, which of course depends on the place considered, the differential energy spectrum of the reactor $\bar{\nu}_e$ covers that of the Boron solar ν_e (integrated flux $\lesssim 2\ 10^6\ \nu_e\ cm^{-2}s^{-1}$ [3]); so that, in that part of the spectrum, the detectors have to be able to discriminate between ν_e and $\bar{\nu}_e$. I emphasize this point because the interest in a determination of the Boron ν_e energy spectrum has been considerably accentuated by the results on possible matter oscillations inside the sun of the emitted neutrinos ([4] and these proceedings).

If we are now interested in the use of far away reactor $\bar{\nu}_e$ to study neutrino oscillations, we note, first, that large length of oscillation could be tested (from 300 to 3000 km, see table I); second, the number of $\bar{\nu}_e$ interactions expected during one year in a 1 kiloton liquid scintillator detector varies from 10 to 10^3 according to the location envisaged (see Fig. 1). These numbers are more than 2 orders of magnitude lower than the numbers obtained for the existing

small oscillation detectors located near one powerful reactor [b]. Then, in order to study neutrino oscillations, the requirements on the backgrounds in large underground detectors are extremely stringent. Furthermore, the $\bar{\nu}_e$ considered originate from numerous sources not operating at the same time, so that it would be difficult to measure the background and to disentangle neutrino oscillations, if any.

3. Nuclear power stations under construction

If we consider now the nuclear power stations under construction, the fluxes expected increase by about a factor 2 in all the laboratories except at Fairport Harbor. There, the flux increases by a large factor ($\approx$ 40) because two nuclear power stations of 3600 MWth each are under construction at about 10 kilometers from the laboratory. A first one will be put in operation this year. The construction of the second one has been stopped but will certainly start again once the first one will be in operation. Then, the underground laboratory at Fairport Harbor will be soon the laboratory with the highest reactor $\bar{\nu}_e$ background ($\approx 4\ 10^7\ \bar{\nu}_e\ cm^{-2}s^{-1}$). The number of counts expected in a 1 kiloton liquid scintillator detector would be only $\approx$ 5 times lower than that in the Göesgen detector at position 3 (65 m) and the length of oscillation tested could be more than 2 orders of magnitude larger.

The $\bar{\nu}_e$ background induced by all the nuclear power stations other than those at $\approx$ 10 kilometers from Fairport Harbor makes up $\approx$ 5% of the total flux. When more than $\approx 10^3$ events are detected, this background dominates over the statistical fluctuations and has to be taken into account.

The detectability of these $\bar{\nu}_e$ depends, of course, on the background. There are two main sources of background: the cosmic rays and the radioactivity outside and inside the detector. The second one increases rapidly when the energy decreases below 10 MeV. The underground detectors are larger ($> 3\ 10^3$ times) than "surface detectors" and thus are more sensitive to backgrounds. But, the flux of cosmic rays in underground laboratories is suppressed by a large factor ($\approx 10^4$ at Fairport Harbor). The local radioactivity is also weak in these laboratories; furthermore, it is possible to shield the detector against it. As for the internal radioactivity, it increases with the volume, so that

b) The far away reactor $\bar{\nu}_e$ at Göesgen and Bugey (respectively $7\ 10^6\ \bar{\nu}_e\ cm^{-2}s^{-1}$ and $10^6\ \bar{\nu}_e\ cm^{-2}s^{-1}$), more than 10^5 times less numerous than the nearby reactor $\bar{\nu}_e$, do not interfere at all with the existing experiments on reactor $\bar{\nu}_e$ oscillations.

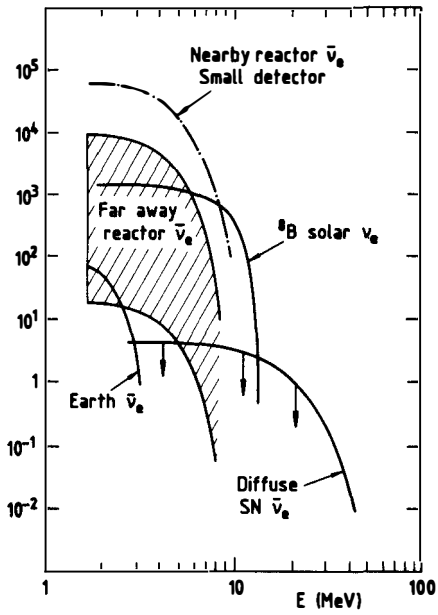


Fig. 1: Number of $\bar{\nu}_e$ (or ν_e) with energy greater than E, interacting per year in a 1 kton scintillator detector, as a function of E. The number of $\bar{\nu}_e$ interactions from reactors (assumed 100% efficient) lie inside the shaded region, according to the location considered; bottom line: Kolar Gold Field, upper line: Fairport Harbor; for comparison, the number of interactions in a 0.3 ton detector at 65 m from a reactor has been indicated (dashed dotted curve). The ^{8}B solar ν_e plotted have a standard spectrum and a total flux of 2 10^6 ν_e cm^{-2} s^{-1}. The upper limit for the diffuse supernova $\bar{\nu}_e$ is from [5]. The earth $\bar{\nu}_e$ are from [6].

high purity materials are required in large detectors. Apart from the above general considerations, the best way to deal with background problems, is to make measurements with prototypes.

4. Moving sources

I turn now to what I call "moving sources", that is the reactors of the fleet with nuclear propulsion. There are as many such sources as nuclear power stations but these sources are less powerful (between 45 MWth to more than 300 MWth), so that the total power available is only ≈ 1/20 of that induced by nuclear power stations. Furthermore, these sources do not operate often at full power. Then, it can be guessed that the $\bar{\nu}_e$ background induced in underground laboratories by these sources is less important than the one due to nuclear power stations.

It is amusing to notice that a 1 kiloton detector located at 700 meters from a small reactor of 100 MWth would count the same number of $\bar{\nu}_e$ events as a 0.3 ton detector located at 65 meters from a nuclear power station . Furthermore,

the background could be reduce by moving the small reactor between two positions. Such an experiment would permit to test oscillation of neutrinos with Δm^2 down to $\approx 10^{-3}$ eV^2 (one order of magnitude lower than currently done with reactor $\bar{\nu}_e$). The Fairport Harbor laboratory, just beside the lake Erie, could be a good site for such a purpose.

5. Discussion

Oscillations of neutrinos with Δm^2 greater than $\approx 10^{-1}$ eV^2 and $\sin^2(2\theta)$ greater than 10^{-2} are well studied with the help of accelerator neutrinos. To test Δm^2 down to 10^{-2} eV^2 with $\sin^2(2\theta) \gtrsim 10^{-1}$, reactor $\bar{\nu}_e$ are used. Solar ν_e, thanks to recent calculations on matter oscillations [4], can be used to test a large region of small Δm^2 (10^{-9}-10^{-5} eV^2), with $\sin^2(2\theta)$ as low as $\approx 10^{-3}$. The atmospheric cosmic ray neutrinos are used to fill the gap between results from reactor $\bar{\nu}_e$ and expected results from solar ν_e ([7] and references therein); but possible matter oscillations inside the earth make the interpretation of the results much more difficult than previously thought ([8] and references therein).

If necessary, the range of the parameter Δm^2 accessible with reactor $\bar{\nu}_e$ could be significantly enhanced with large underground experiments. When we consider the present underground laboratories, the best site, from this point of view, is Fairport Harbor where the reactor $\bar{\nu}_e$ background will be soon dominated by the $\bar{\nu}_e$ emitted by one nuclear power station located at 10 kilometers from the laboratory but no experiments are proposed there. In the other sites, the reactor $\bar{\nu}_e$ are less numerous (by at least a factor 10) and originate from a multitude of nuclear power stations.

References

1) Boehm F., Vogel P.: Ann. Rev. Nucl. Part. Sci. 34, 125 (1984).
2) Lagage P.O.: Nature, 316, 42 (1985).
3) Bahcall J.N., Cleveland B.T., Davis R., Rowley J.K.: Astrophys. J., 292, L79 (1985).
4) Mikheyev S.P., Smirnov A.Yu.: 10th International Workshop, Savonlinna, Finland, June 16-25, 1985.
5) Woosley S.E., Wilson J.R., Mayle R.: Astrophys. J. (in press).
6) Krauss L.M., Glashow S.L., Schramm O.N.: Nature, 310, 191 (1984).
7) LoSecco J.M. et al.: Phys. Rev. Letters, 54, 2299 (1985).
8) Cudell J.R., Gaisser T.K.: Proceedings of 19th Int. Cosmic Ray Conf., Vol.5, p. 124 (1985).

NEUTRINO OSCILLATIONS IN MATTER WITH VARYING DENSITY

S.P.Mikheyev and A.Yu.Smirnov
Institute for Nuclear Research, Academy of Sciences of the USSR
60-th October Anniversary prospect 7a, Moscow 117312, USSR

ABSTRACT

The properties of ν oscillations in matter with varying density are investigated. The following effects have been considered: i) resonant amplification of ν-oscillations, ii) effects on the border between two layers, iii) the propagation of oscillating neutrinos in adiabatic regime, iv) the oscillationless transformation of ν -beam. The consequencies of these effects for ν -propagation in collapsing stars, in the Earth and in the early Universe are represented.

Introduction. (1)

The interaction of neutrino with matter modifies ν-oscillations[1-5]. In some essential aspects matter effect is similar to refraction index appearence and to coherent regeneration of K-mesons.

In matter with a constant density the general view of ν-oscillations remains the same as in vacuum. Values of mixing angle and oscillation length are changed only.

Some applications of matter effect to neutrino astrophysics[1-6,7] and geophysics[1-6,8] have been considered in approximation of constant density. In matter with varying density qualitatively new effects appear. It was remarked[9] that the dependence of mixing angle $\mathrm{Sin}^2 2\theta_m$ on density of matter or energy of neutrino has a resonance character. At definite ρ and E the parameter $\mathrm{Sin}^2 2\theta_m$ reaches the maximal value $\mathrm{Sin}^2 2\theta_m = 1$ for arbitrarely small value of mixing in vacuum. This results in strong oscillation effect in ν -beam even at very small $\mathrm{Sin}^2 2\theta$. Strong unreversable changing in ν -beam occures when neutrinos cross the resonant layer in matter at adiabatic conditions. The applications of these effects for ν -propagation in the Sun have been considered[9].

In this paper we continue to discuss ν -oscillation in matter with varying density. We start with properties of neutrino eigenstates and mixing angle in matter (sect.2). Then the resonant condition and resonant amplification of oscillations in matter (sect.3) will be considered. In section 4 we give a simple geometrical representetion of ν -oscillation which will be very usefull for futher discussions. We describe the dinamics of ν -oscillation in matter with varying density (sect.5-9). Two cases are considered: (i) sudden leap of density (sect.6) and (ii) smooth density changing (sect.7). As the limit case the oscillationless transformation in ν -beam is investigated (sect.8). In section 9 we consider the coherence condition. Sections 10-12 are devoted to the applications of the considered effects to the ν -propagation in collapsing stars (sect. 10), in the Earth (sect.11) and in early Universe (sect.12).

Eigenstates and mixig angle in matter. (2)

Consider two neutrino mixing (for definiteness ν_e and ν_μ):

$$\begin{aligned} \nu_e &= c\,\nu_1 + s\,\nu_2 \\ \nu_\mu &= c\,\nu_2 - s\,\nu_1 \end{aligned} \qquad (1)$$

here ν_1 and ν_2 are the states with definite masses m_1 and m_2, $c=\mathrm{Cos}\theta$, $s=\mathrm{Sin}\theta$, θ is a mixing angle in vacuum. Any neutrino state $\nu(t)$ can be represented as follows:

$$\nu(t) = A_e(t)\,\nu_e + A_\mu(t)\,\nu_\mu \qquad (2)$$

where A_e and A_μ are the amplitudes of probabilities to find ν_e and ν_μ.

A_e and A_μ obey the evolution equations[1)]

$$i\frac{d\bar{A}}{dt} = \hat{M}\bar{A} \qquad (3)$$

where $\bar{A} = (A_e, A_\mu)$ and

$$\hat{M} = \begin{bmatrix} M_e & \bar{M} \\ \bar{M} & M_\mu \end{bmatrix} \qquad (4)$$

Here:

$$M_e = \frac{m_1^2}{2k}c^2 + \frac{m_2^2}{2k}s^2 + \sum_i f_e^i(0)\frac{n_i}{k}$$
$$M_\mu = \frac{m_2^2}{2k}c^2 + \frac{m_1^2}{2k}s^2 + \sum_i f_\mu^i(0)\frac{n_i}{k} \qquad (5)$$
$$\bar{M} = -sc\,\frac{\Delta m^2}{2k}$$

$\Delta m^2 = m_1^2 - m_2^2$, k is momentum of neutrino. In eqs.(5) last two terms describe the changing of wave functions due to neutrino interaction with matter. $f_\alpha^i(0)$ (α =e, μ) is the amplitude of forward ν -scattering on i component of matter (i = e,n,p) n_i is the concentration of i component.

Introduce new states $\vec{\nu}^m = (\nu_1^m, \nu_2^m)$ which diagonalize matrix $\hat{M}$ (4):

$$\vec{\nu}_\alpha = \hat{S}\vec{\nu}^m$$

where $\vec{\nu}_\alpha = (\nu_e, \nu_\mu)$ and matrix

$$\hat{S} = \begin{bmatrix} \mathrm{Cos}\theta_m & \mathrm{Sin}\theta_m \\ -\mathrm{Sin}\theta_m & \mathrm{Cos}\theta_m \end{bmatrix} \qquad (6)$$

is determined from condition

$$\hat{S}^{-1}\hat{M}\hat{S} = \hat{M}^{diag}$$

Here $\hat{M}^{diag}$ is the diagonal matrix. We will refer to $\vec{\nu}^m$, as to eigenstates of neutrino in matter. The angle θ_m which relates the eigenstates of weak interaction and the eigenstates in matter is called the mixing angle in matter.

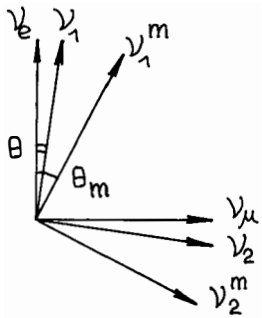


Fig.1 Geometrical relations between the eigenstates of weak interaction, mass matrix and ν -eigenstates in matter.

$$tg2\theta_m = -\frac{2\bar{M}}{M} \qquad (7)$$

where $M = M_e - M_\mu$. From (7):

$$\mathrm{Sin}2\theta_m = -\frac{2\bar{M}}{(M^2+4\bar{M}^2)^{1/2}} \qquad (8)$$

In vacuum ν_i^m coinside with eigenstates of mass matrix: ν_1, ν_2 and $\theta_m = \theta$. In matter with

$$\sum_i f_e^i(0)n_i = \sum_i f_\mu^i(0)n_i \qquad (9)$$

situation is the same, due to (9) $M^{matt} = M_e - M_\mu = M^{vac}$.

If the equality (9) is broken, $\vec{\nu}_i^m$ do not coinside with ν_1, ν_2 and $\theta_m \neq \theta$ (fig.1).

Inequality in (9) means that the transition $\nu_1 \to \nu_2$ exist or that ν_1 and ν_2 are not more the eigenstates of propagation. In matter ν_1 and ν_2 oscillate themself. In vacuum or in matter with a constant density ν_i^m diagonalize not only $\hat{M}$ but all the system (3). That is ν_i^m are the eigenstates of Hamiltonian. This is not the cause for varying density.

In matter with varying density ($n_i=n_i(x)$ or $n_i=n_i(t)$) the mixing angle changes with t; $\theta_m=\theta_m(t)$ and ν_i^m can be introduced only locally (for given point x or given moment t).

Consider the dependence of θ_m on ν-parameters and properties of matter. Using eq.(5) one has:

$$2\bar{M} = -\frac{2\pi}{L_v}\mathrm{Sin}2\theta$$
$$M = \frac{2\pi}{L_v}(\mathrm{Cos}2\theta - L_v/L_o) \qquad (10)$$

where $L_v = 4\pi E/\Delta m^2$ - oscillation length in vacuum, L_o - is the eigenlength in matter.

$$L_o^{-1} = \sqrt{2}\, G_F \rho_{eff}^{\alpha}/m_N \qquad (11)$$

where $\rho_{eff}^{(\alpha)}$ is the effective density $\rho \sim \sum_i f^i(0) n_i$, which depends on type of ν-mixing and properties of matter (see Appendix A). Later on we will omit the index α and eff for simplicity.

Substituting (10) in (8) we obtain :

$$\mathrm{Sin}2\theta_m = \frac{\mathrm{Sin}2\theta}{((\mathrm{Cos}2\theta - L_v/L_o)^2 + \mathrm{Sin}^2 2\theta)^{1/2}} \qquad (12)$$

Note that $L_v/L_o \propto E$. The main feature of relation (12) is that the dependence of $\mathrm{Sin}^2 2\theta_m$ on L_v/L_o or E at small θ has the resonant form[9].

Resonance condition. Resonant amplification of ν-oscillation. (3)

At

$$\mathrm{Cos}2\theta = L_v/L_o \qquad (13)$$

the value $\mathrm{Sin}^2 2\theta_m$ reaches the maximum $\mathrm{Sin}^2 2\theta_m = 1$. We refer to the condition (13) for which $\mathrm{Sin}^2 2\theta_m = 1$ as to the resonance one. Substituting (11) in (13) one has:

$$\rho_{res} = m_N \Delta m^2 / 4\sqrt{2}\pi G_F E \qquad (14)$$

The value of density (energy) which satisfies relation (14) is called the resonant density (energy).

For small mixing in vacuum $\mathrm{Sin}^2 2\theta_m$ is of order of unit in narrow region around $(L_v/L_o)_{res}$ or ρ_{res}. Beyond this region $\mathrm{Sin}^2 2\theta_m$ becames small ($\mathrm{Sin}^2 2\theta_m \ll 1$). The interval of densities $\Delta\rho_{res}$ in which $\mathrm{Sin}^2 2\theta_m > 1/2$ is called the width of resonant layer[9]. From (12) one obtains:

$$\Delta\rho_{res} = \rho_{res}\, \mathrm{tg}2\theta \qquad (15)$$

Similarly the resonant energy E_{res} and the width of resonance in energy (ΔE_{res})

can be introduced.

Consider now the θ_m-dependence on ρ. In terms of ρ_{res} it can be represented as follows:

$$\sin 2\theta_m = \frac{\operatorname{tg} 2\theta}{((1 - \rho/\rho_{res})^2 + \operatorname{tg}^2 2\theta)^{1/2}} \qquad (16)$$

(see fig.2). From (16) one has

$$\theta_m = \begin{cases} \pi/2 & \rho \gg \rho_{res} \\ \pi/4 & \rho = \rho_{res} \\ \theta & \rho \ll \rho_{res} \end{cases} \qquad (17)$$

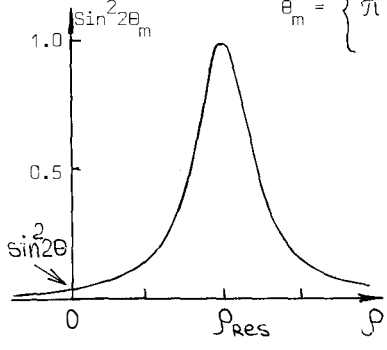


Fig.2 The dependence of $\sin^2 2\theta_m$ on effective density of matter.

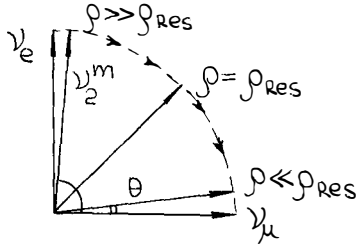


Fig.3 The changing of mixing angle in matter with varying density.

When the density decreases from large values $\rho \gg \rho_{res}$ to zero the mixing angle in matter changes from $\pi/2$ to $\theta_m = \theta$. The eigenstates in matter rotate with respect to the eigenstates of weak interaction on the angle $\pi/2$. This means that if at $\rho \gg \rho_{res}$ some eigenstate ν_i^m coinsides with ν_e then at $\rho \ll \rho_{res}$ it will approach to ν_μ.

What is the physical sence of the resonance dependence of $\sin^2 2\theta_m$? In some cases $\sin^2 2\theta_m$ is equal to the depth of oscillations*). If in these cases the resonance condition is fulfiled the oscillations have the maximal amplitude in spite of arbitrarely small mixing in vacuum. Consider the matter with constant density. Let neutrinos with continuous energy spectrum are generated. Then at definite $E = E_{res}(\rho)$ oscillations with maximal amplitude develope. The energy dependence of the depth of oscillation is determind by resonant curve (12) $\sin^2 2\theta_m (E/E_{res})$. If neutrino beam propagates

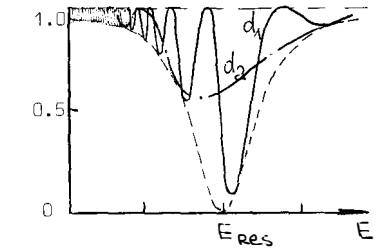


Fig.4 Resonant amplification of ν-oscillations. Effect in matter with constant density and finite size d.

*) We would like to stress that in general this is not the case. The depth of oscillations does not equal to $\sin^2 2\theta_m$ (see sect. 6,7).

through the matter with finite size d, then on the exit the spectra will have oscillating form, modulated by resonant curve (fig.4).

Geometrical representation of oscillations. (4)

Mathematicly oscillations are equivalent to the following geometrical picture. Consider orthogonal basis with axes $\vec{\nu}_1$, $\mathrm{Re}\vec{\nu}_2$ and $\mathrm{Im}\vec{\nu}_2$. Any neutrino state is described by unit vector $\vec{\nu}(t)$ in this basis, so that the projection of $\vec{\nu}$ on $\vec{\nu}_i$ is equal to the amplitude of probability to find $\vec{\nu}_i$ in the state $\vec{\nu}(t)$. Vectors (Cosθ, Sinθ, Sinθ) and (-Sinθ, Cosθ, Cosθ) correspond to $\vec{\nu}_e$ and $\vec{\nu}_\mu$. For amplitude A_e one has: $A_e = (\vec{\nu}_e, \vec{\nu}(t)) = (\mathrm{Re}\vec{\nu}_e, \vec{\nu}(t)) + i(\mathrm{Im}\vec{\nu}_e, \vec{\nu}(t))$. Oscillations are equivalent to the rotation of vector $\vec{\nu}(t)$ arround axis ν_1. The frequency of rotation coinsides with oscillation time $t = L/c$. If the initial state is $\vec{\nu}(0) = \nu_e$, then vector $\vec{\nu}(t)$ will rotate arround ν_1 with angle θ and initial position $\vec{\nu}(0) = \mathrm{Re}\vec{\nu}_e = (\mathrm{Cos}\theta, \mathrm{Sin}\theta, 0)$ (fig.5).

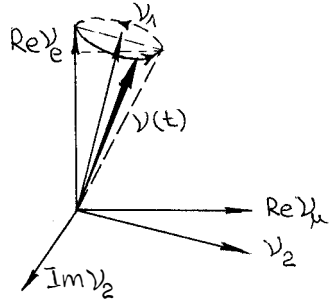


Fig.5 Geometrical representation of oscillations.

The maximal and minimal projections of $\vec{\nu}(t)$ on $\mathrm{Re}\nu_e$ determine the depth of oscillation: $\mathrm{Sin}^2 2\theta_{osc} = |(\vec{\nu}(t)\mathrm{Re}\vec{\nu}_e)|^2_{max} - |(\nu(t)\mathrm{Re}\vec{\nu}_e)|^2_{min}$.

In matter one should introduce (ν_1^m, ν_2^m) instead of (ν_1, ν_2) and substitute θ by θ_m. Vector $\vec{\nu}(t)$ will rotate around ν_1^m now.

Oscillations in matter with varying density. (5)

From system (3) the equation follows for probability $P(t) = |A_e|^2$ of transition $\nu_e \to \nu_e$:

$$\dddot{P} - \dot{M}\ddot{P} + M(M^2 + 4\bar{M}^2)\dot{P} - 2\bar{M}^2\dot{M}(2P-1) = 0 \qquad (18)$$

If electron neutrinos are generated then the initial conditions are

$$P(0) = 1, \quad \dot{P}(0) = 0, \quad \ddot{P}(0) = -2\bar{M}^2 \qquad (19)$$

Futher on we will analize the solution of (18) for two important cases:

i) Sudden leap of density (two layers with different densities).

ii) Smooth varying of density (adiabatic regime).

Note that for constant density ($\dot{M} = 0$) it follows from (18):

$$\dddot{P} + (M^2 + 4\bar{M}^2)\dot{P} = 0 \qquad (20)$$

This eq. gives the Wolfenstein's solution[1]:

$$P = 1 - \frac{1}{2}\mathrm{Sin}^2 2\theta_m \, \mathrm{Sin}^2 \pi x/L_m$$

with

$$L_m = 2\pi(M^2 + 4\bar{M}^2)^{-1/2} = L_V((\mathrm{Cos}2\theta - L_V/L_0)^2 + \mathrm{Sin}^2 2\theta)^{-1/2} \qquad (21)$$

Sudden leap of density. (6)

Let ν-flux propagates through the medium consisting of two layer with different constant densities ρ_1 and ρ_2 (one of these densities can be equal to zero). If neutrino flux (for definitness ν_e) is generated in the first layer then in this layer oscillations will have the usual form.

The depth of oscillation "$\sin^2 2\theta_{osc}$" and the averraged value of probability $\bar{P}$ are determined by mixing angle in matter θ_m: "$\sin^2 2\theta_{osc}$" = $\sin^2 2\theta_m$, $\bar{P}(\nu_e \to \nu_e) = 1 - \frac{1}{2}\sin^2 2\theta_m$. In second layer situation is essentially different. This difference is due to initial conditions. For layer 1: $\nu(0) = \nu_e$ that is $\nu(0)$ coincides with pure eigenstate of weak interaction. For layer 2 the initial conditions are ones on the broad between the layers. In general one has:

$$\nu(x_0) = c_0 \nu_e + s_0 \nu_\mu e^{i\varphi_0} \qquad (22)$$

where $c_0 = \cos\theta_0$, $s_0 = \sin\theta_0$ and φ_0 are determined by oscillations in layer 1.

Considering the evolution of ν-state (22) in layer 2 we obtain for $\varphi_0 = 0$ (the general cause with $\varphi_0 \neq 0$ is discussed in Appendix B):

$$P(\nu_e \to \nu_e) = \bar{P} + \sin^2 2\theta_{osc}(\sin^2 \pi x/L_m - 1/2) \qquad (23)$$

where

$$\bar{P} = \cos^2\theta_0 - \frac{1}{2}\sin 2\theta_m \sin 2(\theta_m - \theta_0) \qquad (24)$$

and

$$\sin^2 2\theta_{osc} = \sin 2\theta_m \sin 2(\theta_m - \theta_0) \qquad (25)$$

It follows from (24) and (25) that both the depth "$\sin^2 2\theta_{osc}$" and the averraged value of P are determined not only by θ_m but by θ_0 (initial conditions) also. In matter with varying density the possibility appears to prepare the complex state which will oscillate with $\sin^2 2\theta_{osc} \neq \sin^2 2\theta_m$.

Consider some special cases. At $\theta_0 = \theta_m$ or $\theta_0 = \pi/2 + \theta_m$ there is no oscillations at all: $\sin^2 2\theta_{osc} = 0$, $\bar{P} = \cos^2\theta_0$. This corresponds to the coincidence of initial ν-state with one of eigenstates in matter.

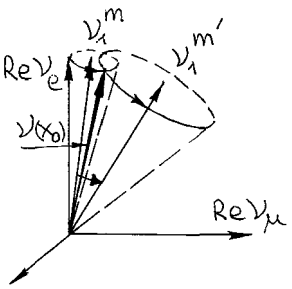


Fig.6 The geometrical representation of ν-oscillations in matter with two densities.

For $\theta_0 = 0$ or $\pi/2$ initial ν-state is the eigenstate of weak interaction and eq.(23-25) reduce to the usual ones.

The maximal value of oscillations depth for given θ_m ($\sin^2 2\theta_{osc} = \sin 2\theta_m$) is reached at $\theta_0 = \theta_m - \pi/2$. The minimal value of $\bar{P}$ ($\bar{P}_{min} = \sin^2\theta_m$ corresponds to $\theta_0 = \pi/2 - \theta_m$. The maximal value $\bar{P}_{max} = \cos^2\theta_m$ one obtains at $\theta_0 = +\theta_m$.

In geometrical picture the transition from one layer to another one corresponds to instantaneous changing of position of ν^m-eigenstate $\nu_1^m \to \nu_1^{m'}$, $\vec{\nu}$-vector will rotate around new position of vector $\vec{\nu}_1^{m'}$. Moreover the rotation

angle is equal to the angle between $\nu_1^{m'}$ and $\nu(t)$ in the moment of crossing the border between two layers (fig.6).

Smooth varying density. Adiabatic regime. (7)

Consider the layer of matter which satisfies following conditions:

i) The density distribution $\rho(r)$ has no pecularities, the derivative $\frac{d\rho}{dr}$ is smooth.

ii) The density changes slowly; so that for given mixing angle inequality is valid

$$\Delta r_{res} = (d\rho/dr)^{-1} \Delta\rho_{res} \gtrsim L_m/2 \qquad (26)$$

where $\Delta\rho_{res} = \rho_{res}\, tg2\theta$ and $L_m = L_0(\rho)/tg2\theta$. We will refer to (26) as to adiabatic condition.

iii) $\rho(r)$ changes monotonically from $\rho = \rho_{max}$ to $\rho = \rho_{min}$.

Let the resonant density for neutrinos with given energy lies in interval $\rho_{min} < \rho_{res}(E) < \rho_{max}$. At this conditions the solution $P(r)$ possesses the universality with respect to density distribution.

Let us introduce $n = (\rho(r) - \rho_{res})/\Delta\rho_{res}$ (27), where ρ_{res} and $\Delta\rho_{res}$ are determined by E and $Sin^2 2\theta$. We will measure the distance in n instead r (this is possible due to monotonic character of $\rho(r)$). Note that in resonance n=0; at $\rho \to \infty$: $n \to \infty$ and at $\rho \to 0$: $n \to (tg2\theta)^{-1}$. Initial conditions are fixed at n_0:

$$n_0 = (\rho(r_0) - \rho_{res})/\Delta\rho_{res} \qquad (28)$$

If $\rho(r_0) \gg \rho_{res}$, then

$$n_0 \simeq \rho(r_0)/\Delta\rho_{res} \simeq \rho(r_0)/(\rho_{res} Sin2\theta) \simeq 1/Sin2\theta_m^0 \qquad (29)$$

n_0 is equal to inverse value of Sin2θ in initial point. n_0 rises when initial point moves away (in ρ-scale) from resonant layer or $Sin^2 2\theta$ decreases.

Introduce $m = (d\rho/dr)^{-1} \Delta\rho_{res}/L_m^{res}$ (30)

m is the number of oscillations length in resonant layer. It rises when $\rho(r)$ becames more flat or $Sin^2 2\theta$ diminishes. Both n and m include the dependence on mixing angle.

When conditions i) - iii) are fulfiled the probability $P(r,E,Sin^2 2\theta)$ turns out to be the function of n, n_0, m: $P = P(n, n_0, m)$ and does not depend on actual density distribution $\rho(r)$.

The solution $P(n, n_0, m)$ have the following properties:

i) P is the oscillating function of n. In resonant layer period is equal on definition to $T_{res} = 1/m_R$. Beyond the resonance one has $T \simeq (m(n^2+1)^{1/2})^{-1}$.

ii) P oscillates around $\bar{P}(n, n_0)$:

$$\bar{P} = \frac{1}{2} + \frac{1}{2} \frac{n_0}{(n_0^2+1)^{1/2}} \frac{n}{(n^2+1)^{1/2}} \qquad (31)$$

iii) The amplitude of P oscillations: $A_p = |P_{max} - P_{min}|$ is maximal in resonant layer

$$A_p \simeq \frac{1}{\sqrt{n_0^2+1}} \qquad (32)$$

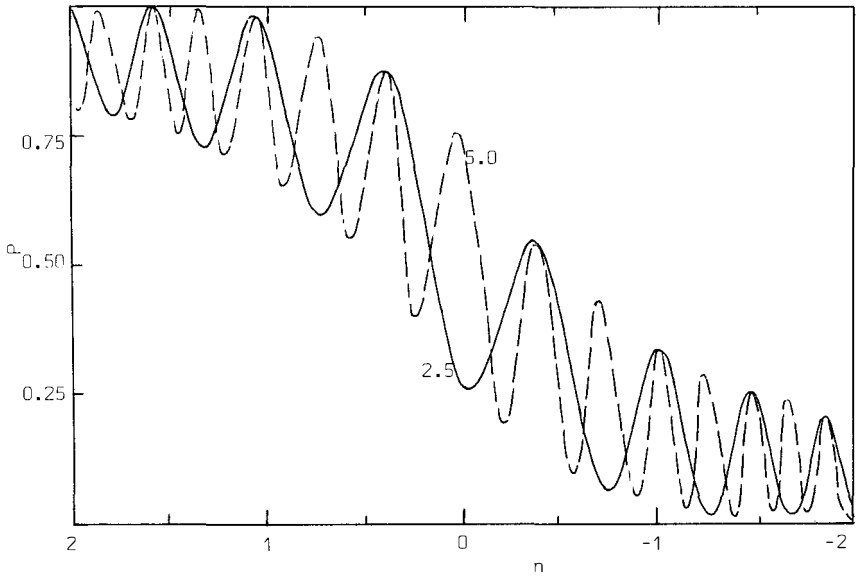


Fig.7 The dependence of oscillations probability on n for different value of m (figers on curves).

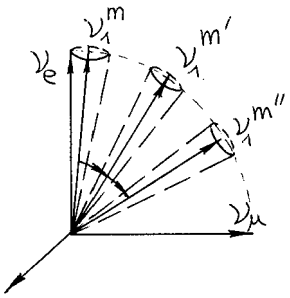


Fig.8 Geometrical represention of ν-oscillations in adiabatic regime.

and it decreases when one moves away from the resonance. Let us underline that A_p does not depend on m (fig.7).

On the exit from the layer ($\rho \to 0$):

$$\bar{P} - \frac{1}{2} - \frac{1}{2} \frac{n_o}{(n_o^2 + 1)^{1/2}} \cos 2\theta \qquad (33)$$

In geometrical representation of oscillations smooth changing of density corresponds to the continuous rotation of eigenstates with respect to ν_e, ν_μ-axes. The adiabatic condition ensure that ν-state has the time to arrange for the density changing. Vector $\vec{\nu}(t)$ will follow the eigenstate so that the "rotation" angle will be approximately the same (fig.8).

Oscillationless transformation in ν-beam. (8)

Let n_o rises. This means that the point of ν-generation moves away from resonant layer. In this cause the amplitude of oscillations decreases (see (32)): $A_p \sim 1/n_o$. The averraged function $\bar{P}(n, n_o)$ converges to the asymptotic one:

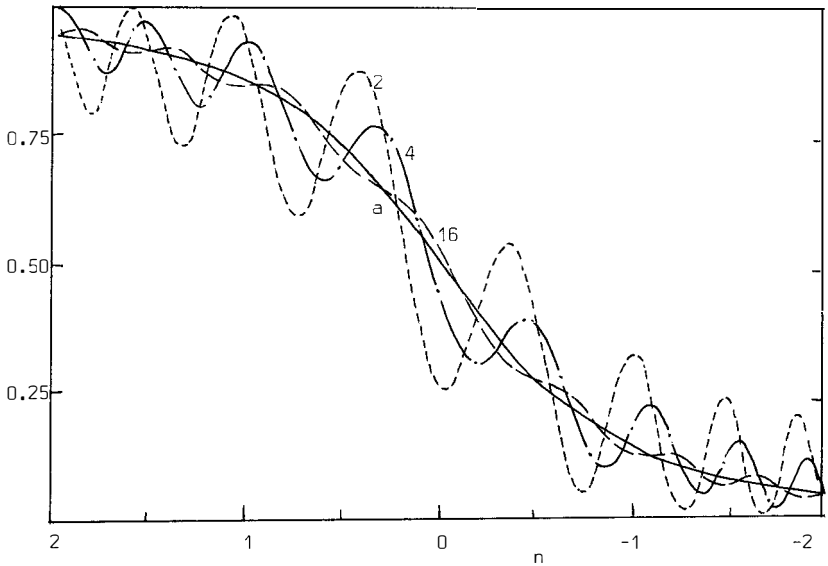


Fig.9 The n dependence of oscillations probability for different initial conditions n_o (figers on curves), a - the asymptotic curve.

$$\bar{P}_{as}(n) = \frac{1}{2} + \frac{1}{2}\,\frac{n}{(n^2+1)^{1/2}} \qquad (34)$$

At the exit ($\rho \to 0$):

$$\bar{P}_{as} \to \mathrm{Sin}^2\theta \qquad (35)$$

See fig.9.

So we conclude that for small value θ and large n_o (when ν -flux generated far from the resonant layer) the propagation of neutrinos takes the form of practically complete oscillationless transformation of one type of neutrino into another one.

The interpretation of such effect is the following one. In initial moment at $\rho_o \gg \rho_{res}$ the mixing angle in matter is very small $\mathrm{Sin}^2 2\theta_m^o = \mathrm{Sin}^2 2\theta(\rho_{res}/\rho_o)^2 \simeq 1/n_o^2 \ll 1$. This means that the initial ν-state coincides with one of the eigenstates in matter:

$$\nu_e = \nu(0) \simeq \nu_2^m(0) \qquad (36)$$

The adiabatic condition ensures that $\nu(t)$ will coincide with $\nu_2^m(t)$ in any moment:

$$\nu(t) \simeq \nu_2^m(t) \qquad (37)$$

When the density $\rho(t)$ changes from $\rho_o \gg \rho_{res}$ to $\rho_{fin} \ll \rho_{res}$, the eigenstate in matter (ν_2^m in particular) rotates on the angle $\pi/2$ (see sect.3). So if $\nu_2^m(0) \simeq \nu_e$, then $\nu_2^m(t_{fin}) \simeq \nu_\mu$. Using (36) and (37) one obtains: $\nu_e = \nu(0) \simeq \nu_2^m(0) \to \nu_2^m(t_{fin}) \simeq \nu_\mu$ (see fig.2).

Note that the conditions for such effect are not exotic. For example if $\mathrm{Sin}^2 2\theta = 10^{-3}$ the amplitude of oscillations: $A_p \lesssim 10^{-2}$ at $n_o = 30$ or $\rho_o = 2\rho_{res}$ (see (29)).

Coherence conditions. (9)

The solutions considered above are correct untill the coherence exists in ν-state. The coherence length L_{coh} is limited by i) opaqueness of medium, that is by the scattering on nonzero angle or inelastic collisions; $L_{coh} \lesssim m_N/\rho\sigma$, where m_N is the nucleon mass, σ is νN-cross section; ii) divergence of wave packets corresponding to different ν-eigenstates.

Consider the second reason in detail. The divergence is negligible if

$$L \ll (c\tau)/\Delta v_g^m \qquad (38)$$

where $c\tau$ is the length of wave packet and $v_g^m = v_1^m - v_2^m$, v_1^m, v_2^m - the group velocity of ν_1^m and ν_2^m.

$$v_i^m = \frac{dE_i}{dk} = 1 + \frac{dM_i^d}{dk}$$

Here M_i^d (i=1,2) are the elements of diagonalized matrix $\hat{M}$ (4). Using (4) and (5) one find: $dM_i^d/dk \simeq m_i^2/2k^2$ or

$$v_i^m \simeq 1 - \frac{m_i^2}{2k^2} = v_i^{vac} \qquad (39)$$

The interactions with matter does not change the group velocities of ν-packets. Group velocities are the same as in vacuum. This results from the fact that the additional terms in $\hat{M}$ describing matter effect do not depend on neutrino momentum k.

According with (38) and (39) we obtain the condition

$$L_{coh} \ll 2\tau k^2/\Delta m^2 \qquad (40)$$

Applications of effects of ν-oscillations in matter. (10)

Typical scale on which the matter effect becames essential is

$$L \gtrsim L_o = 3.5\ 10^4 \mathrm{km}/G_F\rho \qquad (41)$$

From (26) it follows that the thickness of matter (d) should be:

$$d = L\rho \gtrsim 3.5\ 10^9\ \mathrm{g/cm}^2 \qquad (42)$$

This condition is fulfiled for the Earth and the Sun, in the cores and envelopes of collapsing stars, in the Early Universe.

The matter effects take plase in charge asymmetrical medium only. The concentrations of particles and antiparticles should be different. Indeed if $n_i = n_{\bar{i}}$ then $\rho_{eff} \propto f_i(0)n_i + f_{\bar{i}}(0)n_{\bar{i}} = \Delta f_i(0)(n_i - n_{\bar{i}}) = 0$.

If the fluxes of oscillating components (for example $\nu_e - \nu_\mu$) are equal, there are no observable effects.

The considered oscillation effects take place for neutrino or antineutrino only, depending on the sign of the product $\mathrm{Cos}2\theta \cdot f(0)/\Delta m^2$.

Neutrino fluxes from collapsing stars. (11)

We use the density distribution in the envelope at the beginning of collapse which is similar to that in white dwarfs

$$\rho \simeq \rho_0 (R_B/r - 1)^3 \qquad (43)$$

$\rho_0 \simeq (8 - 10)\ 10^5 g/cm^3$, $R_B \simeq 5\ 10^8 cm$, $\rho_{max} \simeq 10^9 g/cm^3$. For massive stars in addition to (43) the extending hydrogen envelope exist with $\rho \simeq 10^{-9} g/cm^3$. The envelope may expand with velocity $v \simeq 5000 km/sec$.

For cores above the neutrinosphere we use electron and nucleon density according with model[10] (ρ_N and ρ_e have approximately exponential dependences on r; neutronization is taken into account; $\rho_{max} = 10^{12} - 10^{13} g/cm^3$).

Using such density distributions we find the region of ν-parameters for which conditions listed in sect.10 are fulfilled. Upper limits on Δm^2_{max} are determind by maximal densities. Lower limit for $Sin^2 2\theta$ follows from adiabatic condition (26). Note that Δm^2_{max} for $\nu_e - \nu_\mu$ and $\nu_e - \nu_s$ oscillations are different: $\Delta m^2_{max}(\nu_e - \nu_\mu) = (10^{-1} \div 10^{-2}) \cdot \Delta m^2_{max}(\nu_e - \nu_s)$, ($\nu_s$ - sterile neutrino). This is related with strong neutronization in core which results in $n_n > n_e$.

For $\nu_e - \nu_s$ oscillation ρ_{eff} changes the sign at $\rho \simeq 10^9 g/cm^3$ in core. The effect on neutrons is compensated by effect on electrons and protons ($\rho_{eff} = 0$). This means that if in core strong transition exists for neutrinos, then in envelopes it will take place for antineutrinos.

Consider the coherence condition (40). The typical length of wave packet for ν is very small $\tau \lesssim 1/kT \simeq 10^{-22} - 10^{-21} sec$. From (40) we obtain that $L_{coh} \ll R_B$ practically for all considered region of Δm^2 (see fig.10). Nevertheless the effect of packets divergence is small. Indeed, for the greater part of the Δm^2, $Sin^2 2\theta$ region one has $n_0 = (\rho_0 - \rho_{res})/\Delta \rho_{res} >> 1$. This means that ν-state consists predominantingly of the one eigenstate in matter. Neglecting the small admixture of another eigenstate we reject the problem of the packets spread. Moreover if the packets diverge before crossing of the resonant layer we may consider the evolution of this packets separately. The results are approximately the same as in the case without divergence: $P \to Sin^2\theta$. So we conclude that in the Δm^2 versus $Sin^2 2\theta$ region (fig.10) the suppresion factor for the flux of neutrino of initial type is $P = (1/4 \div 1/2)\ Sin^2 2\theta$ (see (33)).

Consider some consequencies of the discussed effects for detection of ν-flux from collapsing stars.

Let the conditions of sect.10 are fulfilled for channal $\bar{\nu}_e - \bar{\nu}_\alpha$ ($\alpha = \mu$ or τ). In this case $\bar{\nu}_e$ flux transform in $\bar{\nu}_\alpha$-flux and vice versa. So $\bar{\nu}_e$ and $\bar{\nu}_\alpha$ exchange their spectra. $\bar{\nu}_\mu$ and $\bar{\nu}_\tau$ are supposed to have more hard spectra then ν_e has. So the exchange $F_{\nu e} \leftrightarrow F_{\nu\mu}$ results in strong increasing of number of events in $\bar{\nu}_e$ - detectors. ν_e - flux in this case does not changed.

If the resonant conditions is fulfilled for $\nu_e - \nu_\alpha$ channel the effect, si-

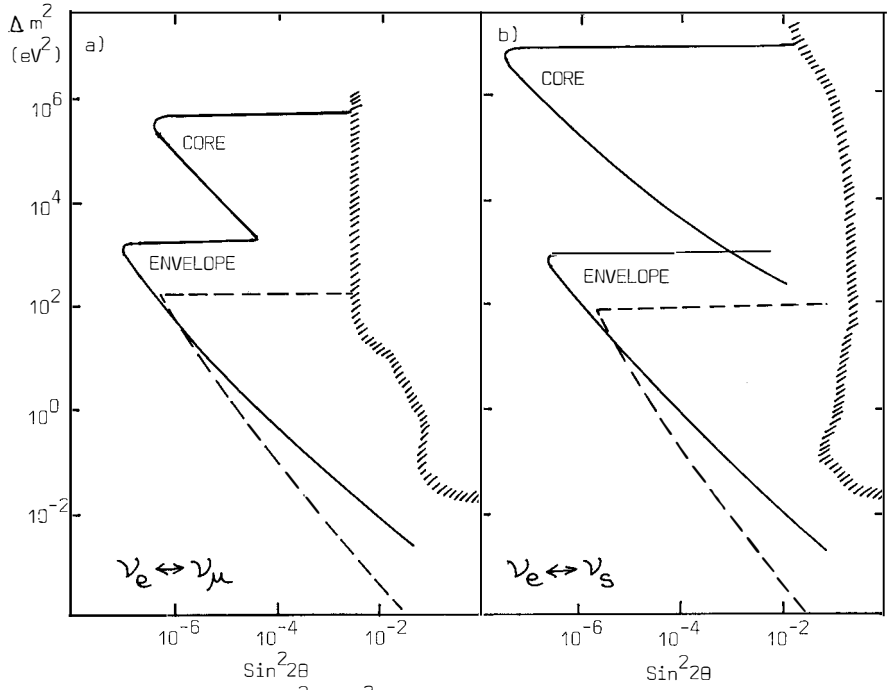


Fig.10 The region of Δm^2, $Sin^2 2\theta$ parametres for which adiabatic conditions are fulfilled in cores and envelopes of collapsing stars, a) $\nu_e - \nu_\mu$, b) $\nu_e - \nu_s$ oscillations. The shaded region is the existing experimental restriction. The dashed lines correspond to the expanded envelope at t=10 sec.

milar to that described above take place for ν_e - detectors (radiochemical). The exchange of $\nu_\alpha \to \nu_e$ or $\bar{\nu}_\alpha - \bar{\nu}_e$ spectra in core results also in a strong increasing of energy release in envelope due to $\nu_e e$ or $\bar{\nu}_e e$ - scattering. This can help to solve the problem of envelope throw off.

Consider now resonance in $\nu_e \to \nu_s$ or $\bar{\nu}_e \to \bar{\nu}_s$ channels. The fluxes of sterile neutrinos are seems to be small. The effect of spin precession in magnetic field for $H \lesssim 10^{12}$G and $\Delta m^2 \leq 10^3 eV^2$ is negligible. So $\nu_e \to \nu_s$ or $\bar{\nu}_e \to \bar{\nu}_s$ transformations results in a strong (up to several orders of magnitude) suppression of ν_e or $\bar{\nu}_e$ fluxes.

Note, because in core and envelopes ρ_{eff} has the opposite signs the strong effect may exist both for ν_e and $\bar{\nu}_e$ with different enegies.

We would like to stress that it is very important to search for ν-fluxes from collapsing stars by ν_e and $\bar{\nu}_e$ - detectors simultaneously. In the cause of three or more neutrinos mixing it is possible that two or more Δm^2 turn out to be in the region of strong adiabatic suppression. Some combinations of the considered

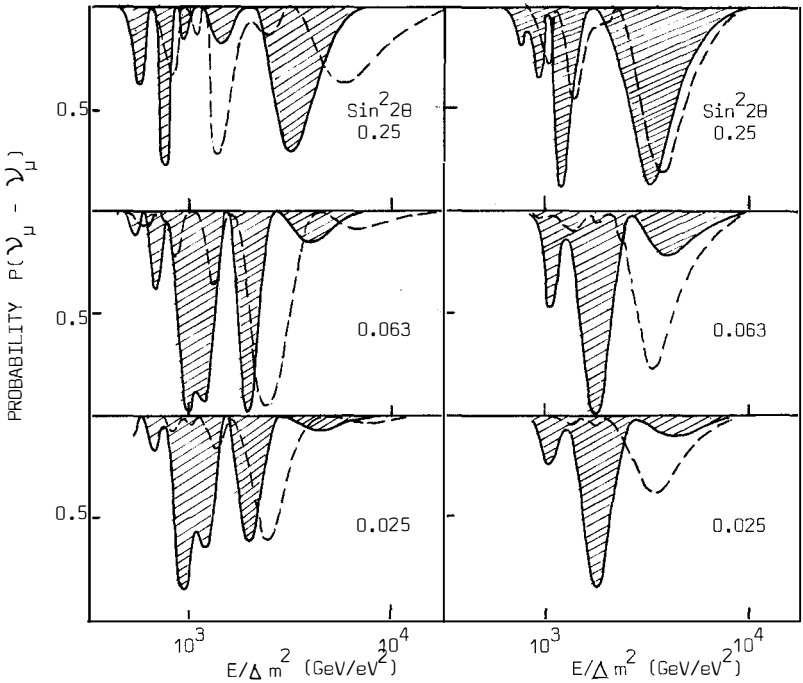


Fig.11 The suppresion factor for ν_μ - ν_e (full curves) and ν_μ - ν_s (dashed curves) oscillations, zenith angle $\cos\Psi=1$.

Fig.12 The same as fig.11, zenith angle $\cos\Psi=0.8$.

effects may be then observed.

Note that the matter effects can be changed during the collapse (Δt = 5-10s). This dependence on time will reflect the changing in structure of cores and envelopes.

The effects in the Earth. (12)

The thickness of matter of the Earth along its diameter is equal to $3\cdot10^9$ g/cm^2. So, for the Earth the condition (42) is fulfilled. It have been pointed out that strong oscillation effect due to resonant amplification can take place[11]. We have found that for sufficiantly large mixing angle $\theta \simeq \theta_C$ the resonance developes completely $L_m/2 \simeq d$, where d is the thickness of regions inside the Earth with slow changing of density. The suppression factors P for ν_μ - ν_e and ν_μ - ν_s oscillations are shown on fig. 11,12.

The matter of the Earth amplifies the ν-oscillations in the regions of energies and Δm^2:

$$E/\Delta m^2 = \begin{cases} (5\cdot10^2 - 5\cdot10^3)\ \text{GeV/eV}^2 & \nu_\mu \to \nu_e \\ (10^3 - 10^4)\ \text{GeV/eV}^2 & \nu_\mu \to \nu_s \end{cases} \qquad (44)$$

and the mixing angles $\sin^2 2\theta \gtrsim 0.02$.

For smaller values of θ the oscillations length L_m becames much larger then diameter of the Earth and strong oscillations effect does not develope.

When zenith angle rises the thickness of the Earth decreases and matter effect disappears (fig.11,12). The dependence of suppression factor P on E and Ψ reflects the density distribution inside the Earth.

Consider now possible consequencies of neutrino propagation through the Earth.

i) Atmospheric neutrinos. One expects the irregular suppression of ν-flux in the region of energies within one order of magnitude $E_{max}/E_{min} \lesssim 10$. The position of this energy interval depends on value of Δm^2. According with (44) the measurements of ν-flux in the region $E = (0.3 - 3\cdot10^4)$ GeV give the information on $\Delta m^2 \simeq (10^{-4} - 10)$ eV^2 and $\sin^2 2\theta \gtrsim .02$ (fig.13,14).

It should be noted that if the charge sign of muons are not determined, the suppresion effect is diminished by the presence of $\nu_\mu, \bar{\nu}_\mu, \nu_e, \bar{\nu}_e$-components in ν-flux: $F_\mu^{osc}/F_\mu \simeq (P F_{\nu_\mu} + F_{\bar{\nu}_\mu} + (1 - P) F_{\nu_e})/(F_{\nu_\mu} + F_{\bar{\nu}_\mu}) \gtrsim 0.3 - 0.4$.

The possibility have been discussed[11] to study density distribution in the Earth by means of resonance effect in accelerator experiments.

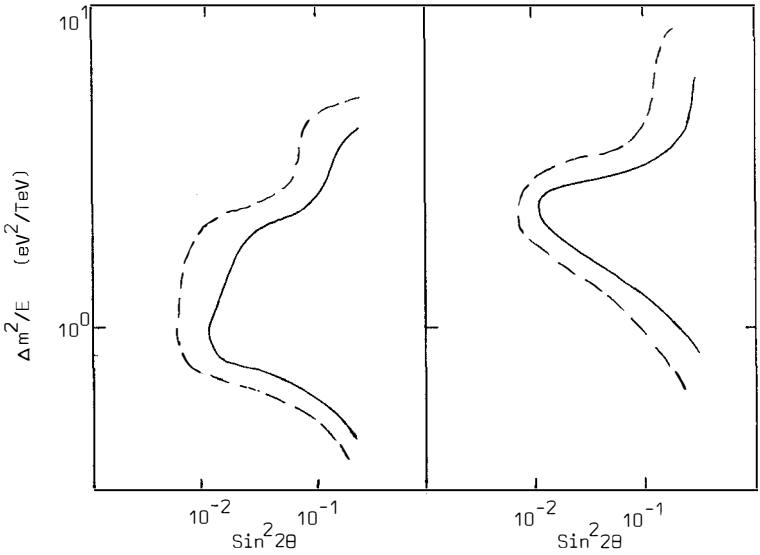


Fig.13 The region of ν_μ - ν_e - oscillations parameters in which the probability $P(\nu_\mu - \nu_\mu)$ is smaller than 0.7 (dashed curves) and 0.5 (full curves.

Fig.14 The same as fig.13 for ν_μ - ν_s - oscillations.

ii) ν-flux from collapsing stars. According with (44) the influence of matter of the Earth takes place for $\Delta m^2 = (10^{-6} - 6\cdot10^{-5})$ eV^2 and $\sin^2 2\theta \gtrsim 2\ 10^{-2}$ (E_ν = 10 - 30MeV). The effects are similar to that considered in sect.11. The value of effects depend on the position of instalation on the Earth and the measured fluxes F_ν will be different for different detectors. This enables to reconstruct the direction on collapsing star.

iii) The Sun (E_ν = (0.2 - 14MeV)). From (44) one finds $\Delta m^2 = (2\cdot10^{-8} - 2\cdot10^{-5})$ eV^2. This values of Δm^2 are in the region of strong effect inside the Sun[9]. So regeneration of initial ν_e-flux will take place. The rotation of the Earth results in day-night modulation of the ν-flux. In experiments with large time of exposition the averraging gives $\simeq$ 10% effect only. The modulation effect can be seen more explicitely in electronic experiments, where time recording of each event is possible.

Early Universe. (13)

Expanding Universe is also the example of matter with varying density in which neutrino fluxes propagate.

Consider changing in ν-fluxes after decoupling of neutrinos from matter ($T \gtrsim$ 0.25 - 0.3sec). Because of ν_e, ν_μ, ν_τ-fluxes are approximately equal the observable effect may appear for $\nu_\alpha - \nu_s$ - oscillations only ($\alpha = e, \mu, \tau$). The density of sterile state is supposed to be small.

For definiteness consider the system of ν_e, $\bar{\nu}_e$, ν_s, $\bar{\nu}_s$-neutrinos. The ν-oscillations in matter results in difference of concentrations of ν_e and $\bar{\nu}_e$: $n(\nu_e) - n(\bar{\nu}_e) = \Psi_A(t) \neq 0$. In the cause of vacuum oscillations[12] such effect exists due to CP - violation in ν - mixing. We don't need CP - violation and the $\nu\bar{\nu}$ - asymmetry appears as matter effect only.

In initial moment the charge asymmetry of matter is related with barion and lepton excesses. It is small ($n_B/n_\gamma \simeq 10^{-9}$) concentratiors of p, n, e trigger the matter effect. As $\nu\bar{\nu}$ asymmetry rises the increasing contribution to effective density give neutrinos themselves ($\nu\nu$ and $\bar{\nu}\nu$ - scattering):

$$\rho_{eff} = \rho_{B,L} + \rho_\nu (P_\nu - P_{\bar{\nu}}) \qquad (45)$$

Here $\rho_{B,L}$ - effective density for p, n, e; $\rho_\nu \propto m_N \cdot n_\nu$ and n_ν is the full concentration of neutrinos. Because of $\rho_\nu / \rho_{B,L} \simeq 10^9$ even very small difference ($P_\nu - P_{\bar{\nu}}$) results in dominance of neutrinos in ρ_{eff}. The expression (45) means that one should now to consider the systems of equations (3) for P_ν and $P_{\bar{\nu}}$ - simultaneously. Moreover these equations became nonlinear in P_ν, $P_{\bar{\nu}}$. The red shift effect must be taken into account also.

The effective density for $\bar{\nu}$ is equal

$$\rho^{\bar{\nu}}_{eff} = -\rho^{\nu}_{eff} = -\rho_{B,L} + \rho_\nu (P_{\bar{\nu}} - P_\nu) \qquad (46)$$

and thus in limit $\rho_{B,L}=0$ the system of equations is symmetrical for $\bar{\nu}$ and ν. It is $\rho_{B,L}$ triggeres the matter effect and determines the sign of $\nu\bar{\nu}$-asymmetry for given moment t.

The asymmetry Ψ_A depends on $\sin^2 2\theta$, $\rho_{B,L}/\rho_{res}$, ρ_{res}/ρ_ν, $\rho_{res}=\rho_{res}(E/\Delta m^2)$ is the resonant density for neutrinos with given energy. At $\rho_{res}(t)/\rho_\nu \ll 1$ the fast changing of density in comparison with L_ν/c suppresses the depth of oscillations. This depth rises when ρ_{res}/ρ_ν approaches to the 1. For moments $0.3\text{sec} < t < 2\text{sec}$ the ratio ρ_{res}/ρ_ν is of order of 1 for $\Delta m^2 \sim 10^{-1} - 10^2\ \text{eV}^2$.

We found that $\Psi_A(t)$ is the oscillating function so that both positive and negative $\nu\bar{\nu}$-asymmetry appears.

The consequencies of these asymmetries for primordial nucleosynthesis, for constrains on the number of neutrino species and others will be represented elsewhere.

Acknowledgements.

We are gratefull to V.S.Berezinsky, A.E.Chudakov, A.Yu.Ignatev, D.K.Nadjozhin, V.A.Rubakov, M.E.Shaposhnikov, G.T.Zatsepin for helpful discussions.

Appendix A.

The eigenlength of matter for oscillations $\nu_\alpha - \nu_\beta$ ($L_0^{\alpha\beta}$) can be written in the following way:

$$L_0^{\alpha\beta\,-1} = \sum_i \frac{\Delta f_i(0)}{k} n_i = \frac{\sqrt{2}\, G_F \rho_{eff}^{\alpha\beta}}{m_N} \qquad (A.1)$$

where

$$\rho_{eff}^{\alpha\beta} = \rho \sum_i x_i q_i^{\alpha\beta} \qquad (A.2)$$

Here x_i - is abundance of i-component of matter, q_i - the difference of amplitudes in units $-\sqrt{2}\, G_F k$. The values of $q_i^{\alpha\beta}$ for different oscillation channels ($\alpha\beta$) and different components i are represented in Table I.

Table I

oscillation species	$f_i(0)/k$ in units $(-\sqrt{2}\, G_F)$*)		
	e	p	n
$\nu_e \leftrightarrow \nu_\mu$ $\nu_e \leftrightarrow \nu_\tau$	1	0	0
$\nu_e \leftrightarrow \nu_s$	$1/2 + 2S_W^2$	$1/2 - 2S_W^2$	$-1/2$
$\nu_\mu \leftrightarrow \nu_s$ $\nu_\tau \leftrightarrow \nu_s$	$-1/2 + 2S_W^2$	$1/2 - 2S_W^2$	$-1/2$
$\nu_\mu \leftrightarrow \nu_\tau$	0	0	0

$S_W^2 = \sin^2\theta_W$, θ_W - Weinberg's angle.

*) The sign of amplitudes corresponds to P.Langacker's analises.

The value ρ_{eff} is called the effective density of matter for oscillation channel $\nu_\alpha - \nu_\beta$.

Consider the most important causes. For $\nu_e - \nu_\mu$ oscillations the matter effect is due to scattering on electrons only, so

$$\rho^{e\mu}_{eff} = \rho X_e \qquad (A.3)$$

For $\nu_e <-> \nu_s$ -oscillations in electrically neutral medium ($X_e = X_p$) one has:

$$\rho^{es}_{eff} = \rho (X_p - \frac{1}{2} X_n) \qquad (A.4)$$

Note that in matter with neutrons dominance over protons ($X_n > 2X_p$) the density ρ^{es}_{eff} becames negative (neutron stars).

For $\nu_\mu - \nu_s$ and $\nu_\tau - \nu_s$ oscillations in electrically neutral medium:

$$\rho^{\mu s}_{eff} = -\frac{1}{2} \rho X_n \qquad (A.5)$$

Appendix B. Oscillations of neutrino state with general form of initial condition.

Consider the oscillation of $\nu(t)$ state in matter with mixing angle θ_m and oscillation length L_m. Let the initial condition has a general form:

$$\nu(0) = \cos\theta_o \nu_e + \sin\theta_o \nu_\mu e^{i\varphi_o}$$

The probability to find ν_e in the moment t is equal to

$$P(t) = |\langle \nu_e | \nu(t) \rangle|^2 = \bar{P} + \sin^2 2\theta_{osc} \left[\sin^2(\pi t/2L_m + \Psi) - \frac{1}{2}\right)$$

where

$$\bar{P} = |A|^2 + |B|^2 + 2\rho_{AB}$$
$$\sin^2 2\theta_{osc} = 4\rho_{AB} = 4\,\mathrm{Mod}(AB^*) \qquad (B.1)$$
$$\Psi = \arg(AB^*)$$

and

$$A = c\,(c_o c - s_o s\, e^{i\varphi_o})$$
$$B = s\,(c_o s - s_o c\, e^{i\varphi_o}) \qquad (B.2)$$

From (B.1) and (B.2) one has

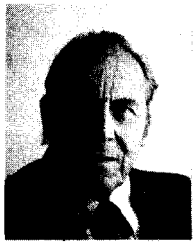
$$\sin^2 2\theta_{osc} = \sin 2\theta\,((\sin 2\theta_m \cos 2\theta_o + \sin 2\theta_o \cos 2\theta_m C_\varphi)^2 + \sin^2 2\theta_o S^2_\varphi)^{1/2} \qquad (B.3)$$

References.

1) L.Wolfenstein Phys. Rev. D17, 2369, 1978
2) L.Wolfenstein Proc. of "Neutrino'78", Purdue Univ., p.C3 1978
3) L.Wolfenstein Phys. Rev. D20, 2634, 1979
4) V.Barger et al Phys. Rev. D22, 2718, 1980
5) V.Barger et al Phys. Rev. D24, 538, 1981
6) S.Pakvasa "DUMAND-80", vol.2, p.45, 1981
7) H.J.Haubold Astrophys. Space Sci. 82, 457, 1982
8) P.V.Ramana Murthy Proc. 18th ICRC, vol.7, p.125 (Bangalore, India, 1983)
9) S.P.Mikheyev, A.Yu.Smirnov Yadernaja Fizika (Sov. Journ. Nuclear Physics) 42, 1441, 1985
10) V.S.Imshennik, D.K.Nadyozhin Preprint ITEP-98, 1980
11) V.K.Ermilova, V.A.Tsarev, V.A.Chechin Preprint-45, Lebedev Physical Institute 1986
12) M.Yu.Khlopov, S.T.Petcov Phys. Lett. 99, 117, 1981

TREATMENT OF $\nu_{\odot}$-OSCILLATIONS IN SOLAR MATTER THE MSW EFFECT

Albert Messiah
Institut de Recherche Fondamentale,
CEN-Saclay, 91191 Gif-sur-Yvette Cedex, France



ABSTRACT

Mikheyev and Smirnov, following Wolfenstein's theory of neutrino oscillations in the presence of matter, have found that the change of flavour of solar neutrinos may be spectacularly enhanced in the presence of solar matter, when the parameters of the neutrino mass operator fall in a suitable range *(MSW effect)*. It is shown that this effect can be readily deduced from the adiabatic solution of the equation of flavour evolution. A complete study of the two-flavour case is given, permitting to calculate, for any set of values of the mass operator parameters, the ν_e suppression factor at the site of detection on earth. The adiabatic approximation holds over a wide range of the parameters, leading to especially simple expressions. Our calculations cover the whole range, including domains where the adiabatic approximation is no longer valid. Some of the results, presented in a form most suited for an analysis of solar neutrino experiments, are displayed for illustration and discussed.

Introduction

Mikheyev and Smirnov[1], using Wolfenstein's formalism[2] of neutrino flavour oscillations in the presence of matter, have found that the change of flavour of solar neutrinos may be spectacularly enhanced by the presence of solar matter, when the parameters of the neutrino mass operator fall in a suitable range. They call it the "resonant amplification effect", a somewhat misleading denomination. It will be referred to thereafter as the Mikheyev-Smirnov-Wolfenstein (MSW) effect.

The main purpose of this work is to show that the MSW effect is readily deduced from the *adiabatic solution* of the equation of flavour evolution in solar matter, and that it occurs only *to the extent* that the adiabatic approximation is valid.

Our final aim is to calculate the probability that a neutrino, produced in flavour ν_e within the sun, is detected as ν_e on earth. We have treated this problem completely *assuming two flavours*, and report below the main features and results of this treatment. Taking into account more flavours complicates matters. One should emphasize however, that many of the features which show up in the two-flavour case, notably all those connected with the adiabatic approximation, can be readily extended to the more general case.

1. The problem of flavour evolution in solar matter

1.1. General

Following Wolfenstein[2], $|\psi(x)\rangle$, the state vector in flavour space, taken as a function of x along the line of travel of the ν, obeys the Schrödinger equation ($\hbar$=c=1):

$$i \frac{d}{dx} |\psi(x)\rangle = M(x) \; |\psi(x)\rangle \tag{1.1}$$

$$M(x) = M_v + M'(x) \tag{1.2}$$

M_v, mass operator in vacuum

$$M'(x) = \sqrt{2}\, G\, n_e(x) \; |e\rangle\langle e| + Cst \tag{1.3}$$

G, Fermi coupling Cst. $|e\rangle$, state vector of flavour ν_e.

$n_e(x)$, number density of electrons: it steadily decreases to 0, as one goes from x=0, where the ν is produced in the solar core, to x=1, where it reaches the solar surface ($R_\odot$=1).

Eq.(1.1) has to be solved with the initial condition

$$|\psi(0)\rangle = |e\rangle \tag{1.4}$$

Thus one gets $|\psi(1)\rangle$, from which $|\psi_f\rangle$, the flavour state at the detection on earth, is readily deduced.

The probability to detect flavour ν_e is $|\langle e|\psi_f\rangle|^2$. The quantity to be considered in practice, denoted below as

$$\left\langle P_{\nu_e \mapsto \nu_e} \right\rangle \qquad \text{(or } \langle P\rangle \text{ in short)},$$

is the average of the latter over all possible lines of travel, i.e. over the sites of ν-production in the sun and over the variations of travelling distance due to the eccentricity of the terrestrial orbit. The net result of this averaging process -in the relevant range of parameters considered here- is to wash out the oscillatory terms in $|\langle e|\psi_f\rangle|^2$.

Instead of considering $|\psi(x)\rangle$, we may, as well, consider the evolution operator, $U(x,x')$, which follows the same Schrödinger Eq.(1.1).

$$|\psi(1)\rangle = U(1,0)\ |e\rangle \tag{1.5}$$

1.2 Two flavours

Using Pauli σ-matrices, the Hamiltonian in Eq.(1.1) reads

$$M(x) = \vec{\sigma}.\vec{W}(x) \tag{1.6}$$

$$\vec{W}(x) = A\ \vec{\nu} + B(x)\ \vec{e} \tag{1.7}$$

$$\vec{\nu}.\vec{e} = \cos 2\theta_\nu \qquad A = \frac{1}{4}\frac{\delta m^2}{q} = .88\times 10^9\ \frac{\delta m^2_{(eV^2)}}{q_{(MeV)}} \tag{1.8}$$

$$B(x) = \tfrac{1}{2}\sqrt{2}\ G\ n_e(x) = 1.3\times 10^4\ \frac{n_e(x)}{n_e(0)} \tag{1.9}$$

θ_ν, mixing angle. $\delta m^2 = m_1^2 - m_2^2$ $(m_1 > m_2)$. q, neutrino energy. $n_e(0)$, density at the center of the sun (taken from Ref.3)

1.3 Relevant range of parameters

From the numbers above, one easily deduces the range of values of $q/\delta m^2$ to be considered in this problem:

$$q/\delta m^2 \qquad \text{from } 10^4 \text{ to } 10^9$$

If $q/\delta m^2 < 10^4$, $B_{max} \ll A$: the matter term acts as a small perturbation.

If $q/\delta m^2 > 10^9$, the vacuum oscillation length exceeds $R_\odot$: $B(x) \gg A$ during most of the travelling within the sun, keeping flavour ν_e up to the solar surface, from where the usual theory of ν-oscillations applies.

2. Outline of the solution

The Schrödinger equation amounts to a system of two (or n, if the number of flavours is n) coupled differential equations, with a Hamiltonian, M(x), which *does not stay constant in "time"*, due to the presence of the matter term:

$$M'(x) = B(x)\,\vec{\sigma}.\vec{e} \qquad B(x) \propto n_e(x)$$

It, at any rate, can be solved numerically.

The solution takes a very simple form, though, if the eigenvectors of M(x) *rotate slowly enough (adiabatic approximation*[4]): the system "follows adiabatically" the eigenvectors of M(x).

To be precise, let

$$\varpi(x) = \frac{|\text{rotation velocity of eigenvector}|}{|\text{level spacing}|} \tag{2.8}$$

If, in a given range $[x_1, x_2]$, $\varpi(x)$ stays small, i.e. $\varpi < \varpi_{max} \ll 1$, the components of $|\psi(x)\rangle$ along the rotating eigenvectors deviate no more than

$$\approx \varpi_{max}$$

from the strict adiabatic result, according to which each one merely picks up a well-defined phase factor.

Hence the method to be followed:

. Solve the eigenvalue problem of M(x) and calculate $\varpi(x)$

. If $\varpi(x) \ll 1$ over the whole range [0,1], the adiabatic solution gives $\left\langle P_{\nu_e \mapsto \nu_e} \right\rangle$ to within $\approx \varpi_{max}^2$

. If not, one needs a better solution, namely apply the adiabatic approximation in all ranges of x where $\varpi(x) < \epsilon$, say, and resort to numerical integration in the remainder. One thus obtains $\left\langle P_{\nu_e \mapsto \nu_e} \right\rangle$ to within $\approx \epsilon$ at worst.

3. Set up of the two-flavour formalism

Our first task is to solve the eigenvalue problem of M(x), as given by Eq.(1.6-7), and to build the unitary operator $\hat{U}(x'',x')$ which rotates the eigenvectors into one another as "time" x develops.

We shall make full use of the σ-formalism and of the geometrical picture in 3D-Eulidean space deduced from the (two-valued) representation in flavour space of the rotation group. To each unit vector $\vec{u}$ corresponds a unit ket vector $|u\rangle$,

$$\vec{u} \longrightarrow |u\rangle \qquad\qquad (\vec{\sigma}.\vec{u})|u\rangle = |u\rangle,$$

and, to the transform of $\vec{u}$ by a rotation, the transform of $|u\rangle$ by the unitary operator representative of this rotation.

Thus, we picture the eigenvalue problem through the motion of the vector $\vec{W}$, as shown on Figs.1a or 1b:

$$\vec{W}(x) \equiv W(x)\,\vec{w}(x) = A\,\vec{v} + B(x)\vec{e} \qquad \vec{w},\ \text{unit vector}$$

$|w_{\pm}\rangle_x$, eigenvectors of $M(x) \equiv \vec{\sigma}.\vec{W}(x)$ eigenvalues: $\pm W(x)$

$$M(x)|w_{\pm}\rangle_x = \pm W(x)|w_{\pm}\rangle_x$$

$|v_{\pm}\rangle$, eigenvectors of $M_v \equiv A\,\vec{\sigma}.\vec{v}$ eigenvalues: $\pm A$

$$M_v|v_{\pm}\rangle = \pm A|v_{\pm}\rangle$$

$|e\rangle$, $|v_{\pm}\rangle$, $|w_{\pm}\rangle_x$ are pictured by unit vectors $\vec{e}$, $\pm\vec{v}$, $\pm\vec{w}(x)$ respectively. They stay in the same plane and transform into each other by rotations around the axis

$$\vec{k} \equiv \vec{v} \times \vec{e}\ /\sin 2\theta_v, \quad \text{unit vector perpendicular to the plane}$$

$$2\theta_v \equiv \text{angle}\left(\vec{v},\vec{e}\right) \qquad\qquad 2\theta(x) \equiv \text{angle}\left(\vec{w},\vec{e}\right)$$

The corresponding operator in flavour space reads

$$\exp\left[-\tfrac{1}{2}\, i\alpha\, \vec{\sigma}.\vec{k}\right] \qquad \alpha,\ \text{angle of rotation}$$

We thus obtain the transformation properties

$$|e\rangle = |v_+\rangle \cos\theta_v + |v_-\rangle \sin\theta_v = |w_+\rangle_x \cos\theta + |w_-\rangle_x \sin\theta \qquad (3.1)$$

$$|\mu\rangle = |v_+\rangle(-\sin\theta_v) + |v_-\rangle \cos\theta_v = |w_+\rangle_x(-\sin\theta) + |w_-\rangle_x \cos\theta \qquad (3.2)$$

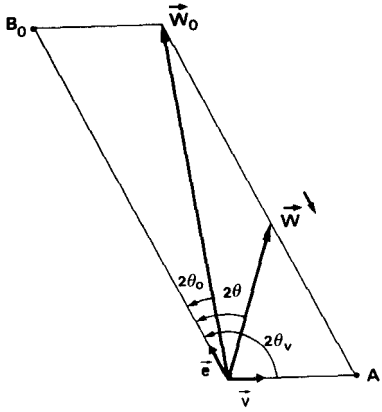


Fig.1b : $\theta_v > \pi/4$
$|e\rangle$ closer to lower mass

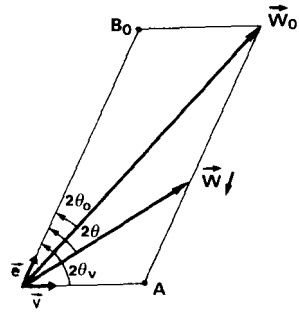


Fig.1a : $\theta_v < \pi/4$
$|e\rangle$ closer to higher mass

and the explicit form of the "rotating axis" operator

$$\hat{U}(x";x') = \exp\left[i(\theta" - \theta')\vec{\sigma}.\vec{k}\right] \tag{3.3}$$

$$\hat{U}(x",x')|w_{\pm}\rangle_{x'} = |w_{\pm}\rangle_{x"} \qquad \hat{U}(x",x')\vec{\sigma}.\vec{w}' = \vec{\sigma}.\vec{w}"\ \hat{U}(x",x') \tag{3.4}$$

When x goes from 0 to 1 - cf. Fig.1a or 1b - B(x) goes from B_0 to 0, and $\vec{W}$ from $\vec{W}_0$ to its value in vacuum A $\vec{v}$. The eigenvalue W varies accordingly, and the "mixing angle in solar matter" $\theta(x)$ goes from its initial value θ_0 to θ_v, mixing angle in vacuum.

$$W(x) = A\sqrt{\kappa^2+2\kappa\cos 2\theta_v+1} \qquad \kappa(x) \equiv B(x)/A$$
$$\cos 2\theta(x) = (\kappa+\cos 2\theta_v)\Big/\sqrt{\kappa^2+2\kappa\cos 2\theta_v+1} \tag{3.5}$$

The Schrödinger Eq. for U(x,x') will be solved by considering the evolution in the "rotating picture".

$$U(x,x') \equiv \hat{U}(x,x')\ \bar{U}(x,x') \tag{3.6}$$

hence

$$i\frac{d\bar{U}}{dx}(x,x') = \left[W(x)\ \vec{\sigma}.\vec{w}(x') + \frac{d\theta}{dx}\ \vec{\sigma}.\vec{k}\right]\bar{U}(x,x') \tag{3.7}$$

If

$$\varpi(x) = \frac{d\theta/dx}{2W(x)} \equiv \frac{\text{ang. velocity of axis}}{\text{level spacing}} \tag{3.8}$$

stays small enough over the range of x, the second term in the l.h.s. of Eq.(3.7) can be neglected, and the equation is readily integrated. This is the *essence of the adiabatic approximation*

$$\bar{U}(x,x') \simeq \bar{U}_{ad}(x,x') = \exp\left[-\tfrac{1}{2}\, i\, (\Phi(x) - \Phi(x'))\ \vec{\sigma}.\vec{w}'\right] \tag{3.9}$$

$$\Phi(x) \equiv 2\int^{x} W(x_1)dx_1 \tag{3.10}$$

It will be discussed in the following sections.

To conclude, note that the Hamiltonian in the Schrödinger equations considered here *anticommute* with the "time reversal" operator[5], namely the *antiunitary* operator K, which reverses the "spin" in flavour space: $K\ \vec{\sigma}\ K^{\dagger} = -\vec{\sigma}$. Hence

$$K\ U(x,x') = U(x,x')\ K$$

from which useful complex conjugaison relations can be obtained for matrix elements of U. In particular, since

$$|v_-\rangle = K\ |v_+\rangle, \quad |w_-\rangle_0 = K\ |w_+\rangle_0, \qquad (K^2 = -1)$$

one gets

$$\begin{aligned} \alpha &\equiv \langle v_+|U(1,0)|w_+\rangle_0 = \langle v_-|U(1,0)|w_-\rangle_0^{*} \\ \beta &\equiv \langle v_-|U(1,0)|w_+\rangle_0 = -\langle v_+|U(1,0)|w_-\rangle_0^{*} \end{aligned} \tag{3.11}$$

with $\quad |\alpha|^2 + |\beta|^2 = 1 \quad$ (Unitarity of U)

For $\langle P \rangle$, the probability of detecting ν_e on earth (with oscillatory terms averaged out), one obtains, from Eq.(3.1) and (3.11), the simple expression

$$\left\langle P_{\nu_e \mapsto \nu_e} \right\rangle = \tfrac{1}{2} \left[1 + \gamma \cos 2\theta_v \cos 2\theta_0\right] \tag{3.12}$$

$$\gamma \equiv |\alpha|^2 - |\beta|^2 \qquad (-1 \leqslant \gamma \leqslant 1) \tag{3.13}$$

4. The adiabatic solution. The MSW effect

Assume that $\varpi(x) \ll 1$ over the whole range $x \in [0,1]$. Then $U(1,0)$ is very well approximated by the adiabatic solution. From Eqs.(3.1 to 10), we deduce

$$|\psi(0)\rangle \equiv |e\rangle = |w_+\rangle_0 \cos\theta_0 + |w_-\rangle \sin\theta_0$$

$$|\psi(1)\rangle \simeq \hat{U}(1,0)\ \bar{U}_{ad.}(1,0)\ |\psi(0)\rangle$$

$$= |v_+\rangle \cos\theta_0 \exp\left[-i \int_0^1 W\, dx\right] + |v_-\rangle \sin\theta_0 \exp\left[+i \int_0^1 W\, dx\right]$$

The essential features of the adiabatic approximation is transparent in this expression: in the travel from solar core to solar surface, the components of $|\psi(x)\rangle$ along the (rotating) eigenvectors of $M(x)$ stay constant to within a well defined phase factor.

A straightforward calculation then leads to

$$\left\langle P_{\nu_e \mapsto \nu_e} \right\rangle \cong \langle P_{ad} \rangle = \tfrac{1}{2} \left[1 + \cos 2\theta_v \cos 2\theta_0\right] \tag{4.1}$$

to be compared with the general result, Eq.(3.12): $\gamma_{ad} = 1$. Here

$$\alpha_{ad} = \exp\left[-i \int_0^1 W\, dx\right] \qquad \beta_{ad} = 0 \tag{4.2}$$

The effect of solar matter will now be discussed, by comparing this rather simple expression for $\langle P \rangle$ with the one that obtains in vacuum:

$$\langle P_v \rangle = \tfrac{1}{2} \left[1 + \cos^2 2\theta_v\right] \tag{4.3}$$

First, the only property of matter which comes into play is the *electron*

density at the center of the sun, $n_e(0)$, through the occurrence of $\cos 2\theta_0$ in expression (4.1):

$$\cos 2\theta_0 = \frac{\kappa_0 + \cos 2\theta_v}{\sqrt{\kappa_0^2 + 2\kappa_0 \cos 2\theta_v + 1}} \qquad \kappa_0 \equiv B_0/A \tag{4.4}$$

It does not depend at all on the detailed behaviour of $n_e(x)$+.

Moreover, if

$$B_0 \gg A, \quad \text{i.e. } q/\delta m^2 \gg 0.7 \times 10^5 \quad (n_e(0), \text{ from Ref.3})$$

then $\cos 2\theta_0 \simeq 1$, the expression further simplifies:

$$\langle P_{ad} \rangle \simeq \cos^2\theta_v \tag{4.5}$$

Comparison with $\langle P_v \rangle$ in this limiting case is plotted in Fig.2.

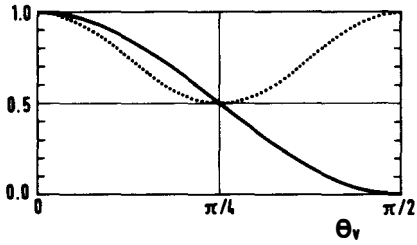


Fig.2 : Solid line : $\langle P_{ad} \rangle$ vs θ_v in the limit $B_0 >> A$
Dotted line : $\langle P_v \rangle$ vs θ_v

Secondly, because $\theta_0 < \theta_v$ (cf. Fig.1), the situation differs qualitatively according as $\theta_v \gtrless \pi/4$:

. $\theta_v < \pi/4$ $\quad \cos 2\theta_v > 0$, $|e\rangle$ closer to state of higher mass (Fig.1a)
$\langle P_{ad} \rangle > \langle P_v \rangle$ $\quad \nu_e$-suppression smaller

. $\theta_v > \pi/4$ $\quad \cos 2\theta_v < 0$, $|e\rangle$ closer to state of lower mass (Fig.1b)
$\langle P_{ad} \rangle < \langle P_v \rangle$ $\quad \nu_e$-suppression greater

---

†It must decrease slowly enough, though, for the adiabatic approximation to be valid (see below).

The MSW effect, namely the occurrence of a spectacular ν_e-suppression, is observed in the $\theta_v > \pi/4$ sector (Fig.1b), when

$$B_0 \gg A \quad \text{and} \quad \theta_v \quad \text{closer to } \pi/2$$

Then (Fig.2), $\langle P_{ad} \rangle$ becomes very small
whereas $\langle P_v \rangle$ gets closer to 1

The MSW effect has been advertised for rather small values of $\sin^2 2\theta_v$. Note however that, for as large a value as .75 ($\theta_v = \pi/3$),

$$\langle P_{ad} \rangle = .25 \qquad \text{whereas} \qquad \langle P_v \rangle = .625$$

5. Validity of the adiabatic solution. Study of $\varpi(x)$

5.1 Conditions of validity and estimate of error

The adiabatic result (4.1) differs from the exact expression for $\langle P \rangle$, Eq.(3.12), merely by

$$|\beta|^2 \cos 2\theta_v \cos 2\theta_0 \tag{5.1}$$

β can be estimated from the first order correction to the adiabatic solution of Eq.(3.7):

$$\beta \simeq \beta^{(1)} = -i\, e^{\frac{1}{2} i(\Phi_1 + \Phi_0)}\, I$$

$$I \equiv \int_0^1 e^{-i\Phi(x)} \frac{d\theta}{dx}\, dx = \int_0^1 \varpi(x)\, e^{-i\Phi} \frac{d\Phi}{dx}\, dx$$

Since $d\Phi/dx = 2\,W(x)$ and $\varpi(x)$ are positive, and since the latter has no more than one maximum, ϖ_{max}, in [0,1], one can show (first integrate by parts, then major all terms) that

$$|\beta| = |I| < 2\,\varpi_{max} \tag{5.2}$$

Conclusion:

. The adiabatic result holds if $\varpi(x) \ll 1$ in [0,1]
. It gives $\langle P \rangle$ with an error smaller than $4\,\varpi_{max}^2 \cos 2\theta_v \cos 2\theta_0$
(in fact, much smaller)

5.2 Study of $\varpi(x)$

Simple geometry leads to

$$\varpi(x) = \frac{(-dB/dx)\ A \sin 2\theta_v}{4\ W^3} \tag{5.3}$$

It depends on x via $n_e(x)$ and dn_e/dx. According to datas from Ref.3), $n_e \propto e^{-\lambda x}$ in most of the range with $\lambda \simeq 9.5$. We continue the discussion assuming this exponential behaviour. Then:

$$\varpi = \frac{\lambda}{4A} F[\kappa,\theta_v] \qquad F = \frac{\kappa \sin 2\theta_v}{\left[\kappa^2+2\kappa \cos 2\theta_v+1\right]^{3/2}}$$

$$\kappa(x) \equiv B(x)/A = \kappa_0\ e^{-\lambda x} \qquad \kappa_0 = 1.48 \times 10^{-5}\ q/\delta m^2 \tag{5.4}$$

The behaviour of ϖ, as a function of x via $\kappa(x)$, is transparent on these expressions: an increase up to a maximum, ϖ_{max}, then a decrease.

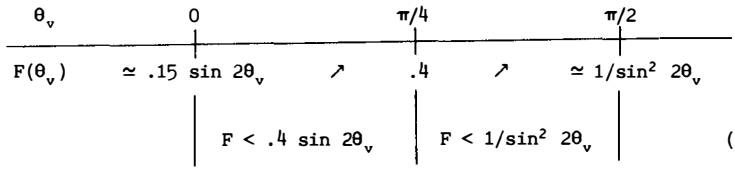
The main features of this maximum are as follows.

Its location on the x-axis, depends mainly on $q/\delta m^2$, but little on θ_v. It is reached when $\kappa = \kappa_m$, a function of θ_v alone, going from ½ to 1 when θ_v goes from 0 to $\pi/2$.

ϖ_{max} is proportional to $q/\delta m^2$:

$$\varpi_{max} = 2.7 \times 10^{-9} \frac{q}{\delta m^2} \times F(\theta_v) \tag{5.5}$$

with $F(\theta_v)$ increasing from 0 to ∞ when θ_v goes from 0 to $\pi/2$:



(5.6)

5.3 Domains of application in diagram $\left[q/\delta m^2, \theta_v\right]$

Using expression (5.5), one can delineate wide domains where the adiabatic approximation applies to within a given level of precision, 1% say. Following the discussion of §5.1, the requirement is

$$\varpi_{max} \lesssim .1$$

leading to $q/\delta m^2 < .4 \times 10^9/F(\theta_v)$ (5.7)

Again, things appear differently according as $\theta_v \gtrless \pi/4$. Using upper limits (5.6), this gives:

if $\theta_v < \pi/4$, $q/\delta m^2 < 10^8/\sin 2\theta_v$ (5.8)

if $\theta_v > \pi/4$, $q/\delta m^2 < .4 \times 10^8 \sin^2 2\theta_v$ (5.9)

Thus, the adiabatic approximation is valid in a large domain of parameters. It breaks down, however,

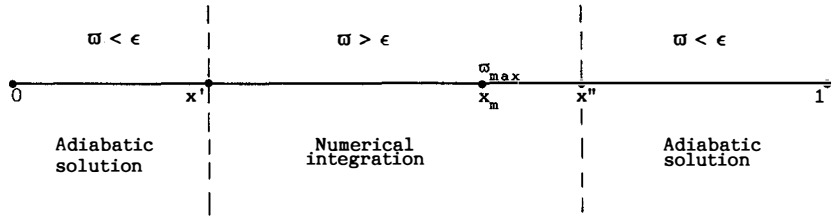
when $q/\delta m^2$ becomes too large

and when, given $q/\delta m^2$, θ_v is too close to $\pi/2$.

6. Beyond the adiabatic approximation. Summary of results

When the eigenvectors rotate too rapidly, the system "does not fully catch up" and deviates from the adiabatic motion. The quantity γ in the exact expression for $\langle P \rangle$, Eq.(3.12), is no longer close to 1.

One must then resort to numerical integration. However it needs not be perform on the whole range [0,1], but only in regions where the rotations of eigenvectors is too rapid, i.e. $\varpi(x) > \epsilon$, hence deviations from the adiabatic motion too large. In practice, since $\varpi(x)$ has no more than one maximum within [0,1], there is at most one limited region, [x',x"], where the numerical integration has to be operated:



The integration in the sensitive region [x',x"] can best be performed by the method devised by Raynal and collaborators[6]. The use of "Raynal's algorithm" is ideally fit for these regions, where not to many oscillations occur. The methods permits to obtain, for each set of parameters $q/\delta m^2$ and θ_v, the value of $\langle P \rangle$ with an error smaller than $\simeq 4\epsilon\,|\beta|\cos 2\theta_v \cos 2\theta_0$.

The computer burden, with this combination of adiabatic solution together with numerical integration in restricted regions where Raynal's algorithm happens to work, is quite limited. All calculations have been performed on our small computer.

We have thus calculated $\langle P \rangle$, for given θ_v, as a function of $q/\delta m^2$ over the whole range of interest of this parameter including the higher values for which the adiabatic approximation is no longer valid. The calculations have been performed for values of θ_v covering the whole range $[0,\pi/2]$.

Some of the plots are shown on Fig.3.

All these curves have a rather simple shape, a shape which varies continuously with θ_v.

So long as $\theta_v < \pi/4$, $\langle P \rangle$ is greater than its vacuum value, Eq.(4.3). The curve displayed on Fig.3a correspond to the value $\sin^2 2\theta_v = .75$, for which the deviation from $\langle P_v \rangle$ is the largest.

The interesting sector is $\theta_v > \pi/4$, for which $\langle P \rangle$ is everywhere smaller than $\langle P_v \rangle$ (ν_e- suppression enhanced). Three plots are given for illustration, Fig.3b, corresponding to $\sin^2 2\theta_v = .01, .1, .75$ respectively. Their shape look all the same: a pit with a flat bottom, a rather steep edge on the left, a more rounded and less steep edge on the right. The pit becomes wider and shallower as $\sin^2 2\theta_v$ gets larger. The adiabatic approximation ($\gamma = 1$), holds on the left part of the plot, as expected from (5.9). $\langle P \rangle$ is then given by (4.1): when $q/\delta m^2$ increases from 10^3, say, θ_o decreases from θ_v down to 0 (cf. Fig.1b). Accordingly, $\langle P \rangle$ decreases (steep edge) from $\langle P_v \rangle$ to its minimum value, expression (4.5), reached circa $q/\delta m^2 \approx 2.10^5$. It, then, stays constant (flat bottom) up to the point where deviations from the adiabatic approximation become significant. γ then starts to decrease from 1 and $\langle P \rangle$ increases steadily up to its value in vacuum.

Note the strikingly similar shape of the right branch of the two upper curves of Fig.3b. It indeed can be shown (cf. Appendix) that, all over the region $B_o \gg A$, $\langle P \rangle$ depend on $q/\delta m^2$ and $\sin^2 2\theta_v$ via the ratio

$$q/\delta m^2 \sin^2 2\theta_v \qquad \text{as} \qquad \sin^2 2\theta_v \to 0$$

As a consequence, on a log plot like that of Fig.3a, the right branch of the curve is merely translated to the left as $\sin^2 2\theta_v$ decreases. The value $\sin^2 2\theta_v = .1$ is about at the edge of this asymptotic region.

The effect of ν-oscillations on the capture rate observed in solar neutrino experiments has been already discussed[1,7]. It obtains by inserting $\langle P \rangle$ in the expression for the capture rate. Contrary to what happens when the effect of solar matter can be ignored, $\langle P \rangle$ depends on q, as seen above, a q-dependence very simple indeed, which makes the analysis rather

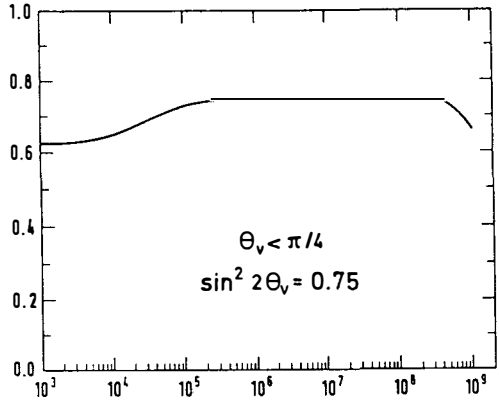


Fig.3 : Plots $\langle P_{\nu_e \to \nu_e} \rangle$ vs $q/\delta m^2$ for given $\sin^2 2\theta_\nu$
a) $\theta_\nu < \pi/4$ $\sin^2 2\theta_\nu = .75$
b) $\theta_\nu > \pi/4$ $\sin^2 2\theta_\nu = .01, .1, .75$

straightforward.

7. Conclusion and comments

. The effect of solar matter on $\nu_\odot$-oscillations cannot be neglected for

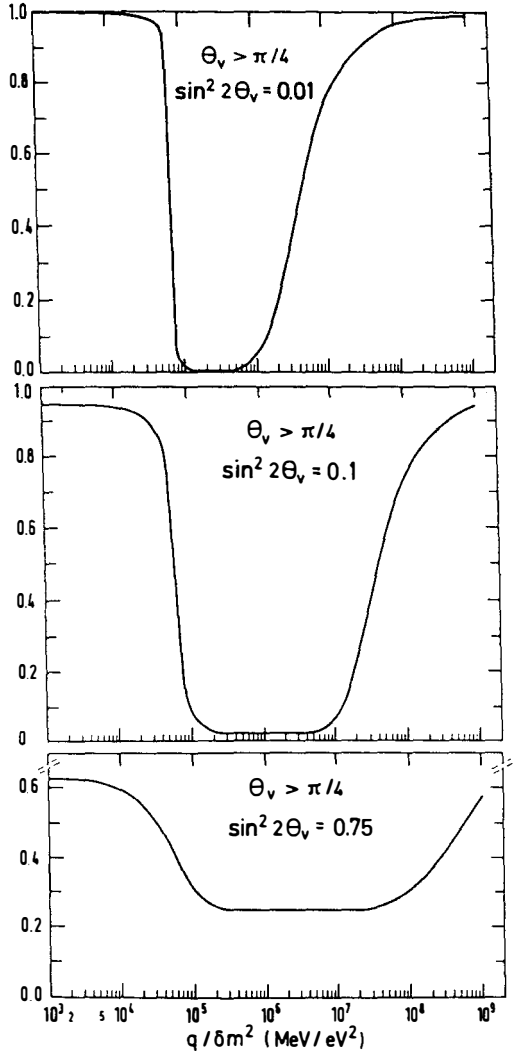
$q_{(MeV)}/\delta m^2_{(eV^2)}$ in the range 10^4-10^9 ,

enhancing the ν_e- suppression if the ν_e state is closer to the state of lower mass ($\theta_\nu > \pi/4$).

. It is easily analysed in the framework of the adiabatic approximation provided the latter is valid.
In particular, the ***MSW effect***, i.e. strong ν_e-suppression for $\theta_\nu \approx \pi/2$ and $q/\delta m^2 > 10^5$, shows up to the extent that the adiabatic approximation is valid ($q/\delta m^2 \sin^2 2\theta_\nu$ small enough) and fades away when it breaks down.
Note that rather large suppression effects still occur with θ_ν far away from $\pi/2$.

. Taking into account this new possibility, the picture regarding solar neutrino experiments must be radically revised.

The averaged "ν-oscillation factor", $\langle P_{\nu_e \to \nu_e} \rangle$, is no longer independent of q, so that the capture rates in different experiments, e.g. in the Cl and in the Ga experiment, are not reduced by the same factor. Thus, the Ga experiment


$\Theta_v > \pi/4$
$\sin^2 2\Theta_v = 0.01$
$\Theta_v > \pi/4$
$\sin^2 2\Theta_v = 0.1$
$\Theta_v > \pi/4$
$\sin^2 2\Theta_v = 0.75$
$q/\delta m^2$ (MeV/eV^2)

cannot be thought any longer as a way to check the Standard Solar Model (SSM), irrespective of any ν-oscillation effect. On the other hand, what can be done (and has been done[7]) is to deduce the values of the ν-oscillation parameters from the measurement of the capture rates, *on the assumption that the* SSM *is correct*. To go further in the analysis would require experiments in which the $\nu_\odot$-spectrum is actually observed, e.g. experiments with D^2O, or with In, the feasibility of which is not yet established.

Note, however, *one very important feature of the Ga experiment*. Suppose that neutrinos do not oscillate. Then one can show that the observed capture rate is at least equal to

75 SNU

to be compared with the 122 SNU predicted by SSM. This lower limit does not depend at all on the details of the solar theory, but on the mere assumption that proton burning into α particles is the unique source of thermonuclear power in the sun. Hence if the experiment gives a smaller capture rate, it will be a *major evidence that neutrinos do oscillate*.

Appendix : Limit $\theta_v \approx \pi/2$

Assume $B_o \gg A$ and $\sin^2 2\theta_v \ll 1$ with $\theta_v > \pi/4$.

This limiting case is best studied in the $\vec{e}$-representation :

$$|\psi(x)\rangle = |e\rangle\, u(x) + |\mu\rangle\, v(x) \qquad \langle P\rangle = \tfrac{1}{2}\left[1 + \cos^2 2\theta_v \left(|u_1|^2 - |v_1|^2\right)\right].$$

Equation of evolution in solar matter :

$$i\frac{d}{dx}\begin{pmatrix} u \\ v \end{pmatrix} = \begin{pmatrix} B+A\cos 2\theta_v & A\sin 2\theta_v \\ A\sin 2\theta_v & -(B+A\cos 2\theta_v) \end{pmatrix}\begin{pmatrix} u \\ v \end{pmatrix} \qquad (A.1)$$

Change the variable : $x \to \xi \equiv -\cot g\, 2\theta$ (Cf. Fig.1a).

$$\xi = -(B+A\cos 2\theta_v)/A\sin 2\theta_v = -(\kappa + \cos 2\theta_v)/\sin 2\theta_v$$

$$i\frac{d}{d\xi}\begin{pmatrix} u \\ v \end{pmatrix} = k\begin{pmatrix} -\xi & 1 \\ 1 & \xi \end{pmatrix}\begin{pmatrix} u \\ v \end{pmatrix} \qquad (A.2)$$

$$k \equiv A\sin^2 2\theta_v/(-d\kappa/dx) \qquad (A.3)$$

Integration of (A.2) from $\xi_o \simeq -\kappa_o/\sin 2\theta_v \approx -\infty$ $\quad u_o=1 \quad v_o=0$
to $\xi_1 = -\cot g\, 2\theta_v \approx +\infty$ gives u_1, v_1 .
The result depend on k, a function of ξ via $d\kappa/dx$. Now, in the limit

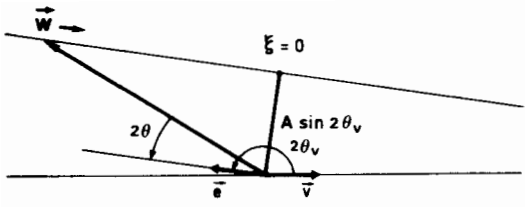


Fig.4 : θ_v close to $\pi/2$. Sensitive region of Fig.1b magnified. Point B_o stays far away on the left.

considered here, the evolution mainly takes place in the region around $\xi = 0$ (Cf. Fig.4). To the extent that $d\kappa/dx$ varies slowly enough within this sentisitive region, $k(\xi)$ can be replaced by $k(0)$, which is thus the unique parameter of the theory: u_1, v_1, and therefore $\langle P \rangle$ (since $\cos^2 2\theta_v \simeq 1$) depend on the mass operator parameters via $k(0)$, i.e. via the combination

$$q/\delta m^2 \sin^2 2\theta_v \qquad \text{if } n_e(x) \text{ follows an exponential law.}$$

Note that $k(0) = 1/4\ \varpi(0)$ and that $\varpi(0) = \varpi_{max}$ at this limit.

Acknowledgements

I was introduced to the work of Mikhayev and Smirnov by the members of the Gallex collaboration in Saclay. I am grateful to them for providing me with all the information that they could get, and gained much from the numerous discussions which followed, especially with J. Rich on the role of the adiabatic approximation in this problem. I am greatly indebted to J. Raynal for his invaluable advices and help on all the computational aspects, and to N. Tichit for her assistance in writing the programs and operating the computer. Fruitful discussions with A.Smirnov and with P.Rosen during the Rencontres at Tignes are also gratefully acknowledged.

References

1) S.P.Mikheyev and A.Y.Smirnov, Yadernaya Fizika, 1441, 42 (1985) *in russian*; Nuovo Cimento A (to be published)
2) L.Wolfenstein, Phys.Rev.D, 2369, 17 (1978) [In eq.(22) - GN_e in front of the mass term should be replaced by + $\sqrt{2}\ GN_e$]
3) J.Bahcall *et al*, Rev.Mod.Phys. 767, 54 (1982)
4) e.g. A.Messiah, Mécanique Quantique II, Dunod, Paris (1960), chap.XVII
5) e.g. A.Messiah, *Ibid*, chap.XV
6) J.Raynal in "Computing as a Language of Physics, IAEA, Vienna (1979); Melkanoff, Raynal and Sawada, Math.Comput.Phys. 6, Acad.Press, New York (1966).
7) S.P.Rosen, Introductory talk to this workshop; J.Bouchez et al., talk presented by M.Spiro at this workshop; see also S.P.Rosen and J.M.Gelb, to be published in Phys.Rev.D.

THERMAL PULSE DETECTION OF PHOTONS AND CHARGED PARTICLES

K.Riisager[1], H.H.Andersen[2], P.Delsing[3], P.G.Hansen[1], B.Jonson[3], G.Nyman[3], B.Ottefjäll[3], and H.L.Ravn[4]

[1] Institute of Physics,
University of Aarhus, DK-8000 Aarhus C, Denmark

[2] H.C.Ørsted Institute,
University of Copenhagen, DK-2100 København Ø, Denmark

[3] Department of Physics
CTH, S-41296, Göteborg, Sweden

[4] CERN
CH-1211 Geneve 23, Switzerland



ABSTRACT

During the last few years the technique of thermal detection has been developed so that high resolution spectroscopy of single particles is possible. This method seems to yield improvements in energy resolution of about a factor 100 and could thus be of decisive importance for neutrino experiments. The theoretical limits for the resolution and the experimental works performed to data are reviewed and the Göteborg detector is briefly described.

1. Introduction

Although calorimetry has been used for detection of nuclear radiation since the turn of the century, it was Simon[1]) who first suggested the use of small low-temperature calorimeters, and Niinikoski[2]) who pointed out about ten years ago that single particles could be detected with this method. Experimental work on thermal detection of single particles started in 1983.

In principle the detectors work as follows. The radiation - e.g., x-rays or α-particles - of energy E is absorbed in a detector with heat capacity C. This gives a temperature rise

$$\Delta T = \frac{E}{C} \qquad (1)$$

In order to get a measurable signal it is necessary to work at a low temperature, since this makes the relative temperature rise larger due to the strong temperature dependence ($C \sim T^3$) of the heat capacity. If a good energy resolution is needed, small size detectors must be used. The experiments have up to now worked at temperatures around 1K and with detectors of size less than 1 mm^3. The temperature rise is normally detected by the voltage drop across a temperature dependent resistor in thermal contact with the detector.

As will be seen in the next section such thermal detectors (also called microcalorimeters or bolometers) seem to promise a resolution superior to that obtainable with standard semiconductor detectors. Thermal detectors would therefore be ideally suited for measurements of tritium beta-decay[3]), internal bremsstrahlung[4,5]) or double beta-decay[6]).

2. Resolution

This section summarizes the theoretical estimates[7-9]) of the resolution of the thermal detectors. Experimental results are reviewed in section 4.

The thermodynamic limit on the resolution of an optimized detector is[7])

$$\Delta F_{FWHM} = \xi(8\ln 2 k_B T^2 C)^{1/2} \qquad (2)$$

where the constant ξ is in the range $1.5 \lesssim \xi \lesssim 2$, k_B is the Boltzmann constant, T is the temperature of the heat sink, and C(T) is the specific heat. Two important effects are here the thermodynamic fluctuations and the Johnson noise of the thermistor. A more intuitive exposition of this limit can be found in ref.10. The limit is shown in figure 1 for a heat capacity C as given in ref.4.

In a realistic thermal detector not all of the energy of the radiation is transformed to heat on a short time scale (the time used for detection of one event should be less than 1 msec if experiments with high count rates are to be performed). Andersen[8,9]) has calculated what the effect of this imperfect thermalization will have on the resolution by following the energy flow in the detector in detail. Creation of lattice defects is important. We refer to refs. 8,9 for details, the resolution for 4 keV internal electrons is also shown in figure 1.

Finally long-term fluctuations in the temperature of the environment will also lead to loss of resolution. For semiconductor thermistors with resistance $R \sim T^{-n}$, $n \gtrsim 4$-9, it is easily shown from (1) that fluctuations δT in the temperature of the reservoir gives fluctuations $\delta(\Delta V)$ of the voltage pulses

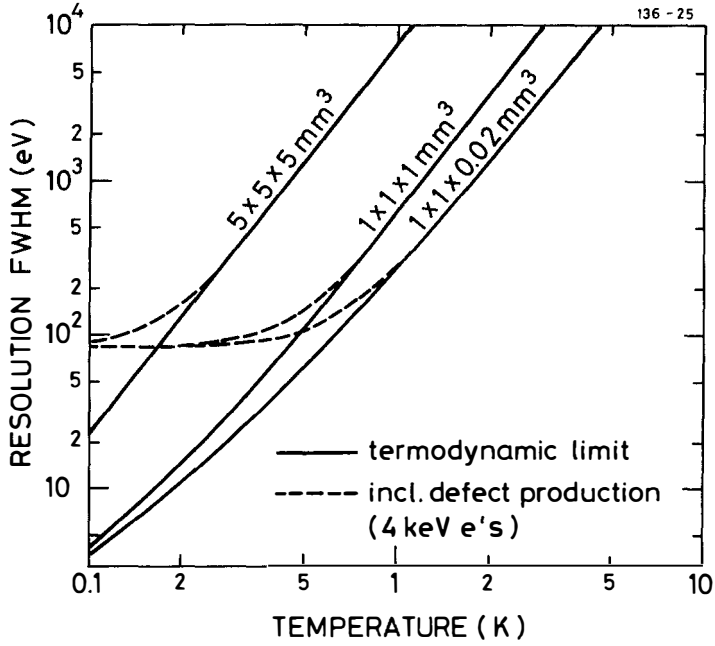


Fig.1. Theoretical limits on resolution for a diamond bolometer (as described in ref.4). The figure is adapted from refs. 4 and 8. Limits are given for several detector volumes. Solid lines give the thermodynamic limits, dashed lines include the effect of defect production and are only valid for 5 keV internal electrons.

given by

$$\frac{\delta(\Delta V)}{\Delta V} = (n+4)\frac{\delta T}{T} , \qquad (3)$$

i.e., the fluctuations are amplified by a factor of order 10. A high temperature stability is therefore important, unless one is able to record the temperature of the environment at each event.

3. Detector designs

Two different types of detectors have been tried in experiments up to now. The first type - advocated by the Goddard Space Flight Center, University of Wisconson collaboration[7]) - uses a semiconductor crystal as detector. The thermistor is here made by ion implantation in a small region of the crystal itself. The second-type - developed by the LPSP group for bolometry and later used as a thermal pulse detector [4]) - is a composite bolometer, where the detector and the thermistor are glued together. A diamond absorber and Ge-thermistor have been used.

We are still in the process of building the detectors and have not yet performed actual experiments. Our final design involves a detector of volume 0.01-0.02 mm^3 etched out of a Si-wafer, with thermistor and contacts implanted from the backside. The fabrication involves only well-known techniques from semiconductor processing. In order to test the electronic and mechanical setup we have made large detectors (size 1.0 mm^3) of Si, both with an implanted thermistor and with carbon thermometers. The latter detector type is shown in figure 2.

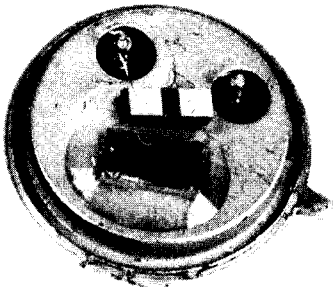


Fig.2. A thermal detector (centered) made of silicon with dimensions 1mmx2.5mmx0.34mm. The thermometer is made by implantation of phosphorus. The gold wires are bonded on gold contacts evaporated upon the thermometer.

Note that very few materials have been tried as detector materials up to now. As argued in ref.9, use of superconductors might be advantageous.

4. Experimental tests

The work of McCammon et al.[3 10-12]) has been concentrated on low-energy x-rays. The best results obtained so far[10]) is a resolution (FWHM) of 35 eV for 6 keV x-rays, a factor about 4 better than obtained with Si(Li) detectors. Experiments were performed at .1-.3K. The work of N.Coron et al.[4-13-14]) was performed at somewhat higher temperatures, 1-4K. Alpha particles, gamma rays, and Auger electrons have been detected[13]), the best result being a resolution of 36 keV on 5-6 MeV α's. Other groups[15 16]) have also reported observations of alpha particles.

The important question of thermalization has been addressed by McCammon et al. They find that more than ~70% of the energy is seen as heat[11]), but also find indications[3 10]) for energy being trapped in semiconductors (they attribute this to electron hole pairs in metastable states) and conclude that the thermodynamic limit of equation (2) can not be reached with silicon as detector material.

Count rates around 100 s^{-1} have already been obtained[13]). As pulse rise times of 1-3μs and decay times of 20μs have been seen[16]), even higher count rates should be possible. The detectors are not expected to be completely linear as the heat capacities change with temperature, still a linearity better

than 1.5% from 20 keV to 6 MeV has been obtained[13]). Digital pulse analysis has been employed in several experiments [12,13]), note in this connection that the pulse shape is not a single exponential[17]).

5. Outlook

We expect to have a working detector within a few months. Systematic studies involving variations of detector parameters and detector materials in order to optimize the bolometer are planned. The results obtained by other groups in the last few years are very promising, and it thus seems realistic to expect vast improvements of the resolution for single particle detection compared with standard semiconductor detectors. The thermal detectors are still in their initial stage. When more developed detectors are available, experiments with tritium will be among the first to be performed. Finally one should not forget the suggestions of using thermal detectors for direct detection of neutrinos[18]). Thus in general thermal detection offers interesting new possibilities in neutrino physics.

One of us, (K.R.) was supported by the Danish Natural Science Research Council.

References

1) S.Simon, Nature 135 (1935) 763
2) T.O.Niinikoski, in "Liquid and Solid Helium" (Halsted, New York, 1975) p.145
3) D.McCammon, M.Juda, D.D.Reeder, R.L.Kelley, S.H.Moseley and A.E.Szymkowiak, in "3rd Telemark Conference on Neutrino Mass and Low Energy Weak Interactions" (AIP Conf.Proc.,1986)
4) N.Coron, G.Dambier, G.J.Focker, P.G.Hansen, G.Jegoudez, B.Jonson, J.Leblanc, J.P.Moalic, H.L.Ravn, H.H.Stroke, and O.Testard, Nature 314(1985)75
5) K.Riisager, these proceedings
6) E.Fiorini and T.O.Niinikoski, Nucl.Instrum.Methods 224 (1984) 83
7) S.H.Moseley, J.C.Mather, and D.McCammon, J.Appl.Phys.56 (1984) 1257
8) H.H.Andersen, Nucl.Instrum.Methods B 12 (1985) 437
9) H.H.Andersen, Nucl.Instrum.Methods B, in press
10) D.McCammon, M.Juda, J.Zhang, R.L.Kelley, S.H.Moseley, and A.E.Szymkowiak, IEEE Trans.Nucl.Sci.33 (1986) 236
11) D.McCammon, S.H.Moseley, J.C.Mather, and R.F.Mushotzky, J.Appl.Phys.56 (1984) 1263
12) S.H.Moseley, R.L.Kelley, J.C.Mather, R.F.Mushotzky, A.E.Szymkowiak, and D.McCammon, IEEE Trans.Nucl.Sci.NS-32 (1985) 134
13) N.Coron, G.Artzner, G.Dambier, G.Jegoudez, J.Leblanc, J.P.Lepeltier, J.Y.Deschamps, R.Rocchia, A.Tarrius, C.Testard, P.G.Hansen, B.Jonson, H.L.Ravn, H.H.Stroke, and E.Turlot, at "2nd Int.Technical Symp.on Optical and Electro Optical Applied Sciences and Engineering", Cannes, 1985
14) H.H.Stroke, G.Artzner, N.Coron, G.Dambier, P.G.Hansen, G.Jegoudez, B.Jonson, J.Leblanc, J.P.Lepeltier, G.Nyman, H.L.Ravn, and O.Testard, IEEE Trans.Nucl.Sci.33 (1986) 759
15) C.Borango, U.Valbusa, G.Gallinaro, D.Bassi, S.Iannotta, and F.Mori, Cryogenics 24 (1984) 681
16) T.O.Niinikoski, A.Rijhart,A.Alessandrello, E.Fiorini, and A.Giuliani, preprint, Milano, 1986
17) G.Gallinaro, C.Salvo, and S.Terreni, Cryogenics 26 (1986) 9
18) B.Cabrera, these proceedings

THE SUPERCONDUCTING TUNNELJUNCTION - A NEW HIGH-RESOLUTION DETECTOR IN THE KEV RANGE

V. Zacek[1]

CERN, Geneva



Abstract:
At the Technical University Munich thin film superconducting tunneljunctions were operated at 0.3 K and irradiated by a ^{55}Fe X-ray source. Pulses due to photo absorption were observed and the Mn-K_α, Mn-K_β lines at 5.89 keV and 6.43 keV could clearly be resolved. Among other applications the expected resolution of several eV could make Tritium loaded tunneljunctions interesting devices for direct neutrino mass determinations.

---

[1] Collaborators: F.v.Feilitzsch, H.Kraus, R.L.Mössbauer, T.Peterreins, F.Pröbst, (Technische Universität München, D-8046 Garching) and E.Umlauf (Walter-Meissner Institut für Tieftemperaturforschung, D-8046 Garching)

1. INTRODUCTION

Superconducting devices offer the interesting possibility of radiation detection in bulk material with an improved energy resolution compared to semiconductor detectors. This expectation is based on the fact that the minimal ionization energy of such detectors is of the order of the binding energy of a Cooper-pair 2Δ, i.e. of a few meV only. Provided that most of the charge carriers released in Cooper-pair breaking can be collected, the statistical limitation on the energy resolution may be lower by more than one order of magnitude compared to other solid state detectors. Furthermore the binding energy of Cooper-pairs is small compared to typical phonon energies. Consequently superconducting detectors could have the unique property that the part of the energy of the incoming radiation, which is spent in phonon excitation can be partially recuperated via Cooper-pair breaking. In order to collect the radiation produced charge carriers a second superconductor can be used as counter electrode, which is seperated from the first by a thin ($\approx$ 20 Å) insulating barrier. A voltage $U < 2\Delta/e$ applied across the junction allows extraction of the free charge carriers via the quantum mechanical tunnel effect. In the following the operation principle of this new type of radiation detector will be descibed in more details, together with results obtained from irradiation tests of $Sn/SnO_x/Sn$ tunnel junctions[1].

2. EXPERIMENTAL METHOD

The principle of the detector is illustrated in fig.1a, which shows the energy level scheme of a junction of two identical superconductors seperated by an insulating layer and biased with voltage U. As long as the voltage drop is less than $2\Delta/e$ only the tunnel current of thermally broken Cooper-pairs, viz. quasiparticles, will be observed. For operation as radiation detector the superconducting tunnel junction is biased by current injection in the high impedance part $U < 2\Delta/e$ of the current voltage characteristic (fig.1b). Incoming radiation

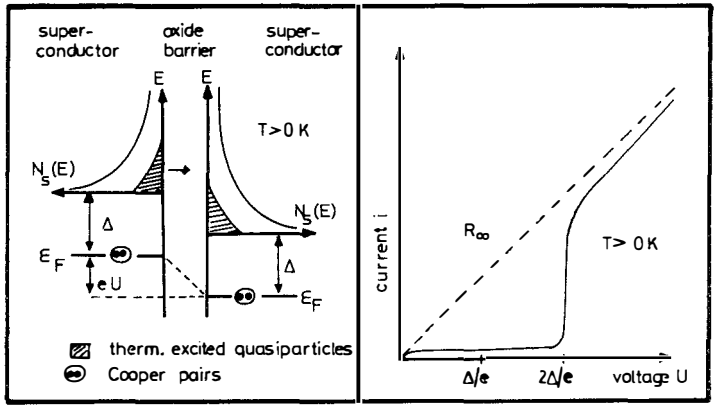


Fig. 1a) Simplified energy level scheme of quasiparticle excitation. $N_S(E)$ is the density of states, ε_F is the Fermienergy. A tunnel current of thermally excited quasiparticles flows between the two superconductors with gap Δ if the junction is biased in the region $0 < U < 2\Delta/e$.

Fig. 1b) Current-voltage characteristic of a tunnel junction with two identical superconductors.

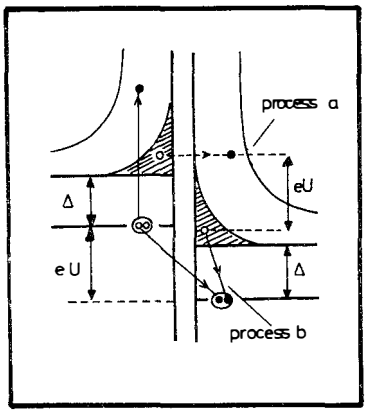


Fig.2) Two processes (a and b) contribute to the tunnel-current, each transferring one electron from the left to the right film. In thermal equilibrium and for superconductors with equal gap, the rates of both processes are identical. As a consequence of processes a and b both superconductors can act as particle detectors.

looses energy by excitation of quasiparticles. These will relax to energetically lower states mainly by emission of phonons, which themselves contribute by pair breaking to the production of additional quasiparticles. After a few psec all quasiparticles will reside above the band gap and give rise to an additional tunnel current,

$$i_T \approx e\, \gamma_T\, n_0 \exp[-(\gamma_T + \gamma_L)\, t] \qquad (1)$$

where e is the electron charge and n_0 denotes the number of broken-up Cooper-pairs. The tunneling rate γ_T can be calculated from the normal conducting properties of the junction:

$$\gamma_T = (R_\infty\, e^2\, N^0\, A\, d)^{-1} \quad \sec^{-1} . \qquad (2)$$

R_∞ denotes the asymptotic resistance of the junction above $U = 2\Delta/e$ (fig.1b). N^0 is the density of electron states of one spin per unit energy and volume at the Fermi energy in the normal conducting metal (e.g. $N^0 = 1.4\times10^{22} eV^{-1}cm^{-3}$ for Sn). A is the area of the junction and d is the thickness of the superconducting film in which the radiation is detected. γ_L denotes the sum of all individual loss probabilities, which can effect quasiparticles before tunneling. Among those the most important processes are recombination back into Cooper-pairs, diffusion of charge carriers out of the tunnelling volume and phonon losses into the substrate.

For effective charge collection the tunnelling rate has to be made as large as possible, which can be achieved by minimizing the thickness of the oxide barrier and the thickness of the superconducting layers themselves. In addition recombination losses can be minimized by reducing the temperature, since the recombination rate γ^{th}_{rec} is proportional to the density of thermally broken Cooper-pairs,which in turn is strongly temperature dependent:

$$\gamma^{th}_{rec} \approx 10^{-10} N_{th} \quad sec^{-1} \qquad (3a)$$

$$N_{th} = N^0 \sqrt{(8\pi\Delta kT)} \exp(-\Delta/kT) \quad cm^{-3} \qquad (3b)$$

where $k=8.617\times10^{-2}$meV/K and N^0 was defined above. This implies that the junctions have to be operated at temperatures such that the number of recombination partners becomes sufficiently small, so that the recombination rate γ^{th}_{rec} is neglibeable compared to the tunneling rate γ_T. For our present choice of junction parameters (i.e. $A\approx100\times100\ \mu m^2$, $d=0.3\mu m$, $R_\infty\approx1\Omega$) this condition is easily fullfilled at our operating temperature of 0.3 K, with $\gamma^{th}_{rec} \approx 0.5 sec^{-1}$ compared to a tunneling probability of $\gamma_T \approx 10^5 sec^{-1}$. At these low temperatures only about 10 thermally excited quasiparticles exsist in our Sn-junctions, compared to a population of about 10^6 radiation induced quasiparticles for a X-ray of several keV! Thus we rather expect from eq.(3a) temperature independent self recombination of the excess charge carriers with a recombination time of tens of μsec, in accord with our observation.

Immediately after production the cloud of quasiparticles is spread by impurity scattering limited diffusion. After 0.5μsec the charge carriers are homogeneously distributed throughout the detector volume. Therefore local variations in barrier thickness which effect the tunneling probability are averaged and the charge collection efficiency via tunnelling is independent of the original position of the radiation induced event.

It is interesting to note that according to fig.2 both superconducting films act as detectors independent from the sign of the applied bias. In process b an excited quasiparticle in the right film recombines into a Cooper-pair by breaking another pair in the left film, causing a net transfer of an electron from the left to the right. The remaining quasiparticle in the left film can tunnel back to the right side and start the same process again. Therefore a nonequilibrium quasiparticle excitation in either film not only results in a same sign tunnel current but in addition the combined occurence of processes a and b offers the possibility of an intrinsic current amplification as pointed out in ref.2.

3. EXPERIMENT AND RESULTS

The geometry of the junctions is shown in the inset of fig.3. The sensitive area is the overlapping region of 100×100 μm^2 of the two films. The junctions were produced by standard techniques, i.e. vacuum evaporation of Sn through suitable masks and barrier formation by glow discharge oxidation. After an initial pressure of 10^{-11} mbar in the recipient, the ambient pressure was increased to 10^{-5} mbar by a continuous flow of pure oxygen, which was found to improve the film quality. Then the bottom Sn-layer with a thickness of 0.3 µm was evaporated from a heated boat at a rate of 10 nm/sec on a silicon substrate at room temperature. Next the 20 Å thin oxide barrier was formed during d.c. glow discharge in an atmosphere of 0.2 mbar of dry oxygene. After pressure reduction to the starting value the second Sn-film was evaporated. In this way high quality junctions with small leakage currents were obtained. The electrical resistance R_∞ of the junctions was typically 0.1Ω at 4.2°K.

The junctions were mounted together with a calibrated resistive Ge-thermometer in a vacuum chamber inside a ^{3}He-cryostate on a copper coldfinger to provide good thermal contact with the ^{3}He-bath. Reliable electrical connections to the Sn-films were obtained with In-pressure contacts. A d.c. bias was applied to the junctions with a voltage driven current source and the signals were fed via 50 Ω VA-microcoax cables into a voltage or charge sensing preamlifier at room temperature. For the irradiation experiments a 34.4 mCi ^{55}Fe source was mounted 14 mm apart from the detector. Following electron capture the source emits Mn-K_α, Mn-K_β X-rays at 5.89 keV (88%) and 6.49 keV (12%), respectively. A weak magnetic field of about 20 G was applied parallel to the tunnelling barrier to suppress the dc-Josephson current.

About 22% of the incoming Mn-K_α, Mn-K_β X-rays interacted in the Sn-films whose thickness of 0.3 µm are roughly matched to the range of the ejected photoelectrons. Below 1 K X-ray induced pulses appeared when the junctions were biased near the point of highest impedance in the current-voltage characteristic.

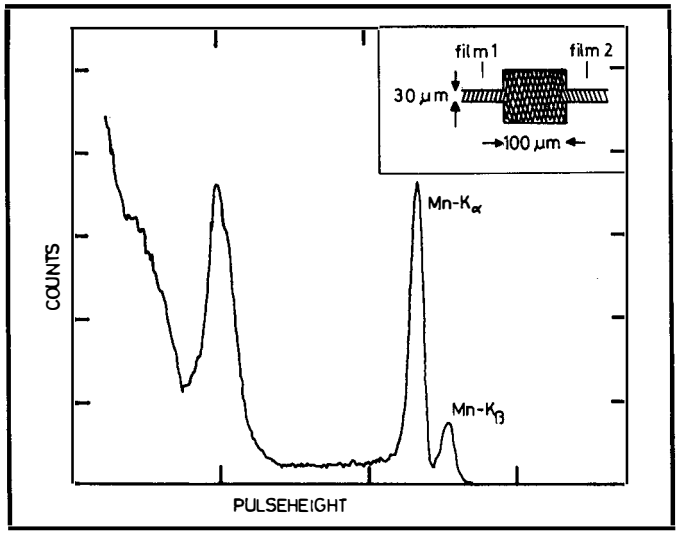


Fig.3) Pulse height spectrum at 0.3 K from a superconducting tunnel junction (Sn/SnO_x/Sn) exposed to a ^{55}Fe X-ray source emitting Mn-K_α, Mn-K_β X-rays with energies of 5.89 keV and 6.49 keV, respectively. The upper pair of peaks is due to X-ray absorption in the 0.3 m thick top film. The lower peak corresponds to X-ray absorption in the bottom film. A resolution of 250 eV (FWHM) can be inferred from the response of the top film. The detection geometry is shown in the inset. The tunnel junction is confined to the overlap of the two superconducting films.

By further cooling a steady increase of the signal amplitude was observed. However, below 0.6 K the pulse height showed no significant further temperature dependence. The risetime of the signals increased up to a value of 8 µsec at 0.3 K. Absolute value and behaviour of the risetime is entirely determined by the intrinsic RC time constant of the junction, where R = (dU/dI) denotes the (temperature dependent) differential resistance at the bias point and C is the junction capacity. In addition an increase of the signal decay time was observed from about 1 µsec to 50 µsec for decreasing temperature from 0.9 K to 0.6 K. Since according to (1) the decay time is affected by the lifetime of excess charge carriers, this can be explained by the continuous freezing-out of thermally excited recombination partners. Below 0.6 K self-recombination of X-ray induced charge carriers takes over.

A pulse height spectrum recorded at 0.3 K is shown in fig.3. A well resolved pair of lines shows up in the upper part of the spectrum, which correponds to absorption of Mn-K_α and Mn-K_β X-rays in the top film. The peak width corresponds to a resolution of 250 eV (FWHM). The lower peak belongs to X-rays detected in the bottom film. Systematic studies with varying film thickness proved, that (as described in fig.2) both films perform as detectors with a tunnelling probability and hence charge collection efficiency inversely proportional to the respective film thicknesses. The observed flat background results from incomplete charge collection due to quasiparticle diffusion out of the detector volume. Adopting an estimated value of 1.7 Δ for the amount of energy necessary to produce a free charge carrier[3], a charge collection efficiency of 19% can be derived from the recorded pulse amplitudes. The enormous countrate immediately above threshold is assigned to X-ray absorption in the substrate, followed by phonon detection in the tunnel junction.

CONCLUDING REMARKS

In this report irradiation tests of $Sn/SnO_x/Sn$ tunnel junctions with ^{55}Fe X-rays were described, as they were performed at the Technical University Munich. Our investigations were originally sparked by our search for a new type of detector allowing for an independent method to precisely determine the effects of a finite neutrino mass in ^{3}H-decay. By doping superconducting tunnel junctions with Tritium one may achieve a high resolution measurement of the β-spectrum without problems due to the source thickness, backscattering and final state effects. With an energy resolution of 250 eV at 6 keV obtained in the first tests reported here and a charge collection efficiency around 20%, our goal is by far not achieved. However, improvements are obvious and possible by straightforward techniques[4]. In the meantime also other groups are pursuing this line of development, exploring the feasability of this new detector concept in various domains, e.g. ββ-decay experiments[5] and detection of solar neutrinos[6].

References:

/1/: H.Kraus et al., Europhys.Lett. 1, 161 (1986)

/2/: K.Gray, Appl.Phys.Lett. 32, 392 (1978)

/3/: M.Kurakado, Nucl.Instr.and Meth. 196, 275 (1982)

/4/: D.Twerenbold, Europys.Lett. 1, 209 (1986)
see also: D.Twerenbold, these proceedings

/5/: B.Cabrera, these proceedings

/6/: N.E.Booth et al., in: Proc. of the Conference on Solar Neutrinos and Neutrino Astronomy, Lead, South Dakota (1984)

SUPERCONDUCTING TUNNELLING JUNCTIONS AS HIGH-RESOLUTION X-RAY DETECTORS

Damian Twerenbold*
Swiss Institute for Nuclear Research
CH-5234 Villigen, Switzerland



ABSTRACT

In a superconducting detector, a superior energy resolution compared to conventional semiconductor detectors is expected owing to the thousand times smaller energy gap Δ. Results are presented from Sn/Sn-ox/Sn junctions exposed to the X-ray photons of a Fe-55 source at a temperature of 0.32 K. The best energy resolution observed is 67 eV (FWHM) at 5.89 keV. When evaporated onto a silicon substrate, most of the pulses originate, via phonon backscattering, from X-ray photons interacting in the substrate. The main features of this detector are well described by dynamical Cooperpair breaking and the relaxation mechanisms of nonequilibrium superconductivity.

* now at: Institut für Hochenergiephysik
ETH-Hönggerberg, CH-8093 Zürich, Switzerland

Introduction

The potentially high resolving power of superconducting detectors arises from the fact that in a superconductor the lowest lying excited electronic states (quasiparticles) are separated from the ground state (Cooperpairs) by a gap Δ of the order of 1 meV. Hence, a thousand times more 'free' charge is expected to be produced than in semiconductor detectors with a gap of the order of 1 eV. In addition, excited phonons are not a priori lost, as their energies (Debye energy is $\approx$ 10 meV) can be considerably larger than the gap Δ, breaking pairs and contributing to the production of free charge in the detector. Assuming no losses, the ideal resolution of a tin detector (Δ_{Sn} = 0.58 meV) would be 0.07 % at an energy of 5.89 keV.

The first to detect alpha particles with superconducting tunnelling junctions were G.H. Wood and B.L. White[1]. The sensitivity to low energy X-ray photons has been established recently [2,3]. Here, the basic results are presented. A describtion of the experimental set-up and a more detailed discussion of the results is presented in references [4,5]. The physics of the junction detector is well described by dynamical Cooperpair breaking and the relaxation processes of nonequilibrium superconductivity.

Results

The films were deposited onto the substrate (fused silica) by thermal evaporation and using the shadow masque technique. The oxide was grown in an oxygen glow discharge. The geometry of our samples is shown in Fig.1.

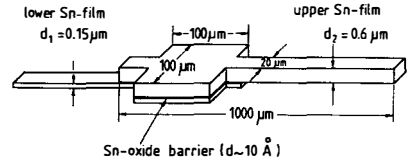


Fig. 1: Geometry of the junction

When applying a voltage across the two films, a current flows owing to the thermally excited quasiparticles. After the absorption of an X-ray, an excess tunnelling current will appear, which decays approximately as $\exp(-t/\tau_{eff})$. The effective relaxation rate τ_{eff}^{-1} of the excess quasiparticles depends on tunnelling rate of the quasiparticles and on the various quasiparticle and phonon relaxation rates. At higher temperatures (T > 0.5 K), quasiparticle relaxation is dominated by the recombination with thermal quasiparticles. This rate is proportional to the density of thermally excited quasiparticles, which depends on temperature as $\exp(-\Delta/kT)$. In order to collect efficiently the produced excess charge,

the tunnelling rate has to be larger, or at least comparable, to the losses in the films. The tunnelling time can be expressed in terms of the normalconducting properties of the junction and the thickness of the film[4,5]. In our detector, the values varied between 1 and 10 μsec.

The excess tunnelling current was integrated by means of a charge sensitive preamplifier. In Fig.2, the pulseheight spectrum of one of our junctions is shown. The most striking property is the doubling of the K_α - K_β structure. This is due to the absorption of X-rays in either films. Electrons always tunnel from the film at the higher potential to the one with the lower. In superconducting tunnelling junction, however, it is possible to exchange quasiparticles in both directions. This can be shown by applying the appropriate Hamiltonian to the problem of tunnelling of electrons between superconducting films[5,6]. As a consequence, the back-tunnelling of quasiparticles leads to an intrinsic amplification of the excess quasiparticle tunnelling current. This effect was first observed by K.E. Gray using the quasiparticle injection method in aluminium double junctions[7]. In our detectors, an intrinsic gain of the order of 2 is deduced[5,6]. As the thickness of the films is much smaller than the attenuation length of the X-rays (≃ 6 μm), the number of events is proportional to the thickness of the respective films. The relative positions of the two K_α peaks in the spectrum is determined by the relaxation processes of each film.

In Fig.3, the corresponding risetime spectrum of the events of Fig.2 is shown. (here one refers to the risetime of the integrated signal, which is essentially the decay time of the excess tunnelling current). The risetime of the thinner film is faster owing to the shorter tunnelling time of that film. This risetime structure makes possible clean pulseheight spectra by applying the appropriate

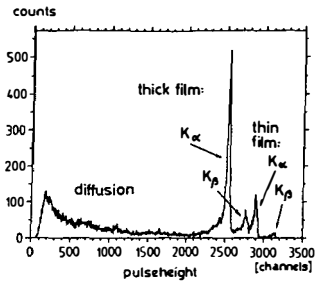


Fig. 2: Pulseheight spectrum.

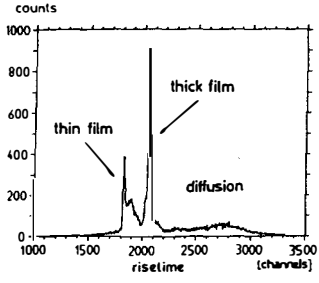


Fig 3: Risetime spectrum
(same events as in Fig.2)

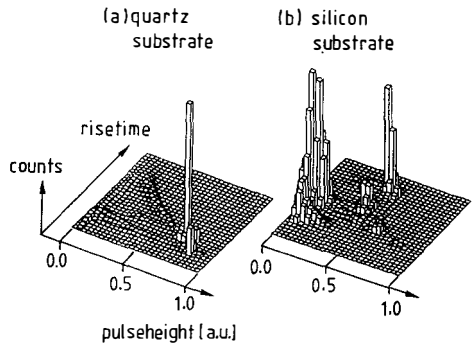


Fig. 4: Comparison of the 2-dimensional spectra from Sn-junctions evaporated onto two different substrates: (a) fused silica, (b) single crystal silicon.

time cuts. The events with lower pulseheights and larger risetimes in Fig.2 and Fig.3, respectively, are due to the diffusion of the quasiparticles produced by X-rays absorbed in the current leads into the tunnelling region[4,5].

Some X-ray measurements were recorded with Sn-junctions evaporated onto a silicon substrate. In Fig.4, the 2-dimensional pulseheight versus risetime spectra of a junction evaporated onto fused silica and onto a silicon substrate are compared. The monocrystalline silicon substrate (same dimensions as the fused silica substrate: 10 x 20 x 0.25 mm^3) was cut from a wafer and the orientation of the surface was in the (1,1,1) direction. The resistivity of the silicon sample was $\simeq$ 5 Ωcm. The exponentially increasing intensity of pulses at smaller pulseheights suggests that they are due to backscattered phonons from X-rays absorbed in the silicon substrate. The phonons with $E > 2\Delta$ break Cooper-pairs in the superconducting films and yield the observed signal. We do not fully understand the reason for the striking differences in the two spectra of Fig.4. The additional peaks in Fig.4 at pulseheights $\simeq$ 0.5 may be due to the specific phonon focussing properties of silicon in the (1,1,1) orientation[8]. These results indicate an interesting possible application of superconducting tunneling junctions: to use them as 'phonon read-outs' in detectors where ballistic phonons are produced by ionizing radiation. A phonon detector of this kind is proposed by B.Cabrera in these proceedings[8].

Energy Resolution

With appropriate cuts in the risetime spectrum, good fits of the total absorbing K_α peaks of either films could be obtained. The best result is shown in Fig.5. This junction had the largest conductance ($4.4 \cdot 10^4$ $(\Omega cm^2)^{-1}$), leading to a fast tunnelling time ($\simeq$ 1 µsec) and consequently to a large amount of accumulated charge ($2.5 \cdot 10^6$ e). The K_α and K_β peaks were fitted at the high energy side of the peaks; the low energetic tail is understood to be due to charge losses depending on the position of X-ray absorption. The K_β peak in Fig.5 is shifted to a lower position in the spectrum. This is due to a pronounced nonlinearity of the detector which is a consequence of the self-recombination of the excess quasiparticles. Two resolutions can be defined in Fig.5:

(1) The differential energy resolution defined by the energy scale owing to the known energy difference of the Mn K_α and Mn K_β X-rays. This yields a $\Delta E(FWHM)$ = 67 eV at 5.89 keV, i.e. 1.14 %, and

(2) an integral resolution $R_{K\alpha}$ which is the FWHM of the K_α peak divided by the position of the peak in the spectrum, yielding 0.90 %.

The electronic noise contribution R_{noise} to the broadening of the K_α is obtained by dividing the FWHM of the testpulse by the channel of the K_α peak and amounts to 0.42 %. By comparing the integral resolutions $R_{K\alpha}$ with the electronic contri-

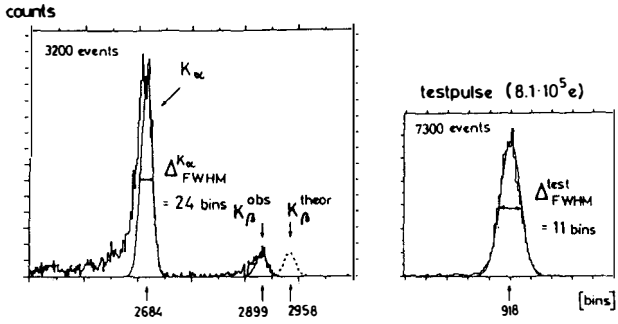


Fig 5: The resolution of the Kα peak and of the corresponding testpulse. The displacement of the observed Kβ peak shows the nonlinearity of the detector, owing to the self-recombination of the excess quasiparticles.

butions R_{noise} of a series of different spectra from four junctions, it was possible to extrapolate the intrinsic resolution of the detector in the limit of vanishing electronic noise. This yielded an intrinsic resolution of our Sn-junction detector of 0.7 % at 5.89 keV.

Conclusion

Superconducting tunnelling junctions were expected to have an energy resolution superior to other ionizing detectors because of the small energy gap Δ of superconductors. We have obtained an intrinsic resolution (FWHM) of 0.7 % at 5.89 keV. This resolution is about a factor of two better than the best results from Si(Li) detectors. Nevertheless, it is ten times worse than theoretically expected from the statistics of the $2.5 \cdot 10^6$ electron charges collected. We believe that this finite resolution is caused by the granularity of the films or by some other geometrical effect.

Solid state detectors with a higher energy resolution than 1o eV could be useful in various applications. Low energy phenomena in fundamental physics (tritium decay, double beta decays, electron capture etc. sensitive to finite neutrino masses) may be investigated more successfully by using calorimetric methods[9]. In addition to the high energy resolution, the superconducting junction detectors also offer the possibility for high spatial resolution by using charge division owing to the diffusion of the excess quasiparticles. Superconducting microstrip detectors would have the great advantage of being virtually massless (thickness < 0.5 μm). A promising application is the possibility of using superconducting tunnelling junctions as phonon sensitive detectors in acoustic crystal detectors[8].

In order to improve the superconducting tunnelling junction detector, however, it is necessary to investigate the geometrical properties of the detector in more detail. The usefulness of these detectors in real experiments also very much depends on the possibility of increasing the size of these detectors, both in area and in film thickness.

References

1) G.H.Wood and B.L.White, Appl.Phys.Letters 15 (1969) 237
2) H.Kraus et al. , submitted to Europhys.Lett.
3) D.Twerenbold, Europhys.Lett.1 (1986) 209
4) D.Twerenbold and A.Zehnder, submitted to Journ.of Appl.Phys.

5) D.Twerenbold, Ph.D. thesis, Eidgenössische Technische Hochschule, Zürich, 1986
6) D.Twerenbold, submitted to Phys.Rev.B, 1986
7) K.E.Gray, Appl.Phys.Letters 32 (1978) 392
8) B.Cabrera, published in these proceedings
9) V.Zacek, published in these proceedings

DETECTING DARK MATTER WITH SUPERCONDUCTING GRAINS

David N. Spergel
Department of Astronomy
Harvard University
Cambridge, MA 02138, USA

ABSTRACT

The use of superconducting micron size grain in the search for the "missing mass" is discussed. The predicted count rates for massive neutrinos and supersymmetric relics from the early universe range from 10^{-1} - 10^{3} counts per kilogram of active detector per day. The earth's motion around the Sun produces a significant annual modulation in this signal. Several experimental challenges remain in the development of this detector.

One of the outstanding problems of astrophysics is that we do not know what comprises 90% of the mass of the galaxy. In recent years, additional evidence continues to accumulate which confirms the presence of "dark matter" in galaxies. Observations of rotation curves of HI gas in spiral galaxies[1] is perhaps the strongest evidence that the amount of gravitational matter exceeds the amount of luminous matter observed in stars, gas, and dust. Observations of hot X-ray emitting gas in elliptical galaxies suggests that the dark matter is pervasive and appears in equal abundance in a variety of galaxies[2]. The success of the inflationary scenario in resolving many of the paradoxes of the big bang cosmology also encourages the prejudice that most of the matter in the universe is not only non-luminous but also non-baryonic.

The range of possible solutions to the "missing mass" problem is enormous: there is a factor of 10^{67} in mass between the 10^{-5} eV "invisible axions"[3] and 10^{6} solar mass black holes[4]. The GeV range candidates offered by supersymmetric models ("sparticles") lie in middle of this range. Since this is a conference on neutrinos, I should not forget to add heavy stable 4^{th} generation neutrinos to the list of GeV range candidates. The effect of all of these "cold dark matter" candidates on galaxy formation is very similar, so we must turn to the laboratory to elucidate the mysteries of the heavens.

If the halo of our galaxy is composed of weakly interacting massive particles (WIMPs), then millions of these particles are streaming through a square centimeter every second. Goodman and Witten[5] realized that this flux could be experimentally detectable. There are, however, two difficulties involved with detecting WIMPs[5].

(1) THEY DON'T DO MUCH: All of the proposed WIMPs have some conserved quantum number (R-parity for SUSY particles and fourth generation lepton number for massive neutrinos); hence, the end-product of an interaction with a nucleus is at best the deposition of a few keV of energy.

(2) THEY DON'T DO IT OFTEN: The lowest mass supersymmetric particle (which is stable in many theories) is usually some linear combination of photino and higgsino interaction eigenstates. This Majorana particle has only axial couplings with quarks and thus has a typical elastic nuclear cross-section $\sim 10^{-37}$ cm^2 for WIMPs through its spin-dependent interactions with nuclei. If these sparticles were the galactic missing mass, they would produce $\sim 10^{-1}$ - 1 counts in a kilogram of detector. Scalar neutrinos and massive Dirac neutrinos have vector couplings with quarks,

and thus the neutrons in the nucleus constructively interfere to yield a much larger cross-section $\sim 10^{-34}$ cm^2 and a higher count rate $\sim 10^3$ counts /kg/day. In either case, the search for WIMPs requires a detector with very good background rejection and a low energy threshold.

In an earlier talk, I noted that we already have limits on weakly interacting halo dark matter from germanium spectrometers. These limits, however, only exclude particles more massive than 16 GeV and it does not seem likely that these limits could be extended below 8 GeV. Unfortunately, the most interesting region for Dirac neutrinos is around 2-3 GeV (the range of the Lee Weinberg limit). Particles with spin-dependent interactions (e.g. photinos, higgsinos, and Majorana neutrinos) also evade detection since most of the abundant isotopes of germanium have zero spin. (They have an even number of both protons and neutrons.) This motivates us to examine the use of new types of detectors in the search for dark matter. I will discuss my work with Andrzej Drukier (Harvard/Smithsonian) and Katherine Freese (ITP, Santa Barbara) on the use of superconducting grains to detect the energy deposited in a nuclear recoil[6].

Grains are not a new, but rather an underutilized, detector technology[7]. They have been suggested for use in the detection of other rare events such as the elastic scatter of solar neutrinos[8] and the monopoles in the galactic halo[9]. Several groups are not actively working on developing grains and grain detectors: A. Drukier (CFA) and his collaborators at UBC, Vancouver; G. Waysand and his collaborators in Orsay, Saclay and Annecy; L. Stodolsky, K. Pretzel and collaborators at MPI für Physik und Astrophysik and F. von Feilitzsch at Technical University in Munich. Blas Cabrerra, in the subsequent talk, will discuss an alternative scheme which involves phonon detections.

In a detector, these grains would be kept in a superheated superconducting state. The deposition of a few keV of energy in an elastic scatter of a WIMP off of a nucleus in the grain heats the grain and flips it from the superconducting to the normal state. The background magnetic field can now permeate the grain. This produces a change in the magentic flux through a loop surrounding the grains equivalent to the addition of a dipole whose strength is proportional to the product of the grain's cross-sectional area and the background magentic field. SQUIDs (superconducting quantum interference devices) would be ideal for detecting this small change in flux. The grain could be composed of any type I superconductor. These include gallium and aluminium, both of which are mostly composed of

isotopes with an odd number of neutrons, and thus have large cross-sections for particles with spin-dependent couplings.

The grains would probably be coated with a dielectric composed of low Z material. This dielectric separates the grains and suppresses diamagnetic interactions with neighboring grains. Another collective grain interaction is the "avalanche effect"[10]. Since the grains are superheated, the change in state of a grain releases energy, which can flip neighboring grains if they are not thermally well separated. This effect can propagate through the detector. Thus if the grains fill most of the detector volume, a single scatter can produce an "avalanche" which results in many grains flipping into the normal state.

The energy threshold of a grain, the minimum amount of energy needed to flip the grain, is set by its composition, size, and temperature. Micron size grains are needed to detect photinos of a few GeV. More massive photino/higgsino particles may arise in superstring theories in which large squark masses are predicted[11]. These 10-80 GeV sparticles could be detected by large grains. Since signal is proportional to the cube of the grain radius, larger grains produce a much stronger signal and thus allow the use of less expensive electronics.

The major source of background in the detector is the radioactive decay of trace contaminants in the grains and the surrounding dielectric. Most of these decays produce MeV electrons. Since the dielectric is composed of low Z material, these electrons, which lose energy through Coulomb interactions, will deposit most of their energy in the grains. Thus radioactive decays will flip multiple grains, which will produce a large change in flux in the SQUID loop. The scatter of a WIMP off of a grain will flip only a single grain. Uniform grains, which have similar energy threshold, are needed for this background suppression mechanism to work. Most of the grains must be in the superheated state so that there is little dead material into which the β particle can deposit its energy.

The problem of grain production is presently the greatest challenge in the development of these detectors. Many of the problems that workers in this field have had with the grains are due to irregularities in grain size and shape. Strong fields near corners of non-spherical grains lead to a spread in energy thresholds. Wide hysteresis curves are a symptom of variations in grain properties. At Vancouver, multiple filtered grains have produced promisingly narrow hysteresis curves which suggest that this process eliminates not only large variations in grain size but also

removes irregular grains. Livermore labs has produced very high quality grains. At this conference, Luis Gonzalez-Mestres has shown me some beautiful new grains that he and his co-workers at Annecy have just obtained from a French industrial producer. If the same techniques that produced these very regular 250 micron diameter cadmium grains can be extended to micron-size gallium or aluminium grains, the future may be very bright for grain dark matter detectors.

Another challenge in dark matter grain detector development will be the integration of the SQUID with the low background technologies. Avoiding background signal due to vibrations producing spurious signals in the SQUID loop will require that the detector is vibrationally well insulated from its environment and may necessitate using multiple SQUID loops as a gradiometer.

Since it is possible for both radioactive decays and the elastic scatter of a halo WIMP to flip a single grain, we must find a characteristic of the signal that will allow differentiation from the background. Failing this, any "detection" could be written off as a misunderstanding of the background. Fortunately, the earth's motion around the Sun provides a significant modulation in the background rate.

The Sun is moving around the Galactic Center at a velocity of about 250 km/s. The non-dissipative dark matter in the galactic halo, on the other hand, never collapsed into a disc; thus, it is not rapidly rotating. As a result of the Sun's motion, the detector is moving relative to the galactic halo. Since the grains have an energy threshold, the anisotropy in the velocity distribution alters the predicted count rate.

The earth's motion around the Sun modulates the velocity of the detector relative to the halo. The earth moves around the Sun with a velocity of 30 km/s. Since the ecliptic is inclined at 62^{o} relative to the galactic plane, only a fraction of this velocity is added to the Sun's motion. In January, when the Sun is in Saggitarius (the location of the Galactic Center), the earth is moving at $\sim$ 235 km/s relative to the halo. (The earth's motion around the Sun is counter-clockwise, while the Sun's motion around the Galactic Center is clockwise.) In June, more energetic particles will stream through the detector when the earth is moving at $\sim$ 265 km/s relative to the galactic halo. Since the detector has an energy threshold, the flux of more energetic particles produces a higher count rate. In reference (6), we estimated a modulation in the signal of $\sim$ 12% in a detector sensitive to 20% of the incident flux. This

calculation assumes that the galactic halo has an isothermal distribution of velocities. More detailed models of the galactic halo[12] that include the effects of the growth of the disc on the halo suggest a more radial distribution of velocities. This would imply a higher modulation rate ($\sim$ 15-25%).

The existence of this modulation effect does not depend upon details of models of the galactic halo. It only requires that the earth's velocity relative to the rest frame of the halo changes with time. The assumption that the halo is composed of WIMPs implies that it is non-dissipative; hence, its rest frame should differ from that of the Sun which is composed of baryons which collected in the disc through dissipation. The only other astronomical requirement for the modulation effect is that the earth moves around the Sun. Seeing the modulation effect, however, requires that grains have a narrow distribution of energy thresholds (< 50%). This is yet another incentive for developing more uniform grains.

In conclusion, a promising application of grain detectors is their use in the search for dark matter. The earth's motion around the Sun produces a significant modulation which can be used to confirm a detection. While hurdles such as the production of uniform spherical grains remain, recent progress, the rewards of detection, and the powerful limits that could be placed on SUSY theories through non-detection will hopefully continue to motivate experimentalists to surmount these problems.

Acknowledgements

D.N.S. is supported by NSF grant PHY-83-06693. I thank my collaborators for allowing me to describe our results before publication.

References

[1]Faber, S.M. and Gallagher, J.S., Ann.Rev.Ast.Astrophys. 17, 135(1979).

[2]Forman, W., Jones, C., and Tucker, W., Ap.J. 203, 102(1985).

[3]Dyne, M., Fischler, W. and Brednicki, M. Phys.Lett. 104B, 199(1984).

[4]Freese, K., Price, R. and Schramm, D.N., Ap.J. 275, 405(1983).

[5]Goodman, M. and Witten, E. Phys.Rev. D31, 3059(1985); Wasserman, I., "On the Possibility of Detecting Heavy Neutral Fermions in the Galaxy," Cornell preprint DE3065 D15-1(1985).

[6]Drukier, A.K., Acta Physica Polonica, in press; Drukier, A.K., Freese, K. and Spergel, D.N., Phys.Rev.D, in press.

[7]Drukier, A.K. and Valette, C. NIM 105, 285(1972); Drukier, A.K., Valette,

C., Waysand, G., Yuan, L.C.L., and Peters, F. Lett. Nuovo Cimento 14, 300(1975); Drukier, A.K. and Yuan, L.C.L., NIM 138, 213(1976); Drukier, A.K. NIM, 173, 259(1980); Drukier, A.K., NIM 201, 77(1982).

[8] Drukier, A.K. and Stodolsky, L. Phys.Rev. D30, 2295(1984).

[9] Drukier, A.K., "Search for Magnetic Monopoles with Use of a Superconducting Colloid," preprint MPI-PAE/Pth 58/83; Gonzalez-Mestres, L. and Perret-Gallix, D., "Detection of Magnetic Monopoles with Superheated Type I Superconductors," LAPP-EXP-85-02. For shorter versions of both proposals, see "Proceedings of 1985 Moriond Conference on Massive Neutrinos in Physics and Astrophysics."

[10] Kouiriti, M., Thesis, Université Paris VI, Dec. 1984; Seidel, W., Thesis, TU Munich, Jan. 1985; Oberauer, L., Thesis, TU Munich, Feb. 1985; Kotlicki, A., Le Gross, M., and Drukier, A.K., Technical Report, UBC/Vancouver, in preparation.

[11] Ellis, J., private communication.

[12] Binney, J., May, A. and Ostriker, J.P., private communication.

CRYOGENIC PARTICLE DETECTORS FOR MAGNETIC MONOPOLES AND NEUTRINOS*

Blas Cabrera
Physics Department, Stanford University
Stanford, California 94305

ABSTRACT

This paper describes particle detectors for magnetic monopoles and neutrinos which are based on cryogenic technology and superconductivity. The first part discusses the status of our search for a cosmic ray flux of magnetic monopoles. We are terminating the operation of the three loop detector and will shortly begin operation of a 1.5 m^2 times 4π sr eight coil detector. The second part describes our more recent work on an entirely new type of particle detector based on ballistic phonon generation in large single crystals of silicon. Such silicon crystal acoustic detectors (SiCADs) would have spatial resolution in three dimensions and would measure the total energy. SiCADs would be particularly useful for neutrino detection experiments where the large cross sections for elastic neutrino scattering off of silicon nuclei can be utilized. Other uses would include high resolution neutron and gamma ray spectroscopy.

PART I: SEARCH FOR MAGNETIC MONOPOLES IN THE COSMIC RAYS

Introduction

In 1931, P.A.M. Dirac proposed the existence of magnetically charged particles to explain the observed quantization of electric charge. He showed that only integer multiples of a fundamental magnetic charge g (Dirac charge) are consistent with quantum mechanics. Many years of experimental searches produced no convincing candidates. In 1974 't Hooft and independently Polyakov showed that in all true unification theories (those based on simple or semi-simple compact groups) magnetically charged particles are necessarily present. The modern theory predicts the same long-range field and thus the same charge g as the Dirac solution; now, however, the near field is also specified leading to a calculable mass. The standard SU(5) model predicts a monopole mass of 10^{16} GeV/c^2, much heavier than had been considered in previous searches. More recent unification theories based on supersymmetry of Kaluza-Klein models yield even higher mass values up to the Planck mass of 10^{19} GeV/c^2.

Such supermassive magnetically charged particles would possess qualitatively different propoerties from those assumed in earlier searches. These include necessarily nonrelativistic velocities from which follow weak ionization and extreme penetration through matter. Thus such particles may very well have escaped detection in earlier searches based on heavy ionization of relativistic monopoles.

Although GUTs theories are very clear in their prediction of the existence of monopoles, cosmological theories based on GUTs lead to impossibly high or unobservably low predictions for monopole particle flux limits with the latter results being exponentially model dependent. Thus, only astrophysical arguments provide guidance for the relevant detector sensing areas for experiments. An upper bound of 10^{-15} cm^{-2} sr^{-1} s^{-1} is obtained assuming an isotropic flux from arguments based on the existence of the 3 microgauss galactic magnetic field (Parker bound). The Parker bound becomes less severe linearly with monopole mass for masses above 10^{17} GeV/c^2. In addition, several authors have demonstrated that models incorporating monopole plasma oscillations would allow a much larger particle flux, approaching in some cases the local galactic dark mass limit (see section on Particle Flux Limits From Our Detector Exposures). All of these bounds assume particle velocities in gravitational virial equilibrium, i.e., very near 10^{-3} c.

Much more severe astrophysical limits can be obtained based on proton decay catalysis. It has been shown theoretically that the supermassive monopoles arising from many grand unification theories would catalyze nucleon decay processes. If the cross section for such events is of order the hadron cross section, as has been suggested, then all attempts at direct detection of the monopoles from such theories may be doomed to failure. Arguments based on x-ray flux limits from galactic neutron stars, which assume a strong interaction cross section for proton decay catalysis, lead to an upper bound for magnetic particle flux of about 10^{-21} cm^{-2} sr^{-1} s^{-1}. There remain unanswered questions concerning the detailed theoretical understanding of the catalysis cross section and concerning the astrophysical arguments based on our incomplete understanding of neutron stars. In addition, proton decay has not yet been observed. Thus, from an experimental point of view more weight should be given to the less model dependent astrophysical limits.

Superconductive technologies, many developed at Stanford University over the last decade, have led naturally to very sensitive detectors for magnetically charged particles. These superconductive detectors directly measure the magnetic charge independently of particle velocity, mass, electric charge and magnetic dipole moment. In addition, the detector response is based on simple and fundamental theoretical arguments which are extremely convincing. Because of their velocity-independent response, these detectors are a natural choice in searches for a particle flux of supermassive (and therefore slow) magnetically charged particles. By far, the most definitive positive identification of a magnetic charge would be made with a superconductive detector.

Recent detailed reviews of the theoretical, the experimental and the atsrophysical work can be found in Magnetic Monopoles (R. A. Carrigan and W. P. Trower, eds., Plenum, 1983) and Monopole '83 (J. Stone, ed., Plenum 1984).

Operation of Three Loop Detector

Beginning in 1982, the research effort at Stanford has been undertaken primarily by B. Cabrera, M. Taber, R. Gardner and M. Huber. Since February, 1983, we have been operating a three loop coincident superconducting magnetic monopole detector[1] (Fig. 1). The rms current noise levels in an effective noise bandwidth of ~0.16 Hz are now 0.02 ϕ_o/L in all three loops, less than 1% of the signal expected from the passage of a Dirac magnetic charge through one of the loops (4 ϕ_o/L). The sensing

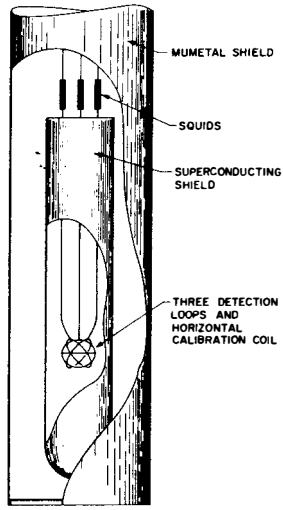


Fig 1 Schematic of three loop detector

area based on this low noise operation is 476 cm^2 (71 cm^2 loop area and 405 cm^2 near miss area) for events greater than 0.1 ϕ_o/L in at least two of the three loops. As of March 20, 1986, the data have been extremely clean and no candidate events have been seen. Based on the 1008 days of accumulated active running time, these data set an upper limit of 4.4×10^{-12} cm^{-2} sr^{-1} s^{-1} (90% C.L.) on any uniform flux of magnetic monopoles passing through the earth's surface at any velocity[2].

Summarizing our results to date on the three loop detector, Figure 2 contains an updated histogram of all the unexplained offsets which have occurred. The largest (loop 2) is

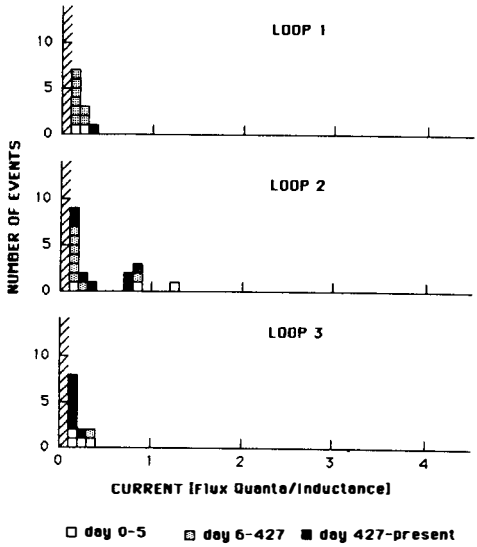


Fig 2 Histogram of all unexplained events for three loop detector. There are no monopole candidates since every event occurred in only one channel.

nearly an order of magnitude smaller than the candidate event observed on the prototype detector (7.5 ϕ_o/L).[3] The unshaded events occurred within the first five days of the run during a settling period of generally noisy data, and the hashed events have occurred most recently after the dewar was moved and a pressure regulation system installed on the helium boiloff exhaust line. Since all of the events were strictly single loop events, with no detectable coincident offsets in the other two channels, they are all excluded as monopole candidates. The probability of a monopole induced event producing a signal above threshold (0.1 ϕ_o/L) in one loop but no detectable offset (0.02 ϕ_o/L) in either of the remaining two loops is $\sim 10^{-4}$. These single loop events are thought to be due to the motion of trapped fluxons in the SQUIDs themselves, but the trigger mechanisms are not understood. A typical eight hour printout of the permanently stored low bandwidth data (0.1 Hz bandwidth) is shown in Fig. 3.

New 1.5 m^2 Detector

During this past year, we have completed the construction of a new larger detector with a sensing area greater than 1.5 m^2 times 4 π sr. This detector[4], shown schematically in Fig. 4, is composed of eight planar

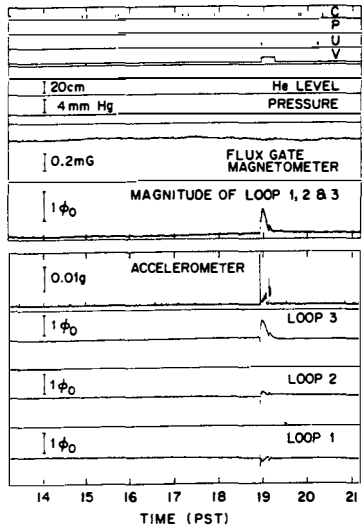


Fig 3 Typical eight hour data record (0.1 Hz bandwidth).

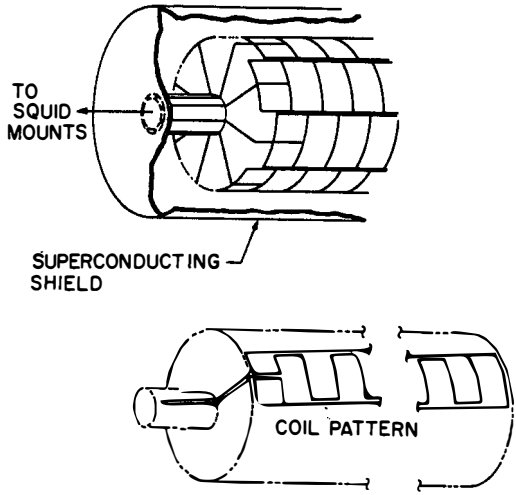


Fig 4 Schematic of new eight SQUID 1.5 m^2 sensing area superconductive detector.

superconducting detection coils arranged around a cylinder with an octagonal cross section. Each coil is a gradiometer 16 cm wide and 6 m long and is connected to a high sensitivity rf SQUID current sensor. The entire assembly is surrounded by a superconducting lead shield and housed in a dewar which is enclosed in a μ-metal shield. This detector has a sensing area 30 times larger than that of the three loop detector.

A very important design feature for the large scale use of superconducting coils as monopole detectors is the use of a gradiometer winding pattern. The sensitivity of a gradiometer to external magnetic field changes is substantially reduced over that from a simple coil whereas the sensitivity to the passage of a magnetic charge remains high since the particle passes through only one element of the gradiometer pattern. We have utilized computer calculations to optimize our coil design under constraints from dewar size and minimum acceptable signal to noise ratio. The optimum pattern which we have used for our design is shown in Fig. 5. It is a repeating rectangular pattern with an aspect ratio of 0.6 to 1.0. A further improvement was achieved by breaking the loop up into a number of parallel elements which are connected together to one SQUID. This technique reduces the coupling losses to the SQUID from a 1/L proportionality

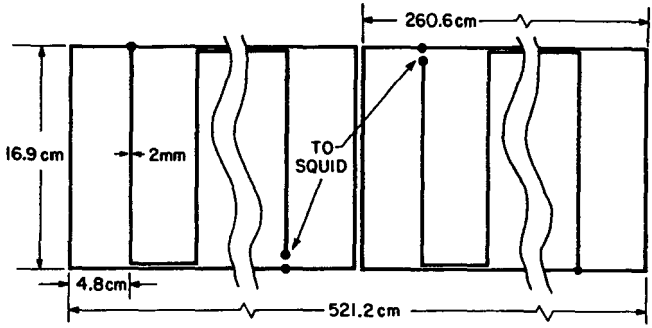


Fig 5 Design of planar gradiometer coils for eight loop detector to $1/\sqrt{L}$, where L us the inductance of the single series loop.

The circuits are mounted on a G-10 structure which provides a rigid support. The entire assembly is shown photographed in Fig. 6. Two of the six cylindrical G-10 sheets which are used as the support structure for the superconducting lead shield are also seen in the photograph. The lead shield, made from 1/32 inch roofing lead, has also been mounted onto the outside of the detector coil assembly. Fig. 7 shows the G-10 detection structure with the lead shield in place as it is being inserted into the cryogenic dewar.

A shield of high magnetic permeability metal (μ-metal) has been designed and constructed to shield the detector from the earth's magnetic field during the initial cooldown, as the inner superconducting lead shield goes through its transition temperature. The external shield consists of 0.038 inch-thick sheets of μ-metal mounted on an aluminum frame. The shield provides an absolute field below 10 milligauss throughout most of its interior.

We have purchased a one liter per hour closed-cycle liquid helium refrigeration system from Cryosystems, Inc. for use with the new 1.5 m^2 detector during continuous operation. There are two significant advantages

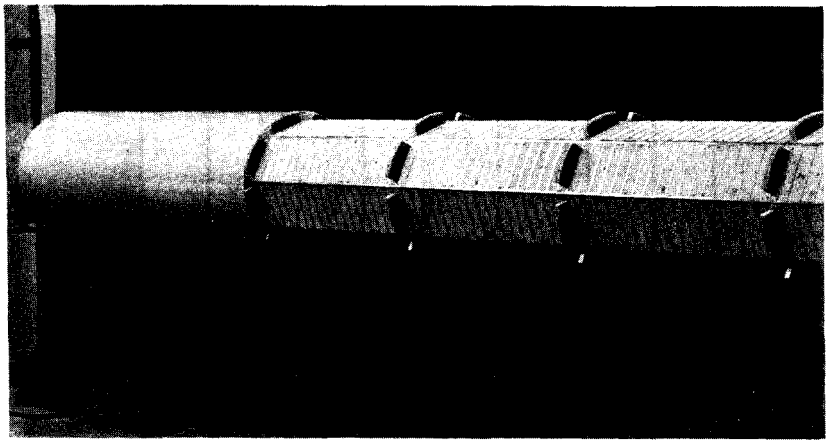


Fig 6 Photograph of detection coil assembly

derived from using this system: lower long-term operating costs, and the virtual elimination of disturbances that are produced by liquid cryogen transfers. Thus, once the new system is cooled down and stabilized, we should be able to achieve essentially 100% live time.

We will utilize the existing computer-based data acquisition system, now in use with the three loop detector, to monitor the new larger detector. Only minor changes are needed in the code to allow use with the new detector. High bandwidth data around any interesting events will be provided as with out existing system.

Particle Flux Limits From Our Detector Exposures

The following points summarize the current status of these research efforts with respect to astrophysical bounds (see Fig. 8).

The Parker bound as modified to include supermassive monopoles has a mass independent floor at $\sim 10^{-15}$ cm^{-2} sr^{-1} s^{-1} and rises linearly with mass above $\sim 10^{-17}$ GeV/c^2 until it intersects the local dark matter bound around the Planck mass, searches at a flux level of $\sim 10^{-13}$ cm^{-2} sr^{-1} s^{-1} are already important. Also shown in Fig. 8 are possible monopole particle flux levels 2 to 3 orders of magnitude above the Parker bound. These

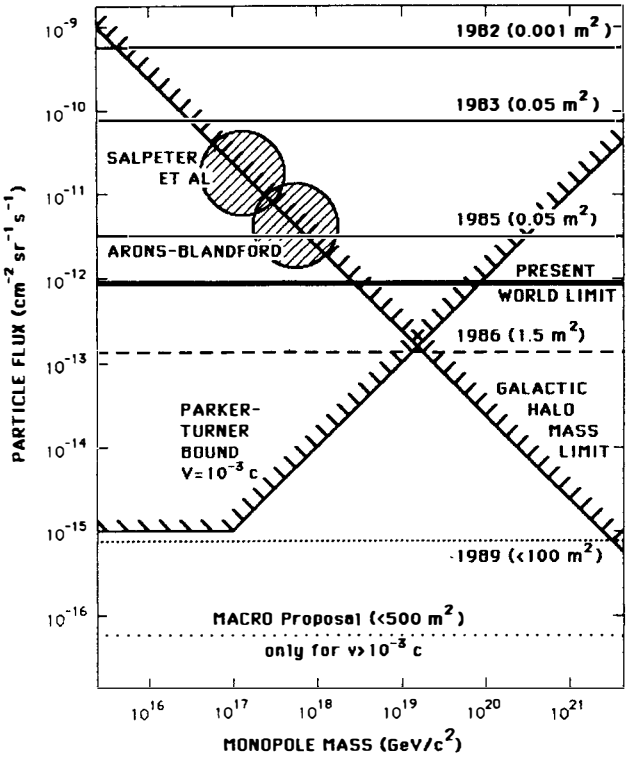


Fig 8 Cosmic ray particle flux limits from our superconductive detectors compared with various astrophysical limits.

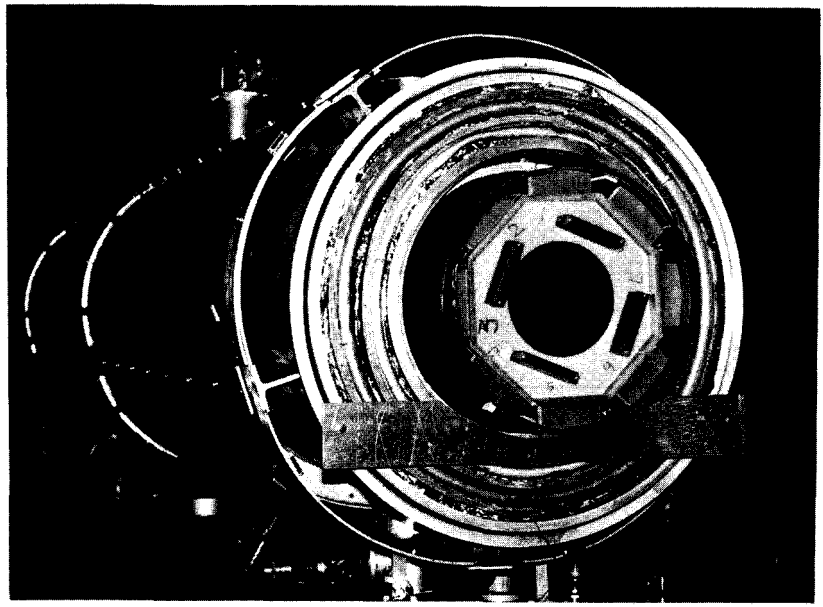


Fig 7 Photograph of the detection coil assembly with surrounding lead superconducting shield being inserted into the cryogenic dewar.

models are based upon monopole plasma oscillations within the galaxy. Detailed computer simulations performed by the Cornell group confirm the stability of such solutions and they are not ruled out by any galactic observations.

The current particle flux limit obtained from our three loop superconductive detector is 4.4×10^{-12} cm^{-2} sr^{-1} s^{-1} at 90% C.L. At this level, monopole plasma oscillation models are more difficult and our limit is within a factor of 50 of the peak of the Parker bound. In fact, four other groups (Chicago-FermiLab-Michigan [5]; IBM, Yorktown Heights[6]; Imperial College[7]; and NBS, Boulder[8]) have obtained similar limits, so that the world limit is now within a factor of ~10 above the peak for the mass-dependent Parker bound (monopole mass ~10^{19} GeV/c^2).

Our Stanford group, as well as the CFM and IBM groups, have constructed larger superconductive detectors with ~1 m^2 x 4π sr sensing areas. Each of these detectors which are now being brought into operation will surpass the peak of the Parker bound in three years of operation. These detectors are

considered prototypes for a future superconductive array with a sensing area of at least 100 m^2 x 4π sr.

Conclusions

We are completing the final assembly phase of construction and beginning the cryogenic testing phase for the first of a new generation of superconductive monopole detector. It has a sensing area of 1.5 m^2, 30 times larger than our existing three loop detector. Each month of operation will equal out total previous area-time exposure.

We have continued operation of our three loop detector in our search for a cosmic ray flux of supermassive magnetic monopoles. As of March 20, 1986 we have accumulated 1008 days of live run time. The data contain no candidate events for the passage of a monopole through the detector and set an upper limit on such a particle flux of 4.4×10^{-12} cm^{-2} s^{-1} sr^{-1} (90% C.L.). This limit is 318 times lower than the original 151 day run with the prototype single loop detector and 5000 above the mass-independent Parker bound. We are terminating the operation of the three loop detector. This research is funded in part by DOE Contract DE-AM03-76-SF00-326.

PART II: SILICON CRYSTAL ACOUSTIC DETECTORS FOR NEUTRINOS

Introduction

Semiconductor diode particle detectors now provide the highest energy resolution (~3 KeV FWHM for 1 kg) and the lowest thresholds available (~4 KeV). In this energy range less than 30% of the deposition energy is converted directly into electron-hole pairs which produce the observed signal in the semiconductors, the rest forming phonons. The characteristic energies of these phonons is ~1 meV, 10^3 less than the excitation energy for an electron-hole pair in a semiconductor (~1 eV). Thus in principle, energy resolutions over an order of magnitude better are possible. In this paper we describe a new class of particle detector which directly senses the phonons produced by an event. Recent work on bolometers, which sense the thermal phonons, has demonstrated an improvement in energy resolution (~30 eV) and threshold (~30 eV) by measuring the temperature rise in a small (~10^{-5} g) ultra-low heat capacity sensor.[9] B. Cabrera, L. Krauss and F. Wilczek suggested scaling bolometers up to a mass ~1 kg.[10]

Motivated by this suggestion, our group at Stanford, B. Cabrera, J. Martoff, B. Neuhauser and B. Young, has proposed direct sensing of the

ballistic phonons produced by an event in a large insulating single crystal.[11] Since this wavefront carries information on the event total energy and location within these silicon crystal acoustic detectors (SiCADs), as well as possible information on the particle direction, substantial improvements in background rejection are possible over detection schemes which measure total energy deposition only. A threshold of 1 KeV or better is important for our primary interest in using SiCADs as neutrino detectors.[10] For example, at power reactors all nuclear recoil signals from elastic neutrino scattering are below 10 KeV with 60% above 1 KeV, and a 1 kg SiCAD would register an event rate of ~100 events/day.

Ballistic Phonons from Point Events in Crystal Cubes

For a deposition of energy in a well localized volume within a single crystal of silicon, a thermal-like spectral phonon distribution is generated with a characteristic temperature of 10-20 K. The reason for this universal spectral distribution is that the first excitations are plasmons or very short wavelength phonons, both of which quickly decay to longer wavelength phonons within less than 10 nsec. Since the decay rates are very strongly dependent on phonon energy and crystal temperature as soon as the distribution has reached wavelengths of even 10 lattice spacings further decays are entirely negligible. These longer wavelength phonons propogate throughout the crystal with no scattering and no dispersion. This mode has come to be called the ballistic phonon mode. Since the discovery of ballistic phonons in 1964 an enormous body of research has established that phonons with wavelengths greater than a few lattice spacings propogate freely without scattering through single crystals such as Si, Ge, CaF_2, SiO_2, Al_2O_3 and other insulating crystals.[12] This work has led to an improved understanding of phonon physics.

An interesting and important aspect of ballistic phonon propogation is that although the propogation is dispersionless, strong focussing effects occur within the crystal. These focussing patterns projected onto each face of a silicon cube cut with its faces orthogonal to the principal axes of the crystal permits three dimensional reconstruction of event locations and can resolve tracks or multiple scattering events. We have performed detailed Monte Carlo calculations[11]. Fig. 9 shows the result of such a calculation for a point energy deposition. The number of points used in the calculation corresponds to the number of phonons expected from a 1 KeV energy deposition at a point within the crystal. It is clear that high

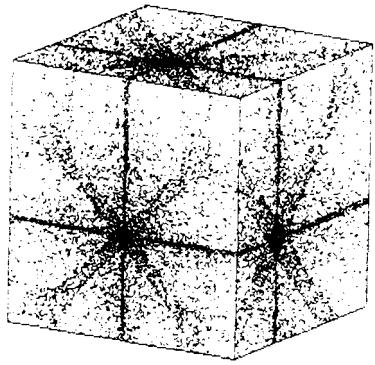


Fig 9 Phonon energy density incident on 100 faces of silicon cube from point event at x/a = 0.7, y/a = 0.5 and z/a = 0.4. (70,000 points in 4 πsr)

in Fig. 9 is shown in Fig. 11. As can be seen for the silicon crystals, sharp peaks in each of the face intensity profiles locate the event to better than the width of a sensor and there is always at least one sensor with an intensity greater than ~2% of the total energy in the event. The lower two rows in Fig. 11 show the time evolution for the peak channel on each face. The time difference on opposing faces also provides position information along that axis through the relation $x_i = a/2 - (T_{ia}-T_{io})V/2$, where $(T_{ia}-T_{io})$ is the resolution information on the event location as well as tracking information is available.

We have considered several phonon sensor configurations for the surface readout. The most promising to date consists of parallel strips on each face (Fig. 10) and provides spatial resolution based on the intensity and arrival time profiles across the sensors on each face. The sensors on the front and back faces perpendicular to the x (y and z) axis have their sensors parallel to the z (x and y) axis and thus can be used to determine the y (z and x) coordinate of the event location. The phonon energy flux intensities incident on each of the 384 strips for the event location

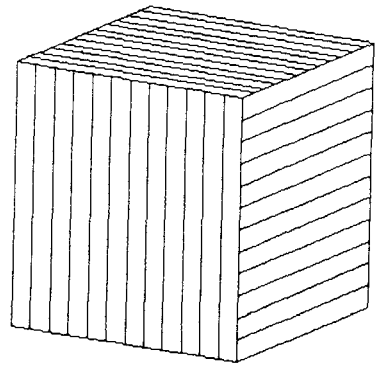


Fig 10 Phonon sensor configuration with parallel sensors on each face (12 shown).

difference in arrival times at the $x_i = 0$ and the $x_i = a$ faces. We have chosen a = 7.5 cm, corresponding to a 1 kg Si cube.

For a = 7.5 cm and using 64 parallel strips per face a spatial resolution of better than 0.25 mm can be achieved by determining the centroid of the peak to one quarter of the width of each sensor. For a 1 KeV energy threshold for event detection within a 1 kg SiCAD cube (for example necessary to detect neutrino-nucleus elastic scattering) then each parallel strip sensor must have an energy sensitivity of ~2% of 1 KeV = ~20 eV. We shall discuss this point further when we consider the use of superconducting tunnel junctions as phonon detectors.

We are extending these calculations to determine the track definition. Multiple point-like interactions appear as the time coincident superposition of two or more single point events.

Superconducting Tunnel Junctions as Phonon Detectors

The most promising sensors for high sensitivity phonon detection are superconducting tunnel junctions. These have been used for many years in condensed matter experiments on phonon and phonon focussing studies.[12] Our proposed application as a SiCAD readout is shown schematically in

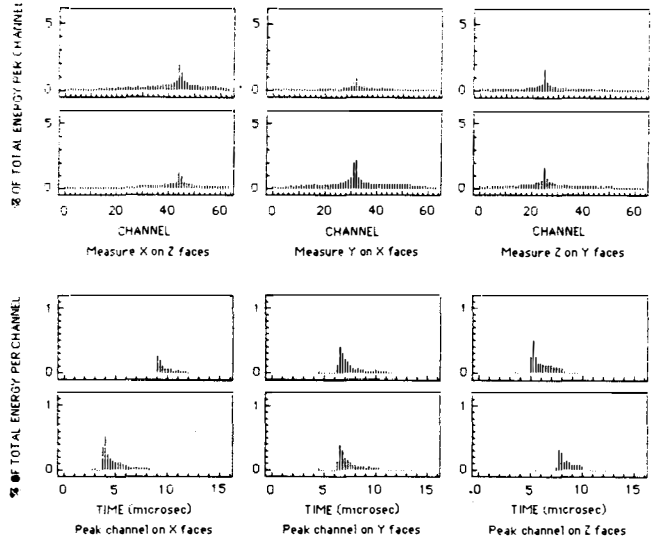


Fig 11 Simulated signals for 64 channels per face in the configuration of Fig. 10 for event location of Fig. 9.

Fig. 12. The junctions are formed by a ~200 nm thick aluminum film deposited directly onto the surface of the silicon cube, followed by the formation of a thin oxide tunnel barrier (~1-2 nm thick) and then deposition of a second aluminum upper film. Phonons from an event within the cube reach the surface and enter the aluminum. Once inside the superconducting aluminum, phonons with energy greater than 2Δ (where Δ is the superconducting energy gap) are strongly absorbed by breaking Cooper pairs and forming electron-like excitations called quasiparticles. In fact, for phonon energies well above threshold, several Cooper pairs will be dissociated. We operate at $T < T_c/10$ (~100 mK for aluminum), where the quasiparticle recombination with thermal quasiparticles is negligible.

Recently the S.I.N. group in Zurich, Switzerland[13] has reported a resolution of ~30 eV for the detection of low energy X-rays (~6 KeV) using a 100 μm x 100 m area Sn - Sn oxide - Sn tunnel junctions operated at ~0.38 K. Pulse rise times of ~15 μsec were observed.

In fact, this sensitivity is already sufficient for our detection threshold requirement of 1 KeV in a 1 kg SiCAD. However, the area of each parallel strip sensor in Fig. 10 is ~0.88 cm^2, a factor of ~10^4 greater than used by the S.I.N. group. We are pursuing several techniques for

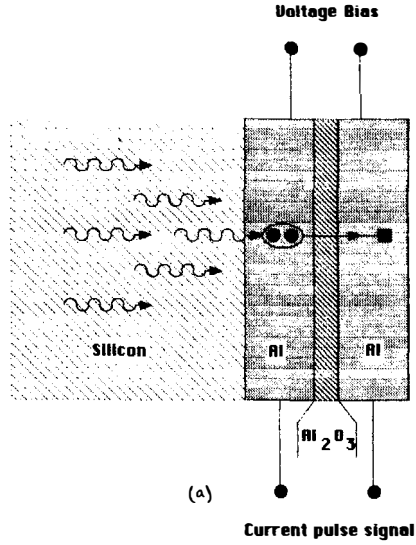


Fig 12 Schematic of superconducting tunnel junctions used as phonon sensors at crystal surfaces.

obtaining comparable energy sensitivity in these much larger area tunnel junctions.

Conclusions

Ballistic phonon focussing effects greatly enhance the spatial resolution in silicon crystal acoustic detectors (SiCADs). Using parallel strip sensors on the faces of a cube, a spatial resolution of ~1/4 mm can be achieved. Utilizing superconducting tunnel junctions as the phonon sensors on the crystal surfaces, we believe that an energy threshold of ~1 KeV can be achieved for a 1 kg SiCAD. Such a detector could be of use for high resolution neutron and gamma ray spectroscopy as well as for our primary interest of high cross section detection of low energy neutrinos. This work has been funded in part by a Research Corporation Grant.

References

[1] B. Cabrera, M. Taber, R. Gardner and J. Bourg, Phys. Rev. Lett. 51, 1933 (1983), and B. Cabrera, R. Gardner and R. King, Phys. Rev. D31, 2199 (1985).

[2] R. Gardner, B. Cabrera, M. Taber and M. Huber, in preparation for Phys. Rev. D.

[3] B. Cabrera, Phys. Rev. Lett. 48, 1378 (1982).

[4] R. Gardner, B. Cabrera, M. Taber and M. Huber, LT-17, U. Eckem, A. Schmid, W. Weber and H. Wuhl (eds.), (Elsevier Science Publishers B.V., 1984).

[5] J. Incandela, M. Campbell, H. Frisch, S. Somalwar, M. Kuchnir and H. Gustafson, Phys. Rev. Lett. 53, 2067 (1984).

[6] S. Berman, P. Chaudhari, C. C. Chi, C. D. Tesche, and C. C. Tsuei, Phys. Rev. Lett. 55, 1850 (1985).

[7] A. D. Caplin, C. N. Guy, M. Hardiman, J. G. Park, and J. C. Schouten, Nature 317, 234 (1985).

[8] M. W. Cramar, A. F. Clark, and F. R. Fickett, preprint.

[9] S. H. Moseley, J. C. Mather and D. McCammon, J. Appl. Phys. 56, 1257 (1984); D. McCammon, S. H. Moseley, J. C. Mather and R. F. Mushotzky, J. Appl. Phys. 56, 1263 (1984).

[10] B. Cabrera, L. Krauss and F. Wilzcek, Phys. Rev. Lett. 55, 25 (1985).

[11] B. Cabrera, J. Martoff and B. Neuhauser, Stanford Preprint No. BC44-86.

[12] See for example, Nonequilibrium Phonon Dynamics, ed. W. E. Bron, NATO ASI Series B124, Plenum Press, N.Y., 1985. An excellent review of recent developments in phonon physics.

[13] D. Twerenbold, preprint.

THE NEUTRINO MASS FROM BETA SPECTRUM (ITEP-85)

Valentin Lubimov
Institute of Theoretical
and
Experimental Physics
Moscow,USSR



ABSTRACT

The new cycle of tritium beta spectrum measurements in valine with the ITEP spectrometer is discussed (ITEP-85). The detailed investigation of the total response function (TRF) has been performed. The special run of beta spectrum measurements carried out in a wide energy interval (3.4 KeV) has turned out to be a sensitive mode for the TRF experimental test. The results confirm the indication of the neutrino nonzero mass.

I. INTRODUCTION

This paper is the further development of the known investigation on the neutrino mass in beta-decay [1-3]. The results of a new series of measurements (ITEP-85) and the analysis of the beta-spectrum of tritium in a valine molecule are presented. The new cycle of measurements was carried out by the authors: S.Boris, A.Golutvin, L.Laptin, V.Lubimov, N.Myasoedov, V.Nagovizin, V.Nozik, E.Novikov, V.Soloshenko, I.Tihomirov, E.Tretjakov. The magneto-electrostatic spectrometer is described in [2]. We note that the beta-spectrum is scanned by electrostatic field variation while the focusing magnetic field was kept constant, i.e. the value of electron energy registered by the detector was fixed. This method of measurement has two considerable advantages:

I) The shape of the observed spectrum is virtually unaffected by the detector efficiency, which gives the possibility to widen the range of measurements. In the given cycle it amounts to 3.4 KeV.

2) There is a possibility to get rid of the main background component caused by the tritium contamination of the spectrometer parts. In the given set of measurements the electrons at the energy 2I.2 KeV. were focused by the magnetic system, which exceeds the electron energy limit of the tritium spectrum.

A proportional chamber with six channels is used as a detector. The measurements are taken with a nonequipotentional source, yielding a continuous focusing potential secured by the backing made of weakly conducting glass. We call such a source "pointlike", since, though the electrons from the entire source surface are focused on a point of the detector focal plane, they are actually emitted from different geometrical points. In this respect the resolution function of the pointlike source differs from the ideal one such as an electron gun. The measurements of the resolution function for 6 channels carried out with the electron gun, generating a narrow monochromatic beam of electrons, passing through the torodial magnetic system not touching the coils are shown in Fig.I. In this case the shape of the line is practically determined by the detector entrance slits alone. The employment of the pointlike source as well as the multichannel detector makes it possible to use the whole available focal plane of the spectrometer to the full. In this way we reached the 20 eV resolution by narrowing the entrance slit and regained intensity by

increasing the number of channels. With the improved resolution we can explore the "mass-sensitive" 25 MeV end portion of the spectrum where the effect and background contributions are nearly equal. The spectrometer calibration was carried out with 29 conversion lines of different gamma-transitions of ^{169}Tm. The calibration coefficients are determined from the energy balance for a conversion electron, the transition energies being known with high precision (not employing the data on electron shell binding energy for ^{169}Tm). From this equations we extracted the differences of binding energies for different shells, they are in good agreement with [4], except for those involving the shell M_3. We estimate the accuracy of the calibration measurements as 5 eV. As before, for the evaluation of the neutrino mass and the end-point energy we used the data fitting procedure employing the model spectrum:

$$
\begin{aligned}
&N^{th}(E)=A\cdot S(E);\\
&S(E)=\int dE' R(E,E')\left[1+\alpha_1(E'-E_0)\right]\left[1+\alpha_s(E'-E_0)^2\right]\\
&\qquad \sum_K W_k f_k(E',M_\nu,E_0);\\
&f_k(E',M_\nu,E_0)=PE_t F(E')(E_0-E_k-E')\left[(E_0-E_k-E')^2-M_\nu^2\right]^{1/2};
\end{aligned}
\qquad (I)
$$

The ITEP-85 investigation was aimed at thorough experimental analysis of the resolution function, involving its optical component and the component determined by the ionization losses in the source. The beta-spectrum measurements performed in a widened energy range are sensitive to the long tails of the function R, as well as to the possible heavy neutrino admixture in the mass below 3 KeV.

II. SPECTROMETER APPARATUS FUNCTIONS

The overall resolution function of the spectrometer is a sum of noninteracting electron spectrum, i.e. the optical resolution function, and its convolution with the ionization loss spectrum, caused by the interaction of the initially monochromatic electrons with the source material (including the spectrum of backward scattering from the backing).

In our analysis, we used the spectrum of conversion electrons of K, L, and M - the lines of different transitions in ^{169}Tm(Yb)

at E=20.7, 63.I, I09.8, I97.9 KeV. The intrinsic widths of these lines were measured by us earlier: $\Gamma(L_I)$=5.2eV, $\Gamma(M_I)$=I4.7 eV, Γ(K)=32 eV.

The collected data are in good agreement with that obtained recently [3]. The broadening of the conversion lines, caused by this effect, was removed by solving the inverse problem for the folding equation.

II.I. Ionization losses in the working source

The procedure we have developed requires measurements of several parameters to determine a mean spectrum of ionization losses in a homogeneously distributed source (the working source).

Let M(E',E) be the known line shape of a test source (the measured shape of the electron conversion line). We cover this test source with a thin layer ΔT of working substance (valine) and determine the line shape $M_{\Delta T}(E',E)$ of this layered source. Deconvoluting $M_{\Delta T}(E',E)$ related to M(E',E) we get the ionization loss spectrum $\varphi_I(E',E,\Delta T)$ of electrons passing through the working substance with thickness ΔT at energy E. This spectrum contains some particles with the probability $W_o=e^{-\Delta T}$ and ionization losses spectrum (ILS) itself. So, we can determine: I) the thickness of the layer ΔT expressed in the lenght of the free run: $\Delta T=\ln(I/W_o)$; 2) the shape of ILS. It is easy to see that $\varphi_k(E',E,K\Delta T)$ the spectrum resulting from the interaction of electrons with the layer of thickness $K\Delta T$ is a K-fold convolution of the primary spectrum $\varphi_I(E',E)$:

$$\varphi_k(E',E)=\varphi_I(E',E)^{(k)}$$

(The designations $\otimes$; $\overset{(k)}{\odot}$ denote the convolution and deconvolution procedure correspondingly).

Ionization losses spectra for three primary sources of different thickness are shown in Fig.2 - a,b,c. In addition the values W_o and ΔT for these sources are given. With the above described method we can reconstruct the desired ILS of thick sources from the thin one by the convolution procedure. The reconstructed and experimental spectra were compared and were found to be in good agreement. Fig.3 shows their comparison that proves the reliability of the procedure.

And finally the spectrum of the sources homogeneously distribu-

ted in the substance (the working source) with the thickness T can be represented as

$$\varphi_{work.s.}(E',E,T)=\frac{\Delta T}{T}\sum_{k=1}^{T/\Delta T}\varphi_k(E',E) \qquad (2)$$

Now the value $T/\Delta T$ remains to be determined for the estimation of the Ionization loss spectrum of the working source. For this purpose the spectrum analogous to that described above but with the working substance of tritiated valine is measured. This spectrum can be represented as a sum of the beta-spectrum which intensity depends on the valine thickness and the electron conversion line (M_I) spectrum the shape of which as mentioned above enables us to estimate the layer thickness (ΔT). The beta- and conversion line spectra can be separated by the fit procedure (Fig.4). From the ratio of intensities of the beta-spectra of the working and test sources is it possible to find the ratio of thicknesses: $T/\Delta T$. Fig.2 shows the ionization losses spectrum for the working source calculated from formula (2). The indexes d, e, and f indicate the spectra obtained from the three primary sources with the indexes a, b and c correspondingly. The histograms of the spectra and the corresponding values $T/\Delta T$ are given in the table.

	$T/\Delta T$ \ ΔE	0-25	25-50	50-75	75--100	100--150	150--200	200--250	250--∞
ILS-1	2.55	0.151	0.274	0.195	0.135	0.146	0.066	0.023	0.010
ILS-2	4.12	0.168	0.273	0.196	0.117	0.135	0.066	0.025	0.020
ILS-3	17.25	0.096	0.250	0.189	0.126	0.171	0.086	0.047	0.035

II.2. The optical resolution function

The optical resolution function (O.L.) could be studied with the help of the electron gun. The advantage of this source lies in its monochromaticity. But its disadvantage non-equivalence to the working source (backing, geometry, angular distribution, focusing conditions) is not compensated by monochromaticity. For the O.L. determination we used spectra of conversion lines. The test source of conversion electrons is completely equivalent to the working

one (geometry, focusing conditions, angular distribution). But the electron conversion line is not monochromatic. It comprises the intrinsic width (we've already discussed it), the spectrum of final states which arises from the conversion of an electron ("shake off" effect) and, finally, the ionization losses in the Yb layer. All these distortions should be taken into account. The Yb layer in the test source was vary thin. Thus the ionization losses effect was insignificant. This has been shown in experiments with sources of different thickness. The "shake off" effect doesn't depend on thickness. It should be determined and excluded from the conversion line spectrum. In principal there are some theoretical calculations of this effect [6] but we obtained it experimentally by using the measurements of conversion lines in the energy range IO-I50 KeV. The analysis is based on the assumption that each line can be represented as a combination of two components:

I) the monoenergetic line which has a constant shape in the relative scale (constancy $\Delta p/p$ for a magnetic spectrometer).

2) the "shake-off" spectrum that is constant in the absolute energy scale.

The intensity of the lines in the "shake-off" spectrum given as the model parameters, it is possible to determine this spectrum and the optical resolution function by fitting several lines simultaneously. The measured spectra K(E =I97.9 KeV), L_I(E =63.IKeV) and M_I(E =20.7 KeV) and the optical resolution function, obtained by the indicated procedure in the relative energy scale are shown in Fig.5. It can be seen that the optical resolution function has the residual asymmetry which can be explained as one caused by the optical properties of the spectrometer. It can be seen from Fig.5. that the higher is the energy of the line, the more insignificant is the correction arising from the "shake-off" spectrum. That is why in the present study the K-line served as basic for the O.L. determination. Fig.6. presents the optical resolution functions for three detector channels. They differ a little in their "trunks" but the tail at a distance more than 50 eV from the maximum acquires a universal character. Its area shaded in Fig.6 amounts to 6,4% (note that in the ITEP-84 data processing the "shake-off" spectrum was determined from the energy range IO-60 KeV and the M_I line served as basic. The tail contribution

was I0.I% of the O.L.).

The O.L. measurement was also carried out in the direct experiment free from any assumptions of the "shake off" behaviour. The shape of the L_I line (E_c - I0.6 KeV)(the intrinsic width L_I = = 5.2 eV is minimal) from rather thick source (to enhance intensity) was thoroughly measured in the accelerating field with the focusing energy E = 2I.2 KeV corresponding to the working cycle of measurements. The line obtained under these conditions is the fold of the sought optical line which corresponds to the working conditions: O.L.(2I.2) with ILS in Yb, with the "shake off" spectrum and a Lorentzian with Γ = 5.2 eV:

$$L_I(2I.2) = O.L.(2I.2) \otimes I.L.S. \otimes "S - O" \otimes \Gamma$$

Then the same line was measured with "deceleration" at E =2KeV:

$$L_I(2) = O.L.(2) \otimes I.L.S. \otimes "S - O" \otimes \Gamma$$

When passing from "accelaration" to "deceleration" ILS, "shake off" and Γ remain unchangeable while O.L. getting narrower by an order of magnitude turning into the δ-function.

Thus, (see Fig.7) we get the sought optical resolution function involving the deconvolution procedure:

$$L_I(2I.2) \odot L_I(2) = O.L.(2I.2) \odot O.L.(2) \simeq O.L.(2I.2)$$

(In reality this problem was solved without the above mentioned approximations made for simplicity).

The contribution of the tail in the O.L. obtained in this way is the intermediate in magnitude (9.3%). In the subsequent analysis we used the O.L. with the minimal tail contribution 6.4% and the spread resulting from different ways of the O.L. determination and particularly the analysis results with the optical resolution function without " a tail ", all this was taken into account in terms of systematic errors.

II.3 Backward scattering and the spectrum "curvature"

Though the complete value of backward scattering is rather high (30%), its differential ampletude is comparable with the back-

ground.

The effect of backward scattering on the backing was studied by comparing base differences of the low and high energy sides of the conversion line peak. It was found that on the low energy side the spectrum was constant from -400 eV down to -2500 eV. The fact that the magnitude of backward scattering is conditioned by the difference of the base hights has been checked in a special experiment using extremely thin backing (4μg/cm of organic). It should be also mentioned that a twofold variation of the BSS is "absorbed" by the fitted values of α_L and α_S without substantial effects on M_V and E_O.

The total resolution function (TRF) is shown in Fig.8.

III. MEASUREMENTS. RESULTS. DISCUSSIONS.

III.I. Single mass fit

The scan of the experimental beta-spectrum was made in two runs. The first one was "standard": 4I points in 50 eV steps (A) and 6I points in 5 eV steps (B), exposition time being I00 sec and 300 sec. at each point correspondingly. On the whole the first run contained 34 series of double (A-B) measurements and covered the interval I7 KeV of the beta-spectrum. The second run: 75px50eVx 200sec contained I4 series and covered the interval 3.4 KeV. The total statistics 55K/I00 eV at the end point energy.

The shorter is the fitting interval from the end of the beta-spectrum the more insignificant is the influence of the total resolution shape on the value of the obtained parameters including those of physical significance such as M_V and E_O. Really, the parameter values don't depend at all on the TRF shape beyond the limits of the fitting interval. On the contrary, the wider is the fitting interval the stronger is the dependence of the parameters on the TRF form. Only when there is a complete adequacy of the TRF to the experimental spectrum the fitting parameters have to be independent on the width of the fitting interval. The broadening of the beta-spectrum range of measurements up to 3.4 KeV made in the present work, appeared to be extremely sensitive mode for choosing the right shape of the TRF. Thus, choosing the shortest fitting interval (so far as statistics makes it possible) we get the physical parameters (M_V and E_O) with the smallest systematic errors

resulting from uncertainty in the O.L. form. At the same time the widest fitting interval serves to test the adequacy of the TRF.

Table I gives the results of the fit of the experimental beta-spectra in the intervals 3.4 KeV (the second run), I.68 KeV and 330 eV (the first run) for different spectra of ionization losses (ILS) in the working source obtained from three test sources, covered with valine of different thickness (I/I7, I/4, I/2.5 from the layer thickness of the working source).

As it can be seen from the table, the obtained parameters M_ν and E_o in the intervals I680 and particularly 330 are stable with regard to the form ILS (parameters variations of the order of statistical errors; for ILS-I and ILS-2 the parameters practically coincide). At the same time the interval 3.4 KeV shows that only ILS-I can be considered as adequate to the experimental spectrum and ILS-2 together with ILS-3 must be rejected.

Let us pass on to the influence of the optical line shape (O.L.). Now consider the optical line admissible symmetrisation (so far as its individual peculiarities allow in some detector channels). For this purpose, the "tail" of the optical line similar for all the channels has to be rejected as shown in Fig.6.

Given in the same table are the results of the fit. The spectrum ILS-2 only is acceptable. The values of the parameters M_ν and E_o for the interval 330 differ (in the hypothesis: "with a tail" and "without a tail") within their statistical errors.

The variation of the working source thickness displays an analogous behaviour:

		3400	I680	330
$\delta\frac{T}{T} = I0\%$	δM_ν^2	422	I36	86
	δE_o	3,2	I,8	I,4

All these examples show that requirements for the parameters independence on the width of the fitting interval and their high sensivity to different variations lead to considerable restrictions on the magnitude of the acceptable variations O.L., ILS, $\Delta T/T$ and so on. The statistical errors of the parameters M_ν^2 and particularly E_o in the interval 3400 eV being 400 eV^2 and I eV, the systematic errors for M_ν^2 due to the above mentioned variations

do not exceed 100 and 60 eV^2 in the intervals 1680 and 330 eV.

Shown in Fig.9 are the experimental and fitted (O.L. with "a tail"; ILS-I) spectra in the range of measurements 1680 eV (run I). The statistics was summed up over all the detector channels and all the runs at each point. The curve with the fitted parameters and at M=0 is taken for the zero line. The values normalized to the standard statistical error are plotted along the ordinate axis.

Having at our disposal the combination: O.L. - with "a tail" and ILS-I we recalculated the experimental spectra of the previous runs: ITEP-84 (Leiptzig[1]). The results are given in Table 2.

The results of the ITEP-84 investigation are in a reasonable agreement with those given in the present work (ITEP-85). The results of the joint data fit (ITEP-84 and ITEP-85) are given in Table 3. The fit of data with the neutrino mass set to zero is also presented in the table). The shape of the curve at M=0 doesn't describe the experimental spectrum in any of the fit intervals, which can be seen from the table. All the given results relate to the spectrum of final states (SFS) for tritium in a valine molecule. This spectrum was calculated by Kaplan et al [7]. The mass difference of the neutral atoms of tritium and gelium can be calculated from the fitted value of the parameter E_o, employing the data [7]. The obtained from E_o value ΔM_{T-He} = 18600.8 ± 5 is in an excellent agreement with the mass measurements of the doublet T-He carried out by Lipmaa et al [8] with the ICR-spectrometer:
ΔM_{T-He} = 18599 ± 2

It is common knowledge that the parameters M_ν and E_o depend on the adopted spectrum of final states (i.e. are model-dependent). Thus, for instance, for an extreme case when the spectrum of final states is represented as the δ-function (the bare nucleus decay), the fitted value of E_o is reduced by 18 eV and becomes incompatible with the Lipmaa data. The limits of the SFS variation agreeble to the Lipmaa data (with the error taken into account in our absolute calibration) lead to the interval:

$$17 < M_\nu < 40 \text{ eV}$$

And now a few remarks about Bergkvist criticism [9] of our results which has become widely known recently. Bergkvist makes essentially two statements:

I) The spectrometer resolution function measured with the gun in

his experiment gives "a symmetric" line (without "a tail"), at the same time the conversion line shape is asymmetric with a long "tail". But it is a symmetric line that must be used in the analysis.

As to this statement it is not new for us. The analysis with a symmetric O.L. (at least as an extreme variant) was under our consideration in Brighton and Leiptzig [3] and was discussed at the Leiptzig conference (summer I984) about a year before Bergkvist's publications. In the present work this problem doesn't exist at all, since the possibility of data fitting in the interval 3400 eV makes it possible to choose the optical resolution function as well as ILS adequate to the experimental beta-spectrum. This is true for ITEP-85 results as well as the reanalysed ITEP-84 data.

2) Bergkvist tries to evaluate the change of the mass parameter with the O.L. (with "a tail") being replaced by the symmetric O.L. To do this he proposes the following formula:

$$\Delta M_\nu^2 = 2\sigma^2_{trunc} \qquad (\text{at } E_{tr} \text{ I50 eV}) \qquad (3)$$

and draws the conclusion that ITEP-84 data are overestimated by

$$\Delta M_\nu^2 = 1400 \pm 200 \text{ eV}^2$$

i.e. compatible with $M_\nu = 0$.

This is a false statement since formula (3) is mathematically unfounded and is not correct at all. We have already seen that the value M_ν at the O.L. variation depends on the range of the fitting interval. Thus the erroneousness of the formula (3) is out of the question. Everyone can make sure of this by turning to the Monte Carlo procedure. As to the real change of ΔM^2 it, as it has been shown above, is $\sim$I00 eV^2 for the fitting interval 330 eV.

III.2. Two masses fit

Strictly speaking, single mass fit gives the effective value of the mass parameter only. The single mass description of the experimental spectrum in the interval ΔE = 3.4 KeV isn't quite satisfactory: X^2 = 5I0/472 (See Table 3). The situation radically changes for the better with the two mass description:

$$M_I^2 = 8I0 \pm 50 \; ; \quad E_o = I8580.5 \pm 0.2; \quad \mathcal{A}_L = -(0.39 \pm 0.I2)I0^{-5};$$

$\alpha_s=(0.32\pm0.02)10^{-8}$; $N=1.0077\pm.0016$; $M_2=(1045\pm25)$ eV

with admixture $P_2=(0.72\pm0.11)\%$; $X^2=475.6/470$

In this case the "wave" which can be seen in Fig. 9 disappears. The limits to the possible heavy neutrino admixture obtained in two masses fit of the beta-spectrum in the interval from 100 to 3000 eV are shown in Fig.10. The peculiarity (See Fig.10) appearing in the region $M_x\sim1000$ eV is reflected in the ITEP-84 data as well as in the ITEP-85 measurements (being quite independent). The nature of this fenomenon hasn't yet been studied well enough. If it is interpreted as an indication of a heavy neutrino then one should expect it in the region 800 ÷ 1200 eV with admixture 0.4 ÷ 1%. Given in Fig.10 also are the limits in the interval 5 - 85 KeV obtained by us in [10] in the beta-spectrum investigation ^{35}S. These data disproved the "Simpson neutrino" [11] with $M_\nu=17.1$ KeV and contribution ~3%.

In conclusion I would like to thank my collegues S.Boris, A.Golutvin and V.Nozik for their help with the report.

REFERENCES

I. V.A. Lubimov et al., Phys.Lett. I980, v.94B, p.266.

2. S. Boris et al., HEP83, Intern. Europhysics Conf. on High energy physics (Brighton I983), p.386.

3. S. Boris et al., Proc. XXII Intern. Conf. on High energy physics (Leipzig I984) Vol.I, p.259; Phys.Lett. I985, v.I59B, p.2I7.

4. K. Sevier, ADNDT v.24, p.323, I979.

5. C.L. Bennet et al., Phys.Rev. I985, v.3IC, p.I97.

6. M. Voloshin, P.Silvestrov, preprint INP-85-70.

7. I. Kaplan et al., DAN USSR I984, v.279, p.III0.

8. E. Lipmaa et al., Phys.Rev.Lett. I985, v.54, p.285.

9. K.E. Bergkvist, Phys.Lett. I985, v.I54B, p.224; K.E. Bergkvist, Phys.Lett. I985, v.I59B, p.408.

I0. A. Apalikov et al., preprint ITEP-II4, I985.

II. J.J. Simpson, Phys.Rev.Lett. I985, v.54, p.II58.

Table I

		Standard O.L. (tail ~ 6.2%)		
	ΔE	3000	I680	330
ILS I	M_y^2	I0I2±409	875±I09	673±I22
	E_0-I8500	8I.9±0.9	82.3±0.6	80.7±.8
	d_L xI0^5	-5.7±0.2	-3.5±0.9	-
	d_S xI0^8	0.I5±0.02	0.9±0.3	-
	N	4806±I6	4866±33	4948±43
	χ^2	426/372	3II/30I	I70/I93
ILS 2	M_y^2	I639±434	896±I05	677±I25
	E_0-I8500	84.4±0.9	82.2±0.7	80.5±0.8
	d_L xI0^5	-5.5±0.2	-I.6±0.9	-
	d_S xI0^8	0.I7±0.02	I.4±0.3	-
	N	4825±I6	4965±34	5070±44
	χ^2	424/372	3I6/30I	I70/I93
ILS 3	M_y^2	2245±260	II43±I30	685±III
	E_0-I8500	87.5±0.8	83.7±0.7	80.5±0.8
	d_L xI0^5	-5.4±0.2	-0.4±0.9	-
	d_S xI0^8	0.I8±0.02	I.8±0.4	-
	N	4833±I5	5026±37	5I93±0.8
	χ^2	422/372	332/30I	I72/I92
		O.L. without a tail		
ILS 2	M_y^2	896±390	7II±II2	560±I33
	E_0-I8500	80.2±0.8	80.3±0.7	79.I±0.9
	d_L xI0^5	-5.8±0.2	-3.5±0.9	-
	d_S xI0^8	0.I3±0.02	0.9±0.3	-
	N	4796±I5	4859±33	4936±45
	χ^2	43I/372	330/30I	I68/I93

Table 2

Standard O.L.; ILS-I; valine

ΔE		I680		330	
ITEP	T	M_V	E_0-I8500	M_V	E_0-I8500
85	I.98	875±I09(200)	82.3±0.6(2)	673±I22(I60)	80.7±0.8(I.6)
84	2.I0	990±I93(I80)	8I.3±I.I(2)	965±260(I30)	8I.2±I.4(I.5)
	2.27	I088±I06(I90)	8I.6±0.6(2)	I094±I52(I40)	8I.6±0.6(I.5)
	2.82	989±I00(200)	82.7±0.6(2)	773±98(I80)	80.9±0.8(I.7)
average		970±(I80)	82.0±(I.8)	870±(I30)	8I.0±(I.4)

M_V= 30.I±(2); E_0= I858I.3±(6)*

*) The absolute calibration error included. The sistematic errors are shown in braks. The total statistics: I30 K/I00 eV

Table 3

ΔE	3400	I680	330
M_v	984±50	966±50	852±66
E_o	8I.7±0.2	8I.5±0.2	80.7±0.4
α_l xI0^5	-I.65±0.I2	-I.60±0.I0	Fix
α_s xI0^8	0.I3±0.02	Fix	Fix
N	0.9896±0.00I6	0.9907±0.00I4	0.999I±0.0039
χ^2	5I0/472	429/407	265/247
$M_v = 0$			
E_o	77.I±0.I	77.0±0.I	74.7±0.2
α_l xI0^5	-0.06±0.I0	-0.00±0.08	Fix
α_s xI0^8	0.35±0.02	Fix	Fix
N	I.0I39±0.00I2	I.0I44±0.00I0	I.0529±0.0024
χ^2	II65/473	I032/408	475/248

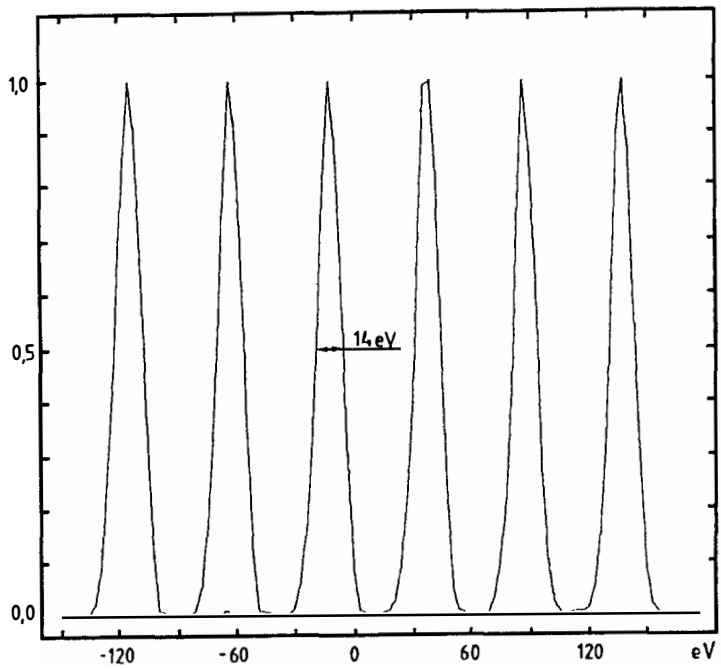


FIG.I. The shape of the spectrometer O.L. for an electron gun in six detector channels (an ideal onepoint source).

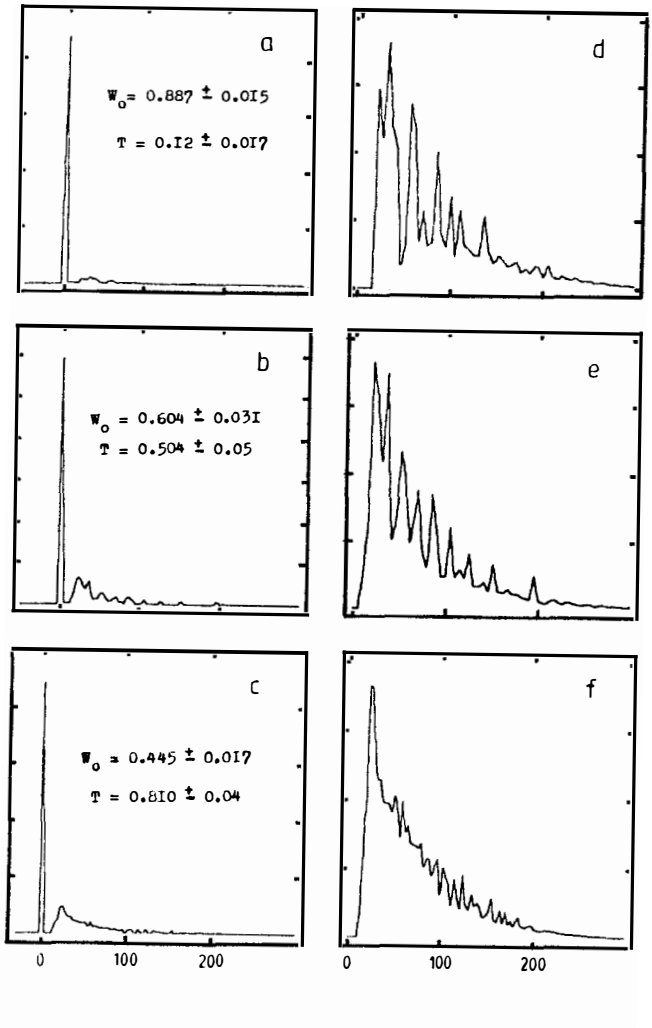
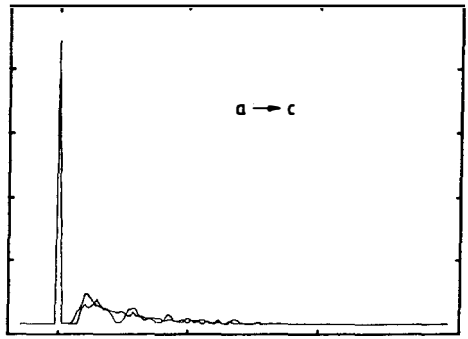


FIG.2. a,b,c - the spectra of ionization losses for three test valine sources of different thickness. The values W_o and T are indicated for each source (see the paper). d,e,f - the spectra of ionization losses for the working source obtained independently from three test sources a,b,c.



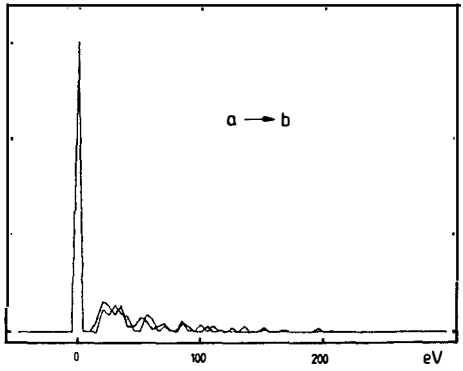


FIG. 3 : The spectra of ionization losses for sources with T corresponding to "b" and "c" reconstructed from the test source "a" in comparison with the measured "b" and "c".

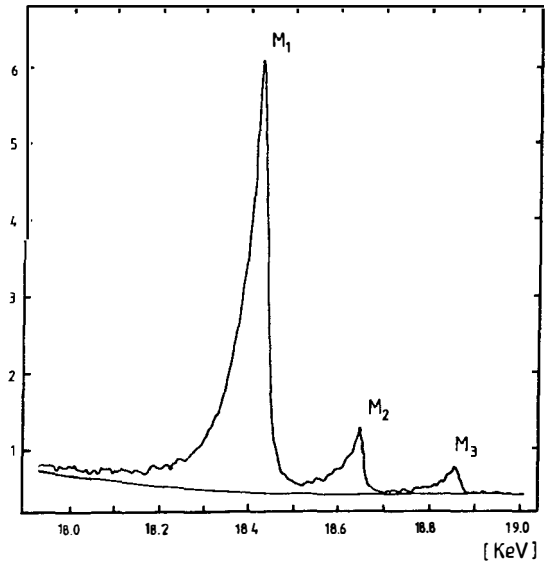


FIG. 4 : The transition spectrum of the M_1 lines passed through the layer of tritiated valine.

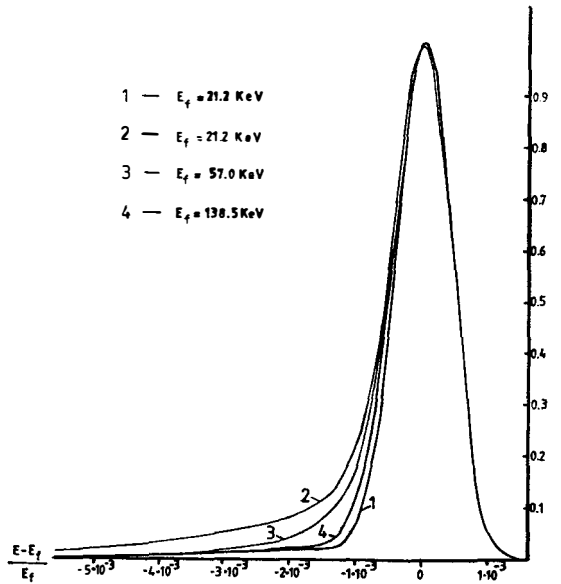


FIG. 5 : The spectra of experimental lines and the O. L. after the subtraction of the "shake off" contribution in the third channel.
I. O.L.
2. $M_I(E_k = 18.4)$
3. $L_I(E_k = 53.0)$
4. $K(E_k = 138.5)$

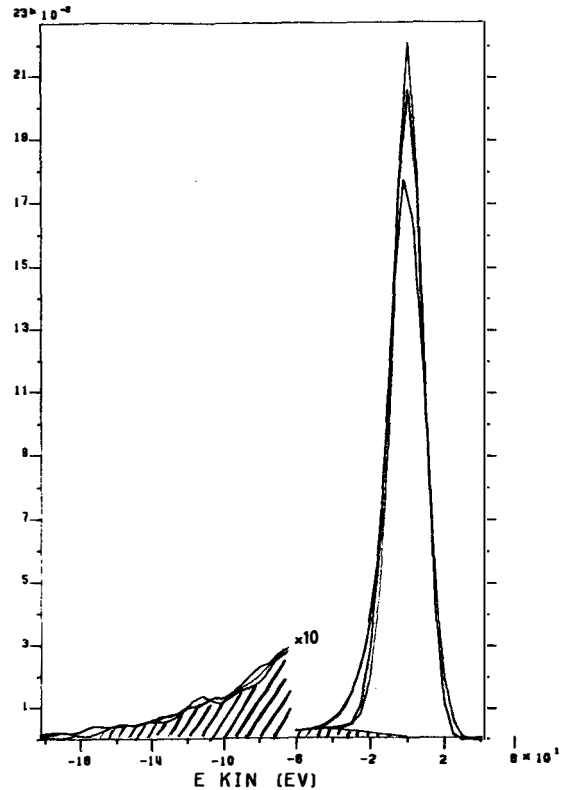


FIG. 6 : The O. L. in I, 3 and 6 channels. The shaded area indicates the "subtracted tail".

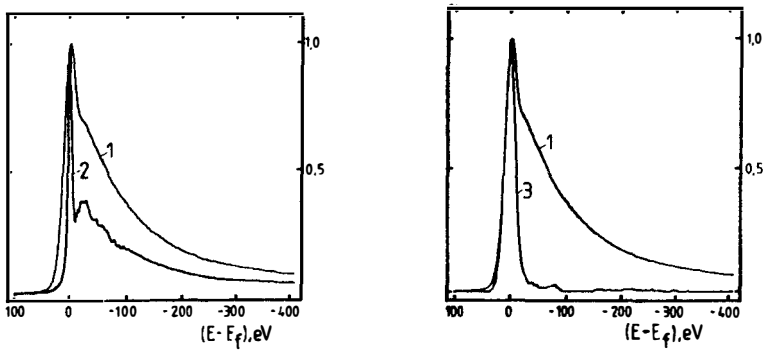


FIG. 7 :The O. L. determination in the direct experiment.
1 - $L_I(2I.2)$
2 - $L_I(2)$
3 - O.L.

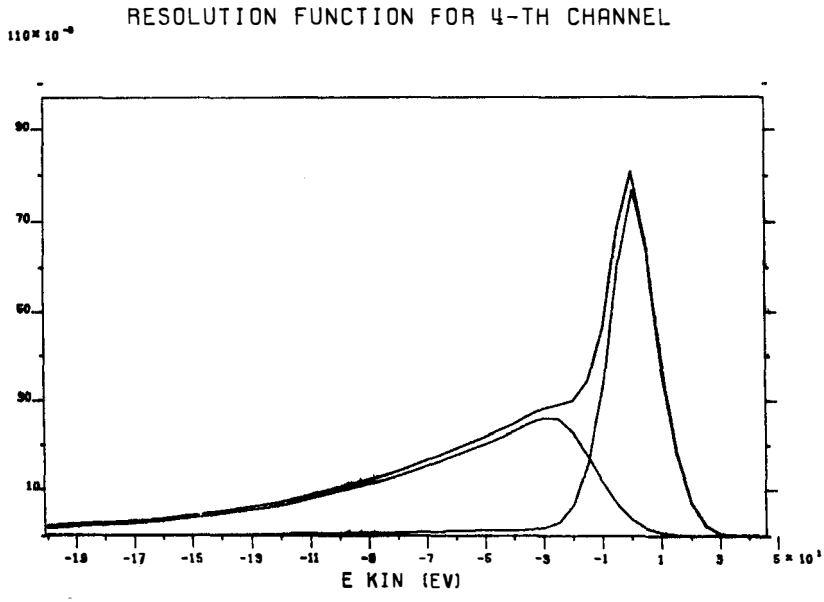


FIG. 8 : The total resolution function (TRF) for the working source. The contributions of the O. L. and ILS are shown.

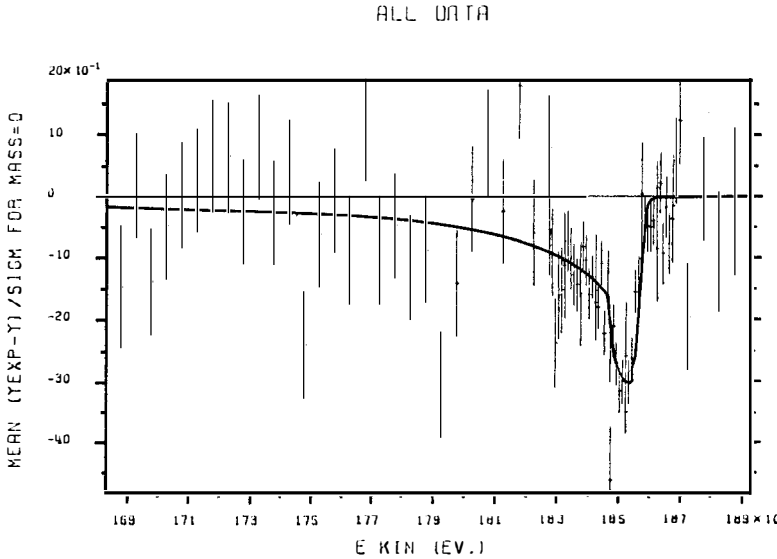


FIG.9. The difference between the experimental data (and the result of the overall fit - the solid curve) and theoretical dependence at M=0 normalized to the experimental errors.

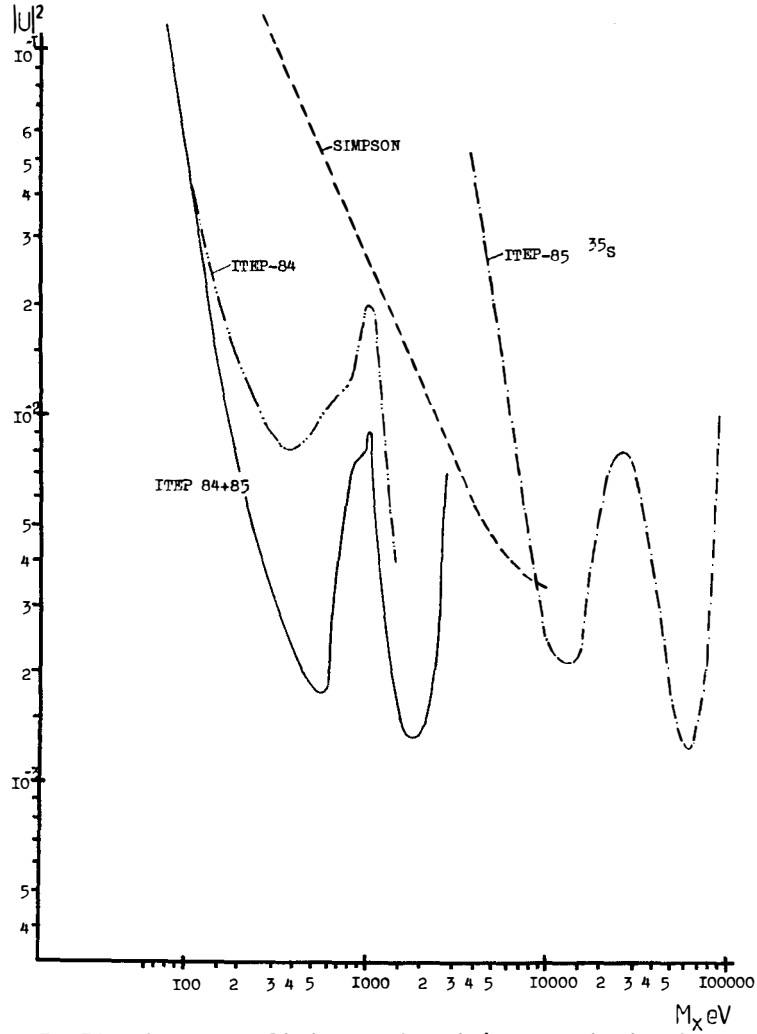


FIG.10. The upper limit to the mixing matrix in the two neutrino model.
Simpson data [11] - the dashed line.
ITEP-84 - the two point dash line.
ITEP-84 and ITEP-85 data (the beta decay of tritium) - - the solid line.
ITEP-85 data (the beta decay of ^{35}S [10]) - the point dash line.

SOME NOTES ON A MATTER OF CONTROVERSY REGARDING THE ITEP CLAIMS OF EVIDENCE OF FINITE NEUTRINO MASS

Karl E. Bergkvist
Research Institute of Physics
S-104 05 Stockholm, Sweden



ABSTRACT

We have earlier remarked that a lack of proper handling of the particle optical response function seems to make a consistent claim of evidence of finite neutrino mass untenable on the basis of the material presented in ITEP-83 and ITEP-84. Our arguments on this point are strongly rejected by V.A. Lubimov in his talk at this workshop. The purpose of the present note is to point at the fact that the basis for our conclusion referred to concerning ITEP-83 and ITEP-84 is actually implicitly essentially fully confirmed by ITEP information issued after our first remarks on the issue. A resulting incompatibility between ITEP-84 and the latest ITEP claim of finite neutrino mass as delivered at this workshop is pointed at.

Based on findings gained in the preparation of a new tritium neutrino mass experiment in Stockholm[1] we have issued some remarks questioning the basis for the earlier claims of evidence of finite neutrino mass as reported by V.A. Lubimov and co-workers. Initially[2] motivated by ITEP-83 (Brighton)[3], our discussion was subsequently[4] applied to ITEP-84 as described[5] in the proceedings of the Leipzig HEP conference, with still some further comments of ours[6] stimulated by the later, more detailed account[7] of ITEP-84. Throughout, our main points concern the handling of the problem of the particle optical response function in the ITEP papers quoted; in our view the finite neutrino mass effect so far reported from ITEP has seemed quite possible to attribute to erroneous assumptions as regards this function. Reported by V.A. Lubimov at this workshop is further neutrino mass experimental work at ITEP[8], sustaining a claim of evidence of finite mass. In his talk[8] V.A. Lubimov also levels very strong criticism indeed on the relevance of our questioning[2,4] of the earlier ITEP claims of finite neutrino mass. Since, actually, our anticipated effects are confirmed by information supplied by the ITEP group itself, there is a striking situation of self-contradiction here which, we feel, warrants some immediate comments.

To be specific we consider our questioning[4] of the basis for a claim of evidence of finite neutrino mass in ITEP-84[5]. Our analysis in Ref. 4 concerns the long-range (1680 eV) data fits, the short range (330 eV) fits being less readily accessible for discussion by an external viewer. Our conclusion that a claim of finite mass based on the long-range fit is not justified is arrived at in two steps: an earlier experimental observation[2] implying that the intrinsic shape of the ITEP-84 reference line departs from the shape assumed in the analysis[5], and a rough analytical estimate[2] — reasonably valid for long-range fits — that the resulting effect on an inferred value of M_ν^2 is readily large enough to endanger the finite mass effect reported in the ITEP-84[5] long-range fits. Accordingly we noted[4] that further arguments are needed to support a consistent claim of evidence of finite neutrino mass from ITEP-84[5].

Actually, we can now see:

(i) Our experimental findings[2] on the intrinsic shape of the ITEP-84 reference line are in essence confirmed by the ITEP studies of K, L and M lines in the energy range E_f = 21–138 keV reported by Lubimov in his talk[8] at this workshop — cf. relevant figure in Ref. 8. Even assuming the low energy tail of the K line shown to be particle optics alone,

the exhibited M_I profile satisfactorily accommodates* and accounts for the truncated mean square energy spread of some (800 ± 200) eV^2 ascribed to shake-up effects in our work[2]. Allowing for such a spread in the ITEP-84[5] reference line essentially means that what is denoted the symmetrized optical line should be employed in a correct analysis of data in this work.

(ii) Our crude estimate in Ref. 4 indicated that the fitted value of M_ν^2 in ITEP-84[5] should be expected to go down by some (1400 ± 400) eV^2 when changing to the symmetric optical line in the long-range fits in this work. Actually, as told in the later version[7] of ITEP-84, the reduction experienced is about 1100 eV^2, from 1215 eV^2 to 140 eV^2, the latter figure stemming from a quoted result $M_\nu = 12 \pm 3$ eV on page 221 in Ref. 7. The reduction in M_ν^2 actually found clearly is in satisfactory agreement with our prediction.

The reduction of the ITEP-84 value of M_ν^2 from the long-range fits by almost an order of magnitude when properly adjusting the particle optical response function clearly amounts to making the claim of evidence of finite neutrino mass as issued in ITEP-84 lack consistency. Having our anticipation[4] on this score confirmed by results delivered by the ITEP team itself, we find it somewhat difficult to understand the complete rejection[8] of our questioning[2,4] from this party at the present workshop.

As to the latest, ITEP-85, claim of finite neutrino mass, presented at this workshop[8], we first note that our anticipated reduction in inferred values of M_ν^2 in Refs. 2 and 4 when going to a symmetrized particle optical response function in ITEP-83 and ITEP-84 does not apply to ITEP-85, since the asymmetry tail — in terms of our analysis in Refs. 2 and 4 — contributes a much smaller mean square spread in the ITEP-85 particle optical response function. Further to be noted in ITEP-85 is an increase from one to two free (fitted) spectrum shape parameters. Observing this, it is not incompatible with our type of analysis in Ref. 2 that removing the tail in the particle optical response function in ITEP-85 makes a much smaller change in M_ν^2. Striking now is, however, that ITEP-84 — as originally[5,7] issued — and ITEP-85 are not really compatible as basis for a claim of finite neutrino mass when proper response functions are used in either case. A convincingly large value $M_\nu^2 \approx 700$ eV^2 is reported in ITEP-85 for the 1680 eV range fits for a symmetrized optical response function,

---

* A certain extrapolation of the M_I tail in Ref. 8 towards lower energies is needed to cover the full truncation interval used in Ref. 2.

compared with the corresponding almost vanishing $M_\nu^2 \approx 140\ eV^2$ told in Ref. 7 to emerge in ITEP-84 with such an assumption.

REFERENCES

1. K.E. Bergkvist, Proc. Fourth Moriond Workshop on Massive Neutrinos in Particle Physics and Astrophysics, p. 243. (Editions Frontières, Paris, 1984)
2. K.E. Bergkvist, Phys. Lett. **154B**, 224 (1985)
3. S. Boris et al., Proc. Intern. Europhysics Conf. on High Energy Physics (Brighton, UK, 1983) p. 386 (Rutherford Appleton Laboratoriy, UK)
4. K.E. Bergkvist, Phys. Lett. **159B**, 408 (1985)
5. S. Boris et al., Proc. 22nd Intern. Conf. on High Energy Physics (Leipzig, DDR, 1984) Vol. 1, p. 257 (Institut für Hochenergiephysik, 1615 Zeuthen, GDR)
6. K.E. Bergkvist, Proc. 1985 Intern. Symp. on Lepton and Photon Interactions at High Energies, Kyoto, Japan, p. 560 (Yukawa Hall, Kyoto University, Kyoto 606, Japan)
7. S. Boris et al., Phys. Lett. **159B**, 217 (1985)
8. V.A. Lubimov, these Proceedings.

AN UPPER LIMIT FOR THE ELECTRON ANTINEUTRINO MASS FROM THE ZURICH EXPERIMENT ON TRITIUM β-DECAY

M. Fritschi, E. Holzschuh, W. Kundig, J.W. Petersen[a],
R.E. Pixley and H. Stuessi
Physics Institute, University of Zurich
8001 Zurich, Switzerland
and
Swiss Institute for Nuclear Research
5234 Villigen, Switzerland

ABSTRACT

The endpoint region of the tritium β-spectrum has been measured with 27 eV resolution using a magnetic spectrometer. The tritium activity was implanted into a thin layer of carbon. The neutrino mass determined is consistent with zero with an upper limit of 18 eV which includes instrumental and statistical uncertainties as well as uncertainties due to the energy loss in the source and the final electronic states.

(a) Present address: CERN, CH-1211 Geneva, Switzerland

I. Introduction

In 1980 the ITEP (Institute for Theoretical and Experimental Physics) group in Moscow published the first of a series of papers[1] claiming evidence for a nonzero mass of the electron antineutrino. The experiment has been improved continuously, the latest result being 20 eV < m < 45 eV with a best value of 35 eV. This result has been subject to criticism[2]. Nevertheless no other experiment has reached sufficient sensitivity to be a true, independent test. Here we report first results of our measurement. The data were taken in four runs with three different sources, representing a total of 27 days of effective measuring time. The analysis of the data gives no indication of a nonzero neutino mass but results in a smaller upper limit for the mass than has been obtained previously from the tritium β-decay.

II. Spectrometer

The instrument employed in the present investigation consists of a toroidal field, magnetic spectrometer of the Tretyakov type[3] with 2662 mm source-detector distance, modified with a radial, electrostatic retarding field around the source. At the exit of the spectrometer, the β-particles are reaccelerated by a voltage of 15 kV before entering a proportional counter (diameter 5 cm, length 10 cm) with a resistive anode wire. Pulse height and position, determined by charge division, are recorded. The source assembly consists of 10 rings, each with 5 cm diameter and 1 cm width, i.e. the total active source surface is 157 cm^2. To compensate for the source length a gradient voltage, proportional to the spectrometer dispersion, is applied along the rings. Spectra are recorded by stepping the retarding voltage while keeping the analysing energy of the magnetic spectrometer constant at 2.2 keV. More details were presented two years ago at the Moriond Workshop in La Plagne[4]. With a set-up as described above, the spectrometer has the following basic properties: 0.6 % transmission, 1.1 eV/mm dispersion, and 27 eV resolution (FWHM).

III. Source Production

The three sources which have been used so far for data taking were prepared by implantation of T_2^+ molecular ions into carbon evaporated onto an aluminum backing. The implantation energies were in the range 100-200 eV per tritium atom yielding activities of typically 0.3 mCi/cm^2 for an effective

thickness of about 2 μg/cm².

Two constraints led to this choice of source. First, hydrogen isotopes implanted into carbon form a strongly bound system leading to a minimal contamination rate of the spectrometer. This is certainly the most important constraint, since the experiment is very sensitive to contamination. Second, implanted sources are inheirently uniform. They tend to have uniform areal density independent of the flatness of the substrate and since both implanted ions and detected electrons enter or leave the source at almost normal incidence the electron energy loss also tends to be uniform. This is essential for an accurate determination of the energy loss part of the overall resolution function. Nonuniformity could be a servere problem if e.g. an evaporated sources were used, since they are notorious for building islands.

The first two sources (T1 and T2) used in the present study were produced in a simple device using the principle of a hot filament ion gauge. This idea was first employed for tritium sources by Bergkvist[5]. Electrons from the filament are accelerated through roughly 50 V toward a spiral grid. Ions produced in the region between the grid and the collector electrode surrounding the grid are accelerated (200 V) toward the collector. Aluminum foil of 0.1 mm thickness evaporated with carbon was mounted on the inside of the cylindrical collector electrode. The system is pumped with a turbomolecular pump. With the valve between turbopump and forepump closed, the pressure of T_2 is adjusted to roughly 10^{-3} mbar. Due to differences in compression ratio of the turbopump, the partial pressure of the normal gases found in the chamber (N_2, O_2, H_2O, etc.) remained very low during the source production. After implantation the tritiated foils were cut into 1 cm wide strips, which were cleaned in a hydrogen gas discharge to remove weakly bound surface tritium prior to being fastened to the source cylinder. This implantation device had the disadvantages of not producing a well-defined implantion energy and of causing unwanted heating of the substrate by the hot filament.

In order to overcome these problems and to circumvent handling tritiated foils, an improved implantation device was developed based on the Bayard-Alpert ion-gauge principle. In this device, electrons are accelerated through approximately 35 V toward a spiral grid, g1, surrounding the filament. Ions produced beyond this grid are accelerated through a small potential (< 10 V) toward a second grid, g2, which surrounds the collector but not g1 or the filament. This geometry allows the collector to be shielded form the direct

radiation of the filament. The main acceleration occurs between g2 and the collector (200 V). Instead of foils as source carriers, solid Al disks, evaporated with carbon were used. The entire assembly of 10 disks was rotated during implantation to achieve uniformity. Surface cleaning was carried out by bombarding with low energy (10 eV) H_2^+ ions. This proved to be effective and resulted in a 15% loss of activity. The source T3 was produced in this way.

IV. Overall Resolution Function

The determination of the overall resolution function (OR) of the experiment is perhaps the most important part of the analysis. The OR can be conveniently divided up into three parts:

1) the spectrometer resolution function (SR) which describes the spectrometer response to monoenergetic electrons leaving the source,

2) the energy loss spectrum (EL) which originates from electrons losing energy in traversing the source substrate and

3) the backscattering spectrum which is due to electrons suffering a combination of inelastic and large angle elastic scattering in the source substrate.

An accurate knowledge of the energy loss distribution is as important as the spectrometer resolution. Clearly, the sensitivity of the measurement is enhanced by keeping the effects of components 2 and 3 as small as possible.

The determination of the spectrometer resolution function was described in considerable detail two years ago,[3] and only a brief summary is given here. Due to the almost cylindrical geometry of the spectrometer the electric and magnetic fields are known analytically. Sufficient mechanical precision is assured by the modest relative resolution (1%) in the magnetic part of the spectrometer allowing an accurate Monte Carlo simulation of the SR (see Fig. 1). Detailed conversion electron measurements have confirmed the calculated shape of the SR, the agreement between calculated and measured width being better than 10%. The determination of the SR from the measured conversion line spectrum is complicated by shake-off effects. The calculated SR is therefore believed to be more reliable and was used in analysing the tritium data.

The EL spectra were determined using experimental results for the energy loss properties of electrons in evaporated carbon[6] in conjunction with the depth profiles measured for our tritium samples. In the following we outline the procedure employed.

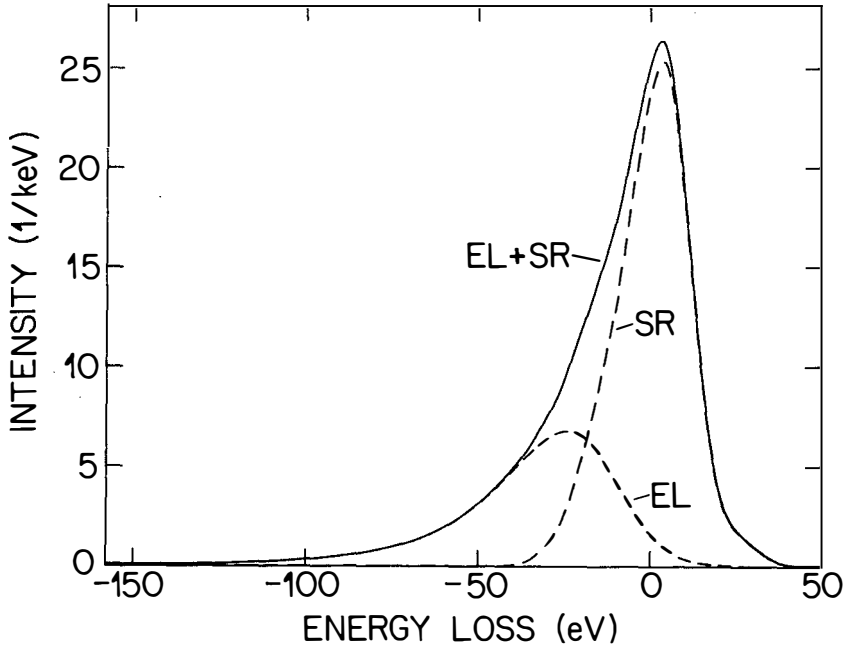


Fig. 1 Spectrometer resolution function (SR), energy loss spectrum (EL) for source T3 convoluted with SR.

The profile for each source was measured using a nuclear recoil method similar to that described in Ref. 7. The energy distribution of tritium recoils produced by 400 keV incident ^{12}C ions was measured. The energy resolution was 5.7 keV corresponding to a depth resolution of 50 Å (FWHM). Care was taken to determine accurately the energy corresponding to tritium at the surface. Fig. 2 shows the profile for source T3. The main source of error is due to the dE/dx values employed and results in a 7% error for the depth scale. The density of evaporated carbon was taken to be 2.1 ± 0.2 g/cm^3.

A fast electron traversing a layer of carbon loses energy mainly due to excitation of plasmons[6]. The probability for exactly n plasmon interactions is given by the Poisson distribution

$$P_n(x) = 1/n!\ (x/\lambda)^n \exp(-x/\lambda), \qquad (1)$$

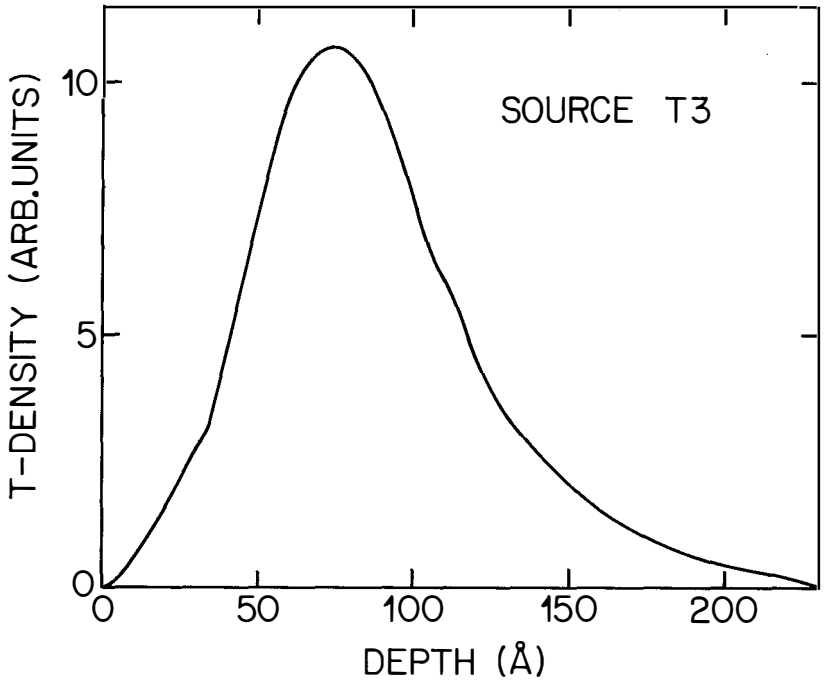


Fig. 2 Tritium depth profile for source T3.

where x is the layer thickness and λ denotes the mean free path. The deflection angle of an inelastically scattered electron is very small and completely negligible in our case. Assuming initially monoenergetic electrons the energy distribution after the layer is given by

$$f(\Delta,x) = \sum_{n=0}^{\infty} P_n(x)\, \omega^{*n}, \qquad (2)$$

where $\omega(\Delta)$ is the normalized energy loss spectrum for a single interaction with energy loss Δ and where

$$\omega^{*n} = \omega * \ldots * \omega \qquad (3)$$

denotes the n-fold convolution of $\omega(\Delta)$ with itself. The no-loss term (n = 0) is defined by $\omega^{*0} = \delta(\Delta)$. For a distributed source Eq. 2 remains unchanged if P_n is replaced by the right side of Eq. 1 averaged over the source depth

profile. In our case an additional averaging over the acceptance angle of the spectrometer is necessary.

We therefore need to know the mean free path λ and the single interaction spectrum $\omega(\Delta)$. These quantities were taken from Burge and Misell[6] who measured energy loss spectra for very thin evaporated carbon foils with initial energies in the range 23 to 70 keV. They used essentially the same procedure as outlined above and obtained good fits to their data assuming a simple Drude type expression for $\omega(\Delta)$ independent of the initial energy. It was necessary to extrapolate λ from 23 keV to the 18 keV energy of the tritium data. We therefore have increased the 5% error given in Ref. 6 to 8% for our analysis.

The uncertainties for the mean free path λ, the depth scale of the profile, and the density have equivalent effects on the calculated energy loss spectra, i. e. there is only one effective length scale which we choose to be the mean source thickness d. The total error in d is thus found to be 15%. Independently the spectrum of various conversion electron sources covered with evaporated carbon has been measured with the spectrometer. This test confirmed the validity of the procedure described above. However, due to the tendency of island formation in thin evaporated layers as well as shake-off effects, we consider the calculated energy loss spectra to be more reliable. The spectrum EL for source T3 obtained by folding with SR is shown in Fig. 1. The sum of SR and EL is the effective resolution function which is also shown in Fig. 1.

Backscattering in the source substrate has been studied by Monte Carlo simulations using the principles of Ref. 8. It was found to be adequately described by a small, energy independent distribution below the no-loss line. Its intensity, however, could not be calculated with sufficient accuracy and was therefore treated as a free parameter in the data analysis (see below). The height of the backscattered spectrum is extremely small compared with the height of the no-energy-loss peak (about 0.2% for the sources and SR employed). Nevertheless, the backscattering must be taken into account in order to obtain a good fit to the tritium data due to the extended energy range of this effect. The integrated contribution corresponds to roughly 6% per keV.

V. Measurement and Data Analysis

The measurements were made by stepping the retarding voltage on the source back and forth between minimum and maximum values in 5 V steps. The energy

range for each source was slightly different, but was typically 17.7 to 19.3 keV. The time per up-down pass was approximately one hour. The time per voltage step was typically 20 s in the 18.4 to 18.7 keV region and 2 s elsewhere. In the measurement with source T3, an additional energy range from 18.0 to 18.4 was measured with 6 s per step. Event data and retarding voltage were recorded for each step. Magnet currents were inspected once per up-down pass. The stability of the entire system was better than ± 1 eV during each measurement. The absolute accuracy of the energy was approximately 10 eV (calibration of retarding voltage, magnet current and position).

In an off-line analysis, the event data were position binned, thereby obtaining an energy spectrum for each position. The bin width was determined such that it was equal to the 5 eV energy steps of the measurement (20 bins over the entire detector). This made it possible to add the energy spectra, shifted by an appropriate energy for each position, thereby obtaining a single energy spectrum for the entire detector. In this analysis, a pulse-height cut on the energy deposited in the proportional counter was applied (typically 0.5 to 1.5 times the peak pulse height). The data were corrected for electronic dead time (approximately 1% for the high counting rate at low energies). Fig. 3 shows a section of the spectra around the endpoint in the form of Kurie-plots.

The β-spectrum was assumed to have the form

$$N(E) = A\, F(E)\, p\, E_t\, (1 + \alpha\varepsilon_o) \sum_i W_i\, \varepsilon_i^2\, (1 - m^2/\varepsilon_i^2)^{1/2} + BG \qquad (4)$$

where $\varepsilon_i = E_{oi} - E$. $F(E)$ is the Fermi function. E, E_t and p are the electron kinetic energy, total energy and momentum, respectively. The sum runs over all electronic final states (FS) with branching fractions W_i and endpoints E_{oi}. Each term in the sum is set to zero for E above the point where the term first reaches zero. The E_{oi} are defined by $E_{oi} = E_{oo} - E_{ex,i}$, where E_{oo} corresponds to the electronic groundstate and is, for m = 0, the true endpoint of the spectrum. $E_{ex,i}$ are excitation energies measured from the groundstate. Backscattering in the source substrate is taken into account by the parameter α which enters in this approximate form by a convolution of the backscattering distribution with a β-spectrum proportional to ε_o^2. The fit function is obtained by convoluting Eq. (4) with the OR function exclusive of backscattering (see Fig. 1). A small correction factor ($<$ 7% variation) for

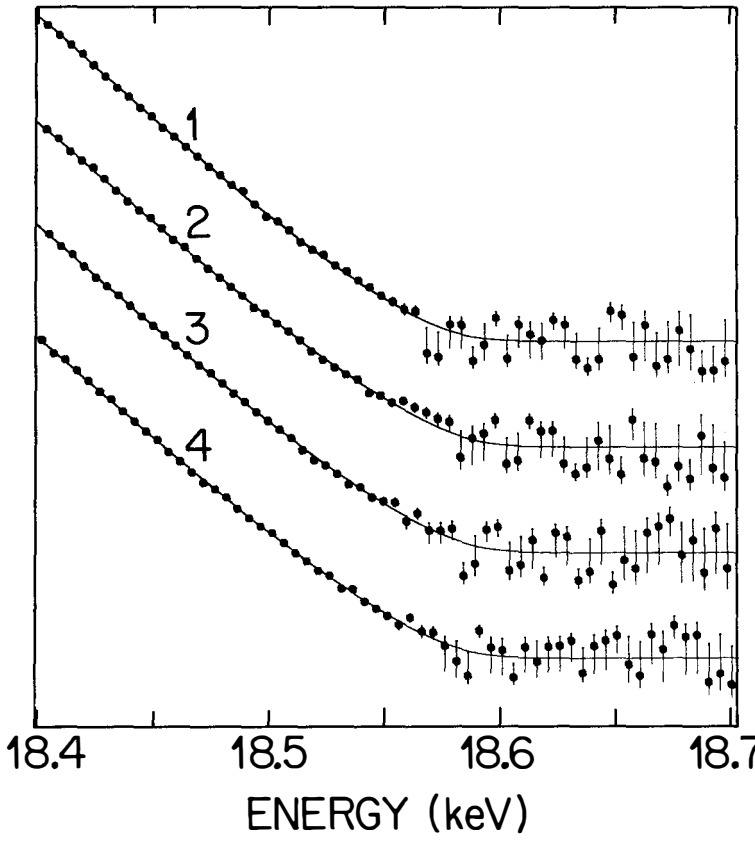


Fig. 3 Selected range of data for runs 1 - 4 in the form of a Kurie-plot and the corresponding best fits obtained with CH_3T FS.

the changing spectrometer acceptance as a function of retarding voltage has been included. The free parameters are α, E_{oo}, an overall normalization A, background BG, and the neutrino mass squared m^2. The latter was allowed to take on nonphysical, negative values, in which case the square root in Eq. (4) was replaced by its first order expansion $|1 - m^2/(2\varepsilon_i|\varepsilon_i|)|$. This gave symmetric, parabola-like curves for χ^2 versus m^2. Our final result is essentially independent of this assumption.

The measured β-spectra were fitted using the FS distributions of the bare nucleus (T^+, one level), the free atom (T), the tritium molecule[9] (T_2), and

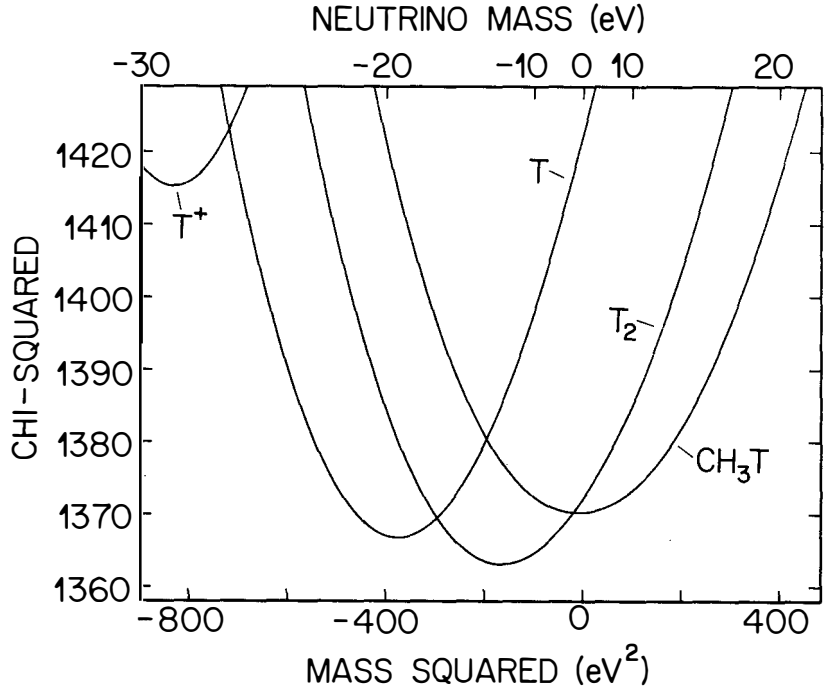


Fig. 4 Plot of χ^2 versus m^2 for the combined set of data with all other parameters fitted. The final states employed are for the bare nucleus T^+, the atom T, the tritium molecule T_2 and methane CH_3T.

the methane molecule[10] (CH_3T). In addition to fitting each spectrum separately, all four spectra were fitted simultaneously with m^2 being the only common parameter. The results for the combined data are shown in Fig. 4 in the form of χ^2 versus m^2 curves (all other parameter fitted for each m^2). The number of degrees of freedom (DOF) for these fits is 1370.

Obviously the best value for m^2 depends on the assumed FS. However, at our present level of precision this dependence is only critically determined by three averaged properties of the FS. These are the groundstate fraction, W_o, the mean energy E_{ex} and the mean width ΔE_{ex} of the excited states (the groundstate excluded from the means). This dependence was confirmed by fitting our data using a variety of FS distributions. It may also be justified

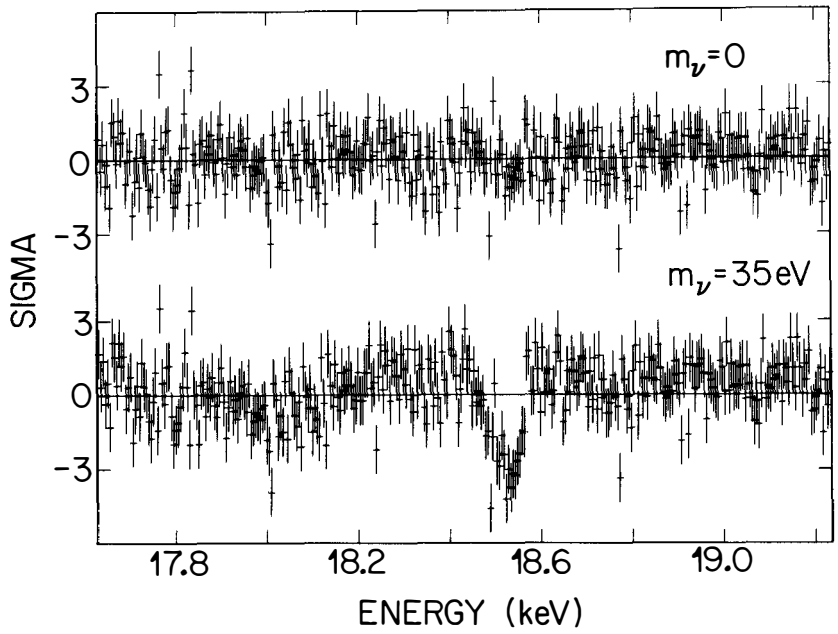


Fig. 5 Plot of the difference between the fitted function and the data divided by the standard deviation for spectrum 4 using fixed values of m. All other parameters were fitted. The FS of CH_3T were used.

analytically[11].

Concerning the FS for our sources we argue as follows. The extremely small diffusion rate of hydrogen isotopes implanted in carbon[12] and the stability of our sources strongly suggest that C-T bonds are formed. Kaplan et al.[10,13] calculated the FS for a variety of molecules with C-T bonds and found very little variation in terms of their averaged properties. Moreover, W_o and E_{ex} can be calculated using groundstate wave functions alone and are thus more reliable than any particular feature in the excited-state distribution. We thus take CH_3T, the simplest case, as an adequate representation for the FS of our sources. The corresponding fit results for the four spectra and the combined data set are listed in Tab. I. Also shown is F_{NL}, the probability of no-energy loss in each source. As can be seen in Fig. 4 and Tab. I, good fits were obtained and m^2 is compatible with zero within one sigma. Statistical upper limits UL for m^2 at the 95% confidence level are also shown. Due to

Table I.

Fit results for four runs with three different sources and the combined set of data using CH_3T final states. Errors indicated are one standard deviation.

Data set	1	2	3	4	all
Source	T1	T2	T2	T3	
F_{NL}	0.573	0.589	0.589	0.662	
Chisquare	328.8	345.6	349.9	343.7	1370.2
DOF	337	356	356	317	1369
E_{oo}	18582.6 ± 0.3	18584.5 ± 0.2	18584.4 ± 0.2	18577.6 ± 0.2	
$\alpha(keV^{-1})$	0.018 ± 0.004	0.020 ± 0.002	0.022 ± 0.002	0.021 ± 0.002	
$m^2(eV^2)$	140 ± 130	-9 ± 140	-22 ± 140	-85 ± 93	-11 ± 63
$UL(95\%)(eV^2)$	356	218	202	70	95

Table II.

Fitted values of m^2 and corresponding shift Δm^2 when the input parameters of the fitted function are changed. Shown are only changes which increase m^2. The complete set of data was fitted for which there are 1369 DOF.

Input parameter	Change	χ^2	$m^2(eV^2)$	$\Delta m^2(eV^2)$
Initial set	--	1370.2	-11	--
Spectrometer resolution	+10%	1370.2	52	63
Mean source thickness	+15%	1373.8	120	131
Groundstate fraction	-2.5%	1370.5	30	41
Mean excitation energy	+6%	1373.2	111	122
Width of excited states	+30%	1386.3	52	63

calibration problems the E_{oo} values show some nonstatistical variation. It may be conceivable that some small fraction of tritium in our sources is in the form of T_2 molecules. It can be seen in Fig. 4 that this would make m^2 only smaller and thus does not invalidate any UL. The m = 35 eV hypothesis was tested by fitting all data with fixed values m = 0 and m = 35 eV, giving χ^2 = 1370.2 and χ^2 = 1773.2, respectively, with 1370 DOF. In fig. 5 the normalized deviations for spectrum 4 are plotted for the two cases. It is seen that the m = 35 eV hypothesis gives a very poor fit, whereas no systematic deviations are discernible for m = 0.

Systematic errors for m^2 were investigated by fitting our data with various values of the nonfitted, input parameters. These are the width of the SR function and the effective mean source thickness d, and the FS parameters W_o, E_{ex}, ΔE_{ex}. The uncertainties for the latter were taken to be the maximum variation in the results for all molecules involving C-T bonds reported in Refs. 10 and 13 and increased generously to account for calculational uncertainties. The effects of altering each input parameter separately are listed in Tab. II. The direction of the changes was chosen such that m^2 was increased. Note that χ^2 stays either constant or is increased in all cases. Making all changes in Tab. II simultaneously shifts m^2 to 398 eV^2 but also increases χ^2 by 28 units and is thus not reasonable. Therefore we treat the shifts of m^2 in Tab. II as independent errors and add them in quadrature. This gives 204 eV^2 as systematic error for m^2. Assuming the best fitted value for m^2 would be exactly zero (and not -11 eV^2) a statistical UL of 106 eV^2 for m^2 at the 95% confidence level was calculated. Adding the systematic error for m^2 linearly with the statistical UL we arrive at our final result, $m^2 < 310$ eV^2 or

$$m < 18 \text{ eV}.$$

In conclusion we find no indication of a nonzero mass for the electron antineutrino, which is in strong contradiction to the results of Ref. 1. We see no possible source of error in our experiment large enough to account for this discrepancy.

A grant from the Swiss National Science Foundation and the continuous support from SIN are gratefully acknowledged. We are particularly indebted to the staff of the Physics Institute machine shop for very close cooperation during the course of this experiment.

References:

1 V.A. Lubimov et al., Phys. Lett. 94B, 266 (1980); Sov. Phys. JETP 54, 616 (1981), [Zh. Eksp. Theor. Fiz. 81, 1158 (1981)] and Phys. Lett. 159B, 217 (1985).

2 J.J. Simpson, Phys. Rev. D 30, 1110 (1984); K.E. Bergkvist, Phys. Lett. 154B, 224 (1985) and Phys. Lett. 159B, 408 (1985).

3 E.F. Tretyakov, Izv. Akad. Nauk SSSR Ser. Fiz. 39, 583 (1975).

4 W. Kundig et al.,Proceedings of the Fourth Moriond Workshop, La Plagne - Savoie, France, 1984, ed. by J. Tran Thanh Van (Edition Frontières, Paris, 1984), p. 261.

5 K.E. Bergkvist, Nucl. Phys. B39, 317 (1972).

6 R.E. Burge and D.L. Misell, Phil. Mag. 18, 251, (1968).

7 G.G. Ross et al., J. Nucl. Mat. 128, 730 (1984).

8 R. Shimizu et al., J. Phys. D; Appl. Phys. 9, 101 (1976).

9 O. Fackler et al., Phys. Rev. Lett. 55,1388 (1985).

10 I.G. Kaplan, G.V. Smelov and V.N. Smutnyi, DAN USSR 279, 1110 (1984).

11 Chin Cheng-rui and HO Tso-hsiu, Phys. Rep. 112, 1 (1984).

12 B.L. Doyle et al.,J. Nucl. Mat. 103, 513 (1981); V. Malka et al., Proceedings Tritium Technology in Fission, Fusion and Isotopic Applications, American Nuclear Society National Topical Meeting, Dayton Ohio, 1980, p.102.

13 I.G. Kaplan, V.N. Smutnyi and G.V. Smelov, Phys. Lett. 112B, 417 (1982).

THE LOS ALAMOS FREE MOLECULAR AND ATOMIC TRITIUM BETA DECAY EXPERIMENT

J.F. Wilkerson, T.J. Bowles, D.A. Knapp, M.P. Maley,
and R.G.H. Robertson,
(presented by J.F. Wilkerson)
Physics Division
Los Alamos National Laboratory, Los Alamos, NM 87545, U.S.A.



ABSTRACT

An initial measurement of the tritium beta decay spectrum spanning an energy range of 16.4 - 18.9 keV has been performed using a free molecular tritium gas source. With the data from this preliminary low statistics measurement (~72 hours of data), we are able to set an upper limit on the electron-antineutrino mass of 36 eV at the 95% confidence level. Measurements with a gaseous source eliminate many of the ambiguities arising from uncertainties associated with solid-source-based measurements. The ultimate neutrino mass sensitivity of our system should be about 10 eV or less.

1. Introduction

The existence of a non-zero electron-antineutrino mass as reported by Lubimov *et al.*[1] would have important consequences in our understanding of physics. A neutrino with mass could account for the dark matter observed in the universe. Many current theories in cosmology require non-baryonic dark matter. Also, in most realistic grand unified theories neutrino masses are quite natural. Thus, it is of critical importance to confirm or refute this result. Unfortunately, the selection of a tritiated complex amino acid, valine, as the measurement source has raised doubts about the current results. With the goal of making the most unambiguous measurement of tritium beta decay possible, a free molecular and atomic gaseous source and a high-resolution iron-free magnetic spectrometer have been constructed at Los Alamos. This system will be described along with the presentation of preliminary results from measurements of the beta spectrum of free gaseous molecular tritium.

2. Measurement Requirements

There are many important factors to consider in designing a tritium beta decay experiment that is capable of determining a neutrino mass of order 30 eV or less. The energy region of the beta decay spectrum which is sensitive to the neutrino mass is the region of about the same size as $m_\nu c^2$ directly below the endpoint energy. There are two consequences of this small region of sensitivity which impact any measurement. First, the count rate near the endpoint will be very small: for example, in the last 100 eV below the endpoint in tritium the decay branch is about 2×10^{-7} of the total decay. Thus, a source of reasonable strength and a measurement system that is efficient and has a good signal-to-background ratio is demanded. The second difficulty results from the small energy region of sensitivity to neutrino mass. Sensitivity to neutrino mass effects in the beta spectrum requires that the total system energy resolution should be comparable to $m_\nu c^2$. Note that the total system resolution is a convolution of the instrumental resolution and the source-related resolution functions. When comparing different experiments it is important to consider the total system resolution and not just the instrumental (spectrometer) resolution.

Thus, source strength, apparatus transmission, background, resolution, and systematic effects must be carefully considered in designing an experiment that is sensitive to neutrino mass. For the Los Alamos experiment we chose to build a Tretyakov type high-luminosity

magnetic spectrometer and to employ an intense gaseous tritium source. The next two sections will detail the reasons for selecting this arrangement and describe the experiment.

3. Properties of a Molecular or Atomic Gaseous Tritium Source

The principal reason for using a gaseous source of free atomic or molecular tritium is that it is the simplest possible system. This eliminates the numerous uncertainties and complications that arise in analyzing data obtained from a solid source. As we shall show, the price one pays for having the simplest data to interpret is that the experimental apparatus necessary to produce a gaseous source and measure the tritium beta spectrum is much more complicated than for a measurement based on a solid source.

There are several clear advantages to using a free gaseous source. First, the source resolution function is the narrowest possible. In a gaseous source the sole contribution to the source resolution function is the energy loss of electrons in the source. But, since a pure tritium source has the highest specific activity per unit mass of any source, then the source thickness and corresponding energy loss is the minimum possible. For all solid sources, except solid tritium, the energy loss per unit activity of tritium must be greater. Another advantage of a gaseous source is that the resolution function resulting from source energy losses can be carefully studied as a function of source thickness. This is because the source thickness is simply determined by the gas pressure in the source region and in our system it is trivial to adjust this pressure.

In addition to the energy-loss mechanism, solid sources have two additional processes which contribute to the source resolution function. One additional resolution smearing process is backscattering from the source backing substrate. The other effect is energy loss from contamination on the front surface of the source. There are ways to minimize the contribution from backscattering and contamination, but these effects are impossible to eliminate.

Another critical reason for choosing a gaseous source of pure tritium is that the so called "final state effects" are minimal and well understood. When a tritium atom decays to a $^3He^+$ ion there is a probability of populating any of the energetically allowed final atomic states of the daughter $^3He^+$ ion. In order to extract a neutrino mass from a tritium beta decay spectrum accurately it is necessary to know precisely

the branching ratios and energies for all possible final decay states and include this in the analysis. This is essential because the reported neutrino mass is of the same order as the binding energy of electrons in ^3He. Since the transition to each atomic state has a different endpoint, the shape of the total spectrum is complicated. Hence when experimental resolutions are folded in, the spectrum can resemble a decay with different branching ratios and a massive neutrino. The only cases for which the decay probabilities can be accurately determined are for atomic tritium ($T \rightarrow {}^3He^+$) and molecular tritium ($T_2 \rightarrow T^3He^+$).

For the simplest case, free atomic tritium decaying to a $^3He^+$ ion, the calculation of branching ratios and final states can be done to great accuracy[2] using the "sudden approximation" wherein the nuclear charge is assumed to change abruptly by one at the instant of β decay (Fig. 1). Recently, more difficult calculations of comparable accuracy to the atomic case have been performed[3,4] for molecular tritium (Fig. 2). In comparing the decay probabilities for the two cases it is obvious that in going from the atomic to the molecular case the branch to the ground state is reduced significantly and that the complexity of the decay scheme is increased. Obviously, the decay schemes from tritium in complex molecules or implanted into solid sources are even more complicated. Unfortunately, calculations of the final states for any systems other than atomic or molecular tritium are much less certain. The final states for many solid sources are for practical purposes impossible to calculate and require making some assumptions or approximations to simpler structures. For most experiments employing complicated molecular solid sources or sources of tritium implanted into solids, the uncertainty in knowledge of the final state effects is the dominant uncertainty in the measurements.

Using a gaseous source of tritium makes for a simple and clean interpretation of the beta decay spectrum, but does introduce certain difficulties into the actual measurement. Fortunately, these problems can all be solved by careful design of the experiment's apparatus. Obviously a gaseous source will be of low density and, thus, thin with low activity. But by building an extended source region with good extraction efficiency of the betas that decay in the region, one can overcome the low density problem. Another potential problem is that of source strength (pressure) fluctuations. It is impossible to have a constant source pressure, but by having a monitor system that measures the source activity at the same time as the beta spectrum measurement it is possible to know the source strength

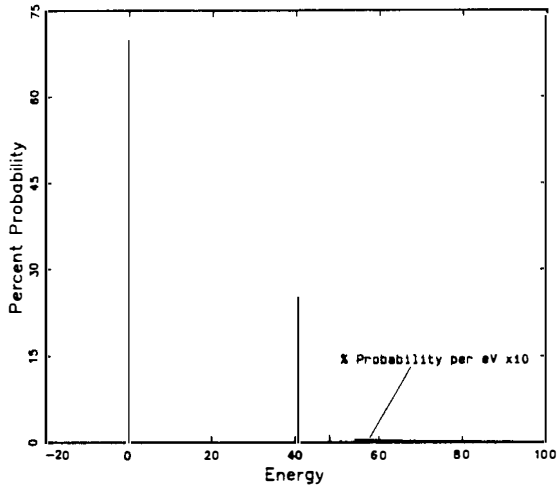


Fig. 1 Decay probabilities for $T \rightarrow {}^{3}He^{+}$ atomic final states versus energy of states. The continuum decay probabilities are multiplied x 10.

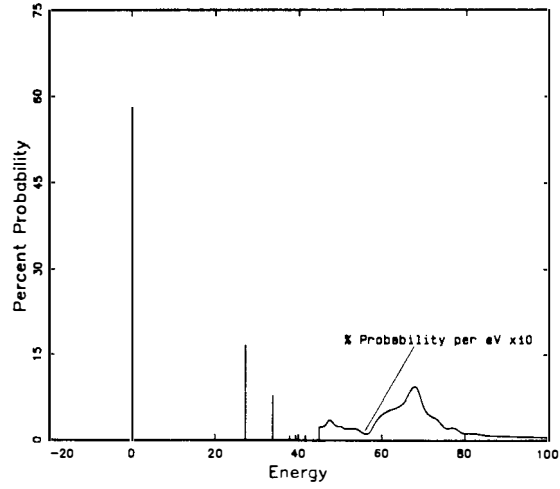


Fig. 2 Decay probabilities for $T_2 \rightarrow T^{3}He^{+}$ molecular final states versus energy of states. The continuum decay probabilities are multiplied x 10.

to great accuracy. One would also expect that contamination of the energy analyzing system would be extremely likely with a free gaseous source. However, as we will show in the next section, this problem is also solvable.

Finally, it is critical in any tritium experiment to be able to make an accurate determination of the total resolution function of the system. Obviously, the resolution of an extended gaseous source is not expected to be the same as for a solid source or an electron gun. There is, however, an ideal gaseous line source available. The short-lived (1.8 hours) ^{83m}Kr isomer, a daughter of 83-day ^{83}Rb isotope, has a narrow conversion line at 17.84 keV. The energy at which this line occurs is well matched with the energy region being measured in the tritium beta decay. Thus, it is possible to determine the instrumental resolution function by using this source and running under conditions essentially identical to those of the tritium source. It is also possible to determine energy loss in the source by mixing the Kr source (which has a negligible thickness) with either hydrogen or deuterium gas and observing the effect on the total resolution. Hence, the total resolution function for the entire measurement system can be experimentally verified.

4. Overview of the Los Alamos Experiment

A schematic view of the Los Alamos experiment is shown in Fig. 3. The apparatus can be divided for discussion purposes into three distinct sections: a source region, a pumping restriction and extraction section, and a toroidal magnetic spectrometer. The extended source is required to reach a sufficient source intensity. Placing this source in a strong axial magnetic field with a pinch at one end allows the extraction of most of the betas from the tritium decays into the extraction region. The pumping restriction and extraction region serves two purposes: to stop tritium molecules from reaching the spectrometer and to focus the betas emerging from the source region into the spectrometer. The toroidal spectrometer analyzes the momentum of the betas, allowing a precise measurement of the tritium energy spectrum near the endpoint.

a. Atomic and molecular source

The source decay region consists of a 3.86-m long 3.8-cm diameter highly polished aluminum tube which is pumped by Hg diffusion pumps located at each end. When running with atomic gas, molecular tritium at 300-mT pressure enters a Pyrex discharge tube where the molecules are dissociated

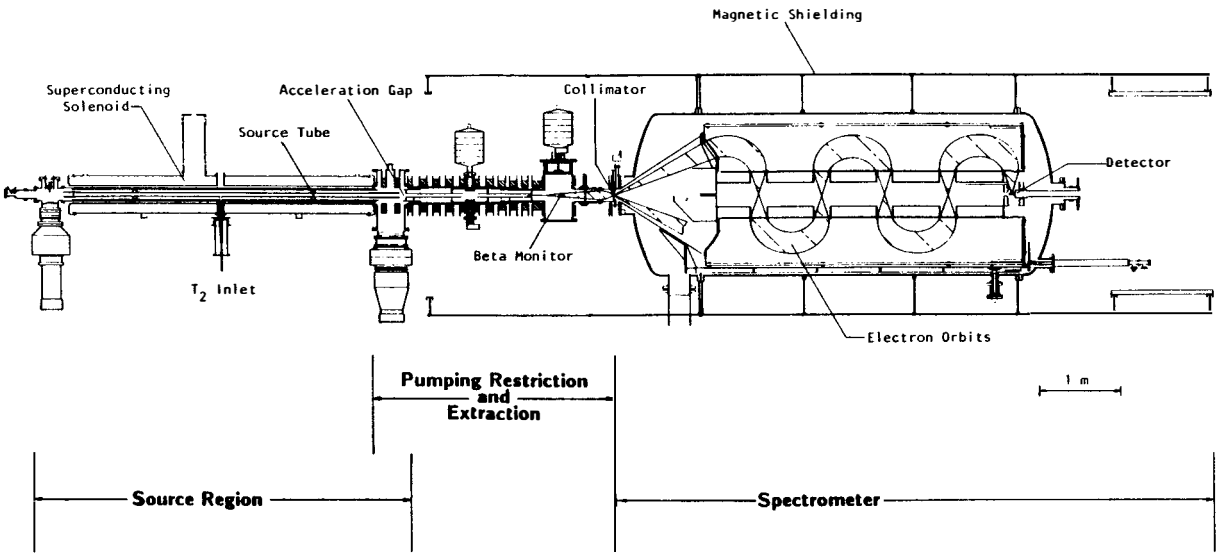


Fig. 3 Cross-sectional view of the Los Alamos gaseous tritium beta decay experiment.

in an RF discharge. The tritium atoms emerge through a small orifice into the source tube at the midpoint between the two pumps. The highly polished aluminum tube's surface has a thin layer of aluminum oxide which inhibits recombination. For hydrogen and deuterium, we have made measurements of recombination rates on aluminum at cyrogenic temperatures. Typically at 140K a hydrogen or deuterium atom can undergo 50,000 "bounces" before recombining. Tritium is not expected to behave very differently.

An equilibrium density of atomic T is built up as established by the influx and the conductance of the tube. The average atom bounces approximately 4,000 times on the walls before being pumped away, so recombination is small. The equivalent source thickness integrated along the axis is conservatively estimated to be 10^{15} - 10^{16} tritium atoms/cm^2 of 85-90% pure atomic tritium. The presence of a molecular component (10-15%) in the source gas is inevitable and not a serious problem if steps are taken to monitor and correct for it. The experimental molecular spectrum can be scaled and subtracted from the total atomic-plus-molecular spectrum to obtain a pure atomic spectrum. The molecular-to-atomic ratio must be known and will be measured by UV absorption spectroscopy. For measurements of the molecular tritium spectrum, the same system is used except that the RF dissociator is turned off. The source strength for molecular tritium can be 5 times higher than atomic, and is limited only by the energy loss in the source gas that can be tolerated.

The source region is in a solenoidal magnetic field of about 1.5 kG with a small axial gradient. The electrons are constrained to spiral about the field lines ($B\rho \leq 463$ Gauss-cm). At one end of the solenoid a pinch coil with a peak field of about 4 kG reflects most of the β's that start with a velocity component directed towards that end; as a result about 90% of the β's reach the weak field end of the solenoid. Sapphire standoffs allow the aluminum source tube to be thermally regulated to minimize recombination, but electrically isolated, so that the potential of the entire decay region can be varied up to 20 kV. (This bias is applied with a highly stable power supply and accurately measured with a voltage divider certified by two independent standards laboratories to be accurate to 2 V at 20 kV.) The biasing of the source tube allows the electrons emerging from the weak field end of the tube to be accelerated through a potential of typically 10 kV.

This acceleration is one of the critical features of the experiment. By biasing the source tube, the betas that decay in the source region are

accelerated when they emerge into the extraction region. This energy gain is never compensated by deceleration later in the apparatus. Hence, the betas decaying in the source region can be differentiated from background tritium decays that occur elsewhere in the system. The second advantage of acceleration is that the spatial component of phase space is reduced. Thus, not only is the background in the region of the shifted endpoint far lower than it would be at 18 keV, but the emittance of the beam is improved. The price paid is, of course, that higher resolving power is required in the spectrometer.

One final feature to note in the source region is the placement of a hot filament in the region of the magnetic pinch. A mechanism exists whereby the source potential might be altered by the space charge built up from positive ions remaining from decays in the source. These ions are effectively trapped by the magnetic field and the potentials at the ends. But thermal electrons emitted from the filament will neutralize these ions. The emission of electrons is self-regulating and depends on the space charge built up in the cell. This prevents the space charge from exceeding 1 V.

The acceleration of betas emerging from the weak field end of the source is accomplished at an acceleration gap located between the source tube and pumping restriction. Spectrum distortion can result from tritium decaying in the acceleration region. However, the fraction of detected decays occurring in the acceleration gap is less than 10^{-3} of the accepted decays from the source region.

Scanning the beta spectrum can be performed in several ways, but the preferred method is to vary the potential of the source tube while maintaining all magnetic fields fixed. While this causes a (smooth) energy-dependence of extraction efficiency, the advantage of presenting the extraction lens, spectrometer and focal plane detector with fixed-energy particles is considerable.

b. Pumping restriction and extraction region

The pumping restriction and extraction region is a differential pumping system that allows a windowless source while limiting tritium contamination of the spectrometer to 0.4 mCi/day. The accelerated beta particles from the source are focused to a collimator located at the object of the spectrometer. The collimator limits the acceptance of the spectrometer so that betas that emerge from or strike the source walls can

be rejected absolutely, independent of aberrations or imperfections in the electron-optical system. This is most important because a monolayer of adsorbed tritium would represent 3 orders of magnitude more activity than the gaseous source.

c. Spectrometer

Our spectrometer design was based on considerations of resolution, acceptance, background, and ease of injecting betas from a gaseous source. The resulting toroidal, iron-free, spectrometer (Fig. 3) is similar to that of Tretyakov[5], but differs in a number of respects. First, electrons enter at an angle of $(24 \pm 5)^{o}$ to the axis because they are essentially injected from a beam instead of emerging from a solid source. Also, several significant improvements over the original Tretyakov design were incorporated in our spectrometer. By using curved non-linear conductors third-order aberrations that degrade the resolution were corrected for yielding a factor of 3 increase in solid angle and improved resolution. Another improvement is the use of thin copper strips (0.5 x 13 x 170 mm) to carry the current where electron orbits cross the axis. Use of these thin strips rather than thick water-cooled conductors allows approximately 75% of the electrons to be transmitted to the focal plane (compared to 4.5% in the original Tretyakov design). The spectrometer itself accepts 53% of the incoming cone of rays. Other transmission factors include detector efficiency (75%) and losses at the magnetic pinch (90% of 4π source is available). These factors lead to a calculated luminosity of 0.14 cm^2. The intrinsic resolution, $E/\Delta E$, of the spectrometer is at present about 1100.

To realize the full capabilities of the spectrometer it is necessary to reduce the influence of external magnetic fields, particularly the earth's field. The permissible transverse field is small, approximately 10^{-2} G, but rather large axial fields (0.1 G) can be tolerated. To achieve this level of magnetic shielding, an active shield comprised of two sine coils (conductors spaced around the vacuum vessel and driven in proportion to the sine of the angle from the transverse field direction) with fluxgate magnetometers to provide feedback to the coils is used. Detailed measurements of ambient and local variations of the magnetic field in the building where the spectrometer and source are situated, together with measurements of spectrometer resolution as a function of beta energy, indicate that this system provides the necessary transverse shielding.

The focal-line detector used in the spectrometer is a gas proportional counter with both position and energy sensitivity. In our present detector, 26 keV electrons are detected with an energy resolution of 20% and a position resolution of 4.0 mm. The efficiency (peak-to-total ratio) and the background count rate are 75% and 0.004 counts/sec, respectively.

Although the spectrometer does have a focal line length of a few resolution widths, it is essentially a point-by-point device. As mentioned earlier there will certainly be intensity fluctuations of the gaseous source. Thus, a satisfactory means of normalizing the intensity during each measurement point is required. This is accomplished by using a solid-state detector (Beta Monitor in Fig. 3) to detect a small fraction of betas which have been accelerated from the source before they are focused onto the spectrometer entrance collimator. As the spectrum is scanned by varying the source potential, it is necessary to float this solid-state detector at the same voltage as the tube to eliminate any variation of detector efficiency that might affect the normalization.

5. System Performance and Resolution Measurements

The entire system became fully operational and the first beta spectrum from a T_2 source was measured in June 1985. A variety of different tests and calibrations to study the electron-optical characteristics of the system has been performed to verify and accurately determine the system parameters. The initial transmission, resolution, and background performances of the system will be presented below. However, please note that in many cases these initial results are not the final values we expect to achieve.

a. Apparatus Transmission

From ray-tracing calculations we expect that about 25% of the effective source area can be extracted with very simple electron-optical design. Measurements with a solid ^{103}Ru source give a 25% focusing efficiency, in agreement with the calculations. However, measurements with the extended gaseous ^{83m}Kr source give a total extraction efficiency times spectrometer transmission a factor of three lower than calculated. This discrepancy is currently being studied.

b. Resolution

A variable-energy photoemissive electron gun (40 kV maximum) can be mounted at the spectrometer collimator position and can be used to measure spectrometer resolution, transmission, scattering effects, and aberrations. This e-gun is not a pencil beam type gun, but in fact fills the full spectrometer aperture. Thus, it can be used to determine the spectrometer's intrinsic resolution and test for resolution degradation resulting from magnetic field non-uniformities. However, the e-gun cannot be used as a substitute for measuring the resolution of the real extended source because it does not fill momentum phase space nor is it an extended source. Tests performed with this e-gun at energies of 18, 26, and 34 keV found the spectrometer intrinsic resolution, $E/\Delta E$, to be a constant 1100. This indicates that the spectrometer resolution is not limited by local magnetic field gradients. The measured resolution function at 26 keV is shown in Fig. 4.

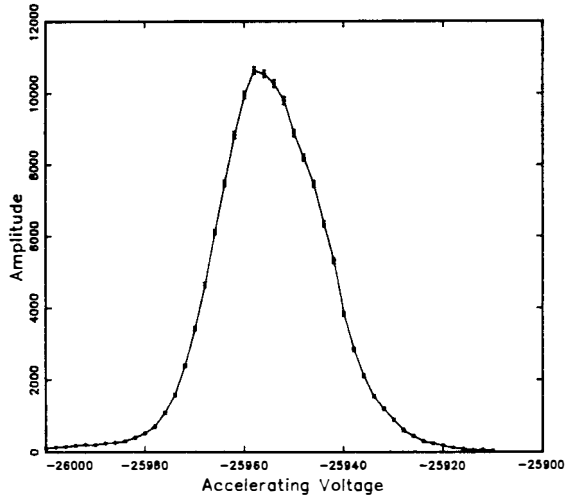


Fig. 4 Intrinsic spectrometer resolution function of 26 eV FWHM measured in 2 eV steps with a photoemissive e-gun and the spectrometer at a fixed energy of 26 keV.

At present, we vary the acceleration of the betas from the source to scan the beta spectrum, and leave the spectrometer at a fixed energy to accept 26 keV betas. The initial observed resolution width of the gaseous ^{83m}Kr isomer in the source was 65 eV FWHM (Fig. 5). Calculations were performed to deconvolute the intrinsic line width[6] of 2.26 eV and shake-up and shake-off effects[7,8,9] from the observed resolution. From our calculations we derive an instrumental resolution of 54 eV FWHM for the total system (Fig. 6). Note that care is needed to ensure that the linewidth, shake-up, and shake-off effects of the Kr source are known to sufficient accuracy. More detailed calculations and experimental studies using synchrotron light are also planned to verify these data.

The molecular tritium spectrum presented in this paper was taken with this 54 eV FWHM instrumental resolution. However, after these data were taken some modifications to the system were implemented and now an instrumental resolution of 37 eV FWHM has been achieved. While this is acceptable for initial data acquisition, we will continue to work to improve the resolution.

For the present molecular tritium data, the other component to the total system resolution, namely the energy loss of betas in the source, is negligible. The source thickness in these early measurements is extremely small, approximately 10^{-3} μg cm^{-2}. However in calculating the energy losses, the effective path length of the betas in the B-field must be taken into account since some electrons can travel up to 40 m in the source gas while spiraling around the field lines. Nevertheless, even for the electrons that travel farthest, the average energy loss is only about 0.5 eV. Fortunately, detailed measurements of inelastic cross sections for electrons on H_2 have been made, and even the small energy loss expected can be corrected. Actual resolution measurements using the Kr line source mixed with hydrogen or deuterium gas to achieve the source pressure used during tritium measurements are planned to verify the energy loss calculations.

c. Background

Background arises from several possible sources: cosmic rays, tritium, other radioactivity, and scattered electrons in the spectrometer. As has been described, rejection of tritium background is very high by virtue of the preacceleration and use of an energy-sensitive detector.

One of the advantages of Tretyakov's spectrometer design is its inherent suppression of scattering backgrounds. The spectrometer is in fact five spectrometers in tandem, and electrons with an energy a few

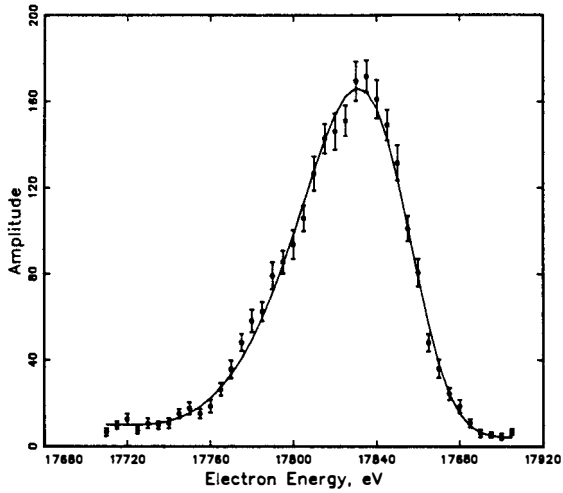


Fig. 5 ^{83m}Kr gaseous source 17.835 keV conversion line measured at a fixed spectrometer energy of 26 keV. The curved line is a calculation used to determine the instrumental resolution function.

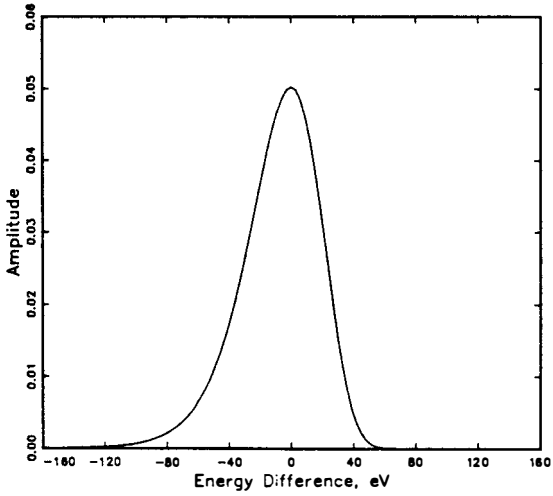


Fig. 6 The instrumental resolution function derived from the ^{83m}Kr gaseous source measurement shown in Fig. 5.

percent away from the focused energy are rejected at the first stage. The main scattering contribution thus comes from collisions with the inner conductors entailing very small energy losses and angular changes. This background scales with the signal and is estimated to be at the level of 10^{-3} or less. Experimental measurements of scattering made with the electron gun have confirmed that scattering is negligible.

Initially our chief background concern was that tritium contamination could eventually build up in the spectrometer and affect our background rate. However, after several months of running tritium, we have not observed any detectable change in the background. Thus, our built-in safeguards of the pumping restriction and a 50,000 ℓ/sec Ti sublimator pump located at the entrance to the spectrometer seem to be working very effectively.

The present background rate using a single-resistive-wire detector is 0.004 counts/sec. Tests indicate that the majority of this background is from cosmic ray muons. To reduce this component even further we are developing a multiwire detector to discriminate between through-going particles and stopping particles.

6. Molecular Tritium Data Acquisition and Analysis

A preliminary 3-day molecular tritium beta spectrum measurement was completed in January 1986. An energy range of 16.44 to 18.94 keV was covered in 10 eV steps. The energy region was scanned in a random fashion to eliminate time dependent systematic errors. To correct for the source strength the counts from the proportional counter were divided by the beta monitor counts. An additional correction for source strength fluctuations and an estimate of systematic errors in the normalized counts was obtained by repeatedly measuring a "calibration" energy point at 16.44 keV in between measurements of the "real" data points. (In other words after one or two measurements of data runs the 16.44 keV energy point would be remeasured.) The data points were measured for 600 secs while the calibration points were measured for 200 secs. The molecular source was run at reduced pressure because of a defect in one of the sapphire high-voltage standoffs. Nevertheless, in the last 100 eV of the spectrum we obtained a count rate of 0.15 sec^{-1}, which compares quite well with the rate obtained by Lubimov *et al.*, 0.04 sec^{-1}. The background count rate during the run was 0.004 sec^{-1}. The measured beta spectrum is shown in Fig. 7 along with a Kurie plot of the data. Note that the error bars include both the

statistical error and the systematic error based on all of the 16.44 keV calibration runs. The absolute energy calibration is based on the 17.835-keV Kr conversion line which is known to an accuracy of 20 eV [10].

These data were taken by keeping the magnetic fields and spectrometer field constant (to accept 26 keV betas), while the source potential was varied to scan the energy region. The advantage of this procedure is that the spectrometer acceptance, the detector background, and backscattering from the detector window are constant (for constant energy particles). Nevertheless, it is still possible for the efficiency of extraction to vary with the acceleration voltage. This is a smooth variation which is generally calculable. But imperfections in the electron-optical system will almost certainly lead to small deviations from this ideal behavior, and an empirical correction similar to that used by Lubimov *et al.* and by Bergkvist[11] is required in fitting the data. However, the normalization of the count rate to the beta monitor, whose extraction efficiency tracks that of the spectrometer, cancels to first order the extraction efficiency variations and produces a very linear Kurie plot (Fig. 7). In fitting the data only a small quadratic correction term, less than 10^{-8} eV^{-2}, is necessary.

7. Data Analysis

The calculation of the predicted beta spectrum includes molecular final state calculations[3], Coulomb corrections, screening corrections, nuclear recoil effects[12], weak magnetism[12], and acceleration gap corrections (the last two corrections are negligible). The total system resolution function is then folded into the calculated data. A four-parameter fit using a non-linear least squares routine[13] is then performed for which the four parameters are: amplitude, endpoint energy, neutrino mass, and a extraction efficiency term.

The accuracy of the fitting code was checked by generating beta spectra including the same corrections listed above from a totally independent data-generation code. These two codes were developed by separate people totally independently to ensure a true check on the accuracy of the fitting code. Beta spectra using a variety of different parameters were calculated using the generation code. These data were then input into the fitting code and the resulting fit parameters were then compared to the original input parameters. Agreement was exceptional even for cases where very small neutrino masses (eV's) and poor resolution

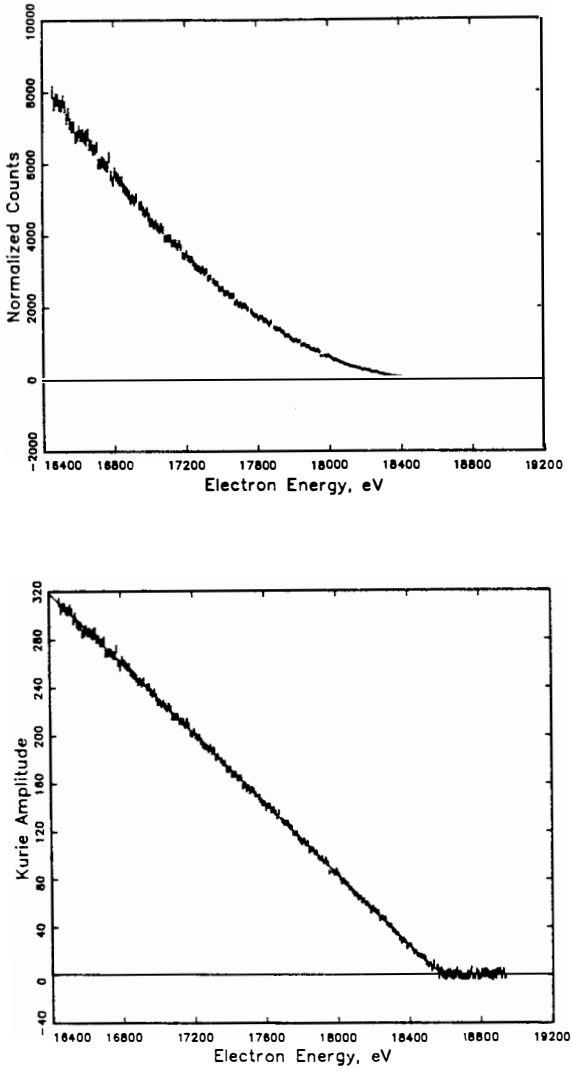


Fig. 7 The molecular tritium beta decay spectrum versus energy and Kurie plot for the same data. The line through the data in the Kurie plot is the calculated best fit for m_ν=0.

functions (50-70 eV) were used. The results from this "blind" check of the fitting code give us a high level of confidence in our analysis procedure.

Another code was written to generate realistic Monte Carlo mock data. This allows us to investigate and determine the effects of various systematics and correlations between variables. It is essentially impossible to gauge these effects any other way. Crude analytical arguments and simplifications are not accurate because of the complicated correlations between parameters.

The molecular beta spectrum from our 3-day run was analyzed using the procedure outlined above. The resolution function used was the 54 eV FWHM total resolution function extracted from the Kr resolution function. A residual plot of the beta spectrum data versus the best fit is shown in Fig. 8. The residual for each data point is the difference between the measured value and calculated value divided by the point's error bar. The endpoint energy from this fit is 18.581 keV which yields an atomic mass difference for T-^{3}He of 18.597 ± 0.020 keV, where the uncertainty is dominated by the uncertainty in the ^{83m}Kr line energy.

From this short 3-day run we find that $m_\nu < 36$ eV at the 95% confidence level. The χ^2 best fit was for m_ν=0. The total χ^2 was 279 for 242 degrees of freedom. Figure 9 is a plot of χ^2 versus neutrino mass.

8. Conclusions

The preliminary 3 days of molecular tritium data we have presented here offers a hint of the eventual results possible using a free gaseous tritium source. With systematic errors at the few eV level and a spectrometer resolution in the 30 eV range (known to 1 eV accuracy), we will be statistics-limited down to a neutrino mass below 10 eV. With our expected event rate of 1 count/sec in the last 100 eV, and our demonstrated background level of 0.004 counts/sec, we should be able to set a limit on a neutrino mass of 10 eV (95% C.L.) using molecular tritium.

However, we are continuing work to improve the spectrometer resolution, increase the transmission and the source strength, and reduce backgrounds. The present limitations on these parameters have been largely identified and tractable solutions have been found. We plan to implement these improvements, perform systematic checks, and acquire sufficient statistics to set a limit of 10 eV or better with molecular tritium. Upon completion of running with molecular tritium, we will then bring the atomic tritium source into operation. Then systematic checks will be performed

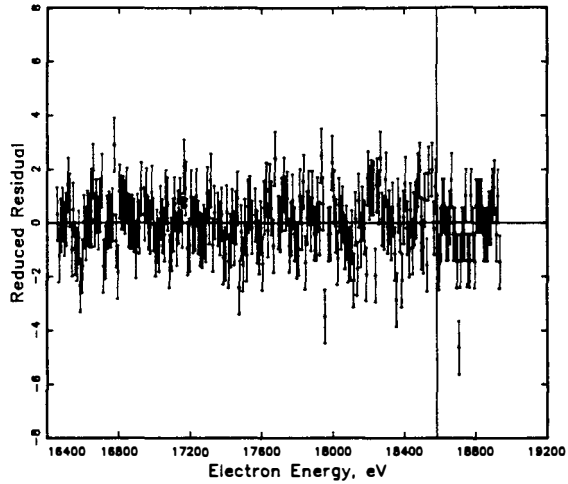


Fig. 8 A plot of reduced residuals calculated from the best fit to the molecular tritium data.

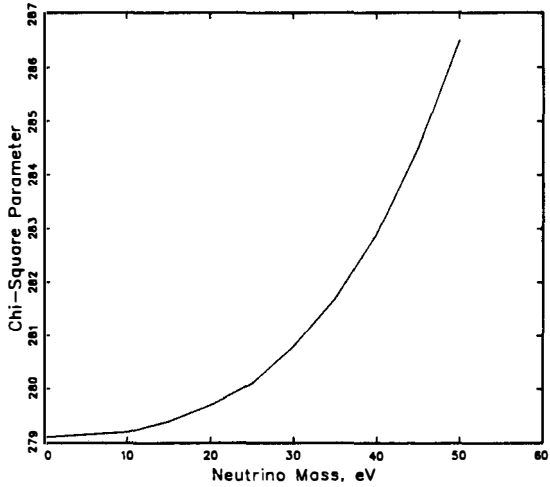


Fig. 9 χ^2 as a function of neutrino mass for the fit to the molecular tritium data.

and sufficient statistics accumulated to set a limit of 10 eV or better with atomic tritium.

Employing a gaseous source is admittedly experimentally complex, but we believe it is the approach that provides the most unambiguous information about a possible neutrino mass in the eV-range.

REFERENCES

1. V. A. Lubimov, E. G. Novikov, V. Z. Nozik, E. F. Tretyakov, V. S. Kosik, and N. F. Myasoedov, Zh. Exp. Teor. Fiz. 81, 1158 (1981) and contributions these proceedings.
2. R. D. Williams and S. E. Koonin, Phys. Rev. C27, 1815 (1983).
3. R. L. Martin and J. S. Cohen, Phys. Lett. 110A, 95 (1985).
4. W. Kolos *et al.*, Phys. Rev. A31, 551 (1985); O. Fackler *et al.*, Phys. Rev. Lett. 55, 1388 (1985).
5. E. F. Tretyakov, Isv. Akad. Nauk. S.S.S.R., Ser. Fiz. 39, 102 (1975).
6. W. Bambynek *et al.*, Rev. Mod. Phys. 44, 716 (1972).
7. T. A. Carlson and C. W. Nestor, Phys. Rev. A8, 2887 (1973).
8. D. P. Spears *et al.*, Phys. Rev. A9, 1603 (1974).
9. J. S. Levinger, Phys. Rev 90, 11 (1953).
10. S. L. Ruby *et al.*, Phys. Lett. 36A, 321 (1971).
11. K. E. Bergkvist, Nucl. Phys. B39, 317 (1972).
12. J. Friar, private communication.
13. The IMSL Library - Mathematics and Statistics, IMSL, Houston, Texas.

NEUTRINO MASS MEASUREMENT AT INS

H. Kawakami, K. Nisimura, T. Ohshima, S. Shibata,
Y. Shoji, I. Sugai, K. Ukai, T. Yasuda*
Institute for Nuclear Study, University of Tokyo

N. Morikawa, N. Nogawa
Isotope Center, University of Tokyo

T. Nagafuchi, F. Naito, T. Suzuki, H. Taketani
Tokyo Institute of Technology

M. Iwahashi
Kitasato University

K. Hisatake
Jissen Women's University

M. Fujioka
Cyclotron-Radioisotope Center, Tohoku University

and

Y. Fukushima, T. Matsuda
National Laboratory for High Energy Physics, KEK

Abstract

Our first measurement of the neutrino mass has been successfully carried out at INS. Extended and cooled ^{3}H source and 40 cell proportional counters are simultaneously used to improve statistics. Energy resolution, not be excluded the shake off effect yet, is 12 eV. Reliable response function is obtained by using the ^{109}Cd reference source with the same chemical form as ^{3}H source. The preliminary result of the electron anti-neutrino mass has been obtained to be less than 34 eV

Present address ; * North Eastern University, Boston, MA 02115

(I) Introduction

This project started in 1980 just after ITEP data was published, and it took five years to get the first data obtained on last Autumn.

The principle of neutrino mass measurement with ^3H ß-decay is to detect a non-zero mass effect as a phase space modification on the ß-spectrum at the end-point energy region. In our experiment, following key points to detect the mass effect are considered. Some parts of our measurement was already described in INS-Report-561[1].

(II) Key points

In this type experiment, there are four key points to achieve high quality data.

(1) Good energy resolution : The mass effect shows up at only the energy range with the order of the M_ν below the end-point, so that $\Delta E < M_\nu$ is obviously required.

(2) High statistics : Decay fraction of the mass sensitive energy range is very small, for instance it is 3×10^{-7} in the range of 100 eV below the end-point. To obtain high enough event rate or statistics, some special devices or approaches are required.

(3) Low background : Because the background contribution easily masks the mass effect, it is essential to suppress the background as low as possible. Main background in the case of ITEP[2] was the ß-decay of ^3H molecule which was evaporated from the ^3H source itself.

(4) Reliable response function : In the data analysis the response function of the whole spectrometer system including the effect of the source determines reliability of the final result, thus very reliable response function is required.

The INS iron-free ß ray spectrometer makes it possible to realize the first point. The maximum momentum resolution and coil current stability are

0.013% and 3 x 10^{-5}, respectively. External field contribution is cancelled to less than 10 γ (= 10^{-4} Gauss) which corresponds to $\sim$ 1 x 10^{-5} of the field strength in the ^{3}H measurement. Momentum resolution of 0.020% is obtained in the ^{3}H ß ray measurement, which corresponds to energy resolution of 8eV.

The second point is achieved with use of a extended source by the non-equipotential method, which was originally developed by Bergkvist[3], and simultaneously use the spectrographical data taking.

Low background counting rate is realized by a very small size (2^{mmW} x 2^{mmD}) proportional counter surrounded by five VETO-counters. Moreover, background count due to the evaporation of the ^{3}H source is sufficiently reduced by cooling down the ^{3}H source to -35 C.

Reliable response function is obtained by use of ^{3}H and reference ^{109}Cd sources with the same chemical form. The KLL Auger lines ($E_e \simeq$ 18 keV) following the decay of ^{109}Cd are used for obtaining the response function and calibrating the absolute energy of the system.

(III) Experimental device

3-1 The iron-free ß-ray spectrometer

This spectrometer was built on 1967, and has been used for study of the nuclear physics and chemical physics. The specification of the spectrometer is listed in Table 1. The bird's-eye figure of the iron-free ß-ray spectrometer facility is given in Fig. 1. Top cross-sectional view of vacuum chamber is shown in Fig.2. DC-components

Table 1. Parameters of the INS ß-ray spectrometer (constructed ; 1967)

Type	:	$\pi\sqrt{2}$ Double focusing, Iron-free, Current loop
Mean Radius	:	ρ = 75 cm
Resolution	:	0.013% (for E_e = 624 keV)
Solid Angle	:	6.5 x 10^{-4} (for 0.01% and an extended source)
Max. Current	:	100A (208 Gauss)
Energy Range	:	6 keV to 4 MeV (6 keV is due to the cut off energy of counter window)
Current Stability	:	3 x 10^{-5} /d
Cancellation of External Field	:	< 10 γ (10^{-4} Gauss)
Focal Plane	:	4% in Momentum (120 mm)

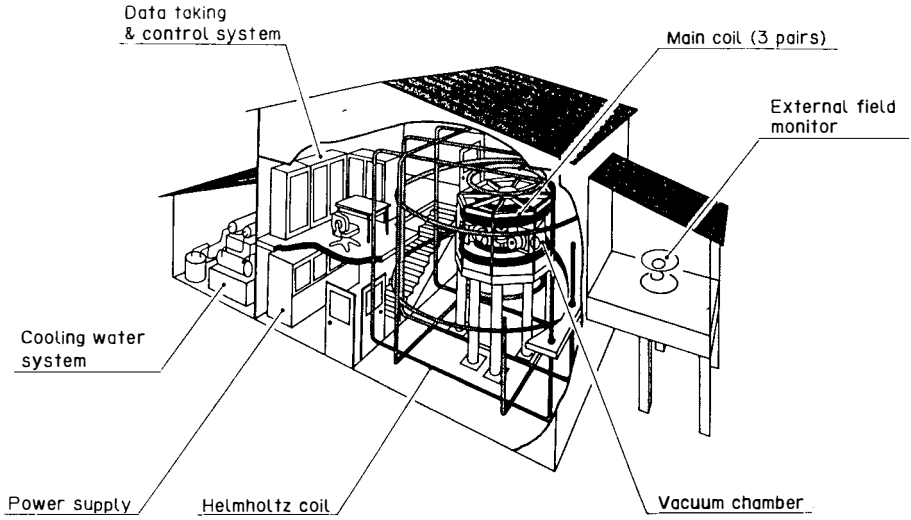


Fig. 1 Bird's-eye figure of the INS $\pi/2$ double focusing ß-ray spectromenter.

of external field are compensated by helmholtz coils which are installed in vertical, north-south and east-west directions. The fluctuation of the vertical component is detected with a probe and compensated by another helmholtz coil which is wound on the same flame as the vertical coil. The suppression of less than 10 is achieved.

3-2 Extended ^{3}H source and ^{109}Cd reference source

To achieve high counting rate, a extended source of 25^{mmH} x 100^{mmW} is used by applying the focusing electric potential on each 5^{mm} distance. The source is mounted on a conductive plate with resistivity of 10 MΩ.

Actual applied voltage is 500 volts in 18.5 keV electron measurement. The tilted angle of the extended source is 67.5 for the normal direction.

In order to suppress the evaporation rate (∿ 1%/day at room temperature) of the ^{3}H source in vacuum, the source is cooled down to -35 C by liquid nitrogen. The evaporation rate is reduced to order of 10^{-5}.

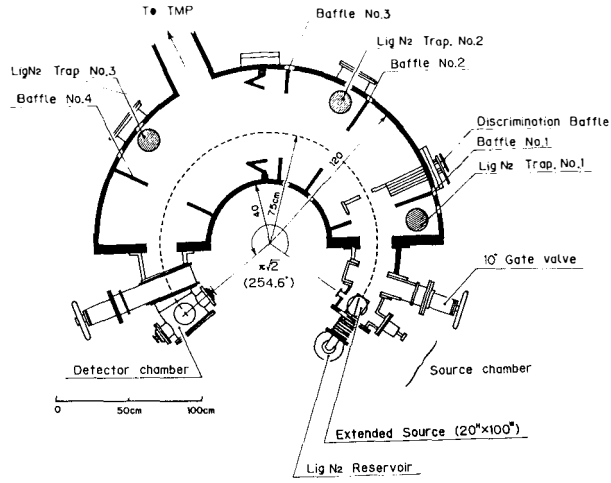


Fig. 2 Top cross-sectional view of the vacuum chamber of the spectrometer.

The source chamber system is illustrated in Fig. 3. ^{3}H and ^{109}Cd reference sources are mounted to upward and downward as shown in Fig.3.

Both sources are made by the same chemical material of a kind of acid. The part of the chemical structure are shown in Fig. 4. And also both sources are prepared by the same technique which makes it possible to controll the source thickness in unit of the molecular monolayer with high uniformity.

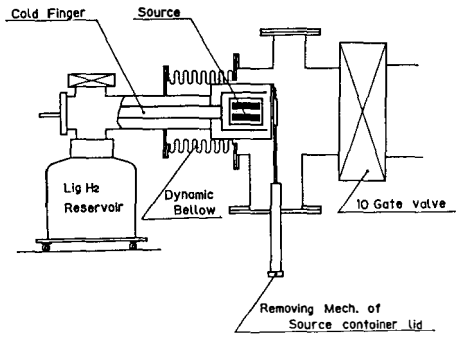


Fig. 3 Side view of the cooled source chamber system.

Due to above reason, the energy loss and backscattering in both sources are essentially same. Thus, very reliable resolution function can be obtained experimentally from the

measured Ag KLL Auger spectra by subtracting only contributions of their shake off, and the natural line width.

The atomic effect such as shake off for ^{109}Cd and shake up for ^{3}H is now theoretically estimated.

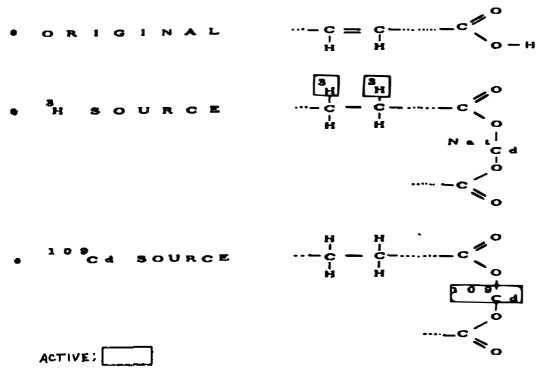


Fig. 4 Chemical structure of the original acid, ^{3}H and ^{109}Cd reference sources.

In the first measurement the intensities of the source with 2 molecular layer thickness of 0.6 $\mu g/cm^2$ are $\sim$6 mCi and 120 μCi for ^{3}H and ^{109}Cd sources, respectively.

3-3 Electron counter and data taking system

One more approach to obtain higher counting rate is to take data with the spectrographic method. In our spectrometer facility, a single wire proportional counter has been successfully used. However, the position resolution of this type counter for 18 keV electron is 2 mm which corresponds to 0.07% momentum resolution. Thus, we made a small-size ($2^{mmW} \times 2^{mmD} \times 50^{mmH}$) 40 channel multi-cell proportional counter. Forty slits of each 0.5mm width are set at the front of the counter window. Position is read out by a delay line of which time interval between adjacent wires is 20 ns. Electrostatic scanning method is employed to obtain the spectrum at the intervals between slits of the ß-detector.

Data are taken with the PDP 11/40 computer through the CAMAC system, and stored on the magnetic tape with the event by event.

(IV) Preparatory works

Before the ^{3}H ß-spectrum measurement, we carried out some preparatory works as follows :

1) evaporation rate measurement of the ^{3}H source in vacuum at room temperature and at -100°C
2) test of the non-equipotential method with five ^{109}Cd sources of line style and a extended source
3) dispersion measurement by the ^{109}Cd source
4) energy loss effect by source thickness
5) peak shift by source up and down
6) line shape difference by source temperature
7) energy calibration of KLL Auger lines in Ag by the ^{169}Yb source

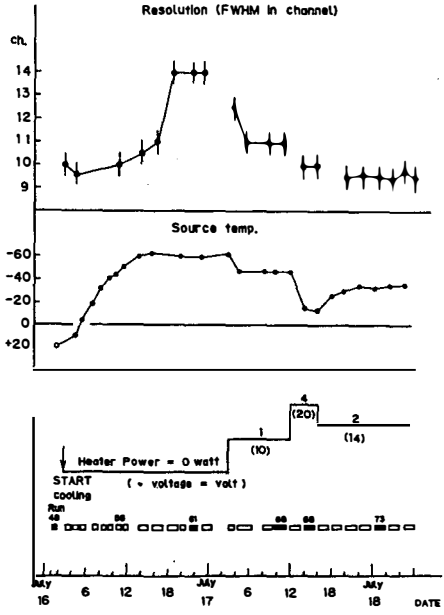


Fig. 5 Time sequence at the measurement of the line shape vs. source temperature. Source temperature and resolution (FWHM) are also shown.

Here we report only the result of line shape difference by source temperature. The other items of the preparatory works are already reported in ref.1.

Source temperature is controlled by consumed power in resisters which are attached on the back of the source holder. The heater powers supplied on the resisters were 0, 1, 2 and 4 watts, and the KLL Auger spectra in Ag were measured. The vacuum is 8 x 10^{-7} Torr during the measurement. The time sequence is shown in Fig. 5, together with the source temperature and the resolution (FWHM) observed. Fig. 6 illustrates the temperature dependence of line shape. It is worth saying that the resolution is more fastly recovered than we

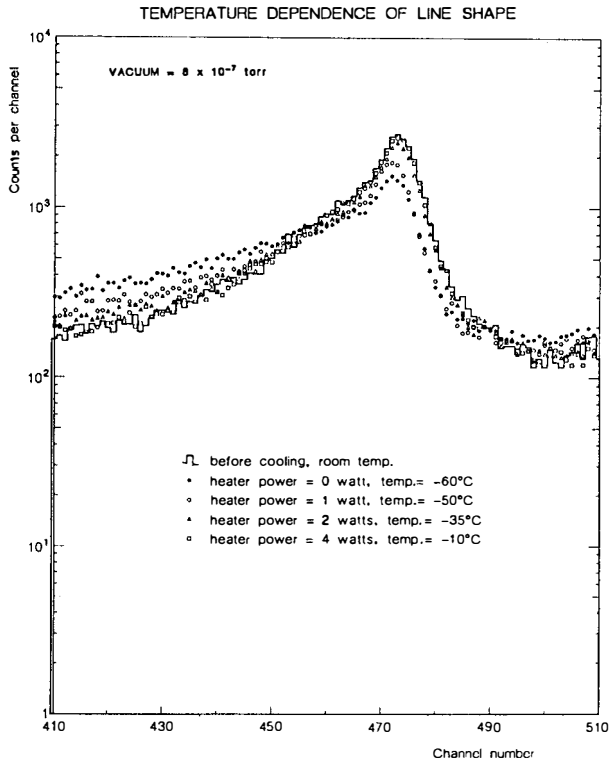


Fig. 6 Temperature dependence of KL_2L_3 spectrum.

initially considered, even after the resolution is getting worse by out-gas adsorption on the cold source. The measurement of ^3H ß-spectra was carried out at the temperature of -35°C. The temperature was determined by taking into account the balance between the evaporation rate of ^3H source and the line shape. The line shape difference between at room temperature and at -35°C is displayed in Fig. 7.

(V) Measurement of H^3 ß spectrum

Following 4 type measurements are performed, in which ^3H and ^{109}Cd sources are exchanged by moving up or down;

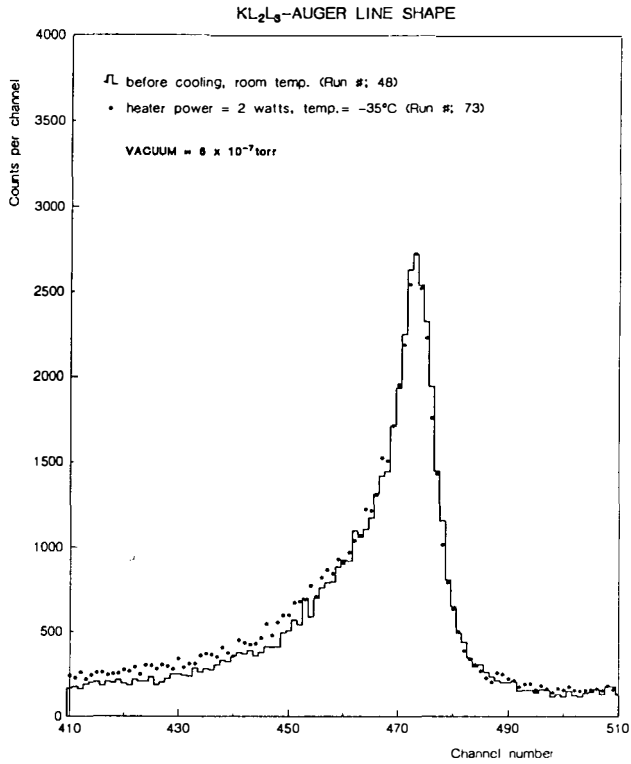


Fig. 7 KL_2L_3 spectrum at room temperature and at -35°C.

1) Type-1 (^3H; fine step) :

^3H spectrum at the end-point region between 17.5 and 19 keV is measured at once. Scanning step is 2.4 eV and scanning range is 119 steps of which 102 steps are overlapped with those of the neighbouring cells. (The slit distance of 3 mm corresponds to 17 steps.) Time duration of a step is 30 seconds and about 65% of the experimental time is spent for this measurement.

2) Type-2 (^3H; wide step) :

Scanning step is 17 x 2.4 eV and scanning range is 22 steps. With this measurement, many of the cells cover the same region so

that data can be also used for the correction of the relative detection efficiency of the individual cell, as same as type 1. About 10% of experimental time is assigned.

3) Type-3 (^{109}Cd; Auger line) :

KLL Auger spectra in Ag are measured. Scanning step is 2.4 eV and scanning range is 17 steps. This scan is repeated 10 times, and time duration of a step is 30 seconds. This measurement is used for monitoring the system stability and for obtaining the response function.

4) Type-4 (^{109}Cd; Auger tail) :

Tail spectrum of the KL_1L_1 line is observed by the same manner with Type-3. These data are used to know the tail shape of the response function observed by type-3 measurement.

During those type measurements, acceleration voltage of 2.8 kV and source potential of 500 V are supplied, respectively. The stabilities of the coil current, acceleration voltage and external field cancellation, and TDC and ADC spectra from the proportional counter, and total counting rate are always monitored and stored on the magnetic tape together with spectrum data. Fig. 8 shows the coil current stability, as an example, of which

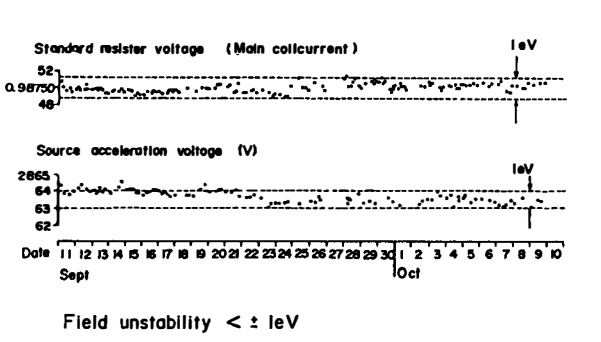


Fig. 8 Fluctuation of the coil current and the acceleration voltage.

fluctuation is 1 eV equivalent to 18 keV electron energy. The fluctuation of the source acceleration voltage of 2.8 KV was found to be the nearly same as that of the coil current stability.

This measurement took just one month and accumulated about 5 K events in the energy range of 100 eV below the end-point.

No appreciable increase of the background rate was detected. The background rate was 0.005/sec/cell.

A tritium monitor was equipped at outlet of the rotary pump of the vacuum chamber evacuation system, and also a gas sampler was set in the spectrometer room. We did'nt detect any contaminations by the monitors during the ^{3}H measurement.

(VI) Analysis

After correcting the detection efficiency, dead time of the computer system, fluctuation of coil current and acceleration voltage, we obtained the final ß-spectrum. Its Kurie plot is given in Fig. 9. Response function

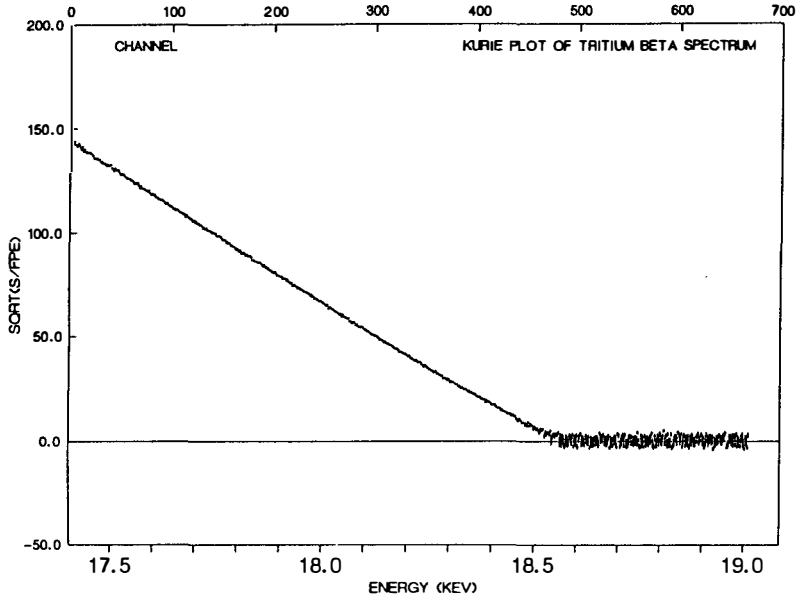


Fig. 9 Kurie plot of the ß spectrum obtained.

from KL_2L_3 spectrum was obtained by convoluting the natural line width of 12 eV, and is shown in Fig. 10.

Excitation energies and probabilities of final states of our source were calculated by Prof. J. Arafune, Prof. K. Morokuma Dr. N. Koga and T. Watanabe. The result is shown in Fig. 11.

Taking into account the excitation probabilities for the final state, the ß-spectrum with above response function was calculated.

The preliminary result of the neutrino mass has been obtained to be less than 34eV. The fitted spectra is given in Fig. 12.

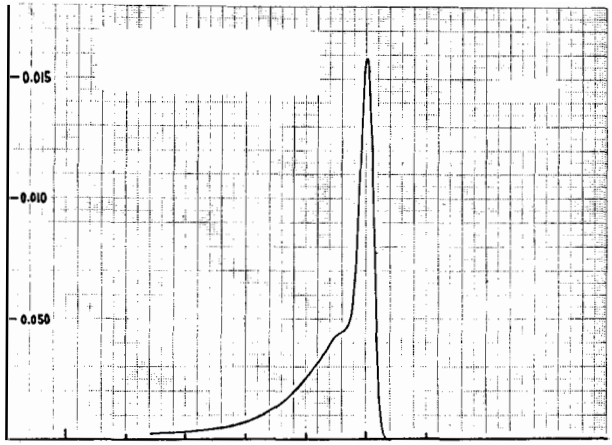


Fig. 10 The response function deconvoluted by the natural line width of 12 eV. The resolution (FWHM) is 12 eV.

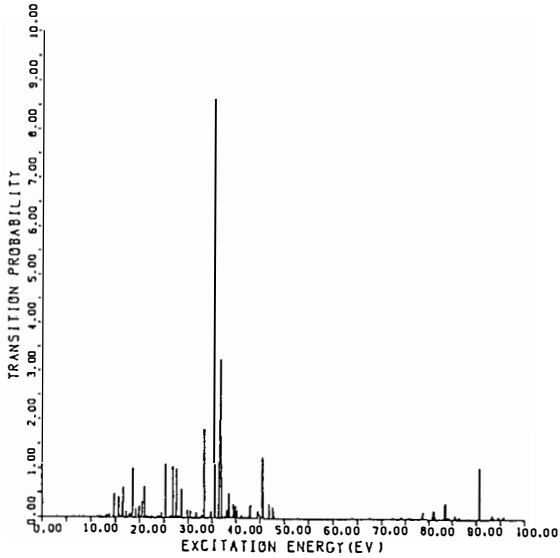


Fig. 11 Transition probabilities to the final state in the case of our ^3H source.

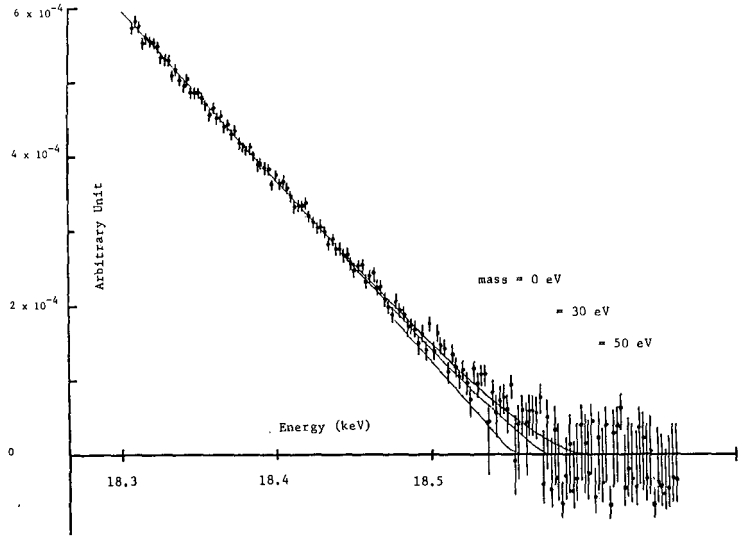


Fig. 12 Comparison between the calculated spectra for neutrino mass of 0, 30 and 50 eV and the experimental spectra.

Reference

1) H. Kawakami et al., INS-Rep-561,Nov., 1985, and proceedings of INS International Symposium on "Composite Models of Quarks and Leptons, INS, Tokyo, Aug. 11-13, 1985, edited by H. Terazawa

2) E. T. Tretyakov et al., Proc. Intern Neutrino Conf., Aachen, 1976 ; V. A. Lubimov et al., Phys. Letters 94B (1980) 266; S. Boris et al, proc. of HEP83, Intern. Europhusics Conf. on HEP, Brington, 1983; S. Boris et al., Proc. of XXII Intern. Conf. on ITEP, Leipzig, 1984

3) K. E. Bergkvist, Nucl. Phys. B39 (1972) 317

4) Y. Fujita, H. Kawakami and M. Hosoda, Nucl. Instr. and Meth. 196 (1982) 271

5) J. Arafune, K. Morokuma and N. Koga, private communication, and the results will be published in near future.

Molecular Effects in the Neutrino Mass Determination From Beta-Decay of The Tritium Molecule

O.Fackler[a,b], B.Jeziorski[c], W.Kolos[c], H.J.Monkhorst[d], M.Mugge[a] and K.Szalewicz[c]

a Lawrence Livermore National Laboratory, University of California, Livermore, California 94550, USA

b Department of Physics, The Rockefeller University, New York, New York 10021, USA

c Quantum Chemistry Laboratory, Department of Chemistry, University of Warsaw, 02-093 Warsaw, Poland

d Quantum Theory Project, Departments of Chemistry and Physics, University of Florida, Gainesville, Florida 32611, USA

Abstract

Molecular final state energies and transition probabilities have been computed for beta-decay of the tritium molecule. The results are of sufficient accuracy to make a determination of the electron neutrino rest mass with an error not exceeding a few tenths of an electron volt. Effects of approximate models of tritium beta-decay on the neutrino mass determination are discussed

I. Introduction

Experiments are being prepared or performed in several laboratories aiming at electron neutrino mass determination from measurements of the tritium β-decay spectrum near the endpoint. These experiments can be separated into (1) those dealing with atomic, molecular or solid state tritium, and (2) those in which the decaying tritons have a more complex molecular or solid state surrounding. Only in the first case can one perform reliable quantum mechanical computations for the final states of the daughter system, and therefore only in these experiments will the accuracy of the neutrino mass determination depend solely on the experimental resolution. In the second group of experiments the inherently less accurate theoretical results for the final states will always introduce an additional uncertainty into the determined value of the neutrino mass.

In the present paper we give a summary of our accurate theoretical treatment of molecular effects[1-5] accompanying the β-decay of T_2. We consider transitions to the electronic ground state of HeT^+, to excited bound states of this ion, as well as to the resonance and scattering states. In the case of transitions to lowest electronic states we explicity consider excitations to all possible rovibrational (rotational and vibrational) states. These results are used to construct the Kurie plots and to perform numerical experiments that show the magnitude of error in the neutrino mass determination arising if the accurate treatment of the final states is replaced by a more approximate one. We also discuss the solid state effects in frozen T_2 and show that they are either small or computable.

The results presented below will be used to interpret the data from the frozen tritium experiment now under way at LLNL (see the accompanying contribution in these proceedings).

II. Kurie plots and their accuracy

It is well known that to extract the neutrino rest mass from the β-decay spectrum one must compute the Kurie plots[6] defined as

$$K(E;m_\nu) = [\sum_n P_n K_n^2(E;E_n,m_\nu)]^{1/2} \qquad (1)$$

$$K_n(E;E_n,m_\nu) = (m_\nu + E - E_n)^{1/2}[(m_\nu + E - E_n)^2 - m_\nu^2]^{1/4} \qquad (2)$$

where E denotes the β-electron energy relative to the endpoint energy, m_ν the neutrino rest mass, P_n the transition probability to the n-th final state of the daughter ion, and E_n the energy of this final state measured relative to the lowest state energy.

The process under consideration is

$$T_2 \rightarrow {}^3He^+ + e^- + \bar{\nu}_e$$

Since the ground state of T_2 is a $^1\Sigma_g^+$ state, n in Eq.(1) labels all $^1\Sigma$ rovibronic (rotational, vibrational and electronic) states of the $^3He^+$. The values of E_n and P_n for all these states are needed to calculate the Kurie plots (1).

The following basic methods and techniques have been applied in our work to provide the necessary input for the Kurie plots:

1. First-order time-dependent perturbation theory,
2. Neglect the β-electron interaction with the molecular electrons,
3. Adiabatic approximation,
4. Expansion of the electronic wavefunction in elliptic coordinates,
5. Numerical solution of the vibrational equation.

Since we do not use any new approaches we will not present the details of the above steps 1-5, and only their accuracy and reliability will be discussed:

1. The applicability of first-order perturbation theory follows from the smallness of the weak interaction operators.

2. In this Born approximation one essentially neglects the following effects: (a) screening of the active nucleus and the final state dependence of this screening, (b) exchange of the β-electron with the molecular ones, (c) correlation of the β-electron in its continuum orbital with the bound state electrons. Since in the case of tritium decay the momentum of the β-electron is relatively large, all three effects should be small, with effect (a) being probably the largest one. It has been shown[7] that for the two lowest states of the T atom the effects (a) and (c) change the transition probability by only 0.17%. There is no reason to suppose that the molecular binding in T_2 may change this value significantly.

3. The adiabatic approximation consists of factoring the molecular wavefunction into electronic and rovibrational wavefunctions. For the ground states of T_2 and $^3HeT^+$ one may expect[8] the relative value of the nonadiabatic effects in the energy to be less than 10^{-6}. They may be larger for some higher excited states but since the transition

probabilities to these states are considerably smaller than to the ground state we conclude that the adiabatic approximation is very reliable.

4. The expansion of the electronic wavefunction in terms of the basis set expressed in elliptic coordinates and depending explicitly on the interelectronic distance (r_{12}^n, with $n < 4$) is known to be very rapidly converging (see Ref.1 and references therein). Most of our computations have been carried out with 200-term expansions and the results indicate that for a few lowest bound states the error in the probabilities is approximately 0.00001. The error may be larger for high lying Rydberg states and also for the resonance states. We have shown, however, by performing numerical experiments, that this effect has no effect on our final results relevant to the neutrino mass determination.

5. The vibrational equation has been solved numerically for all bound rovibrational and continuum states[2] resulting from the nuclear motion in the electronic states 1-4 and 6. Using sum rules we have shown that for each considered electronic state of $^3HeT^+$, and a given rotational quantum number j, the error in the transition probabilities summed over the whole spectrum amounts to less than 0.0001.

Concluding this section we can say that in our computation of the Kurie plots for the T_2 molecule the largest error arises from approximations 1 and 2, but not from molecular computations. In our opinion, the accuracy of the Kurie plots for molecular T_2 computed in the present work is equally as accurate as that which can be calculated for atomic T.

III. Computation of wavefunctions and of transition probabilities

For the electronic ground state of T_2 we have used the previously determined wavefunctions[9,10] different for different regions of the internuclear distance. For HeT^+ six lowest electronic states have been considered explicitly. For each of these states a selection of terms in the expansion of the electronic wavefunction has been made and the nonlinear parameters have been optimized. Transition probability to the electronic ground state of HeT^+, computed for the equilibrium internuclear distance in T_2, R = 1.4 bohr, amounts to 58.2%, and to the five lowest excited states 26.4%. By diagonalizing the Hamiltonian matrix we get, however, more eigenvalues below the ionization continuum. With our best 249-term wavefunction we obtained 16 states in this region. Transition probabilities to the 10 highest of these states, for which the nonlinear parameters in the wavefunctions have not been individually optimized, sums

to 1.1%. Thus the total transition probability to all bound excited states is 27.5%.

For resonance states the energies have been computed using the stabilization method.[11] The reliability of this method has been demonstrated by performing (in elliptic coordinates) computations for the united atom as well as for the separated atoms, and reproducing the corresponding atomic resonance energies.[4,5]

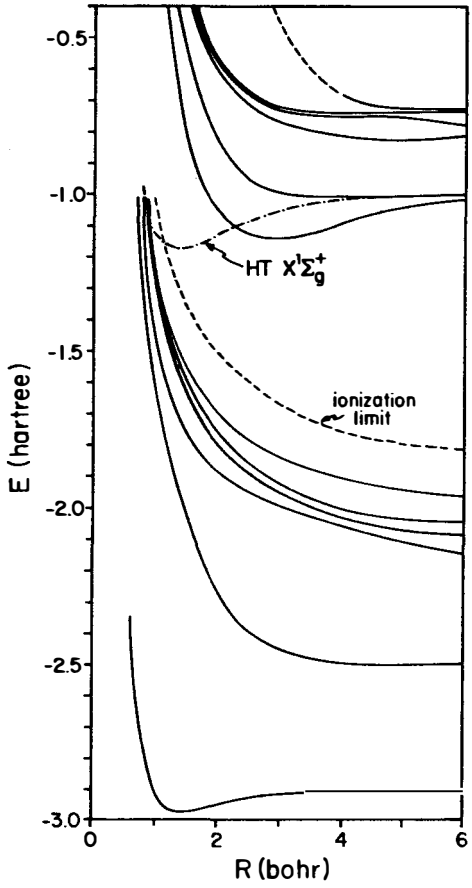


Fig. 1. Potential energy curves for HeT^+

The transition probability to all resonance and scattering states in the continuum amounts to 14.3%. In our most accurate computations we have used 249 terms in the expansion of the H matrix, and the sum of transition probabilities to all these 249 states amounts to 1.00000.

Some of the computed potential energy curves are shown in Fig.1. The equilibrium internuclear distance for T_2 is 1.4 bohr, and due to the slow motion of the nuclei the transitions to the various electronic states of HeT^+ occur without any change of R (Franck-Condon-type transitions). It is seen in Fig.1 that only transitions to the ground state can end up in a stable rovibrational state of the daughter molecular ion. For all other states the internuclear distance R = 1.4 bohr corresponds to a

strongly repulsive part of the potential energy curve and no stable vibrational states are possible.

To compute the transition probabilities to the rovibrational states in the electronic states of HeT^+ we had to solve the rovibrational Schrodinger equation

$$\frac{d^2f}{dR} + 2\mu[E - U_{nj}(R)]f(R) = 0 \qquad (3)$$

where $U_{nj}(R)$ denotes the potential governing the nuclear motion and μ is the reduced mass of the nuclei. Equation (3) is obtained if the adiabatic, i.e. factorized form of the molecular wavefunction is assumed

$$\Psi = \Psi_n(\vec{r}_1,\vec{r}_2;R)f_{nvj}(R)R^{-1}Y_{jm}(\theta,\phi) \qquad (4)$$

In the above wavefunction $\Psi_n(\vec{r}_1,\vec{r}_2;R)$ denotes the electronic wavefunction computed for the fixed internuclear distance R, $Y_{jm}(\theta,\phi)$ is the rotational wavefunction and $f_{nvj}(R)$ describes the vibrational motion. The dependence of the vibrational wavefunction on the rotational quantum number j arises from the centrifugal term in the nuclear motion potential U_{nj} appearing in Eq.(3). This potential has the form

$$U_{nj}(R) = \frac{j(j+1)}{2\mu R^2} + U_n^{BO}(R) + U_n^{ad}(R) + U_n^{rel}(R) \qquad (5)$$

where $U_n^{BO}(R)$ denotes the Born-Oppenheimer (or clamped nuclei) potential for the n-th electronic state, obtained by solving the electronic Schrodinger equation, $U_n^{ad}(R)$ is the diagonal correction for nuclear motion,[9] and $U_n^{rel}(R)$ is the relativistic correction to the potential which is small[9] and has been included only for T_2.

If the direction of the emitted β-electron does not coincide with the direction of the molecular axis, rotation of the molecule is excited. This rotation gives rise to the centrifugal potential barrier in the potential, leading to rotational dissociation from the quasibound vibrational and scattering states whose energies are above the dissociation limit. In the electronic ground state of $^3HeT^+$ there are 300 stable rovibrational states. Transition probabilities to all rovibrational states and to the region of the continuum spectrum have been computed[2] and the resulting probability histogram is shown if Fig.2. The ground state dissociation limit is at E = 0. Thus transitions to the E > 0 region include transitions to the quasibound and continuum states. It follows from the histogram that they

occur with a probability of 16.57%, which is only smaller by a factor of 2.5 than the transition probability to the bound rovibrational states, the latter amounting to 40.84%.

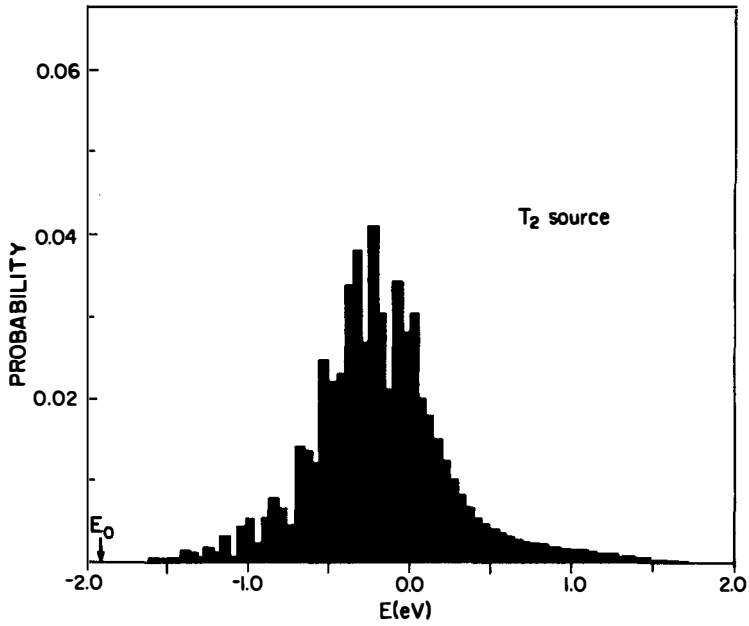


Fig.2. Probability histogram for transitions to the ground electronic state of $^3HeT^+$.

IV. Results and discussion

The best probability distribution, computed as described in the previous section, has been used to calculate the Kurie plots[3]. In Fig.3 we show some Kurie plots obtained for $m_\nu = 30$ eV using various models of the decaying system. The curves labeled "nuclear" and "atomic" show the results obtained for bare triton and for the T atom, respectively. The remaining results are for molecular T_2. The $T_2(R = 1.4)$ curve shows results computed for the equilibrium internuclear distance $R = 1.4$ bohr. The "R-averaged" results which on the graph are indistinguishable from the previous one, have been obtained by averaging the electronic transitions over the zero-point vibrations in the initial state of T_2. The "T_2(final)" curve has been computed taking explicitly into account all transitions to

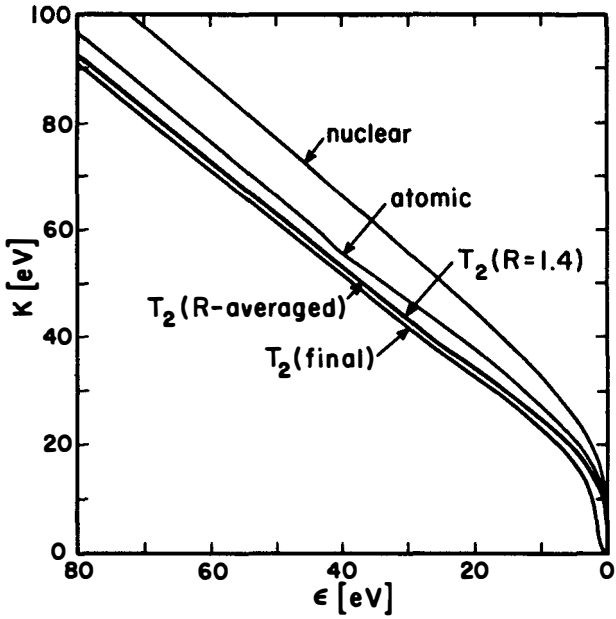


Fig. 3. Comparison of pure nuclear, atomic, and molecular T_2 Kurie plots for tritium β decay and for $m_\nu = 30$ eV.

rovibrational and continuum states in the lowest electronic states of $^3HeT^+$. These transitions considerably change the Kurie plot near the end point, and may have a large effect on the determined value of the neutrino mass if the latter is small, i.e. of the order of 1 eV or less.

We have also studied[5] the effect of various models of tritium β-decay and of the experimental resolution on the determined value of the neutrino mass. The following procedure was employed: We have used our best probability function, assumed $m_\nu = 30$ eV or $m_\nu = 1$ eV, and the spectrum thus obtained was convoluted with two different resolution functions. Next we generated the "experimental" spectrum by the Monte Carlo method, fitted the spectrum with various models, and for each model we determined m_ν.

The results are shown in Table 1. It is seen that they are sensitive to the resolution function, and if $m_\nu = 30$ eV one can expect that any reasonable molecular model would give fairly reliable[5] results. The entry GTO CI in Table 1 corresponds to a configuration interaction type wavefunction in which Gaussian type orbitals have been used[12]. This wavefunction gives considerably worse energies for HeT^+ as compared with our values but, in spite of that, it would lead to a fairly accurate value of m_ν. This situation changes considerably for $m_\nu = 1$ eV. In this case very accurate results are needed to derive an m_ν value with, say, 50% accuracy. One may expect that if m_ν equals a few eV the situation will be less optimistic than for $m_\nu = 30$ eV, and fairly accurate Kurie plots will be needed for a reliable determination of m_ν.

The results presented above refer to molecular T_2. The question arises, how big are the solid state effects that will have to be taken into account to extract the m_ν value from the LLNL frozen tritium experiment. Five such effects can be considered:

1. The fractional change of the T_2 wavefunction, $\Delta\Psi/\Psi$, caused by the binding in the crystal lattice. This is a small effect and amounts to $< 0.1\%$[13] in the wavefunction.

2. Perturbation due to the interaction of the HeT^+ ion (treated as a point charge) with the induced dipoles of the surrounding T_2 molecules results in less than an 0.8 eV shift of all excitation energies[5]. In the lowest approximation this energy is independent of the HeT^+ state, and in such a case it affects only the end-point energy but not the value of m_ν. Since in a higher approximation the interaction depends on the state of HeT^+, it has some effect on m_ν but being of a higher order this effect can be expected to be small.

Table 1. Effect of various model spectra on neutrino mass

	Resolution Function			
	ITEP 1984 Forward half width 22 eV		Gaussian FWHM = 4.7 eV	
	m_ν	Δm_ν	m_ν	Δm_ν
Reference m_ν = 30 eV				
Bare nucleus	6.4	24	12.3	18
Two-level atomic	25.5	5	25.4	5
Atomic	25.2	5	25.3	5
GTO CI, R = 1.4 bohr	29.2	<1	29.3	<1
This work r = 1.4 bohr	30.0	<1	30.0	<1
" " R-averaged	30.2	<1	30.3	<1
" " final	29.9	<1	30.2	<1
Reference m_ν = 1 eV				
Bare nucleus			0.00	1
Atomic			0.00	1
GTO CI, R = 1.4 bohr			0.00	1
This work R = 1.4 bohr			0.42	≤1
" " R-averaged			1.92	≤1
" " final			1.00	≤1

3. Recoilless β-decay ("Mossbauer effect") has been found to be completely negligible[5].

4. The sudden charge change of the decaying nucleus may induce excitations not only of the daughter ion but also of the surrounding T_2 molecules. This effect is expected to be small and will be computed in the near future.

5. Multiple scattering of the β-electron by surrounding T_2 molecules. This effect will be computed in the near future using the methods developed earlier[14]. It may be added that the multiple scattering effect is source thickness dependent and its magnitude can be studied experimentally by varying the thickness of the T_2 layer.

V. Conclusions

1. If m_ν is about 30 eV or larger a considerably less sophisticated approach than that presented above is sufficient to extract a reliable m_ν value from the experimental data.

2. If m_ν is less than about 1 ev, and the experimental resolution reaches this high degree of accuracy, both the theory and its numerical implementation must be improved.

3. In any case, we can say that results have been obtained needed for a neutrino mass determination with an error not exceeding a few tenths of an eV.

This work was supported under the auspices of the U.S. Department of Energy by Lawrence Livermore National Laboratory under Contract No.W-7405-ENG. It was also supported in part by National Science Foundation Grant No. CHE-82007220, Division of Sponsored Research of the University of Florida, and Polish Academy of Sciences Grant MR.I.9.

References

1. W.Kolos, B.Jeziorski, K.Szalewicz and H.J.Monkhorst,Phys.Rev. A 31, 551 (1985).
2. B.Jeziorski, W.Kolos, K.Szalewicz, O.Fackler and H.J.Monkhorst, Phys.Rev. A 32, 2573 (1985).
3. O.Fackler, B.Jeziorski, W.Kolos, H.J.Monkhorst and K.Szalewicz, Phys.Rev.Lett. 55, 1388 (1985).
4. W.Kolos, B.Jeziorski, H.J.Monkhorst and K.Szalewicz, Intern.J.Quantum Chem. S 19, 000 (1985).
5. O.Fackler, B.Jeziorski, W.Kolos, H.J.Monkhorst and K.Szalewicz, to be published.
6. F.N.D.Kurie, J.R.Richardson and H.C.Paxton, Phys.Rev. 49, 368 (1936).
7. R.D.Williams and S.E.Koonin, Phys.Rev. C 27, 1815 (1983).
8. L.Wolniewicz, J.Chem.Phys. 78, 6173 (1983).
9. W.Kolos and L.Wolniewicz, J.Chem.Phys. 41, 3663 (1964).
10. W.Kolos and L.Wolniewicz, J.Mol.Spectrosc. 54, 303 (1975).
11. H.S.Taylor, G.V.Nazaroff and A.Golebiewski, J.Chem.Phys. 45, 2872 (1966); H.S.Taylor, Adv.Chem.Phys. 18, 91 (1970).
12. O.Fackler and N.Winter, Unpublished; O.Fackler, M.Mugge, H.Sticker, N.Winter and R. Woerner, Proceedings of the Fourth Moriond Workshop on Massive Neutrinos in Astrophysics and Particle Physics, La Plague, Savoie, France 1984, edited by J.Tran Thanh Van (Edition Frontiers, Paris), p.273.
13. L.Z.Stolarczk and H.J.Monkhorst, unpublished.
14. W.Kolos, H.J.Monkhorst and K.Szalewicz, J.Chem.Phys. 77, 1323, 1335 (1982); K.Szalewicz, W. Kolos, H.J.Monkhorst and C.Jackson, J.Chem.Phys. 80, 1435 (1984).

A Status Report on the Livermore-Rockefeller-Fermilab Neutrino Mass Experiment

O. Fackler[a,b], M. Mugge[c,d], H. Sticker[a,e],
R. M. White[b], R. Woerner[b,f]

a The Rockefeller University, New York, NY 10021
b Lawrence Livermore National Laboratory, Livermore,CA 94550
c Fermilab, Batavia, IL 60510
d Now at Lawrence Livermore National Laboratory
e Now at Bell Communications
f Now at Wells Fargo

ABSTRACT

We are performing an experiment to determine the electron neutrino mass with the precision of a few eV by measuring the tritium beta decay energy distribution near the endpoint. Key features of the experiment are a 2 eV resolution electrostatic spectrometer and a high-activity frozen tritium source.

Now is an exciting time because, after a six year startup time, the neutrino mass determination experiments are coming to fruition. We have been setting up an experiment at Lawrence Livermore National Laboratory for the last three years and expect to be taking data this year.

Our approach to this measurement is to use frozen tritium as the source and an electrostatic spectrometer to measure the decay electron energy spectrum. Frozen tritium as a source offers a number of unique features. First, tritium molecules allow precise calculation of final state effects as was discussed in detail at this meeting by Professor Kolos. Binding the molecules in solid tritium results in a perturbation of less than 0.1 eV and are of no consequence to present generation experiments. Second, it offers the highest activity tritium source for a given dE/dx energy loss. With the counting rate near the endpoint being so low, having a high activity source is important to making a neutrino mass determination at the few eV level. Third, techniques exist to determine the dE/dx loss precisely by electron scattering experiments using gaseous hydrogen and deuterium beams. These features make frozen tritium a very attractive source. Since Professor Kolos discussed the final state effects in substantial detail, we refer the reader to his work in these proceedings, and continue with a discussion of our experiment.

For a finite neutrino mass, the Kurie plot significantly deviates from a zero mass straight line within about five neutrino masses from the zero mass endpoint. Actually, the major deviation is within two m_ν of the endpoint. In order to see the mass effect on the Kurie plot, one would ideally have a spectrometer resolution at least comparable to m_ν if not several times smaller. With an appropriate source, an experiment with sufficiently high resolution, can clearly see the finite mass, the final state and the dE/dx effects.

We have designed a system with a resolution of less than 1 eV. This high resolution was achieved by an appropriate choice of the source and

system. The spectrometer has three parallel grids, the outer of which are at ground potential. The potential on the center grid is varied to allow only those electrons with an energy greater than the potential of the grid to pass through. The wire diameter, wire spacing, and grid spacing determine the depth of the potential well between the center grid wires. Choosing a 2 eV well depth gives an effective resolution of less than 1 eV.

With our grid plane design, the spectrometer resolution is primarily determined by the angle of the electrons with respect to the electric field in the spectrometer. Electrons entering at an angle to the spectrometer axis actually follow a parabolic path and the spectrometer determines the axial momentum component of the electron. Thus to get 1 eV level resolution it is important to collimate the electrons to be nearly coaxial. We found that a beam collimated to within 14 milliradians of the spectrometer axis gave a change in acceptance from ten to ninety per cent in a 3 eV range. This resolution from our integral spectrometer corresponds to a differential resolution, such as obtained by a magnetic spectrometer, of about 2 eV. We made the collimator adjustable in length because the resolution gets better as the electrons are more tightly collimated. On the other hand, the counting rate drops as the square of the collimation angle. The collimator has been designed to give resolutions between 1 and 20 eV.

The electrons passing through the center grid are accelerated back to their incoming energy as they leave the spectrometer. They then pass through a three lens system focussing them into a 5 cm diameter spot at either a solid state detector or a microchannel plate. The solid state detector has about a 1.5 KeV energy resolution which discriminates against any background electrons which may migrate about the vacuum vessel.

We originally planned to put in a large diameter source which faced downstream. After initial setup, we found that a background resulting from photon-to-electron-conversions in the spectrometer center grid plane turned out to be much worse than expected. Because a tritium source gives rise to a large photon background from atomic deexciataion and electron

Bremstrahlung in the source backing, we made a simple modification to our design. We turned the source around, decreased its diameter, and gathered the emerging electrons in the electrostatic analog of an optical parabolic reflector with the source at its focus. The emerging electron beam is parallel and heading downstream. This technique allowed a much smaller source to give us nearly the same rate by gathering electrons from a much larger solid angle. The smaller source decreased the number of photons and it also shielded the grids from the photons since it points upstream.

The apparatus has been thoroughly tested but further work is necessary to fully realize the original design. The present spectrometer is actually a low-resolution version of our original design. When various materials compatability problems prevented early completion of the 1 eV spectrometer, we built a lower-resolution spectrometer for initial use. We found that this spectrometer had a 4 eV FWHM resolution when measuring the 7.3 keV cobalt line. This resolution is good enough for initial studies and allows work to continue on other aspects of the experiment until 1 eV resolution is required.

A second major effort required to meet our original design is to complete the cryogenic tritium source. We expect this work to take the rest of this year. While completing the cryogenic version, we are using tritium implanted in aluminum foil as a source. The tritium is held very stably in the aluminum oxide layer, leading to minimal contamination. This foil has the further advantage of being much easier to handle than a cryogenic tritium source. Unfortunately, lack of calculable final state effects prevent a determination of the neutrino mass to better than 10 eV with this source.

The cobalt resolution measurements were made using a microchannel plate and a phototube in place of the solid state detector. We are currently installing the solid state detector and expect it to be operational soon. This detector will have a low enough background rate to allow measurements very near the endpoint. During the course of these

measurements, we plan to complete the cryogenic components and perhaps install the high resolution spectrometer.

We would like to thank Professor J. Tran Thanh Van for his remarkable efforts these past twenty years in organizing these Moriond meetings. It has been a real pleasure to work with him, his family, and his staff on this meeting. Professor Tran's dedication to bringing together the right people, the right topics, and the right atmosphere for highly stimulating physics meetings has been highly successful. We all hope that the next twenty years will continue this tradition.

Finally, let us thank the sponsoring agencies, the Centre National de la Recherche Scientifique, the Commissariat a l'Energie Atomique, and the Lawrence Livermore National Laboratory for their joint sponsorship of this meeting.

The research described in this contribution is the result of the efforts of many people in the physics departments of the supporting institutions. This work is performed under the auspices of the U.S. Department of Energy by the Lawrence Livermore National Laboratory under contract NO. W-7405-eng-48, by Fermilab and by The Rockefeller University.

New Upper Limit for the Muon Neutrino Mass

R. Abela, M. Daum, G. H. Eaton*, R. Frosch, B. Jost, P.-R. Kettle, and E. Steiner

SIN, Schweizerisches Institut für Nuklearforschung,
CH-5234 Villigen, Switzerland

*Present adress: Rutherford and Appleton Laboratory, Chilton, Didcot,
Oxon OX 11 OQX, England



Presented by Manfred Daum

Abstract

At the Schweizerisches Institut für Nuklearforschung (SIN) we have measured the muon momentum p_{μ^+} in the pion decay $\pi^+ \rightarrow \mu^+ \nu_\mu$ at rest using a magnetic spectrometer. Our result is $p_{\mu^+} = (29.79139 \pm 0.00083)$ MeV/c. The consequences of this value for the rest masses of the muon neutrino and of the charged pion are discussed.

In recent years the question of whether neutrinos have finite rest masses has attracted considerable attention. In tritium beta-decay Lubimov et al. [1] have found a deviation near the end piont of the beta-spectrum which may suggest a ν_e mass between 14 and 46 eV/c^2. The measurements of m_{ν_μ} have so far been much less accurate. The world average of p_{μ^+} before our measurement, (29.794 ± 0.010) MeV/c, gave an upper limit of m_{ν_μ} around 1 MeV/c^2. Clark et al. [2] have determined m_{ν_μ} from the upper end of the invariant $(\pi^\pm\mu^\mp)$ mass distribution in the decay $K_L^0 \to \pi^\pm\mu^\mp\nu_\mu$; they find an upper limit of 0.65 MeV/c^2 (90 % c. l.) for m_{ν_μ}. Anderhub et al. [3] have investigated the decay of π^+ in flight and obtained the result $m_{\nu_\mu} < 0.50$ MeV/c^2 (90 % c. l.).

The large difference between the upper limits for m_{ν_e} and m_{ν_μ} can be understood by considering that the ideal decay process for the determination of a neutrino mass must satisfy three conditions:
(a) The kinetic energy of the observed particle must be small, so that the absolute uncertainty of the measured energy is small.
(b) The momentum of the neutrino must be small (zero if possible) so that the neutrino energy depends strongly on its rest mass, and
(c) The investigated decay process must occur with a sufficiently large branching ratio.
All three conditions are well satisfied for tritium beta-decay near the end point, whereas in the case of the muon neutrino no similarly advantageous process has been found; e. g., the decays in flight $K_L^0 \to \pi^\pm\mu^\mp\nu_\mu$ and $\pi^+ \to \mu^+\nu_\mu$ studied in references [2] and [3] respectively are suitable concerning conditions (b) and (c) but not (a), whereas the decay $\pi^+ \to \mu^+\nu_\mu$ at rest, used in our experiment, adequately satisfies conditions (a) and (c) but not (b); the neutrino has a momentum of about 29.8 MeV/c and therefore its energy depends only weakly on m_{ν_μ}.

Our experiment is based on the kinematics of the decay $\pi^+ \to \mu^+\nu_\mu$ at rest. The muon neutrino rest mass is related to the momentum of the muon and the rest masses m_{π^+} and m_{μ^+} by energy and momentum conservation:

$$m_{\nu_\mu}^2 = m_{\pi^+}^2 + m_{\mu^+}^2 - 2m_{\pi^+}(m_{\mu^+}^2 + p_{\mu^+}^2)^{1/2} \quad (1)$$

The experimental arrangement for the measurement of p_{μ^+} is shown in fig. 1. Positive pions with a momentum of 150 MeV/c from the SIN πE1 high intensity channel are stopped in a small NE102A plastic scintillator (S1) inside a homogeneous magnetic field which is used to analyze the momenta of the decay muons. The pions of interest are those which come to rest close to the downstream face of the scintillator, because their decay muons can leave the scintillator with little or no energy loss. A muon which is created at the scintillator surface and which starts along the central trajectory of the spectrometer travels

along this trajectory if the magnetic field is about 2760 Gauss. It is identified after passing through two copper collimators in a silicium surface barrier detector (Si), also placed inside the homogeneous magnetic field region. At higher magnetic fields one expects the muon rate to decrease to zero because the trajectories in the spectrometer become too strongly bent and the muons miss the silicium detector. At lower field values, muons are detected which are generated farther inside (→ 50 μm) in the scintillator and therefore lose part of their energy in leaving the scintillator.

Our data taking runs consisted of registering pulses from the silicium detector gated by pion stop signals from the scintillation counter S1. Pulse height spectra are obtained for a series of 21 magnetic field values closely spaced in and around the field region for which muons that leave the scintillator without energy loss are accepted by the spectrometer. In this field region and below the pulse height spectra of the silicium counter contain a narrow peak due

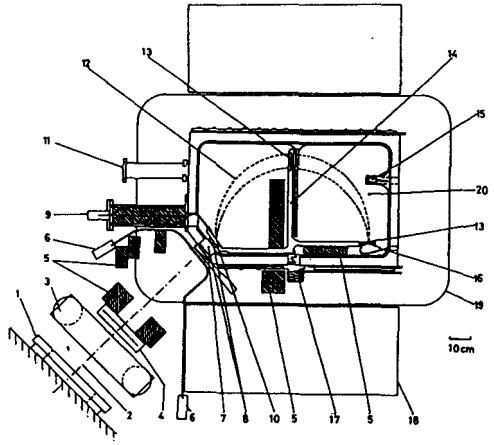


Figure 1: Experimental arrangement for the muon momentum measurement; 1. Exit vacuum window of the pion channel; 2. central trajectory of pion beam; 3. horizontal beam steering magnet; 4. multi wire proportional chamber; 5. lead collimator; 6. light guides of the two scintillation counters used for beam steering 7. remotely controlled pion degrader; 8. fixed graphite degrader; 9. S1 scintillation counter light guide; 10. S1 scintillator (NE102A); 11. port for the vacuum pump; 12. accepted muon trajectory; 13. copper collimators; 14. aluminium T-arm supporting scintillator, collimators and silicium counters, removable for distance measurements; 15. nuclear magnetic resonance probe for magnetic field measurements and stabilization; 16. silicium surface barrier detector; 17. cooling spiral for temperature control of T-arm and vaccuum chamber; 18. yoke of spectrometer magnet; 19. magnet coils; 20. ^{241}Am source for calibration of silicium detector.

to the good events produced by stopping muons from the decay of pions at rest in the scintillator; see fig. 2.

A detailed description of the apparatus, and the experimental methods, as well as first results are given in ref. [4]. Since then the statistical uncertainty has been reduced substantially by taking advantage of the increased SIN proton current and also by redesigning the π^+-beam entry and stopping region: In the new design (fig. 1) the downstream face of the pion energy degrader is much closer to the pion stop scintillator than in ref. [4]. Also most of the non-statistical uncertainties have been reduced considerably as described in ref. [5].

The momentum of a particle in a magnetic field is defined by

$$p = \eta \cdot B \cdot \rho \,. \qquad (2)$$

Here η is a constant related to the velocity of light, η = 0.0299792458 MeV/(c kG m), B is the magnetic field and ρ is the radius of the particle trajectory in the spectrometer. We have used a semicircular magnetic spectrometer with homogeneous field (cf. fig. 1 and ref. [4]). Thus our momentum measurement relies on the measurements of the homogeneous magnetic field and the size and distances of both detectors and collimators. These elements were mounted on a T-shaped aluminium arm (fig. 1), which was positioned in the vacuum chamber during data taking. For position measurements the T-arm was placed on the coordinate table of a milling machine. The critical distances were determined

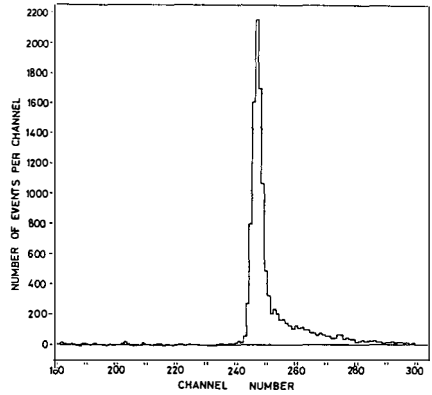


Figure 2: Pulse height spectrum in the silicium detector, taken at a magnetic field value of 2730 Gauss. The dominant peak is due to μ^+ produced by π^+-decays at rest in the scintillator S1 and accepted by the magnetic spectrometer. The tail to the right of the peak is due to e^+ from μ^+-decay and has been included in the good-event count.

with a laser interferometer to a precision of ± 10 μm. The temperature of tne T-arm was remotely sensed and stabilized to (20.0 ± 0.5) °C.

The magnetic field during data taking was stabilized to ± 8 mG by remote control once every second at a reference point (fig. 1) using a nuclear magnetic resonance (NMR) probe. Between data-taking periods complete field maps in the region of the accepted muon trajectories were taken with twenty NMR probes placed at several sets of suitable positions inside the vacuum chamber. These field maps are used to determine the difference δB between the mean effective field B_{eff} experienced by the muons and the field B_{ref} at the reference point. The combined uncertainty of the magnetic field measurements was $\Delta B = \pm 0.042$ Gauss.

In the data analysis the dependence of the good event rate (cf. fig. 2), after background subtraction, on magnetic field is fitted with curves generated by a Monte-Carlo computer program. The inputs for this program were:
(a) The spatial distribution of stopped pions,
(b) the effective magnetic field,
(c) size and positions of the detectors and collimators, and
(d) energy loss and multiple scattering of the muons in the scintillator.
The fitting procedure involves only two free parameters, namely the decay momentum p_{μ^+} and a normalization factor for the ordinate of fig. 3. The final result is:

$$p_{\mu^+} = (29.79139 \pm 0.00083) \text{ MeV/c.} \quad (3)$$

The uncertainty quoted here was obtained by quadratic summing of independent statistical and non-statistical uncertainties; cf. refs. [4] and [5].

The squared neutrino rest mass $m^2_{\nu_\mu}$ was calculated from eq. (1) inserting p_{μ^+} from eq. (3) and $m_{\mu^+} = (105.65932 \pm 0.00029)$ MeV/c^2 from the latest Particle Data Group compilation [6]. We assumed $m_{\pi^+} = m_{\pi^-}$ (CPT theorem) and used $m_{\pi^-} = (139.56761 \pm 0.00077)$ MeV/c^2, the world average of the direct π^--mass measurements [6], which is dominated by ref. [7]. The result is

$$m^2_{\nu_\mu} = (-0.163 \pm 0.080) \text{ (MeV/c}^2)^2 \quad (4)$$

The confidence level of this result is 4 %. In a new measurement of the π^--mass with improved accuracy Jeckelmann et al. [8] found $m_{\pi^-} = (139.56871 \pm 0.00053)$ MeV/c^2, from which we calculate

$$m^2_{\nu_\mu} = (-0.097 \pm 0.072) \text{ (MeV/c}^2)^2 \quad (5)$$

The confidence level of this result is 17 %. The value of eq. (5) together with the procedure recommended by the Particle Data Group and described in ref. [4] (probability function set to zero for $m^2_{\nu_\mu} < 0$) yields an upper limit

$$m_{\nu_\mu} < 0.27 \text{ MeV/c}^2. \quad (90\ \%\ \text{c. l.}) \qquad (6)$$

which is at present the lowest experimental upper limit for the muon-neutrino rest mass. The upper limit obtained from eq.(4) is $m_{\nu_\mu} < 0.25$ MeV/c^2 with 90 % confidence.

The p_{μ^+} result (3) can be interpreted in a second way: From cosmological arguments using the big bang hypothesis an upper limit of 40 eV/c^2 has been derived for the neutrino rest mass [9]. With this limit and the above value of the muon mass one can calculate the pion-muon mass difference or the mass of the π^+ from the p_{μ^+} value of eq. 3 with strongly improved precision from our measurement. The results are

$$\Delta m = m_{\pi^+} - m_{\mu^+} = (33.9111 \pm 0.0011) \text{ MeV/c}^2 \qquad (7)$$

or

$$m_{\pi^+} = (139.5704 \pm 0.0011) \text{ MeV/c}^2. \qquad (8)$$

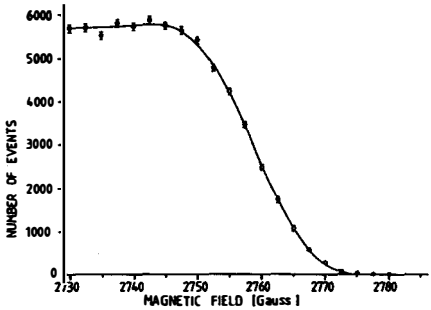


Figure 3: Spectrum of muon momenta from pion decay at rest. Ordinate: Events in muon peak of silicium counter pulse height spectrum normalized to pion stops. Abscissa: Magnetic field of spectrometer. Points with uncertainty bars are experimental data. The curve is the theoretical spectrum from a Monte Carlo calculation and is fitted to the experimental data with two free parameters (see text). χ^2 is 15.2 for 19 degrees of freedom.

References:

[1] V. A. Lubimov et al., Phys. Lett. 94B, 266 (1980).
[2] A. L. Clark et al., Phys. Rev. D9, 533 (1974).
[3] H. B. Anderhub et al., Phys. Lett. 114B, 76 (1982).
[4] M. Daum et al., Phys. Rev. D20, 2692 (1979).
[5] R. Abela et al., Phys. Lett. 146B, 431 (1984).
[6] Particle Data Group, Rev. Mod. Phys. 56,No 2, part II (1984).
[7] D. C. Lu et al., Phys Rev. Lett. 45, 1066 (1980).
[8] B. Jeckelmann et al., to be published in Phys. Rev. Lett. (1986).
[9] B. W. Lee et al., Phys. Rev. Lett. 38, 165 (1977).

NUCLEAR-MUON CAPTURE IN ^{3}He AND MASSIVE NEUTRINO SEARCH IN THE 10-100 MEV RANGE†

Baudouin Tasiaux
Institut de Physique Nucléaire
Université Catholique de Louvain
B - 1348 Louvain-la-Neuve
Belgium



ABSTRACT

In the following we show how muon-capture in ^{3}He can be used to reveal the possible existence of massive neutrinos and generations mixing among the different neutrino flavors. A detector aimed to take advantage of this feature is briefly reported. Finally, we show what limits on the mixing angle could be expected in such an experiment.

†Part of this talk is based on the letter of intent SIN R-82-14 of the SIN-Louvain collaboration (J. Egger, H. Kaspar, Cl. Petitjean ; B. Tasiaux, J. Deutsch, Gh. Grégoire, R. Prieels).
I thank, in particular, J. Deutsch for useful discussions.

1. Introduction

Within the Standard Model, all neutrinos are massless and lepton number is conserved for each generation separately.

But there are no bovious reasons for it. There might be neutrinos with mass-eigenstates of non-zero mass and those states could be mixed, leading to flavor-mixing in the coupling to the charged leptons :

$$|\nu_\ell\rangle = \Sigma\, U_{\ell m}\ |\nu_m\rangle$$

where $|\nu_\ell\rangle$ (ℓ = e, μ, ...) are the states of definite flavor-coupling ; $|\nu_m\rangle$ (m = 1, 2, 3, ...) are the mass-eigenstates, and $U_{\ell m}$ are the mass-mixing matrix elements, with $U_{\ell m}$ ($\ell \neq m$) not necessarily zero.

Leptons would then look more similar to quarks as required by various scenarios of grand-unification. Massive neutrinos could explain experimental anomalies, like missing solar ν_e on earth, or missing mass in the galactic halo ... They would also help to explain cluster formation in the universe, double beta-decay suppression ...

2. Muon-capture in ^{3}He

Muon-capture in general could bring about many consequences of new physics beyond the Standard Model [1]. For the present we shall be concerned with the possible evidence of non-vanishing neutrino mass and neutrino-mixing in the muon flavor-state.

The principle of the experiment [2] consists essentially in a precision spectroscopy of the charged partner emitted in conjunction with the neutrino $|\nu_\ell\rangle$: a mixture of non-vanishing mass-eigenstates would be revealed by peaks of "anomalous" momentum in the charged particle spectrum.

Though very sensitive to $U_{\ell m}$, the typical energy-resolution achievable limits this method to the observation of neutrinos having masses in the MeV-range at least.

Such massive neutrinos can be accomodated by astrophysical evidence only if they are unstable. The mixing mechanism itself provides however the required decay mechanism of sufficient rapidity [8].

In this case, $\mu + {}^3\mathrm{He} \rightarrow {}^3\mathrm{H} + \nu + 105.6$ MeV, the triton recoil energy is ranging from 0.8 MeV to 1.9 MeV for neutrino masses diminishing from 80 MeV/c^2 to a few MeV/c^2. This region is of particular interest [3] since there is a gap to fill in the (m_ν, $|U_{\mu H}|^2$) plane, between 30 MeV/c^2 and 80 MeV/c^2 (see figure 2).

Below 30 MeV/c^2, the sensitivity of the $\pi \to \mu\nu$ decay [4] was limited by the π/μ mass difference, while over 80 MeV/c^2, the $K \to \mu\nu$ decay experiment [5] was limited by the momentum resolution of its muon spectrometer. Limits extracted [3] from previous non-dedicated experiments [6] far above $|U_{\mu H}|^2 = 0.01$.

We are intended [7] to explore this region, building a ^{3}He living target featuring much better energy resolution and background rejection than 6).

3. Detection of ^{3}H

There are 3 main experimental constraints : the low triton energy ($0.8 < T_{^3H} < 2$ MeV), the beam features (FWHM $\Delta p/p = 2.5$ % at 30 MeV/c ; $\Delta x \,.\, \Delta\theta_x = 3$ cm x 0.6 rad ; $\Delta y \,.\, \Delta\theta_y = 5$ cm x 0.1 rad) and the finite beam time (in-beam time $\sim 10^6$ sec).

In order to be as sensitive as possible on the mixing angle over the widest neutrino mass range, we require :- good energy resolution ($\sim$ 3 %) in the 0.8 - 2 MeV range : to improve signal to noise ratio, $|U|^2$-limits, neutrino mass resolution (if a heavy neutrino is found) and increase the sensitivity to smaller neutrino masses.

- good particle separation : to be able to tell tritons from μ-decay electrons, protons and deutons (at least for the most numerous deutons at high energy), coming from the break-up channels of the capture.

- good stop localisation : to avoid uncontrolled energy-loss at the borders of the fiducial volume.

- reasonable triton-rate.

The low triton energy implies the target to be also the detection medium. A Gas Scintillation Proportional Counter [9] (GSPC) was prefered to a proportional counter (slow, unstable, $\frac{\Delta E}{E} \gtrsim 5$ %) or to the gas scintillation counter ($\frac{\Delta E}{E} \gtrsim 15$ %) used in 6).

A first prototype [10] was built to solve the specific problem of maintaining the required field intensity ($\gtrsim 3$ V/torr-cm) in helium. Using special electrode- and feed-through designs, this problem was solved and 4 % FWHM energy resolution was readily achieved with alpha-particles in a mixture of 90 % He-10 % Xe. Other mixtures were also successfully tested. Thanks to the drift time of about 1 cm/μs, very good localization of the deposited charges could be obtained in the drift direction. The charges deposited bythe muon and the particle emitted with some delay can also be separated by a suitable inversion of the drift field.

A second prototype is now under construction, and should be tested in beam by September 86. This detector is a 5-liter-vessel made out of 4 cm-stesalit steel-reinforced walls working at 5 atm. A schematic lay-out is given in figure 1.

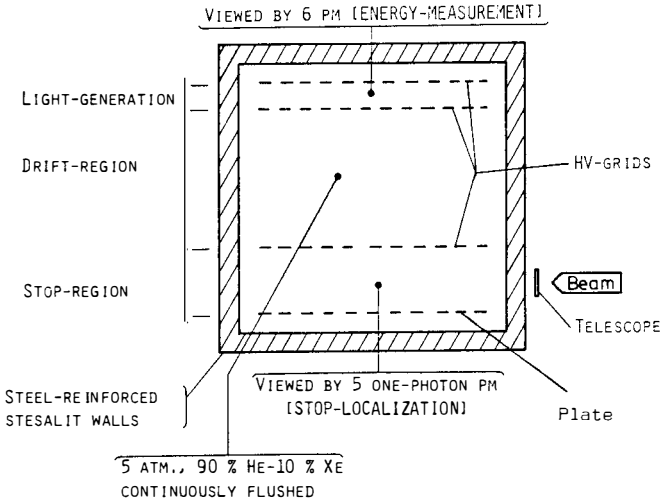


Figure 1 : Schematic lay-out of the detector
(not to scale)

It provides a 4 x 5 x 9 cm^3 fiducial volume (630 mgr) for the low energy muons coming in through a ø 4 cm havar window. Muons are stopping between a plate at positive voltage and a grid at negative voltage, placed 7 cm apart, so that this region is clear from background charges. Five one-photon PM's are watching this gap to detect the emission, after a suitable time, of decay particles, and trigger the field inversion towards the analyzing region. They also localize the stop-position with a precision expected to be about 5 x 5 mm^2 in a plane parallel to the electrodes.

If a heavy charged decay particle is emitted, the electron swarm newly created and the muon electron swarm are drifted up to the high field region, where they will be viewed by 6 low gain PM's. Energy will be measured and additional directional information will be extracted from the light pulse shape. The energy measurements and localization allow an excellent separation of tritons from other particles, excepted, possibly, from 1-2 MeV deuton of very small number. And so, the background is expected to lie at a very low level.

4. Count rate estimate

At 30 MeV/c the SIN μE4-beam should supply 2.10^4 muons/s crossing the detector window. One third of those will stop in the fiducial region, a quarter being captured by ^{3}He. The triton yield can then be evaluated to 6/s, half of those being emitted late enough to be analyzed.

Figure 2 shows the mixing angle limits expectation versus GSPC energy-resolution and background.

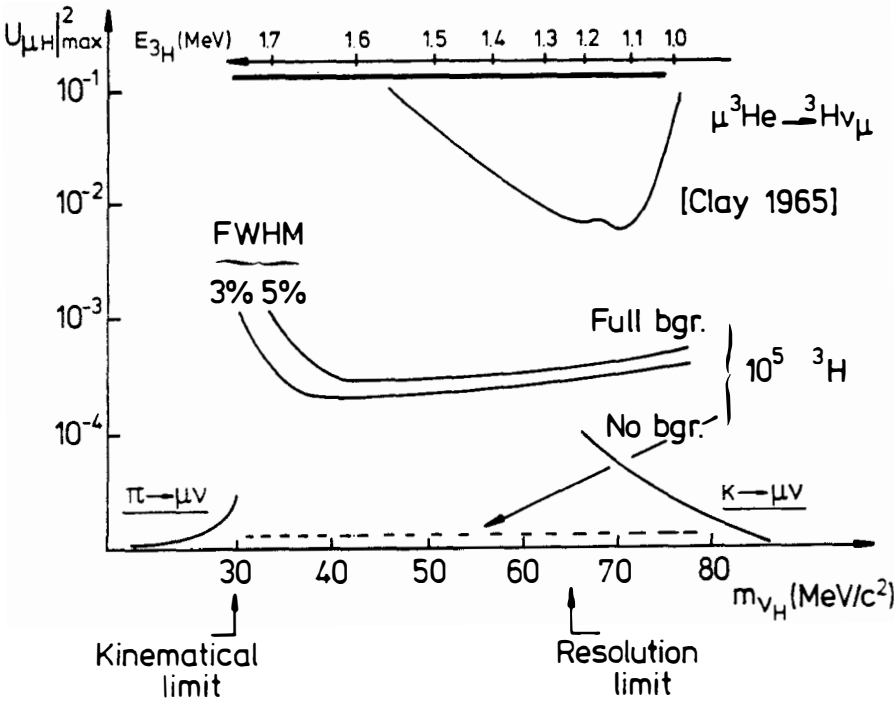


Figure 2 : Mixing angle enlarged view.
$|U_{\mu H}|^2$-limits expected observing 10^5 ^{3}H.

1) For recent information on this subject, see J. Deutsch "Workshop on Fundamental Muon Physics : Atoms, Nuclei and Particles" Los Alamos Nat. Lab. LAMPF, Jan 20-22, 1986

2) For a general discussion, R.E. Schrock, Phys. Rev. D24 (1981) 1232

3) J. Deutsch et al., Phys. Rev. D27 (1983) 1644

4) R. Abela et al., Phys. Lett. 105B (1983) 263 ; R.C. Minehart et al., Phys. Rev. Lett. 52 (1984) 804

5) T. Yamazaki, Proc. 22nd Int. Conf. on High Energy Physics (1984) eds. A. Meyer and E. Wieczorek, Vol. I, pg 262

6) L.B. Auerbach et al., Phys. Rev. 138 (1965) B127 ; D.R. Clay et al, Phys. Rev. 140 (1965) B586

7) J. Egger, H. Kaspar, Cl. Petitjean ; B. Tasiaux, J. Deutsch, Gh. Grégoire, R. Prieels, SIN R-82-14

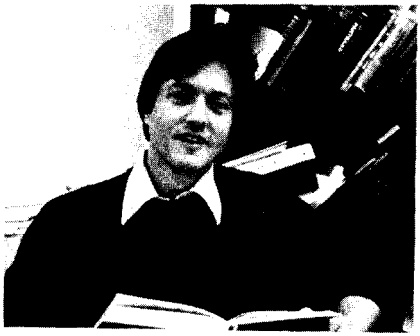
8) E.g. : J. Schechter and J.W.F. Valle, Phys. Rev. D25 (1981) 774

9) A.J.P.L. Policarpo, Space Sc. Instr. 3 (1977) 77 and ref. therein

10) J. Deutsch et al., S.I.N. Jahresbericht (1983) NL26

SEARCH FOR NEUTRAL HEAVY LEPTONS

David S. Koltick
Purdue University
West Lafayette, Indiana 47907



ABSTRACT

Searches for massive neutral leptons in e^+e^- collisions are reviewed. Upper limits found using the HRS and Mark II detectors at PEP and the JADE and CELLO detectors at PETRA are presented.

In e^+e^- annihilation at PEP and PETRA energies, the effects of the weak neutral boson, Z°, have been observed through its interference with the photon.[1] Measurement of the production of $e^+e^- \to \mu^+\mu^-$, $\tau^+\tau^-$ and more recently charm production[2] all confirm the standard model predictions. Another prediction of the standard model is that neutral leptons will be produced in this energy range through direct couplings to the Z°. The cross section for $e^+e^- \to L^\circ\bar{L}^\circ$ shown in Fig. 1a is given by,[3]

$$\sigma_{Stan} \sim \frac{G_F^2 M_Z^4}{96\pi} \left[\frac{S}{(S-M_Z^2)^2}\right] \frac{\beta(3+\beta^2)}{4} \sim \frac{8}{9} \frac{\pi\alpha^2 S}{(S-M_Z^2)^2} \sim 3.10^{-37} \text{ cm}^2 \qquad (1)$$

where I have written the cross section in terms of electromagnetic parameters so it can easily be compared with production by annihilation through a single photon. Data sets as large as ~300 pb^{-1} have been accumulated at PEP, while at PETRA sets between 30 and 40 pb^{-1} have been obtained. This means up to ~100 $L^\circ\bar{L}^\circ$ pairs per generation have been produced per PEP experiment and up to ~30 per PETRA experiment. If the standard model is correct and each generation has only massless neutral leptons then the only way to "observe" the production of these states would be through radiative effects.[4] There are not enough events yet to carry out such a program. Nonetheless, many questions can be asked to check the standard model and to look for the unexpected.

INVERTED GENERATION

Suppose that the 4th generation is inverted[5] so that $M_{L^\circ} > M_{L^-}$. But such heavy leptons can be ruled out for $M_{L^\circ} < 23$ GeV/c^2, because no new heavy charged leptons have been observed up to a center of mass energy of 46.3 GeV in e^+e^- collisions. This is true whether or not the lepton generations mix with one another.

MIXING BETWEEN GENERATIONS

If the 4th generation neutral lepton is massive and has a mixing as is shown in Fig. 1b, then we would expect to observe its decays if its lifetime is less than ~10^{-11} M_{L°(GeV/c^2) seconds (prompt decays).

In order to separate the very rare $L^\circ\bar{L}^\circ$ events from the ~10^5 hadronic events in an experiment, two main features of L° decay can be employed. The first is illustrated in Fig. 2. Here the probability of L° decay into two charged tracks is plotted[6] as a function of M_{L°. The prediction is that the two charged track decay mode dominates for $M_{L^\circ} < 1.5$ GeV/c^2. At higher masses the two charged track mode is still expected to make up

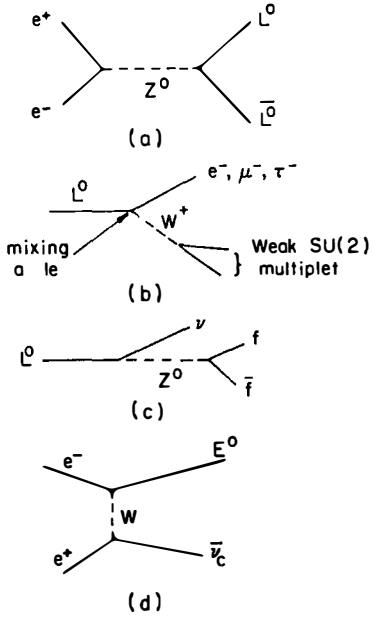


Fig. 1(a) The production heavy neutral leptons in e^+e^- annihilations.
(b) The decay of a heavy neutral lepton via mixing with other generations. Flavor changing currents are disallowed.
(c) A flavor changing neutral current decay.
(d) Production of a heavy electron-type neutral lepton.

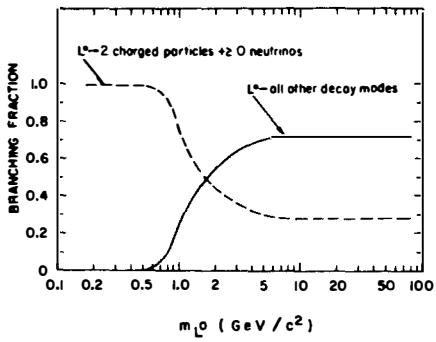


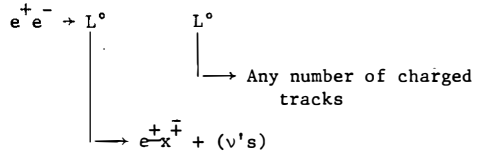
Fig. 2. The branching fractions for the decay of an L° via the weak charged current.

~30% of the total decays. This is in sharp contrast to the average hadronic jet multiplicity, $\langle n_{jet} \rangle \approx 6$-7 charged tracks.

A further rejection of hadronic background can be obtained by demanding a lepton in the final state. An electron or muon in the final state is a strong indicator that a weak interaction has taken place.

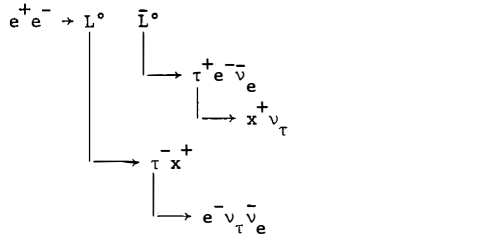
HRS

The HRS group has utilized this approach in searching for the decay,[7,8]



(2)

A very striking event is shown in Fig. 3. Notice that the event contains two like sign electrons. If the L° is mixed with the lower mass leptons, then it may mix most strongly with the τ just as the b-quark mixes most strongly with the c-quark. A possible explanation for this event is then,



(3)

where x represents any particle which is not an electron. The minimum mass of this event is $M_{L^\circ} \geq 6.3$ GeV/c^2. The HRS group finds 6 events of this type in the data. The expected background is 5.5 events coming from charm production, hadrons mimicking an electron and the effects of a non-hermetic detector. Considering these events to be background the corresponding upper limits are shown in Fig. 4.

MARK II PROMPT SEARCH

At PEP and PETRA there are relatively few events produced with four charged particles, no photons, and total charge zero. The major source of such events are purely electromagnetic processes. There are also relatively few events containing only two charged tracks, no photons and total charge zero once the Bhabha scattering events and $\mu^+\mu^-$ pair production has been eliminated. In many models production proceeds as shown in Fig. 1b. For $M_{L^\circ} \leq 1$ GeV/c^2 a substantial branching fraction exists into two charged particles with and without neutrinos in the final state. Based on this criteria and using 220 pb^{-1} of data, the MARK II group has conducted two searches.[6] The first uses 443 candidate events with four charged particles in the final state and the second uses 249 candidate events with only 2 charged particles in the final state.

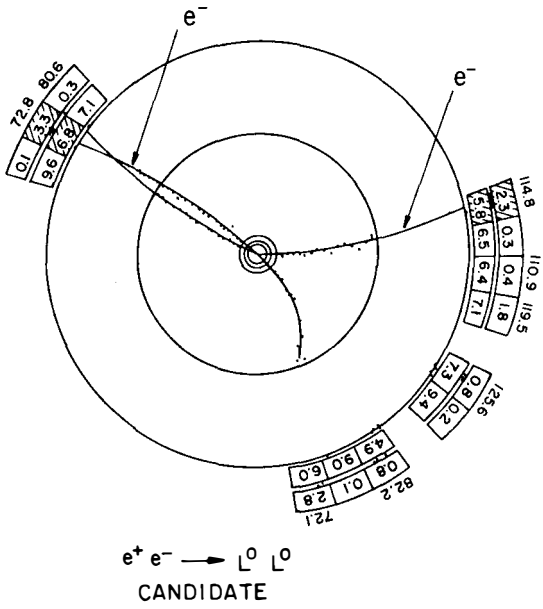


Fig. 3. A candidate event for $e^+e^- \to L^\circ\bar{L}^\circ$.

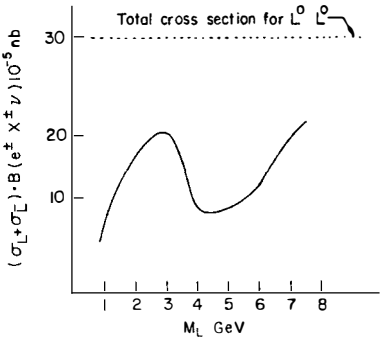


Fig. 4. Upper limits at 95% C.L. for heavy lepton production from the HRS.

The events that contain four charged particles in the final state can be used to search for the decays

$$L^\circ \to \omega^+ + x^-$$
$$L^\circ \to y^+ + z^- + \nu \qquad (4)$$
$$L^\circ \to y^+ + z^- + 2\nu\text{'s}$$

where the roman letter stands for any charged final state particle. Most of the candidate events result from $e^+e^- \to \tau^+\tau^-$ and are easily eliminated. A further reduction of the sample is achieved by elimination of low mass e^+e^- pairs and demanding the events to conserve energy. There are no events found consistent with $0.11 \leq M_{L^\circ} \leq 5.4$ GeV/c^2. Eleven events are found consistent with $M_{L^\circ} > 6.0$ GeV/c^2 but represent a cross section much larger than standard model predictions allow for such massive states. Mainly because the prob-

ability for such massive L°'s both decaying with only 2 charged tracks in the same event is quite small.

The upper limit for heavy neutral leptons having a 100% branching into 2 charged tracks ($M_{L^\circ} \leq 1$ GeV/c^2) is $\sigma_{L^\circ\bar{L}^\circ}/\sigma_{Stan} \leq 0.2$. If the branching fractions shown in Fig. 2 are used, then $M_{L^\circ} \leq 2$ GeV/c^2 are ruled out at the 90% confidence level.

Similarly the two charged track data can be used to search for the decays

$$\begin{aligned} L^\circ &\to \nu\ \nu\ \nu \\ \bar{L}^\circ &\to e^{\pm} + \chi^{\mp} + \nu \end{aligned} \tag{5}$$

the all neutrino decay mode can result from a flavor changing neutral current interaction shown in Fig. 1c. The major backgrounds in the sample can be removed by dropping events with low mass e^+e^- pairs and demanding a large transfer momentum with respect to the beam direction, effectively eliminating the two-virtual photon events. With this criteria no events are observed consistent with $M_{L^\circ} \leq 3.2$ GeV/c^2. The 90% C.L. upper limit for this mass range is

$$Br(L^\circ \to \nu\nu\nu)Br(L^\circ \to e^{\pm}\chi^{\mp}\nu)\sigma_{L^\circ\bar{L}^\circ}/\sigma_{Stan} \leq 0.2 \tag{6}$$

MARK II LONG LIVED SEARCH

If a GIM mechanism is operational in L° decay then the L° will only be able to decay into a known charged lepton and virtual W. Its lifetime is completely calculable but will depend on an unknown mixing angle ε (Fig. 1b). In this model each L° must decay into at least 2 charged particles.

Using these ideas the MARK II group at PEP[9] has conducted a search for long lived, heavy neutral leptons. The strategy was to look for events with two vertices separated from the interaction point and containing no tracks coming directly from the interaction point. No events were found. At 90% confidence level, decay lengths between 1 and 20 cm are excluded for $1 < M_{L^\circ} < 13$ GeV/c^2. The excluded contours are shown in Fig. 5.

JADE - HEAVY ELECTRON-TYPE LEPTON

The JADE group at PETRA[10] has searched for a heavy, neutral, electron-type lepton E°, having the same quantum numbers as the electron. The production of such a state $e^+e^- \to E^\circ\bar{\nu}_e$ proceeds through the diagram shown in Fig. 1d. The E° subsequently decays to E° → e + W. The W then decays in a conventional manner to the known quarks and leptons. There are two main characteristics of these events which allow them to be separated from the

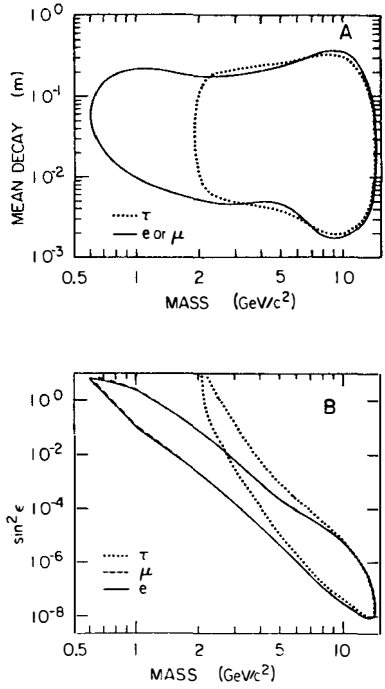


Fig. 5. Excluded region for L° at 90% confidence level for (a) mean decay length as a function of mass and (b) since as a function of mass.

hadronic background. The first is that they have a large amount of missing energy as compared to hadronic events. The second is the events are extremely acoplanar or non jet like. This is obvious in the case of low mass E°'s. Similarly the high mass states have an acoplanarity distribution extending well above the hadronic background as is shown in Fig. 6.

Comparing the number of surviving events after all cuts to the number expected using a Monte Carlo simulation, the JADE group is able to set a 95% C.L. upper limit of $M_{E^\circ} > 22.5$ GeV/c^2 when combined with the previous SPEAR result of $M_{E^\circ} > 1.5$ GeV/c^2.

CELLO

The CELLO group at PETRA[11] using a data set of ~22 pb^{-1} has recently completed a series of heavy neutral lepton searches. For the production $e^+e^- \to L^\circ\bar{L}^\circ$ as has been discussed earlier, they exclude the mass region $3.2 < M_{L^\circ} < 17.4$ GeV/c^2 at 95% C.L., if the mixing shown in Fig. 1b is dominantly to the muon. They exclude the region $3.1 < M_{L^\circ} < 18.0$ GeV/c^2 if the mixing is dominantly to the electron.

A search has also been carried out for $e^+e^- \to E^\circ\nu_e$. The improved limits for a V-A coupling are $M_{E^\circ} > 34.6$ GeV/c^2 and for a V+A coupling $M_{E^\circ} > 37.4$ GeV/c^2, both at 95% C.L. A more thorough discussion of the CELLO results is presented elsewhere in these Proceedings.

CONCLUSION

In e^+e^- collisions at both PEP and PETRA we are producing the 4th generation of neutral leptons if they exist and if their mass is less than ~15 GeV/c^2. All searches have produced only null results. This

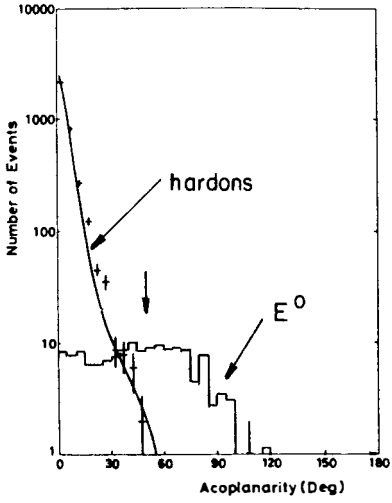


Fig. 6. The acoplanarity distribution for $M_{E^0} = 17$ GeV/c^2 compared to that of hadronic events.

suggests either that the 4th generation is not doing anything peculiar at the level of ~100 events or that it does not exist.

REFERENCES

1. D.S. Koltick, in Symposium on High Energy e^+e^- interactions, Vanderbilt U. (1984).

2. D.H. Miller in Proceedings of the International Europhysics Conference on High-Energy Physics, Bari, Italy, Ed. L. Nitfi, G. Preparata (1985).

3. I.J.R. Aitchison and A.J.G. Hey, Gauge theories in Particle Physics, (Adam Hilger LTD, Bristol 1982).

4. Proceeding of the SLC workshop on Experimental use of the SLAC linear collider, March 1982 - SLAC-Report-247.

5. M.L. Perl, in Proceedings of the Sante Fe Meeting of the Division of Particle and Fields of the American Physical Society, edited by T. Goldman and M.N. Nieto (World Scientific, Philadelphia and Singapore, 1985).

6. M.L. Perl et al., Physical Review D B2, 2859 (1985).

7. R. Thun, Physics Letters 134B, 459 (1984).

8. D. Errede et al., Phys. Lett. 149B, 519 (1984).

9. G.J. Feldman, Preceedings of the Annual Meeting of the Division of

Particles and Fields of the APS, Eugene, Oregon, August 1985.

10. W. Bartel, et al., Phys. Lett. 123B, 353 (1983).

11. Aleksan, these proceedings.

LIMITS FOR THE ELECTRON NEUTRINO MASS FROM INTERNAL BREMSSTRAHLUNG

K.Riisager
Institute of Physics, University of Aarhus
DK-8000 Aarhus C, Denmark



ABSTRACT

Numerical non-relativistic calculations of internal bremsstrahlung spectra are described and compared with recent experiments. The spectra of the nuclei ^{193}Pt (wherefrom m_ν limits have already been obtained) and ^{125}I have been measured, both agreeing well with theory. From the measurements of ^{125}I it is possible to deduce limits on the mixing parameter for heavy neutrinos in the mass range 15 keV to 45 keV. Predictions are presented for the spectrum of ^{163}Ho, upto now the preferred nucleus for neutrino mass measurements using internal bremsstrahlung.

1. Introduction

Internal bremsstrahlung following electron capture (IB) is the second-order process in which a photon is emitted in a normal nuclear electron capture:

$$A_Z \rightarrow A_{(Z-1)}{}^h + \nu + \gamma. \qquad (1)$$

The final state thus consists of the daughter nucleus with a hole h in an atomic shell (normally an s-hole or a p-hole), an electron neutrino and a photon. In general, only the photon is measured. The end point of the photon spectrum, which corresponds to emission of neutrinos of low energy, carries information on the neutrino mass in the same way as the tritium end point carries information on the anti-neutrino mass. Use of IB is the most obvious way to obtain direct mass limits on neutrinos to complement the limits on anti-neutrinos from tritium decay.

Interesting mass limits require IB-spectra with high relative intensity at the end point. This will occur for nuclei where the Q-value equals an atomic s-state binding energy B_{ns}. The reason is that all p-IB spectra (final state with a p-atomic hole) exhibit resonances at low photon energies, namely the x-rays. X-ray emission after electron capture is normally treated as a two-step process, but is covered by eq.(1). The x-rays are an integral part of the IB spectrum. Requiring the internal bremsstrahlung end point to lie at the position of an x-ray gives the mentioned relation $Q=B_{ns}$. For the resonant enhancement to work fully, this relation should be fulfilled within the width of an x-ray, i.e., O (10 eV). Untill now no nuclei has been found for which this is the case; the seemingly most promising candidate for neutrino mass measurements is ^{163}Ho with [1]) $Q-B_{3s} \sim 750$ eV.

Experimentally the IB-technique offers several advantages, as photons are detected instead of electrons, and as the shakeup and shake-off problems which plague the tritium experiments are virtually nonexisting here. The two main disadvantages are as follows. First the total IB-spectrum is intrinsically composite. Many atomic final states (though a finite number) are allowed in eq.(1), each with an associated partial IB-spectrum. The end points of the different spectra do not coincide. However, this can sometimes be turned into an advantage (this was the case for the ^{125}I experiment of section 4) as a neutrino signal must occur at several correlated positions in the spectrum. Alternatively coincidence measurements can be used to pick out a single spectrum. Second we need to have reliable calculations of the matrix elements. The resonances which make IB-experiments possible stem from the atomic matrix elements. These matrix elements can in principle be calculated, the next section summarizes our (partial) solution of this problem. Experiments on ^{197}Pt and ^{125}I to test these calculations are then described, the limits one can extract on neutrino masses from these experiments are also given. At last some conclusions on the future work with IB will be given.

2. Calculations of IB spectra

The standard treatment of internal bremsstrahlung is due to Glauber and Martin[2]). They were mostly interested in predicting the spectrum above the x-ray region and used hydrogenic wave functions. DeRujula[3]) extended their work to include the low

photon energies as well and suggested an empirical procedure in order to place the x rays at their experimentally observed positions. In subsequent works[4]) screening has been taken into account by use of non-relativistic wave functions. This brings the predicted x-ray energies in much closer agreement with the experiments than by use of hydrogenic wave functions.

A detailed discussion of the theory of p-IB is given in ref.4, we here just give the final formula. The intensity of np-IB (final state atomic np-hole) per decay as a function of photon energy K is:

$$\frac{1}{\omega_{tot}} \frac{d\omega_{np}}{dK} = \frac{2e^2}{\pi\hbar^3 c^3} \frac{S\,|M_{np}(K)|^2}{\sum_{n'l} |\psi^{Z}_{n'l}(0)|^2 (Q-B^{Z-1}_{n_p})^2} \tag{1}$$

$$S = \sum_i c_i K(Q-B^{Z-1}_{np}-K)((Q-B^{Z-1}_{np}-K)^2 - m_i^2c^4)^{1/2} \tag{2}$$

$$M_{np}(K) = \sum_{j=1}^{N} \frac{\psi^{Z}_{js}(0)(B^{Z-1}_{np} - B^{Z-1}_{js})}{K+B^{Z-1}_{np} - B^{Z-1}_{js} + i\frac{\Gamma_{nj}}{2}} \int(\psi^{Z-1}_{js})^* \, z \, \psi^{Z-1}_{np} d\tau \tag{3}$$

$$+ \sum_{j=N+1}^{\infty} \frac{\psi^{Z}_{js}(0)(B^{Z}_{np} - B^{Z}_{js})}{K + B^{Z}_{np} - B^{Z}_{js}} \int(\psi^{Z}_{js})^* \, z\psi^{Z}_{np} d\tau \ .$$

Here Q is the nuclear Q-value, B and $\psi(0)$ the atomic binding energy and wave function at origin values with the subscript giving the atomic orbital and the superscript the nuclear charge (Z in the mother atom, Z-1 in the daughter atom). S is the kinematic factor which depends on the neutrino mass. Here the general formula is given for several neutrino masses m_i of relative strength c_i (this is only relevant if neutrino mixing occurs). M_{np} is the second-order matrix element, the integrals stem from the atomic dipole matrix elements. Only the wave functions for the occupied levels are used, the last term in eq.(3) is approximated by a term $T_{np}/(K+t_{np})$, which is evaluated by means of sum rules (see ref.4 for details).

The corresponding formula for ns-IB is simply:

$$\frac{1}{\omega_{tot}} \frac{d\omega_{ns}}{dK} = \frac{c^2}{\pi m^2 \hbar c^5} \frac{|\psi^{Z}_{ns}(0)|^2 \, S}{\sum_{n'l} |\psi^{Z}_{n'l}(0)|^2 (Q-B^{Z-1}_{n'l})^2} \tag{4}$$

with S given in eq.(2) and the same notation as above.

3. The IB-spectrum of ^{193}Pt

The isotope ^{193}Pt is ideally suited for a test of the low energy IB theory as its Q_{EC}=56.6±0.3 keV is less than the 1s-binding energy. For our measurements[5,4]) of its IB-spectrum we used a source of 7×10^{13} atoms produced at the ISOLDE facility at CERN. The setup used a 200 mm^2 intrinsic Ge detector and a 100 mm^2 Si(Li) detector so that the total IB-spectrum as well as the

IB coincident with L x-rays (i.e. 2p-IB) could be measured. Refs.4,5 give the experimental details.

A comparison of the experimental and theoretical total IB spectrum is given in figure 1a on an absolute scale. The shape is reproduced very well by theory, while the absolute magnitude is good to within a factor of 2 only. Figure 1b gives the corresponding comparison for the 3p+4p+... IB-spectra. Again the shape fits well, while the absolute magnitude is somewhat off. Note the interference dip at 20 keV which arises when the amplitudes in the matrix element in eq.(3) sum to zero. As already reported[5]) a 90% conf. upper limit on the electron neutrino mass (m_1 of eq.(2), assuming $c_1 \simeq 1$) of 500 eV can be put from this experiment.

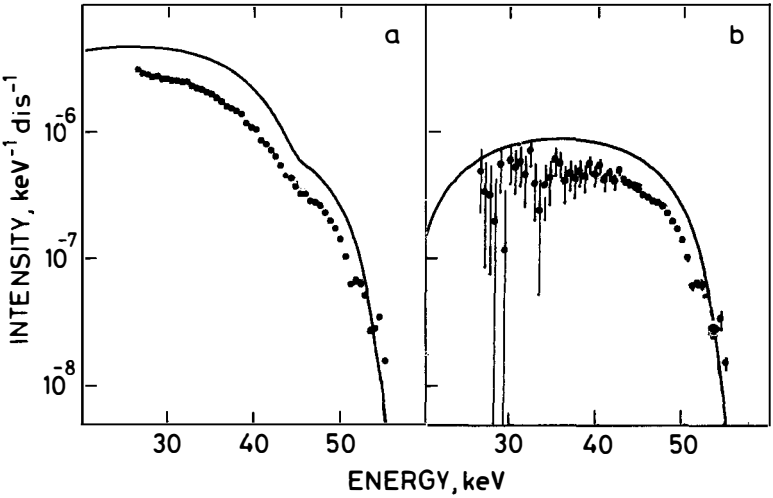


Fig.1. The internal bremsstrahlung spectra of ^{193}Pt taken from ref.4. The solid line is the theoretical curve (see section 2), dots are experimental points. Figure 1a shows the total IB spectrum, figure 1b shows the (3p+4p+...)-IB spectrum.

4. The IB-spectrum of ^{125}I

The isotope ^{125}I has a Q_{EC}=186.1±0.3 keV somewhat higher than atomic binding energies. For this reason both s-IB and p-IB can be seen, the latter dominating at lower energies. A source of about 7×10^{14} atoms was produced at ISOLDE. The total IB-spectrum was measured with two 200 mm^2 intrinsic Ge detectors. Reference 6 gives the experimental details.

Figure 2 gives the theoretical and experimental IB-spectrum on an absolute scale. Again the shape is reproduced very well, the absolute magnitudes agree within the 30% ,uncertainty on the normalization of the experimental spectrum. The data yield limits on neutrino-mixing. Assuming that only two neutrino masses are present, one of them very light, we get 90% conf.

upper limits on the mixing parameter c_2 of eq.(2) of 1-2% for neutrino masses m_2 in the range 15-45 keV. This excludes the suggested[7]) 3% 17 keV neutrino in accordance with experiments[8]) on ^{35}S.

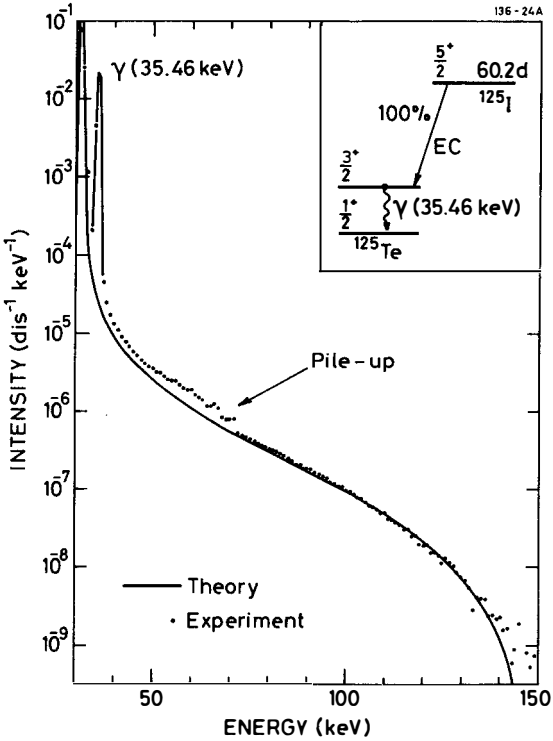


Fig.2. The total IB spectrum of ^{125}I, the inset gives the decay scheme. The experimental spectrum is unfolded for detector response but not corrected for pile-up, which gives the structure in the spectrum below 70 keV.

5. Outlook

From the two comparisons we conclude that theory can give the shape of IB-spectra with high accuracy and absolute intensities within a factor 2 as long as we are well away from interference dips, where we are very sensitive to small changes in atomic parameters. The predicted spectrum[4]) for ^{163}Ho, the most promising candidate for neutrino mass measurements, is given in figure 3. The most noticable feature is the interference dip right at the end point. We can not determine the exact position of this interference dip[4]), however, it will lie within 0.5 keV of the spectral end point, thus making neutrino mass measurements more difficult. We feel that to put interesting limits on m_ν from the IB-spectrum of ^{163}Ho, it is necessary to use high efficiency detectors with better

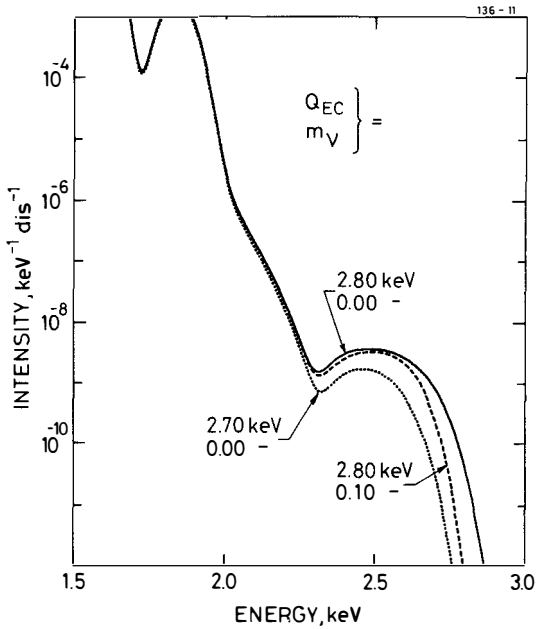


Fig.3. The theoretical total IB spectrum of ^{163}Ho.A detector resolution (FWHM) of 0.1 keV has been folded in. Predictions are given for three sets of values of Q and m . The exact position of the interference dip is uncertain by about 0.5 keV.

resolution than offered by Si(Li) detectors. The possibility of finding a better isotope should not be excluded. Calorimetric measurements[9]) on ^{163}Ho still seem promising as we here measure both the IB ("tails of x rays") and ejected electrons ("tails of Auger lines"), the last process being the dominating one.

Acknowledgement

The work reported here was carried out in collaboration with M.J.G.Borge, A.DeRújula, P.G.Hansen, B.Jonson, G.Nyman, and H.L.Ravn. K.R.was supported by the Danish Natural Science Research Council.

References

1) E.Lægsgaard, J.U.Andersen, G.J.Beyer, A. DeRújula, P.G.Hansen, B.Jonson and H.L.Ravn, Proc.7th Int.Conf.on Atomic Masses and Fundamental Constants (AMCO-7), Darmstadt 3-7 September 1984, p.652
2) R.J.Glauber and P.C.Martin, Phys.Rev.104 (1956) 158, P.C.Martin and R.J.Glauber, Phys.Rev.109 (1958) 1307
3) A.DeRújula, Nucl.Phys.B188 (1981) 414
4) K.Riisager, A.DeRujula, P.G.Hansen, B.Jonson, and H.L.Ravn, Physica Scripta 31 (1985) 321
5) B.Jonson, J.U.Andersen, G.J.Beyer, G.Charpak, A.DeRujula, B.Elbek, H.Å.Gustafsson, P.G.Hansen, P.Knudsen, E.Lægsgaard, J.Pedersen and H.L.Ravn, Nucl.Phys.A396 (1983) 479c
6) M.J.G.Borge, A.DeRujula, P.G.Hansen, B.Jonson,G.Nyman, H.L.Ravn and K.Riisager, submitted to Nucl.Phys.A
7) J.J.Simpson, Phys.Rev.Lett.54 (1985) 1891
8) T.Altzitzoglou, F.Calaprice, M.Dewey, M.Lowry, L.Piilonen, J.Brorson, S.Hagen and F.Loeser, Phys.Rev.Lett.55 (1985) 799 J.Markey and F.Boehm, Phys.Rev.C32 (1985) 2215
9) A.DeRujula and M.Lusignoli, Phys.Lett.118B (1982) 429

EVIDENCE FOR A 17-KEV NEUTRINO IN ^{3}H AND ^{35}S β SPECTRA

J.J. Simpson
Guelph-Waterloo Program for Graduate Work in Physics
and
Department of Physics
University of Guelph
Guelph, Ontario N1G 2W1, Canada



Abstract

New data obtained from ^{3}H in a silicon detector is presented confirming the distortion 17 keV below the end-point seen in an earlier experiment. In addition, a critical analysis of five ^{35}S β spectra is given. It is shown that two ^{35}S spectra have distorted Kurie plots which are in agreement with the Kurie plot of tritium, strengthening the earlier suggestion that the distortion seen in the β spectrum of tritium is due to the emission of a 17-keV neutrino.

Introduction

As this workshop demonstrates, there is considerable interest in whether or not neutrinos have non-zero rest mass, and associated with this, whether or not the weak eigenstate neutrinos are also mass eigenstates. Since it has been known for some time that energy spectra of β decay will show a distortion at the threshold energy for the emission of a heavy neutrino[1-3], the spectra can be used to look for such a neutrino and to determine its amplitude of mixing with the predominantly emitted light neutrino. (See this workshop for discussion of the mass of the dominant neutrino emitted in tritium decay.)

It is useful to assume that the electron neutrino is predominantly a linear combination of two mass eigenstates ν_1 and ν_2, of masses m_1 and m_2,

$$\nu_e = \nu_1 \cos\theta + \nu_2 \sin\theta \qquad [1]$$

where θ is the mixing angle. Then the β spectrum is

$$N_\beta(E,Z) = N_\beta(E,Z,m_1)\cos^2\theta + N_\beta(E,Z,m_2)\sin^2\theta \qquad [2]$$

where $N_\beta(E,Z,m)$ is the usual β-energy spectrum[4] with the emission of one neutrino of mass m. A heavy neutrino produces a distortion at an energy m_2c^2 below Q, the end-point energy of the β spectrum. A measurement of the size of the distortion gives $\tan^2\theta$, the mixing probability. Below the threshold for emission of a heavy neutrino, one would observe a deviation ΔK from the straight line Kurie plot K (for allowed decay) of

$$\frac{\Delta K}{K} = \frac{\tan^2\theta}{2}\left[1 - \frac{m_2^2c^4}{(Q-E)^2}\right]^{1/2}. \qquad [3]$$

Tritium β-spectra

In 1985 I reported[5] a distortion of the β-spectrum of tritium. The only cause for this distortion which was both sudden and pronounced (see fig. 3 of ref. 5 and fig. 4 below) seemed to be the emission of a massive neutrino. I suggested that the distortion was well-fitted by a neutrino of mass about 17.1 ± 0.2 keV with a value of the mixing probability ranging from about 2% to 4%, smaller mixing being correlated with smaller neutrino masses.

I have now examined the spectrum of tritium in a second detector. This detector was implanted at a different tritium energy and with a very low dose (about 1/40 of the first detector) originally for the purpose of trying to determine accurately the end-point energy of tritium. The implantation of this detector and various tests on it are described in detail in ref. 6. Fig. 1 shows the tritium shape spectrum from this

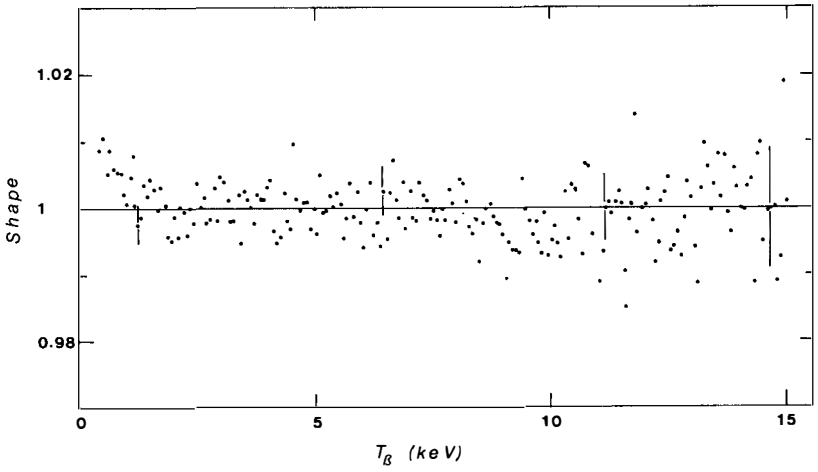


Fig. 1. The shape spectrum of ^3H obtained with the detector with a low ^3H dose as a function of the β-kinetic energy. Representative error bars are given.

detector and fig. 2 from the earlier detector. The shape is the ratio of the experimental spectrum to the theoretical spectrum for an allowed decay with a massless neutrino. The distortion at low energies is clearly seen in both. The only parameters in the fits are the tritium end-point energy and the overall normalization. The end-point energy for both fits is in reasonable agreement with the known Q-value for tritium decay, having a value of 18.56 keV for the new detector and 18.58 keV for the earlier detector.

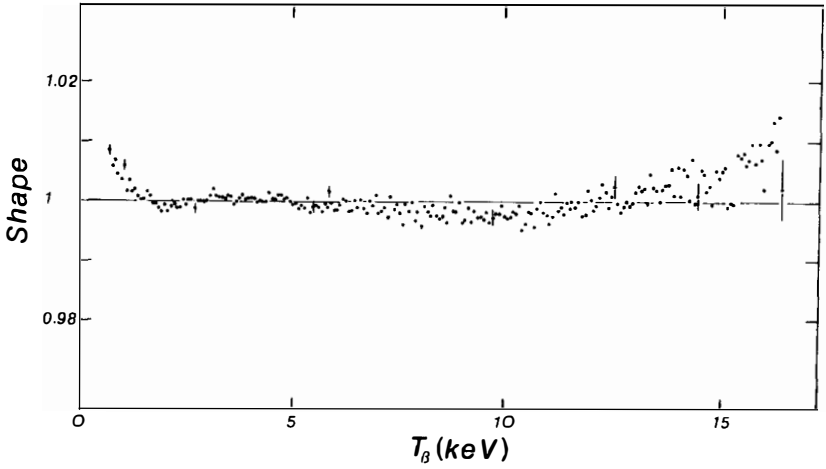


Fig. 2. The shape spectrum of ^{3}H obtained with the original detector. Representative error bars are given.

Fig. 3 shows $\Delta K/K$ for the recent data and it is seen that this data is completely consistent with that from the earlier detector and with the emission of a 17.1 keV neutrino with a mixing probability between 2 and 3%. It would seem to be not accidental that two detectors by different manufacturers implanted quite differently with very different amounts of tritium should show the same distortion of the β-spectrum of tritium.

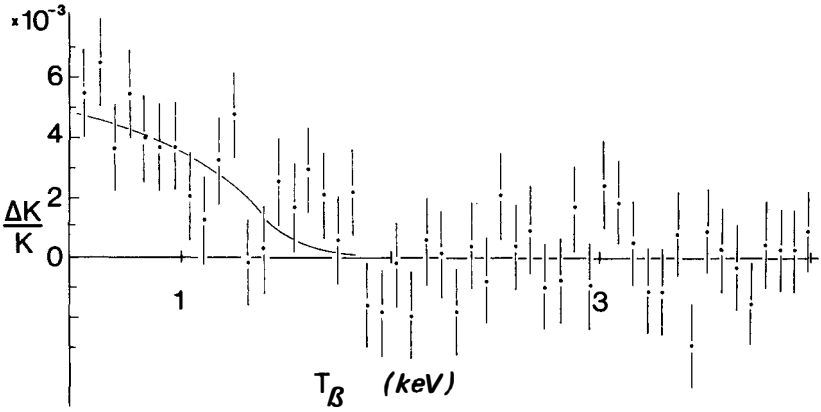


Fig. 3. Distortion of the Kurie plot of ^3H obtained with the low dose detector as a function of the β-kinetic energy. The smooth curve is an example with $\tan^2\theta = 0.027$ and threshold energy of 1.5 keV derived from the fitted β spectra including resolution effects.

Because the distortion is at very low energy (~ 1.5 keV β-particles) there is some question about the adequacy of the Fermi function and, in particular, the screening correction to it. Exchange corrections[7] and variations in the screening potential[8] all produce smoothly-varying changes to the β-spectrum and to $\Delta K/K$. It was partly to minimize the uncertainty arising from incomplete knowledge of the correct Fermi function that only a limited portion of the spectrum around the distortion was used in ref. 5 for actual analysis and determination of the mixing probability. The effect of

a large reduction in screening is shown in fig. 4, and while this reduces the magnitude of $\tan^2\theta$ by about 20%, it does not remove the kink in the spectrum.

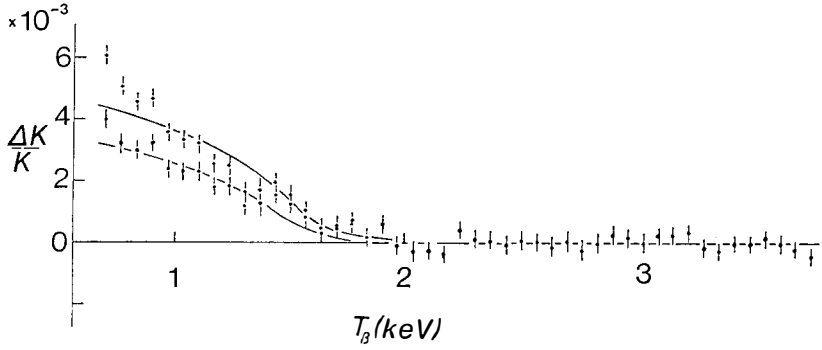


Fig. 4. The effects of screening on the deviation of the Kurie plot. The same data, which is new data from the original detector, has been analyzed twice. The upper crosses are derived using the same screening potential as in ref. 5 (99 eV), lower dots with a screening potential of 41 eV. The upper curve is the fit to the upper data and gives $\tan^2\theta$ of 0.028 and threshold energy of 1.57 keV and the lower curve the fit to the lower data with $\tan^2\theta$ of 0.022 and threshold energy of 1.53 keV.

If, as suggested, the distortion in the tritium spectrum is caused by the emission of a "normal" neutrino, that is, normal within the context of the model given by eq. [1], then a distortion should be seen in other β-spectra which have large enough Q-values.

β spectra of ^{35}S

A number of groups[9-13] have examined the β spectra of ^{35}S for a distortion which would signal the emission of the 17-keV neutrino. The end point energy of ^{35}S is about 167 keV so that the end-point of the spectrum associated with the heavy neutrino would be at 150 keV. All of these groups report that they do not see the distortion expected for a 17-keV

neutrino, with various upper limits for the mixing probability considerably below 3%. After examining only the data presented by these groups in their published work, I am of the opinion that in all cases the conclusion that a 17-keV neutrino is excluded is overstated, and that three of the five reported experiments show a distortion in their spectra consistent with the emission of this neutrino with about the same intensity as in tritium.

The ITEP group[9] carried out a high-resolution (130 eV) and the highest statistics measurement of the ^{35}S spectrum using their famous toroidal β-spectrometer. By fitting the whole region from 75 to 165 keV and from 145 to 165 keV they conclude that a 17-keV neutrino would have an intensity of less than 0.3% at 90% confidence. (The fitting required two adjustable parameters α_1 and α_2 which appeared in the factors $(1 + \alpha_1 (Q-E))\cdot(1 + \alpha_2 (Q-E)^2)$ multiplying the theoretical β spectrum. After fitting, these parameters were not negligible.) However, examination of their raw data gives a different result. In fig. 5 I show a reproduction of their Kurie plot (fig. 1 of ref. 9). In particular their figure shows an expanded portion of the Kurie plot from 148 to 152 keV spanning the sensitive region for a 17-keV neutrino. There is an evident distortion in the Kurie plot at 150 keV. Furthermore, the size of this distortion is almost exactly the same as the distortion seen in the tritium spectrum (see fig. 2 of ref. 5) which is as it should be, because all Kurie plots are the same as a function of (Q-E). (If one overlays the tritium Kurie plot on the present one, an almost perfect fit is obtained.) From the points on the Kurie plot near 148 keV one can estimate that $\tan^2\theta$ is about 0.02. The agreement is so remarkable as to demand an explanation, and certainly the most obvious one is that here, in the ITEP data, is confirmatory evidence of the emission of a neutrino of about 17 keV in mass.

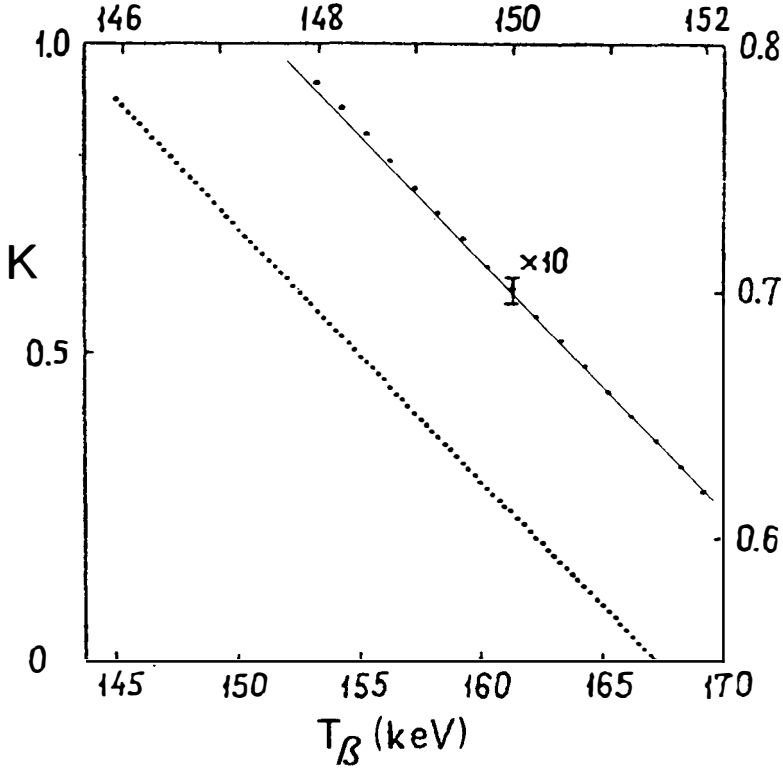


Fig. 5. The Kurie plot of ^{35}S (fig. 1 of ref. 9). The straight line on the portion of the Kurie plot around 150 keV has been drawn by the present author.

A different type of experiment was carried out by Ohi et al.[10]. They used a solid state detector to measure the energies of the ^{35}S β particles, with a second detector to veto the β-particles backscattered from the main detector. By fitting the whole spectrum from 120 keV to 160 keV they quote an upper limit of 0.15% at the 90% confidence level. This analysis seems flawed, however, because after fitting their shape spectrum without a 17 keV neutrino, they then appear to hold the parameters fixed and permit only

the 17-keV neutrino's intensity to vary thereafter. In addition they seem to have ignored an obvious anomaly at 150 keV, such that in the shape spectrum (their fig. 3a) almost all the data points between 150 keV and 156 keV lie one standard deviation or more above unity. I have read the data from their fig. 3a and reconstructed the β spectrum. The Kurie plot appears to be slightly convex, but if one looks only at the data near 150 keV one obtains the ΔK/K plot shown in fig. 6. The smooth curve is what one expects for a 17-keV neutrino with a mixing probability of 2% and the data supports this conjecture fairly well. Thus two independent experiments on ^{35}S show a distortion consistent with the emission of a 17-keV neutrino, and consistent with the tritium spectrum.

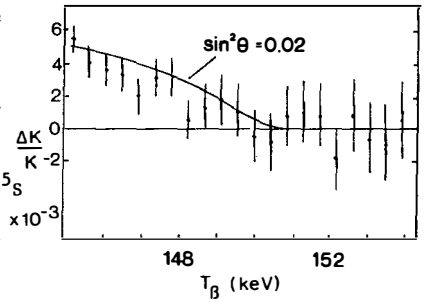


Fig. 6. ΔK/K vs the kinetic energy of the β particles from ^{35}S, derived from the data in ref. 10 by the present author. The smooth curve is that expected for a 150 keV threshold with an intensity of 2%, including a gaussian resolution function with σ = 1.02 keV.

A somewhat similar experiment was performed by Datar et al.[11], who however simply used one solid state detector to measure the energies of β-particles emitted from a source of ^{35}S. They conclude that the intensity of a 17-keV neutrino is less than 0.6% at the 90% confidence level. Their analysis is also flawed, however, because they have allowed only the mixing probability to vary after fitting their shape spectrum without a 17-keV

neutrino. Fig. 7 shows their data upon which I have superimposed the expected curve for a 2% mixing of the heavy neutrino. One sees some similarity between the data and the curve. By fitting their data, a minimum in χ^2 is found for a 0.8% branch of a 17-keV neutrino, with a 2% branch allowed at the 10% confidence level and a 2.6% branch at the 1% level. Clearly their data is consistent with a 17-keV neutrino, but unfortunately they do not have sufficient statistics for a more definite conclusion.

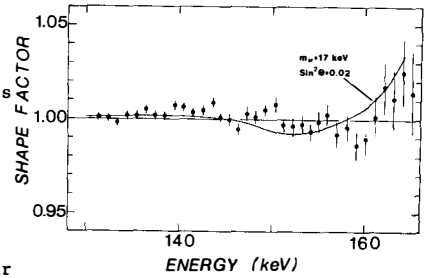


Fig. 7. The shape spectrum for ^{35}S from ref. 11 with that expected for a 17-keV neutrino of 2% intensity, calculated by the present author, as the smooth curve.

The earliest experiment reported[12] was carried out using an iron-free intermediate-image magnetic spectrometer. The resolution was 4.8 keV and the data was taken in ~ 2 keV steps. (It should be pointed out that the kink caused by a 17-keV neutrino is a very sharp function of energy. Neglecting resolution it reaches 45% of its full change by 2 keV below the end-point energy (eqn. [3]). There is thus an advantage to good resolution and small energy steps.) They report that the upper limit (at 99%

confidence) is 0.4%. In fig. 8 I show a shape spectrum reconstructed from data presented in ref. 12. The points A are essentially the shape spectrum of ref. 12 and the smooth curve is a polynomial fit to the shape of the form $S(E) = a + bE + cE^2$, where $a = 0.833$, $b = 2.2 \times 10^{-3}/\text{keV}$, and $c = -7.1 \times 10^{-6}/\text{keV}^2$. A distortion about this smooth curve was sought as the signal for a 17-keV neutrino. However, this solution is not unique, as the points B show. These points are the same data, but with a spectrum associated with a 2% branch of a 17-keV neutrino subtracted off, and fitted, as above, by varying the end-point energy and normalization to get the result shown. The smooth curve is a polynomial fit with $a = 1.224$, $b = -4.12 \times 10^{-3}/\text{keV}$ and $c = 1.88 \times 10^{-5}/\text{keV}^2$. Clearly there is no reason to choose A over B without independent knowledge of the shape to be expected, and certainly B is not sufficiently distorted to be ruled out on some arbitrary concept of smoothness. Thus this experiment is unable to rule out a 17-keV neutrino at 2% intensity.

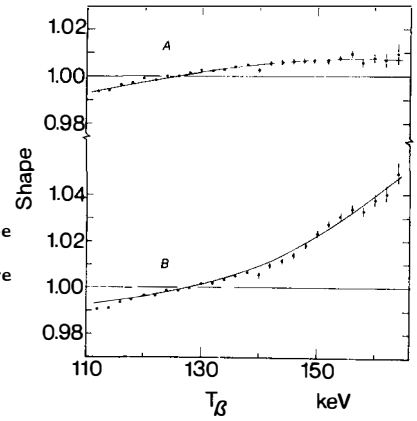


Fig. 8. The shape spectrum of ^{35}S. The points A are essentially the data after adjustment of end-point energy and normalization as presented in ref. 12. The points B are the same data, but with the spectrum associated with a 2% branch of a 17-keV neutrino subtracted off by the present author, and the normalization and end-point energy readjusted. The smooth curves are polynomial fits with parameters given in the text.

Markey and Boehm[13] have used an iron-free double-focussing magnetic spectrometer with a resolution of about 0.9 keV. They also took data every 2 keV. Their shape spectrum is consistent with unity, and they put a limit of 0.3% at 90% confidence on a 17-keV neutrino. However, since there is no

independent evidence presented as to what the true shape factor of their experimental set-up would be and recalling the discussion of ref. 12 one can only conclude from their data that a 17-keV neutrino is not confirmed.

Conclusions

In view of the preceding discussion, it may seem curious that all groups measuring the β spectrum of ^{35}S ultimately put very low limits on the occurrence of a threshold at 17 keV below the end-point. One reason seems to be that, in trying to fit a very large portion of the β spectrum, the danger that slowly-varying distortions of a few percent could bury a threshold effect seems to have been disregarded. One cannot emphasize too strongly how delicate is the analysis when searching for a small branch of a heavy neutrino, and how sensitive the result may be to apparently innocuous assumptions. For example, downward from about 34 keV below the Q-value, the Kurie plot of a β-spectrum with a 17-keV neutrino branch looks about the same as if there were no heavy neutrino (i.e. it is linear and extrapolates to the Q-value). It would seem that the safest approach to search for the presence of a threshold is to test for it initially in a limited region about the expected energy, since the narrower the region the less the test is likely to be troubled by experimental distortions. This requires high statistical accuracy and good resolution, and not all the ^{35}S experiments carried out have them.

Finally, it must be emphasized that it has not been merely shown that the previous analyses of the five ^{35}S experiments are inadequate to decide on a distortion at about 150 kev. More importantly, it has been shown that three of the experiments[9-11] actually have a distortion 17 keV below the end-point and that two of them[9,10] with sufficient statistics have Kurie plots which are in very good agreement with the Kurie plot of tritium. That

two tritium experiments and two ^{35}S experiments are in agreement among themselves is not likely to be a coincidence. One is justified in concluding that there is a distortion 17 keV below the end-point of β spectra and the hypothesis that a neutrino is the cause of the distortion seen in the β spectrum of tritium is the most plausible one.

The author acknowledges discussions with V. Lubimov, F. Boehm, G. Karl and correspondence with V.M. Datar. This work was supported by a grant from the Natural Sciences and Engineering Research Council of Canada.

References

1. R.E. Shrock, Phys. Lett. 96B, 159 (1980).
2. B.H.J. McKellar, Phys. Lett. 97B, 93 (1980).
3. I. Yu. Kobzarev, B.V. Martemyanov, L.B. Okun, M.G. Schepkin, Yadernaia Fizika 32, 1590 (1980).
4. J.J. Simpson, Phys. Rev. D23, 649, (1981).
5. J.J. Simpson, Phys. Rev. Lett. 54, 1891 (1985).
6. J.J. Simpson, W.R. Dixon and R.S. Storey, Phys. Rev. C31, 1891 (1985).
7. W.C. Haxton, Phys. Rev. Lett. 55, 807 (1985).
8. B. Eman and D. Tadić, private communication.
9. A. Apalikov et al., ITEP-114 (1985).
10. T. Ohi et al., Phys. Lett. 160B, 322 (1985).
11. V.M. Datar et al., Nature 318, 547 (1985).
12. T. Altzitzoglou et al., Phys. Rev. Lett. 55, 799 (1985).
13. J. Markey and F. Boehm, Phys. Rev. C32, 2215 (1985).

MEASUREMENT OF THE MASS OF THE ELECTRON NEUTRINO USING ELECTRON CAPTURE IN ^{163}Ho

S. YASUMI*, M. ANDO, H. MAEZAWA, H. KITAMURA, T. OHTA, F. OCHIAI and A. MIKUNI
National Laboratory for High Energy Physics, KEK, Ibaraki-ken 305 Japan
M. MARUYAMA
Osaka University, Toyonaka, Osaka 560 Japan
M. FUJIOKA, K. ISHII, T. SHINOZUKA, K. SERA, T. OMORI, G. IZAWA,
M. YAGI and K. MASUMOTO
Tohoku University, Sendai 980 Japan
K. SHIMA
University of Tsukuba, Niihari, Ibaraki 305 Japan
T. MUKOYAMA and Y. INAGAKI
Kyoto University, Kyoto 606 Japan
I. SUGAI
Institute for Nuclear Study, University of Tokyo, Tanashi, Tokyo 188 Japan
A. MASUDA and O. KAWAKAMI
University of Tokyo, Tokyo 113 Japan

Presented by Shinjiro Yasumi



ABSTRACT

Combining an M X-ray spectrum from ^{163}Ho with fluorescence spectra of Dy excited with monochromatic photons, two partial decay constants of ^{163}Ho, λ_{M1} and λ_{M2}, have been determined. Undulator photon beams, with a crystal monochromator, from 2.5 GeV Electron Storage Ring in the Photon Factory of KEK have been used as a light source for the fluorescence measurement on Dy. Using λ_{M1}, λ_{M2} and λ_t which was also independently determined, we obtain 400 eV for an upper limit of the mass of the electron neutrino.

* Permanent Address: Teikyo University, 359 Ohtsuka, Hachioji, Tokyo 192-03 Japan.

§1. Introduction

The mass of the electron antineutrino has been studied for a long time using the tritium β- ray spectrum[1,2,3], while the mass of the electron neutrino has been recently investigated using electron capturing isotopes including ^{163}Ho[4,5,6], ^{193}Pt[7] and so on. In the latter there are two ways to measure m_{ν_e}; one proposed by A. De Rújula[8] of CERN which is essentially based on three body phase space in radiative electron capture process[9], and another that utilizes the m_{ν_e}-dependence of the electron capture rate, which was discussed by Bennett et al.[10] In both cases, electron capturing nuclei having a low Q value seem to be favorable. A nucleus that decays by electron capture with the lowest Q value of any known β-decay process is holmium-163, which was discovered by Princeton group in 1968[11]. Considerations of the intensity of internal bremsstrahlung at electron capture in a ^{163}Ho source, indicate that the first approach is very difficult for measuring m_{ν_e}[12,13], although Bennett et al.[14] reported an upper limit of m_{ν_e} using internal bremsstrahlung in ^{163}Ho. Thus, for the time being, we decided to pursue the second approach[15].

§2. Principle of the method[15]

At first we reduce λ_{M1} and λ_{M2} (partial M1 and M2 subshell electron capture decay constants, respectively) from an M X-ray spectrum of ^{163}Ho. If S_p^{163Ho} stands for a photon spectrum from ^{163}Ho, where the number of photons per atom per second is plotted as a function of the energy of the photons, we then have

$$\begin{aligned} S_p^{163Ho} &= \frac{1}{N_o}\frac{d}{dt}\{S_{M1}\cdot N_{M1} + S_{M2}\cdot N_{M2}\} \\ &= \frac{d}{dt}\{S_{M1}\cdot n_{M1} + S_{M2}\cdot n_{M2}\} \\ &= S_{M1}\cdot\frac{dn_{M1}}{dt} + S_{M2}\cdot\frac{dn_{M2}}{dt} \\ S_p^{163Ho} &= \lambda_{M1}\cdot S_{M1} + \lambda_{M2}\cdot S_{M2} \qquad (1) \end{aligned}$$

where

S_{Mi} : M X-ray spectrum in the case where there is one vacancy in the M_i subshell only,

N_{Mi} $(i = 1,2)$: number of vacancies produced in the M_i subshell in the decay $^{163}Ho \xrightarrow{EC} {}^{163}Dy$,

n_{Mi} $(i = 1,2)$: $\equiv N_{Mi}/N_o$,

N_o : total number of ^{163}Ho atoms in the source,

λ_{Mi} $(i = 1, 2)$: partial Mi-capture decay constant.

Equation (1) tells us that when we reconstruct S_p^{163Ho} using the S_{M1} and S_{M2} spectra, the coefficients of S_{M1} and S_{M2} used in the reconstruction correspond to λ_{M1} and λ_{M2}, respectively.

The experimental procedures for obtaining the S_{M1} and S_{M2} spectra for dysprosium are as follows. If $S_{E\alpha}$ denotes an M X-ray fluorescence spectrum from Dy ions excited by monochromatic photons having an energy E_α, $S_{E\alpha}$ is represented by the following equation,

$$S_{E\alpha} = N^{E\alpha} m \sum_i \sigma_i^{E\alpha} \cdot S_{Mi} \quad (i = 1 \sim 5, \alpha = a \sim e) \qquad (2)$$

where

$\sigma_i^{E\alpha}$: photoionization cross section of M_i subshell for a photon of energy E_α,

$N^{E\alpha}$: total number of incident photons of energy E_α per second,

m : number of dysprosium atoms in a target per cm^2.

$S_{E\alpha}$ includes data of the same number as the one of ADC channels used in the experiment, and implicitly comprises the Auger and the Coster-Kronig transition probabilities and the X-ray transition probabilities related to it.

For E_α, we take five different energies: E_a, E_b, E_c, E_d and E_e where $E_a > E_{M1} > E_b > E_{M2} > E_c > E_{M3} > E_d > E_{M4} > E_e > E_{M5}$, and E_{Mi} ($i = 1 \sim 5$) stands for the binding energy of the Mi subshell of the dysprosium atom.

Then equation (2) becomes

$$\begin{aligned}
S_{Ea} &= N^{Ea} m \{ \sigma_1^{Ea} \cdot S_{M1} + \sigma_2^{Ea} \cdot S_{M2} + \sigma_3^{Ea} \cdot S_{M3} + \sigma_4^{Ea} \cdot S_{M4} + \sigma_5^{Ea} \cdot S_{M5} \}, \\
S_{Eb} &= N^{Eb} m \{ \sigma_2^{Eb} \cdot S_{M2} + \sigma_3^{Eb} \cdot S_{M3} + \sigma_4^{Eb} \cdot S_{M4} + \sigma_5^{Eb} \cdot S_{M5} \}, \\
S_{Ec} &= N^{Ec} m \{ \sigma_3^{Ec} \cdot S_{M3} + \sigma_4^{Ec} \cdot S_{M4} + \sigma_5^{Ec} \cdot S_{M5} \}, \\
S_{Ed} &= N^{Ed} m \{ \sigma_4^{Ed} \cdot S_{M4} + \sigma_5^{Ed} \cdot S_{M5} \}, \\
S_{Ee} &= N^{Ee} m \{ \sigma_5^{Ee} \cdot S_{M5} \}. \qquad (3)
\end{aligned}$$

If $\sigma_i^{E\alpha}$, $N^{E\alpha}$ and m are known, one can obtain S_{Mi} ($i = 5 \sim 1$) by using the above five equations, (3). Spectra S_{M1} and S_{M2} thus obtained can be used to reconstruct the S_p^{163Ho} spectrum for obtaining λ_{M1} and λ_{M2}. On the other hand, λ_t (total decay constant) can be determined with the isotope-dilution mass spectrometry[23]. Using λ_{M1}, λ_{M2} and λ_t, the three quantities, $m_{\nu e}$, the Q-value, and the nuclear matrix element relevant to the decay of ^{163}Ho, can be simultaneously determined.

§3. Experiments

Holmium-163 nuclei were produced with the $^{164}Dy(p,2n)$ reaction. An enriched ^{164}Dy metal target was irradiated by 20 MeV protons for 24.1 hours with an average current of 100 μA using the AVF cyclotron of the Cyclotron and Radioisotope Center, Tohoku University[16], followed by elaborate chemical separation and purification processes including the ion-exchange method[17]. Finally ^{163}Ho was electroplated onto a nickel foil by the electrolysis.

The photon spectrum from a ^{163}Ho source was measured in vacuum with a Si(Li) detector (ORTEC) having a Be window 0.3 mil thick (nominal). The

geometry of the Si(Li) detector, including the effective area of a silicon crystal and the solid angle, was carefully measured using several radioactive sources[18]. The thickness of the Be window of the Si(Li) detector was also checked by comparing a photon spectrum measured using this detector with the one measured using a windowless Si(Li) detector (HORIBA, Japan).

The total number of ^{163}Ho atoms in the source, N_o, was measured with the isotope-dilution mass spectrometry. This measurement yielded $N_o = 6.481 \pm 0.012 \times 10^{15}$ atoms, which is in good agreement with the value determined by the PIXE method[5] within experimental uncertainties.

The experimental setup of fluorescence spectra measurement on dysprosium is shown in Fig. 1. Undulator radiation from the BL2 line of the 2.5 GeV Electron Storage Ring was monochromated by a double reflection crystal monochromator made of beryl for photons of lower energies and InSb for photons of higher energies and directed onto a Dy target. The incident photon beams were monitored with a photon detector(SPD). We used monochromatic photon beams with five different energies; $E_a = 2.250$ keV, $E_b = 1.944$ keV, $E_c = 1.758$ keV, $E_d = 1.504$ keV and $E_e = 1.314$ keV. The energy widths of these photon beams are a few eV and sharp enough to remain distinct from each subshell level. M X-rays emitted by dysprosium ions excited with the incident photon beams, were measured by two Si(Li) detectors having a Be window, one was set in the direction of the polarization of the photon beams (horizontal) while the other was set at an angle of 90° to that direction (vertical), as shown in Fig. 1. It should be noted that the horizontal detector is free from the influence of the large tail of the elastic scattering of the incident photons, because the undulator photon beam is almost completely polarized[19] in a horizontal direction. The vertical detector was used as a overall monitor.

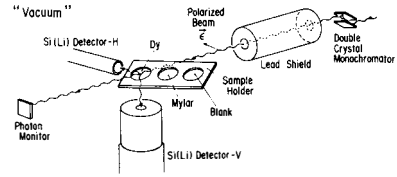


Fig. 1 Experimental setup using undulator radiations from the 2.5 GeV Electron Storage Ring of the Photon Factory in KEK.

The half life of ^{163}Ho was determined by measuring the production rate of ^{163}Dy due to the electron capture decay of ^{163}Ho with the isotope-dilution mass spectrometry. Our result was

$T_{1/2} = 4572 \pm 39$ Yr. ($\lambda_t = 4.8074 \pm 0.0410 \times 10^{-12}$ sec.$^{-1}$),

which is in excellent agreement with Baisden et al.'s[20].

§4. Some results and conclusions

Figure 2 shows a photon spectrum from the ^{163}Ho source as measured in the horizontal Si(Li) detector. In this measurement, a 100 mm thick lead shield was used. In the figure only five peaks each of which, in fact, consists of several characteristic X-ray lines except the peak of the highest energy, washed out by the finite energy resolution of the Si(Li) detector. We decomposed the ^{163}Ho spectrum into above-mentioned five peaks, using response functions corresponding to the peak energies which were also measured with monochromatic photon beams in the present experiment. In Figure 2, spectra corresponding to S_{Ea} and S_{Eb} are also shown. Similarly, Dy fluorescence spectra were decomposed into the peaks corresponding to the peaks in the ^{163}Ho spectrum. In comparing S_p^{163}Ho with S_{Ea} in Fig. 2, no appreciable energy shifts can be seen for five peaks including the 5p-3s line. This fact partly guarantees the validity of this method for determining m_{ν_e}.

In spite of much efforts for it [21], we still do not have reliable data on $\sigma_i^{E_\alpha}$ and N^{E_α}. So we analysed the data using theoretical S_{Mi} spectra calculated by T. Mukoyama[22] whose validities were checked using experimental $S_{E\alpha}$ spectra. It turned out that S_{M4} and S_{M5} spectra corresponding to the lowest energy peak and the second lowest energy peak, could not fit with the experimental $S_{E\alpha}$ spectra. Therefore, substructing the amplitudes corresponding to these two peaks from S_p^{163}Ho, S_{M1} and S_{M2} spectra, the reconstruction of S_p^{163}Ho using S_{M1} and S_{M2} was performed to obtain λ_{M1} and λ_{M2}. Thus we obtained $\lambda_{M1} = (1.0262 \pm 0.0044) \times 10^{-12}$ sec^{-1}, $\lambda_{M2} = (0.0806 \pm 0.0057) \times 10^{-12}$ sec^{-1}.

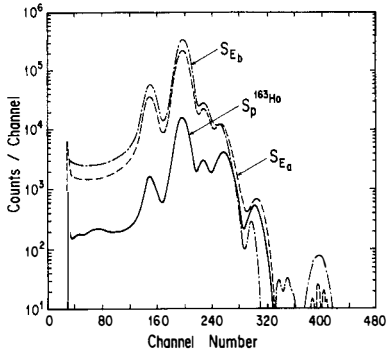


Fig. 2 Photon spectrum from a ^{163}Ho source and fluorescence spectra (S_{Ea} and S_{Eb}) of Dy.

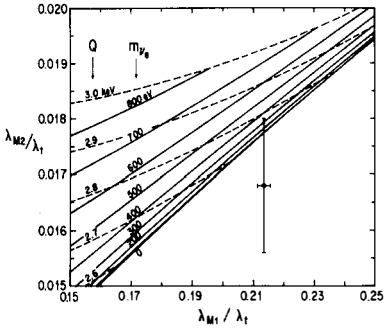


Fig. 3 Summary of the results.

These two values divided by λ_t are plotted in Fig. 3. From this figure we conclude

$m_{\nu_e} < 400$ eV (68% CL).

It should be noted that this procedure to measure m_{ν_e} is free from the uncertainty of the nuclear matrix element relevant to the electron capture decay of ^{163}Ho.

References

1) K.E. Bergkvist, Nucl. Phys. B39 (1972) 317.
2) V.A. Lubimov et al., Phys. Lett. 94B (1980) 266; S. Boris et al., Phys. Lett. 159B (1985) 217.
3) J.J. Simpson, Phys. Rev. D23 (1981) 649.
4) J.U. Andersen et al., Phys. Lett. 113B (1982) 72.
5) S. Yasumi et al., Phys. Lett. 122B (1983) 461.
6) F.X. Hartmann and R.A. Naumann, Phys. Rev. C31 (1985) 1594.
7) B. Jonson et al., Nucl. Phys. A396 (1983) 479C.
8) A. De Rujula, Nucl. Phys. B188 (1981) 414.
9) R.J. Glauber and P.C. Martin, Phys. Rev. 104 (1956) 158; P.C. Martin and R.J. Glauber, Phys. Rev. 109 (1985) 1307.
10) C.L. Bennett et al., Phys. Lett. 107B (1981) 19.
11) P.K. Hopke, J.S. Evans and R.A. Naumann, Phys. Rev. 171 (1968) 1290.
12) S. Yasumi, Proc. the International Europhysics Conference on High Energy Physics, Brighton, UK, July 1983. p. 391; S. Yasumi et al., KEK Preprint 83-17 August 1983 E.
13) K. Riisager et al., Physica Scripta 31 (1985) 321.
14) C.L. Bennett, Proc. the Telemark Conference, Telemark Lodge, Cable, Wisconsin, Oct., 1984. p.128.
15) S. Yasumi et al., Proc. Neutrino '84, Nordkirchen near Dortmund, June 11-16, 1984. p. 202; S. Yasumi et al., KEK Preprint 84-9 September 1984 H.
16) K. Ishii et al., Nucl. Instr. Meth., 205 (1983) 563.
17) S. Yasumi et al., Proc. Neutrino '82, Balatonfüred, Hungary, June 1982. p.59.
18) K. Shima, Nucl. Instr. Meth., 165 (1979) 21.
19) H. Kitamura, Japanese J. Appl. Phys. 19 (1980) L185.
20) P.A. Baisden et al., Phys. Rev. C28 (1983) 337.
21) S. Yasumi et al., Proc. the Telemark Conference on Neutrino Mass and Low Energy Weak Interactions, Telemark Lodge, Cable, Wisconsin, October 25-27, 1984 p. 398; S. Yasumi et al., KEK Preprint 85-45 October 1985 H.
22) T. Mukoyama and H. Adachi, J. Phys. Soc. Japan 53 (1984) 984.

2β-DECAY AND THE PION INDUCED DOUBLE CHARGE EXCHANGE NUCLEAR REACTION

C.R. Ching* and T.H. Ho*

(CERN, Geneve)

ABSTRACT

It is shown that by applying PCAC, the 2β-decay process can be directly related to the pion induced double charge exchange (DCX) nuclear reaction. Thus, if the experimental data of forward-angle cross section on Ca^{40} with pion beam at 164 MeV is used and extrapolated to Ca^{48}, then the calculated life time of Ca^{48} will be much larger than the old theoretical estimations by a factor 10^5~10^6.

* On leave from Institute of Theoretical Physics, Academia Sinica, P.O.Box 2735, Beijing, People's Republic of China.

A serious problem occured in 2β-decay is that the theoretical estimations of the 2ν-2β life time are too optimistic by a factor of $10\sim10^3$[1,2] A new approach is to connect the process of 2ν-2β decay

$$(Z,N) \rightarrow (Z+2,N-2) + 2e^- + 2\bar{\nu}_e \qquad (1)$$

with the pion induced double charge exchange nuclear reactions

$$\pi^+ + (Z,N) = (Z+2,N-2) + \pi^- \qquad (2)$$

Practically, all the 2β-decay nuclear transitions are of $J^P=0^+\rightarrow0^+$ type and with $\Delta T=2$, so that only the Gamow-Teller transition is the dominant one. It is wellknown that the axial vector current can be connected with the pions by means of PCAC, i.e.,

$$\partial A_\mu/\partial x_\mu = F_\pi m_\pi^2 \phi_\pi, \qquad (3)$$

This leads to the speculation that the 2ν-2β-decay can be related to the DCX, provided the soft-pion approximation is valid.[3] The proof cen be shown in the following:

If one starts from the Lehman-Symansik-Zimmermann's representation, it is easily to show

$$^{out}\langle N_f,\pi^-|\pi^+,N_i\rangle^{in} = -(2\pi)^4/(4K_{10}K_{20})^{\frac{1}{2}}\delta^4(K_1+P_i-K_2-P_f)$$
$$d^4x e^{i(K_1+K_2)x}(D^2+m_\pi^2)(D^2+m_\pi^2)\langle P_f|T(\phi_\pi(x)\phi_\pi(-x))|P_i\rangle \qquad (4)$$

By using the PCAC and soft pion approximation, one obtains that

$$^{out}\langle N_f,\pi^-|\pi^+,N_i\rangle^{in} \simeq -(2\pi)^4/[4F_\pi^2(K_{10}K_{20}P_{i0}P_{f0})^{\frac{1}{2}}]$$
$$\delta^4(K_1+P_i-K_2-P_f)K_{1\mu}K_{2\mu}M_{\mu\nu}, \qquad (5)$$

where

$$M_{\mu\nu}=(4P_{i0}P_{f0})^{\frac{1}{2}}\int d^4x e^{i(K_1+K_2)x}\langle P_f|T(A_\mu^+(x)A_\nu^+(-x))|P_i\rangle \qquad (6)$$

is just the same expression which occurs in 2ν-2β-decay. Finaly, one can obtain the following expressions, for DCX,

$$d\sigma/d\Omega \simeq [g_A^4(\vec{K}_1\cdot\vec{K}_2)^{\frac{1}{2}}|G|^2/(64\pi^2M_iM_fF_\pi^4)][|\vec{K}_2|/|\vec{K}_1|]F(Z_i,\nu_1)F(Z_f,\nu_2)$$

(7)

in which F is the Coulomb distortion factor.

$$F(\pm Z,\nu) = \pm 2\pi Z\nu(1-\exp(\mp 2\pi Z\nu))^{-1}$$

$$\nu_i = \alpha m_\pi/|\vec{K}_i| \ , \quad i=1,2$$

G is the nuclear transition matrix element in allowed approximation. As for 2ν-2β-decay, one has

$$\Gamma(i\to f2e2\tilde{\nu}_e) = 9g_a^4G_F^4\cos^4\theta_c m_e^{11}/(64\pi^7M_iM_f)F^2(Z_f)|G|^2 \cdot 16/(11!)T_0^7(T_0^4+22T_0^3+220T_0^2+990T_0+1980) \qquad (8)$$

where T_0 is the total kinetic energy in unit of m_e and

$$F(Z_f) = 2\pi\alpha Z_f(1-\exp(-2\pi\alpha Z_f))^{-1}$$

However, up to now there does not exist any experimental DCX data on 2β-radiative isotopes such as Ca^{48}, Ge^{76}, Se^{82} and Te^{130}. But fortunately, there has been a systematic study of $\pi^+(Z,Z+2)\pi^-$ reactions with pion beam at 164 MeV on C^{12}, O^{16}, Mg^{24}, Si^{28}, S^{32} and Ca^{40}. All of them are of $J^P=0^+\to0^+$ and $\Delta I=2$ transitions[4]. These experiments have indicated that the forward-angular cross section falls roughly as $A^{-4/3}$, or more exactly, it can be fitted well with an empirical fofrmula

$$\sigma(5^\circ,164\text{MeV}) = 21.06A^{-1.354}\ \mu\text{b/sr.} \qquad (9)$$

Since Ca^{48}, the lightest 2β-radioactive isotope, is of the same type of nuclei with close shell or sub-shell, one can expect that the empirical law can be extrapolated to Ca^{48}. Using the experimental data on Ca^{40}, one gets

$$\sigma(5^\circ,164\text{MeV},A248) \simeq 0.111\mu\text{b/sr.} \qquad (10)$$

Then from Eqs.(7) and (10), the squared nuclear matrix element is obtained

$$G^2 = 8.70,$$

where g_A=1.251, F_π=130 MeV are used.

Using the value of G^2, the half-lifetime for Ca^{48} 2ν-2β-decay is obtained

$$T_{\frac{1}{2}}^{2\nu} \simeq 2.2\times10^{25}\ \text{yrs.}$$

It is, however, interesting to compare the lifetime of Ca^{48} with the experimental data[5] as well as that of theoretical calculations carried out by various authors for Ca^{48} decay:

$T_{\frac{1}{2}}^{2\nu}(\text{exp}) > 3.6\times10^{19}$ yrs.[5]

$T_{\frac{1}{2}}^{2\nu}(\text{Th}) = 2.7\times10^{19}$ yrs.[6]

$T_{\frac{1}{2}}^{2\nu}(\text{Th}) = 4.1\times10^{19}$ yrs.[7]

It can be seen that since the experiment only indicates the lower limit of the lifetime, hence our result is not in contradiction with this value, but it is about 10^5~10^6 times larger than that of all the theoretical estimations previously obtained by using the closure approximation.

REFERENCE

[1] W.C. Haxton and G.J. Stephenson Jr., Progress in Particle and Nuclear Physics, Vol.13, 409(1984).

[2] C.R. Ching and T.H. Ho, Phys. Rept. 112 , 1(1984).

[3] C.R. Ching and T.H. Ho, Commun. Theor. Phys. 4 ,51(1985).

[4] L.C. Blend et al., Phys. Letters, 128B ,157(1983).

[5] R. Bardin et al., Nucl. Phys. A158 ,337(1970).

[6] W.C. Haxton, G.J. Stephenson Jr., and A.D. Strottman, Phys. Rev. D25 ,2360(1982).

[7] J.D. Vergados, Nucl. Phys. B218 ,109(1983); L.D. Skouras and J.D. Vergrdos, Phys. Rev. C28 ,2122(1983).

NEW THEORETICAL DEVELOPMENTS ON THE DOUBLE BETA DECAY AND THE PATTERN OF NEUTRINO MIXINGS

Eiichi Takasugi
Institute of Physics, College of General Education
Osaka University
Toyonaka, Osaka 560, Japan



ABSTRUCT

Some new theoretical developments on the double beta decay are discussed. The theorem, "the neutrinoless double beta decay occurs if and only if the electron neutrino is a massive Majorana particle." is discussed. Next the effects of the P-wave and the nucleon recoil terms to the neutrinoless double beta decay is estimated. The very tight bound on one of the right-handed parameters is obtained.

By integrating the information on the neutrino mass from the ITEP result, the double beta decay and the neutrino oscillations, the pattern of neutrino mixings is discussed in the framework of Stech type mass matrices of quarks and leptons which are derived from the SO(10) model with reasonable assumptions. It is shown that only the possible solution is the type that ν_{eL}, $\nu_{\tau L}$ have almost degenerate masses and form a pseudo-Dirac neutrino, while $\nu_{\mu L}$ is a heavier Majorana neutrino by 10 - 50 times than ν_{eL}, $\nu_{\tau L}$. The general features of this model is discussed.

The question whether neutrinos have non-zero masses is one of the most fundamental problems in physics. There are various experiments going on to attack this question. Among them, the neutrinoless double beta decay $(\beta\beta)_{0\nu}$ has the special interest. This is because it occurs if and only if the electron neutrino is a massive Majorana particle. In this report, I will discuss new developments on the $\beta\beta$ decay from the theoretical side. The bounds on the effective neutrino mass and the right-handed parameters are given by analyzing the recent data. By integrating all experimental informations on neutrinos, the patterns of neutrino mixings are discussed in the framework of Stech type mass matrices for quarks and leptons which is based on SO(10).

1. New theoretical developments on $\beta\beta$ decay

The detailed discussions on the theory and the analysis of the experimental data are presented in our recent review article.[1] Here I forcus on two topics.

The Majorana neutrino theorem: The theorem states that "the $(\beta\beta)_{0\nu}$ decay takes place if and only if the electron neutrino ν_{eL} is a massive Majorana particle." We obtain the interesting corollary, "if ν_{eL} is massless, the $(\beta\beta)_{0\nu}$ decay does not take place independently whether neutrinos are Weyle or Majorana particle." The theorem is proved in the framework of gauge theory[2,1] and independently of the mechanisms for the $(\beta\beta)_{0\nu}$ decay. Thanks of this theorem, we can safely say that ν_{eL} is massive Majorana, if the $(\beta\beta)_{0\nu}$ is observed. This decay is commonly discussed in the 2n-mechanism where ν_{eL} must be massive Majorana. However, there may be some other mechanisms such as the superweak interaction where neutrino does not involve directly. In such cases, the theorem still holds.

The P-wave and nucleon recoil effects for the $(\beta\beta)_{0\nu}$ decay: I shall concentrate on the $0^+ \to 0^+$ transition. Since these effects appear only when the right-handed parameter involves in, I start to define the right-handed current interaction:

$$H_W = G/\sqrt{2}\ [\ j_L^\rho J_{L\rho}^\dagger + \kappa j_L'^\rho J_{R\rho}^\dagger + \eta j_R'^\rho J_{L\rho}^\dagger + \lambda j_R^\rho J_{R\rho}^\dagger\ ] + \text{h.c.}, \qquad (1)$$

where

$$\begin{pmatrix} j_L^\rho \\ j_L'^\rho \end{pmatrix} = \bar{e}\,\gamma^\rho(1-\gamma_5)\begin{pmatrix} \nu_{eL} \\ \tilde{\nu}_{eL} \end{pmatrix}, \quad \begin{pmatrix} j_R^\rho \\ j_R'^\rho \end{pmatrix} = \bar{e}\,\gamma^\rho(1+\gamma_5)\begin{pmatrix} \nu'_{eR} \\ \tilde{\nu}'_{eR} \end{pmatrix}, \qquad (2)$$

$$\begin{pmatrix} \nu_{eL} \\ \tilde{\nu}_{eL} \end{pmatrix} = \begin{pmatrix} U_{ej} \\ U'_{ej} \end{pmatrix} N_{jL}, \quad \begin{pmatrix} \nu'_{eR} \\ \tilde{\nu}'_{eR} \end{pmatrix} = \begin{pmatrix} V_{ej} \\ V'_{ej} \end{pmatrix} N_{jR}. \qquad (3)$$

Here N_j is the mass-eigenstate Majorana neutrino. In gauge theory, the mixing parameters should satisfy the following constraints;

$$\text{Normalization: } \Sigma_j |U_{ej}|^2 = \Sigma_j |U'_{ej}|^2 = \Sigma_j |V_{ej}|^2 = \Sigma_j |V'_{ej}|^2 = 1, \qquad (4)$$

$$\text{Orthogonality: } \Sigma_j U_{ej} V_{ej} = \Sigma_j U_{ej} V'_{ej} = \Sigma_j U'_{ej} V_{ej} = \Sigma_j U'_{ej} V'_{ej} = 0, \qquad (5)$$

Orthogonality condition guarantees that ν_{eL} ($\tilde{\nu}_{eL}$) is independent of ν'_{eR} and $\tilde{\nu}'_{eR}$. These independency among weak eigenstate neutrinos is necesessary in gauge theories because they behave differently under the gauge transformation. It may be instructive to consider some examples: (a) $SU(2)_L \times SU(2)_R \times U(1)$ model without mirror leptons: $\nu_{eL} = \tilde{\nu}_{eL}$ ($U_{ej} = U'_{ej}$), $\nu'_{eR} = \tilde{\nu}'_{eR}$ ($V_{ej} = V'_{ej}$), $\kappa = \eta = \eta_0 \cong -\tan\zeta$ and $\lambda = \lambda_0 \cong (M_L/M_R)^2$, where ζ is the mixing angle between W_L and W_R. (b) $SU(2)_L \times U(1)$ with mirror leptons: $\eta = 1$, $\kappa = \lambda = 0$ and $\tilde{\nu}_{eL}$ is the mirror neutrino of ν_{eL}. The additional orthogonality condition, $\Sigma_j U_{ej} U'^{*}_{ej} = 0$ is required to guarantee the independence between ν_{eL} and $\tilde{\nu}_{eL}$.

The important message is that in the framework of gauge theory, the following commonly used phenomenological Hamiltonian[3] is not allowed (ν_e is a Majorana particle):

$$H_W = G/\sqrt{2}\,[\,\bar{e}\,\gamma^{\rho}\{(1-\gamma_5) + \eta(1+\gamma_5)\}\,\nu_e\,J^{+}_{L\rho} + \text{h.c.}]. \qquad (6)$$

Now I talk about the half-life formula whose detailed derivation is given in Ref.(1). The result for ^{76}Ge is:

$$[T_{0\nu}(0^+\to 0^+)]^{-1} = 9.232\cdot 10^{-5}\,\text{yr}^{-1}\,|M^{(0\nu)}_{GT}|^2\,[\,\left(\frac{\langle m_\nu\rangle}{m_e}\right)^2 - 0.3517\langle\lambda\rangle\frac{\langle m_\nu\rangle}{m_e}\cos\psi_1$$
$$+(C_3/C_1)\langle\eta\rangle\frac{\langle m_\nu\rangle}{m_e}\cos\psi_2 + 1.013\langle\lambda\rangle^2 + (C_5/C_1)\langle\eta\rangle^2 - 0.8007\langle\lambda\rangle\langle\eta\rangle\cos(\psi_1-\psi_2)] \qquad (7)$$

where ψ_1 and ψ_2 are phases and take 0 or π if CP is conserved and

$$C_3/C_1 = -0.1011 - 24.27(\chi'_P - 7.661\chi'_R),\ C_5/C_1 = 0.2265 + 646.1(\chi'_P - 7.440\chi'_R)^2, \qquad (8)$$

$$\langle m_\nu\rangle = |\Sigma'_j m_j U^2_{ej}|\ ,\quad \langle\eta\rangle = \eta|\Sigma'_j U_{ej}V'_{ej}|,\quad \langle\lambda\rangle = \lambda\left|\Sigma'_j U_{ej}V_{ej}\frac{g'_V}{g_V}\right|. \qquad (9)$$

Here I assumed a rather simple situation where there are only two groups of neutrinos, light ones (m_j < 10MeV) and heavy ones (m_j > 1GeV). Then the primed sum extends over only the light neutrinos because heavy neutrinos are suppressed by the potential $e^{-m_j r}/r$. If some neutrinos are inbetween, the careful treatment is necessary. In the above expression the coeficients C_i are the functions of ratios of nuclear matrix elements (NM). In general ratios are more reliablly estimated than the absolute magnitude, $M^{(0\nu)}_{GT} = \langle\vec{\sigma}_n\cdot\vec{\sigma}_m h_+(r_{nm})\rangle$, where $\langle O_{nm}\rangle \equiv \langle 0^+_f \| \Sigma_{n,m}\tau^+_n\tau^+_m O_{nm} \| 0^+_i\rangle$. The terms involving χ'_P and χ'_R correspond to the P-wave and nucleon recoil terms. Aside from them, the estimates of Haxton et al.[4] are used for the ratios of NM. The numerical values for other nuclei are given in Ref.1. As for the P-wave term, Haxton et al. gave $\chi'_P = 0.270$, while Tubingen group[5] gave $\chi'_P = -0.218$. Although this discrepancy has to be settled, the P-wave effect is certainly important.

The nucleon recoil term is expressed in a good approximation as,[5,6]

$$\chi'_R = (4.7/3)(g_V/g_A)\,\langle\vec{\sigma}_n\cdot\vec{\sigma}_m h_R(r_{nm})\rangle\,/M^{(0\nu)}_{GT}\ , \qquad (10)$$

where the neutrino potential h_R is given as

$$h_R(r) = \frac{R^2}{M}\int\frac{d^3q}{2\pi^2}\frac{q^2}{q(q+\mu_0 m_e)}e^{i\vec{q}\cdot\vec{r}} = \frac{R^2}{M}\int\frac{d^3q}{2\pi^2}\left[1 - \frac{\mu_0 m_e}{q} + \frac{(\mu_0 m_e)^2}{q(q+\mu_0 m_e)}\right]e^{i\vec{q}\cdot\vec{r}}$$

$$= (R^2/M)[\ 4\ \delta(\vec{r}) - (2/\pi)\mu_0 m_e/r + (\mu_0 m_e)^2\ \phi/r\ ], \qquad (11)$$

where ϕ is a function of $\mu_0 m_e r$ and takes the value nearly equal to 1, R and M are the nuclear radius and nucleon mass, and $\mu_0 m_e$ is the average excitation energy.

In our previous paper[6], the $\delta(\vec{r})$ term is dropped because neutrino should propagate from one nucleon to another ($r_{nm} \neq 0$) due to $\tau_n^+\tau_n^+ = 0$ (point nucleon case). However if the nuclear extension is considered (extended case), this contribution may not be neglected. Tubingen group did this analysis and got the large contribution.[5] There are some confusions on the work by Tubingen. In their first paper,[7] they stressed the importance of the recoil term and obtained the tight bound on $\langle\eta\rangle$. We also analyzed χ_R' semi-quantatively[6] and confirmed the **effect from recoil term comparable** with the P-wave term. **Shortly** after this, Tubingen group wrote a revised version[8] and claimed that the P-wave and recoil terms cancell completely each other and thus the bound on $\langle\eta\rangle$ became very loose. In their new paper,[5] they claimed that the recoil effect is dominant. In view of this situation, I feel obliged to tell something about their work in order to clarify the situation. Let us discuss the $\delta(\vec{r})$ term by taking the nuclear extension into account.

The nucleon size is taken into account by introducing the nucleon form factor. That is, the neutrino potential is modified as (Λ = 850MeV)

$$h_R(r) = \frac{R^2}{M}\int\frac{d^3q}{2\pi^2}\left[\ 1 - \frac{\mu_0 m_e}{q} + \frac{(\mu_0 m_e)^2}{q(q+\mu_0 m_e)}\ \right]\left(\frac{\Lambda^2}{q^2+\Lambda^2}\right)^4 e^{i\vec{q}\cdot\vec{r}}. \qquad (12)$$

Here I make the brief explanation of our rough (semi-quantative) estimation.[9] There are five Gamow-Teller type NM in the double beta decay. I write them in the form of ratios,

$$M_{GT}^{(0\nu)}/M_{GT}^{(2\nu)} = \langle\vec{\sigma}_n\cdot\vec{\sigma}_m h_+(r_{nm})\rangle\Big/\langle\vec{\sigma}_n\cdot\vec{\sigma}_m\rangle \equiv \langle\langle h_+\rangle\rangle,$$

$$\chi_R' = (4.7/3)(g_V/g_A)\langle\vec{\sigma}_n\cdot\vec{\sigma}_m h_R(r_{nm})\rangle/\langle\vec{\sigma}_n\cdot\vec{\sigma}_m h_+\rangle \equiv (4.7/3)(g_V/g_A)\frac{\langle\langle h_R\rangle\rangle}{\langle\langle h_+\rangle\rangle}, \qquad (13)$$

and $\chi_{GT}' \equiv \langle\langle h_+'\rangle\rangle/\langle\langle h_+\rangle\rangle$, $\chi_{GT}^{(0)} \equiv \langle\langle h_0\rangle\rangle/\langle\langle h_+\rangle\rangle$. The evaluation of these ratios is nothing but estimation of average potentials. The approximation we use is to estimate the average potentials by assuming the uniform distribution of nucleons between r_c (hard core, 0.5fm) to $\tilde{R}$ (effective range of interaction between two nucleons). The $\tilde{R}$ is introduced to include the short range correlation and is determined so that the theoretical estimation of $M_{GT}^{(0\nu)}/M_{GT}^{(2\nu)}$ is reproduced by the average potential of h_+. The theoretical value of it is 1.64 (Haxton et al.) and 1.66 (Tubingen). With thus obtained $\tilde{R}$, $\langle\langle h_R\rangle\rangle/\langle\langle h_+\rangle\rangle$ is estimated. The result

is as follows: The contributions to χ_R' from the 1st, 2nd and 3rd terms in the parenthesis of potential in Eq.(12) are refered to as χ_{R1}', χ_{R2}' and χ_{R3}'.

	"pot" point	"pot" extended	Tubingen extended + SRC
χ_{R1}'	0	0.236	0.452
χ_{R2}'		-0.028	-0.033
χ_{R3}'		0.003	0.003
χ_R'	-0.021	0.211	0.423 (0.422)

	"pot" point	"pot" extended
^{48}Ca	-0.021	0.447
^{82}Se	-0.025	0.258
^{128}Te	-0.032	0.207
^{130}Te	-0.034	0.207

The values of χ_R'

The singular term $\delta(\vec{r})$ (χ_{R1}') is certainly important and gives the dominant contribution. The agreement of the naive estimate (semi-quantative) and that of Tubingen group is fairly well. The smaller value of my estimate is resonable because more strong short range correlation is expected for the singlar potential. I presented the values of χ_R' for other nuclei. The value in the parenthesis for Tubingen is the one when all other minor contributions for χ_R' aside from $\vec{\sigma}_n \cdot \vec{\sigma}_m$ termis included. The definitions of some NM by Tugingen group are different from ours:

$$[\chi_R']_T = (1/m_e R)\chi_R', \quad [M_{GT}^{(2\nu)}]_T = (1/2)M_{GT}^{(2\nu)}, \quad [M_{GT}^{(0\nu)}]_T = (1/2R)M_{GT}^{(0\nu)}, \qquad (14)$$

where the subscript T indicates the definition of Tubingen group.

The nucleon recoil term certainly gives the dominant contribution to $\langle\eta\rangle$ and thus the much tighter bound on $\langle\eta\rangle$ is derived. From the recent Santa-Barbara data $T_{0\nu}(0^+ \to 0^+) > 2.5 \cdot 10^{23}$yr,[10] we obtain (see also Ref. 1)

$$\langle m_\nu \rangle < 7.5\text{eV}, \quad \langle\lambda\rangle < 1.2 \cdot 10^{-5}, \quad |\langle\eta\rangle| < (3 \sim 4) \cdot 10^{-7}, \qquad (15)$$

where $\chi_R' = 0.422$ is used and 3 and 4 in the parenthesis correspond to $\chi_P' = -0.218$ (Tubingen) and 0.270 (Haxton et al.). These bounds are considered to be very conservative because $|M_{GT}^{(0\nu)}| = 1.59$ is used. If the value 4.18 (Haxton et al.) or 10.4 (Klapdor et al.) is used, the bounds become tighter by 2.6 or 6.5.

From the geochemical data for $^{128}Te/^{130}Te$ by MPI at Heidelberg,[11] I find

$$\langle m_\nu \rangle < 8\text{eV}, \quad \langle\lambda\rangle < 2.8 \cdot 10^{-5}, \quad |\langle\eta\rangle| < (3 \sim 7) \cdot 10^{-7}, \qquad (16)$$

where $\chi_R' = 0.207$ is used and 3 and 7 for $\langle\eta\rangle$ correspond to $\chi_P' = -0.272$ and 0.272 (Haxton et al.).

2. The pattern of neutrino mixings: It is an interesting question what is the pattern of neutrino mixings if the ITEP data[15] of the electron neutrino from the tritium beta decay is right; 17eV < $m_{\bar{\nu}_e}$ < 40eV. Apparantly, this data contradict with the bounds on $\langle m_\nu \rangle$ from the $(\beta\beta)_{0\nu}$ decay if ν_{eL} does not mix with other neutrinos. There are several story to solve this: (a) The ν_{eL} and $\nu_{\tau L}$ form a pseudo-Dirac neutrino (the destructive interference between almost degenerate neutrinos). (2) The destructive interference between light and heavy neutrinos. If the mass of

heavy neutrino is above 100MeV, the suppression depends sensitively on A of nuclei. That is, it seems not possible to suppress both ^{76}Ge and ^{128}Te. However the data show the suppression both for ^{76}Ge and ^{128}Te as seen from Eqs.(15)-(16). Therefore the mass of heaver neutrino should be less than around 100MeV. However this type of story is not very attructive because the cancellation requires the very fine tuning of parameters which is unstable under perturbation. I feel the possibility (1) is most attractive. Kotani, Taruya and I[12] made the study of neutrino mixings in SO(10) model, in particular the model by Stech.[13] This model is interesting because Stech mass matrices for quarks and leptons are derived in pretty general assumptions. Kim and Nishiura[14] made the study of this model and claimed that only hierarchical pattern of neutrino masses is allowed and moreover the mass of ν_{eL} is less then 10eV. This made the belief that the pattern of pseudo-Dirac neutrino is not allowed in SO(10). This lead us to reexamine the Stech type model. In this model, the mass matrices are expressed as

$$M_u = S\ ,\quad M_d = \alpha S + S' + A\ ,\quad rM_e = \alpha S - 3S' + A\ ,\quad [M_\nu]_{light} = (\beta/t)S'\ , \qquad (17)$$

where S and S' are from the Yukawa coupling with 10 and 126 Higgs bosons and thus they are symmetric matrices, while A is from 120 Higgs and anti-symmetric. α and β are ratios of vacuum expectation values of Higgs and assumed to be real and r and t are effect due to renormalization for the enegy rescaling, $r \sim 3$. All mass matrices are assumed to be Hermitian. Under these simplification, we can choose the basis where M_u is diagonal, i.e., $M_u = \mathrm{diag}(m_u, m_c, m_t)$. Then the diagonalization of M_d is made essentially by the Kobayashi-Maskawa matrix K: $M_d = U D_d U^\dagger = (P_u^\dagger K P_d) D_d (P_u^\dagger K P_d)^\dagger = P_u^\dagger K D_d K^\dagger P_u$, where $D_d = \mathrm{diag}(m_d, m_s, m_b)$ and P_u and P_d are phase matrices, i.e., $P_u = \mathrm{diag}(\exp i\gamma_1, \exp i\gamma_2, \exp i\gamma_3)$. The matrices S' and A are obtained by taking the symmetric and anti-symmetric part of M_d. By substituting them into M_e and diagonalizing M_e, we have three constraints which determine m_t, α and δ. Now we examine $[M_\nu]_{light}$, the light left-handed neutrino mass matrix. Only parameters which are free are phases, $\gamma_{12} = \gamma_1 - \gamma_2$ and $\gamma_{23} = \gamma_2 - \gamma_3$ and K which is almost known. By varying γ_{12} and γ_{23}, the neutrino mixing is examined. First we imposed the constraint $\langle m_\nu \rangle / m_{\nu_e} < 1/4$ from the ITEP data and the $\beta\beta$ decay constraint. Then the neutrino mixing is restricted in the following form:

$$\begin{pmatrix} \nu_{eL} \\ \nu_{\mu L} \\ \nu_{\tau L} \end{pmatrix} = \begin{pmatrix} 0.762 & i0.647 & 0.035\, e^{i247^\circ} \\ 0.040 & i0.039\, e^{i55^\circ} & 0.998\, e^{i21^\circ} \\ 0.647 & i0.761 & 0.044\, e^{i161^\circ} \end{pmatrix} \begin{pmatrix} N_{1L} \\ N_{2L} \\ N_{3L} \end{pmatrix}\ , \qquad (18)$$

and $|m_1/m_2| \sim 1$.

Now if the masses of N_1 and N_2 are not almost degenerate ($\Delta m_{12}^2 = |m_1^2 - m_2^2| < 10^{-3}$ eV^2), the large oscillation between ν_{eL} and $\nu_{\tau L}$ occurs. To prevent this, the almost degeneracy of them is required. That is, ν_{eL} and $\nu_{\tau L}$ should form a pseudo-Dirac neutrino. Notice that i sign for N_2 in the mixing matrix. The $\nu_{\mu L}$ is about

10 ∿ 50 times heavier than the pseudo-Dirac neutrino, $\psi = (N_1 + iN_2)/\sqrt{2}$. The neutrino oscillation in the laboratory experiments for this almost degenerate case is expressed as

$$P(\nu_\ell \to \nu_{\ell'}) = 2\,|U_{\ell 3}U^*_{\ell' 3}|^2 \quad \text{for } \ell \neq \ell' . \tag{19}$$

Therefore the predictions of oscillations from the mixing matrix (18) are $P(\nu_e \to \nu_\mu) = 0.00237$, $P(\nu_e \to \nu_\tau) = 4.7 \cdot 10^{-6}$ and $P(\nu_\mu \to \nu_\tau) = 0.0039$, which are consistent with the present data. Although the mass difference is small, it is generally expected that $\Delta m^2_{12} > 10^{-10}$ eV^2 due to the radiative correction. Then the reduction of 1/2 of solar neutrino is predicted.

Another interesting result is that the top quark is restricted to be very heavy, m_t = (110 ∿140)GeV. Also we found no other solution other than the above scheme in order to satisfy the ITEP data, the ββ decay and the neutrino oscillations. Finally we mention why we got the different result from Kim and Nishiura. In their paper, P_u is assumed to be one although there is no reason to do so. By using this phase freedom, we are able to obtain the solution.

References

1. M.Doi, T.Kotani and E.Takasugi, Suppl. of Theor. Phys. in press.
2. E.Takasugi, Phys. Lett.149B (1984),372.
   J.F.Nieves, Phys. Lett.147B (1984),375.
3. H.Primakoff and S.P.Rosen, Phys. Rev. 184 (1969), 1925.
4. W.C.Haxton and G.J.Stephenson Jr., Progress in Particle and Nuclear Physics 12 (1984), 409.
5. T.Tomoda et al., Tubingen preprint, **July 1985.**
6. M.Doi, T.Kotani and E.Takasugi, Phys. Lett. 158B (1985), 164.
7. T.Tomoda et al., Tubingen preprint, **January 1985.**
8. T.Tomoda et al., Phys. Lett. 157B (1985), 4.
9. E.Takasugi, in preparation.
10. D.O.Caldwell et al., Santa Barbara-LBL preprint (1985).
11. T.Kirsten et al., Phys. Rev. Lett. 50 (1983), 474.
12. T.Kotani, E.Takasugi and K.Taruya, in preparation.
13. B.Stech, Phys. Lett. 130B (1983), 189.
14. C.W.Kim and H.Nishiura, Phys. Lett. 139B (1984), 57.
    H.Nishiura, C.W.Kim and J.Kim, Phys. Rev. D31 (1985), 2288.
15. L.Lubimov, a talk given at the VI Moriond Conference at Tignes, January, 1986.

DOUBLE BETA DECAY RATES AND THE NEUTRINO MASS

H.V.Klapdor
Max-Planck-Institut für Kernphysik
6900 Heidelberg, Germany



Abstract

Predictions for 2ν and 0ν double beta decay rates are given for all nuclei with $A \geq 70$, for which double beta decay is energetically allowed. These predictions are based on detailed nuclear structure studies of the beta strength distribution and replace earlier estimates basing mostly on phase space considerations. New and more stringent limits on the Majorana neutrino mass are deduced from existing double beta decay experiments. Since the collective effects arising from spin-isospin as well as quadrupole-quadrupole forces are found to lead to a strong reduction of the nuclear matrix elements for two-neutrino double beta decay, but to have only minor influence on the matrix elements $M^{0\nu}$ for the neutrinoless decay mode, the smaller limits for m_ν result mainly from the fact that the widely used scaling procedure underestimates the 0ν matrix elements.

1. Introduction - The neutrino mass and GUTs

The exploration of the nature of the neutrino at the lower end of the mass hierarchy of elementary particles is a great challenge. Nuclear physics can contribute to the solution of the question of neutrino masses and mixing by the investigation of neutrinoless double beta decay ($0\nu\ \beta\beta$). The latter is a sensitive probe for a Majorana mass of the neutrino [1], which might be a unique property of the neutrino among the elementary fermions.

Neutrinos with Majorana masses would correspond to the breaking of B-L symmetry and should manifest themselves in the appearance of neutrinoless double beta decay. We shall briefly repeat the motivation from grand unified theories (GUTs) for searching for Majorana neutrinos by double beta decay experiments (see also [2]).

It is known that, starting from the standard SU(5) model, the prediction for the neutrino mass is zero, because on one hand in minimal SU(5) the right-handed neutrino ν_R (not to be confused with the normal antineutrino conventionally denoted by $\overline{\nu}$; $\overline{\nu} = (\nu_L)^C$) does not exist at all; hence no Dirac mass is possible, and on the other hand SU(5) invariant Majorana couplings are not possible with the Higgs content of the minimal model. However, it is also well known that this result should not be taken too seriously, because there are many shortcomings of this model, for example it does not naturally include CP violation.

Extending the standard model naturally leads to nonvanishing neutrino masses. In SO(10), for example (finite neutrino mass can, of course, also be generated in models based on the SU(5) gauge group with enlarged particle content) the elementary fermions of one family are placed in a 16-dimensional spinor representation, which consists of the 5- and 10 dimensional SU(5) representations and one additional neutral fermion, which has to interpreted as the right-handed neutrino ν_R. From this arrangement it is already clear that the neutrino mass must be related to the masses of the other elementary fermions of the same family. In this model the neutrino has a Dirac mass proportional to the u-quark mass, both masses being equal in the simplest case. Although there is a possibility of making this Dirac mass term for the neutrino vanish by a very delicate choice of model parameters, the most natural prediction is a neutrino Dirac mass in the MeV range. An attractive model for the generation of fermion masses has recently been considered by Stech [3].

It is the exceptional position of the neutrinos that could solve this apparent conflict with reality. An interplay between the large Dirac mass terms, which can hardly be avoided, and an additional Majorana mass term could lead to the phenomenologically desired small neutrino mass eigenstate. As considered by [4], in the presence of a right-handed Majorana term $m_R^M(\overline{\nu_R})^C\ \nu_R$ much larger than

m^D, related to the breaking of a global B-L symmetry, the neutrino mass matrix simplified to the one-flavor case (for n flavors m^D and m_R^M have to be replaced by n x n matrices) would have the form

$$(\bar{\nu}_L \overline{(\nu_R)^C}) \begin{pmatrix} 0 & m^D \\ m^D & m_R^M \end{pmatrix} \begin{pmatrix} (\nu_L)^C \\ \nu_R \end{pmatrix} \qquad \begin{matrix} m_R^M >> m^D \\ m^D = 0(\text{MeV}) \end{matrix} \tag{1}$$

Diagonalisation yields one very light Majorana neutrino with

$$m_1 \simeq \frac{(m^D)^2}{m_R^M}$$

consisting mostly of ν_L, and one very heavy one with $m_2 \simeq m_R^M$. For $m_R^M \gtrsim 10^3$ GeV $m_1 \lesssim 0$(eV) would result. The simple model illustrates the general mechanism of generating small Majorana neutrino masses by the mixing of the unavoidable (except in SU(5)) large Dirac mass terms with even larger Majorana mass terms.

2. Neutrinoless double beta decay and neutrino mass

The lepton number conserving process

$$^A_Z X \longrightarrow {}^A_{Z+2}X + 2e^- + 2\bar{\nu} \quad (2\nu \text{ decay}) \tag{2}$$

is already allowed in the standard Fermi theory and, as far as particle physics is concerned, can be parameter-free predicted.

The more interesting lepton number violating neutrinoless (0ν) decay,

$$^A_Z X \longrightarrow {}^A_{Z+2}X + 2e^- \qquad (0\nu \text{ decay}) \tag{3}$$

not possible in the standard model, becomes allowed in the case of right-handed current admixtures or for a finite Majorana mass of the neutrino (a detailed description of the general formalism can be found in [5]).

We neglect right-handed current contributions in the following. In this case the relation between the 0ν decay rate $\omega_{0\nu}$ observable in the experiments and the effective neutrino mass

$$\langle m_\nu \rangle = \Sigma\, U_{e_i}^2\, m_i$$

is given by (see, e.g. [2,6]):

$$\omega_{0\nu} = f^{0\nu} |1 - x_F|^2 |R_0 M^{0\nu}|^2 \langle m_\nu \rangle^2 / m_e^2 \tag{4}$$

Relation (4) is based on the closure approach, in which case the phase space $f^{0\nu}$ can be factorized from the nuclear structure part $|1 - x_F|^2 |R_0 M^{0\nu}|^2$. The closure treatment, which neglects the structure of the intermediate 1^+ spectrum, is well

justified only for the 0ν decay, where the intermediate energy denominator is dominated by the virtual neutrino. In the case of 2ν decay the intermediate states must be treated properly [7]. $M^{0\nu}$ is the closure matrix element for Gamow-Teller transitions (arising from the axial vector coupling) and x_F is the relative fraction of Fermi (vector coupling) to Gamow-Teller contributions:

$$M^{0\nu} = \langle F|\Sigma\vec{\sigma}(i)\tau^-(i)\vec{\sigma}(j)\tau^-(j)H(i,j)|I\rangle \tag{5}$$

$$x_F = \left(\frac{g_V}{g_A}\right)^2 \frac{\langle F|\Sigma\tau^-(i)\tau^-(j)H(i,j)|I\rangle}{M^{0\nu}}$$

$H(i,j)$ is the potential describing the exchange of the virtual neutrino and is dominated by a $1/r_{ij}$ dependence. A major problem in applying eq. (4) to deduce limits on the neutrino mass arises from the fact that such nuclear structure calculations up to now predicted much too high decay rates for the conventional allowed 2ν decay as compared to the geochemical total decay rates for ^{82}Se and $^{128,130}Te$ (these are the only nuclei where positive evidence for $\beta\beta$ decay was found). For the sometimes used calculation by Haxton et al. [8] this discrepancy with experiment is a factor 100 compared to the geochemical result for ^{128}Te and 150 for ^{130}Te [9]. Since the calculated matrix elements for 2ν were too large, up to now it was widely believed that similarly the matrix elements for the 0ν decay $M^{0\nu}$ resulting from the same nuclear structure calculations are too large, too, and cannot be used without modification in analyzing experimental data.

A usual procedure was therefore to scale $M^{0\nu}$ down according to the observed discrepancy on the 2ν sector:

$$M^{0\nu}_{scaled} = M^{0\nu}_{calc}\,(\omega_{2\nu_{exp}}/\omega_{2\nu_{calc}})^{1/2} \tag{6}$$

Implicitly this scaling assumes that the 2ν and 0ν matrix elements are reduced proportional to each other by some unknown reduction mechanism. As will be discussed below, we find that such a scaling procedure underestimates systematically the 0ν matrix element and leads to too large neutrino mass limits.

3. Nuclear structure studies of 2ν and 0ν $\beta\beta$ decay

The decay rate for 2ν double beta decay between 0^+ states is given by [2,7]:

$$\omega_{2\nu} = \frac{F_A^4 G^4}{32\pi^7} \int_{m_e}^{t_o+m_e} F(Z,\epsilon_1)|k_1|\epsilon_1 d\epsilon_1 \int_{m_e}^{t_o+2m_e-\epsilon_1} F(Z,\epsilon_2)|k_2|\epsilon_2 d\epsilon_2 \tag{7}$$

$$\times \int_0^{t_o-\epsilon_1-\epsilon_2+2m_e} \nu_1^2 \nu_1^2 d\nu_1 \sum_{MM'} A_{MM'}$$

with

$$A_{MM'} = \langle F||\sigma\tau^-||M\rangle\langle M||\sigma\tau^-||I\rangle\langle F||\sigma\tau^-||M'\rangle\langle M'||\sigma\tau^-||I\rangle$$
$$\times \frac{1}{3}\,(K_M K_{M'} + L_M L_{M'} + \frac{1}{2} K_M L_{M'} + \frac{1}{2} L_M K_{M'}) \quad .$$

There have been used several approaches to calculate nuclear matrix elements for double beta decay.

The straightforward method is to use conventional shell model techniques [8,10,11] . This method, however, is limited to light double beta emitters. For heavy nuclei the model space and configurations have to be seriously truncated and the collective effects important in double beta decay can only partly be included. It is difficult or even impossible to treat explicitly the intermediate 1^+ spectrum, which could be compared with results from (p,n) experiments, within this approach. This has only been done for ^{48}Ca [12] . In the other calculations [8,10,11] the detailed structure of the intermediate states was neglected and the closure approximation was used. In this approximation eq. (7) is replaced by the analogue of eq. (4).

$$\omega_{2\nu} = f^{2\nu}\,\frac{|M^{2\nu}|^2}{\langle E\rangle^2} \text{ with } M^{2\nu} = \langle F|\sum_{ij}\vec{\sigma}(i)\tau^-(i)\vec{\sigma}(j)\tau^-(j)|I\rangle \qquad (8)$$

This greatly simplifies the calculations, but is not justified for 2ν decay- [2,7,12].

Table 1. Nuclear matrix elements for double beta decay calculated a) using only particle number projected BCS wave functions (pairing), and b) with additional spin-isospin and quadrupole-quadrupole forces.

	$R_o\|M^{0\nu}\|$		$\|M^{2\nu}\|$		
	Pairing	Pairing $+\sigma\tau\sigma\tau$ +QQ	Pairing	Pairing $+\sigma\tau\sigma\tau$ +QQ	ξ
^{76}Ge	12.5	10.4	7.1	1.93	5.4
^{82}Se	9.7	8.2	5.5	1.38	5.9
^{128}Te	12.3	10.0	6.3	0.52	19.3
^{130}Te	11.9	9.4	5.9	0.48	19.7
^{134}Xe	14.7	11.2	8.0	0.77	14.6
^{136}Xe	6.0	3.9	3.6	0.08	50.8
^{142}Ce	7.7	6.2	3.3	1.30	4.8

The most important collective effect in double beta decay comes from pairing correlations. They lead to the fact that many shells contribute all coherently to double beta decay. This effect is included in calculations using BCS wave functions [11,13], or in an HFB approach [14]. However, taking into account only pairing forces yields much too large matrix elements for the 2ν decay (see table 1). The next step is to include besides pairing also neutron-proton forces, the most important of these for double beta decay being the spin-isospin part, which leads to the concentration of the GT strength for single β^- decay in the Gamow-Teller giant resonance and also to a reduction of the total β^- strength and more important of the β^+ strength. The spin-isospin (GT) force together with the pairing forces can be included in an RPA approach based on BCS wave functions [15]. It is important to note that in this approach the closure approximation is avoided.

We have performed such RPA calculations using a deformed Nilsson potential for all double beta emitters with $A \geq 70$ [2,6]. The BCS wave functions were separately optimized for parent and daughter nucleus (taking into account the change in proton and neutron numbers). The results are given in table 2. (A somewhat simplified approach of this type containing, however, some questionable points, has been used recently for a few $\beta\beta$-emitters in [16]). Unfortunately this approach is not suitable to calculate explicitly the 0ν matrix elements. One step beyond this RPA treatment is to include besides the spin-isospin part also other neutron-proton forces. We have done this for the strongest part of the neutron-proton interaction, the quadrupole-quadrupole force [2,7]. This force especially in the isotopes ^{128,130}Te and ^{128,130}Xe leads to low-energetic 2^+ phonons, which are admixed to the 0^+ ground states and give rise to destructive contributions to the 2ν double beta matrix elements. We have performed these calculations for several nuclei using particle number projected BCS wave functions (PBCS) in large model spaces (12 subshells). The strength of the pairing interaction was deduced from existing pickup and stripping data. The neutron-proton Hamiltonian

$$H_{np} = 2\chi\Sigma\vec{\sigma}(i)\tau^-(i)\vec{\sigma}(j)\tau^+(j) - \kappa QQ \qquad (9)$$

was then diagonalized in this model space. Ground state correlations involving four quasiparticles arising from the spin-isospin part were included by exact diagonalization. The spin-isospin force was also applied to the intermediate 1^+ spectrum and the force strength χ was adjusted to reproduce the known position of the GTGR. The quadrupole term κQQ was treated by RPA (lowest order ground state correlations = four quasiparticle excitations are not sufficient for this strongly attractive interaction). The parameter κ was adjusted to reproduce the position of the collective 2^+ states (one-phonon states). A consistency test of

Table 2. Calculated matrix elements and half-lives in the quasiparticle RPA (QRPA) treatment for $\beta\beta$ emitters with $A \geq 70$. Results from the more refined treatment including quadrupole correlations [2,7] are marked with an asterisk. T_0 denotes the Q-value for double beta decay, δ the deformation parameter used in the calculation, $M^{2\nu}$ is defined in eq. (8). The 0ν half-lives are neutrino-mass dependent and the given figures correspond to $\langle m_\nu \rangle = 1$ eV (from [6]).

			QRPA			
	T_0 (MeV)	δ	$M^{2\nu}$	$T^{2\nu}_{1/2}$ (years)	$T^{2\nu *}_{1/2}$ (years)	$T^{0\nu}_{1/2} \times \langle m_\nu \rangle^2$ (years x eV^2)
^{70}Zn	1.00	0	6.79	1.9×10^{22}		7.6×10^{23}
^{76}Ge	2.04	0.2	5.54	1.1×10^{20}	2.2×10^{20}	2.6×10^{23}*
^{80}Se	0.136	0.2	5.33	9.0×10^{28}		6.7×10^{25}
^{82}Se	3.01	0.2	4.47	4.5×10^{18}	1.5×10^{19}	9.5×10^{22}*
^{86}Kr	1.25	0	1.63	3.5×10^{22}		5.0×10^{24}
^{94}Kr	1.15	-0.1	4.63	4.1×10^{21}		6.2×10^{23}
^{96}Zr	3.35	-0.12	4.83	5.2×10^{17}		1.6×10^{22}
^{98}Mo	0.111	-0.19	4.33	1.6×10^{29}		7.3×10^{25}
^{100}Mo	3.03	-0.24	3.81	1.8×10^{18}		3.3×10^{22}
^{104}Ru	1.30	-0.26	3.81	1.8×10^{21}		5.0×10^{23}
^{110}Pd	2.01	-0.23	3.56	5.0×10^{19}		1.3×10^{23}
^{114}Cd	0.54	0.14	1.80	2.7×10^{24}		1.7×10^{25}
^{116}Cd	2.81	0	1.63	8.3×10^{18}		1.7×10^{23}
^{122}Sn	0.36	0	1.75	1.4×10^{26}		3.6×10^{25}
^{124}Sn	2.28	0	1.65	9.3×10^{19}		3.1×10^{23}
^{128}Te	0.87	0.15	2.36	1.2×10^{23}	5.7×10^{23}	9.8×10^{23}*
^{130}Te	2.53	0.10	2.55	1.9×10^{19}	1.2×10^{20}	4.6×10^{22}*
^{134}Xe	0.84	0	3.18	5.1×10^{22}	2.5×10^{23}	8.7×10^{23}*
^{136}Xe	2.48	0	1.22	6.0×10^{19}	3.3×10^{19}	3.0×10^{23}*
^{142}Ce	1.41	0	1.21	2.8×10^{21}	4.1×10^{20}	4.7×10^{23}*
^{146}Nd	0.061	0	3.38	2.9×10^{30}		5.6×10^{25}
^{148}Nd	1.93	0.18	2.63	2.5×10^{19}		1.1×10^{23}
^{150}Nd	3.37	0.24	2.17	4.8×10^{17}		2.4×10^{22}
^{154}Sm	1.25	0.28	3.10	9.5×10^{20}		2.4×10^{23}
^{160}Gd	1.73	0.29	3.46	4.4×10^{19}		6.4×10^{22}
^{170}Er	0.66	0.27	2.80	6.6×10^{22}		9.1×10^{23}
^{176}Yb	1.08	0.26	2.69	1.1×10^{21}		2.5×10^{23}
^{186}W	0.49	0.20	2.46	3.2×10^{23}		1.2×10^{24}
^{192}Os	0.41	-0.15	2.32	1.7×10^{24}		1.6×10^{24}
^{198}Pt	1.04	-0.10	0.78	1.2×10^{22}		1.6×10^{24}
^{204}Hg	0.41	0	0.47	4.6×10^{25}		2.6×10^{25}
^{232}Th	0.85	0.23	3.57	1.6×10^{20}		3.8×10^{22}
^{238}U	1.15	0.24	2.87	2.2×10^{19}		2.4×10^{22}

the parameters is given by the fact that only with the pairing strength used, κ varies smoothly between neighbouring isotopes, and B(E2) values are in reasonable agreement with experiment.

The 2ν decay rates resulting from this more refined (compared to the RPA) treatment are also given in table 2. It is seen that inclusion of the κQQ term in some cases leads to a further strong reduction of the decay rates (especially for ^{128,130}Te). The discrepancy with the experiments on the 2ν sector is considerably reduced compared to the calculations of [8]. While in the detailed treatment leading to the half-lives given in table 2 we include the intermediate 1^+ spectrum explicitly and do not use the closure approximation, the closure matrix elements are given in table 1 for demonstration of the collective effects on the nuclear matrix elements. It is seen that $M^{2\nu}$ is strongly reduced by the spin-isospin and quadrupole-quadrupole correlations compared to the value obtained with pairing wave functions only.

The influence of these long-range correlations on the 0ν matrix elements $M^{0\nu}$, which we have calculated using the same wave functions described above on the other hand is found to be rather weak [6]. 0ν and 2ν matrix elements are, therefore, not proportionally reduced as assumed by the scaling procedure, but $M^{0\nu}$ remains large. The reason for this is the neutrino potential H, which favors the decay of neutrons close to each other. Long-range correlations are therefore less important. One can express this result also by the ratio of closure matrix elements $\xi = R_o M^{0\nu}/M^{2\nu}$. As can be seen from table 1 we find for ξ a strong dependence on the considered nucleus and generally large values. Using these results for $M^{0\nu}$ we obtain for the 0ν half-lives given in table 2. For the nuclei which we have treated only in RPA and for which we did not calculate $M^{0\nu}$ explicitly, a mean value for ξ was used, deduced from the calculated $M^{0\nu}$ values (see [6]).

Table 3. Limits for the neutrino mass deduced directly from the matrix elements $M^{0\nu}$ of table 1 (unscaled) and from matrix elements reduced according to the discrepancy between calculation and experiment on the 2ν sector (scaled).

	$T^{0\nu}_{1/2}$ experiment (years)			$\langle m_\nu \rangle$ (eV) This work unscaled	This work scaled	Haxton et al.[+] scaled
^{76}Ge	$>2.5 \times 10^{23}$		[17]	<1.0	<3.1	<6.3
^{82}Se	$>3.1 \times 10^{21}$	(1σ)	[18]	<5.5	<17	<32
^{128}Te	$>8 \times 10^{24}$	(2σ)	[9]	<0.35	<1.6	<8.8
^{130}Te	$>2.2 \times 10^{21}$	(2σ)	[9]	<4.5	<21	<108

[+] Deduced from the calculated matrix elements of [8].

4. Results for the neutrino mass

Using the matrix elements of table 1, we get the reduced limits on the neutrino mass $\langle m_\nu \rangle$ shown in table 3. The sharpest limits are obtained at present from the direct measurements of ^{76}Ge and from the geochemical result for ^{128}Te. Depending on whether we use directly the calculated $M^{0\nu}$ or scale according to the remaining discrepancy on the 2ν sector, we obtain a limit of 0.35 eV or 1.6 eV for $\langle m_\nu \rangle$. In the case that the still-remaining discrepancy for the 2ν rates could be explained by some refined treatment of long-range nuclear structure correlations, we would expect the lower limit of 0.35 eV to be the more realistic one. The deduced values correspond to effective neutrino masses. It is discussed in detail in [2], that considering possible interference effects between light and heavy neutrinos, consistent with these effective masses the true mass of the lightest (electron) neutrino in the case of mixing with a heavy neutrino of mass larger than 100 MeV could still be as large as 25 eV.

Acknowledgement : The author would like to thank his colleague Dr. K. Grotz for the fruitful cooperation on this subject and Prof. B. Stech for useful discussions.

References

[1] H. Primakoff and S.P. Rosen, Ann. Rev. Nucl. Part. Sci. 31 (1981) 145
[2] K. Grotz and H.V. Klapdor, Proceed. 1st. Symposium on Underground Physics, Saint Vincent, Italy, April 25-28 (1985), and submitted to Nucl. Phys. A
[3] B. Stech, Phys. Lett. 130B (1983) 189
[4] M. Gell-Mann, P. Ramond and S. Slansky, in : Supergravity, eds. P. van Nieuwenhuizen and D.Z. Freedman (North-Holland, Amsterdam, 1979).
[5] M. Doi, T. Kotani, H. Nishiura, K. Okuda and E. Takasugi, Prog. Theor. Phys. 66 (1981) 1739.
[6] K. Grotz and H.V. Klapdor, Phys. Lett. 153B (1985) 1 and 157B (1985) 242
[7] H.V. Klapdor and K. Grotz, Phys. Lett. 142B (1984) 323
[8] W.C. Haxton, G.J. Stephenson, Jr., and D. Strottmann, Phys. Rev. Lett. 47 (1981) 153; W.C. Haxton, Phys. Rev. D 25 (1982) 2360; Comm. Nucl. Part. Phys. 11 (1983) 41; Progr. Part. Nucl. Phys. 12 (1984) 409.
[9] T. Kirsten, H. Richter and E. Jessberger, Phys. Rev. Lett. 50 (1983) 474; T. Kirsten, in: Proc. Workshop on Science Underground (Los Alamos 1982).
[10] V.A. Khodel, Phys. Lett. 32B (1970) 583.
[11] L. Zamick and N. Auerbach, Phys. Rev. C 26 (1982) 2185
[12] T. Tsuboi, K. Muto and H. Horie, Phys. Lett. 143B (1984) 293
[13] W.C. Haxton and G.J. Stephenson, Jr., Phys. Rev. C 28 (1983) 458
[14] T. Tomoda, A. Faessler, K.W. Schmid and F. Grümmer, Phys. Lett. 157B (1985) 4
[15] A.H. Huffmann, Phys. Rev. C 2 (1970) 741
[16] P. Vogel and P. Fisher, Phys. Rev. C 32 (1985) 1362, and P. Vogel, contrib. to this conference
[17] F.T. Avignone, private communication
[18] B.T. Cleveland et al., Phys. Rev. Lett. 35 (1975) 757

DOUBLE BETA DECAY AND NUCLEAR STRUCTURE

Petr Vogel
Physics Department
California Institute of Technology
Pasadena, CA 91125, USA



ABSTRACT

The decay rate of the 2ν double beta decay is calculated as a test of our understanding of the nuclear structure problems involved. The effects of pairing, static quadrupole deformation, spin-isospin polarization, and the Δ isobar admixtures are analyzed. The calculation, which is parameter free, predicts a faster decay rate than has been observed experimentally in ^{82}Se, ^{130}Te, and ^{150}Nd.

Double beta decay ($\beta\beta$) is the process where a nucleus (Z,A) undergoes a transition to (Z+2,A), while the transition to the intermediate nucleus (Z+1,A) is energetically forbidden. The extra stability (pairing energy) of the initial and final even-even nuclei makes such a transition possible. There are two modes of double beta decay; the 2ν mode involves emission of two electrons and two antineutrinos, and the 0ν mode involves the emission of two electrons only. (For general reference on $\beta\beta$ decay see Refs.1 and 2).

The 0ν mode has long been recognized as a sensitive test of lepton number conservation, the mass of electron neutrino, and of weak interactions involving right-handed lepton currents. This mode can proceed only if electron neutrinos are Majorana particles. On the other hand, the 2ν mode is expected to occur from standard theory; it can proceed irrespective of the neutrino mass with both Dirac and Majorana neutrinos. Study of the 2ν $\beta\beta$ decay allows us to gauge our ability to solve the nuclear structure problems involved. Without solving these problems it is difficult to interpret correctly results of experimental searches for the 0ν mode in terms of the neutrino Majorana mass or the strength of right-handed current weak interactions.

In this talk I discuss primarily calculations of the 2ν $\beta\beta$ decay rate[3]. The half-life for the transition between two 0^+ ground states of even-even nuclei is given by the formula

$$\left[T^{2\nu}_{1/2}(0^+ \to 0^+)\right]^{-1} = G_{GT}(E_{max},Z)\left|\sum_m \frac{\langle f|\sum_n \sigma_n \tau_n^+|m\rangle\langle m|\sum_k \sigma_k \tau_k^+|i\rangle}{E_m - (M_i + M_f)/2}\right|^2 \qquad (1)$$

Here $|i\rangle$ ($|f\rangle$) is the initial (final) nucleus in the 0^+ ground state with the mass M_i (M_f); $|m\rangle$ are the 1^+ states of the intermediate odd-odd nucleus with energies E_m, σ_k is the Pauli spin operator for the nucleon and τ_k^+ changes a neutron into a proton. The function G_{GT} results from lepton phase space integration; it contains all the relevant constants as well as the relativistic Coulomb term. Evaluation of G_{GT} is straightforward and in the

following we consider it as given and concentrate on the evaluation of the sum in (1). We are not going to use the customary closure approximation which allows one to avoid the sum over the intermediate states $|m\rangle$. Instead, the summation is performed explicitly. Thus our goal is evaluation of the quantity

$$M_{GT} = \sum_m \frac{\langle f|\sum_n \sigma_n \tau_n^+|m\rangle\langle m|\sum_k \sigma_k \tau_k^+|i\rangle^2}{E_m - (M_i + M_f)/2} \qquad (2)$$

as indicated schematically in Fig. 1.

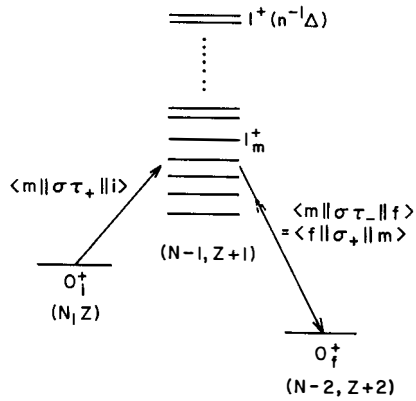


Fig. 1. Schematic illustration of the summation in Eq. (2)

Note that the individual terms in Eq. (2) have a straightforward physical interpretation. The matrix element $\langle m|\Sigma\sigma\tau^+|i\rangle$ describes the amplitude of the Gammow-Teller β^- transition or, alternatively, the amplitude of the (p,n) forward angle reaction at a suitable energy. Similarly, the $\langle f|\Sigma\sigma\tau^+|m\rangle$ matrix element (or its complex conjugate as indicated in Fig. 1) describes the β^+ transition amplitude, or the (n,p) reaction on the final nucleus. These

matrix elements obey the model independent sum rule

$$S^- - S^+ = \sum_m |\langle m|\Sigma\sigma_k\tau_k^+|i\rangle|^2 - \sum_m |\langle m|\Sigma\sigma_k\tau_k^-|i\rangle|^2 = 3\,(N-Z). \qquad (3)$$

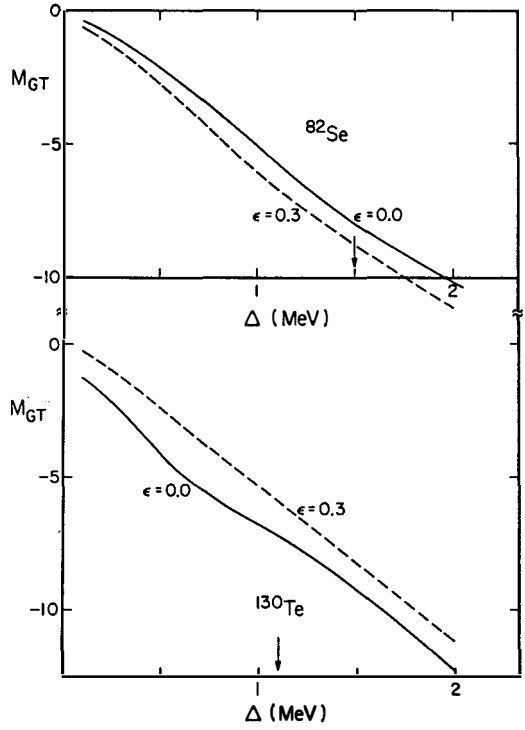


Fig. 2 The matrix elements M_{GT} in closure approximation as a function of the pairing gap Δ for two values of the deformation parameter ε.

For non-magic nuclei one can, in a reasonable approximation, replace $|i\rangle$ by $|f\rangle$ in the second term and obtain a sum rule restricting the sum of squares of the terms in the numerator of Eq. (2).

The first important point deals with the role of pairing correlations in ββ decay. Most ββ decay candidates have a sizable neutron excess and thus neutron and proton Fermi levels are in different shells. Consequently, the S^+ strength (second term in (3)) vanishes or is strongly supressed in the extreme shell model. The smearing of occupation probabilities caused by pairing correlations opens the β^+ channel and allows the ββ decay to proceed. In agreement with this finding our numerical calculation shows that M_{GT} in (2) is approximately proportional to the pairing gap Δ, as illustrated in Fig. 2. Note that the value of Δ is not an adjustable parameter; it is determined by the excess binding energy of the even-even nucleus when compared to its odd-A neighbors.

The next important ingredient of the calculation is the effect of nuclear spin-isospin polarization force. This force is responsible for concentration of the S^- strength in the "Giant Gamow-Teller Resonance", observed in the (p,n) reactions[4]. In the calculations the simplest form of such force was chosen,

$$V_{12} = \chi \vec{\sigma}_1 \cdot \vec{\sigma}_2 \vec{\tau}_1 \cdot \vec{\tau}_2 \qquad (4)$$

The coupling parameter χ was fixed by requiring that the giant GT state is approximately at the experimentally determined energy; the value $\chi = 23/A$ MeV fulfills that requirement. The 1/A dependence of χ reflects the volume nature of the interaction (4).

The force (4) was treated in the customary quasiparticle random phase approximation and its effect is illustrated in Fig. 3 (prepared by P. Fisher). Note the emergence of the giant resonance in the β^- channel. The strength in the β^+ channel, which is small to begin with, is further reduced and the β^+ strength remains spread. As the consequence of the inclusion of spin-isospin polarization the M_{GT} sum (3) is reduced by a factor of about 5. Calculation without such a force would be of little relevance.

Several ββ decay candidates are deformed nuclei. Inclusion of the static quadrupole deformation in the framework of our calculation is concepturally simple (it turns out that it is important to perform the summation in (3) explicitly; the closure approximation gives erroneous results). Inclusion of deformation

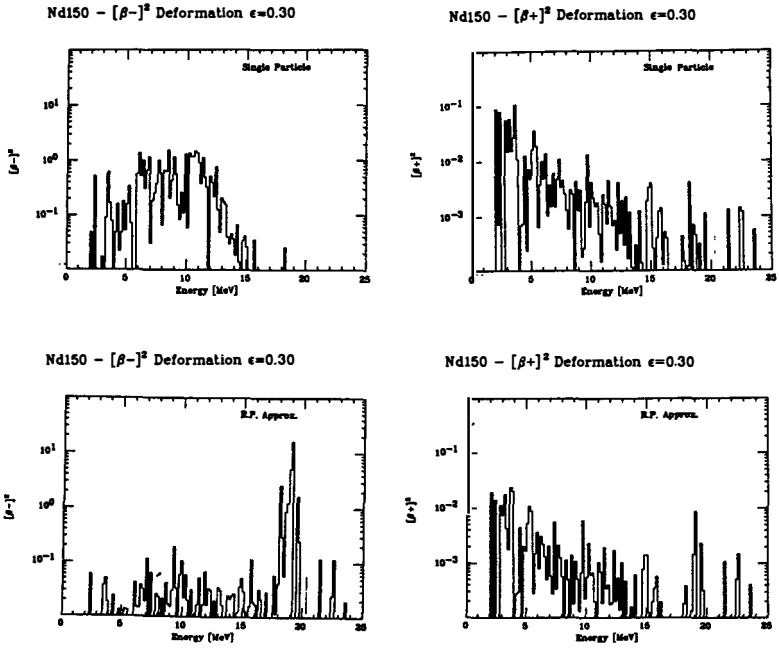


Fig. 3 β^- strength and β^+ strength in ^{150}Nd for indicated deformation. Upper part for independent quasiparticles, lower part with spin-isospin polarization includes.

leads to the reduction of $\beta\beta$ decay rate in ^{150}Nd by a factor of ~ 4. The effect, however, is different in different nuclei.

It is known from (p,n) reaction studies[4] that the observed strength does not obey the sum rule (3). In fact, 30-50% of the strength is "missing". It has been suggested that the mixing of the 1^+ states in the intermediate odd-odd nucleus with the Δ_{33} isobar-nucleon hole states is responsible for this "missing strength" effect.

We have included the Δ_{33} -nucleon hole states in the calculation using the simplest quark model of the Δ_{33} and nucleon.

Two additional states of ∿ 300 MeV, indicated in Fig. 1, must then be considered. The first one corresponds to a nucleon hole in the initial nucleus, combined with Δ^{++} or Δ^{+}. This state has a large β^{-} strength but vanishing β^{+} strength. The second state represents a nucleon hole in the final nucleus, combined with Δ^{-} or Δ^{o}. It has a large β^{+} strength connecting it to the final nucleus but vanishing β^{-} strength. When these two states are included in the RPA equations of motion the strength in the "giant" is reduced by ∿ 35% in agreement with experiment. The effect on the ββ decay, or the sum (3), is only indirect; the two states at 300 MeV cancel each other. The sum over low lying states is reduced by 30-50% Note that in order to keep the giant resonance at the same energy it is necessary to choose another value of the coupling parameter χ (χ_{eff} = 28/A MeV). The final results in Table I were calculated in this way.

TABLE I

Summary of calculation: matrix elements, lifetimes and related quantities.

Nucleus	T_o (MeV)	G_{GT} (yr^{-1}) x 10^{-20}	M_{GT}	calc $T_{1/2}$ (yr) x 10^{20}	exp $T_{1/2}$ (yr) x 10^{20}
^{76}Ge	2.05	13	0.066	1.8×10^{1}	>0.8
^{82}Se	3.00	450	0.082	0.33	1.7(>1.0)
^{100}Mo	3.03	900	0.23	0.021	-
^{128}Te	0.87	0.085	0.10	1.1×10^{3}	$>8 \times 10^{4}$
^{130}Te	2.53	480	0.09	0.23	25
^{136}Xe	2.48	460	0.098	0.23	-
^{150}Nd	3.37	1.1×10^{4}	0.064	0.022	>0.13
^{238}U	1.15	63	0.11	1.4	-

The results of our calculations are summarized in Table I. The experimental data in the last columns (for detailed references see[3]) are by Caldwell et al. (^{76}Ge), Elliott et at. (^{82}Se limit),

Kirsten (^{82}Se value, ^{128}Te, ^{130}Te), and Klimenko et al. (^{150}Nd). The calculated lifetimes are shorter than the experimental ones in ^{82}Se, ^{128}Te, ^{130}Te and ^{150}Nd. The discrepancy in ^{130}Te is specially disturbing. Several further improvements in calculation are possible but none of them is expected to change the calculated rate very much. Note that our calculation is parameter free and that our results agree well with the results obtained elsewhere using very different techniques. So further development in theory is clearly needed. On the other hand the prospects in experimental searches are encouraging. In ^{76}Ge the experimental sensitivity is approaching the calculated rate while in ^{100}Mo, ^{136}Xe and ^{238}U experiments are planned or in progress.

References

1) W.C. Haxton and G.J. Stephenson, Jr., Progr. Part. Nucl. Phys. 12, 409 (1984).
2) M. Doi, T. Kotani, and E. Takasugi, preprint, Osaka Univ. 1985.
3) P. Vogel and P. Fisher, Phys. Rev. C32, 1362 (1985).
4) C. Gaarde, Nucl. Phys. A396, 127c (1983).

A Low Background Study of Ge^{76} Neutrinoless Double Beta Decay in the St. Gotthard Tunnel

Peter Fisher*
California Institute of Technology
Pasadena, California, 91125

March 19, 1986



Abstract

A high purity germanium detector has been run in an underground laboratory for a period of 6728 hours, giving a lower limit for the half-life of Ge^{76} neutrinoless double beta decay of $t_{1/2} \geq 3.2 \times 10^{22}$ years (90% cl) or 6.2×10^{22} years (68% cl).

*Present address SIN, CH-5234 Villigen, Switzerland

The measurement of the neutrinoless double beta decay provides a sensitive test of the structure of weak interactions. The observation of such a lepton number non-conserving process would be evidence that the neutrino is a massive Majorana particle which could possibly be coupled to right handed weak currents [1]. Neutrinoless double beta decay has been searched for, but not observed, which places an upper limit on the Majorana mass of the neutrino. Currently, the best limit is about $m_\nu \sim 2$ to 3 eV (at 68% confidence level)[3].

One such decay is $Ge^{76} \rightarrow Se^{76} + 2e^-$. The two electrons in the final state have a total kinetic energy of 2040.7 ± 0.5 keV and, by measuring ionization energy deposited by these electrons, such a decay can be detected. Natural germanium has an isotopic abundance of 7.76% Ge^{76}, so a semiconductor detector made from germanium and held under reverse bias may be used to search for $\beta\beta$ decay of Ge^{76} inside the detector itself. These detectors have excellent energy resolution and stability, which serves to separate $\beta\beta$ decay events from background events.

In our experiment, a detector with fiducial volume of 90 cm^3 was first operated for 3820 hours in a subbasement room at Caltech (3 meters water equivalent, [2]). To reduce the cosmic ray induced background, the detector was then moved to the St. Gotthard road tunnel (4000 m.w.e.)in Ticino, Switzerland, where a run of over 6728 hours has now been completed. The energy resolution over the run was 2.6 keV at 1.3 MeV.

To reduce background from natural radiation inside the tunnel, the detector is surrounded by 11 cm electrolytic copper, followed by 15 cm lead (Figure 1). The lead is surrounded by an airtight aluminum container which is continuously purged by nitrogen gas. The entire setup is surrounded by 20 cm borated polyethylene to absorb thermal neutrons. Output pulses from the detector were fed through a pre-amp and a Canberra 2010 spectroscopy amplifier followed by an 8192 channel ADC. The ADC operated over a region from 9 keV to 2.8 Mev. Data was also collected over a range from 100 keV to 4.4 MeV in a 1024 channel multichannel analyzer. A pulser was automatically run at constant voltage at 1 Hz for 10 minutes every six hours as a stability check. The pulser peak had a FWHM of 3 keV over the entire run.

Although the 4000 m.w.e. overburden cut the cosmic muon flux by a factor of 10^6, the background in the 2 MeV region was decreased by only a factor of 16 from the Caltech run (Figure 2). Radiation from inside the tunnel caused the remaining background.

Gamma ray photons from the natural decay chains of Th^{232} and U^{238} may cause counts in the 2 MeV region by Compton scattering in the detector or shielding. In particular, Tl^{208} has a strong line at 2614 keV and Bi^{214} has weaker lines at 2447 keV and 2204 keV. Care was taken during the construction of the detector to make sure no thallium contaminated materials were used. The bismuth lines came mostly from Ra^{226} gas which can seep inside the shielding. Purging the aluminum container with nitrogen gas eliminated almost all the bismuth contamination.

Neutron interactions may also produce gamma ray photons two ways. First, high energy neutrons may interact with the copper or germanium to produce radioactive isotopes (Table 1). Since the overburden eliminates the high energy neutrons, only the products of interactions before the detector and shielding were installed in the tunnel are observed. The intensity of these lines are seen to decay exponentially with the correct half life. Sec-

Table 1: Neutron Reactions

Reaction	Gamma Energies	$t_{1/2}$
$Cu^{63}(n,\alpha 2n)Co^{58}$	810.8 keV	70.9 days
$Cu^{63}(n,2\alpha 2n)Mn^{54}$	834.8 keV	312.5 days
$Cu^{63}(n,\alpha)Co^{60}$	1173.2 keV	5.3 years
	1332.5 keV	
$Cu^{63}(n,\alpha 4n)Co^{56}$	1238.3 keV	78.8 days
	846.9 keV	
$Cu^{63}(n,\alpha p)Fe^{59}$	1099.3 keV	44.5 days
$Cu^{63}(n,\alpha 3n)Co^{57}$	122.1 keV	271.8 days
$Ge^{70}(n,\alpha 2n)Zn^{65}$	1124.1 keV	244.1 days

Table 2: Thermal Neutron Reactions

Reaction
$Ge^{70}(n,\gamma)Ge^{71} \rightarrow Ga^{71} + \gamma(9\text{ keV})$, $t_{1/2,EC}$ =11.2 days
$Ge^{74}(n,\gamma)Ge^{75}m \rightarrow Ge^{75} + \gamma(139.7\text{ keV})$
$Ge^{76}(n,\gamma)Ge^{77}m \rightarrow Ge^{77} + \gamma(159.7\text{ keV})$

ond, thermal neutrons may be captured in the germanium, resulting in several low energy lines (Table 2). The borated polyethylene reduces the thermal neutron flux by a factor of 150 and no neutron capture lines were observed (Figures 3 and 4).

Figure 3 shows the full energy spectrum. Lines from both the natural decay chains are evident, as are the lines from the high energy neutron interactions. Figure 5 shows the region between 2.0 and 3.0 MeV, which includes the 2041 keV $\beta\beta$ decay energy and the Tl^{208} line. The average background for a 200 keV region centered on 2041 keV is 2.3×10^{-4} /keV-h and the rate in the Tl^{208} photopeak is 8×10^{-3} /h.

In a 5.5 keV region centered around 2041 keV, there are a total of 10 counts. The average background in this region gives a total of 9.6 counts in this window. To calculate the upper limit of the number of counts from $\beta\beta$ decay with a given confidence level (CL), a background fluctuation of 1-CL is assumed. This gives 5.5 counts from background and an upper limit of 4.5 counts from $\beta\beta$ at 90% CL, which gives an upper limit on the halflife of $t_{1/2} \geq 3.2 \times 10^{22}$ years. At 68% CL, $t_{1/2} \geq 6.2 \times 10^{22}$ years. In comparison, Caldwell et. al.[3], using a large detector array have recently obtained $t_{1/2} \geq 2.5 \times 10^{23}$ years (68%cl).

A larger detector will be installed needed to continue this measurement. An array of eight 140 cm^3 crystals has been designed by the Caltech-SIN-Neuchatel collaboration and a single crystal prototype is currently being tested. A signifincant amount of the running time of the 90 cm^3 detector was used to test candidate materials used in the construction of the large system. The author wishes to acknowledge the support of his colleagues E. Bovet, K. Gabathuler, H. Henrikson, J-L. Vuilleumier and F. Boehm. The work was supported in part by the US Department of Energy.

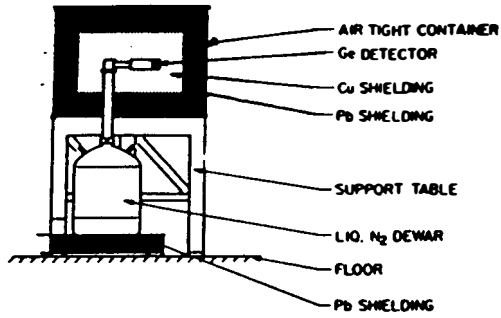


Figure 1: The Detector setup.

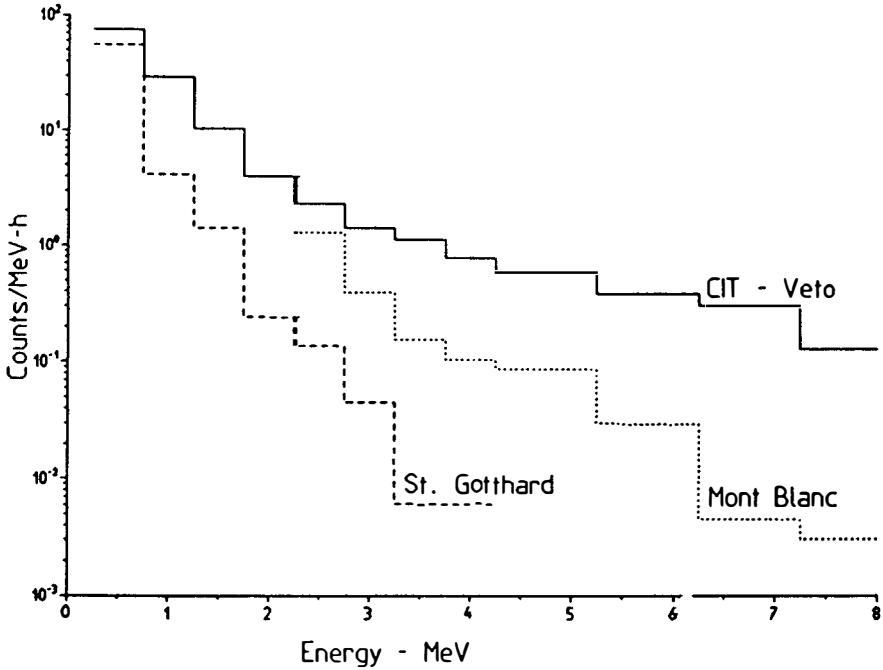


Figure 2: Count rate vs. energy for 90 cm^3 detector at Caltech [2], the Mont Blanc detector [4],and the 90 cm^3 detector in the St. Gotthard tunnel.

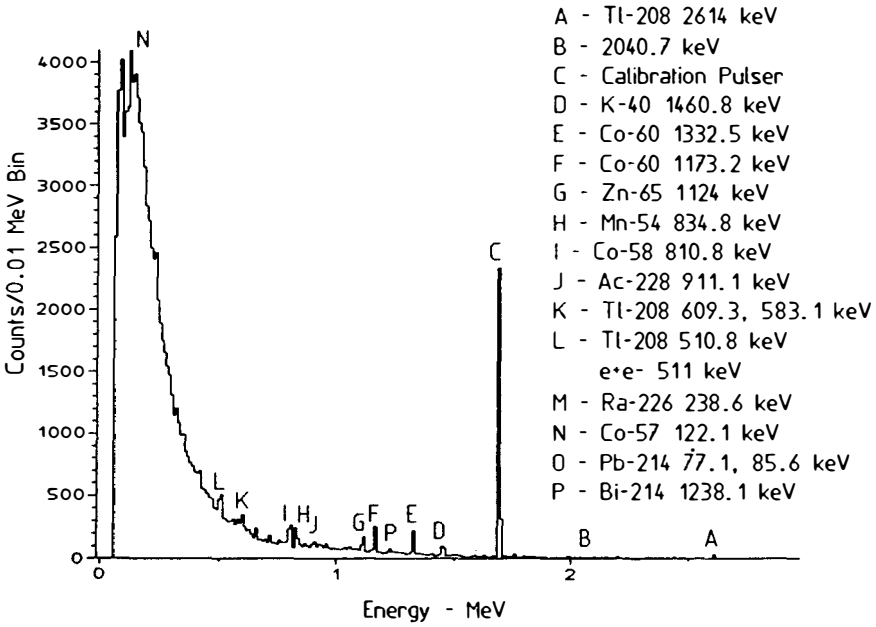


Figure 3: The full spectrum for a 6728 hour run in the St. Gotthard tunnel.

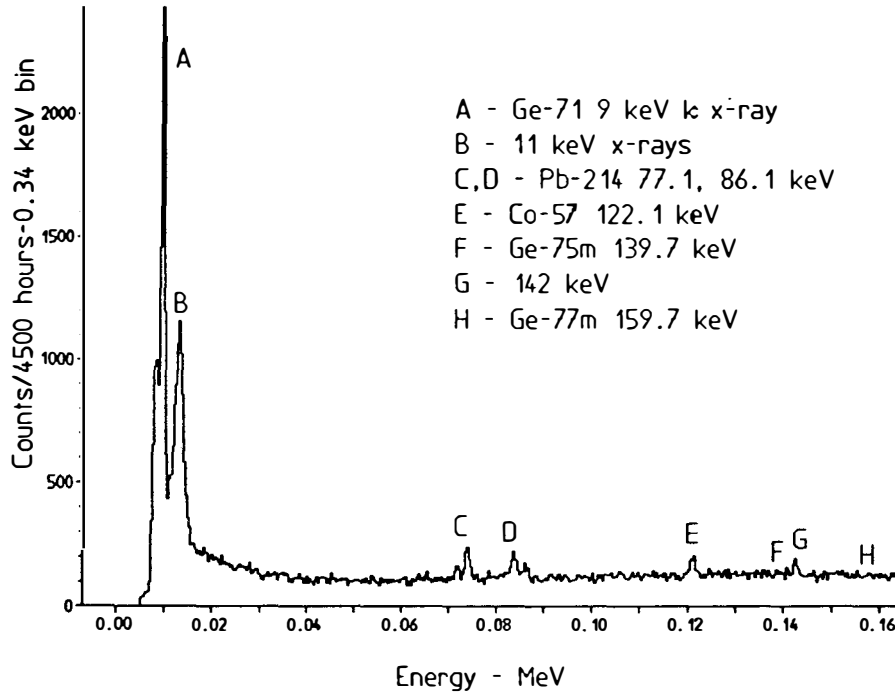


Figure 4: The low energy portion of the 6728 hour spectrum.

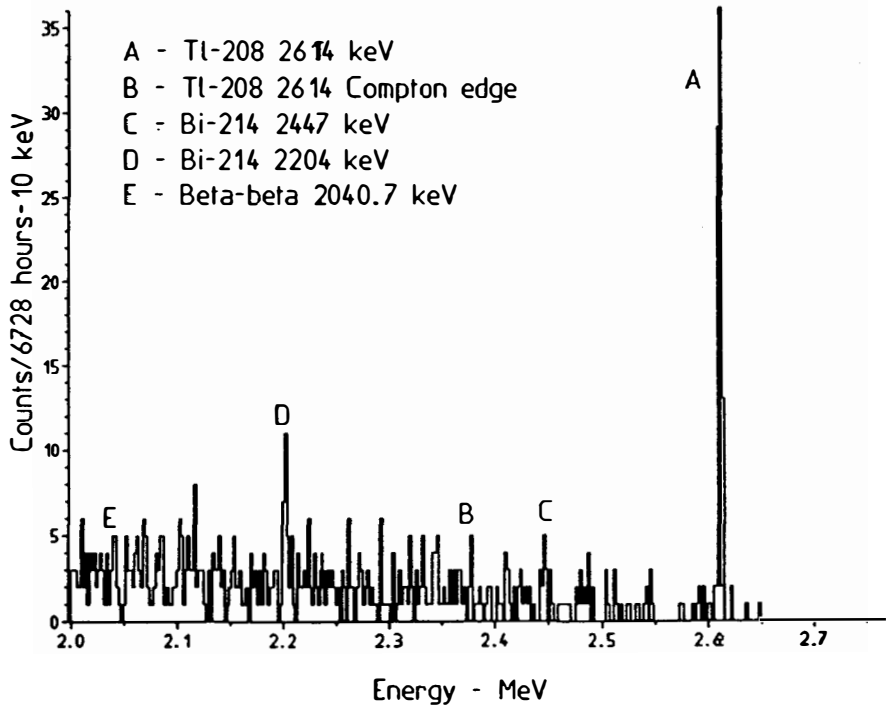


Figure 5: The region above the 2040.7 keV $\beta\beta$ energy.

References

[1] W.C. Haxton and G.J. Stephenson, Prog. Part. Nucl. Phys. 12,409,(1984).

[2] A. Forster, et.al., Phys. Lett. 138B(1984)301.

[3] D.O. Caldwell et. al., Preprint, Sept. 1985.

[4] E. Bellotti et. al., Proc. Int. Conf. High En. Phys., Brighton,1983.

PRESENT AND FUTURE EXPERIMENTS ON DOUBLE BETA DECAY

presented by Ettore Fiorini
Dipartimento di Fisica and Sezione INFN - Milano - Italy

Milano Group (+)

ABSTRACT

The final results of the Milano experiment on double beta decay of ^{76}Ge are presented together with the status and performance of the present Xenon set-up to be installed in the Gran Sasso Laboratory. Finally the possibility is investigated to study double beta decay using low temperature calorimetry, and preliminary results on this technique are reported.

(+)
A. Alessandrello, E. Bellotti, D. Camin, O. Cremonesi, E. Fiorini, A. Giuliani, C. Liguori, A. Pullia, L. Rossi, P. Sverzellati and L. Zanotti.

I would like to discuss briefly here the present and future activity of the Milano group in the field of double beta decay, which has been extensively treated in this Conference both from the theoretical and experimental point of view, and reviewed recently[1]. I will only remind that direct, or instrumental, experiments can be carried out either with a double beta source "external" to the detector, or using as a source the material of the detector itself. This approach has been first adopted by T. der Mateosian and M. Goldhaber with a CaF_2 scintillator to investigate ^{48}Ca[2], and by our group with a GeLi diode to search for double beta decay of ^{76}Ge[3]. Natural germanium contains in fact 7.67% ^{76}Ge, which could decay into ^{76}Se with a transition energy of (2040.71 ± 0.52) keV.

The experiment reported here has been carried out with two true coaxial GeLi diodes with total volumes of 143 and 169 cm^3 and fiducial volumes of 116 and 138 cm^3 operating in a laboratory located in the Mont Blanc Tunnel at a depth of about 5000 hectograms of standard rock. The two detectors have been operated for a total of 21,000 and 12,000 hour of effective running time respectively. No evidence has been found for any type of double beta decay and the final limits, at the 68% confidence level, are:

(1) 1.7×10^{23} years for neutrinoless double beta decay;

(2) 2.2×10^{19} y for two neutrino double beta decay; and

(3) 1.5×10^{20} y for neutrinoless double beta decay accompanied by the emission of a Majoron.

This limit on the neutrinoless decay corresponds to an upper limit on the average neutrino mass ranging from 3.2 eV to 1.3 eV corresponding to the calculations by the Los Alamos[4] and Heidelberg[5] groups.

A second experiment, presently running in Milano, is aiming to detect double beta decay of ^{136}Xe whose isotopic aboundance is 8.86%. The detector is an horizonthal cylinder of 40 cm diameter and 110 length containing a multielement proportional chamber consisting of 61 cells arranged in a honeycomb structure (Fig. 1). Each cell has a length of 80 cm and an exagonal section of 2.5 cm side with anodes made with 20 μm diameter wires. The cathode consists of 24 wires of 100 μm diameter. All materials were pre-tested and selected for their low content of intrinsic radioactive impurities. The operating pressure of the detector is ten bars and a purification pneumatic circuit keeps the oxigen-like impurities below 0.2 ppm.

As shown by the Monte Carlo simulated neutrinoless double beta decay of Fig. 2 an event normally involves more than one cell, and the drift times are considerably long. The aim of the electronic read-out system is to read the

energy deposit in each individual cell of the chamber for every event and to acquire and record on magnetic tape for further analysis the time development of the signals.

Each anode wire is connected to a charge sensitive preamplifier where the current pulse is integrated in the 1.5 pF feedback capacitor; the decay time constant is 1.5 ms. The charge signal is further amplified and digitized by a flash ADC CAMAC module using 7 bit flash encoders which can work down to a sampling period of 100 ns. This period is however set to 1 μs to keep into the buffer memory 256 points describing the time development of the signal covering the whole rise time up to its maximum. The flash ADC CAMAC module continuously digitizes its imput signal and, upon reception of a delayed trigger signal, freezes the buffer content which holds the description of the charge pulse. The trigger pulse is generated in a group of NIM modules which adds all the auxiliary charge pulses comings from the preamplifiers. During the tests the CAMAC dataway has been controlled by a CAVIAR microcomputer, but in the final version a μVax II with a Gec-Elliot interface will handle the data acquisition. A single board computer will read the different parameters of the system like high voltage, pressure, total anode current and temperature: it will be connected through a serial link to the μVAX.

At present the set-up is operating in Milano with a 10 cm lead shielding and a trigger rate of 200 Hz when the total energy deposited in the chamber is above 200 keV. This rate is expected to be reduced to about 2 Hz when the detector will be installed in the Gran Sasso tunnel.

A spectrum of pulses from a single cell with pure Xenon filling at 4.5 bar and ^{241}Am and ^{57}Co is shown in Fig. 3. The energy resolution is 7.5% FWHM for the 122 keV line of ^{57}Co, very near to the theoretical expectation. Events where the energy is released in two adjacent cells were also measured and no noticeable loss of charge was found within 0.5% after adding both signals.

A preliminary spectrum has been obtained in a measurement totaling 40 hours of effective running time at 7 bar adding the signals of the 24 central cells. The overall energy resolution at 511 keV was 9% (FWHM) corresponding to 4% at 2500 keV.

With a better equalization of the pulses from the various anode wires and and an improved time analysis of the pulses, which will be allowed by the use of the μVax computer and by the lower counting rate underground, we expect to reach a resolution of about 3% in the region of neutrinoless double beta decay. Since the fiducial volume at 10 bar is approximately 45 dm^3, which corresponds to 10^{24} nuclei of ^{136}Xe, and the background rate mass unity of the detector is expected to be similar to the one obtained in our ^{76}Ge experiment we are confident to reach in a year a sensitivity of 10^{23} y for neutrinoless dobule beta decay and of a few 10^{21} y for two neutrino and Majoron decays. This expectation could be in principle peximistic since it is based only on

the measurement of the energy and not on the "visualization" of the event.

A third possibility considered by our group to investigate double beta decay, always in the detector=source approach, is provided by the very low heat capacity at low temperature of a crystal made by a pure insulator where impurities of conductive type are strongly reduced[4]; In this case the heat capacity is only due to the phonon propagation and is given by:

$$C = 1944 \left(\frac{V}{V_m}\right) \cdot \left(\frac{T}{\Theta_D}\right)^3 J/°K \qquad (4)$$

where V is the volume of the detector, V_m the molecular volume, and T and Θ_D are the absolute and Debye temperatures, respectively. At very low temperature the heat capacity becomes so small that the energy released by double beta decay inside the crystal is revealed by the increase of the temperature, which can be measured from the change of the resistence. The energy resolution is expected to be:

$$\Delta E = \alpha \sqrt{8 \cdot \ln 2 \cdot C \cdot T^2} \qquad (5)$$

where α ranges from 1 to 2.

This new technique has been recently successfully used to detect and measure X-rays[5,6] and alpha particles[6-9]. In particular the CERN-Milano collaboration has used as detector of alpha particles a Silicon chip of 1 x .5 mm^2 surface and .3 mm thickness implanted with phosphorus ions up to a depth of 1000 A°, the implanted region acting as thermometer of the temperature increases due to the absorbed particles. The excellent time structure of the pulses is shown in Fig. 4: the rise time, related to the velocity of sound (propagation time of the phonons), is lower than the rise time of the preamplifier, while the decay time, related to the heat dissipation from the bolometer is of a few tens of microsecond. The height of the pulses allow to obtain from the know energy delivered by the alpha particle the heat capacity of the bolometer as a function of the temperature. Measurements carried out at temperatures ranging from .3 to 1°K yield values for the heat capacity of the bulk crystal proportional to the cube of the temperature and in excellent agreement with theory, while the contribution due to the implanted region is found to be one order of magnitude larger than expected, probably due to incomplete annealing of this region after implantation.

This technique seems to us very promising for searches on double beta decay. A ultra pure crystal of a double beta active element could be implanted in a very small region, with this active zone acting as a thermometer of the temperature increases due to the energy delivered by the decay. A few isotopes, which are very promising for double beta decay and present at the

same time a large Debye temperature, and therefore a small expected heat capacity, are listed in Table I, together with the expected energy resolution at 0.005°K for a crystal with a mass of one kilogram. We would like to stress that there is in principle no limitation to the mass of the detector: one could use for instance a 400 kg detector made of natural germanium, and the energy resolution would still be below one keV.Our group is presently considering a large ultrapure germanium crystal with a small doped germanium bolometer sinterized on it and acting as thermometer.

(T.O.Niinikoski and A.Rijllart from CERN have partecipated to the test of a low temperature bolometer reported in ref. 9)

T A B L E I

ISOTOPE	DEBYE TEMP. (°K)	RESOLUTION (1 Kg) (eV)
^{76}Ge	370	85
^{96}Zr	291	140
^{100}Mo	460	50
^{116}Cd	210	300
^{124}Sn	200	310
^{128}Te	150	500
^{130}Te	"	"
^{150}Nd	160	400

REFERENCES

1. D.O. Caldwell: Double beta decay - current status. Invited Talk to the Sixth Workshop on Grand Unification - University of Minnesota, Minnesota, April 18-20, 1985.

2. E. der Mateosian and M. Goldhaber: Phys. Rev. 146, 810 (1966).

3. E. Fiorini et al: Phys. Lett. 25 B, 602 (1967).

4. E. Fiorini and T.O. Niinikoski: Nucl. Instr.and Methods 224, 83 (1984) also for previous references.

5. D. Mc Cammon, S.H. Moseley, J.C. Mather, and R.F. Mushotzki: J. Appl. Phys. 58, 1263 (1984).

6. D. Mc Cammon, M. Juda, J. Zhang, R.L. Kelley, S.M. Moseley, and A.E. Szymkowiak: I.E.E.E. NS 33, 236 (1986) also for previous references.

7. C. Boragno, U. Valbusa, G. Gallinaro, D. Bassi, S. Iannotta, and F. Mori: Cryogenics 24, 681 (1984).

8. N. Coron et al: Nature 75, 314 (1985).

9. T.O. Niinikiski, A. Rijllard, A. Alessandrello, E. Fiorini, and A. Giuliani (CERN-MILANO Collaboration): Europhysics Lett. (in the press), also for previous references.

FIGURE CAPTIONS

Fig. 1: Cross section of the Multiwire Proportional Chamber and details of a single cell

Fig. 2: Tipical Monte Carlo generated neutrinoless double beta decay event in Xenon at 10 bar

Fig. 3: Single wire spectrum with ^{57}Co and ^{241}Am souces with pure Xenon at 4.5 bar

Fig. 4: A tipical pulse obtained by the CERN-MILANO collaboration with a Silicon chip exposed to alpha particles at 500 m K. In the inset, the imput circuit

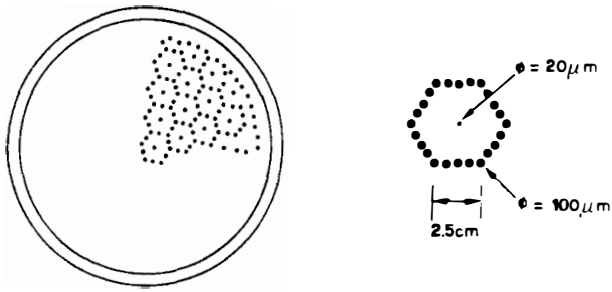

ϕ = 20μm
ϕ = 100μm
2.5cm
MULTIPROPORTIONAL COUNTER
PROPORTIONAL CELL

Fig. 1

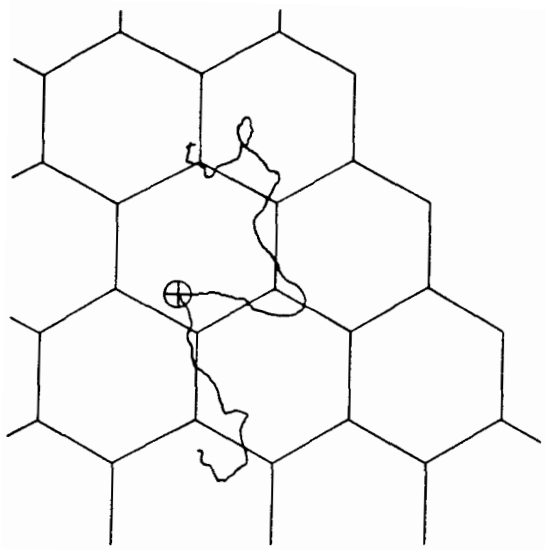


Fig. 2

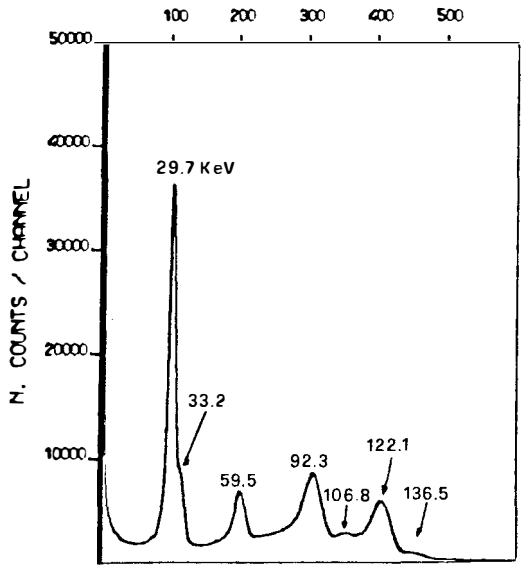

100
200
300
400
500
50000
40000
30000
20000
10000
N. COUNTS / CHANNEL
29.7 KeV
33.2
59.5
92.3
106.8
122.1
136.5

Fig. 3

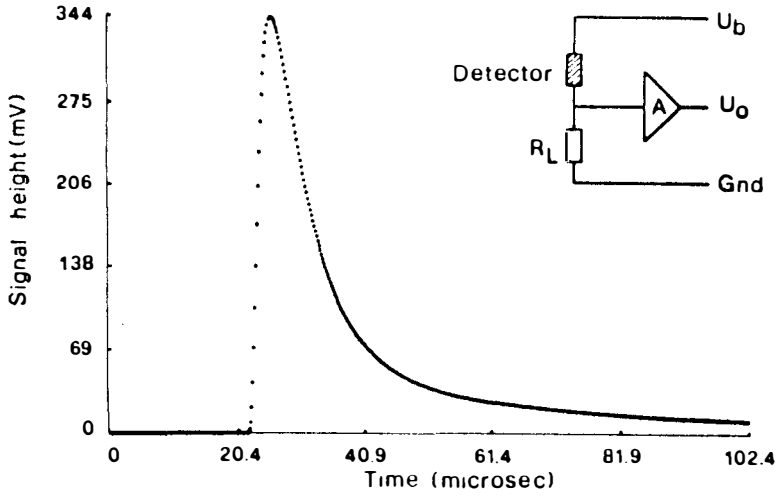

344
275
206
138
69
0
Signal height (mV)
0
20.4
40.9
61.4
81.9
102.4
Time (microsec)
Detector
A
R_L
U_b
U_o
Gnd

Fig. 4

NEUTRINOLESS DOUBLE BETA DECAYS OF ^{76}Ge AND THE PRESENT STATUS OF ^{100}Mo DOUBLE BETA DECAYS

Yasuki Nagai
Department of Applied Physics
Tokyo Institute of Technology
Oh-okayama, Meguro, Tokyo 152, Japan



ABSTRACT

The neutrinoless double beta ($0\nu\ \beta\beta$) decays of ^{76}Ge to 0^+ and 2^+ states in ^{76}Se were studied by the β-γ coincidence method, where a 171 cc Ge detector is surrounded by a 4π NaI detector. The half-lives for the $0^+ \rightarrow 0^+$ and $0^+ \rightarrow 2^+$ $0\nu\ \beta\beta$ decays were obtained as $T_{1/2}(0^+ \rightarrow 0^+) \geq 7.4 \times 10^{22}$ years and $T_{1/2}(0^+ \rightarrow 2^+) \geq 5.6 \times 10^{22}$ years.

The present status of ^{100}Mo double beta decays by using Si(Li) detectors were discussed.

Introduction

The study of the neutrinoless double beta ($0\nu\ \beta\beta$) decay has been of great interest as it reveals the important questions on the neutrino mass and/or the right-handed current (V + A) admixture in the weak interaction[1-2]. The observation of the $0\nu\ \beta\beta$ process, which violates the lepton number conservation rule, would indicate the massive Majorana neutrino and/or the finite amplitude of the V + A current. These neutrino properties are considered to be quite important to formulate the grand unified theories[2]. In the possible $0\nu\ \beta\beta$ decays the $0^+ \rightarrow 0^+$ decay occurs via the Majorana mass term and/or the V + A term. The $0^+ \rightarrow 2^+$ decay is only due to the V + A term[2]. Thus the detection of the $0 \rightarrow 2^+$ $0\nu\ \beta\beta$ decay gives the amplitude of the V + A term unambiguously.

In the present work the $0^+ \rightarrow 2^+$ $0\nu\ \beta\beta$ decay of the ^{76}Ge nucleus is intensively studied as well as the $0^+ \rightarrow 0^+$ $0\nu\ \beta\beta$ decay with use of the ELEGANTS (ELEctron GAmma-ray NeuTrino Spectrometer)[3]. The experiment of the ^{100}Mo $0\nu\ \beta\beta$ process is being prepared and its characteristic points are briefly discussed.

Neutrinoless double beta decays of ^{76}Ge

As the $\beta\beta$ decay is considered to be due to a second order weak process, the expected count rate is extremely small compared to the natural background counts. Thus it is essential to develop a low background system to study the $\beta\beta$ decay process. The ELEGANTS, which was developed for this study, is shown in fig.1. It consists of a 171 cc pure Ge detector surrounded by a 4π NaI(Tℓ) detector with the sizes of 10" ϕ × 12" and 8" ϕ × 3". The NaI(Tℓ) detector is used to reject the background counts and select the $0^+ \rightarrow 2^+$ decay by detecting the 559 keV $2^+ \rightarrow 0^+$ γ-transition in ^{76}Se. Thus the Ge-cryostat, the end cap and the inner side of the NaI(Tℓ) detector are made of thin and low-Z materials in order not to attenuate the γ-rays. Radioactivities of these materials were prechecked to be less than $0.5 - 2 \times 10^{-15}$ Curie/gram. All the energy and timing signals from the Ge and NaI(Tℓ) detectors are recorded event by event in a magnetic tape.

The experiment has been carried out both at the sea level laboratory (Osaka) and at the Kamioka underground laboratory at 1000 m depth (2700 m water equivalent). The enlarged energy spectra of our interest, which was measured at Kamioka for about 7000 hours, is shown in fig.2. Figs.2(a) and 2(b) show the spectra for the $0^+ \rightarrow 0^+$ and $0^+ \rightarrow 2^+$ $0\nu\ \beta\beta$ decays, respectively. So far no appreciable peaks appeared in both spectra. By assuming the Poisson distributions both for the true and background events one can get the lower limits on the half-life of the $0\nu\ \beta\beta$ decay. The limits are 7.4×10^{22} years for the $0^+ \rightarrow 0^+$ and 5.6×10^{22} years for the $0^+ \rightarrow 2^+$ $0\nu\ \beta\beta$ decays with the 68 % confidence level. The latter is the best value so far obtained and gives crucial informations on the mechanism of the $0\nu\ \beta\beta$ process. The former is the same order of magnitude as the previous

ones[4].

The half-life, $T_{0\nu}$, for the 0ν ββ decay of ^{76}Ge is connected with the neutrino mass and the right-handed current admixture as follows[5].

$$[T_{0\nu}(0^+ \to 0^+)]^{-1} = 9.23 \cdot 10^{-5} \cdot |M_{GT}^{(0\nu)}|^2 \cdot [m^2 - 0.352 \cdot \langle\lambda\rangle \cdot m \cdot \cos\psi_1 + (C_3/C_1) \cdot \langle\eta\rangle \cdot m \cdot \cos\psi_2 + 1.01 \cdot \langle\lambda\rangle^2 + (C_5/C_1)\langle\eta\rangle^2 - 0.801 \cdot \langle\lambda\rangle \cdot \langle\eta\rangle \cdot \cos(\psi_1 - \psi_2)]$$

where $m = \langle m_\nu \rangle / m_e$. (Detailed formulas of the parameters in the above equation are given in ref.5)). The present data of the 0ν ββ decay half-lives give the upper limits on the neutrino mass m_ν and the right-handed current admixture ε. The use of the Gamow-Teller matrix element calculated by Haxton[6] gives $m_\nu \leq 4.7$ eV and $\varepsilon \leq 9 \times 10^{-6}$. As discussed before the $0^+ \to 2^+$ 0ν ββ decay is caused only via the right-handed current admixture. Problems, however, remain to calculate the $0^+ \to 2^+$ 0ν ββ process and the nuclear matrix element. It is highly appreciated that these problems are solved.

Origins of background counts

Let me discuss briefly on the origins of the background counts in the Ge spectra shown in fig.3. The spectra were measured at the Kamioka underground laboratory, in which G and A stand for the single and anti-coincidence spectra, respectively. In the single spectrum below 3 MeV there are discrete lines coming from the decays of ^{232}Th and ^{238}U chain isotopes. Detailed analysis of these discrete lines with different γ-ray energies indicates that these γ-intensities are balanced each other after correcting for the efficiency of the Ge detector and the γ-ray branch. Thus these activities are considered to be located near the Ge detector. Otherwise the intensities of low energy γ-rays would be smaller due to absorption if these activities would be in the materials far from the Ge detector. The large reduction of the intensities of γ-rays by the anticoincidence with the NaI detector is consistent with the above argument. The background counts in the anticoincidence spectrum are about 7×10^{-4} C/(keV·hr) at around 2040 keV (corresponding to the energy of the $0^+ \to 0^+$ 0ν ββ decay of ^{76}Ge). The counts are quantitatively explained as the Compton scattered γ-rays from the decays of ^{208}Tl and ^{214}Bi isotopes. Thus the identification of the materials containing these activities is quite important to develop an ultra low background system. The energy spectrum of the NaI detector is shown in fig.4. The spectrum was measured in coincidence with 352 keV γ-ray detected by the Ge detector. The γ-ray comes from the decay of ^{214}Pb, which is the decay product of ^{238}U. Thus some fractions (∿30%) of the activities are considered to locate in the materials close to the NaI crystal, most probably in the teflon seat used as a reflector.

This is because the γ-ray only coincides with the β-ray and the observed highest energy is closed to the maximum electron kinetic energy of 672 keV. Similar analysis indicates that some fractions of ^{208}Tl activities also locate in the materials close to the NaI crystal. However it should be noted that there are no clear β-ray signals in the Ge spectra, which were measured in coincidence with the γ-rays detected by the NaI detector. Furthermore there are no α signals in the energy region of 5 ∿ 8 MeV in fig.3. Thus the Ge crystal and its closest environment are considered to be free from these activities.

Status of ^{100}Mo double beta decays

Because of the three body phase space for the 0ν ββ process the decay rate is proportional to T^5, where T stands for the maximum kinetic energy release[2]. Thus the ββ decay experiment on ^{100}Mo with high T value of 3.03 MeV seems to be interesting. (In case of ^{76}Ge T = 2.04 MeV). The preparation for the experiment on ^{100}Mo 0ν ββ process is being made, where ten foils of ^{100}Mo with thickness of 50 mg/cm^2 are sandwiched by eleven Si(Li) detectors as shown in fig.5. The Si(Li) detectors of transmission types with sizes of 1500 × 4 mm^3 are operated at liq. N_2 temperature. They are placed into the 4π NaI(Tℓ) detector, where the detector is used again to reject background counts and selest the $0^+ \rightarrow 2^+$ 0ν ββ process.

The ^{100}Mo project has following characteristic points. Namely

(1) The high T value of 3.03 MeV leads to the high decay rate as discussed above.

(2) The background counts decrease sharply with increasing the energy as shown in fig.3. Thus the S/N ratio for the $0^+ \rightarrow 0^+$ 0ν ββ decay may be much improved.

(3) The angular correlation of two electrons can be measured, which gives crucial informations on the mechanism of the 0ν ββ process[2].

In addition to the above features the project has another interesting point. The high T value also leads to the high decay rate for the 2ν ββ process. (Note that the decay rate is proportional to T^{11}). Being combined with the large calculated value for the 2ν Gamow-Teller matrix element, the half-life $T_{1/2}(2\nu)$ is estimated to be $T_{1/2} \cong 2 \times 10^{18}$ years[7], which is about 1000 times shorter than that of the ^{76}Ge. Thus we may have much chance to observe the 2ν ββ process, which is quite important as it gives the experimental value for the Gamow-Teller matrix element.

The first run has started since this March.

References

1) H. Primakoff and S.P. Rosen, Phys. Rev. 184(1969) 1925.

2) M. Doi et al., Phys. Lett. 103B(1981) 219.

M. Doi, T. Kotari and E. Takasugi, Suppl. of Theor. Phys. in press.

3) H. Ejiri et al., Nucl. Phys. A 448(1986) 271.

4) E. Bellotti et al., Phys. Lett. 146B(1984) 450.
D.O. Caldwell et al., Phys. Rev. Lett. 54(1985) 281.

5) E. Takasugi, a talk given at this work shop.

6) W.C. Haxton and G.J. Stephenson Jr., Prog. Part. Nucl. Phys. 12(1984) 409.

7) P. Vogel, a talk given at this work shop.

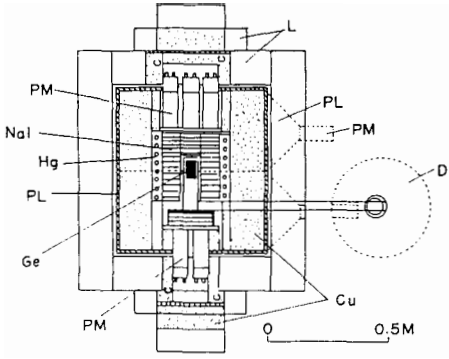


Fig. 1: Schematic top view of the ELEGANTS: Ge - Ge detector; D - dewar; NaI - 4π NaI(Tl) detectors; PL - 2π plastic scintillators; PM - photomultiplier; Hg - pure mercury; Cu - oxygen free copper L - lead

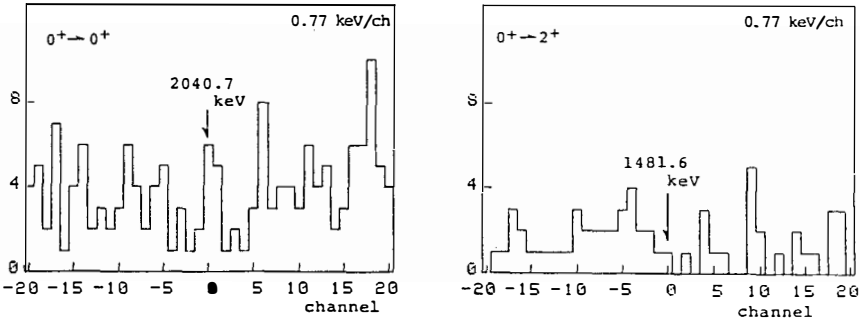


Fig. 2: The enlarged spectra around the energies of our interest. The spectra was taken at the Kamioka underground laboratory for about 7000 hours.

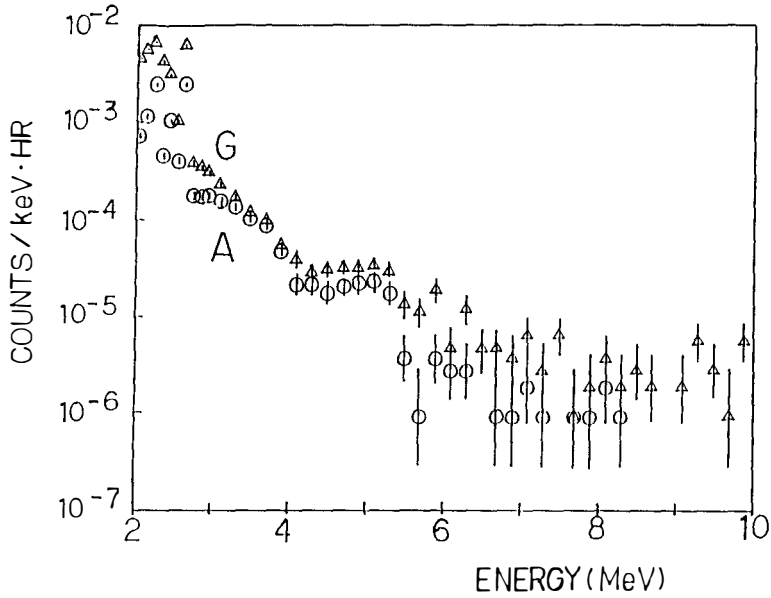


Fig. 3: The background spectra above 2 MeV measured at the Kamioka underground laboratory. G and A stand for single and anticoincidence spectra.

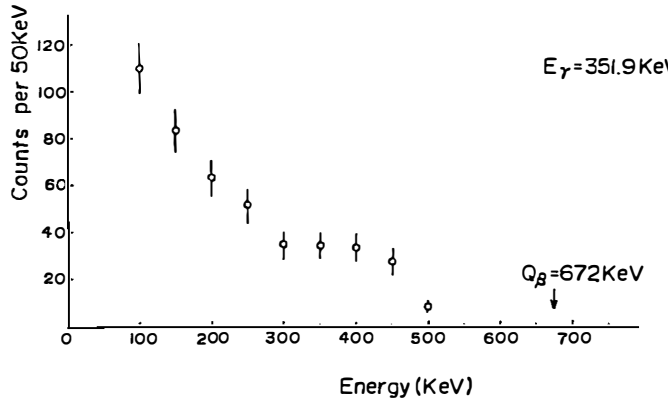


Fig. 4: The beta-ray spectra from ^{214}Pb in coincidence with 352 keV gamma-ray detected by the NaI. The encpoint energy of beta-ray is 672 keV.

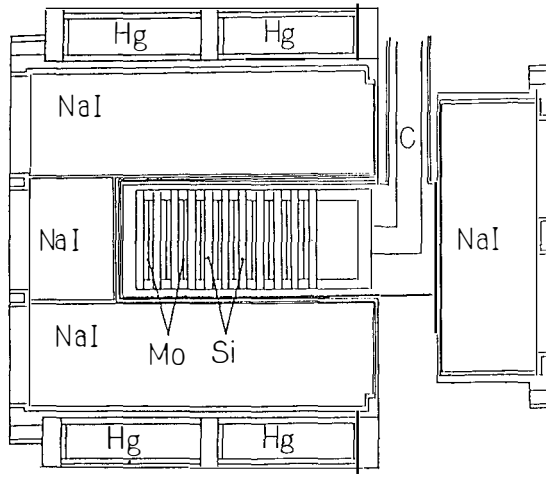


Fig. 5: ^{100}Mo foils sandwiched by 11 Si(Li) detectors,which are set inside the well of the 4π NaI(Tℓ).

COMMENT ON THE IMPORTANCE OF THE TWO NEUTRINO DOUBLE BETA DECAY STUDY FOR UNDERSTANDING OF THE INTERNAL STRUCTURE OF NUCLEI

A.A. Pomansky
Institute for Nuclear Research
Academy of Sciences, USSR

117312 Moscow, 60th October Anniversary Prospect 7a

ABSTRACT

We discuss the discrepancy between the $\beta\beta$ (2ν) experimental results and calculations. An understanding of the source of this disagreement can promote the understanding of nuclear structure.

When we are speaking about double beta decay, physicits normally think about the importance of this process mainly from the point of view of search for the possible violation of lepton number conservation. There is a general selfconfident opinion of the elementary particle physicist community that baryon number conservation is a very serious matter in contrast to lepton number conservation which, this community believes, it can violate when necessary for baryon decay. But who knows, it may be that we are not seeing proton decay because of the veto of lepton number conservation. As a conclusion of these words, the neutrinoless double beta decay is a ghost which we try to catch. However, it is probable that we are not to have the ghost of a chance. May it be that lepton number conservation is an exact symmetry of nature ?

In the same time the usual two neutrino double beta decay, $\beta\beta(2\nu)$, must occur in the second order of weak interactions. However, we do not know why we greatly overestimate the predicted rate of this process. I finished my talk at the Neutrino'84 Conference with the words : "thus our preliminary results indicate once again the existing discrepancy between theory and experiment"[1]. After this Conference, the situation became even worse due to the new data of Mike Moe's ^{82}Se experiment. He closed the previous positive result[2] and presently gives [3] only a limit of the $\beta\beta(2\nu)$ half time which is very close to the geochemical result[4] and is very far from theoretical estimations[5].Where is the clue to this enigma ?

The recently discovered EMC effect exhibits distorsions of the structure functions of bound nucleons inside the nucleus. This suggests that multiquark bags may play an important role inside the nucleus. The bags can be considered as six-quark clusters inside the nucleus. In this case, a more realistic way for an explanation of the double beta decay process can be found, since the two interacting quarks involved in double beta decay can be very close to one another. Although the EMC measurements strongly suggested that the confinement size for quark inside the nucleus is inflated, we do not know absolutely what is the scale of this inflation for different nuclei.

If we consider double beta decay as a process of the six-quark appearance, one can obtain unique information about nuclei from the $\beta\beta(2\nu)$ rate measurements.

Papers have appeared where the $\beta\beta(0\nu)$ process mediated by heavy Majorana neutrinos or Higgs particles is studied in the presence of six-quark clusters in nuclei. Vergados made explicit calculations[6] for the case of the experimentally interesting ^{48}Ca-^{48}Ti decay.

However, as we have stressed many times before and Vogel and Fisher emphasized recently[7], without a solution to the discrepancy between the calculated and experimental life times of the ββ(2ν) mode, it will be difficult to interpret the results of searches for the ββ(0ν) mode in terms of the Majorana neutrino mass and the parameters of the right-handed current weak interactions.
Therefore we believe that it is necessary to speed up the ββ(2ν) measurements for all possible nuclei and then by the way of the reverse solution we can advance in understanding of the ββ(2ν) and to deepen our knowledge about nuclei structure. After this step, one can speak more definitely about the neutrino mass and right-handed current constraints following from the ββ(0ν) experiments.
And finally : because of our absolute ignorance in the understanding of the ββ(2ν,) process one can accidentally meet unexpected results, e.g. short ββ(2ν) life time for nuclei with not very high transition energy.

References

1. A.A. Klimenko, A.A. Pomansky and A.A. Smolnikov, in Neutrino'84, edited by K. Kleinknecht and A. Paschos (World Scient. Singapore 84).
2. M.K. Moe and D.D. Lowental, Phys. Rev. C22 (1980)2186.
3. M.K. Moe, private communication November 1985.
4. T. Kirsten, in Science Underground (Los Alamos), AIP Conf. Proc. No 96, edited by M.N. Nieto et al. (AIP, New York,1983)
5. W.C. Haxton and G.J. Stephenson, Jr., Prog. Part. Nucl. Phys. 12 (1984)409
6. J.D. Vergados, Nucl. Phys. B250 (1985)618.
7. P. Vogel and P. Fisher, Phys. Rev. C32 (1985)1362.

THE FIFTH FORCE*

S. L. Glashow
Lyman Laboratory of Physics
Harvard University
Cambridge, Massachusetts 02138, U.S.A.



*Research supported in part by the National Science Foundation under Grant No. PHY82-15249.

Fischbach *et al.*[1] recently published a reanalysis of the Eötvös experiment in which they present three *raisons d'être* for the existence of a new long-range force in Nature, a force beyond the strong and weak interactions, electromagnetism, and gravity. Its claim to being the *fifth* force is justifiable since there is not yet seen any direct manifestation of the Higgs-mediated force nor of the GUT force leading to proton decay. Their report has been the subject of intense scrutiny in the popular press, since doubt has been cast upon venerable considerations of Galileo, Newton, and Einstein.

One of the three arguments is based upon an alleged indication of energy dependence of the neutral kaon decay parameters. This evidence is marginally suggestive, and very far from compelling. Without further experimental confirmation, it is not to be taken at all seriously and I will discuss it no further.

The second argument relates to the reanalysis of the more than half-century old Eötvös data. Fischbach *et al.* claim to discern a small departure from the principle of equivalence, suggestive of the existence of a new long-range force mediated by an almost massless vector boson coupled to baryon number. As J. Faller[2] has pointed out, Fischbach *et al.* were selective in the data they presented. A more complete display of the Eötvös data and the subsequent Renner data appears to be less decisive. Moreover, there is an apparent error of sign in the Fischbach analysis.

The final argument for the fifth force emerges from geophysical measurements of the variations of the local acceleration of gravity at depth in mines or at sea. That there is a severe and inexplicable anomaly in these data has been stressed since 1978 by F. D. Stacey.[3] In recent years, the existence of a geophysical anomaly has become better established, and its resolution in terms of the existence of a non-Newtonian force is not beyond the realm of

possibility. Fischbach *et al.*, and the permissive editors of the Physical Review Letters, are to be commended for bringing to a wide audience the geophysical evidence for something new and exciting.

Gibbons and Whiting[4] examine the limits that may be placed upon a new long-range force which couples (at least roughly) to mass. Let its strength be αG_N where G_N is Newton's constant and α is a material-dependent parameter depending upon the composition of the source and test masses. Its range is denoted by λ. If the new force is attractive, it is presumably mediated by a new light scalar boson; if repulsive, by a new vector boson. In Figure 1, we show the deduced allowed domain in α and λ for a conjectured repulsive force. A similar result is obtained for a new attractive force.

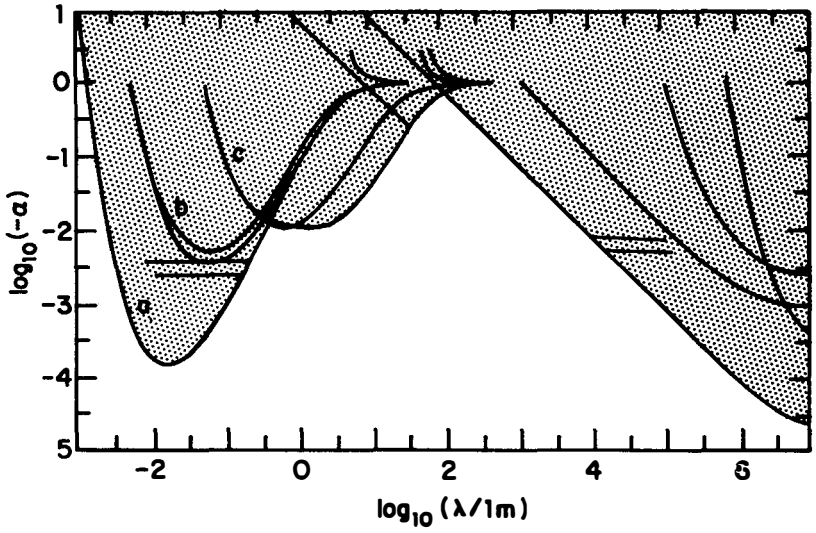


Figure 1. Window of opportunity for a supra-Newtonian repulsion whose strength is α times gravitation and whose range is λ. The unshaded region is allowed. A similar window exists for a possible supra-Newtonian attraction. From G. W. Gibbons and B. F. Whiting, Nature 291, 636 (1981). [We show only the results of experiments that have been done, not those displayed by the above authors that could be done, but haven't been.]

Currently available data admit a rather large window of opportunity. For $\lambda \sim 100$ m, α can be as large as 0.1! For $\alpha \sim 0.01$, λ can range from one meter to ten kilometers! Gibbons and Whiting conclude that "further large scale experiments are essential to improve bounds."

Not only is a new force permissible, but there is some positive evidence that it exists. The most reliable measurement of G_N results from the Cavendish experiment, the direct measurement of the force between two laboratory masses at a separation of one meter or less. The "wallet-card" result is

$$G_N = (6.6720 \pm 0.0041) \times 10^{-8} \mathrm{cm}^3 \mathrm{g}^{-1} \mathrm{s}^{-2} \ . \qquad (1)$$

In principle, G_N can also be deduced from observations of the gravity gradient in mines. Here, the statistical accuracy can exceed that in (1), though there are uncontrollable errors resulting from unknown mass distributions at great depth. In any case, here are the results to four independent determinations with high quoted precision:

$$G_N = \begin{cases} 6.7390 \pm 0.0025 \\ 6.7427 \pm 0.0024 \\ 6.7334 \pm 0.0037 \\ 6.7340 \pm 0.0020 \end{cases} \qquad (2)$$

The first three are from an analysis of prior experiments by Stacey and Tuck,[5] while the last value represents a new determination by Holding and Tuck[6] who conclude: "Although we are not prepared, at this stage, to assert that a non-Newtonian effect is clear and proven, the circumstantial evidence is very clear indeed. The need for a deep sea experiment as originally proposed [see reference 3] is now urgent."

The two determinations of G_N, geophysical and direct, are both precise to better than a part per thousand. Yet, they disagree by

one percent. They can be reconciled by the existence of a new component to the "gravitational" force, a repulsion with a strength $\sim 10^{-2}$ gravity with a range from meters to kilometers.

Let me sketch the nature of the geophysical anomaly under idealized circumstances. For a spherically symmetric earth of surface density ρ we expect a gravity gradient at and below the surface given by

$$\frac{dg}{dh} = (2 - 3\rho/\rho_E)\frac{g}{R} \tag{3}$$

where R is the radius of the Earth and ρ_E is its mean density as determined by the laboratory measurement of G_N, $\rho_E = 5.522$. For the situation discussed by Holding and Tuck ($\rho = 2.75$ and $g = 978.6$ gal) the anticipated gravity gradient is about 80 m gal/km. After making corrections for local density variations and tidal effects, the authors are left with a negative anomalous gravity gradient of about 2 m gal/km. This could be explained in an internally self-consistent fashion by replacing the canonical value of ρ_E with a value about 1% smaller. This is logically equivalent to a purely geophysical determination of G_N: the last quoted result in Eq. (2), with a value 1% in excess of the laboratory value.

Now suppose that there exists in nature a new component to the gravitational force, a repulsive force coupled at least approximately to the product of the masses of two bodies, with a strength αG_N and a range λ from 100 meters to 10 km. The new component of the force is equivalent to an extra (negative) component to the "gravitational" acceleration on earth given by

$$\Delta g = -\frac{3}{2}\alpha g(\rho/\rho_E)(\lambda/R)e^{-d/\lambda} \tag{4}$$

where d is the distance above or below the surface. The underground gravity gradient is given by

$$\frac{dg}{dh} = (2 - 3\rho/\rho_E)\frac{g}{R} - 3\alpha(1 - \frac{1}{2}e^{-d/\lambda})\frac{\rho}{\rho_E}\frac{g}{R} \tag{5}$$

where again ρ_E equals its canonical value. The negative anomaly has two components: one arises from the fact that the Cavendish experiment is a mismeasurement of ρ_E, the other arises from the contribution of the new force. We have neglected terms of order α^2 and of order λ/R.

The anomalous observed gravity gradient may be explained by a value of $\alpha = 1\%$ and $\lambda \sim 100$ m, or by $\alpha = 2\%$ and $\lambda \geq 1$ km, or by an intermediate possibility.

Experiments performed in deep sea water are much less dependent upon deep-lying mass anomalies because the experiment may easily be performed at a variety of different sites in the ocean. Moreover, the seawater density may be determined with precision by measurements of pressure, salinity, and temperature. The new force should generate a negative anomaly in the measured gravity gradient of about one m gal/km. A measurement of its depth dependence could establish the functional form given by Eq. (5) and determine both the strength and the range of the putative new force. Parts per thousand precision measurements of the gravity gradient at the surface and at depth in the deep ocean are required.

A calculable background results from thermal variations and salinity variations with depth. By far the largest conventional contribution to d^2g/dh^2 arises from the hydrostatic compressability of water

$$\frac{d^2g}{dh^2} = \frac{6g}{R^2}\left[1 - \frac{\rho}{\rho_E}\left(1 + \frac{R\rho'}{2\rho}\right)\right] , \qquad (6)$$

where $\rho'/\rho \sim 5 \times 10^{-6}\ m^{-1}$. This background value of $d^2g/dh^2 \sim 0.3$ m gal/km^2 is of comparable magnitude to the anticipated depth-dependence of the anomaly due to the new force, but its expected value can be known with precision. Since experiments can be performed upon g to an accuracy of a few microgals, it seems feasible to mount a search for gravitational anomalies at sea. Such an

experiment, involving the submersible vehicle Alvin, was proposed to the U.S. government (and, rejected) by a Texas A & M group in 1981. Under present circumstances, this experiment or one like it demands the highest priority. We have, after all, spent tens of millions of dollars on neutrino mass effects and have little to show for it. The possible detection of a new force of nature, while perhaps unlikely, presents the potential for a discovery of incomparable significance.

Suppose that there really does exist a new force mediated by an exceedingly light vector boson. I would prefer to believe that the corresponding current is a conserved one, at least from the point of view of the standard model. Thus, it is coupled to a linear combination of proton number, neutron number, and electron number. Since bulk matter is electrically neutral, it suffices to consider a coupling to a linear combination of N and Z. There is no compelling reason to assume, as Fischbach *et al.* do, that this linear combination is simply N + Z. Other linear combinations have an equal claim to uniqueness. The combination N - Z is particularly amusing since

$$\frac{\langle N - Z \rangle}{\langle N + Z \rangle} \cong 10^{-3}$$

for the material of the Earth's crust. The negative contribution of crustal hydrogen nearly cancels the effect of heavier nuclei. This suggests a Cavendish-like experiment comparing neutron-rich material like uranium or gold to neutron-poor materials like water or polyethylene.

Within the context of familiar fermions, the only anomaly-free current is B - L, which reduces to neutron number for neutral matter. Both N and N - Z are interesting possibilities, but we must imagine (and search for) a force depending upon an arbitrary and unknown linear combination of N and Z.

In Figure 2, we present a plot of (N - Z)/M versus (N + Z)/M for various materials. A "Complete Cavendish Experiment" would compare the gravitational forces among pairs of a trio of carefully chosen materials, say water, lithium, and copper. It should be pursued to an accuracy of 10^{-3} at least, and 10^{-4} if possible. This would exclude a wide variety of "fifth forces" that we might imagine.

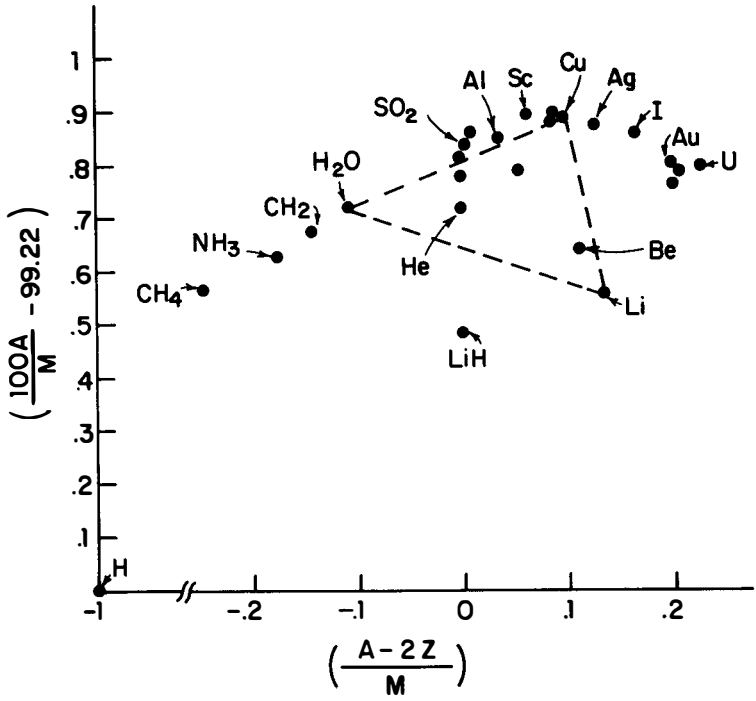


Figure 2. This is a plot of A/M and (N - Z)/M, the two parameters that could govern the fifth force couplings of a light vector boson to a conserved current. The values of A/M are subtracted so as to put H at zero and multiplied by 100. The complete Cavendish experiment, involving three disparate materials (as in Li, H_2O, and Cu) could reveal the new force and identify its current.

In summary, Fischbach *et al.* impel a wide variety of feasible but neglected experiments:

(1) A redo of "Eötvös" experiments, or of falling-body "Galileo" experiments, or of "Cavendish" experiments utilizing a trio of materials spanning the N,Z plane.

(2) Careful gravimetric experiments performed in the deep ocean, or from the frozen and stable surface of Lake Baikal.

Acknowledgements

Discussions with Alvaro De Rújula, Jim Faller, Bob Pound, and Ed Purcell have been invaluable.

References

1. E. Fischbach *et al.*, Phys. Rev. Lett. 56, 3 (1986).
2. J. Faller, private communication.
3. F. D. Stacey, Geophys. Res. Lett. 5, 377 (1978).
4. G. W. Gibbons and B. F. Whiting, Nature 291, 636 (1981).
5. F. D. Stacey and G. J. Tuck, Nature 292, 230 (1981).
6. S. C. Holding and G. J. Tuck, Nature 307, 714 (1984).

SUMMARY TALK

Ettore Fiorini

Dipartimento di Fisica dell'Universita' di Milano
Istituto Nazionale di Fisica Nucleare - Sezione di Milano,
Italy



ABSTRACT

Experimental results presented at the Conference are compared and discussed with special enphasis to solar neutrino experiments, neutrino masses and oscillations, new techniques mainly at low temperatures, lepton non conservation and related topics.

Many important and sometimes exciting new results have been presented to this Rencontre de Moriond: the present Summary does not pretend to be a review of them, but only a discussion on a few problems of experimental neutrino physics and particularly on those who still remain open. During this Rencontre I very much enjoyed enlighting conversations with many colleagues to which I want to express my gratitude, even if the responsibility of the opinions expressed in this talk remains obviously mine.

1. SOLAR NEUTRINO EXPERIMENTS

This is probably the subject where neutrino physics and astrophysics are more strictly connected. The main physics implication, namely neutrino oscillations, will be taken up later on. From the astrophysics point of view one could note that neutrinos of monocromatic and continous type are copiously generated by the various fusion processes inside the Sun as shown by Fig. 1. Being very penetrating they easily excape from the star, reach the surface of our Planet with an intensity expected to be about $6 \times 10^{10} cm^{-2} s^{-1}$ and represent in fact the only way to test directly the various Solar models. It always was, and still is, for me a reason of surprise the fact that only one experiment on solar neutrinos has been carried out so far. It searches, since twenty five years for the reaction:

$$\nu_e + {}^{37}Cl \rightarrow e^- + {}^{37}Ar \qquad (1)$$

The detector consists in 615 tons of $C_2 Cl_4$, where neutrino interactions are revealed by the presence of few (one every two days) atoms of radioactive ^{37}Ar. The experiment does indicate the presence of interacting solar neutrinos (which represents already a great result!), but the obtained rate is only $2.1 \pm .3$ SNU (one SNU corresponds to 10^{-36} neutrino captures per atom) versus a value around 7 SNU predicted by the Standard Solar Model (SSM). If neutrinos do not oscillate this disagreement would cast doubts on the present theory of the solar system. The threshold for reaction (1) is however considerably large (814 keV) and only 10^{-4} of solar neutrinos, mainly from the decay of ^{8}B, have an energy sufficient for the interaction.

Many experiments to search neutrino interactions on various nuclei have been proposed, but only one has been recently definitely approved, and this passage "from hope to reality" has been announced for the first time to this conference[1]. This experiment, GALLEX, is going to be carried out by an european collaboration (Heidelberg, Grenoble, Karlsruhe, Milano, Munich, Nice, Rehovot, Rome, Saclay) on the reaction:

$$\nu_e + {}^{71}Ga \rightarrow e^- + {}^{71}Ge \qquad (2)$$

where ^{71}Ge decays by electron capture with a lifetime of 11.4 days and can therefore be detected. Since the threshold is in this case of 233 keV only, low energy neutrinos will also be detected: in fact most of the signal (70%) will be produced by neutrinos from the pp reaction, the best known ones. The target will consist of an acid solution of $GaCl_3$, containing 30 tons of Gallium, where ^{71}Ge will be extracted in form of volatile $GeCl_4$ and then purified and counted (Fig. 2). This detector will be installed in the Gran Sasso Laboratory, an impressive underground facility suggested and directed by

Antonino Zichichi, presently being built in Central Italy. This laboratory, whose total volume will approach 100,000 m^3, will mainly consist of three large "halls", two of which (A and B) are already excavated, while the entire facility will be available on 1987. Many experiments, of which a few reported here, will be housed in this international laboratory, which will undoubtely play an essential role in the development of "passive" physics. GALLEX, which will be housed in Lab. A, will reach in a year of running time a sensitivity of about 125 SNU. Another essential feature of this experiment, discussed here by M. Spiro[2], will be the possibility to test the performance of the detector with "artificial" neutrinos produced by electron capture in a source of ^{51}Cr, with an activity around one megacurie.

Two other proposals for Gallium experiment have been presented to this conference. One (GAUSCAN), reported by Robertson[3], is very similar to GALLEX and should be carried out by a USA-Canada collaboration in the Nichel Sunbury mine in North Ontario (Fig. 3) at a depth of about 6000 hectograms of standard rock. The other one, reported here by A. Pomanski[4] will be carried out in the Baksam Underground Laboratory in Caucasus. This group already owns a considerable (almost sufficient!) amount of Gallium in metallic form, but cannot treat it chemically. The experiment will therefore be carried out with liquid Gallium (the melting point is 39-C°) which will make extraction of ^{71}Ge considerably difficult.

Other solar neutrino experiments have been discussed here:

a. the study[5] of the reaction

$$\nu_e + {}^{98}Mo \rightarrow e^- + {}^{98}Tc \qquad (3)$$

where ^{98}Tc has a lifetime of 4.2 megayears. Production of ^{97}Tc is also possible but should occur at a lower rate. The samples of Molibdenum mineral will be extracted from great geological depths (1132 m) to avoid contaminations induced by cosmic rays, and the presence of 99 Tc ($\tau = 10^5$ y) produced by natural fission of Uranium will be used as a test. The threshold for this reaction is large (1.74 MeV), but the expected sensitivity of 17.5 $\pm$ 5.5 SNU will allow an interesting comparison with the results of the Clorine experiment.

b. An experiment by a Canadian-U.K.-USA collaboration, also to be carried out in the Sunbury mine, and reported here by J. Simpson[6] is intended to search for interactions of solar neutrinos on electrons and deuterons in 1000 tons of heavy water viewed by photomoltipliers to detect the Cerenkov light (Fig. 4).

c. the 4500 tons liquid argon TPC detector ICARUS proposed for installation in the Gran Sasso Laboratory (Hall C) will also allow to detect neutrino interactions on electrons as well as the superallowed interaction on

^{40}Ar leading to the exited ^{40}K state at 4.38 MeV, as suggested here by Milla Baldo Ceolin[7].

2. SEARCH FOR PENETRATING PARTICLES COMING FROM POINT-LIKE SOURCES IN THE SKY

I will discuss this topic only briefly, since, it is, at least at present, only marginally connected to massive neutrinos in particle physics and astrophysics. The main interest last year was concentrated on Cygnus X-3, a binary system where a compact object, very likely a pulsar, orbits around a companion of lower density. The system has been unambiguously recognized to be a source of radiowaves and X-rays, but recent evidence has been presented for energetic (10^{12} - 10^{15}eV) gamma rays pointing to it. At this conference E. Bellotti[8] has discussed, two underground experiments, initially planned to search for proton decay, were evidence for muons has been found:

a. the Soudan experiment in the USA, running at a depth of about 1800 hectograms of standard rock corresponding to a muon minimum energy of 600 GeV, indicates an excess of muons coming from, and with the same periodicity of Cignus X-3. The intensity is evaluated to be about 2×10^{-11} cm^{-2} s^{-1}.

b. the Nusex nucleon decay experiment, carried out in the Mont Blanc Tunnel at a depth of 5000 h.s.r. corresponding to a minimum muon energy of 2 TeV indicates a flux of 2×10^{-12} cm^{-2} s^{-1}. The peak in phase for events in the direction of Cygnus X-3 is shown in Fig. 5.

There are in these results two unexplained facts:

a. the intensity is much larger (by about two orders of magnitude) than that expected for muons produced by gamma rays. One has however to stress that there is no real experimental prove that the extensive showers in the direction of Cygnus X-3 are indeed due to gamma rays. In fact one of the "gamma" experiments, carried out by the Kiel group, measures also muons and find them at a rate an order of magnitude larger than expected.

b. in the Nusex results the muons are distributed around the direction of Cignus X-3 with an angular spread much larger than the experimental resolution.

These results find some confirmation from the Japanese "mu-tron" experiment, a large muon spectrometer operating on surface; but lack of evidence for underground muons pointing to Cignus X-3 has been reported here by two experiments. The Frejus experiment[9] carried out at a similar depth, but on a different period of time, than Nusex, finds an upper limit of 3×10^{-12} cm^{-2} s^{-1}, while the Baksam experiment[10], carried out at lower depth, set an upper limit of 3×10^{-12} for muon of energy larger than 500 GeV.

The problem remains obviously open, but results should be compared only at similar depths, and especially for the same period of time, since the intensity of radiation from this binary system could vary considerably. Let me report as an example what happened in the second half of last October as it

was totally informally communicated to me:

a. the intensity of radiowaves was found to be up to 300 times above the normal values (Bonn);

b. the Wisconsin group searching for gamma rays with energy above 300 GeV found large bursts on October 12 and 13, the only two days analysed;

c. Soudan claims for the first half of October 8 events in the phase interval .725 - .745, over an expected background of less than one event;

d. Nusex finds in the same period 4 events in the phase region .8 - .9 and only one in all the other 9 regions, but does not consider this effect to be statistically significant.

I believe that we owe an apology to astrophysicists: these underground detectors were dedicated to search nucleon decay and not to detect muons on large surfaces[11]. New underground experiments with large surface like LVD or Macro already approved for the Gran Sasso Laboratory will definitely clear up this point.

3. NEUTRINO MASSES

Let me, unlike the biblical father, forget for the moment the prodigal sons and quickly review the results presented at this conference which are in agreement with the standard present theory of weak interactions:

a. no evidence has been obtained for heavy leptons different from the τ at $e^+ - e^-$ machines[12] and in the CHARM experiment at CERN[13]. The upper e^+-e^- limits on the square of the coupling constant range from 10^{-4} to 10^{-8} in the energy region 1 - 10 GeV.No neutrino decay has been observed[14] and no massive neutrino in muon capture[15];

b. the present upper limit on the mass of the muon neutrino, obtained at SIN is 270 keV[16]

c. an excellent upper limit of 56 MeV has been presented by Koltick[17] for the mass of the τ-neutrino.

Let us now move with caution in the mined field of the electron neutrino mass. The most sensitive way so far to measure the mass of the electron neutrino (as a matter of fact antineutrino) is offered to us by the tritium decay:

$$ {}^{3}_{1}H \rightarrow {}^{3}_{2}He + e^- + \bar{\nu}_e \qquad (4) $$

due to the very low transition energy (~18.6 keV). In order to understand the intrinsic difficults of these experiments, at least at the present level of sensitivity, let us consider the Curie plot of Fig. 6. If the neutrino mass would be exactly zero and the energy resolution infinite one would obtain the straight line a . The curve b refers to a measurement with infinite precision and massive neutrino, while curve c would be obtained with a massless neutrino

and finite resolution. It is therefore obvious that finite resolution and neutrino mass act in opposite way: a straight line would in itself indicate a massive neutrino, since actual resolution cannot be infinite. In addition the transition energy E_0 is not know better than the resolution of the experiment and has to be taken as a third parameter with the neutrino mass and the resolution. Another experimental difficulty comes from the fact the tritium decay can also occur to an excited state of ^3He, and that molecular or atomic effects of the same order of magnitude as the sensitivity on neutrino mass are present. Last, but not least, experimental problem is the very low counting rate at the end of the spectrum. The integral percentage of counts from an energy E and the transition energy E_0 is:

$$P = (2.3 \times 10^{-12}) \left(\frac{E_0 - E}{2eV}\right) \qquad (5)$$

This percentage in the last 100 and 10 eV regions is of only 3×10^{-6} and 3×10^{-7}, respectively. The hystory and difficulties of the tritium experiment have been discussed here comprehensively by O. Fackler[18]. Let me only remind you that, before the ITEP result, the mass of the electron neutrino was considered to be zero with an upper limit of 60 eV, obtained by Berkvist since 1972. In 1980 the Moscow group presented evidence in a magnetic spectrometer experiment for a neutrino with mass in the range 14 to 46 eV, at the 99% confidence level. At the Brighton conference in 1983 Lubimov reported results obtained with a new electro-magnetic spectrometer and a consequent better resolution, claiming a neutrino mass larger than 20 eV at 95% confidence level. A more elaborated analysis based on measurements carried out with valine targets of three different thicknesses and a careful study of the molecular and atomic effects was reported at the Leipzig conference. The most probable value for neutrino mass was 35 eV, which became 9 eV in the worst and extreme case (decay of a free tritium nucleus). These results were criticized by Berkvist, who suggests that the ITEP group overestimates the neutrino mass as a consequence of an underestimation of the resolution. It is the first time in my life that I hear somebody blaiming an experimenter because it measures too well and the experimenter strongly denying it! The situation before this conference was the following: Berkvist criticized the ITEP group for not taking into account the intrinsic width of the line of the ^{169}Yb source used for calibration of the spectrometer, thus underestimating resolution. As a consequence the ITEP group introduced in the evaluation of the resolution function a line with finite width and of a gaussian type, still obtaining a non-zero neutrino mass, but Berkvist was not satisfied on the grounds that the intrinsic curve of the ^{169}Yb line, which he measured, was not gaussian. His conclusion was that the Moscow experiment was indeed proving that neutrino is massless!

At this conference Lubimov has reported a new analysis of the 1984 data re-elaborated taking into account the real shape of the line and concluding that the neutrino mass is between 17 and 40 eV and that the transition energy is of 18600.8 ± 6 eV in excellent agreement with the recent measurement by Lippmaa (18599.4 ± 3) and with the wordl average (18599 ± 2). I will not repeat here the points made during the long quarrel[19] between Lubimov[20] and the still unsatisfied Berkvist[21], but only pose the audience my question: "should such an important item like the neutrino mass be based only on this damned line?" I believe that the most important problem at present is to determine the resolution function in a totally independent way, for instance with an electron gun delivering electrons of known energy. In addition I thinck a final answer will only come after combining results from experiments with: a. sources made by different molecules and atomic or nuclear tritium; b. different methods of measurements; c. a resolution better by an order of magnitude than the present ones.

Many experiments have been reported here. I find of particular interest the one carried out at SIN[22] based on electric deceleration of electrons in a special focalizing magnetic field(Fig. 7), where a 27 eV resolution (FWHM) has been obtained. In this experiment, where tritium is implanted in a carbon target, there is no evidence for a non zero neutrino mass (Fig. 8) with a "best" upper limit of 9 eV at the 95% c.l.. I do not consider this result to be yet in contraddiction with the ITEP one, since with some "extreme" treatment of the data, a value like 20 eV cannot be excluded.

The Los Alamos experiment[23] where calibration with an electron gun is easy since the source is tritium gas (Fig. 9) is just starting operation, but is already yielding an upper limit of 36 eV at the 95% confidence level.

The INS experiment, presently running in Japan[24], is carried out with an iron-free electro-magnetic spectrometer and a source made by an acid compound of tritium. The present best value for the neutrino mass is 12.5 eV, but this result is not incompatible with zero or with the value obtained by the ITEP group.

The Lobashov experiment[25], is based on the use of a longitudinal magnetic field an of a source initially made by Li H deposited on carbon, and later by tritium gas.

The Rockfeller-Fermilab-Livermore experiment[26] adopts an electro-magnetic spectrometer and uses targets of different thicknesses, made with frozen tritium, while in the Texas-Brandeis set-up the performance of the electrical cilindrical mirror analysis will be tested with scattering on the gas by electron accelerated by a gun[27].

As suggested a few years ago by A.de Ruhula, an independent way to investigate the neutrino mass would be the study of the gamma spectrum produced by the radioactive electron capture:

$$e^- + (A,Z) \rightarrow (A,Z-1) + \nu_e + \gamma \qquad (6)$$

Experiments of this type carried out at CERN[28] and Tokio[29] with ^{193}Pt and ^{163}Ho, respectively, have both obtained the same upper limit of 400 eV for electron neutrino .

The last part of the neutrino mass session has seen J. Simpson[30], who has recently proposed the existence of a massive neutrino at 17.1 keV based on the deformation at low energy of the spectrum from tritium implanted in a silicon detector, bravely fighting against the evidences brought by other experiments against his result. Among the various sons, Simpson is undoubtly the most prodigal of all, and fully justifies the italian sentence "Molti nemici, molto onore" (Many enemies, great the Honour). Negative results against this massive neutrino state have been reported recently by Altzitzoglu et al, Markey and Boehm, Ohi et al, Datar et al and Apalikov et al on the basis of the decay spectrum of ^{35}Si, and at this conference by A.de Ruhula from the decay of ^{63}Ni. Criticisms on Simpson experiment have been mainly based on the difficulties to treat correctly implanted tritium, and on improper coulomb corrections in particular.

4. NEUTRINO OSCILLATIONS

One of the most dramatic consequences of finite neutrino mass and lepton flavour non conservation are neutrino oscillations, proposed by B.Pontecorvo since 1957. Let us limit ourselves for the moment to the electron and muon neutrinos. Their fields can be written in term of two majorana neutrinos ν_1 and ν_2, with masses m_1 and m_2:

$$\begin{aligned} \nu_e &= \nu_1 \cos\alpha + \nu_2 \sin\alpha \\ \nu_\mu &= -\nu_1 \sin\alpha + \nu_2 \cos\alpha \end{aligned} \qquad (7)$$

where α is the mixing angle. In this case an initially pure ν_μ beam would contain, at a distance L from the origin, a ν_e impurity, or vice versa. Also "majorana" oscillations of the type ν-$\bar{\nu}$ are in principle possible. The ν_e impurity in a ν_μ beam would be:

$$P(\nu_e/\nu_\mu) = 0.5 \sin^2(2\alpha)\sin^2 \frac{1.27 \cdot \Delta \cdot L}{E_\nu} \qquad (8)$$

where L is in metres, $\Delta = |m_1^2 - m_2^2|$ in eV^2 and the neutrino energy E_ν in MeV. The experiment could search either for the appearance of the wrong flavour neutrino, or for disappearance of the right flavour one.

In the high energy accelerator experiments, reviewed in this conference

by Shaevitz[31] L ranges usually from hundreds to thousands of metres and E_ν from a few GeV to tens of GeV. As a consequence these experiments are not particularly sensitive to Δ, but to α, since the particle composition of the beam is generally well known. No evidence for oscillations has been found and allowed regions are shown in Fig. 10 and 11[32]. Vannucci has however reported at this conference[33] that in an appearance experiment carried out at CERN at moderate energy on $\nu_\mu - \nu_e$ oscillation, 35 $\pm$ 7 electron neutrino events have been detected versus the 11.5 $\pm$ 2.9 expected ones. A new experiment is going to be carried out in Brookhaven to clear up this point.

Pion factories are going to be very useful tools to investigate neutrino oscillations[34, 35], also due to the very interesting time structure and energy distribution of neutrinos emitted as consequence of dumping of the proton beam. Negative pions are imediately absorbed, while π^+'s decay with a mean life of 26 ns and the emission of 29.8 MeV monocromatic ν_μ's. The produced μ^+ decays with a mean life of 2.2 μ s, producing "later" electron neutrinos and muon antineutrinos with continous spectra ranging from zero to 52.8 MeV.

Results on oscillations of atmospheric neutrinos can only be obtained in experiments carried out underground, where the background due to charged cosmic rays is strongly reduced. They are based on possible differences between downwards neutrinos, which have crossed only up to a few km of rock, and upward going ones, which have crossed the entire diameter of the Earth. One can search either for irregularities in the angular distribution of upward muons produced by atmospheric neutrinos in the rock and crossing the detector, or for up-down asymmetries in neutrino interactions produced inside the detector itself. The best results have been obtained[36] by the IMB underground nucleon decay experiment, where a fiducial mass of 3300 tons has been exposed for 417 days of effective running time, totaling 187 upward muons and 401 contained events. No deviation from predictions is found (Fig. 12) in the angular distribution, while the ratio of up-down neutrino induced contained events is 1.06 $\pm$ 0.10. From the latter result one extracts the excluded regions of Fig. 13, which shows the excellent sensitivity on Δ, and the much poorer one on the mixing angle.

An excellent tool to investigate oscillations will be provided by solar neutrino experiments, and particularly by the newly approved Gallex. The sensitivity of such an experiment is shown in Fig. 14[3], in absence of oscillations in solar matter. The presence of such effects would require the comparison among the results from experiments with different target nuclei, and therefore with different thresholds, but will make the subject even more interesting.

Of particular sensitivity are experiments on oscillations carried out at power reactors where intensities of $10^{-13}\bar{\nu}$ cm^{-2} s^{-1} antineutrinos or more can

be obtained in a set-up located near the core. Results from four reactors (two for the first time) have been reported to this conference and refer all to the "inverse beta decay"reaction:

$$\bar{\nu}_e + p \rightarrow e^+ + n \qquad (9)$$

In the experiment carried out at the Goesgen reactor[37] at distances of 37.9, 45.9, 64.7 m, the set-up consists of liquid scintillator and ^3He proportional chambers to detect the positron and neutron, respectively. The results are negative and yield the allowed regions to the left of courve 1 of Fig. 15.

The Bugey experiment[38] has been carried out at 13.6 and 18.3 m from the centre of the core of a reactor of the same power (2.8 Gwatt) and with a similar set-up as for the preceding one. An indication for neutrino oscillations has been found and is represented by the region at the right of the curve 2 in Fig. 15. However the effect, as pointed out by the authors themselves at this conference, is only a three standard deviations one.

The new Savannah River experiment, reported here for the first time [39] is being carried out at a 2.1 Gwatt military reactor, where neutrons produced in (9) are detected in the gadolinium enriched scintillation detector. No evidence for oscillations has been found in preliminary runs at 18.2 and 23.8 m, yielding an allowed region shown by curve 3 of Fig. 15. The detector will be moved soon to a third, farer, position.

Results from an experiment running at 18.06 m from the centre of the core of the Rovenskaia (Figs. 16 and 17) 1.375 Gwatt reactor have been reported here for the first time[37]. The negative evidence for neutrino oscilations obtained in this experiment is shown by curve 5 in Fig. 15.

While concluding this subject I would like to stress that all preceding considerations have been obtained on the semplifying, but obviously wrong hypothesis of the existence of two neutrino flavours only [40]. Inclusion of the third flavour is obviously needed, but would not modify the final conclusion that no evidence has been found for neutrino oscillations, so far.

5. LEPTON NUMBER NON CONSERVATION AND DOUBLE BETA DECAY

Let us now move quickly to an excellent tool provide to us by nuclear physics to investigate conservation of total lepton number. This peculiar process involves a triplet of isotopes, (A, Z), (A, Z+1), (A, Z+2), where single beta decay from (A, Z) to (A, Z+1) is forbidden, or at least strongly hindered. Double beta decay can occur to (A, Z+2) in three different modes:

$$(A, Z) \rightarrow (A, Z+2) + 2\,e + 2\,\bar{\nu}_e \quad (10)$$

$$(A, Z) \rightarrow (A, Z+2) + 2\,e \quad (11)$$

$$(A, Z) \rightarrow (A, Z+2) + 2\,e + X \quad (12)$$

Two neutrinoless double beta decay (10) is a process rare, but allowed by the standard electroweak theory, while decay mode (11) which we will call neutrinoless decay implies violation of lepton number conservation. In mode (12), also violating lepton number, a neutral scalar boson, named "majoron" is emitted. Process (11) is characterized by a very large available phase space and should therefore dominate on (10) even for a tiny violation of lepton number. The two electrons should moreover share the total transition energy, and this also helps in distinguishing neutrinoless from two neutrino modes. In the process with majoron emission the sum spectrum of the two electron energies has a continuous shape, even if peaked towards higher energies than for (10). Distinction between these two decay modes is therefore much more difficult.

Two methods have been used used so far to search for double beta decay. In geochemical experiments, not discussed at this conference, a rock of known geological age containing the father nucleus is searched for abnormal aboundance of the daughter isotope. Double beta decay of ^{82}Se and ^{130}Te has been definitely proved, while some evidence for decay of ^{128}Te waits for confirmation. These experiments are unable to discriminate directly between two neutrino and neutrinoless modes.

Direct experiments, where one tries to detect the two electrons and possibly measure their energy, have been unable so far to find evidence for any type of double beta decay, lepton conserving or not. Same of them are carried out with set-ups where the double beta active source is separated from the detector material. Negative results on neutrinoless double beta decay using scintillators as detector have been reported at this conference for ^{150}Nd[41] and ^{100}Mo[42]. Of particular interest I consider the report by the Irvine group[43], which a few years ago found evidence in a cloud chamber experiment for two neutrino double beta decay of ^{82}Se with a rate an order of magnitude larger than found in geochemical experiments, a very disturbing fact indeed. A new experiment being carried out by the same group with a Time Projection Chamber finds no evidence either for neutrinoless or for two neutrino decays, with lower limits on the half life of 7×10^{21} and 1×10^{20} years, respectively. The latter limit is of the same order of the geochemical result. The contraddiction between the conclusions of this very different experiments has therefore faded away.

A different approach in direct experiments is the use of detectors made themselves with double beta active materials. The best results have been

obtained so far with Germanium detectors which naturally contain 7.76% ^{76}Ge, which could double beta decay to ^{76}Se. The sum of the energies of the two emitted electrons is measured with great precision by the detector itself, and a peak should appear in this sum spectrum at the transition energy if double beta decay occurs in the neutrinoless mode. Three negative results on neutrinoless double beta decay obtained with this technique have been reported at this conference by the Caltech[44], Osaka[42], and Milano[45] groups with lower limits for the half lifes of 0.3, .7 and 1.7 in unity of 10^{23} years, respectively. I was informed, just before leaving to Tignes, that a limit of 2.5×10^{23} years is presently being obtained by the Santa Barbara - Berkeley collaboration with a set-up made by a composite system of intrinsic Ge diodes.

The possible use of ultralow temperature detectors in double beta decay experiments is presently being studied by the Milano group and will be considered in the next chapter.

One of the main problems in the study of double beta decay was the difficulty to compare experimental findings with threoretical predictions, which were quite uncertain, mainly for poor determination of the nuclear matrix elements involved in the process. I intentionally say "was" and strongly welcome recent excellent theoretical calculations, some of which have been discussed here by Ho, Klapdor, Rosen, Takasugi, Vogel and others!

Double beta detectors have peculiar features: they measure very precisely low energies delivered to the set-up by any type of particle, in very low background conditions, and in experiments often installed deep underground. They could therefore yield very important subproducts, and one of them has already be considered at this confererence by Spergal: interactions with dark matter!

6. LOW TEMPERATURE DETECTORS

We have seen in the preceding sections that all experiments reported here are indeed pushing the techniques up to their ultimate possibility: experiments on neutrino mass are an obvious example. There is a fundamental difference with respect to the "classical" accelerator physics: measurements have to be carried out generally on relatively small energy releases, with excellent precision and in a low background environment of spurious counts. Of the unconventional techniques which have to be studied and possibly adopted, the low temperature ones, amply discussed here, seem to me particularly promising. Two approaches look interesting:

a. the use of Superconducting Tunnel Junctions (STJ) as discussed here by Zacek[46] and Twernbold[47], based on the fact that when two superconductors are separated by a thin layer (a few tens of A°) it takes only 10^{-3} eV to produce a free charge carrier. The junction can therefore be used for particle spectroscopy like normal semiconductor detectors, but with a much higher

expected resolution. In particular clear separation was obtained of the 5.89 and 6.49 keV X lines produces by a 55 Fe source with a small STJ detector operated at 0.32 °K[47].

b. particle detection at low temperatures by measurements of the heat delivered to a bulk crystal, as discussed here by Riisager[48], Cabrera[49] and myself (45). In a crystal of pure insulator at low temperature the only expected contribution to heat capacity comes from phonon propagation and is given by:

$$C_V = 1944 \left(\frac{V}{V_m}\right) \left(\frac{T}{\theta_d}\right)^3 JK^{-1} \tag{13}$$

where V and V_m are the detector and molecular volume and T and θ_d the absolute and Debye temperatures, respectively. At low temperature the heat capacity becomes so small that the energy lost by a particle can be measured by the increase of the temperature of the bolometer via the consequent variation of the resistence.

The expected resolution in energy is given by:

$$\Delta E \simeq \sqrt{8 \cdot l_n 2 \cdot k \cdot C \cdot T^2} \tag{14}$$

In a 1 x 1 x 0.1 mm 2 Si detector operated at .1 m°K it could be as low as 1 eV. The results of actual measurements are still far from theoretical expectations, mainly because the "thermometer", which is a doped semiconductor glued to the crystal or a small implanted region of the crystal itself, does not follow the Debye low and can have an heat capacity larger than that of the bolometer itself. Interesting experimental results have however been obtained. In particular the NASA-Wisconsin group was able to measure the above mentioned X-lines of 55 Fe with a resolution of 35 eV, while Coron et al.[48] have obtained the alpha particle spectrum shown in Fig. 18. The Cern-Milano collaboration, concentrated efforts on the time behaviour of the pulses and obtained with alpha particles the shape shown in Fig. 19, when operating at 500 m°K.

7. CONCLUSIONS

I would like to close this admittedly incomplete summary with a few personal conclusions:

a. after 25 years of continous running of the Davis experiment, a second solar neutrino detector (Gallex) is being build and will explore a totally different energy region of solar neutrino spectrum. Other experiments are hopefully joining soon these two;

b. there is no evidence (yet) for any type on neutrino flavour or Majorana oscillation;

c. the possibility that electron antineutrino mass be larger that ten electronvolt is under considerable difficulty. Zurich, Los Alamos and Tokio groups have already joined the club and they should be able to prove or disprove shortly the ITEP result;

d. unlike those on neutrino mass, all direct double beta decay experiments give negative results, which are particularly stringent for the neutrinoless lepton non conserving mode;

e. the neutrino and its problems represent an excellent common field to be studied contemporarily, and with mutual help, by particle physics and astrophysics;

f. new interdisciplinary techniques are required to solve many of the open experimental problems. We will need the help from other fields of science, particularly by chemistry, geology, solid state, and obviously low energy nuclear physics. Many of us, including myself, had to look again to the textbooks used in our graduate or even undergraduate studies. I find this "unification" of techniques as attractive as the unification of forces;

g. we experimentalists are receiving a great help from theorists, who fortunately do not disdain any more to involve themselves in detailed atomic, molecular and nuclear physics calculations which, incidentally, we are generally able to understand. Calculations on neutrino masses and oscillations and on double beta decay are obvious examples;

h. massive neutrino physics and astrophysics is a wonderful field of research, the most exciting I happened to work in!

REFERENCES

1. T. Kirsten: From hope to reality - the Gallex project, this conference.
2. M. Spiro: Chromium source of monoenergetic ν_e, this conference.
3. R.G.H. Robertson: A gallium solar neutrino experiment, this conference.
4. Report by A.A. Pomanski on the present status of the Gallium solar neutrino project in USSR.
5. W.C. Haxton: Solar neutrinos - The Molybdenum experiment, this conference.
6. J. Simpson: Feasibility study for a neutrino observatory based on a large heavy water detector deep underground, this conference.
7. M. Baldo Ceolin: Direct observation of solar neutrinos from 8 B cycle in Icarus, this conference.
8. E. Bellotti: Cygnus X-3 with Mont Blanc Underground Experiment, this conference.
9. G. Chardin: report on the result by the Frejus collaboration.
10. A.Yu. Smirnov: New Baksam data on Cygnus X-3, this conference.
11. "I did not know that you were an astronomer!" comment adressed to me by Mariotta, my mother's maid after evidence on Cygnus X-3 by NUSEX.
12. Reports by Aleksan and Koltic on experiments carried out at Petra.
13. Report by Santoni on Charm results.
14. J.M. Levy: The neutrino decay search in the P.S. beam, this conference.

15. B. Tasiaux: Nuclear muon capture in ^{3}He and massive neutrino search in the 10-100 MeV range, this conference.
16. M. Daum: New upper limit for the muon-neutrino mass, this conference.
17. D. Koltic: Review of tau neutrino mass limits, this conference.
18. O. Fackler: Tritium beta decay neutrino mass determination: an introduction, this conference.
19. "We quarrel only between brothers, with the others we are too far to do so", A. Einstein.
20. V. Lubimov: The neutrino mass from beta spectrum, this conference.
21. K.E. Berkvist: Neutrino mass situation as of Jan. 30, 1986, this conference.
22. J.W. Petersen: An upper limit to m_{ν_e}, this conference.
23. J.F. Wilkerson: The Los Alamos free molecular and atomic tritium beta decay experiment, this conference
24. H.Kawakami et al.: Neutrino mass measurement by ^{3}H beta spectrum at INS, this conference.
25. V.M. Lobashev and P.E. Spivak: Nucl. Instrum. and Methods A238, 496 (1985) and A240, 305 (1985), also for previous references.
26. M. Mugge: A neutrino mass experiment using frozen tritium, this conference. A detailed calculation of the molecular effects in neutrino mass determination by O. Fackler et al has been reported here by W. Kolos
27. H. Wellenstein: The beta spectrum from gaseous T_2, this conference.
28. K. Riisager: Internal bremsstrahlung in electron capture beta decay, this conference.
29. S. Yasumi: Measurement of the mass of the electron neutrino using electron capture in Holmium 163, this conference.
30. J. Simpson: A possible 17.1 keV neutrino - a review, this conference.
31. See the review by Shaevitz at this conference
32. S. Katsanevas: Search for oscillations using BEBC, this conference.
33. F. Vannucci: Did neutrinos oscillate at CERN in July 1984? Will neutrinos oscillate in BNL in March 1986, this conference.
34. The new experiment KARMEN (for Karlsruhe Rutherford Medium Energy Neutrinoexperiment) has been described at this conference by Mashow.
35. The proposal E645-LAMPF by the ANL, Caltech, LBL, Lampf, LSU and Osu collaboration has been described here by Smith.
36. J. Lo Secco: Physics results from IMB, this conference
37. J.L. Vuilleumier: Recent results on $\bar{\nu}_e$ oscillations at reactors, this conference.
38. J. Bouchez: Report by the Bugey collaboration and the report by Cavaignac on a new possibility to detect reactor neutrinos, this conference.
39. H. Sobel: UCI mobile neutrino oscillation experiment, this conference.
40. H. Blumer and K. Kleiknecht: Experimental constraints on lepton mixing angles and neutrino mass differences from three simultaneously oscillating neutrino flavours, submitted to Phys. Lett.
41. A.A. Pomanski, report to this conference.
42. Nagay: Neutrinoless double beta decay of Ge-76, this conference.
43. A. Hahn: Recent results from the UCI Se-82 two neutrino double beta decay experiment, this conference.
44. P. Fisher: The Ge-76 double beta decay experiment in the Gotthard tunnel, this conference.
45. E. Fiorini: Present and future double beta decay experiments, this conference.
46. V. Zacek: Particle spectroscopy with Superconducting Tunnel Junctions (STJ), this conference.
47. Twerenbold: Su-junction detector, this conference.
48. K. Riisager: Calorimeters for nuclear radiation detection, this conference.
49. B. Cabrera: Crystal acoustic detector for neutrinos, this conference.

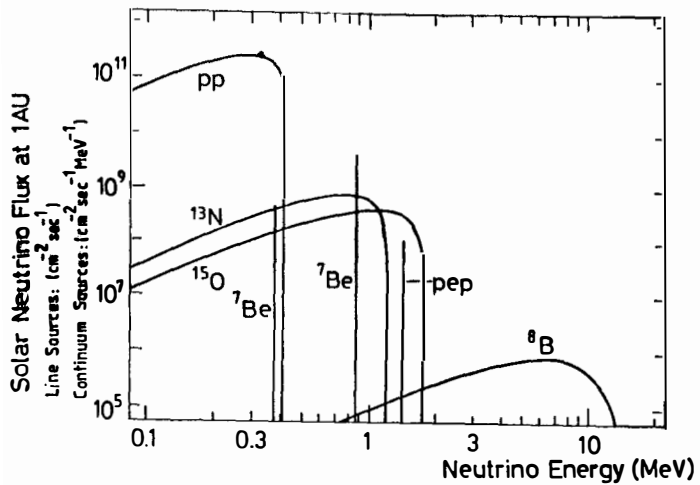
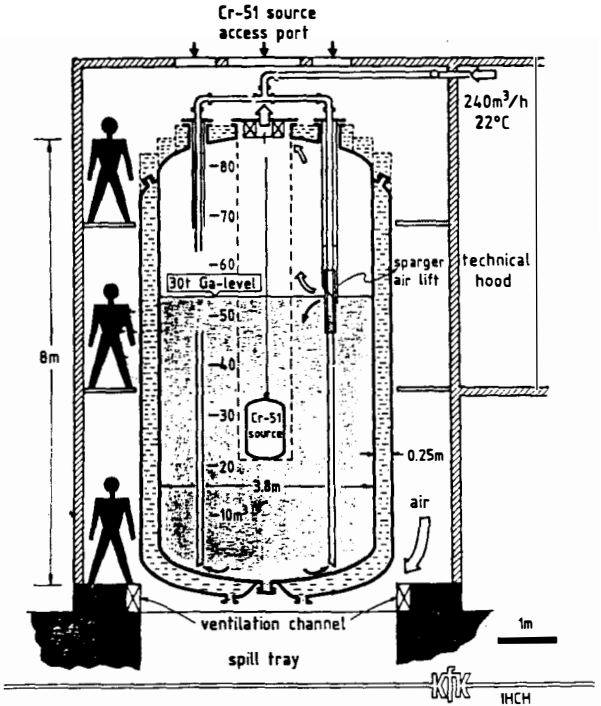


Fig. 1



GALLEX TARGET TANK

Fig. 2

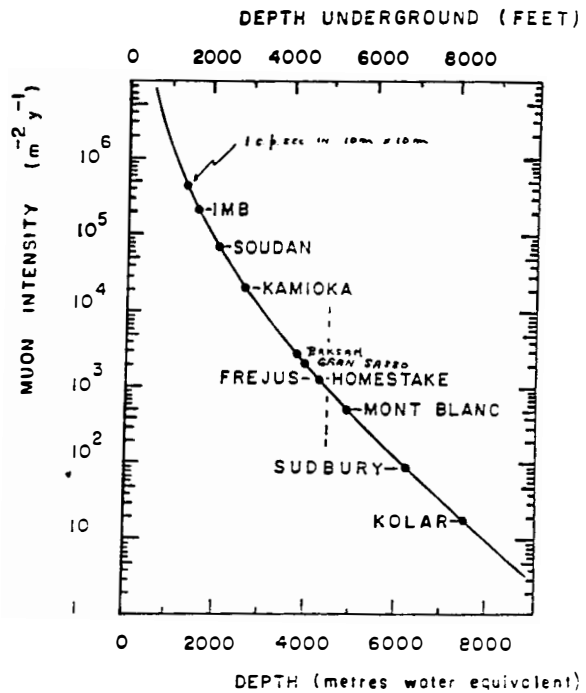

DEPTH UNDERGROUND (FEET)
0
2000
4000
6000
8000
MUON INTENSITY (m^{-2} y^{-1})
10^6
10^5
10^4
10^3
10^2
10
1
IMB
SOUDAN
KAMIOKA
BAKSAN
GRAN SASSO
FREJUS
HOMESTAKE
MONT BLANC
SUDBURY
KOLAR
0
2000
4000
6000
8000
DEPTH (metres water equivalent)

Fig 3

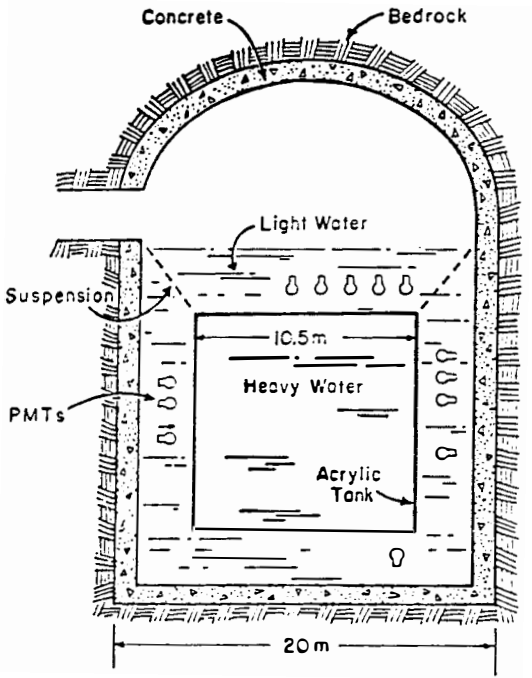

Concrete
Bedrock
Light Water
Suspension
10.5m
Heavy Water
PMTs
Acrylic Tank
20m

Fig.4

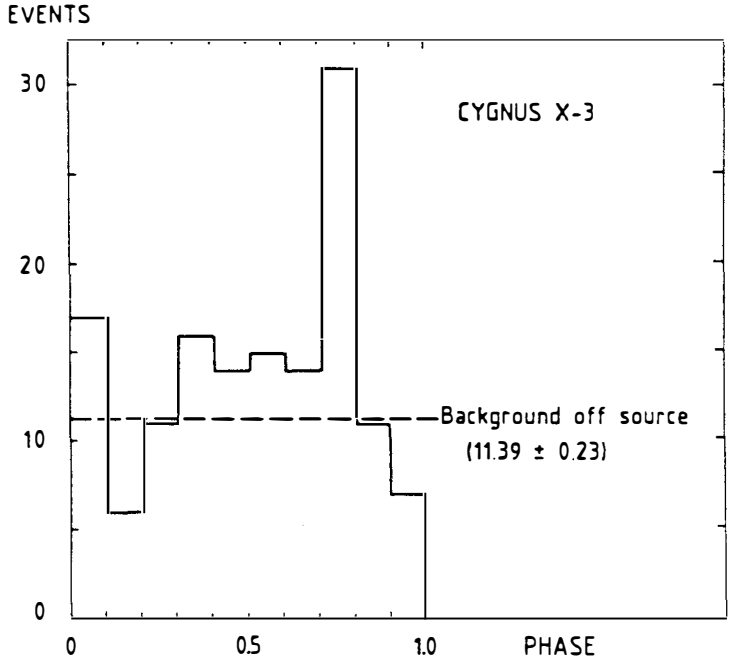

EVENTS
30
20
10
0
CYGNUS X-3
Background off source
(11.39 ± 0.23)
0
0.5
1.0
PHASE

Fig. 5

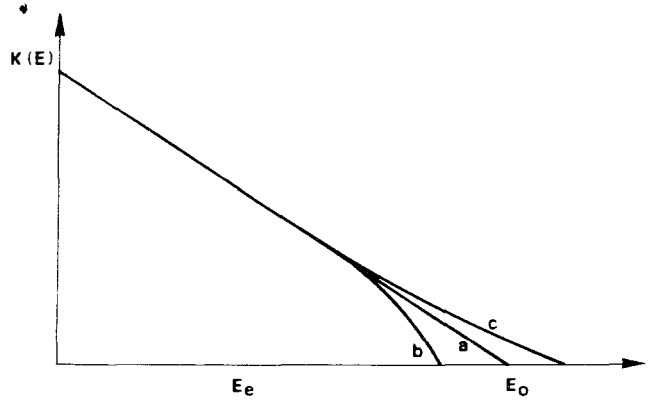

K (E)
c
b
a
E_e
E_o

Fig. 6

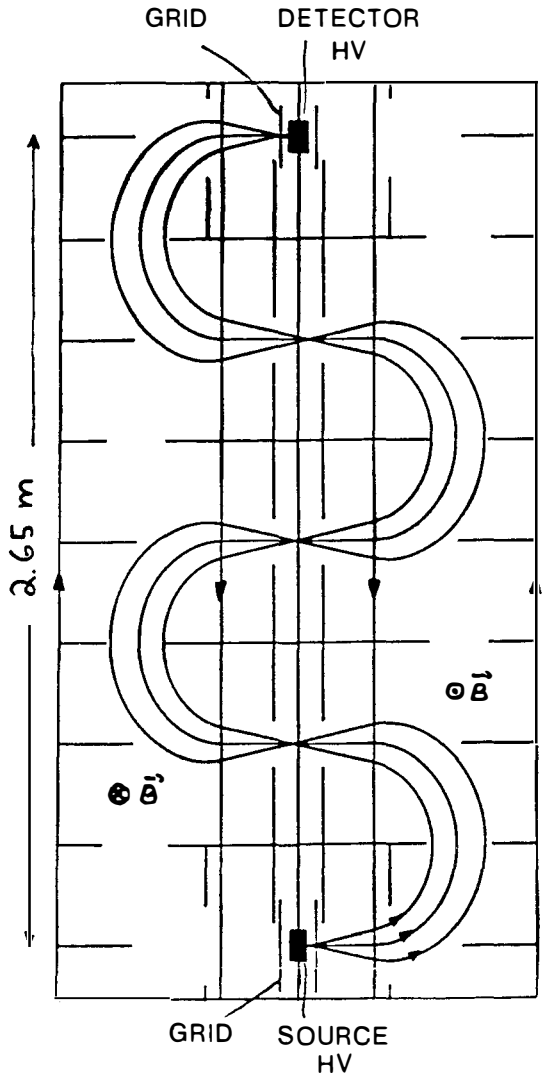


Fig. 7

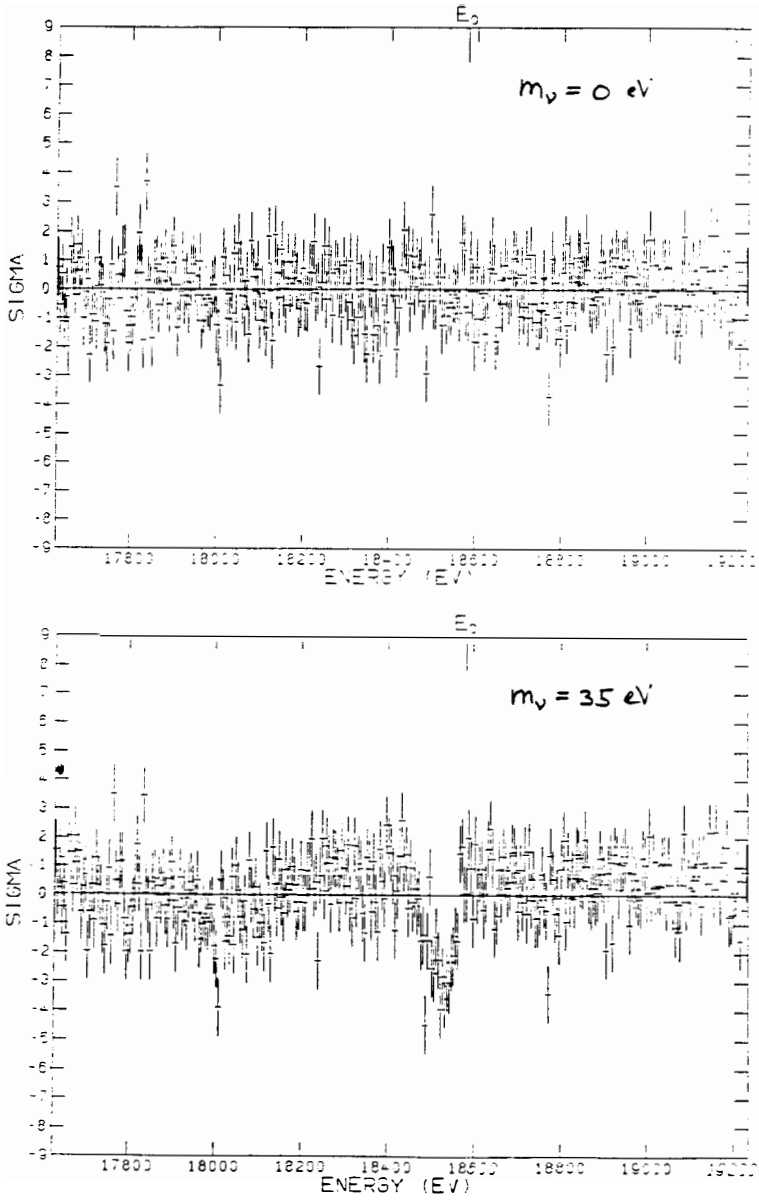

E0
mν = 0 eV
SIGMA
ENERGY (EV)
E0
mν = 35 eV
SIGMA
17800
18000
18200
18400
18600
18800
19000
ENERGY (EV)

Fig. 8

LOS ALAMOS TRITIUM BETA DECAY EXPERIMENT

APPARATUS OVERVIEW

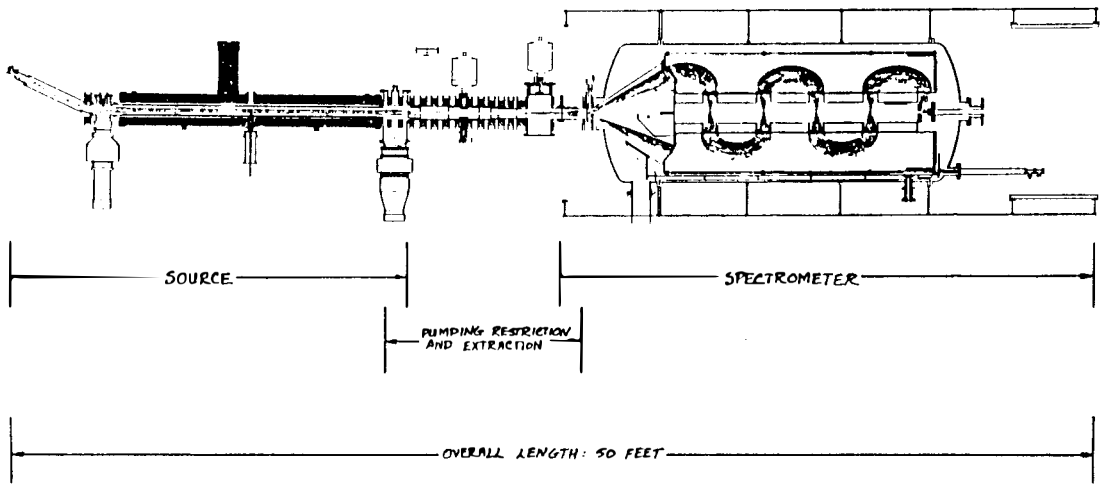


Fig. 9

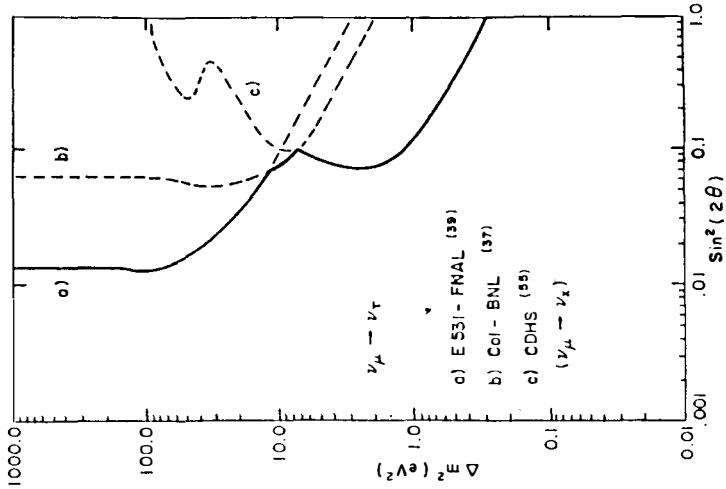

a)
b)
c)
$\nu_\mu - \nu_\tau$
a) E 531 - FNAL (39)
b) Col - BNL (37)
c) CDHS (55)
$(\nu_\mu - \nu_x)$
Δm^2 (eV^2)
$\sin^2(2\theta)$
1000.0
100.0
10.0
1.0
0.1
0.01
.001
.01
.1
1.0

Fig. 10

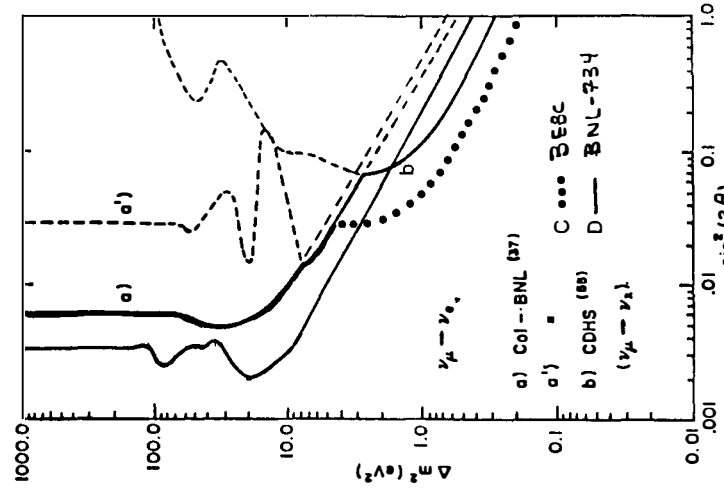

a)
a')
b
$\nu_\mu - \nu_e$
a) Col - BNL (37)
a') "
b) CDHS (55)
$(\nu_\mu - \nu_x)$
C ••• BEBC
D — BNL-734
Δm^2 (eV^2)
$\sin^2(2\theta)$
1000.0
100.0
10.0
1.0
0.1
0.01
.001
.01
.1
1.0

Fig. 11

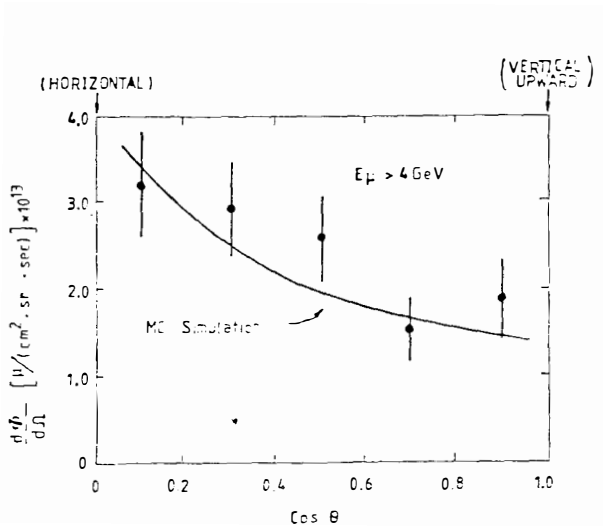

(HORIZONTAL)
(VERTICAL UPWARD)
Eμ > 4 GeV
MC Simulation
4.0
3.0
2.0
1.0
0
0.2
0.4
0.6
0.8
1.0
Cos θ
$\frac{d\psi}{d\Omega}$ [μ/(cm².sr.sec)] ×10¹³

Fig. 12

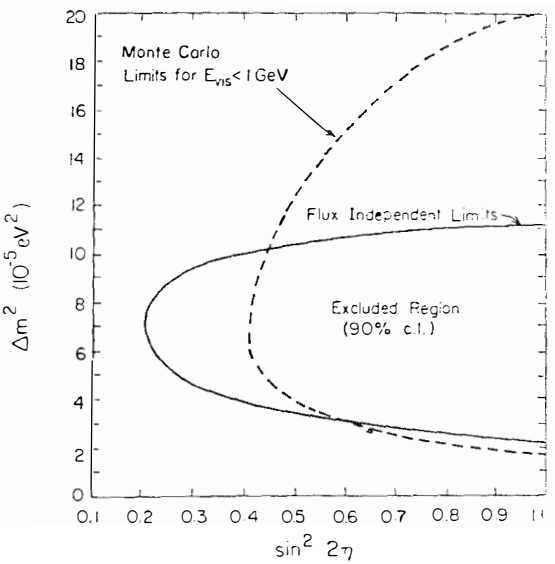
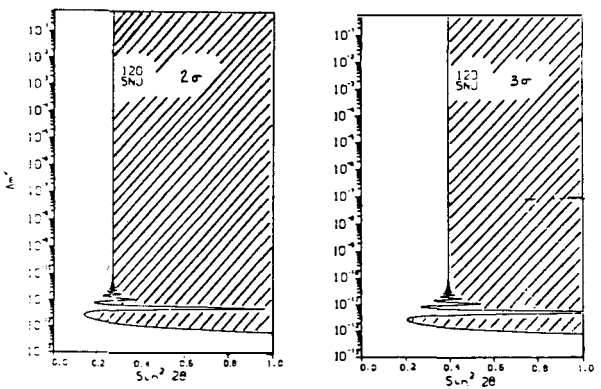

Monte Carlo
Limits for E_{vis}< 1 GeV
Flux Independent Limits
Excluded Region
(90% c.l.)
20
18
16
14
12
10
8
6
4
2
0
0.1
0.2
0.3
0.4
0.5
0.6
0.7
0.8
0.9
Δm^2 (10^{-5} eV^2)
$\sin^2 2\eta$

Fig 13



EXCLUSION LIMITS ON ν_e DISAPPEARANCE FROM A GALLIUM SOLAR NEUTRINO EXPERIMENT

[WITHOUT MATTER OSCILLATIONS !]

Fig. 14

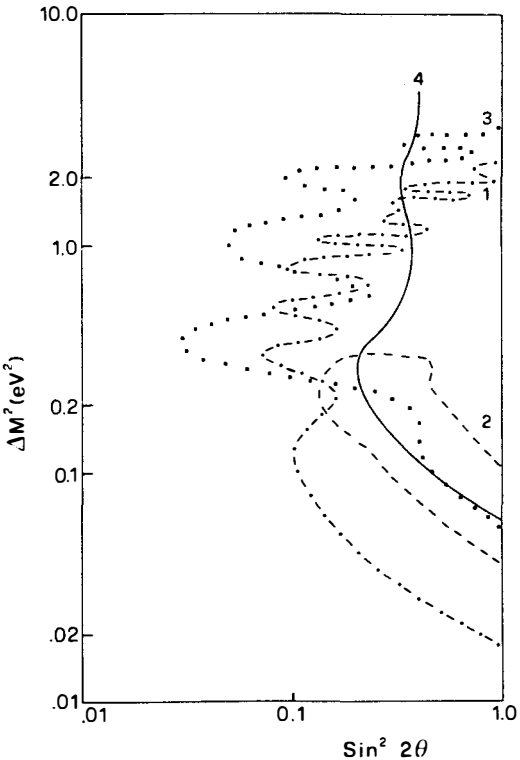
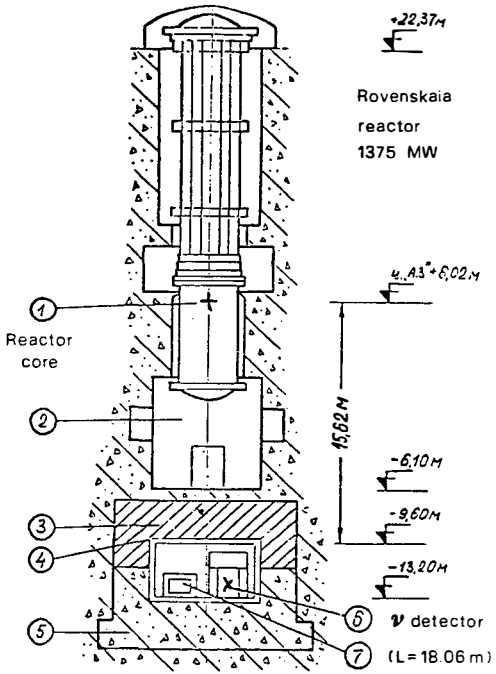
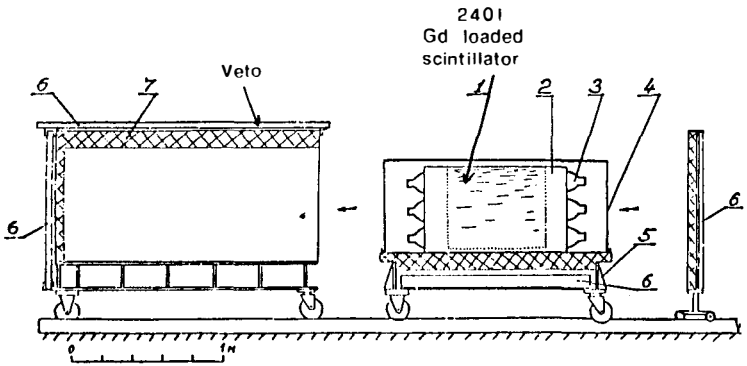


Fig. 15



Kurtchatov Institute, Moscow

Fig. 16



Rovenskaia

Fig. 17

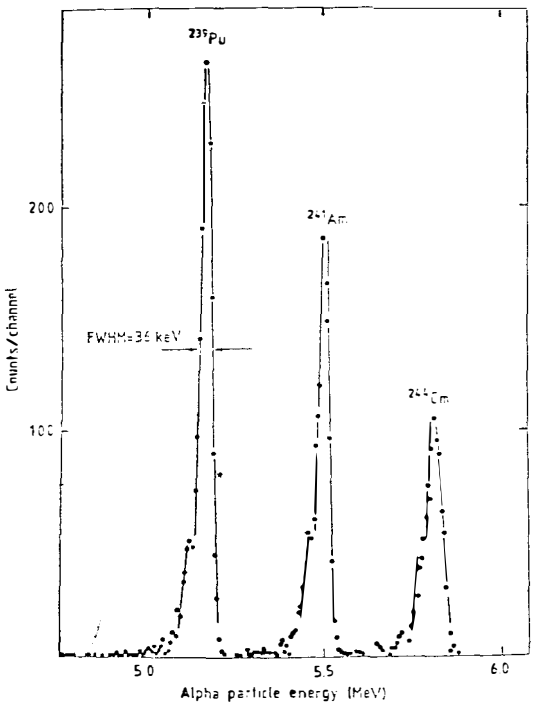

239Pu
241Am
244Cm
FWHM=36 keV
200
100
Counts/channel
5.0
5.5
6.0
Alpha particle energy (MeV)

Fig 18

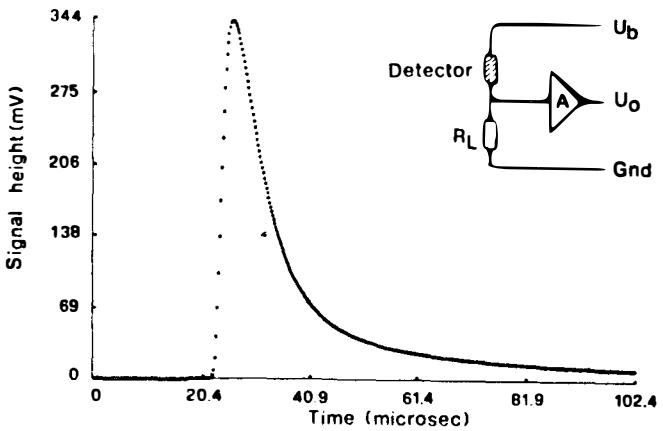

344
275
206
138
69
0
Signal height (mV)
0
20.4
40.9
61.4
81.9
102.4
Time (microsec)
Detector
A
Ub
Uo
RL
Gnd

Fig. 19

SUMMARY IN THEORY

Gary Steigman
Bartol Research Foundation
University of Delaware
Newark, DE 19716, USA



ABSTRACT

This is a much abbreviated guide to some of the theoretical results discussed during the Sixth Moriond Workshop on Massive Neutrinos in Particle Physics and Astrophysics. Since the reader may consult the beautiful introductory lecture of Rosen, as well as the specific theoretical papers in this volume, I devote most of my effort here to setting the stage for the roles of massive neutrinos in astrophysics and cosmology.

INTRODUCTION

I must begin with an apologia to all my friends and colleagues whose contributions to this Workshop have been valuable but, which are unreferenced in this summary. I will comment only very briefly about only very few of the theoretical results presented. Indeed, from my perspective, and with all due respect to my theoretical colleagues, the most interesting results presented at Moriond were the experimental results. I, therefore, urge the reader to consult the experimental summary of Fiorini.

Kang, Langacker and Petcov reviewed for us the expectations for the nature and magnitude of neutrino masses in current theories. We were reminded that the "standard" model (SU(3) x SU(2) x U(1)) makes a very definite prediction for neutrino masses: $m_\nu = 0$. Neutrinos may, in Grand Unified extensions of the standard model, acquire masses which in the most "natural" models are very small ($\lesssim 10^{-3}$eV). These and other speakers noted that for "interesting" masses (~10eV and higher) there were a variety of laboratory and astrophysical constraints on masses, lifetimes and mixings (in this regard see, especially, Langacker's paper).

Halprin called attention to possible (future) laboratory constraints on the properties of the superpartners of the neutrinos.

Most theoretical interest in massive neutrinos seems to be motivated by astrophysical problems. There are, of course, DARK MATTERS. Most of the mass in the Universe is dark - not shining in the optical part of the spectrum. Neutrinos don't shine. If they had a mass, perhaps----. Klinkhammer reviewed for us the Death and Resurrection of the light but massive (~tens of eV) neutrinos. Roos mentioned the possibility of detecting the photons from the decay of a long-lived massive neutrino.

Straying further from the fold, Hall introduced us to the Shadow World and Schramm sold us on Cosmic Strings. Glashow reviewed the evidence (?) for a Repulsive New Force. As an aside, it is worth emphasizing here that the "hyperphoton", the hypothetical carrier of the hypothetical fifth force, could not be the dark matter in the Universe. The hyperphoton would have a tiny mass, some 18 orders of magnitude less than the mass of a nucleon. However, relic hyperphotons should be roughly 7 orders of magnitude more abundant than nucleons. As a result, hyperphotons would contribute $\sim 10^{-11}$ as much as nucleons to the total universal mass density. Worse yet, such light particles would be relativistic today (the thermal energy corresponding to the microwave temperature of ~3K is $\sim 10^{-4}$eV, some 5 orders of magnitude higher than the rest energy of the hypothetical hyperphoton).

Light but massive (~30eV) neutrinos are candidates for "hot" dark matter. Hot dark matter clusters on very large scales but damps inhomogeneities on small scales. In contrast, massive ($\gtrsim$GEV) WIMPs (Weakly Interacting Massive Particles) are candidates for "cold" dark matter. Cold dark matter can cluster on all scales. Indeed, if they are dynamically important, such WIMPs may dominate the mass of the halo of our Galaxy. Among the exciting results presented at this Workshop were those of Spergel and Steigman who emphasized that many such cold dark matter candidates, although dark, are not invisible.

Not the mass but, rather, the number of flavors of light neutrinos is of importance for primordial nucleosynthesis. As Steigman, Schramm and Gunn[1] noted, extra flavors of neutrinos results in more ^{4}He being produced primordially. The "standard" model predicts a mass fraction, $Y_p \simeq 0.24$, for $N_\nu = 3$, in excellent agreement with current observational data[2]. Since stars produce ^{4}He, some of the ^{4}He

presently observed in the Galaxy ($Y_0 \simeq 0.30$) is the result of galactic evolution. In this sense, it should be expected that the solar helium abundance would be close to the galactic helium abundance (actually, $Y_\odot$ should reflect the galactic helium abundance 4.5 billion years ago at the formation of the Sun). Cahen presented here results of recent calculations which suggest that $Y_\odot \simeq 0.28$, in better agreement with Y_0 than previous solar model calculations. The models that Cahen referred to do, however, still predict at least 3 times as many neutrinos as "seen" in the Davis[3] experiment.

That last remark brings me to the most exciting new theoretical result discussed at this Workshop: the "Mikheyev - Smirnov - Wolfenstein" mechanism[4]. This effect, resonant amplification of neutrino oscillations in matter, provides perhaps the most elegant solution to the solar neutrino problem. Although I will have some very brief, qualitative remarks about the M-S-W mechanism later, the reader is strongly urged to consult the articles in this volume by Smirnov, Rosen, Messiah and, Spiro.

Given the important experimental results presented at this meeting, I am led to conclude that some of my colleagues may have spent a significant fraction of the last few years in the bowels of the Earth (or, the bowels of CERN). It may, then, be of some value to present here an overview of the astrophysical framework on which many current ideas concerning massive neutrinos are hung.

DARK MATTERS

There is not one (or two, or three) dark matter problem. Rather, there appears to be a continuum of problems: from scales smaller than galaxies to larger than rich clusters of galaxies, some - often most -

of the mass is invisible[5]. What is the dark mass? Is it "normal" nucleonic material which is dark (dead or failed stars, hot gas, etc.) or, is it an exotic escapee from the particle physics zoo?

There is a "local" missing light problem. In the disk of the Galaxy, in the vicinity of the Sun, the total mass - inferred from the dynamics of stars - exceeds that which can be "seen" (stars, gas, dust, etc.) by a factor of ~50 - 100% (i.e.: $M_{TOT}/M_{seen} \simeq 1.5 - 2$). Most would, however, agree that the dark mass in the disk of the Galaxy is nucleonic in origin. The reason is that, to have collapsed into a flattened disk, the material must have been dissipative. WIMPs cannot dissipate.

If we consider galaxies as a whole, the dark matter problem grows. From simple Newtonian mechanics we can relate the total - dynamical - mass to the observations of the motions (velocities) of "test" particles (stars or gas).

$$v^2 = GM(r)/r \qquad (1)$$

Evidence for Galactic Halos is provided by "flat" rotation curves[4]: far out from the centers of galaxies, the observed velocity is constant (independent of the distance from the center of the galaxy). From (1) we infer that the mass is growing ($M \propto r$), whereas past a certain point - the Holmberg radius - the light falls off exponentially. Beyond the Holmberg radius there is (virtually) no more light but, there is additional mass; on sufficiently large scales the "dynamical" mass exceeds, significantly, the "luminous" mass.

The trend continues on still larger scales. Not only galactic halos, but also among pairs of galaxies and in small groups, rich

clusters and, even in the Virgo supercluster, most of the mass is dark. To quantify the situation consider the mass associated with the luminous parts of galaxies ($\lesssim$ Holmberg radius) and compare this to the amount needed to just "close" the Universe,

$$\Omega_{GAL} = \rho_{GAL}/\rho_{CRIT} \simeq 0.01 \qquad (2)$$

In (2), ρ_{GAL} is the average mass density associated with the luminous parts of galaxies and $\rho_{CRIT} = 3H_0^2/8\pi G$ is the critical value of the density separating those low density universes ($\rho < \rho_{CRIT}$) which will expand forever from those ($\rho > \rho_{CRIT}$) which will eventually recollapse; $H_0 = 50h_{1/2}$ $kms^{-1}Mpc^{-1}$ is the present value of the Hubble parameter. In contrast, the average density of material inferred from the dynamics of halos, groups, clusters, etc. is much larger.

$$\Omega_{DYN} \sim 0.2 \pm 0.1. \qquad (3)$$

It is worth emphasizing not only that $\Omega_{GAL} << \Omega_{DYN}$ (most of the mass in the Universe is "dark" - the "missing light" problem) but, also that $\Omega_{DYN} \neq 1$ (the "observed" Universe is a low density Universe).

Can the dark mass be nucleonic? To answer this question we must compare ρ_{DYN} to ρ_N, the universal density of nucleons. Comparison of the predictions of big bang nucleosynthesis with the observed abundances of the light elements[2] (D, ^{3}He, ^{4}He, ^{7}Li) constrains the ratio of nucleons to photons to lie in the range: $3 \lesssim 10^{10}N/\gamma \lesssim 7$; this corresponds to,

$$0.04 \lesssim \Omega_N h_{1/2}^2 \lesssim 0.11. \qquad (4)$$

Since it is likely that $1 \lesssim h_{1/2} \lesssim 2$ ($H_0 \simeq 50 - 100$ kms^{-1}Mpc^{-1}), $0.01 \lesssim \Omega_N \lesssim 0.1$. Nucleons, then, can account - at most - for ~ 10% of the critical density. It must, however, not be ignored that the lower end of the range of the estimates for Ω_{DYN} overlaps with the upper end of the range of the estimates for Ω_N: all the dark mass in the Universe may be nucleonic; the Universe, however, cannot be closed by nucleons.

Is Ω=1? There are many avenues to approach this question. One path is to note that Ω, the ratio of the total universal mass density to the critical density is, in general, time dependent. Early on, Ω may be very large. As the Universe evolves, Ω will decrease. The "natural" time scale for the evolution of the Universe is the Planck time, $t_p \simeq 10^{-43}$sec. Why, then, at present ($t_0 \simeq 10$Gyr $\simeq 10^{17}$sec), some 10^{60} Planck times after the "bang" is $\Omega \simeq O(1)$? Perhaps Ω has always been equal to unity; if Ω=1 at any time then, Ω=1 for all times.

Another path is Inflation[6]. In this scenario the Universe, during its early evolution, experienced an epoch of "inflation" - exponential expansion - which left the spatial curvature exponentially small. In this case, in the absence of a significant cosmological term, the present value of Ω will be arbitrarily close to unity.

Perhaps the strongest hint that Ω may exceed the dynamical estimates comes from the formation of structure in the expanding Universe. Small density perturbations are amplified gravitationally as the Universe evolves. The growth of perturbations (in the linear regime) is, however, slow. Furthermore, during early epochs when radiation dominated the universal mass density, matter perturbations barely grow at all. The smaller Ω, the more recently in the past was the Universe "radiation dominated" and the less time was available for small

perturbations to grow to non-linearity and form the observed large scale structure of the Universe. In a low density Universe, therefore, the initial perturbations should have large amplitudes. However, such large amplitudes would be reflected in observable anisotropies in the cosmic background radiation. The - as yet - unobserved anisotropies suggest that $\Omega_0 \gtrsim 0.2\text{-}0.4$. Here is an observational - albeit not entirely direct - hint that $\Omega_0 \gtrsim \Omega_{DYN}$.

Shortly, we will compare the density of some relic, X, from the big bang with the critical density. What limits can we place on $\rho_X = \Omega_X \rho_{CRIT}$? From observational data we may infer that $\Omega_{DYN} \lesssim 0.3$ and $h_{1/2} \lesssim 2$ so that: $\Omega_X h_{1/2}^2 \lesssim 1.2$. We have, however, noted that, perhaps, $\Omega_0 \gtrsim \Omega_{DYN}$. Suppose that $\Omega_X \simeq \Omega_0 = 1$. Such a critical density Universe expands quickly and is, at present, "young". For $\Omega_0 = 1$, for a "matter dominated" Universe, the present age is,

$$t_0 = 2/3H_0^{-1} \simeq 13 h_{1/2}^{-1} \text{ Gyr.} \qquad (5)$$

Since the oldest stars, those in globular clusters, seem to be <u>at least</u> 10-13 Gyr old, $h_{1/2} \lesssim 1\text{-}1.3$ and $\Omega_X h_{1/2}^2 \lesssim 1\text{-}1.7$. It must be emphasized that, in the absence of a cosmological term, $\Omega_0 = 1$ and $H_0 = 100 \text{ kms}^{-1}\text{Mpc}^{-1}$ is excluded since such a Universe would be only ~ 6.5 Gyr old. For subsequent estimates we will assume an upper limit, $\Omega_X h_{1/2}^2 \lesssim 1$.

A NEUTRINO DOMINATED UNIVERSE - MUCH ADO ABOUT NOTHING?

Light but massive (<<MeV) neutrinos would have been produced copiously in the early Universe. Relic neutrinos are, today, nearly as common as black body photons: $n_\nu/n_\gamma = 3/11\ (g_\nu/2)$, where g_ν is

the number of neutrino helicity states. Since there are, for $T_\gamma = 2.7K$, $N_\gamma \simeq 400$ photons per cm^3, there are, approximately, 10^2 $(g_\nu/2)$ neutrinos (of each flavor) in every cubic centimeter (on average). If the neutrinos are massive, the current mass density in relic neutrinos is

$$\rho_\nu = \Sigma m_\nu n_\nu \simeq 1/4 \times 10^4 \ \Omega_\nu h_{1/2}^2 \ eVcm^{-3}. \tag{6}$$

In (6), the neutrino mass is in eV and the sum is over neutrino flavors. Since $\Omega_\nu < \Omega_o$, there is an upper bound to the sum (weighted by $g_\nu/2$) of neutrino masses.

$$\Sigma m_\nu \lesssim 24 \ \Omega_o h_{1/2}^2 \ eV \lesssim 24 - 41 \ eV. \tag{7}$$

For the cosmological implications of such massive, relic neutrinos see Klinkhammer (and references therein).

BORN AGAIN NEUTRINOS

The most exciting new work discussed at this Workshop is that relating to the interconversion of neutrinos by the Mikheyev-Smirnov-Wolfenstein mechanism[4]. The resonant amplification of neutrino oscillations in matter is described elsewhere - and often - in these Proceedings. Here, I will merely review some of the salient features and comment on the relevance for the Sun and for the early Universe.

It is well understood that, if neutrinos have non-zero masses, the mass eigenstates and the weak interaction eigenstates need not coincide. As a result, vacuum oscillations among different flavors of neutrinos are possible. Such vacuum oscillations are characterized by the mass-squared differences ($\Delta m^2 = m_1^2 - m_2^2$) and by the vacuum

mixing angles θ_V. As such neutrinos propagate through matter, the eigenstates of the full Hamiltonian will differ from those in vacuum. Another scale then, depending on the strength of the weak interaction and the amount of matter is introduced into the problem. Further, since ordinary matter consists of protons and electrons unbalanced by equal numbers of antiprotons and positrons, neutrinos and antineutrinos will have different oscillation properties in matter. For example, it may turn out that at high density the lowest energy eigenstate is closest to the e-neutrino whereas, at low density it is the μ-neutrino which is closest to the lowest energy eigenstate. It is then possible that e-neutrinos produced at high density, emerge as μ-neutrinos at low density; the antineutrinos may be unaffected. This is the M-S-W effect.

The vacuum mixing is, in the presence of matter, modified to

$$\sin 2\theta_M = \sin 2\theta_V [(\cos 2\theta_V - \ell_\nu/\ell_0)^2 + \sin^2 2\theta_V]^{-1/2} \qquad (8)$$

ℓ_ν is the usual vacuum oscillation length ($\ell_\nu \propto E_\nu/\Delta m^2$) and $\ell_0 \propto (G_F n)^{-1}$ is the scale set by the matter (G_F is the Fermi constant and n is the number density). It follows from (8) that at high density ($\ell_0 \ll \ell_\nu$), $\sin 2\theta_M \simeq (\ell_0/\ell_\nu) \sin 2\theta_V \ll \sin 2\theta_V$ and oscillations are suppressed. In contrast, at low density ($\ell_\nu \ll \ell_0$), $\sin 2\theta_M \simeq \sin 2\theta_V$ and vacuum oscillations are recovered. In between, however, there is a density such that $\ell_\nu = \ell_0 \cos 2\theta_V$. In this case we have maximal oscillations: $\sin 2\theta_M = 1$.

As Mikheyev and Smirnov[4] have realized, e-neutrinos produced in the high density of the solar core may emerge from the Sun as a different flavor neutrino, thus providing an elegant solution to the solar neutrino problem[3]. It is noted in several places in these

Proceedings that there are two "branches" in the Δm^2-$\sin^2 2\theta_V$ plane which "solve" the solar neutrino problem. Solution(I) corresponds to $\Delta m^2 \simeq 10^{-4} eV^2$ and $\sin^2 2\theta_V \gtrsim 10^{-3}$; Solution(II) requires that $\Delta m^2 \sin^2 2\theta_V \simeq 10^{-7.5}$. The implications of these solutions for the Gallium experiment are also discussed elsewhere. For (I), there is no suppression of the expected neutrino flux in that experiment whereas for (II), in the small Δm^2, large $\sin^2 2\theta_V$ limit, suppression by a factor of 3-4 is predicted.

It has been noted elsewhere[7] that the "see-saw" mechanism predicts small mixing angles ($\sin^2 2\theta_V \lesssim 10^{-3}$) and Δm^2 which could be appropriate for the solar neutrino problem ($\Delta m^2 \simeq 10^{-6 \pm 2} eV^2$) provided that the mixing is e-τ and not e-μ. For the cosmologically "interesting" case[7], however, $\sin^2 2\theta_V \gtrsim 0.1$ and $\Delta m^2 \lesssim 10^{-6} eV^2$ and the Gallium experiment should see a very much reduced flux.

Finally, we comment on the possible role of M-S-W oscillations in the early Universe - in particular, the effect of an ν_e - $\bar{\nu}_e$ asymmetry on primordial nucleosynthesis (see Smirnov, this Volume). As the Universe expands the density decreases. Although at early times when the temperature is high ($T \gtrsim$ MeV) the abundance of positrons is high, there is, nevertheless, an excess of electrons over positrons. It is this excess density, Δn_e, which could be responsible for converting e-neutrinos into some other flavor of neutrino while leaving the anti-e-neutrinos untouched or, vice-versa. Smirnov (this Workshop) has noted that if $\bar{\nu}_e$ can be rotated into a "sterile" neutrino, a ν_e excess would be generated. An excess of ν_e will drive the neutron abundance down and result in less ^{4}He being produced primordially[2]. In this case, the number of additional flavors of neutrinos allowed by

primordial nucleosynthesis[8], ΔN_ν, increases. These new, sterile neutrinos, with the appropriate masses and mixings to generate a ν_e excess are ad hoc and unnatural[7]. It is, however, of interest to investigate the effect of M-S-W conversions in the early Universe for those parameters (Solutions I and II) which "solve" the solar neutrino problem[7]. In this case a $\bar{\nu}_e$ excess is developed which tends to increase the neutron abundance and, therefore, increase the predicted abundance of ^{4}He produced primordially[7]. The magnitude of the effect, however, is very small; the predicted helium mass fraction Y increases by only $\Delta Y \lesssim 0.0013$ and the limit on the number of neutrino flavors decreases by $\Delta N_\nu \lesssim 0.09$.

CONCLUSIONS

As a theorist, my strong impression at this meeting was, "plus ca change, ---". The experimental results are driving nails in the coffin of (astrophysically interesting) neutrino masses. Still, neutrinos may have very small masses and the solar neutrino problem may yet have a particle physics solution. As we have heard at this meeting, it is perhaps surprising but, nevertheless true, that just as our particle physics theory colleagues are constrained by laboratory data, we astrophysicists must, too, contend with an increasing body of astronomical observations. Although reports of the cosmological demise of ~30 eV neutrinos may be premature, such neutrinos may still be terminally ill. More massive neutrinos ($\gtrsim$ GeV) should have already been detected and, in any case, are unlikely to be stable. Consistency with big bang nucleosynthesis suggest all lepton flavors may have already been found. Laboratory and astronomical data, hand in hand with careful theoretical analysis, seems capable of providing important answers to

the interesting questions of the masses, couplings and lifetimes of known - and yet to be discovered - particles. We are all grateful to the organizers of the Workshop - Tran in particular - for bringing together in such a pleasant and stimulating environment, such an interdisciplinary gathering of scientists to address these fascinating issues.

ACKNOWLEDGEMENTS

I have benefited from conversations with many people at this Workshop. Special thanks are due E. Fiorini, P. Langacker, S. Petcov, P. Rosen, D. Schramm, A. Yu. Smirnov and D. Spergel. This research is supported by the DOE through grant DE-AC02-78ER-05007.

REFERENCES

1. G. Steigman, D. N. Schramm and J. E. Gunn, Phys. Lett. B66, 202 (1977).
2. A. M. Boesgaard and G. Steigman, Ann. Rev. Astron. Astrophys. 23, 319 (1985).
3. J. K. Rowley, B. T. Cleveland and R. Davis, AIP Conf. Proc. 126, 1 (1985).
4. S. P. Mikheyev and A. Yu. Smirnov, INR Preprint (1985).
5. S. M. Faber and J. S. Gallagher, Ann. Rev. Astron. Astrophys. 17, 135 (1979).
6. A. H. Guth, Phys. Rev. D23, 347 (1981).
7. P. Langacker, S. Petcov, G. Steigman and S. Toshev, CERN Preprint (1986).
8. J. Yang, M. S. Turner, G. Steigman, D. N. Schramm and K. A. Olive, Ap. J. 281, 493 (1984).

LIST OF PARTICIPANTS

ALEKSAN Roy	DPhPE CEN Saclay 91191 GIF SUR YVETTE Cedex FRANCE
ASTIER Pierre	LPNHE, Université Paris VII 4, Place Jussieu, Tour 32 75230 PARIS Cedex FRANCE
AUDI Georges	Lab. René Bernas, CSNSM B. P. N°1, Bâtiment 108 91406 ORSAY FRANCE
AVENIER Michel	Institut des Sciences Nucléaires 53, avenue des Martyrs 38026 GRENOBLE Cedex FRANCE
BALDO-CEOLIN Milla	Physics Dept. "G. Galilei" Via Marzolo 8 35131 PADOVA ITALY
BASSOMPIERRE Gabriel	L.A.P.P. Chemin de Bellevue 74019 ANNECY-LE-VIEUX Cedex FRANCE
BELLOTTI Enrico	University Milano Physics Dept., Via Celoria 16 20133 MILANO ITALY
BERGKVIST Karl. E.	Research Institute of Physics Roslagsvagen 100 10405 STOCKHOLM 50 SWEDEN
BJORKEN James	Fermilab Box 500 60510 BATAVIA IL USA
BOEHM Felix	California Institute of Techn. Physics Department, 161-33 91125 PASADENA CA USA
BOGGILD Hans	Niels Bohr Institute Blegdamsveg 17 2100 COPENHAGEN DENMARK

BORCHERT Gunther L.	Institut für Kernphysik Kernforschungsanlage 5170 JÜLICH GERMANY F.R.
BOUCHEZ Jacques	DPhPE / SEPh CEN Saclay 91191 GIF SUR YVETTE Cedex FRANCE
CABRERA Blas	Physics Department Stanford University 94305 STANFORD CA USA
CAHEN Sébastien	Service d'Astrophysique CEN Saclay 91191 GIF SUR YVETTE Cedex FRANCE
CAVAIGNAC Jean-F.	Institut des Sciences Nucléaires 53, avenue des Martyrs 38026 GRENOBLE Cedex FRANCE
CHARDIN Gabriel	DPhPE CEN Saclay 91191 GIF SUR YVETTE Cedex FRANCE
CHING Cheng Rui	Inst. of Theor. Physics. P.O. Box 2735 BEIJING CHINA
CONFORTO Gianni	Ist. di Fisica, Univ. di Firenze Largo Enrico Fermi 2 50125 FIRENZE ITALY
DAR Arnon	Technion Israel Inst. of Techn. 32000 HAIFA ISRAEL
DAUM Manfred	Schweiz. Inst. f. Nuklearforsch. SIN 5234 VILLIGEN SWITZERLAND
DE RUJULA Alvaro	CERN TH Division 1211 GENEVE 23 SWITZERLAND
DECLAIS Yves	CPPM, Fac. Sciences Luminy Route Leon Lachamp 13288 MARSEILLE FRANCE

FACKLER Orrin	Lawrence Livermore Lab. Univ. of California P.O. Box 808 94550 LIVERMORE CA USA
FAVIER Jean	L.A.P.P. B. P. 909 74019 ANNECY-LE-VIEUX FRANCE
FERRONI Fernando	Istituto Nazionale di Fisica Nucleare Sezione di Roma, Piazzale Aldo Moro 2 00185 ROMA ITALY
FIORINI Ettore	Dipartimento di Fisica Via Celoria 16 20133 MILANO ITALY
FISHER Peter	CALTEC Physics Dept, 161-33 91125 PASADENA CA USA
FRITSCHI Markus	Physik Inst. der Univ. Zürich Schönberggasse 9 8001 ZÜRICH SWITZERLAND
GLASHOW Sheldon L.	Lyman Physics Laboratory Harvard University 02138 CAMBRIDGE MA USA
GONZALEZ-MESTRES Luis	L.A.P.P. B.P. 909 74019 ANNECY-LE-VIEUX Cedex FRANCE
GORITCHEV Peter	Inst. for Theor. and Exp. Physics B. Cheremushkinskaya ul. 25 117 259 MOSCOW USSR
HAHN Alan	Physics Department University of Calif. at Irvine 92717 IRVINE CA USA
HALL Lawrence	Lyman Physics Laboratory Harvard University 02138 CAMBRIDGE MA USA
HALPRIN Arthur	Physics Dept University of Delaware 223 Sharp Laboratory 19711 NEWARK DE USA

HAXTON Wick	Physics Dept. Univ. Washington F.M -15 98195 SEATTLE WA USA
HO Tso Hsin	Inst. of Theor. Physics P.O. Box 2735 BEIJING CHINA
HOLZSCHUH Eugen	Physik Inst., Universität Zürich Schönberggasse 9 8001 ZÜRICH SWITZERLAND
KANG Kyungsik	Brown University Department of Physics 02912 PROVIDENCE RI USA
KATSANEVAS Stavros	CERN EP Division CH-1211 GENEVE SWITZERLAND
KAWAKAMI Hirokane	Inst. for Nuclear Study, Nuclear Physics Div. Univ. of Tokyo, Tanashi-shi 188 TOKYO JAPAN
KAYSER Boris	Division of Physics National Science Foundation 20550 WASHINGTON DC USA
KELLS William	Fermilab P.O. Box 500 20510 BATAVIA ILL USA
KIRSTEN Till	Max-Planck-Institut für Kernphysik Postfach 103 980 6900 HEIDELBERG GERMANY F.R
KITAGAKI Toshio	Tohoku University Physics Dept., Aramaki 980 SENDAI JAPAN
KLAGES Hans O.	Institut für Kernphysik Postfach 3640 7500 KARLSRUHE 1 GERMANY F.R
KLAPDOR Hans Volker	Max-Planck Institut für Kernphysik Postfach 103980 6900 HEIDELBERG GERMANY F.R.

KLEINKNECHT Konrad	Universität Dortmund Institut für Physik, Postfach 500500 4600 DORTMUND 50 GERMANY F.R
KLINKHAMER Frans R.	Lawrence Berkeley Lab. Nuclear Science Division 94720 BERKELEY CA USA
KOLOS Wlodzimierz	Quantum Chemistry Lab. University of Warsaw, Pasteura 1 02-093 WARSAW POLAND
KOLTICK David	Physics Department Purdue University 47907 W. LAFAYETTE IN USA
KUNDIG Walter	Physik Institut Schönberggasse 9 8001 ZÜRICH SWITZERLAND
LABERRIGUE-FROLOW J.	LPNHE, Université Paris VII 4, Place Jussieu, Tour 32 75230 PARIS Cedex 05 FRANCE
LAGAGE Pierre-Olivier	CEN Saclay Service d'Astrophysique 91191 GIF SUR YVETTE Cedex FRANCE
LANGACKER Paul	Department of Physics University of Pennsylvania 19104-6396 PHILADELPHIA PA USA
LANOU Robert	Department of Physics Brown University 02912 PROVIDENCE RI USA
LETESSIER André	LPNHE,Université Paris VII 4, Place Jussieu, Tour 32 75230 PARIS Cedex 05 FRANCE
LEVY Jean-Michel	LPNHE, Université Paris VII 4, Place Jussieu, Tour 32 75230 PARIS Cedex 05 FRANCE
LOSECCO John	Department of Physics University of Notre Dame 46556 NOTRE DAME IN USA

LUBIMOV Valentine	Inst. for Theor. and Exp. Physics B. Cheremnshkinskaya ul. 25 117 259 MOSCOW USSR
MARTIN Thierry	Lab. de Phys. Corp. , Collège de France 11, Place Marcellin-Berthelot 75230 PARIS Cedex 05 FRANCE
MASCHUW Reinhard	Institut für Kernphysik Postfach 3640 7500 KARLSRUHE 1 GERMANY F. R.
MENNRATH Pierre	Centre d'Etudes Nucléaires Le Haut-Vigneau 33170 GRADIGNAN FRANCE
MESSIAH Albert	CEN Saclay Inst. de Rech. Fondam. 91191 GIF SUR YVETTE Cedex FRANCE
MONKHORST Hendrik J.	Physics Department University of Florida 32611 GAINESVILLE FL FRANCE
MORALES Angel	Depart. di Fisica Nucl. Facultad de Ciencias, Univ. Zaragoza 50009 ZARAGOZA SPAIN
MÖSSBAUER Rudolph. L	Physik Department E-15 Techn. Universität München 8046 GARCHING bei München GERMANY F.R
MUGGE Marshall	Lawrence Livermore Nat. Lab. Univ. of California, P.O. Box 808 94550 LIVERMORE CA USA
MURSULA Kalevi	Nordita Blegdamsveg 17 2100 COPENHAGEN DENMARK
NAGAI Yasuki	Tokyo Institute of Technology Dept. of Applied Phys., Oh-Okayama 152 TOKYO JAPAN
O'DONNELL Patrick	University of Toronto Department of Physics M5S 1A7 TORONTO, Ontario CANADA

PERRET-GALLIX Denis	L.A.P.P. B.P. 707 74019 ANNECY-LE-VIEUX Cedex FRANCE
PETCOV Sergey	Elem. Part. Theory Group Bulgarian Academy of Science, Bd. Lenin 72 1184 SOFIA BULGARIA
PETERSEN Jon Wulff	CERN EP Division 1211 GENEVA 23 SWITZERLAND
PIERRE François	DPhPE CEN Saclay 91191 GIF SUR YVETTE Cedex FRANCE
PILKUHN Hartmut	Inst. für Theor. Kernphysik Kaiserstrasse 12, Postfach 6380 7500 KARLSRUHE 1 GERMANY F.R
PIRAN Tsvi	Hebrew Univ. Physics Racah Institute of Physics 91 904 JERUSALEM ISRAEL
POMANSKY Alexandr	Institute for Nuclear Research 60 October Anniversary, Prospect 7a 117312 MOSCOW USSR
RIISAGER Karsten	Institute of Physics Univ. of Aarhus 8000 AARHUS C DENMARK
ROBERTSON Hamish	MS-D449 Physics Division Los Alamos Nat. Lab. 87545 LOS ALAMOS NM USA
ROOS Matts	Dept. of High Energy Physics Siltavuorenpenger 20 C 00170 HELSINKI FINLAND
ROSEN Peter	T-DO M.S. B288 Los Alamos Nat. Lab. 87545 LOS ALAMOS NM USA
SANTONI Claudio	CERN Division EP 1211 GENEVE 23 SWITZERLAND

SCHATZMAN Evry	Observatoire Université de Nice, B.P. 139 06003 NICE Cedex FRANCE
SCHRAMM David	University of Chicago Astronomy Dept., 5640 South Ellis Av. 60637 CHICAGO IL USA
SCHRECKENBACH Klaus	Inst. Laue - Langevin B.P. 156 X 38042 GRENOBLE Cedex FRANCE
SHAEVITZ Michael H.	Columbia University Dept. of Physics 10027 NEW YORK N.Y. USA
SIMPSON John	University of Guelph Dept. of Physics GUELPH, Ontario CANADA
SMIRNOV Alexei	Inst. for Nuclear Research 60th October Anniversary, Prospect 7a 117312 MOSCOW USSR
SMITH Elton	Ohio State University 174 W 18th Av. 43210-1106 COLUMBUS OH USA
SOBEL Henry	University of California Department of Physics 92717 IRVINE CA USA
SONA Pietro	Istit. Naz. di Fisica Nucl. Largo E Fermi 2 (Arcetri) 50125 FIRENZE ITALY
SPERGEL David	Center for Astrophysics Harvard Observatory, 60 Garden Str. 02138 CAMBRIDGE MA USA
SPIRO Michel	DPhPE CEN Saclay 91191 GIF SUR YVETTE Cedex FRANCE
STEIGMAN Gary	Bartol Research Foundation University of Delaware 19711 NEWARK DE USA

TAKASUGI Eiichi	Inst. of Physics, Coll. of Gen. Education 1-1 Machikaneyama-cho, Toyonaka-shi 560 OSAKA JAPAN
TASIAUX Baudouin	Inst. de Physique, Univ. Cathol. de Louvain 2, chemin du Cyclotron 1348 LOUVAIN-LA-NEUVE BELGIUM
TOUCHARD Anne Marie	LPNHE, Université Paris VII 4, Place Jussieu, Tour 32 75230 PARIS Cedex 06 FRANCE
TRAN THANH VAN Jean	L.P.T.P.E Batiment 211, Univ. Paris Sud 91405 ORSAY Cedex FRANCE
TWERENBOLD Damian	Schweizerisches Institut für Nuklear Forschung 5234 VILLIGEN SWITZERLAND
VANNUCCI François	LPNHE, Université Paris VII 4, Place Jussieu, Tour 32 75230 PARIS Cedex FRANCE
VOGEL Petr	Physics Dept. 161-33 California Institute of Technology 91125 PASADENA CA USA
VON FEILITZSCH Franz	Physik Dept. E 15 Techn. Univ. München 8046 GARCHING bei München GERMANY F.R
VUILLEUMIER Jean-Luc	Inst. de Phys., Université de Neuchatel Rue A.L. Breguet 1 2000 NEUCHATEL SWITZERLAND
WAYSAND Georges	Gr. de Phys. des Solides de l'ENS Univ. Paris VI, 2 Pl. Jussieu, Tour 23 75251 PARIS Cedex 05 FRANCE
WELLENSTEIN Hermann F.	Brandeis University Physics Department 02254-9110 WALTHAM MA USA
WILKERSON John	Los Alamos National Lab. MS-D-449 87545 LOS ALAMOS NM USA

YAMAGUCHI Akira
Department of Physics
Tohoku University, Aramaki
980 SENDAI
JAPAN

YASUMI Shinjiro
Nat. Lab. High Energy Phys.(KEK)
Oho-Machi, Tsukuba-gun
305 IBARAKI-KEN
JAPAN

ZACEK Viktor
CERN
E.P. Division
1211 GENEVE 23
SWITZERLAND